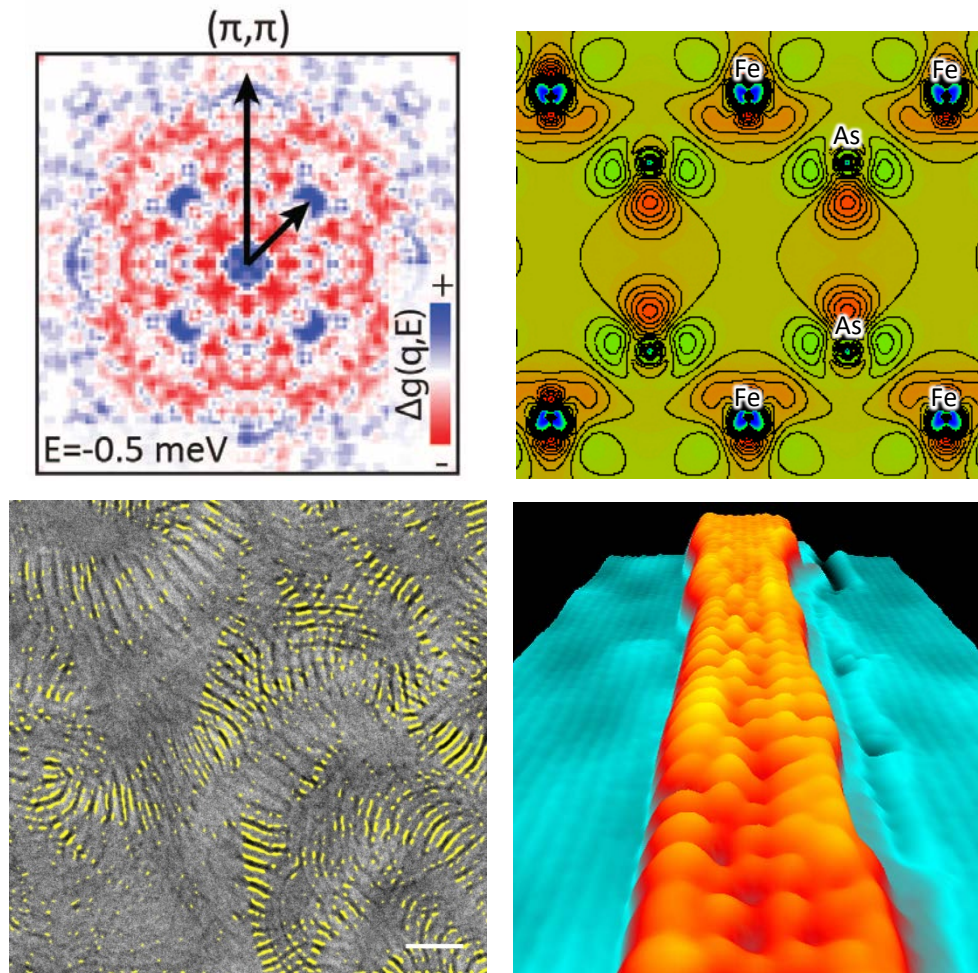


Electron and Scanning Probe Microscopies

2014 Principal Investigators' Meeting



Hilton Washington DC North/Gaithersburg
Gaithersburg, Maryland
October 20-22, 2014



U.S. DEPARTMENT OF
ENERGY

Office of
Science

Office of Basic Energy Sciences
Materials Sciences and Engineering Division

On the Cover

- Top Left:** *Demonstration of Magnetic Cooper Pairing Mechanism for Superconductivity in CeCoIn₅.* Figure shows a measured response of scattering interference in superconducting CeCoIn₅ in magnetic field using scanning tunneling microscopy (STM). Precision measurements of the heavy-fermion band structure using quasiparticle interference imaging (QPI) unveil the momentum (k-space) structure of the magnetic 4f-electron interactions in CeCoIn₅. Work published in *Proc. Nat. Acad. Sci.* **111**, 11663 (2014).
Courtesy: Séamus Davis, Brookhaven National Laboratory
- Top Right:** *New Path to Loss-Free Electricity.* Orbital electron redistribution map using quantitative electron diffraction in BaFe₂As₂ after Co atoms are doped. The lines are density contours. The red areas indicate where the orbital electrons are increased (quadrupole around Fe and dipole around As) after doping which can be directly related to the induced superconductivity state. The experimental results show that orbital fluctuation and electronic polarization are strongly coupled in an iron-based superconductor. Work published in *Phys. Rev. Lett.* **112**, 077001 (2014).
Courtesy: Yimei Zhu, Brookhaven National Laboratory
- Bottom Left:** *Water Uptake and Proton Conductivity of a Model Fuel Cell Membrane.* Cryo-STEM image of hydrated polystyrenesulfonate-block-polyethylene-block-polystyrenesulfonate (S-SES). The darkest phase represents polyethylene while hydrated polystyrenesulfonate (PSS) phase is heterogeneous. Scale bar represents 200 nm. Work published in *Nano Letters* **14**, 4058 (2014).
Courtesy: Nitash Balsara, Lawrence Berkeley National Laboratory
- Bottom Right:** *Edging a Gap in Graphene.* STM image shows a variable width graphene nanoribbon supported on graphene/SiC(0001) in 3D perspective view. Experimental results confirm that interactions of spin-polarized edge states open an energy gap in graphene. Work published in *Nature Communications* **5**, 4311 (2014).
Courtesy: Lian Li, University of Wisconsin

This document was produced under contract number DE-AC05-06OR23100 between the U.S. Department of Energy and Oak Ridge Associated Universities.

The research grants and contracts described in this document are supported by the U.S. DOE Office of Science, Office of Basic Energy Sciences, Materials Sciences and Engineering Division.

Foreword

This volume comprises the scientific content of the 2014 Electron and Scanning Probe Microscopies Principal Investigators' Meeting sponsored by the Materials Sciences and Engineering Division (MSED) in the Office of Basic Energy Sciences (BES) of the U. S. Department of Energy (DOE). The meeting, held on October 20–22, 2014, in Gaithersburg, Maryland, is the fifth biennial Principal Investigators' Meeting in the Electron and Scanning Probe Microscopies area and is one among a series of research theme-based Principal Investigators' meetings conducted by BES.

The purpose of the Principal Investigators' Meeting is to bring together researchers funded in the Electron and Scanning Probe Microscopies core research area to facilitate the exchange of new results and research highlights, to foster new ideas and collaborations among the participants, and to discuss how to advance electron and scanning probe microscopy and spectroscopy, as well as the associated theoretical tools, in order to address forefront scientific challenges. In addition, the meeting affords BES program managers an opportunity to assess the state of the entire program collectively on a periodic basis, in order to chart future directions and identify new programmatic needs.

The Electron and Scanning Probe Microscopies Core Research Activity supports basic research in materials sciences using advanced electron and scanning probe microscopy and spectroscopy techniques to understand the atomic, electronic, and magnetic structures and properties of materials. This activity also supports the development of new instrumentation and techniques to advance basic science and materials characterizations for energy applications. Topical areas highlighted in this year's meeting include two-dimensional materials, magnetic hybrid structures, complex functional oxides & ferroelectrics, electron/spin order & spintronics, materials for energy storage and generation, strongly correlated materials, electron tomography, and novel microscopy methods.

I thank all the meeting attendees for their active participation and sharing their ideas and new research results. Special thanks are given to the Meeting Chairs, Hari Manoharan and Yimei Zhu, for their dedicated efforts towards organizing this meeting. I would also like to express my appreciation to Teresa Crockett in MSED, and to Tammy Click and Verda Adkins-Ferber at the Oak Ridge Institute for Science and Education for their assistance with the logistics of this meeting.

Jane G. Zhu
Program Manager, Electron and Scanning Probe Microscopies
Division of Materials Sciences and Engineering, Basic Energy Sciences
Office of Science
U. S. Department of Energy

AGENDA

2014 Electron and Scanning Probe Microscopies Principal Investigators' Meeting

*Materials Sciences and Engineering Division, Office of Basic Energy Science
U. S. Department of Energy*

SUNDAY, OCTOBER 19, 2014

*****Arrival, Dinner on Your Own*****

MONDAY, OCTOBER 20, 2014

- 7:00 – 8:30 am *****Breakfast *****
- 8:30 – 9:00 am Introductory Remarks
Linda Horton
Director, Materials Sciences and Engineering Division, Basic Energy Sciences
- 9:00 – 9:20 am **Jane Zhu**
Program Manager, Electron and Scanning Probe Microscopies
Meeting Chairs: **Hari Manoharan** and **Yimei Zhu**
SLAC, Stanford University/ Brookhaven National Laboratory
- Session I Two-Dimensional Materials**
Chair: **Markus Raschke**, University of Colorado
- 9:20 – 9:45 am **Amir Yacoby**, Harvard University
Transport and Imaging of Mesoscopic Phenomena in Single and Bilayer Graphene
- 9:45 – 10:10 am **Wu Zhou**, Oak Ridge National Laboratory
Scanning Transmission Electron Microscopy: Atomic Structure and Properties of Materials
- 10:10 – 10:20 am Chair-Led discussion
- 10:20 – 10:50 am *****Break*****
- Session II Magnetic Hybrid Structures**
Chair: **Yimei Zhu**, Brookhaven National Laboratory
- 10:50 – 11:15 am **Amanda Petford-Long**, Argonne National Laboratory
3D Visualization of Emergent Behavior in Nanoscale Functional Heterostructures
- 11:15 – 11:40 am **Dan Dougherty**, North Carolina State University
The Nature of the Spin-Dependent Surface Chemical Bond: The Role of Surface States

11:40 – 12:05 pm **David Muller**, Cornell University
Using Interfaces to Create Strongly-Coupled Magnetic-Ferroelectrics

12:05 – 12:15 pm Chair-Led discussion

12:20 – 1:30 pm *****Working Lunch*****

Session III

Complex Functional Oxides

Chair: **Sergei Kalinin**, Oak Ridge National Laboratory

1:30 – 1:55 pm **Weida Wu**, Rutgers University
In Situ Scanning Probe Microscopy Studies of Cross-Coupled Domains and Domain Walls

1:55 – 2:20 pm **Myung-Geun Han**, Brookhaven National Laboratory
Electric Field Effects in Complex Functional Oxides

2:20 – 2:45 pm **Ward Plummer**, Louisiana State University
Emerging Functionality in Transition-Metal Compounds Driven by Spatial Confinement

2:45 – 3:10 pm **Laurence Marks**, Northwestern University
New Strategies to Image Surfaces

3:10 – 3:20 pm Chair-Led discussion

3:20 – 5:00 pm ******* Poster Session I (and refreshments/coffee break) *******

Session IV

Electron Tomography

Chair: **Jim Zuo**, University of Illinois

5:00 – 5:25 pm **Marc De Graef**, Carnegie Mellon University
Materials Applications of Aberration-Corrected Lorentz Microscopy

5:25 – 5:50 pm **Jianwei (John) Miao**, University of California, Los Angeles
Atomic Resolution Electron Tomography

5:50 – 6:15 pm **Ian Robertson**, University of Wisconsin-Madison
Four-Dimensional Characterization of Dislocation-Defect Interactions in Aggressive Environments – A New Approach

6:15 – 6:25 pm Chair-Led discussion

6:30 – 8:00 pm *****Working Dinner*****

8:00 – 9:30 pm Poster Session I continued and Discussions

TUESDAY, OCTOBER 21, 2014

- 7:00 – 8:30 am *****Breakfast*****
- Session V** **Electron and Spin Order**
Chair: **Hari Manoharan**, SLAC/Stanford University
- 8:30 – 8:55 am **Shoucheng Zhang**, Stanford Institute for Materials and Energy Sciences
Spin Physics and Nanoscale Probes of Quantum Materials
- 8:55 – 9:20 am **Vidya Madhavan**, University of Illinois, Urbana-Champaign
STM Studies of Spin-Orbit Coupled Phases in Real- and Momentum-Space
- 9:20 – 9:45 am **Susanne Stemmer**, University of California, Santa Barbara
Probing Correlated Phenomena in Oxide Structures with Quantitative STEM
- 9:45 – 9:55 am Chair-Led discussion
- 9:55 – 10:25 am *****Break*****
- Session VI** **Ferroelectrics**
Chair: **Xiaoqing Pan**, University of Michigan
- 10:25 – 10:50 am **Albina Borisevich**, Oak Ridge National Laboratory
Probing Phase Transitions, Chemical Reactions, and Energy Transfer at the Atomic Scale
- 10:50 – 11:15 am **P. Maksymovych**, Oak Ridge National Laboratory
Probing Coupled Bias- and Pressure Induced Metal-Insulator and Ferroic Transitions on the Mesoscopic Scale
- 11:15 – 11:40 am **Keji Lai**, University of Texas at Austin
Microscopy of Electrostatic Field Effect in Novel Quantum Materials
- 11:40 – 12:05 pm **Long-Qing Chen**, Pennsylvania State University
Structure and Dynamics of Domains in Ferroelectric Nanostructures – Phase-field Modeling
- 12:05 – 12:15 pm Chair-Led discussion
- 12:20 – 1:30 pm *****Working Lunch*****
- Session VII** **Spintronics**
Chair: **Maria Iavarone**, Temple University
- 1:30 – 1:55 pm **Chris Hammel**, Ohio State University
Understanding Microscopic Mechanisms of Spin Pumping and Magnetization Dynamics in Novel, Tailored Magnetic Material Systems

1:55 – 2:20 pm	Jesse Berezovsky , Case Western Reserve University <i>Towards Mapping Interactions in Hybrid Systems with Active Scanning Probes</i>
2:20 – 2:45 pm	Arthur Smith , Ohio University <i>Spin-Polarized Scanning Tunneling Microscopy Studies of Nanoscale Magnetic and Spintronic Nitride Systems</i>
2:45 – 2:55 pm	Chair-Led discussion
3:00 – 4:40 pm	***Poster Session II (and refreshments/coffee break)***
Session VIII	Materials for Energy Storage and Generation Chair: Haimei Zheng , Lawrence Berkeley National Laboratory
4:40 – 5:05 pm	Shirley Meng , University of California, San Diego <i>New In Situ Analytical Electron Microscopy for Understanding Structure Evolution and Composition Change in High Energy Density Electrode Materials in Lithium Ion Batteries</i>
5:05 – 5:30 pm	Santiago Solares , George Washington University <i>Trimodal Tapping Mode Atomic Force Microscopy: Simultaneous 4D Mapping of Conservative and Dissipative Probe-Sample Interactions of Energy-Relevant Materials</i>
5:30 – 5:55 pm	Peter Crozier , Arizona State University <i>Development and Application of In Situ Nanocharacterization to Photocatalytic Materials for Solar Fuel Generation</i>
5:55 – 6:05 pm	Chair-Led discussion
6:30 – 8:00 pm	***Working Dinner***
8:00 – 9:30 pm	Poster Session II continued and Discussions

WEDNESDAY, OCTOBER 22, 2014

7:00 – 8:00 am	***Breakfast***
Session IX	Strongly Correlated Materials Chair: Seamus Davis , Cornell University/Brookhaven National Laboratory
8:00 – 8:25 am	Ali Yazdani , Princeton University <i>Probing Correlated Superconductors and Their Phase Transitions on the Nanometer Scale</i>
8:25 – 8:50 am	David Cobden , University of Washington <i>Combined Microscopy Studies of Complex Electronic Materials</i>

8:50 – 9:15 am **Benjamin Lev**, Stanford University
Scanning Quantum Gas Atom Chip Microscopy of Strongly Correlated and Topologically Nontrivial Materials

9:15 – 9:25 am Chair-Led discussion

9:25 – 10:00 am *** **Break*****

Session X **Novel Methods**
Chair: **Phil Batson**, Rutgers University

10:00 – 10:25 am **Benjamin McMorran**, University of Oregon
Electron Microscopy with Vortex Beams Carrying Orbital Angular Momentum

10:25 – 10:50 am **Sok Pantelides**, Vanderbilt University
Physics of Complex Materials Systems through Theory and Microscopy/EELS

10:50 – 11:00 am Chair-Led discussion

11:00 – 12:00 pm *Wrap-up: Remarks, Concluding Comments & Discussions*
Hari Manoharan and **Yimei Zhu**, Meeting Chairs
Jane Zhu, Program Manager, Electron and Scanning Probe Microscopies

POSTER SESSIONS

2014 Electron and Scanning Probe Microscopies Principal Investigators' Meeting

Poster Session 1: Monday, 3:20–5:00 & 8:00–9:30 pm

- P-I.1 Structure and Dynamics of Domains in Ferroelectric Nanostructures – Phase-Field Modeling
Long-Qing Chen, The Pennsylvania State University
- P-I.2 Trimodal Tapping Mode Atomic Force Microscopy: Simultaneous 4D Mapping of Conservative and Dissipative Probe-Sample Interactions of Energy-Relevant Materials
Santiago D. Solares, George Washington University
- P-I.3 Materials Applications of Aberration-Corrected Lorentz Microscopy
Marc De Graef, Carnegie Mellon University
- P-I.4 The Nature of the Spin-Dependent Surface Chemical Bond: The Role of Surface States
Dan Dougherty, North Carolina State University
- P-I.5 Time-Resolved Electrical, Optical, and Thermal Probes of Topological Spin Textures in Magnetic Nanostructures
Gregory Fuchs, Cornell University
- P-I.6 Cryogenic Nano-Scale Optical Spectroscopy in Correlated Systems
Adrian Gozar, Brookhaven National Laboratory
- P-I.7 Polarization-Coupled Tunable Resistive Behavior in Oxide Ferroelectric Heterostructures
Alexei Gruverman, University of Nebraska
- P-I.8 Electric Field Effects in Complex Functional Oxides
Myung-Geun Han, Brookhaven National Laboratory
- P-I.9 High Speed SPM of Functional Materials
Bryan D. Huey, University of Connecticut
- P-I.10 Probing Coupled Metal-Insulator and Ferroic Transitions from the Atomistic to Mesoscopic Scales
S. V. Kalinin, Oak Ridge National Laboratory
- P-I.11 Microscopy of Electrostatic Field Effect in Novel Quantum Materials
Keji Lai, University of Texas at Austin
- P-I.12 Tailoring the Electronic Properties of Graphene via Nanostructuring: An Integrated Atomic Resolution STM and Non-contact AFM Study
Lian Li, University of Wisconsin

- P-I.13 STM Studies of Spin-Orbit Coupled Phases in Real- and Momentum-Space
Vidya Madhavan, University of Illinois
- P-I.14 Probing Coupled Bias- and Pressure Induced Metal-Insulator and Ferroic Transitions on the Mesoscopic Scale
P. Maksymovych, Oak Ridge National Laboratory
- P-I.15 New Strategies to Image Surfaces
Laurence Marks, Northwestern University
- P-I.16 Atomic Resolution Electron Tomography
Jianwei (John) Miao, University of California
- P-I.17 Using Interfaces to Create Strongly Coupled Magnetic-Ferroelectrics
David A. Muller, Cornell University
- P-I.18 Structure and Dynamics of Domains in Ferroelectric Nanostructures – In Situ TEM Studies
Xiaoqing, Pan, University of Michigan
- P-I.19 3D Visualization of Emergent Behavior in Nanoscale Functional Heterostructures
Amanda K. Petford-Long, Argonne National Laboratory
- P-I.20 Emerging Functionality in Transition-Metal Compounds Driven by Spatial Confinement
Ward Plummer, Louisiana State University
- P-I.21 Nano-Imaging and -Spectroscopy of Complex and Correlated Materials
Markus B. Raschke, University of Colorado
- P-I.22 Four-Dimensional Characterization of Dislocation-Defect Interactions in Aggressive Environments – A New Approach
Ian M. Robertson, University of Illinois
- P-I.23 Quantum Control of Spins in Diamond for Nanoscale Magnetic Sensing and Imaging
Gurudev Dutt, University of Pittsburgh
- P-I.24 Understanding the Emergent Phenomena Arising from Competing Degrees of Freedom in Doped Manganites
Jing Tao, Brookhaven National Laboratory
- P-I.25 Scanning Transmission Electron Microscopy: Atomic Structure and Properties of Materials
Maria Varela, Oak Ridge National Laboratory
- P-I.26 In Situ Scanning Probe Microscopy Studies of Cross-Coupled Domains and Domain Walls
Weida Wu, Rutgers, the State University of New Jersey
- P-I.27 Transport and Imaging of Mesoscopic Phenomena in Single and Bilayer Graphene
Amir Yacoby, Harvard University

- P-I.28 Spin Physics and Nanoscale Probes of Quantum Materials
Shoucheng Zhang, Stanford University
- P-I.29 Scanning Transmission Electron Microscopy: Atomic Structure and Properties of Materials
Wu Zhou, Oak Ridge National Laboratory
- P-I.30 Dynamics of Topological Nano-Magnetism with Broken Symmetry
Yimei Zhu, Brookhaven National Laboratory
- P-I.31 Current Trends in STM at the Center for Nanoscale Materials
Nathan Guisinger, Argonne National Laboratory

Poster Session 2: Tuesday, 3:00–4:40 & 8:00–9:30 pm

- P-II.1 Soft Matter Electron Microscopy
Nitash Balsara, Lawrence Berkeley National Laboratory
- P-II.2 Discovery of Dielectric Response and Forces in Sub-nanoscale Objects
P. E. Batson, Rutgers, the State University of New Jersey
- P-II.3 Towards Mapping Interactions in Hybrid Systems with Active Scanning Probes
Jesse Berezovsky, Case Western Reserve University
- P-II.4 Probing Phase Transitions, Chemical Reactions, and Energy Transfer at the Atomic Scale
Albina Y. Borisevich, Oak Ridge National Laboratory
- P-II.5 Application of STEM/EELS to Plasmon-Related Effects in Optical Spectroscopy
Jon P. Camden, University of Notre Dame
- P-II.6 Complex Fundamental Mechanisms of Transient States in Materials Quantified by DTEM
Geoffrey H. Campbell, Lawrence Livermore National Laboratory
- P-II.7 Combined Microscopy Studies of Complex Electronic Materials
David H. Cobden, University of Washington
- P-II.8 Spectroscopic Imaging STM and Complex Electronic Matter
J. C. Séamus Davis, Brookhaven National Laboratory
- P-II.9 Probing Correlated Superconductors and Their Phase Transitions on the Nanometer Scale
Ali Yazdani, Princeton University
- P-II.10 Scanning Quantum Gas Atom Chip Microscopy of Strongly Correlated and Topologically Nontrivial Materials
Benjamin Lev, Stanford University

- P-II.11 Mapping Valence Electron Distribution using Quantitative Electron Diffraction to Understand Orbital Fluctuation and Superconductivity
Lijun Wu, Brookhaven National Laboratory
- P-II.12 Electron Microscopy with Vortex Beams Carrying Orbital Angular Momentum
Benjamin J. McMorran, University of Oregon
- P-II.13 Physics of Complex Materials Systems through Theory and Microscopy/EELS
Socrates T. Pantelides, Vanderbilt University
- P-II.14 Imaging Point Defects with Quantitative STEM
Paul M. Voyles, University of Wisconsin
- P-II.15 Electron Density Determination, Bonding and Properties of Tetragonal Ferromagnetic Intermetallics
Jörg M. K. Wiezorek, University of Pittsburgh
- P-II.16 Photon and Surface Plasmon Dynamics Studied in Photoemission Electron Microscopy (PEEM)
Rolf Koenenkamp, Portland State University
- P-II.17 Dynamical Nanoscale Electron Crystallography
Chong-Yu Ruan, Michigan State University
- P-II.18 Scanning Transmission Electron Microscopy: Atomic Structure and Properties of Materials
Andrew R. Lupini, Oak Ridge National Laboratory
- P-II.19 Study of Nanoscale Heat Transport and Dissipation
Pramod Reddy, University of Michigan
- P-II.20 Real Time TEM Imaging of Materials Transformations in Liquid and Gas Environments
Haimei Zheng, Lawrence Berkeley National Laboratory
- P-II.21 In-Situ TEM Observations of Degradation Mechanisms in Next-Generation High-Energy Density Lithium-Ion Battery
Shen J. Dillon, University of Illinois
- P-II.22 Development and Application of In Situ Nanocharacterization to Photocatalytic Materials for Solar Fuel Generation
Peter A. Crozier, Arizona State University
- P-II.23 New In Situ Analytical Electron Microscopy for Understanding Structure Evolution and Composition Change in High Energy Density Electrode Materials in Lithium Ion Batteries
Shirley Meng, University of California
- P-II.24 Vortex Matter in Confined Superconductors and Mesoscopic Hybrid Heterostructures
Maria Iavarone, Temple University

- P-II.25 Spin-Polarized Scanning Tunneling Microscopy Studies of Nanoscale Magnetic and Spintronic Nitride Systems
Arthur R. Smith, Ohio University
- P-II.26 Medium-Range Order in Amorphous Materials Studied by Fluctuation Electron Microscopy
M. M. J. Treacy, Arizona State University
- P-II.27 Probing Correlated Phenomena in Oxide Structures with Quantitative STEM
Susanne Stemmer, University of California
- P-II.28 Understanding Microscopic Mechanisms of Spin Pumping and Magnetization Dynamics in Novel, Tailored Magnetic Material Systems
P. Chris Hammel, Ohio State University
- P-II.29 Electron Nanocrystallography of Complex Materials and Processes
Jian-Min Zuo, University of Illinois
- P-II.30 Surface Electronic Magnetism Probed by STM, Transport, and Magneto-optics
Hari Manoharan, SLAC/Stanford University
- P-II.31 Beneath and Between: Structural, Functional, and Spectroscopic Measurements of Buried Interfaces and Interactions
Paul S. Weiss, University of California

Table of Contents

Table of Contents

Foreword	i
Agenda	ii
Poster Sessions List	vii
Table of Contents	xiv

Laboratory Projects

Soft Matter Electron Microscopy

Nitash Balsara, Kenneth Downing, Andrew Minor, Ronald Zuckermann, Jeffrey Kortright, and David Prendergast	2
---	----------

Probing Phase Transitions, Chemical Reactions, and Energy Transfer at the Atomic Scale

Albina Y. Borisevich, Sokrates T. Pantelides, Jae Hyuck Jang, Qiuhan He, and Rohan Mishra	6
--	----------

Complex Fundamental Mechanisms of Transient States in Materials Quantified by DTEM

Geoffrey H. Campbell, Melissa K. Santala, Joseph T. McKeown, Robert E. Rudd, Linh Nguyen, and Tae Wook Heo	10
---	-----------

Spectroscopic Imaging STM for Complex Electronic Matter

J. C. Séamus Davis	14
---------------------------------	-----------

Cryogenic Nano-scale Optical Spectroscopy in Correlated Electron Systems

Adrian Gozar	18
---------------------------	-----------

Electric Field Effects in Complex Functional Oxides

Myung-Geun Han, Joseph Garlow, and Yimei Zhu	22
---	-----------

Probing Coupled Metal-Insulator and Ferroic Transitions from the Atomistic to Mesoscopic Scales

S. V. Kalinin, P. Maksymovych, R. Vasudevan, A. Tselev, A. Gianfrancesco, and W. Lin	26
---	-----------

Scanning Transmission Electron Microscopy: Atomic Structure and Properties of Materials

Andrew R. Lupini, Maria Varela, Wu Zhou, and Matthew F. Chisholm	30
---	-----------

<i>Probing Coupled Bias- and Pressure Induced Metal-Insulator and Ferroic Transitions on the Mesoscopic Scale</i> P. Maksymovych, S. V. Kalinin, R. Vasudevan, A. Tselev, A. Gianfrancesco, and W. Lin	34
<i>3D Visualization of Emergent Behavior in Nanoscale Functional Heterostructures</i> Amanda K. Petford-Long, Seungbum Hong, and Charudatta Phatak	38
<i>Understanding the Emergent Phenomena Arising from Competing Degrees of Freedom in Doped Manganites</i> Jing Tao and Yimei Zhu	42
<i>Scanning Transmission Electron Microscopy: Atomic Structure and Properties of Materials: Complex Oxide Functionality</i> Maria Varela, Matthew F. Chisholm, Andrew R. Lupini, and Wu Zhou	46
<i>Mapping Valence Electron Distribution using Quantitative Electron Diffraction to Understand Orbital Fluctuation and Superconductivity</i> Lijun Wu, Chao Ma, and Yimei Zhu	50
<i>Spin Physics and Nanoscale Probes of Quantum Materials</i> Shoucheng Zhang, Hari C. Manoharan, David Goldhaber-Gordon, and Joseph Orenstein	54
<i>Real Time TEM Imaging of Materials Transformations in Liquid or Gas Environments</i> Haimei Zheng	58
<i>Scanning Transmission Electron Microscopy: Atomic Structure and Properties of Materials Nanomaterials: Defects in 2D Materials</i> Wu Zhou, Matthew F. Chisholm, Andrew R. Lupini, and Maria Varela	62
<i>Dynamics of Topological Nano-Magnetism with Broken Symmetry</i> Shawn D. Pollard, Javier F. Pulecio, Vyacheslav V. Volkov, and Yimei Zhu	66
University Grant Projects	
<i>Discovery of Dielectric Response and Forces in Nanoscale Objects</i> P. E. Batson and M. J. Lagos	72
<i>Towards Mapping Interactions in Hybrid Systems with Active Scanning Probes</i> Jesse Berezovsky	76
<i>Application of STEM/EELS to Plasmon-Related Effects in Optical Spectroscopy</i> Jon P. Camden	80

<i>Superconducting Properties of the LaAlO₃/SrTiO₃ Interface</i> Venkat Chandrasekhar	84
<i>Structure and Dynamics of Domains in Ferroelectric Nanostructures—Phase-Field Modeling</i> Long-Qing Chen	88
<i>Combined Microscopy Studies of Complex Electronic Materials</i> David H. Cobden	92
<i>Development and Application of In Situ Nanocharacterization to Photocatalytic Materials for Solar Fuel Generation</i> Peter A. Crozier	96
<i>Materials Applications of Aberration-Corrected Lorentz Microscopy</i> Marc De Graef, Emma Humphrey, and Prabhat Kc	100
<i>In-Situ TEM Observations of Degradation Mechanisms in Next-Generation High-Energy Density Lithium-Ion Battery Systems</i> Shen J. Dillon	104
<i>The Nature of the Spin-Dependent Surface Chemical Bond: The Role of Surface States</i> Dan Dougherty	108
<i>Quantum Control of Spins in Diamond for Nanoscale Magnetic Sensing and Imaging</i> Gurudev Dutt	112
<i>Time-Resolved Electrical, Optical, and Thermal Probes of Topological Spin Textures in Magnetic Nanostructures</i> Gregory Fuchs	116
<i>Polarization-Coupled Tunable Resistive Behavior in Oxide Ferroelectric Heterostructures</i> Alexei Gruverman, Chang-Beom Eom, and Evgeny Tsymbal	118
<i>Understanding Microscopic Mechanisms of Spin Pumping and Magnetization Dynamics in Novel, Tailored Magnetic Material Systems</i> P. Chris Hammel	122
<i>High Speed SPM of Functional Materials</i> Bryan D. Huey	126
<i>Vortex Matter in Confined Superconductors and Mesoscopic Hybrid Heterostructures</i> Maria Iavarone	130

<i>Photon and Surface Plasmon Dynamics Studied in Photoemission Electron Microscopy (PEEM)</i> Rolf Könenkamp	134
<i>Microscopy of Electrostatic Field Effect in Novel Quantum Materials</i> Keji Lai	138
<i>Scanning Quantum Gas Atom Chip Microscopy of Strongly Correlated and Topologically Nontrivial Materials</i> Benjamin Lev	142
<i>Tailoring the Electronic Properties of Graphene via Nanostructuring: An Integrated Atomic Resolution STM and Non-contact AFM Study</i> Lian Li	146
<i>STM Studies of Spin-Orbit Coupled Phases in Real- and Momentum-Space</i> Vidya Madhavan	150
<i>New Strategies to Image Surfaces</i> L. D. Marks	154
<i>Electron Microscopy with Vortex Beams Carrying Orbital Angular Momentum</i> Benjamin J. McMorran	158
<i>New In Situ Analytical Electron Microscopy for Understanding Structure Evolution and Composition Change in High Energy Density Electrode Materials in Lithium Ion Batteries</i> Shirley Meng, Feng Wang, Huolin Xin, Nancy Dudney, Nina Balke, and Oleg Shpyrko	162
<i>Atomic Resolution Electron Tomography</i> Jianwei (John) Miao	166
<i>Using Interfaces to Create Strongly Coupled Magnetic-Ferroelectrics</i> David A. Muller, Craig J. Fennie, Darrell G. Schlom, and Peter Schiffer	170
<i>Structure and Dynamics of Domains in Ferroelectric Nanostructures – In Situ TEM Studies</i> Xiaoqing Pan	174
<i>Physics of Complex Materials Systems through Theory and Microscopy/EELS</i> Sokrates T. Pantelides, Mark P. Oxley, and Kalman Varga	178
<i>Emerging Functionality in Transition-Metal Compounds Driven by Spatial Confinement</i> Ward Plummer	182

<i>Nano-Imaging and -Spectroscopy of Complex and Correlated Materials</i> Markus B. Raschke	186
<i>Study of Nanoscale Heat Transport and Dissipation</i> Pramod Reddy	190
<i>Four-Dimensional Characterization of Dislocation-Defect Interactions in Aggressive Environments – A New Approach</i> Ian M. Robertson	194
<i>Dynamical Nanoscale Electron Crystallography</i> Chong-Yu Ruan	198
<i>Spin-Polarized Scanning Tunneling Microscopy Studies of Nanoscale Magnetic and Spintronic Nitride Systems</i> Arthur R. Smith and Jeongihm Pak	202
<i>Trimodal Tapping Mode Atomic Force Microscopy: Simultaneous 4D Mapping of Conservative and Dissipative Probe-Sample Interactions of Energy-Relevant Materials</i> Santiago D. Solares	206
<i>Probing Correlated Phenomena in Oxide Structures with Quantitative STEM</i> Susanne Stemmer	210
<i>Medium-Range Order in Amorphous Materials Studied by Fluctuation Electron Microscopy</i> M. M. J. Treacy	214
<i>Imaging Point Defects with Quantitative STEM</i> Paul M. Voyles and Dane Morgan	218
<i>Beneath and Between: Structural, Functional, and Spectroscopic Measurements of Buried Interfaces and Interactions</i> Paul S. Weiss	222
<i>Electron Density Determination, Bonding and Properties of Tetragonal Ferromagnetic Intermetallics</i> Jörg M. K. Wiezorek	225
<i>In Situ Scanning Probe Microscopy Studies of Cross-Coupled Domains and Domain Walls</i> Weida Wu	229
<i>Transport and Imaging of Mesoscopic Phenomena in Single and Bilayer Graphene</i> Amir Yacoby and Pablo Jarillo-Herrero	233

<i>Probing Correlated Superconductors and Their Phase Transitions on the Nanometer Scale</i>	
Ali Yazdani	237
<i>Electron Nanocrystallography of Complex Materials and Processes</i>	
Jian-Min Zuo	241
Author Index	246
Participant List	248

LABORATORY PROJECTS

Soft Matter Electron Microscopy

Principal Investigators: Nitash Balsara*, Kenneth Downing, Andrew Minor, Ronald Zuckermann, Jeffrey Kortright, David Prendergast

*Materials Sciences Division, Lawrence Berkeley National Laboratory, Berkeley, CA 94709.
email: nbalsara@lbl.gov

Program Scope

Soft polymer materials are an integral part of the emerging clean energy landscape. Our current focus is on ion-containing polymers for clean energy applications. The integration of state-of-the-art synthesis with electron-based imaging and spectroscopy enables understanding of the underpinnings of macroscopic behavior of soft materials. The synthetic approaches include recently developed methods for synthesizing polypeptoids using solid-phase synthesis. This

approach allows synthesis of sequence-specific polymers that are inaccessible by other means. Complemented by X-ray spectroscopy and microscopy, the focus of this program is the development and use of electron microscopy (EM) techniques for characterizing soft matter. A combination of quantum mechanical calculations and molecular dynamics will be used to interpret data obtained from the electron- and X-ray-based experiments.

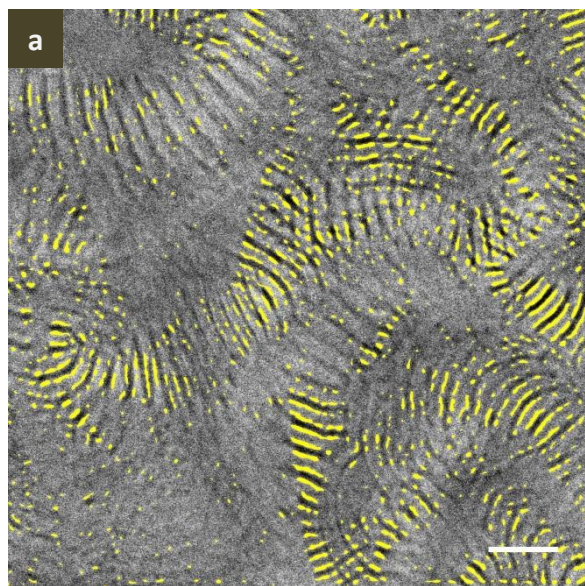


Figure 1. S-SES membrane hydrated in liquid water. (a) Cryo-STEM image of hydrated S-SES. The darkest phase represents polyethylene while hydrated polystyrenesulfonate (PSS) phase is heterogeneous. Scale bar represents 200 nm. (b) A zoomed-in view of a showing the heterogeneous nature of the hydrated channels: two bright stripes (PSS-rich) sandwiching a gray stripe (water-rich). A schematic of the hydrated channels is shown next to the image.

Recent Progress

Morphology of Nanoscale Hydrated Channels in Block Copolymer Electrolyte Membranes

Fuel cells, which hold promise for providing energy without pollution, rely on proton transport through a polymer electrolyte membrane (PEM). It is widely accepted that when PEMs absorb water, nanoscale water channels form inside the membrane and proton conduction occurs. However, there is considerable debate surrounding the structure of the hydrated channels within PEMs.

Recently, we have made a breakthrough using cryogenic TEM to discover the nanoscale morphology of the hydrated channels in a model PEM.

Specifically, we studied the water uptake and proton conductivity of a model fuel cell membrane comprising a triblock copolymer, polystyrenesulfonate-*block*-polyethylene-*block*-polystyrenesulfonate (S-SES), as a function of water activity in both humid air and liquid water. We demonstrate that the water uptake and proton conductivity of S-SES membranes equilibrated in liquid water are fundamentally different from values obtained when they were equilibrated in humid air. We use humidity-controlled cryogenic scanning transmission electron microscopy (STEM) to identify the morphological underpinnings of our observations. The STEM data revealed that the discontinuous increase in conductivity when nearly saturated humid air is replaced with liquid water coincides with the emergence of heterogeneity in the hydrated channels: a water-rich layer is sandwiched between two polymer-rich brushes (Figure 1). While the possibility of obtaining heterogeneous hydrated channels in polymer electrolyte membranes has been discussed extensively, this is, to our knowledge, the first time that direct evidence for the formation of water-rich subdomains is presented (ref. 1).

Sequence-Specified Polypeptoids for Proton Conduction

Polypeptoids are a family of comb-like polymers based on an N-substituted glycine or polypeptoid backbone. They offer tremendous advantages for material science in the solid state. The iterative solid-phase submonomer synthesis method allows for the efficient synthesis of polymers with exact monomer sequence from an extremely diverse set of side chain functionalities. In combination with high-resolution characterization techniques like TEM, we have established a powerful feedback loop between synthesis and characterization. In the process, we are developing a new class of nanoscale phase-separated materials, and uncovering new polymer physics rules that govern the fundamental assembly behavior of block copolymers.

In the past two years we have successfully synthesized EO-based peptoids to enable the transport of lithium ions (ref. 6-8). In recent months we synthesized polypeptoids with strong anionic groups such as phosphonate groups to mediate proton transfer (Figure 2). There are numerous choices of readily available hydrophobic peptoid monomers to include in the non-polar block. Based on our research of diblock copolypeptoid electrolytes, the relatively short polymer chain lengths and monodispersity will enable us to obtain small domain sized hydrophilic channels, which have been shown to help achieve high proton conductivity at elevated temperatures. Furthermore, the fine tunability of the polypeptoids will establish a relationship between the channel size and proton conductivity. Since materials comprising low molecular weight polymers are mechanically weak, mechanically robust membranes will be obtained by combining self-assembly with specific chemical crosslinking. We are making efforts to image these polymers in dry and hydrated states.

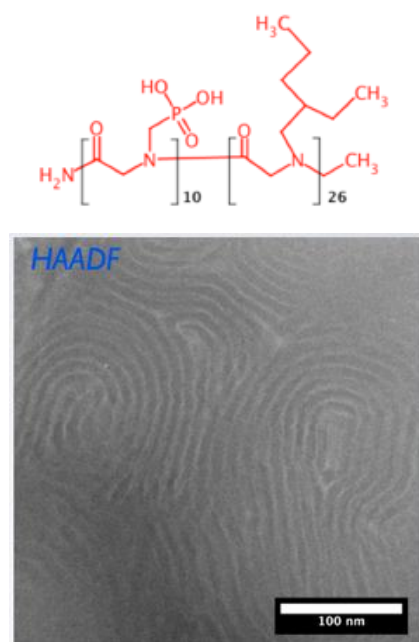


Figure 2. A phosphonate-containing peptoid diblock copolymer for proton conduction. The unstained STEM image shows its lamellar morphology. Bright phase represents the phosphorous-rich phase.

Dendrite Growth in Block Copolymer Lithium Metal Batteries

There has been a renewed interest on electrochemical deposition of metals such as zinc and lithium due to their relevance to rechargeable batteries. An overarching challenge in lithium metal anodes in rechargeable batteries today is the formation of dendrites during charge/discharge cycles. It is therefore critical to discover the underpinnings that govern dendrite growth and design cells that can best prevent it. However, (1) imaging the dendrite that spans the distance between the electrodes remains an unresolved challenge; (2) information concerning the morphology of the nanostructured electrolyte at the electrode-electrolyte interface is lacking.

We have made attempts to tackle both problems. It should be self-evident that high resolution TEM is entirely unsuitable for identifying singular dendrites that are located on a macroscopic electrode within a cell; the probability of choosing a section at random such that it contains the dendrite is very low. We are faced with a "needle-in-a-haystack" problem and all of the high resolution approaches discussed thus far would result, in all probability, in high resolution images of the "haystack". Instead, we imaged the "needle" in a two-pronged approach: First we image the entire cell using (relatively) low resolution synchrotron X-ray microtomography, and mark the location of the electrolyte-spanning dendrite. In the second step, we use a focused ion beam mill to isolate that small portion of the cell, and then use high resolution EM to resolve the fine-structure of the dendrite.

In preliminary work on the cells with cross-sectional area in the 1 cm^2 range, we have cycled lithium-SEO-lithium cells and imaged entire cells using X-ray microtomography. The unexpected finding thus far is that dendritic growth begins within the electrode, underneath the electrode-electrolyte interface (ref. 9). All of the previous work on lithium dendrites had focused on protrusions from the lithium surface. It is obvious however, the we only have a very coarse

view of the dendritic structure. In Figure 3 we show a low-resolution X-ray tomogram of a dendritic structure in a cycled cell. The cell was opened in a glovebox, the lithium electrode was separated from the electrolyte by dissolving the electrolyte, and taken into a FIB instrument. Figures 3b and c show our attempts to use FIB to section the dendrite to obtain a high resolution image of the dendrite. Our ultimate goal is to quantify the 3D nature of dendritic structures formed at the lithium/block copolymer interface as a function of charge passed.

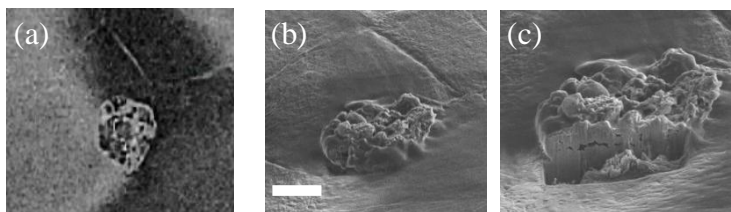


Figure 3. Low resolution X-ray tomography (a) and high resolution SEM (b) of the same dendrite. (c) Use of FIB to section the dendrite to obtain internal structure. Scale bar is $50\ \mu\text{m}$.

Future Plans

Our work described above lays the groundwork for our future studies on nanostructured ion-containing polymers. We will use the approaches established to image hydrated proton-conducting channels to explore more PEM systems. We are particularly excited to characterize the precise polypeptoids as the morphology in these systems should be better defined than that in synthetic polymers (all of our imaging work thus far is restricted to synthetic polymers with some polydispersity). The imaging of nanostructures near the lithium electrode and identifying

dendrites in lithium batteries remains a challenge. Finally, we will the use of theory to understand both structure-property relationships in our systems and interpret the microscopy and spectroscopy experiments.

In summary, in the coming years we will:

- Image the proton-conducting domains in hydrated in fuel cell membranes.
- Characterize morphology and function of sequence-specified polypeptoids for proton conduction.
- Image block copolymer electrolytes and the interface between them and lithium metal electrodes.
- Image nanostructures including dendrites at the lithium-electrolyte interface.
- Utilize soft X-ray to study ionic species in polymer electrolytes.
- Use theory and modelling to interpret our experimental results.

Publications

1. "Effect of Morphology of Nanoscale Hydrated Channels on Proton Conductivity in Block Copolymer Electrolyte Membranes", X.C. Chen, D.T. Wong, S. Yakovlev, K.M. Beers, K.H. Downing, N. P. Balsara, *Nano Letters*, vol.14, pp 4058–4064, **2014**.
2. "Design of Cluster-free Polymer Electrolyte Membranes and Implications on Proton Conductivity", K.B. Beers, N.P. Balsara, *Macro Letters*, vol. 1(10), p. 1155-1160, **2012**.
3. "Deciphering the Three-Dimensional Morphology of Block Copolymer Thin Films by Transmission Electron Microscopy", F.I. Allen, P. Ercius, M.A. Modestino, R.A. Segalman, N.P. Balsara, A.M. Minor, *Micron*, vo. 44, p. 442-450, **2013**.
4. "Design of a Humidity Controlled Sample Stage for Simultaneous Conductivity and Synchrotron X-ray Scattering Measurements", A. Jackson, K.B. Beers, X.C. Chen, A. Hexamer, J.A. Pople, J.B. Kerr, N.P. Balsara, *Review of Scientific Instruments*, vol. 84, 075114, **2013**.
5. "Insights on the Study of Nafion Nanoscale Morphology by Transmission Electron Microscopy", S. Yakovlev, N.P. Balsara, K.H. Downing, *Membranes (An Open Access Journal)* vol. 3, p. 424-439, **2013**.
6. "Nanoscale Phase Separation in Sequence-Defined Peptoid Diblock Copolymers", J. Sun, A.A. Teran, X. Liao, N.P. Balsara, R.N. Zuckermann, *Journal of the American Chemical Society*, vol. 135, p. 14119-14124, **2013**.
7. "Peptoid Polymers: A Highly Designable Bioinspired Polymer", J. Sun, R.N. Zuckermann, *ACS Nano*, vol. 7, p. 4715-4732, **2013**.
8. "Crystallization in Sequence-Defined Peptoid Diblock Copolymers Induced by Microphase Separation", J. Sun, A.A. Teran, X. Liao, N.P. Balsara, R.N. Zuckermann, *Journal of the American Chemical Society*, vol. 136, pp 2070–2077, **2014**.
9. "Detection of Subsurface Structures Underneath Dendrites formed on Cycled Lithium Metal Electrodes", K.J. Harry, D.T. Hallinan, D.Y. Parkinson, A.A. MacDowell, N.P. Balsara, *Nature Materials*, vol. 13, p. 69-73, **2014**.

Probing Phase Transitions, Chemical Reactions, and Energy Transfer at the Atomic Scale

PI: Albina Y. Borisevich¹ Co-PI: Sokrates T. Pantelides^{2,1}

Postdocs: Jae Hyuck Jang,¹ Qiuhan He,¹ Rohan Mishra²

¹Materials Science and Technology Division, Oak Ridge National Laboratory

²Department of Physics and Astronomy, Vanderbilt University, Nashville, TN 37235

Program Scope

The focus of the program is on probing the mechanisms of reversible and irreversible bias-induced transformations in solids at the atomic level of individual defects using a combination of scanning transmission electron microscopy (STEM) and local-field confinement in *ex-situ* and *in-situ* active device configurations. We aim to unravel the complex interplay between order parameter dynamics, ionic flows, electrochemical reactions, and mechanical behavior by studying three classes of phenomena: (A) irreversible electrochemical processes including oxygen vacancy injection and vacancy ordering (B) hysteretic processes including electrostatically-driven structural changes and phase transitions in ferroelectrics and at ferroelectric interfaces and ultimately (C) kinetics of reversible electronic transfer, ionic polarization and interfacial reactions at oxide interfaces and oxide grain boundaries. We aim to uncover the mechanisms of these transformations at the nanometer-scale, and ultimately, the single-atom and single electron level, and link these to atomistic and mesoscopic models. The experimental and quantification approaches are developed for *ex situ* experiments, in particular systems with built-in electric fields or compositional gradients. They are subsequently used in *in situ* studies, where types of information inaccessible by other techniques can be obtained, such as direct images of metastable states and real-time compositional snapshots. The transformation mechanisms uncovered in this project will help establish a sound scientific basis for optimization and engineering of materials for a broad range of energy and information technologies from solid oxide fuel cells to memristive data storage and logic devices, as well as elucidate the role of vacancies in physical functionality of surfaces and interfaces.

Recent progress

1. *In situ* studies of early stages of conductive filament formation in amorphous TiO₂ thin films

As a prototypical system to explore hysteretic and irreversible vacancy dynamics, we have studied bias-induced electrochemical processes in TiO₂, a key material for resistive switching memories (ReRAM), and memristors. In a ReRAM, two different resistive states – high resistance state (HRS) and low resistance state (LRS) – are controlled by voltage sweep.¹ Some *in-situ* observations of prototype ReRAM devices indicate presence of conducting filaments (CFs) in otherwise insulating oxide matrix. It is therefore important to investigate how the oxide film is changed by external voltage in order to understand the mechanism of CF formation in the oxide. Studying the initial electroforming is particularly important,

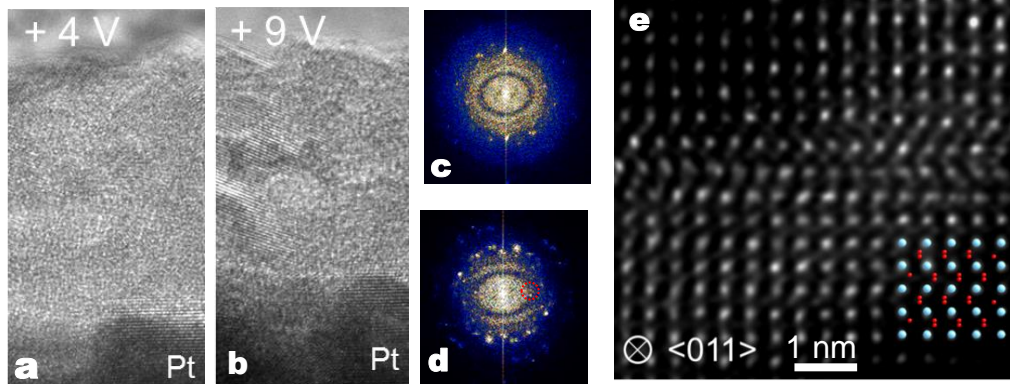


Fig.1. (a,b) TEM images and (c,d) diffractograms of the amorphous TiO₂ thin film at different stages of the initial electroforming. While (c) only shows stoichiometric TiO₂ reflections, higher spacings are evident in (d) (red circle) indicating formation of reduced Magneli phases. (e) Intermediate stage of reduction showing stacking faults in rutile.

because the filament structure established in this process is modified very slightly during subsequent cycling.

Here, TiO₂ thin film was deposited on Pt as a bottom electrode, and STM tip (Pt-Ir) was used as the top electrode within

STM-STEM setup inside the electron microscope. A sudden increase of current level was observed near +4V applied to tip (top electrode), which was coincident with emergence of crystalline features in the initially amorphous TiO_2 film (Fig. 1a,c). The highest characteristic d-spacing of the initially forming $c\text{-TiO}_2$ is about 0.24 nm, which could correspond to the (013) spacing of anatase or (212) spacing of rutile structure. As the voltage is increased, the area of the crystalline TiO_2 is gradually extended from the bottom electrode to the top electrode. In addition to the voltage-dependent crystallization of TiO_2 , which starts happening at very low voltages, higher voltages ($\sim 9\text{V}$ and up) induce stacking faults in grains near bottom electrode (Fig. 1e), and eventually much higher lattice spacings characteristic of Magneli phases (Fig.1b,d). The formation of these defects is caused by voltage-induced transport of oxygen ions. This work follows our extensive studies of the effect of voltage cycling on memristive [4] and fuel cell materials [5,7,9,10] and is currently submitted for publication.

2. Coupling of oxygen vacancies and polar behavior in oxide thin films and heterostructures.

Perovskite oxides offer a rich playground of varied physical properties, from polar to magnetic to electrical transport behavior.² However, it becomes evident that oxygen sublattice is not a passive background but rather an active contributor to behavior of oxide thin films.

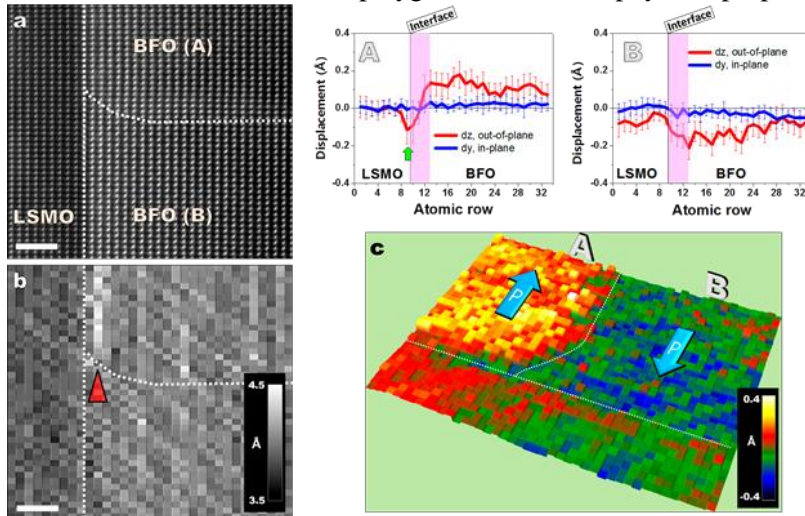


Fig.2. Lattice spacing and polarization changes at the interface of BFO-LSMO: (a) ADF image of $[110]_{pc}$ oriented BFO/LSMO/STO thin film. (b) Out-of-plane lattice spacing map showing local lattice expansion and (c) polarization map and profiles of BFO film on LSMO showing antiparallel domain configuration. Scale bars are 2 nm.(from [13]).

For example, changing the octahedral tilt pattern by varying interface termination can lead to emergence of metastable antiferroelectric state in stoichiometric BiFeO_3 [6]. While oxygen vacancies were always a known possibility for oxide thin films, now there is an emerging consensus that oxygen chemical potential should be considered as another moveable variable, alongside electric, magnetic, and strain fields, determining the properties of the system [3].

As an example of a system with built-in electric field, we studied a domain wall/interface junction in $\text{BiFeO}_3/(\text{La,Sr})\text{MnO}_3/\text{SrTiO}_3$ heterostructure with two antiparallel domains (Fig. 2a). Lattice spacing map shows that there is a localized expansion at the interface with negative polarization charge, but not with positive (Fig.2b). Additionally, the polarization at the interface shows a double-layer-like structure for negative polarization charge, while for positive polarization charge it simply decreases to zero (Fig.2c). In combination with EELS data on oxygen content and localized oxidation states of intermixed Mn ions inside BFO (not shown), as well as theoretical modeling, these results led us to conclude that while positive polarization charge is compensated by electrons, negative polarization charge is compensated by oxygen vacancies, which are forming a double layer at the interface. These results have major implications for switching domains of different orientations. While dynamic switching studies have shown that, depending on polarization direction, some domains can be impossible to switch completely³, our study is the first to directly demonstrate different screening species for two polarization directions [13].

While the above example shows oxygen vacancy motion induced by polarization charge at ferroelectric interface, we have also reported on electrical polarization induced at the interface between two metallic oxides due to vacancy accumulation [2] and polar behavior in non-polar superlattice induced by oxygen

vacancy ordering [11], highlighting that coupling goes both ways and that controlling local oxygen chemical potential can lead to better materials and possibly new device paradigms.

3. *In situ* dynamics of oxygen vacancies

Unlike oxide electronics devices, where pivotal role of oxygen vacancies is only now becoming to be fully recognized, for materials such as solid oxide fuel cells, gas sensors and catalysts *basic functionality* is dependent on the distribution and transport behavior of oxygen ions. We have recently demonstrated that, for a static case, oxygen vacancy distribution and vacancy ordering can be characterized at an atomic scale using quantitative aberration-corrected STEM. [1] In further work, we used this approach to observe

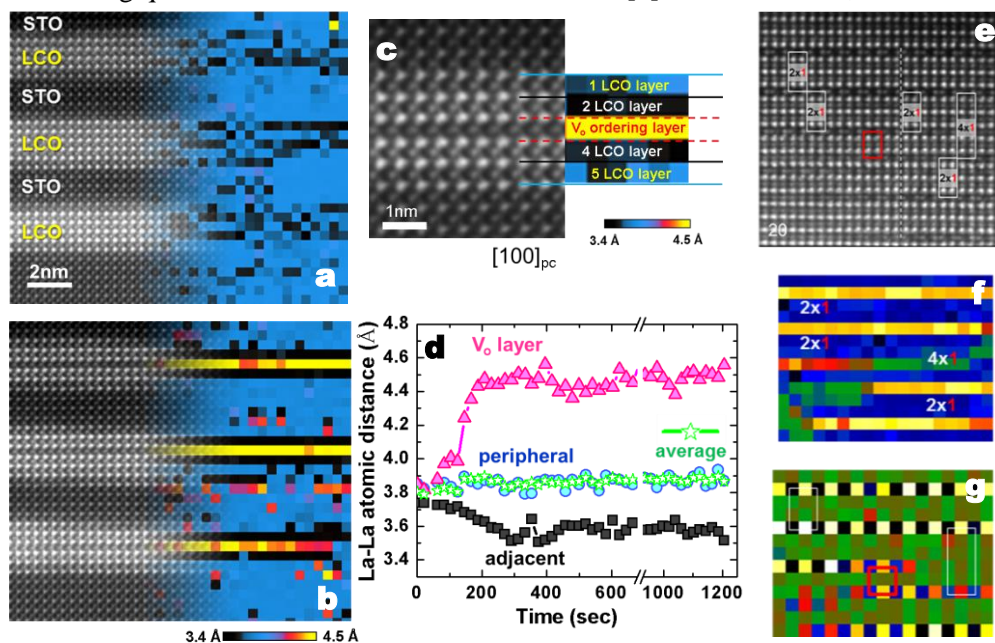


Fig.3. HAADF images and spacing maps for LCO/STO heterostructures (a) before and (b) after electron beam exposure for ~20 minutes. (c) Quantification schematic and (d) time evolution of local spacings in the superlattice suggesting vacancy redistribution (e-g) HAADF image, La spacing map, and Co shift map of a snapshot in LCO film time series showing coexistence of multiple phases (white boxes) and a metastable configuration (red box).

the dynamics of vacancy ordering and vacancy injection under the electron beam in $\text{LaCoO}_3/\text{SrTiO}_3$ (LCO/STO) superlattices and LaCoO_{3-x} thin films. We found that we can observe the transition from the initial disordered state (Fig.3a) to ordered state (Fig.3b) on the time scale of 20 minutes, taking an image every second. Quantifying the results for the superlat-

tice (Fig. 3c,d) led us to conclude that, rather than injecting vacancies, electron beam primarily orders vacancies already present in the sample. In the case of 15 u.c. LCO film, beam exposure leads to a sequence of different phases, starting from disordered perovskite LaCoO_{3-x} to a brownmillerite polytype $\text{La}_3\text{Co}_3\text{O}_{8-x}$ (2 perovskite layers), to eventually brownmillerite $\text{La}_2\text{Co}_2\text{O}_{5-x}$, which is similar to the phase evolution observed in the bulk.⁴ In these series of images, we have detected localized intermediate stages and phases, including metastable ones (Fig.3e-g). Theoretical analysis of relevant energy barriers is currently ongoing.

Future Plans

Utilizing the portfolio of imaging and analysis methods and hardware developed in the preceding periods, we plan to further integrate these areas, bringing in situ biasing studies to atomic level. With this approach we can explore (a) electronic and vacancy mediated phenomena at moving ferroelectric domain walls, (b) electromigration in the metal-mixed electronic/ionic conductors, and (c) static electrochemical properties and bias controlled polarization at oxide-oxide interfaces. We will also continue to develop new methods of structural characterization from STEM images, including 3D characterization. These studies will reveal the interplay between polarization and structural order parameters, strain, and vacancy-controlled electrochemistry in oxides, and will enable optimization of a broad range of energy and information technologies from fuel cells to memristive data storage and logic devices.

References

- ¹R. Waser, et al., *Adv. Mater.* **21** 2632 (2009).
²H.-U. Habermeier, *Materials Today*, **10**, 34 (2007).
³M.-G. Han, et al., *Nat Commun* **5**, 4693 (2014).
⁴Ole H. Hansten et al., *J. Mater. Chem.* **8**, 2081 (1998)

Selected DOE-sponsored publications in the last 2 years [in total 15 journal papers supported or partially supported by the project were published –2 *Nature Mater.*, 1 *Adv. Mater.*, 2 *Adv Mater* family, 1 *Nanolett.*, 2 *ACS Nano* (plus 1 *Nature Mater.* and 1 *Adv. Mater.* Interfaces accepted for publication), 1 patent disclosure]

- [1]. Young-Min Kim, Jun He, Michael D. Biegalski, Hailemariam Ambaye, Valeria Lauter, Hans M. Christen, Sokrates T. Pantelides, Stephen J. Pennycook, Sergei V. Kalinin & Albina Y. Borisevich, Probing oxygen vacancy concentration and homogeneity in solid-oxide fuel-cell cathode materials on the subunit-cell level, *Nature Materials*, **11** (10), 888-894 (Oct 2012).
- [2]. Albina Y Borisevich, Andrew R Lupini, Jun He, Eugene A Eliseev, Anna N Morozovska, George S Svechnikov, Pu Yu, Ying-Hao Chu, Ramamoorthy Ramesh, Sokrates T Pantelides, Sergei V Kalinin, Stephen J Pennycook, Interface dipole between two metallic oxides caused by localized oxygen vacancies, *Physical Review B* **86** (14), 140102 (Oct 2012).
- [3]. Sergei V Kalinin, Albina Borisevich, Dillon Fong, Beyond Condensed Matter Physics on the Nanoscale: The Role of Ionic and Electrochemical Phenomena in the Physical Functionalities of Oxide Materials, *ACS Nano* **6**, 10423–10437 (Dec 2012)
- [4]. Yunseok Kim, Jae Hyuck Jang, Sang-Joon Park, Stephen Jesse, Leonard Donovan, Albina Y Borisevich, Woo Lee, Sergei V Kalinin, Local probing of electrochemically induced negative differential resistance in TiO₂ memristive materials, *Nanotechnology* **24**, 085702 (2013).
- [5]. Donovan N. Leonard, Amit Kumar, Stephen Jesse, Michael D. Biegalski, Hans M. Christen, Eva Mutoro, Ethan J. Crumlin, Yang Shao-Horn, Sergei V. Kalinin, Albina Y. Borisevich, , Nanoscale probing of voltage activated oxygen reduction/evolution reactions in nanopatterned (La_xSr_{1-x})CoO_{3-δ} cathodes , *Adv. Energy Mater.* **3**(6), 788 (2013).
- [6]. Young-Min Kim, Amit Kumar, Alison Hatt, Anna N. Morozovska, Alexander Tselev, Michael D. Biegalski, Ilya Ivanov, Eugene A. Eliseev, Stephen J. Pennycook, James M. Rondinelli, Sergei V. Kalinin, and Albina Y. Borisevich, Interplay of octahedral tilts and polar order in BiFeO₃ films, *Adv. Mater.*, **25** 2497 (2013).
- [7]. Amit Kumar , Donovan Leonard , Stephen Jesse , Francesco Ciucci , Eugene A. Eliseev , Anna N. Morozovska , Michael D. Biegalski, Hans M. Christen , Alexander Tselev , Eva Mutoro , Ethan J. Crumlin , Dane Morgan , Yang Shao-Horn , Albina Borisevich , and Sergei V. Kalinin, Spatially Resolved Mapping of Oxygen Reduction/Evolution Reaction on Solid-Oxide Fuel Cell Cathodes with sub-10 nm Resolution, *ACS Nano* **7**, 3808-3814 (2013).
- [8]. YW Yin, JD Burton, YM Kim, AY Borisevich, SJ Pennycook, SM Yang, TW Noh, A Gruverman, XG Li, EY Tsymbal, Qi Li, Enhanced tunnelling electroresistance effect due to a ferroelectrically induced phase transition at a magnetic complex oxide interface, *Nature Mater.*, **12**, 397–402 (2013).
- [9]. Amit Kumar, Francesco Ciucci, Donovan Leonard, Stephen Jesse, Mike Biegalski, Hans Christen, Eva Mutoro, Ethan Crumlin, Yang Shao-Horn, Albina Borisevich, Sergei V. Kalinin, Probing Bias-Dependent Electrochemical Gas–Solid Reactions in (La_xSr_{1-x})CoO_{3-δ} Cathode Materials, *Adv. Func. Mater.*, **23** 5027 (2013).
- [10]. N. Yang, S. Doria, A. Kumar, J.H. Jang, T.M. Arruda, A. Tebano, S. Jesse, I.N. Ivanov, A.P. Baddorf, E. Strelcov, S. Licoccia, A.Y. Borisevich, G. Balestrino, S.V. Kalinin, Water-mediated electrochemical nano-writing on thin ceria films, *Nanotechnology* **25**, 075701 (2014).
- [11]. Rohan Mishra, Young-Min Kim, Juan Salafranca, Seong Keun Kim, Seo Hyoung Chang, Anand Bhattacharya, Dillon D Fong, Stephen J Pennycook, Sokrates T Pantelides, Albina Borisevich, Oxygen-vacancy-induced polar behavior in (LaFeO₃)₂/(SrFeO₃) superlattices, *Nano Lett.*, **14** (5), pp 2694–2701 (2014).
- [12]. Michael. D. Biegalski, Yayoi Takamura, Apurva Mehta, Zhang Gai, Sergei V. Kalinin, Haile Ambaye, Valeria Lauter, Dillon Fong, Sokrates T. Pantelides, Young M. Kim, Jun He, Albina Borisevich, Wolter Siemons, Hans M. Christen, Interrelation between Structure – Magnetic Properties in La_{0.5}Sr_{0.5}CoO₃, *Adv. Mater. Interfaces*, in press (2014).
- [13]. Y.-M. Kim, A. N. Morozovska, E. A. Eliseev, M. P. Oxley, S. T. Pantelides, S. V. Kalinin, and A. Y. Borisevich, "Direct observation of ferroelectric field effect and vacancy-controlled screening at the BiFeO₃-La_xSr_{1-x}MnO₃ interface", *Nature Mater.* in press (2014).

Complex Fundamental Mechanisms of Transient States in Materials Quantified by DTEM

Geoffrey H. Campbell (PI), Melissa K. Santala, Joseph T. McKeown, Robert E. Rudd, Linh Nguyen, and Tae Wook Heo

**Condensed Matter and Materials Division, Physical and Life Sciences Directorate,
Lawrence Livermore National Laboratory, PO Box 808, Livermore, CA 94550, Email:
ghcampbell@llnl.gov**

Program Scope

The thrust of this project is to measure rates of processes occurring during solid – solid phase transformations in materials, explore the variability of these rates as they depend on processing parameters of the materials, and compare with simulations of the phase transformations to reveal and quantify the fundamental controlling mechanisms. To make measurements of the dynamic event *in situ*, we use a time resolved transmission electron microscope (DTEM) that is still unique in the world because of its single shot imaging capability (as opposed to stroboscopic). Since it is a high-resolution real space imaging capability, it allows us to identify and measure rates of individual processes, for example nucleation or growth, which other methods cannot deconvolve.

Recent Progress

One type of initial phase transformation we are studying is crystallization of an amorphous phase. We have chosen to initially study crystallization of amorphous films of Ge. It has been known for some time that amorphous Ge films, when heated rapidly by a laser pulse [1] or an electron pulse [2], will generate a complex crystallization pattern. A similar pattern has also been observed in Si [3]. A low magnification image of such a pattern in Ge is shown in Figure 1. It consists of three concentric zones, with zones I and II roughly corresponding to the size of the laser spot on the film at FWHM. The morphologies of the microstructure in the zones are distinctly different. Zone I has a nanocrystalline, equiaxed structure. Zone II has

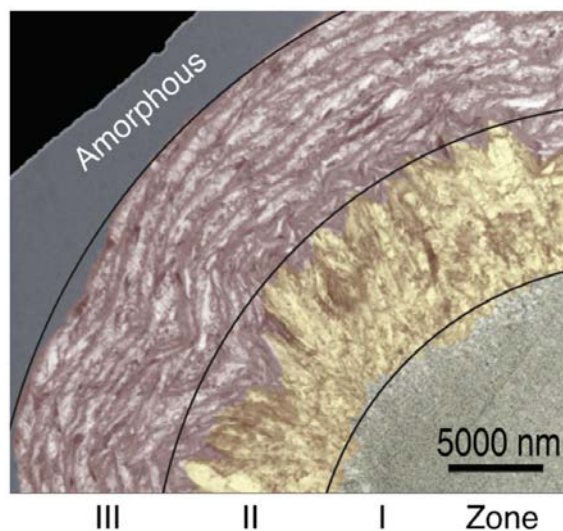


Figure 1 – Conventional bright-field TEM image of a laser crystallized area in 110 nm thick amorphous Ge. The three distinct microstructural zones are labeled. False color added for clarity.

much larger grains that are elongated along the radial direction. Zone III also consists of large, elongated grains, but they are oriented in the tangential direction and are layered with fine grain regions in between.

A time resolved sequence of images acquired in the movie mode operation of the DTEM is shown in Figure 2. A spot on the film is irradiated with a pulse of 532 nm light with a duration of 12 ns at $t = 0$. The time after $t = 0$ is shown in the upper right hand corner of each frame, so the irradiation has ended long before the sequence begins. Zone I is formed by the first frame at 100 ns. In fact this zone may be completely formed within 55 ns [4]. Zone I has a distinct boundary

from which Zone II starts to grow. The shape of the laser irradiation on the specimen is gaussian and the distinct boundary suggests a critical temperature threshold, above which the equiaxed nanoscale grains can form. Zone II is seen to grow outwards from this boundary over the nine frames of the movie. The speed of this zone as it grows into the amorphous matrix is constant at 11.0 m/s. In multiple instantiations of this same experiment the speed of growth of the Zone II varies from about 7 to 12 m/s, but in each case the speed is constant over the interval measured. We would expect that neither the temperature nor the temperature gradient would necessarily be constant over the width of the zone, therefore this

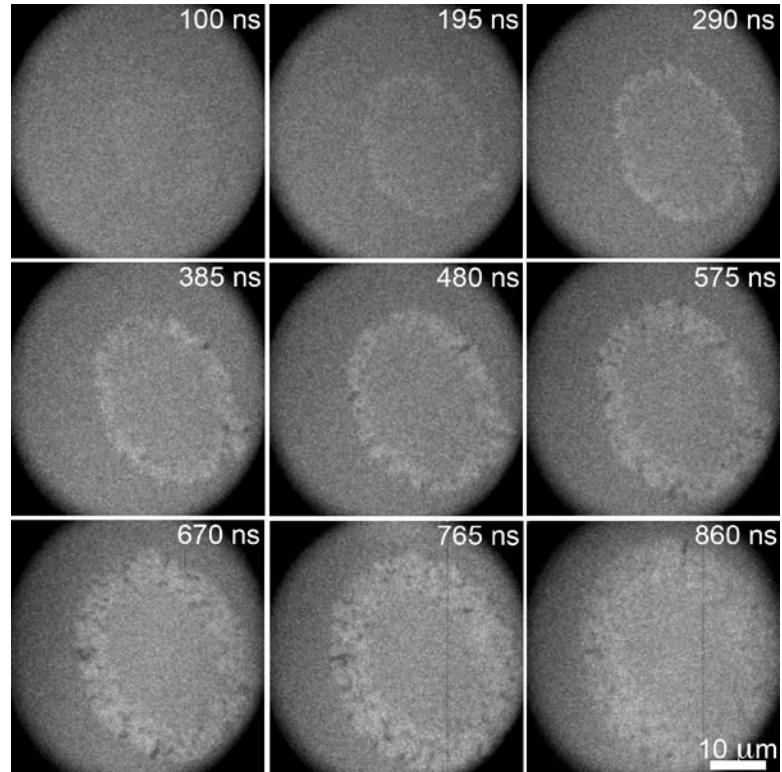


Figure 2 – Time resolved movie mode DTEM sequence of images showing the crystallization evolution of amorphous Ge when subjected to rapid heating by a 12 ns laser pulse.

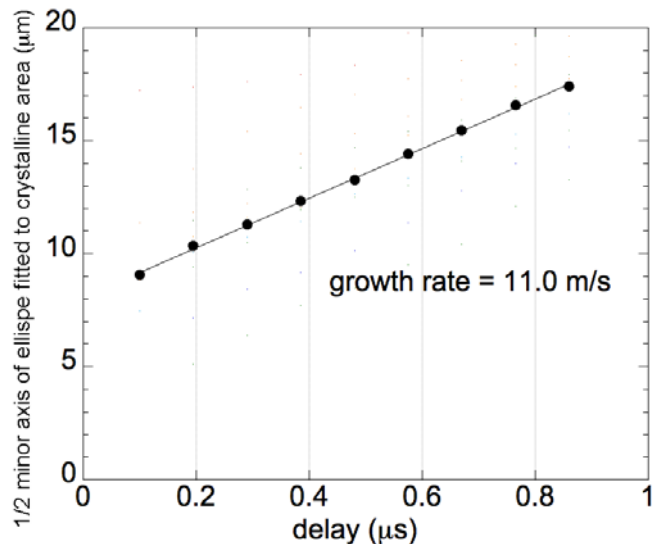


Figure 3 – Plot of the measured size of the ellipse formed by Zone II growth in Figure 2 as a function of time. The constant slope shows constant growth front velocity.

result appears somewhat surprising and will require further investigation. After approximately 1.5 – 2.0 μs , the growth of Zone II stops and the much slower growth of Zone III proceeds for several 10s of μs [5].

Future Plans

We will be making thin films of Ge under differing deposition conditions, for example by changing the substrate temperature during deposition, in order to change the structure of the amorphous phase. The amorphous structure will be characterized and quantified with fluctuation electron microscopy (FEM) and then their crystallization kinetics measured in the DTEM. The differing structures of the amorphous phase should change the available free energy change upon transformation and thus should have an affect on the kinetics. We will use atomistic simulations to create model amorphous structures and simulate FEM data based on these structures to quantitatively compare to the experimental results. With these representative structures as initial conditions we will simulate crystallization and compare differences we observe in the kinetics with the experimental results.

References

- [1] O. Bostanjoglo, E. Endruschat, "Kinetics of Laser-Induced Crystallization of Amorphous-Germanium Films," *Physica Status Solidi a-Applied Research*, **91** [1] 17-28 (1985).
- [2] O. Bostanjoglo, G. Hoffmann, "Time-Resolved Tem of Transient Effects in Pulse Annealing of Ge and Ge-Te Films," *Physica Status Solidi a-Applied Research*, **73** [1] 95-105 (1982).
- [3] O. Bostanjoglo, "Time-Resolved Tem of Pulsed Crystallization of Amorphous Si and Ge Films," *Physica Status Solidi a-Applied Research*, **70** [2] 473-481 (1982).
- [4] L. Nikolova, T. LaGrange, B.W. Reed, M.J. Stern, N.D. Browning, G.H. Campbell, J.C. Kieffer, B.J. Siwick, F. Rosei, "Nanocrystallization of Amorphous Germanium Films Observed with Nanosecond Temporal Resolution," *Applied Physics Letters*, **97** [20] (2010).
- [5] L. Nikolova, T. LaGrange, M.J. Stern, J.M. MacLeod, B.W. Reed, H. Ibrahim, G.H. Campbell, F. Rosei, B.J. Siwick, "Complex Crystallization Dynamics in Amorphous Germanium Observed with Dynamic Transmission Electron Microscopy," *Physical Review B*, **87** [6] 064105 (2013).

Publications

M.D. Grapes, T. LaGrange, L. Friedman, B.W. Reed, G.H. Campbell, T.P. Weihs, and D.A. LaVan, "Combining nanocalorimetry and dynamic transmission electron microscopy for *in situ* characterization of materials processes under rapid heating and cooling," *Rev. Sci. Instr.* **85** 084902 (2014).

J.T McKeown, A.K. Kulovits, C. Liu, K. Zweiacker, B.W. Reed, T. LaGrange, J.M.K. Wiezorek, G.H. Campbell, "In situ transmission electron microscopy of crystal growth-mode transitions during rapid solidification of a hypoeutectic Al-Cu alloy," *Acta Mater.* **64** 56 – 68 (2014).

L. Sandoval, G.H. Campbell, and J. Marian, “Thermodynamic interpretation of reactive processes in Ni-Al nanolayers from atomistic simulations,” *Model. Sim. Mater. Sci. Eng.* **22** 025022 (2014).

G.C. Egan, K.T. Sullivan, T. LaGrange, B.W. Reed, M.R. Zachariah, “In situ imaging of ultra-fast loss of nanostructure in nanoparticle aggregates,” *J. Appl. Phys.* **115** [8] 084903 (2014).

K. Fisher, S.C. Barron, M.A. Bonds, R. Knepper, K.J.T. Livi, G.H. Campbell, N.D. Browning, T.P. Weihs, “Phase transformations, heat evolution, and atomic diffusion during slow heating of Al-rich Al/Zr multilayer foils,” *J. Appl. Phys.* **114** [24] 43509 (2013).

J.A. Aguiar, B.W. Reed, Q.M. Ramasse, R. Erni, and N.D. Browning, “Quantifying the low-energy limit and spectral resolution in valence electron energy loss spectroscopy,” *Ultramicroscopy* **124** 130 – 138 (2013).

M.K. Santala, B.W. Reed, S. Raoux, T. Topuria, T. LaGrange, and G.H. Campbell, “Irreversible reactions studied with nanosecond transmission electron microscopy movies: Laser crystallization of phase change materials,” *Appl. Phys. Lett.* **102** [17] 174105 (2013).

L. Nikolova, T. LaGrange, M.J. Stern, J.M. MacLeod, B.W. Reed, H. Ibrahim, G.H. Campbell, F. Rosei, and B.J. Siwick, “Complex crystallization dynamics in amorphous germanium observed with DTEM,” *Phys. Rev. B* **87** [6] 064105 (2013).

S. Mehraeen, J.T. McKeown, P.V. Deshmukh, J.E. Evans, P. Abellan, P.H. Xu, B.W. Reed, M.L. Taheri, P.E. Fischione, and N.D. Browning, “A (S)TEM gas cell holder with localized laser heating for *in situ* experiments,” *Microsc. and Microanal.* **19** [19] 470 – 478 (2013).

L. Piazza, D.J. Masiel, T. LaGrange, B.W. Reed, B. Barwick, and F. Carbone, “Design and implementation of a fs-resolved transmission electron microscope based on thermionic gun technology,” *Chem. Phys.* **423** 79 – 84 (2013).

T. LaGrange, B.W. Reed, M.K. Santala, J.T. McKeown, A. Kulovits, J.M.K. Wiezorek, L. Nikolova, F. Rosei, B.J. Siwick, and G.H. Campbell, “Approaches for ultrafast imaging of transient material processes in the transmission electron microscope,” *Micron* **43** [11] 1108 – 1120 (2012).

J.T. McKeown, N.A. Roberts, J.D. Fowlkes, T.B. LaGrange, B.W. Reed, G.H. Campbell, and P.D. Rack. “Real-time observation of nanosecond liquid-phase assembly of nickel nanoparticles via pulsed-laser heating,” *Langmuir* **28** [49] 17168 – 17175 (2012).

M.K. Santala, B.W. Reed, S. Raoux, T. Topuria, T. LaGrange, and G.H. Campbell, “Nanosecond-scale time-resolved imaging during laser crystallization of GeTe,” *Phys. Stat. Sol. B* **249** [10] 1907 – 1913 (2012).

K.J. Koski, C.D. Wessells, B.W. Reed, J.J. Cha, D.S. Kong, and Y. Cui, “Chemical Intercalation of zerovalent metals into 2D layered Bi₂Se₃ Nanoribbons,” *J. Am. Chem. Soc.* **134** [33] 13773 – 13779 (2012).

K.J. Koski, J.J. Cha, B.W. Reed, C.D. Wessells, D.S. Kong, and Y. Cui, “High-density chemical intercalation of zero-valent copper into Bi₂Se₃ nanoribbons,” *J. Am. Chem. Soc.* **134** [18] 7584 – 7587 (2012).

Spectroscopic Imaging STM and Complex Electronic Matter

J. C. Séamus Davis

CMP&MS Department, Brookhaven National Laboratory, Upton, NY 11973, USA

LASSP, Physics Department, Cornell University, Ithaca, NY 14853, USA.

Office: 607-254-8965 / Mobile: 607-220-8685 / Email: jcdavis@ccmr.cornell.edu

Research Objectives

Our long-term research objectives are focused on the *DoE Grand Challenge for Science and the Imagination*: “How do remarkable properties of matter emerge from complex correlations of atomic or electronic constituents and how can we control these properties?”. Recently our focus has been on understanding heavy fermion and topological superconductors.

Program Scope

We address these issues by direct atomic scale visualization of electronic structure in a variety of materials using our suite of specialized SI-STM systems.

Recent Progress

- *First Visualization of Heavy Fermions*

We originated dilution-refrigerator-based millikelvin SI-STM for mapping simultaneously the r -space and k -space electronic structure of heavy fermion systems at temperatures down to 50 mK. This approach was expected to be powerful because it is hybridization between f -electrons $\varepsilon_{\vec{k}}^f$ localized in r -space and free electrons $\varepsilon_{\vec{k}}^c$ in k -space that generates the heavy fermion state.

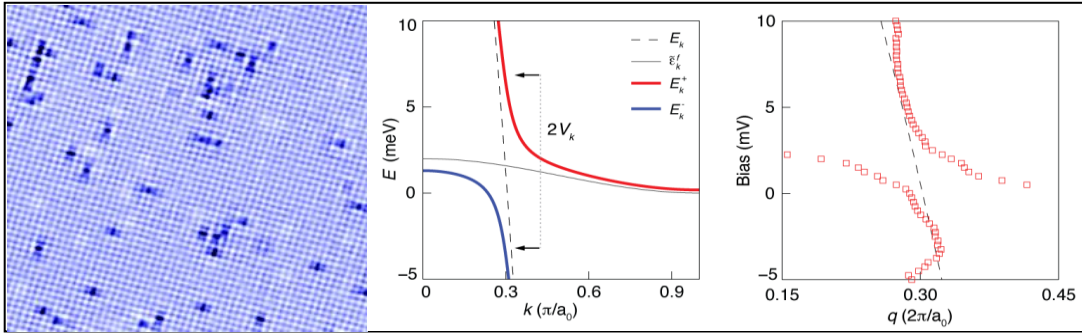


Figure 1. a) URu₂Si₂ surface with Th substitution sites dark; b) the expected heavy bands within standard theory of heavy fermion formation e.g. Eqn. 1; c) the measured heavy bands of URu₂Si₂ using QPI (**Nature** 465,570(2010)).

We carried out the first imaging of heavy-fermion scattering interference patterns in the heavy fermion compound URu₂Si₂ and thereby achieved the direct observation of splitting of the light k -space band into two heavy-fermion bands $E_{\vec{k}}^{\alpha,\beta}$

$$E_{\vec{k}}^{\alpha,\beta} = \frac{\varepsilon_{\vec{k}}^c + \varepsilon_{\vec{k}}^f}{2} \pm \sqrt{\left(\frac{\varepsilon_{\vec{k}}^c - \varepsilon_{\vec{k}}^f}{2}\right)^2 + s_{\vec{k}}^2} \quad (1)$$

By demonstrating feasibility of millikelvin QPI for determining heavy band-structures with $dE < 100$ meV, this result launched the field of STM studies of heavy fermions[1]; **Nature** 465, 570 (2010).

- *Visualizing a ‘Kondo Hole’*

Replacing a magnetic atom by a spinless atom in a heavy fermion compound generates a special many-body quantum state referred to as a ‘Kondo-hole’. We visualized a Kondo-hole [2] by imaging the electronic structure at a spinless Thorium atom substituted for magnetic Uranium atom in the heavy fermion compound URu₂Si₂. Surrounding each Thorium atom the heavy-fermion hybridization modulations predicted to occur at Kondo-holes were observed. We also discovered nanoscale hybridization heterogeneity due to the randomness of Kondo-hole doping and these long-range hybridization oscillations; *PNAS* **108**, 18233 (2011).

- *First k -Space Visualization of Heavy Fermion Cooper Pairing*

The Cooper pairing mechanism of heavy-fermion superconductors [3-4,5,], while long hypothesized as due to spin fluctuation exchange [6,7], had proved impossible to determine in the decades since the discovery of such materials. It is the k -space structure of the two superconducting energy gaps $\Delta_{a,b}(k)$ on the heavy bands a,b that encodes specifics of this Cooper pairing mechanism. However, because the energy scales are so low, it was impossible to directly measure $\Delta(k)$ for any heavy-fermion superconductor.

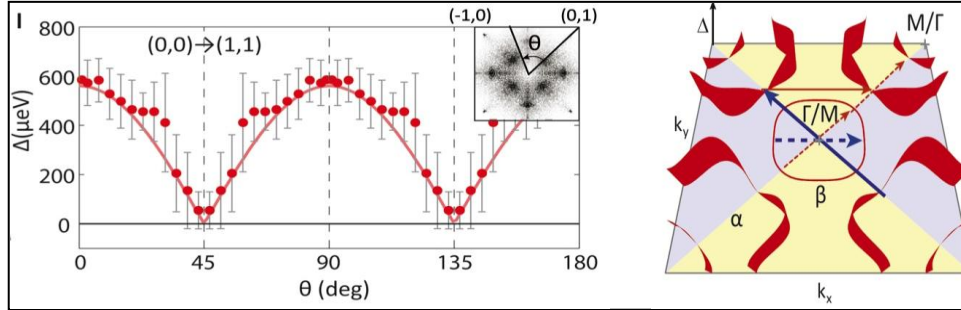


Figure 2. a) Measured superconducting energy gap magnitude on the a-band of CeCoIn₅; b) the overall determination of $\Delta(k)$ for CeCoIn₅. (*Nat. Phys.* **9**, 458 (2013)).

The technique of Bogoliubov quasiparticle interference (QPI) imaging was recently proposed [8] as a new method to measure $\Delta(k)$ in heavy-fermion superconductors - specifically CeCoIn₅. By implementing this method in CeCoIn₅, we discovered the complex band structure and Fermi surface of its heavy-fermion bands $E_{\vec{k}}^{\alpha,\beta}$, that the primary $\Delta(k)$ with maximum 600 μ eV and nodal structure opens on a complex a-band surrounding the p,p point, and that the quasiparticle interference patterns are most consistent with $d_{x^2-y^2}$ symmetry. This innovative technique for heavy band-structure $E_{\vec{k}}^{\alpha,\beta}$ and $\Delta_{a,b}(k)$ determination reveals an exciting new approach to identifying the mechanism of heavy fermion superconductivity; *Nature Physics* **9**, 458 (2013).

- *Demonstrated Magnetic f -Electron Mediated Cooper Pairing Mechanism in CeCoIn₅*

Magnetically mediated Cooper pairing has been the conjectured basis of heavy-fermion superconductivity but no direct verification of this mechanism existed. To explore this issue, we used our newly developed capability to measure the hybridized heavy-fermion band structure using quasiparticle interference (QPI) imaging, to determine the k -space structure of the f -electron magnetic interactions of CeCoIn₅. Then, by solving the superconducting gap equations on its two heavy-fermion bands $E_{\vec{k}}^{\alpha,\beta}$ with the hypothesis that these interactions mediate the Cooper pairing,

we generated a series of quantitative predictions about the superconductive state. We then showed them in excellent agreement with numerous experiments; (*PNAS III*, 11663 (2014)).

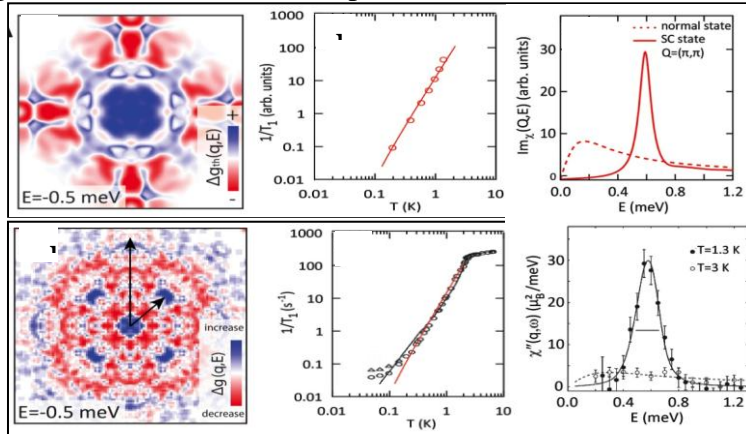


Figure 3. a) Magnetic-field induced alterations predicted in CeCoIn_5 , b) predicted $T_1(T)$ with f -electron magnetism as pairing mechanism c) predicted spin-resonance; d) magnetic-field induced changes in CeCoIn_5 QPI; e) measured $T_1(T)$ of CeCoIn_5 ; f) measured spin resonance of CeCoIn_5 .

This provides strong and direct evidence that heavy fermion Cooper pairing is mediated by the f -electron magnetism; *PNAS III*, 11663 (2014).

- *Visualizing Electronic Structure of a Topological Superconductor*

Sr_2RuO_4 has long been the leading candidate to exhibit phenomena expected of topological superconductivity. To establish the mechanism and topology of order-parameter of superconductivity in Sr_2RuO_4 , a prerequisite is direct information concerning the energy gaps $\Delta_i(k)$, and whether the pairing is stronger on the quasi-1D or on the quasi-2D Fermi surfaces.

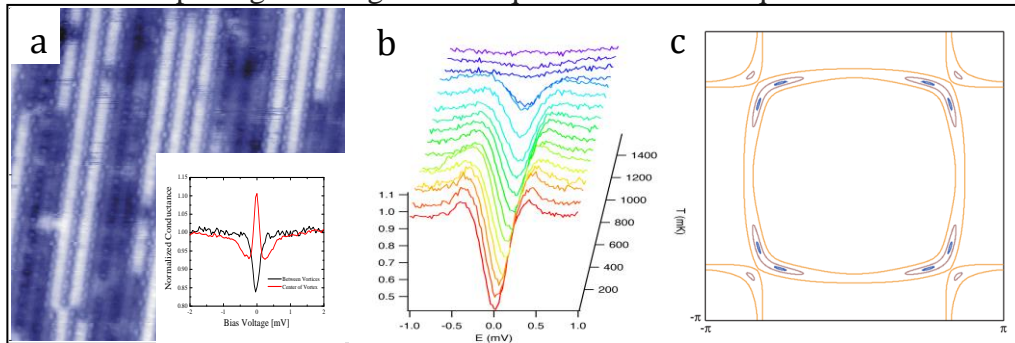


Figure 4 a) Topographic image of RuO_2 layer b) T dependence of $\text{DOS}(E)$ spectrum of Sr_2RuO_4 ; c) Theoretically predicted contours of constant energy of Bogoliubov quasiparticles for the $D(\)$ predicted within one-dimensional pairing mechanism (*PRB 88*, 134521 (2013)).

We achieved the first STM measurements of the density-of-states spectra in superconducting Sr_2RuO_4 for $0.1T_c < T < T_c$ (Fig. 4b). Analysis shows that the gap scale with maximum value $2\Delta \approx 5 T_c$ along with a spectral shape indicative of line nodes (Fig. 4b) is consistent with magnetically mediated odd-parity superconductivity (topological) superconductivity.

- *Unifying magnetic interactions, coincident electronic orders and correlated superconductivity*

We introduced a simple conceptual framework providing a unified explanation of the relationship between antiferromagnetic electron-electron interactions, coincident broken-

symmetry phases, and the correlated superconductivity. We demonstrated that this approach is equally successful in explaining the cases of copper-based, iron-based and heavy-fermion superconductors; *Proc. Nat. Acad. Sci.* **110**, 17623 (2013).

Future Plans

- *Visualizing CDW/SC Quantum Critical Point*

We plan to study the interplay of a CDW critical point under a superconducting “dome” with the superconductivity itself. In 2H-type Cu_xTaS_2 , for $0 \leq x \leq 0.12$, the charge density-wave (CDW) is destabilized with Cu doping while the superconducting T_c , increases to 4.5 K at the optimal composition $\text{Cu}_{0.04}\text{TaS}_2$, and then decreases at higher x . We plan a doping dependence study of the electronic structure of Cu-TaS_2 as it is evolved through the critical point.

- *Bogoliubov QPI and $\Delta(k)$ of Topological Superconductor in Sr_2RuO_4*

We plan to apply our experience of this compound in combination with our new $dE \sim 75\text{meV}$ resolution Bogoliubov QPI techniques to the superconductive state at $T \sim 250\text{mK}$ in Sr_2RuO_4 . Figure 4c shows the approximate predicted Bogoliubov contours of constant energy of this compound. Since there are four nodes in a tetragonal arrangement, we expect a QPI signature in the form of a classic ‘octet’ of dispersive scattering interference wavevectors.

Publications

1. How Kondo Holes Create Intense Nanoscale Heavy-Fermion Hybridization Disorder, M.H. Hamidian, et al *Proc. Nat. Acad. Sci.* **108** 18233 (2012).
2. Imaging Cooper Pairing of Heavy Fermions in CeCoIn_5 , M. P. Allan, et al *Nature Physics* **9**, 468 (2013).
3. Concepts Relating Magnetic Interactions, Intertwined Electronic Orders and Strongly Correlated Superconductivity J.C. Davis and D.-H. Lee, *Proc. Nat. Acad. Sci.* **110**, 17623, (2013).
4. Evidence from Tunneling Spectroscopy for a Quasi-One Dimensional Origin of Superconductivity in Sr_2RuO_4 ; I. A. Firmo, et al *Phys. Rev. B* **88**, 134521 (2013).
5. Direct Evidence for Magnetic f -Electron-Mediated Mechanism for Pairing of Heavy Fermions in CeCoIn_5 , J. Van Dyke, et al *Proc. Nat. Acad. Sci.* **111**, 11663 (2014).

References

-
- ¹ A. Schmidt *et al*, *Nature* **465**, 570 (2010).
 - ² M.H. Hamidian et al *Proc. Nat. Acad. Sci.* **108** 18233 (2011).
 - ³ Superconductivity without phonons; P. Monthoux, D. Pines, G. G. Lonzarich, *Nature* **450**, 1177-1183 (2007) .
 - ⁴ The Challenge of Unconventional Superconductivity; Norman; M. R. *Science* **332**, 196 (2011)
 - ⁵ A Common Thread: The Pairing Interaction for Unconventional Superconductors; Scalapino, D. J. *Rev. Mod. Phys.* **84**, 1383–1417 (2012)
 - ⁶ Spin-fluctuation-mediated even-parity pairing in heavy-fermion superconductors; Miyake, K., Schmitt-Rink, S., and Varma, C. M. *Phys. Rev. B* **34**, 6554 (1986)
 - ⁷ d-wave pairing near a spin-density-wave instability; Scalapino, D. J., Loh Jr., E., and Hirsch, J. E. *Phys. Rev. B* **34**, 8190 (1986)
 - ⁸ Quasiparticle interference in the heavy-fermion superconductor CeCoIn_5 ; Akbari, A., Thalmeier, P., and Eremin, I. *Phys Rev.* **84**, 134505 (2011)

Cryogenic Nano-Scale Optical Spectroscopy in Correlated Systems

PI: Adrian Gozar (the only person working on the project)

Brookhaven National Laboratory, Upton, NY

Program Scope:

The purpose of this project is twofold. First, to develop new instrumentation which enables performing infrared optical spectroscopy measurements with nano-scale spatial resolution within a variable temperature environment. Second, to use this tool in order to address physics problems which are either difficult/impossible by other techniques or to bring complementary information from a new perspective. The key features of the Scanning Near Field Optical Microscopy (SNOM) were aimed at studying competing phases in correlated systems (e.g. phase transitions, the role of intrinsic/extrinsic inhomogeneities) and emergent phenomena associated with surfaces or buried interfaces in artificial structures. Our current work is focused on three projects:

- 1) Electronic properties of graphene. Here we are interested in the origin of damping in a quasi-2D electronic gas with relevance for graphene-based electronics. We use near-field plasmon interferometry which allows us to extract temperature dependent energy-momentum information about collective electronic excitations [1]. We obtain this information from real-space mapping of plasmonic scattering around defects and sample edges (see Fig.1).
- 2) Metal-Insulator (M-I) transition and ferromagnetism in thin sub-surface EuO films. This project serves as a starting point for our studies of properties of surfaces and buried interfaces. We want to address the following questions. Can the M-I transition in EuO be detected optically by a non-invasive probe like SNOM? What is the relation between metallic and ferromagnetic orders? Does the giant magneto-resistance exhibited by EuO [2] belong to the paradigm of manganites (i.e. related to inhomogeneous behavior) ? Given the almost full spin polarization of the electronic bands, can we offer insights for a roadmap to spintronics application? (see Fig.2).
- 3) Enhanced high-temperature interface superconductivity: Previous work of the PI reported 25% enhancement of the maximum bulk T_c for ultra-thin interfacial superconducting layers in LaSrCuO based heterostructures [3]. Here we exploit the capability of SNOM to image superfluid-polaritons in the superconducting states in order to answer the following questions. What is the cause of the enhanced critical superconducting temperature? What is the true maximum critical superconducting temperature for copper-oxide based materials and can one use interface physics to further increase the maximum T_c ? (see Fig.3).

Recent Progress

All data reported here are the result of work performed only during the past 7-8 months, after the PI moved his lab to a new location. Our Early Career project was delayed by almost two years due to inadequate mechanical and electrical conditions in a previous laboratory space. *A telling*

example in this respect are the data in Fig.1, acquired in March 2014: back in November 2012 we used the same system to measure the same sample but the signal was buried in noise.

1) Electronic properties of graphene. Panels (a) and (b) of Fig.1 show AFM and SNOM data taken in ambient conditions single layer graphene (SLG) sample. The near field scan reveals information beyond the usual optical contrast between the SLG/SiO₂ and other topographic AFM features. We observe 'halos' and 'highways' which surround and connect these features and we associate them with heavily damped standing waves due to plasmon scattering [1]. The efficiency by which folds or sub-nanometer cracks in SLG scatter the plasmons is remarkable.

Our aim is to discriminate between intrinsic and extrinsic electronic scattering by monitoring the temperature dependent complex conductivity as inferred from near-field plasmon interferometry. Performing this experiment with the sample in Fig. 1a,b “as is” was not possible: the Fermi level changed with desorption of particles once the sample was placed in vacuum and the plasmon interference pattern disappeared. Accordingly, our future low temperature experiments will be performed on very high mobility samples, Fig.1c, which will be patterned to allow in-situ gating for Fermi level control during measurements.

2) Metal-Insulator (M-I) transition in thin sub-surface EuO films. Fig.2 shows typical low temperature data obtained in EuO. The 20 nm thick film is protected by a layer of amorphous Si in order to preserve stoichiometry. The data so far allow for two observations: the signal measured at $T > T_c = 69$ K is about 50% lower in intensity and an optically homogeneous sample is observed at all measured temperatures. These preliminary results indicate that SNOM can probe the subsurface M-I transition in EuO and that the paradigm of manganites may not be applicable to EuO, i.e. the giant magneto-resistance is not related to inhomogeneous behavior.

The data in Fig.2 were obtained on the sample “as grown”. In order to make our previous observations quantitative, i.e. extract the complex dielectric function of the film, one needs a reference material. For this purpose we recently deposited 20 nm strips of Au, see Fig.2a. Our next set of measurements will consist of SNOM data of EuO with in-situ reference to Au as well as MFM measurements to correlate the metallic and ferromagnetic orders.

3) High-temperature superconductivity. We are about to demonstrate low-temperature SNOM operation in the 0.1 – 1 THz range, which was one of our main project goals. We report progress in two areas. First, all equipment needed for the THz setup is already in place. The remaining effort is to replicate the currently working mid-infrared setup with the THz one. Second, in order for AFM tips to perform as good “antennas” in the sub-1 THz region they need to have shaft lengths comparable to the wavelength of radiation ($\lambda \sim 0.3 - 3$ mm). We had to replace the currently used Akiyama probes (shaft length ≤ 30 μ m) with etched wires attached directly to quartz tuning forks, see Fig.3a. We established procedures to obtain sharp tips by etching W and Au-wires, see Fig.3. Room temperature tests show excellent behavior of these probes, low-temperature tests are currently underway.

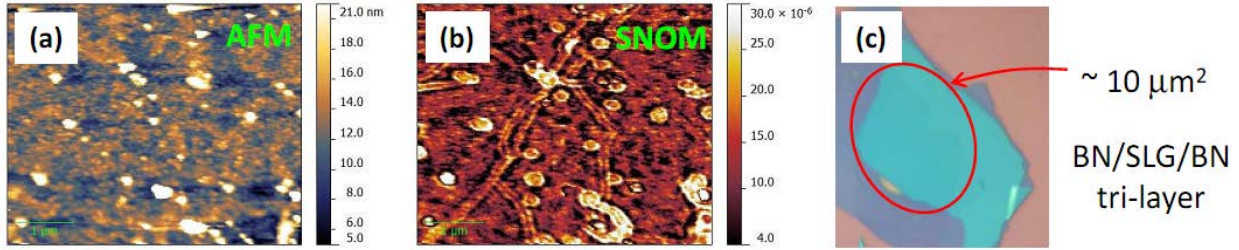


Fig. 1: Panels (a) and (b) show $4 \times 5 \mu\text{m}^2$ AFM and SNOM scans respectively in a commercially available single layer graphene (SLG) sample, Graphene Supermarket. The data were taken at $T = 300 \text{ K}$ in air with a laser excitation light $\lambda = 10.6 \mu\text{m}$. The SNOM data display near-field plasmonic interference effects around the defects seen in AFM [1]. For a temperature dependent study in-situ gating for Fermi level control is necessary (see text): panel (c) shows the high mobility SLG sample sandwiched between two boron nitride (BN) layers which will be used for the low-temperature experiments once the contact pads are defined by lithography (work in progress, collaboration with Philip Kim's group, Columbia/Harvard University).

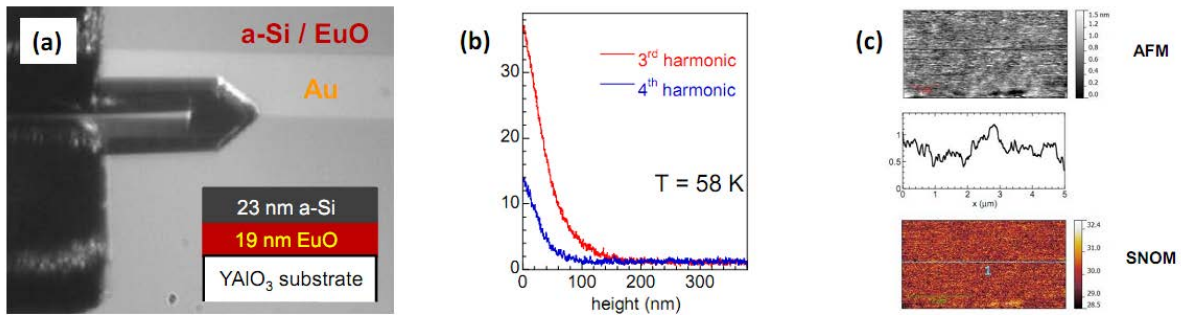


Fig. 2: a) The EuO sample onto which reference Au-strips were deposited (see text). The film is covered by a protective layer of a-Si, inset of panel (a). Panels (b) and (c) show data taken at $T = 58 \text{ K}$. SNOM approach curves at the 3rd and 4th harmonic of the tapping frequency are shown in (b) and $5 \times 3 \mu\text{m}^2$ AFM and SNOM scans along with a AFM profile are shown in panel (c). These data are representative for measurements taken at *all* temperatures, i.e. an optically homogeneous sample is observed both above and below $T_c = 69 \text{ K}$ (work in progress, collaboration with Darrell Schlom's group, Cornell University).

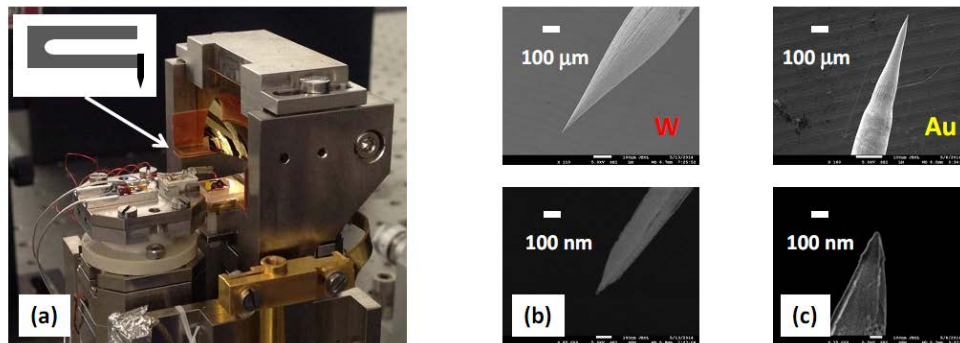


Fig. 3: Panel (a) is a close-up view of the AFM/SNOM head showing the quartz tuning fork (TF) based AFM probes to be used for measurements in the far-infrared (0.1 – 1 THz) range. Typical SEM pictures of the AFM tips obtained so far are shown in the middle, W tips panel (b), and on the right, Au tips, panel (c).

Future Plans

Our near-future plan is to complete the three projects described above: 1) Graphene: perform low-temperature surface plasmon interferometry measurements in high mobility samples with in-situ gating; 2) EuO: quantitatively characterize the M-I transition; 3) demonstrate SNOM operation in the sub-1 THz range and understand enhanced superconductivity in $\text{La}_2\text{CuO}_{4+\delta}$ / $\text{La}_{1.55}\text{Sr}_{0.45}\text{CuO}_4$ bilayers.

Longer term plans depend substantially on the size of the group possibly working on this project in the future. The projects we want to pursue include the following topics: 1) Probing the locally inhomogeneous behavior in the pseudo-gap phases of correlated electron materials. 2) Superconductivity and symmetry breaking at the meso- and nano-scales: high-Tc cuprates and Fe-based materials. 3) emergent phenomena associated with surface and/or interface layers; critical length-scales.

References

- [1] Fei et al., Nature 487, 82 (2012); Fei et al., Nature Nanotechnology 8, 821 (2013).
- [2] Schmehl et al., Nature Materials 6, 882 (2007).
- [3] Gozar et al., Nature 455, 782 (2008); Logvenov et al., Science 326, 699 (2009).

Publications

- Pereiro et al., Philos. Trans. Roy. Soc. A 370, 4890 (2012).
- Stilp et al., Phys. Rev. B 88, 064419 (2013).
- Logvenov et al., J. of Supercond. Novel Magn. 26, 2863 (2013)

Electric Field Effects in Complex Functional Oxides

Myung-Geun Han, Joseph Garlow, and Yimei Zhu
Condensed Matter Physics and Materials Science Department
Brookhaven National Laboratory, Upton, NY 11973

Program Scope

The focus of this research task under the FWP Number MA-015-MACA is to study charge-lattice-spin interplays and dynamics in complex oxides under external stimuli to unveil the underpinning physical principles that control emergent macroscopic functionalities. The research areas include (i) cross-coupled domains and domain walls in novel ferroelectrics and multiferroics, (ii) emergent electronic or magnetic phenomena at surfaces or interfaces in heterostructures, and (iii) dynamics of conventional and unconventional spin/charge density waves. Our approach is to integrate electron microscopy characterization with macroscopic property measurements inside a transmission electron microscope (TEM) to uncover property-dictating structural entities and elucidate the atomistic origins of emergent physical properties in complex functional materials. Various advanced electron microscopy techniques including holography, electron-beam-induced-current (EBIC), and aberration-corrected imaging under external stimuli such as electromagnetic fields, cooling/heating, optical excitations, strain, etc. are developed and extensively utilized to study dynamic responses of complex oxides.

Recent Progress

Multiferroic hexagonal manganites have been a current focus in studies of multiferroics since the seminal report on interlocking between structural boundaries and ferroelectric domain walls in topological vortex domains¹. Although topological defects in hexagonal manganites, such as vortices and domain walls, attracted much attention, their exact roles on the dynamic switching process were not clearly understood. Recently, we have studied ErMnO_3 crystals and directly observed unique dynamics of domain switching around a vortex core that we termed “topologically guided partner changing”², as shown in Fig. 1.

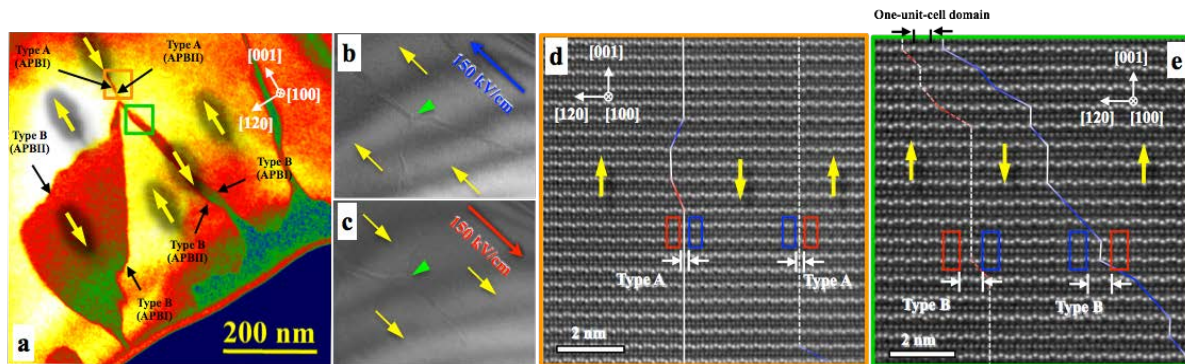


Fig. 1. False-colored dark-field TEM image (a) showing a vortex domain. Dark-field TEM images after electric poling with -150 kV/cm electric field (b) and 150 kV/cm (c) along the c axis. Note that the vortex core, marked with green arrow, is immobile and domain walls are paired but not annihilated in each poled states. HAADF STEM images showing two configurations of paired domain walls: neutral pair (d) and oppositely charged pair (e). Note that two types of domain walls are distinguishable with different separations of unit cells across domain walls.

Six domain walls emerging from a topologically protected and immobile vortex core are paired in a poled state, and each of the three pairs changes partners (i.e., neighboring domain walls) in the process of switching to the oppositely poled state. Atomic resolution high-angle annular dark-field (HAADF)

scanning transmission electron microscopy (STEM) imaging further revealed the unique topological $Z_2 \times Z_3$ symmetry (two additive cyclic groups of order 2 and 3, respectively) originated from the ferroelectric domain walls interlocked with antiphase boundary near a vortex core, as shown in Fig. 1d-e. In addition, employing shear strain with a large gradient, we demonstrated transformations of vortices and antivortices into stripes³. The stripe domain structure was monochiral and showed the alternations domain walls with distorted and undistorted rare-earth ions. Our findings reveal unusual behaviors of topological defects under an electric field and unexpected relation between vortex and stripe domains in hexagonal manganites, providing a novel way of controlling topological defects.

We also studied interface-induced nonswitchable domains in ferroelectric thin films. Engineering domains in ferroelectric thin films is crucial for realizing technological applications including non-volatile data storage and solar energy harvesting. Interfacial band bending and mobile charge effects have been speculated to play important roles in domain structures and switching behavior. By mapping electrostatic potentials and electric fields using off-axis electron holography and electron-beam-induced-current with *in situ* electrical biasing in TEM, we show that electronic band bending across the film/substrate interfaces locks local polarization direction and further produces unidirectional biasing fields, inducing nonswitchable domains near the interface⁴. Presence of oxygen vacancies near the film surface, as revealed by electron-energy loss spectroscopy, stabilizes the charged domain walls. The observations advanced our understanding on ground-state domain structures and switching behaviors in ferroelectrics. The formation of charged domain walls and nonswitchable domains reported in this study can be an origin for imprint and retention loss in ferroelectric thin films, major obstacles for commercialization.

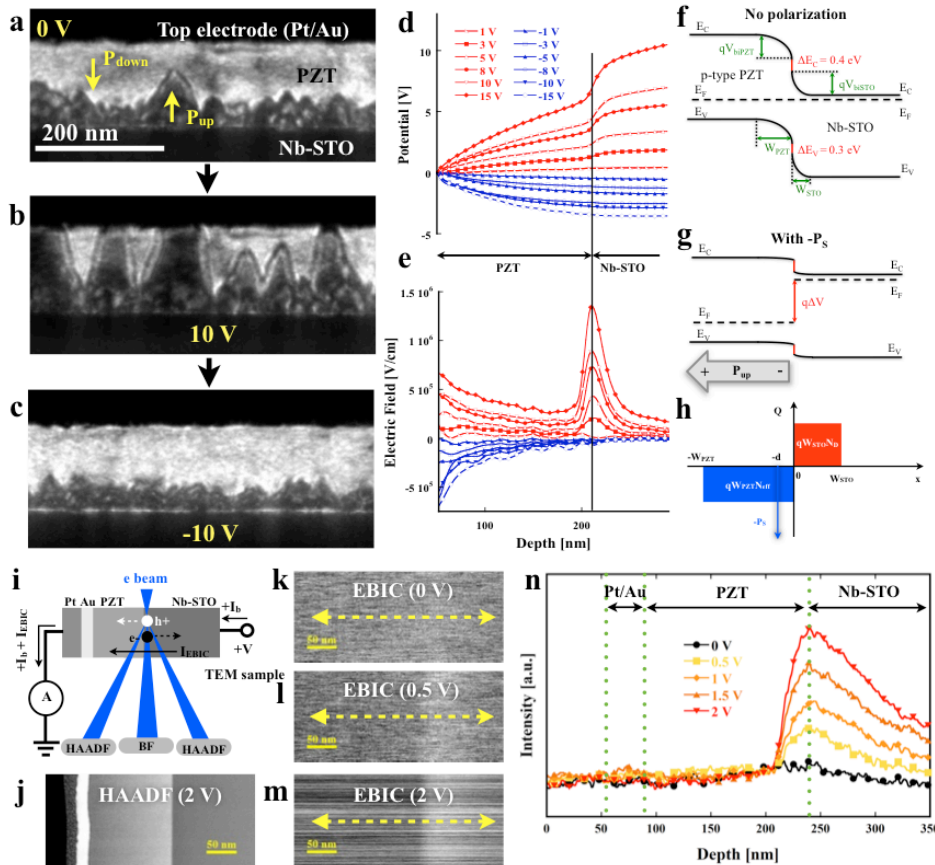


Fig. 2. Dark-field TEM images showing ferroelectric domains structures of epitaxial $\text{PbZr}_{0.2}\text{Ti}_{0.8}\text{O}_3$ thin films grown on Nb-doped SrTiO_3 substrate: as grown (a), after 10 V (b), and after -10 V (c), respectively. Electrostatic potential line profiles (d) and electric fields (e) along the c axis, obtained by electron holography. Schematics of band diagram without (f) and with (g) negative polarization charge ($-P_s$). Schematic (i) of simultaneous electron-beam-induced current (EBIC) and STEM images with various biases. Line profiles of EBIC (n) showing electric field distributions that are consistent with holography data (e), indicating unidirectional electric fields at the interface.

Future Plan

Knowledge of dynamic responses to external stimuli can reveal the atomistic mechanisms of a material with exotic properties. In this task, we will continue to combine advanced electron microscopy techniques with simultaneous macroscopic property measurements to establish structure-property correlations. Various external stimuli including cooling/heating, strain, electromagnetic fields, optical pumping, etc. will be utilized to give further insights towards understanding of emergent phenomena in complex materials. Specifically, we will exploit reconstruction of spin, lattice, and charge states in heterostructure-based complex materials for understanding and discovery of technologically important functionalities. Examples include (i) emergent electronic or magnetic phenomena at/across interfaces and (ii) development of an experimental framework to study previously inaccessible dynamics of charge density waves using *in situ* electrical biasing at low temperatures.

Emergent electronic or magnetic phenomena at/across interfaces We will investigate reversible reconstructions of electronic states by ferroelectric control and octahedral engineering at oxide heterointerfaces where two dissimilar tilting patterns are coupled to trigger charge transfers for depletion or accumulation of atomically confined charges. Direct imaging of octahedral tilting patterns by annular bright-field (ABF) STEM and mapping of charge distributions by electron holography will be directly complemented with *in situ* electronic transport measurements for bistable states. As an example, we will study $\text{PbZr}_{0.2}\text{Ti}_{0.8}\text{O}_3$ (PZT)/ LaNiO_3 (LNO) grown on LaAlO_3 substrate, as shown in Fig. 3. DFT calculations predict reversible oxygen octahedral tilting patterns and large charge depletion/accumulation to give rise to a significant modulation in *in-plane* electronic conduction. Further investigation will be made to confirm DFT results with ABF STEM and electron holography.

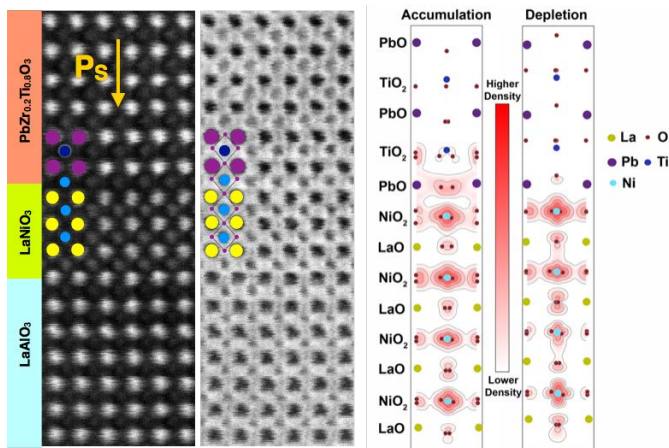


Fig. 3. HAADF STEM (a) and ABF STEM (b) images of $\text{PbZr}_{0.2}\text{Ti}_{0.8}\text{O}_3/\text{LaNiO}_3$ film grown on LaAlO_3 substrate. Polarization direction is indicated with an arrow. Charge density maps above Fermi level for accumulation and depletion, calculated by DFT. Note there is additional charge densities in PbO and TiO_2 layers adjacent to the interface, giving higher *in-plane* electronic conductance. Oxygen columns are visible in the ABF-STEM image showing a longer O-Ni bond, in agreement with depletion states in DFT results.

Dynamics of charge density waves As noted by Frohlich in 1954, charge density wave can carry superconducting current in the absence of pinning and damping⁵, which are very important to understanding superconductivity. Although, in reality, it has been predicted that the charge condensate moves in the field of randomly distributed pinning potentials due to chemical disorder or defects, no experimental observation has been made up to date and thus its dynamics remains elusive. We will directly observe dynamics of charge density waves in complex materials with highly anisotropic band structures such as IrTe and TaS_2 , using *in situ* electrical biasing at low temperatures (down to 6 K). Our study will generate a broad impact on understanding the competing degrees of freedom in condensed matter, especially between the charge-order state and superconductivity, as it manifests as the key to superconductivity in iron-based superconductors.

References

1. Choi, T., Horibe, Y., Yi, H.T., Choi, Y.J., Wu, W., Cheong, S.-W., “Insulating interlocked ferroelectric and structural antiphase domain walls in multiferroic YMnO_3 ”, *Nature Materials*, **9**, 253-258 (2010).
2. Han M.-G., Zhu, Y., Wu, L., Aoki, T., Wang, X., Chae, C., and Cheong, S.-W., “Ferroelectric switching dynamics of topological vortex domains in a hexagonal manganite”, *Advanced Materials*, **25**, 2415-2421, (2013).
3. Wang, X., Mostovoy, M., Han, M.-G., Horibe, Y., Aoki, T., Zhu, Y., and Cheong, S.-W., “Unfolding of vortices into topological stripes in a multiferroic material”, *Physical Review Letters*, **112**, 247601 (2014).
4. Han, M.-G., Marshall, M.S.J., Wu, L., Schofield, M.A., Aoki, T., Twosten, R., Hoffman, J., Walker, F.J., Ahn, C.H., and Zhu, Y., “Interface-induced nonswitchable domains in ferroelectric thin films”, *Nature Communications*, **5**:4693 (2014).
5. Gruner, G., “The dynamics of charge-density waves”, *Reviews of Modern Physics*, **60**, 4, 1129-1181 (1988).

Publications

1. Patete, J., Han, J., Tiano, A., Liu, H., Han, M.-G., Simonson, J., Li, Y., Santulli, A., Aronson, M., Frenkel, A., Zhu, Y., and Wong, S.S., “Observation of ferroelectricity and structure-dependent magnetic behavior in novel one-dimensional motifs of pure, crystalline yttrium manganese oxides”, *Journal of Physical Chemistry*, accepted (2014).
2. Liu, S., Akbashev, A., Yang, X., Liu, X., Li, W., Zhao, L., Li, X., Couzis, A., Han, M.-G., Zhu, Y., Krusin-Elbaum, L., Li, J., Huang, L., Billinge, S., Spanier, and J., O’Brien, S., “Hollandites as a new class of multiferroics”, *Scientific Reports*, accepted (2014).
3. Han, M.-G., Marshall, M.S.J., Wu, L., Schofield, M.A., Aoki, T., Twosten, R., Hoffman, J., Walker, F.J., Ahn, C.H., and Zhu, Y., “Interface-induced nonswitchable domains in ferroelectric thin films”, *Nature Communications*, **5**:4693 (2014).
4. Wang, X., Mostovoy, M., Han, M.-G., Horibe, Y., Aoki, T., Zhu, Y., and Cheong, S.-W., “Unfolding of vortices into topological stripes in a multiferroic material”, *Physical Review Letters*, **112**, 247601 (2014).
5. Bansal, N., Koirala, N., Brahlek, M., Han, M.-G., Zhu, Y., Cao, Y., Waugh, J., Dessau, D.S., and Oh, S., “Robust topological surface states of Bi_2Se_3 thin films on amorphous SiO_2/Si Substrate and a large ambipolar gating effect”, *Applied Physics Letters*, **104**, 241606 (2014).
6. Jiang, L., Choi, W.S., Jeon, H., Dong, S., Kim, Y., Han, M.-G., Zhu, Y., Kalinin, S., Dagotto, E., Egami, T., Lee, and Ho, N., "Tunneling electroresistance induced by interfacial phase transitions in ultrathin oxide heterostructures", *Nano Letters*, **13**, 12, 5837-5843 (2013).
7. Liu, X., Liu, S., Han, M.-G., Zhao, L., Deng, H., Li, J., Zhu, Y., Krusin-Elbaum, L., and O'Brien, S., “Magnetoelectricity in CoFe_2O_4 nanocrystal-P(VDF-HFP) thin films”, *Nanoscale Research Letters*, **8**, 374 (2013).
8. Volkov, V.V., Han, M.-G., and Zhu, Y., “Double-resolution electron holography with simple Fourier transform of fringe-shifted holograms”, *Ultramicroscopy*, **134**, 175-184 (2013).
9. Han M.-G., Zhu, Y., Wu, L., Aoki, T., Wang, X., Chae, C., and Cheong, S.-W., “Ferroelectric switching dynamics of topological vortex domains in a hexagonal manganite”, *Advanced Materials*, **25**, 2415-2421, (2013).
10. Polking, M. J., Han, M.-G., Yourdkhani, A., Petkov, V., Kisielowski, C. F., Volkov, V., Zhu, Y., Caruntu, G., Alivisatos, A. P., and Ramesh, R., “Ferroelectric order in individual nanometer-scale crystals”, *Nature Materials*, **11**, 700-709, (2012).
11. Zhu, Y., Milas, M., Han, M.-G., Rameau, J.D., and Sfeir, M., “Multimodal optical nanoprobe for advanced in-situ electron microscopy”, *Microscopy Today*, **20** (6), 32-37 (2012).

Probing Coupled Metal-Insulator and Ferroic Transitions from the Atomistic to Mesoscopic Scales

S.V. Kalinin and P. Maksymovych
(sergei2, maksymovych@ornl.gov)

Postdocs: R. Vasudevan, A. Tselev (Res. Prof.), A. Gianfrancesco (student), W. Lin (now at LANL)

Oak Ridge National Laboratory, Oak Ridge, TN 37831

Research scope

The coupling between electronic and ferroic behaviors has emerged as one of the most intriguing aspects of condensed matter physics, with examples including phase separation in complex oxides, metal-insulator transitions in ferroelastic oxides, and complex electronic ordering patterns in superconducting and charge-density wave materials. Both structural and electronic aspects of these behaviors are currently of interest for energy generation and storage and information technology applications, and are uniquely accessible through high-resolution probe-based studies. The goal of this project is to reveal the mechanisms of coupled electronic (metal-insulator) and ferroic (ferro- and antiferroelastic, ferro and antiferroelectric) transitions on the atomic level by exploring coupled structural and electronic phenomena on the surfaces of *in-situ* grown oxides. The research will develop and exploit the synergy between advanced scanning probe microscopy, artificial-intelligence and multivariate methods for theory-experiment matching, and established methodologies of surface science and oxide growth. This will provide a fundamental scientific basis for optimization and engineering of energy-related materials, with enormous potential benefits to fuel cells, batteries, solar energy, data storage, energy transport, and other vital energy technologies.

Recent Progress

In the concurrence period, the research was focused on exploring the coupling between ferroic behavior, chemical degrees of freedom, and electronic phenomena on atomic and mesoscopic level. Specifically, effort has been focused on the atomic-level studies of the surface functionalities of the *in-situ* grown oxide films, as well as development of big- and deep- data analysis tools for multivariate imaging data sets in real space (local crystallography), k-space (RHEED), and spectral domains (tunneling spectroscopy). The enabling step was the introduction of the laser heating system that enabled high-quality film growth. The progress on atomic level studies summarized below.

Structure-order parameter coupling on the atomic level in model systems. To develop the necessary know-how for probing the coupling between electronic properties and structural order parameters, we explore superconducting $\text{Fe}(\text{Te}_x\text{Se}_{1-x})$ system. These materials offer the advantage of atomically flat defect-free surfaces that can be prepared by cleaving and readily identifiable from dI - dV curves electronic structure and superconductive order parameter. Spatial variability of electronic structure in Fe-based superconductor $\text{FeTe}_{0.55}\text{Se}_{0.45}$ is explored on the atomic level using continuous imaging tunneling spectroscopy (CITS). Multivariate statistical analysis of the data differentiates regions of dissimilar electronic behavior that can be identified with the segregation of chalcogen atoms, as well as boundaries between terminations and near neighbor interactions. Subsequent clustering analysis allows identification of the spatial localization of these dissimilar regions. Statistical analysis of calculated density of states of chemically inhomogeneous structures further confirms that the two types of chalcogens – (Te,Se), can be identified by their electronic signature and further differentiated by their local chemical environment. This approach allows detailed chemical discrimination of the STM data including separation of atomic identities, proximity and local configuration effects, and can be universally applicable to chemically- and electronically inhomogeneous surfaces.

In-situ oxide growth: SrRuO₃. We further aim to extend the mesoscopic studies of order parameter-electronic property couplings and atomic level studies to realistic oxide surfaces. Yet, the study of the reactive surface on length scales over which reaction occur has not been forthcoming, due to difficulties in surface preparation, necessitating an *in-situ* approach. Via a user project, the CNMS NanoTransport system combining PLD growth and surface characterization, was used to grow and characterize by atomically resolved STM surfaces of SrRuO₃. We have grown SrRuO₃ films on etched SrTiO₃ substrates by pulsed laser deposition, and studied them with Scanning Tunneling Microscopy (STM) and X-Ray Photoelectron Spectroscopy (XPS), without exposure of the sample surface to air. An AFM topography of this film is shown in Fig. 1(a) below. STM topography image of the surface shown in Fig. 1(b), and much smaller views are shown in Fig. 1(c,d). Fig. 1(c) indicates that the surface is covered by an adatom layer of oxygen arranged in a zigzag-type pattern. However, on the surface of this sample, rectangular packing could also be observed (Fig. 1(d)). DFT modeling for this system indicates a surprising pseudo-gap in the density of states in the majority spin state of the surface SrO layer just above the Fermi level, paving the way towards half-metallicity in SRO. These studies reveal the key role of surface oxygen in affecting the properties of complex oxides, and highlight the utility and necessity of *in-situ* approaches in unravelling their physics and local behaviors.

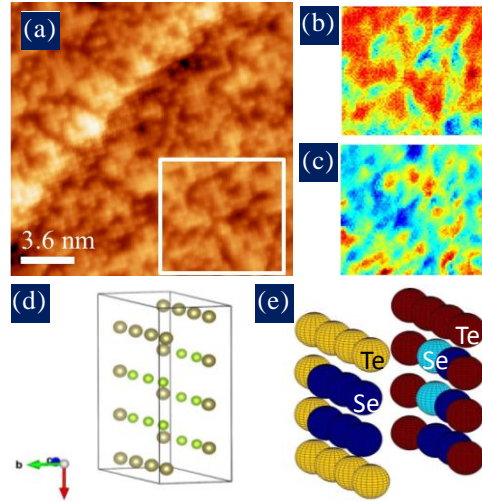


Figure 1: Multivariate Results of CITS Data. (a) Topographical STM of FeTe_{0.55}Se_{0.45}, T = 82K 18x18nm², 50mV, 100pA, white rectangle represents area where CITS was performed. (b) Loading map for the first eigenvector. (c) Loading map for the fourth eigenvector. (d) Calculated FeSe_{0.5}Te_{0.5} model of the Se cluster - green are Se atoms, gray are Te atoms. (e) K-means clustering result for a Se cluster, DOS trimmed to -2 eV to 1.82 eV, yellow and red atoms correspond to Te atoms, two types of blue are the Se atoms

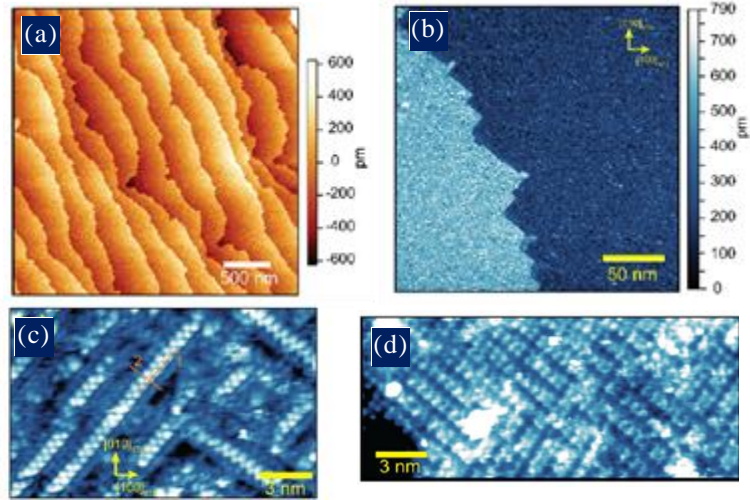


Figure 2. *In-situ* study of surface of SRO. (a) AFM Topography, (b) STM image ($V_t = 2V$, $I_t = 15pA$) of SRO/STO. (c,d) STM Image of surface reconstructions on SRO. Images are from Tselev *et al.* [4].

Atomic level physics and electrochemistry of La_xCa_{1-x}MnO₃ Surfaces

The manganese oxides (manganites) display properties ranging from charge and orbital ordering, to colossal magnetoresistance, and tunable, spatially inhomogeneous metal-insulator transitions. We explored in detail thickness, laser fluency, and substrate effects on surface structure of LCMO films. XPS confirms that the surface is primarily MnO₂ terminated. Surface diffraction data indicates films shows layer by layer growth for all films. The general trends from the growth experiments are

summarized in STM topography images in Fig. 3(a,b). Initially, there are a large number of layers exposed to the surface, but as the growth proceeds the mode of growth changes, and indeed at the thickest film, it is extremely flat. Films begin with mostly MnO_2 -terminated, but with small islands of $(\text{La,Ca})\text{O}$, but at large thicknesses the fraction of $(\text{La,Ca})\text{O}$ islands is reduced until the film becomes uniformly MnO_2 -terminated.

Single atom electrochemistry experiments were also performed on the surface (Fig. 3(c,d)), and suggest that oxygen atoms can be extracted from the $(\text{La,Ca})\text{O}$ termination at $\sim +2.2\text{V}$. These experiments show that tip-induced electrochemistry can provide a template for studying physical and electrochemical processes at the single atom scale, and paves the way for better understanding of surface oxygen reactions in the manganites. In forthcoming studies, we will attempt to quantify threshold potentials required to control oxygen atoms on the surfaces with the aim of differentiating between electron-induced and field-induced mechanisms, identifying the dominant mechanism for atom motion in mesoscale experiments and directly measuring the electronic phase changes caused by local redox reactions from tunneling spectroscopy experiments

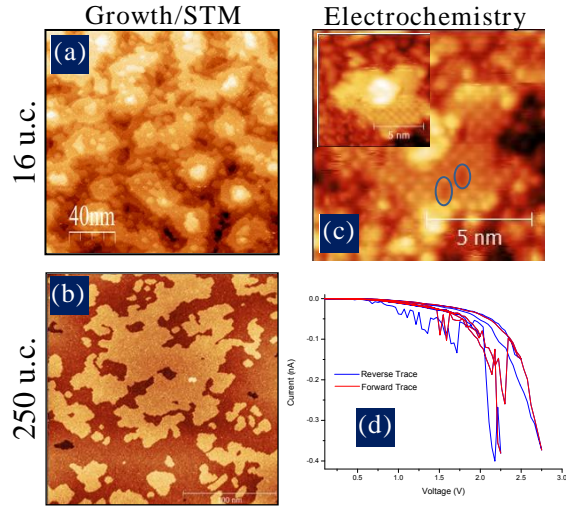


Figure 3. Growth and STM Topography images of LCMO films for two different thicknesses, (a) 16 u.c. and (b) 250 u.c. The film morphology changes from being mixed-terminated and having many layers exposed to being completely flat and single terminated at 250 unit cells. Single atom electrochemistry (c) on the a 25 unit cell sample of LCMO shows that oxygen vacancies can be created by applying positive voltage to the tip (image before STM tip bias application inset). (d) The formation of the two vacancies (circled) is correlated with spikes in the current trace.

Future plans:

Understanding of the fundamental physics of coupling between electronic properties and ferroic behaviors on strongly correlated oxide surfaces necessitates a synergistic view of (a) local *in-situ* studies of surfaces via high-resolution imaging, (b) development of data analytics tools that allow extraction of chemical, physical, and structural information from multidimensional data sets, and (c) theoretical framework that allows describing the coupling between structural degrees of freedom, at mesoscopic and atomic levels. Our research will pursue these directions, aimed at the following fundamental issues:

- **Atomic phenomena during oxide growth:** We will utilize multivariate statistical methods to analyze *in-situ* surface diffraction data captured by reflection high energy electron diffraction (RHEED) apparatus during deposition of films, to determine growth modes, onset of 2D-3D growth transitions, and types and degrees of surface disorder. The results of analysis will be directly compared with real-space atomic-level *in-situ* imaging to confirm its validity, and test the viability of scattering models. These studies will (a) greatly reduce the time spent on optimizing growth parameters, (b) provide a wealth of hitherto generally discarded information pertaining to the surface, and (c) potentially provide the link to theory via separating time dynamics in different regions and k-spaces and finding reliable descriptors.
- **Atomistic origins of order parameters and defect interactions.** We aim to reveal the atomistic structure of the order parameter and defect interactions in ferroic materials using comprehensive data analytics. We will directly correlate structural and functional data via multimodal atomically resolved imaging. The questions include (a) can we understand the atomistic aspects of collective interactions leading to the emergence of polar and structural order parameters, (b) how the

localized disordered defects give rise to mesoscopic order parameter fields, and (c) can the order parameter be manipulated and used to tailor local electronic properties of surfaces.

- **Local electrochemical probing on atomic level.** We aim to use the STM tip as an electrochemical probe by application of bias on the surfaces of oxides. We aim to answer (a) whether oxygen vacancies can be formed on manganites and other oxides by STM tip, and (b) the stability of e.g. surface reconstructions in manganites after removal of oxygen, indicating the strength of e.g. polaronic couplings, and (c) spatial correlations of multiple formed vacancies indicating preferred orientations. We will utilize tunneling spectroscopy and *in-situ* growth and imaging, and compare results from density functional theory/Monte-Carlo approaches to extract the vacancy formation energies and density of states that will provide insight to tailor the surface properties of manganites. We will further (d) probe the feasibility of defect engineering on correlated electron surfaces; (e) control electronic phases by defect patterning, from single, to sparse-random to ordered defect patterns, thereby amplifying the effect of broken symmetry and providing the “chemical libraries” for theory-experiment matching of both electronic structure and phase transitions.

Research supported by the U.S. Department of Energy Office of Basic Energy Sciences Division of Materials Sciences and Engineering and performed at the Center for Nanopahse Materials Sciences supported by Division of Scientific User Facilities (SVK, PM, YK WL, and AT).

DOE-sponsored publications 2012-2014 [27 peer-reviewed papers including 2 *Nature Mat.*, 1 *Sci Rep.*, 1 *Phys. Rev. Lett.*, 3 *ACS Nano*, 2 *Nano Lett.*, 5 *Adv. (Func, En.) Mat.*, 2 plenary, 2 keynote, and 12 invited talk at conferences)]

1. Y.M. KIM, J. HE, M.D. BIEGALSKI, H. AMBAYE, V. LAUTER, H.M. CHRISTEN, S.T. PANTELIDES, S.J. PENNYCOOK, S.V. KALININ, and A.Y. BORISEVICH, *Local Measurements of Oxygen Vacancy Concentration and Homogeneity in Solid Oxide Fuel Cell Cathode Materials on the (sub) Unit Cell Level*, *Nat. Mater.*, 11, 888 (2012)
2. E.A. ELISEEV, P.V. YUDIN, S.V. KALININ, N. SETTER, A.K. TAGANTSEV and A.N. MOROZOVSKA, *Structural phase transitions and electronic phenomena at 180 degree domain walls in rhombohedral BaTiO₃*, *Phys. Rev. B* **87**, 054111 (2013).
3. Y.M. KIM, A. KUMAR, A. HATT, ANNA MOROZOVSKA, A. TSELEV, M. BIEGALSKI, I. IVANOV, E. ELISEEV, S.J. PENNYCOOK, J.M. RONDINELLI, S.V. KALININ, and A.Y. BORISEVICH, *Interplay of octahedral tilts and polar order in BiFeO₃ films*, *Adv. Mat.* **25**, 2497 (2013).
4. A. TSELEV, P. GANESH, L. QIAO, W. SIEMONS, Z. GAI, M. BIEGALSKI, A.P. BADDORF, and SERGEI V. KALININ, *Oxygen Control of Atomic Structure and Physical Properties of SrRuO₃ Surfaces*, *ACS Nano* **7**, 4403 (2013).
5. W. LIN, Q. LI, A. BELIANINOV, B.C. SALES, A. SEFAT, Z. GAI, A.P. BADDORF, M. PAN, S. JESSE, and S.V. KALININ, *Local crystallography analysis for atomically resolved scanning tunnemling microscopy images*, *Nanotechnology* **24**, 415707 (2013).
6. Y. KIM, E. STRELCOV, I.R. HWANG, T. CHOI, B.H. PARK, S. JESSE, and S.V. KALININ, *Correlative Multimodal Probing of Ionically-Mediated Electromechanical Phenomena in Simple Oxides*, *Science Reports* **3**, 2924 (2013).

Scanning Transmission Electron Microscopy: Atomic Structure and Properties of Materials

Physics of Electron Microscopy

Principal Investigators: Andrew R. Lupini, Maria Varela, Wu Zhou, Matthew F. Chisholm

Materials Science & Technology Division, Oak Ridge National Laboratory, TN 37831

Sub-Program Scope

This task is aimed at exploring the frontiers of new techniques in the aberration-corrected scanning transmission electron microscope (STEM), aiming for the highest resolution and sensitivity. Examples include optimizing the fifth-order aberrations of a quadrupole-octupole based aberration-corrected microscope [1] and demonstration of better than 0.57 Å resolution in a Nion UltraSTEM operating at 200 kV.

Recent Progress

Quantitative Mapping of Sample Thickness at Atomic Resolution: One long-standing obstacle in analyzing atomic resolution electron microscope images is that the sample thickness is usually unknown or has to be fitted from parameters that are not accurately known. Previous work has shown that by normalizing the detected intensities to the incoming beam, it is possible to *quantitatively* compare experimental STEM images to simulations¹. To accurately track and analyze single dopants, we needed a parameter free measure of thickness, ideally with column-by-column resolution and single atom precision. To achieve this accuracy, we prepared samples without ion milling and removed surface contamination. By considering sources of error and the properties of our detector system, we were able to identify signals from single electrons and map sample thickness at atomic resolution with an uncertainty corresponding to about ± 1 atom [2].

Depth detection of single optically active dopants: Many materials properties, such as optical and electronic responses, can be greatly enhanced by isolated single dopant atoms [3]. Determining the full three-dimensional single-dopant defect structure and spatial distribution is therefore critical to understanding and adequately tuning functional properties. Building on our quantitative measurements of the sample thickness at atomic resolution we were able to measure the depth of a single dopant atom with a precision of about one unit cell [4]. In order to control the electron dose and to better examine the repeatability of such measurements, we implemented a fast scan sequential imaging approach [5], recording multiple images, which allows recording movies and provides a wealth of statistical information (Fig. 1). This technique allowed us to capture the motion of single dopants. We were able to use the depth measurements to verify that the atoms were in the bulk and not on the surface, meaning that it is now possible to image bulk diffusion of single dopant atoms inside a crystal. Detailed comparisons to density functional theory were able to reveal which diffusion mechanisms are active in this sample. Moreover, we

are able to predict dopants that should be more stable, and to experimentally verify those predictions.

Combined Tilt and Focal Series Tomography: The traditional method to obtain 3-dimensional images in electron microscopy is to use tilt-series tomography. However, one of the implications of aberration-correction is

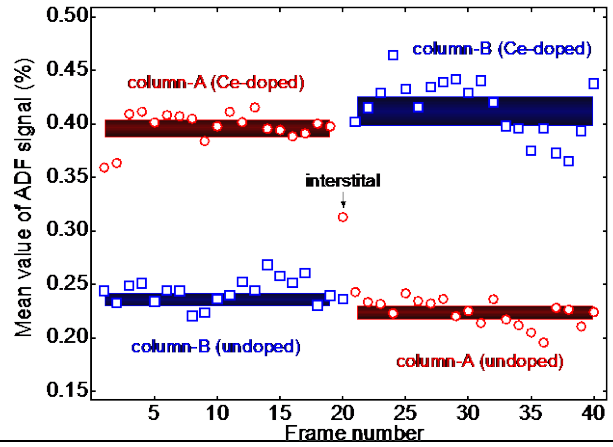
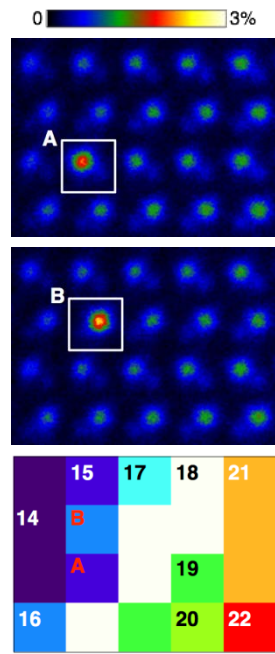


Figure 1. Single Ce dopant atom in a *w*-AlN crystal. (Left) the dopant sits at the site labelled A, moving to site B via an interstitial; and the sample thickness in atomic layers for the same area. (Right) The intensities of columns A and B over the series. [4]

that in order to improve image resolution, the beam-limiting aperture is made larger, resulting in a reduced depth of field. This reduced depth of field makes obtaining a tilt-series much more difficult, because different parts of each frame will be at different focal positions; a problem which will be exacerbated at high tilts. We have previously used this reduced depth of field to obtain 3-dimensional information from a variety of samples in a manner analogous to optical sectioning². Although that work opened a new dimension in STEM imaging, the depth resolution is still many times lower than the transverse resolution. We have recently developed a combined tilt and focal series reconstruction algorithm, which allows thick samples to be examined at high-resolution and requires fewer tilts to obtain the same quality of reconstruction as a conventional tilt-series.

Novel Imaging Modes: One of the traditional limitations of all electron microscopy is the phase problem; that the complex electron wave-function contains most information about the sample, but the detectors record only intensity. Pioneering work by Rodenburg and Nellist showed that by recording a suitably redundant set of data in a STEM, a diffraction pattern for every probe position, it is possible to reconstruct the complex wave-function and image beyond the conventional resolution limits³. Following the successful correction of aberrations, faster computers and multi-channel detection systems have raised intriguing possibilities. For example, in a STEM, it is usually necessary to use a small-angular detector to obtain a large-spatial coherence envelope. However, we have recently shown that it is possible to record images on a pixelated detector and make more efficient use of the transmitted electrons.

Synergy with theory: An important result in collaboration with dynamical diffraction theory [7] is the demonstration that near edge structure varies as a function of probe position due to dynamical scattering alone, and not simply due to a mixing of spectra from distinct atomic sites. This can be understood by considering each energy loss event as a separate “experiment” with its own inelastic scattering potential. Figure 2 shows the projected structure of SrTiO₃ along the [001] zone axis. The simulated potential constructed by integrating over the O K-shell edge has the usual symmetry associated with isolated atomic models. If however we consider the potentials from individual energy losses within the O K-shell edge, we see that they have not only significantly different delocalizations, but substantially different shapes. This means that different parts of the spectrum will change at different rates within the unit cell.

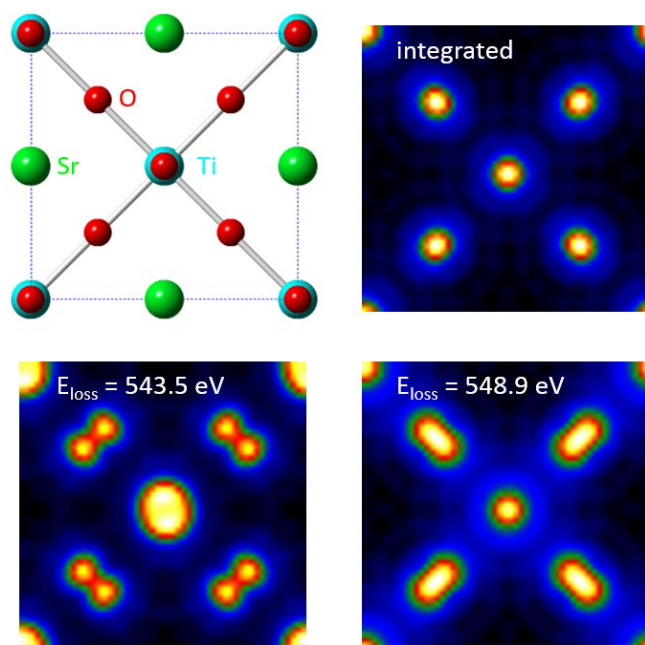


Figure 2. Projected structure of SrTiO₃ along the [001] zone axis (Top left). The simulated projected O K-shell ionization potential, integrated over 20 eV above the edge onset is shown for 200 kV electrons (Top right). Also shown are O K-shell scattering potentials for two distinct energies within the edge [7].

Applications to Energy Materials: We have ongoing collaborations with other programs for the study of catalytic nanoparticles [10-11] and photovoltaic materials. For example we have used a variety of techniques such as combining imaging with spectroscopy, cathodoluminescence and measuring electron-beam induced current to uncover the roles played by defects and grain boundaries in CdTe [12-14]. Developments include potential new photovoltaic systems that self-assemble [15] or have other desirable properties, such as superhydrophobic coatings [16].

Future Plans

The 200 kV Nion UltraSTEM can be operated at voltages between 40-200 kV, allowing the accelerating voltage to be optimized for particular samples. This machine has a stage that allows electrical contacts to be made to the specimen, even though there is no sample rod. We have recently developed an interface allowing us to use conventional TEM-heating chips in the cartridges for this microscope and obtained initial results. We will use these capabilities to investigate the effects of thermal excitation and to explore electrical properties *in situ*.

References

- ¹ LeBeau, J.M., Findlay, S.D., Allen, L.J. & Stemmer, S. Quantitative atomic resolution scanning transmission electron microscopy. *Phys. Rev. Lett.* **100**, 206101 (2008).
- ² Borisevich A Y, Lupini A R, and Pennycook S J. Depth sectioning with the aberration-corrected scanning transmission electron microscope. *Proc. Natl Acad. Sci. USA* **103** (3044–3048). (2006)

³. P. D. Nellist, B. C. McCallum, J. M. Rodenburg, Resolution beyond the 'information limit' in transmission electron microscopy, *Nature* **374** (1995) 630.

Selected Publications in the last 2 years

1. Lupini, A.R. & Pennycook S.J. Tuning Fifth-Order Aberrations in a Quadrupole-Octupole Corrector. *Microscopy and Microanalysis* **18** 699-704 (2012).
2. Ishikawa, R.; Lupini A.R.; et al. Quantitative Annular Dark Field Electron Microscopy Using Single Electron Signals. *Microscopy and Microanalysis* **20**, 99-110 (2014).
3. Ishikawa, R., et al. Atomic Structure of Luminescent Centers in High-Efficiency Ce-doped w-AlN Single Crystal. *Scientific Reports* **4** 3778 (2014).
4. R. Ishikawa, R, Lupini, AR, Findlay, SD; Taniguchi, T; Pennycook, SJ. Three-Dimensional Location of a Single Dopant with Atomic Precision by Aberration-Corrected Scanning Transmission Electron Microscopy. *Nano Letters* **14**, 1903-1908 (2014).
5. Zhou, W.; Oxley, M.P.; Lupini, A.R.; et al. Single Atom Microscopy. *Microscopy and Microanalysis* **18**, 1342-1354 (2012).
6. Dahmen, T.; Baudoin, J.P.; Lupini, A.R., et al. Combined Scanning Transmission Electron Microscopy Tilt- and Focal Series *Microscopy and Microanalysis* **20**, 548-560 (2014).
7. Oxley, M. P.; Kapetanakis, M.D.; Prange, M.P.; Varela M.; Pennycook, S.J. & Pantelides, S.T. Simulation of Probe Position-Dependent Electron Energy-Loss Fine Structure. *Microscopy and Microanalysis* **20**, 784-797, (2014).
8. Lin, J.; Fang, W.; Zhou, W.; Lupini, A.R.; Idrobo, J.C.; et al. AC/AB stacking boundaries in bilayer graphene. *Nano Letters*, **13**, 3262-3268 (2013)
9. Gong, Y.; Liu, Z.; Lupini, A.R.; Ajayan, P.M.; et al. Band gap engineering and layer-by-layer mapping of selenium-doped molybdenum disulfide. *Nano Letters* **14**, 442-449 (2014).
10. Veith, G.M.; Lupini, A.R.; et al. Evidence for the Formation of Nitrogen-Rich Platinum and Palladium Nitride Nanoparticles. *Chemistry of Materials* **25**, 4936-4945 (2013).
11. Gold on carbon: one billion catalysts under a single label. Prati, L.; Villa, A.; Lupini, A.R.; et al. *Phys. Chem. Chem. Phys.* **14**, 2969-2978 (2012).
12. C. Li, Y. Wu, J. Poplawsky, T. J. Pennycook, N. Paudel, W. Yin, S. J. Haigh, M. P. Oxley, A. R. Lupini, M. Al-Jassim, S. J. Pennycook, and Y. Yan, Grain-boundary-enhanced carrier collection in CdTe solar cells. *Phys. Rev. Lett.* **112**, 156103 (2014).
13. Li, C.; Poplawsky, J.; Wu, Y.; et al. From atomic structure to photovoltaic properties in CdTe solar cells *Ultramicroscopy* **134**, 113-125 (2013).
14. Li, Chen; Wu, Yelong; Pennycook, T. J.; et al. Carrier Separation at Dislocation Pairs in CdTe *Phys. Rev. Lett.* **111**, 096403 (2013).
15. Polat, O.; Aytug, T.; Lupini, A. R.; et al. Nanostructured columnar heterostructures of TiO₂ and Cu₂O enabled by a thin-film self-assembly approach: Potential for photovoltaics *Materials Research Bulletin* **48**, 352-356 (2013).
16. Aytug, T.; Simpson, J.T.; Lupini, A. R.; et al. Optically transparent, mechanically durable, nanostructured superhydrophobic surfaces enabled by spinodally phase-separated glass thin films. *Nanotechnology* **24**, 315602 (2013).
17. Cantoni, C.; Gazquez, J.; Granozio, et al. Electron Transfer and Ionic Displacements as the Origin of the 2D Electron Gas at the LAO/STO Interface: Direct Measurements with Atomic-Column Spatial Resolution. *Advanced Materials* **24**, 3952-3957 (2012).

Probing Coupled Bias- and Pressure Induced Metal-Insulator and Ferroic Transitions on the Mesoscopic Scale

P. Maksymovych and S.V. Kalinin
(sergei2_maksymovych@ornl.gov)

Postdocs: R. Vasudevan, A. Tselev (res. prof), A. Gianfrancesco (student), W. Lin (now at LANL)

Oak Ridge National Laboratory, Oak Ridge, TN 37831

Research scope

The overarching goal of this research is to reveal the mechanisms of coupled electronic (metal-insulator) and ferroic (ferro- and antiferroelastic, ferro and antiferroelectric) transitions on the mesoscopic scale and explore associated time scales. The SPM tip will act as a local probe of the ferroic and electronic state of matter, communicating local properties to the outside world through measured electronic current, dynamic and static electromechanical response, resonant frequency and quality factor of the cantilever, and microwave response, thus *exploring* and *actively manipulating* local order parameters in nanoscale volumes. Unraveling and subsequently understanding the energy balance between competing interactions will pave the way to deterministic design of novel electronic materials, and reveal the key structural and electronic mechanisms involved in energy storage, generation and dissipation processes.

Recent Progress

In the concurrence period, the program was focused on exploring the coupling between ferroic behavior, chemical degrees of freedom, and electronic phenomena on the mesoscopic level. Our studies focused on conductance of topological defects in ferroelectric materials and pressure-induced morphological changes of mixed electron ionic materials. Although involving quite different material classes and electronic behaviors, the emerging theme of these studies is a control of vacancy density and order parameters in a combined stress-electric field to create new electronic and prospectively optical behaviors or control phase transitions themselves. These studies were further extended to probe relaxation processes in disordered ferroelectrics.

Metal-insulator transitions in ferroelectric domain walls?

The discovery of finite conductivity on ferroelectric domain walls in paradigmatic ferroelectric materials, such BiFeO_3 and $(\text{Pb}_x\text{Zr}_y)\text{TiO}_3$, urges a number of questions including: (1) properties of the metallic state created in the vicinity of tilted or distorted domain walls in ferroelectrics, including the role of electron correlations or electron-phonon coupling in this case; (2) origin of carriers that cause metal-insulator transitions in ferroelectrics – ionization of donor/acceptor levels, inversion layer or in-situ electrochemical process associated with vacancy creation or redistribution; (3) possibility of a metal-insulator be caused *within* a domain wall, e.g. by continuous variation of the tilting angle and associated carrier density of other properties responsible for local electronic changes. Our first step to address these questions has been to compare various compositions of epitaxial PZT films, intentionally chosen from a variety of growth conditions. Coupling between ferroelectric and resistive switching has been observed in all PZT films, with the overall similar trends to our original observation of insulator-metal transition [1]. The variability primarily manifested in the overall magnitude of local current, which ranged by up to ten orders of magnitude between different films, Fig .1. However, even for the most insulating lead zirconate, ferroelectric nanodomains exhibited small activation of local transport, with the largest activation barrier of only ~ 50 meV. As with our earlier findings, this is the hallmark of a new transport channel through the film created and controlled by ferroelectric domain walls. The very low activation barrier height is particularly noteworthy as it is well within the range of polaron hopping conduction, by analogy with 50-100 meV

activation energy in macroscopically doped BaTiO₃. At the same time, it rules out traps and Schottky barriers as the limiting resistance. Therefore, conductive tilted domain walls of ferroelectric nanodomains can be both metallic and insulating, the latter presumably due to small polaron hopping. It may be possible that depending on the specific configuration of the domain wall, one will observe transitions between band-transport, small polaron hopping and, at lower temperature, reentrant small polaron band transport. Controlling these crossovers will ultimately lead to much larger local conductance (well beyond typical 10⁻⁷-10⁻⁸ S), possibility to stabilize conducting walls and observe optoelectronic effects.

Pressure-induced modification of complex oxides

Recently, we demonstrated that applied stress can control the density of oxygen vacancies in polycrystalline NiO [2] and local conductance on the surface of colossal magnetoresistive manganite LCMO [3]. The basis for electrochemical manipulation in the studied cases is that the chemical potential of charged impurities will be approximately linearly dependent both on external potential *and* stress, where the latter is related to the change of the molar volume upon ionization. Since local probes can achieve quite large pressures of a few GPa, “poling” of electrochemical materials can be achieved by simply making contact to the surface. We have witnessed these effects in NiO and La_{0.7}Ca_{0.3}MnO₃, as well in the “clean limit” of single crystal La_{2-2x}Sr_{1+2x}Mn₂O₇ (Fig. 2). In all cases, local conductance was found to depend strongly on tip mechanical contact and the history of contact (i.e. applied pressure, repeated rastering etc). Mechanical control of oxide materials is very attractive, because it can potentially have much broader applicability and it does not require electronic circuitry. These observations also cast new light onto metal-insulator transitions in manganites, and more generally raises a possibility to locally pole the phase states in correlated electron materials. These questions will be explored going forward using atomically-resolved probes and growth methods that are under development within this FWP.

Ferroelectricity in layered sulphides: Exploration of ferroelectricity in thin CuInP₂S₆ films has produced fruitful results in exfoliated films that are 0.5 μm to less than 50 nm thick. Strong domain contrast was detected with BE-PFM in flakes at thicknesses of ~50 nm (Fig. 3); beyond that we found the response may be too weak to be observed, or the *T_c* (315 K) is suppressed, Fig. 3b. Regions that are a hundred or more nanometers thick exhibit bulk behavior, with excellent domain contrast; and at 50 nm domains are still discernable in amplitude and phase signals.

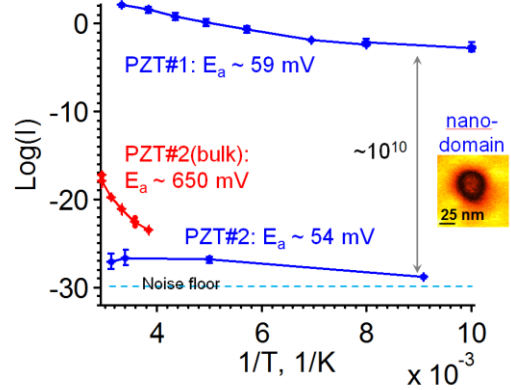


Figure 1. Despite 10 decades difference in local conductance, nanodomains maintain a very low thermally activated transport with a barrier of ~50 mV, which is at least 10-fold smaller than that in bulk.

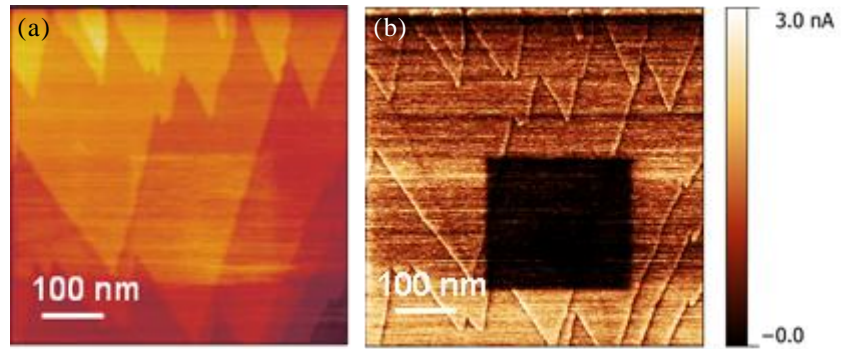


Figure 2: (a) Topography of vacuum-cleaved La_{2-2x}Sr_{1+2x}Mn₂O₇ single crystal with clear single-atom steps. (b) Conduction of La_{2-2x}Sr_{1+2x}Mn₂O₇ locally modified by combination of mechanical and electrical forces.

To quantify this behavior, we assumed the applicability of a Landau-Ginzburg-Devonshire (LGD) theory for a proper ferroelectric. The critical thickness can be found from the Euler-Lagrange boundary problem. Depending on the material parameters and screening length critical thickness can vary in a wide range of 50 nm to 1 μm . Moreover, ferroelectric semiconductors may exhibit a phase diagram in coordinates "film thickness – temperature" due to temperature dependence of the screening length.

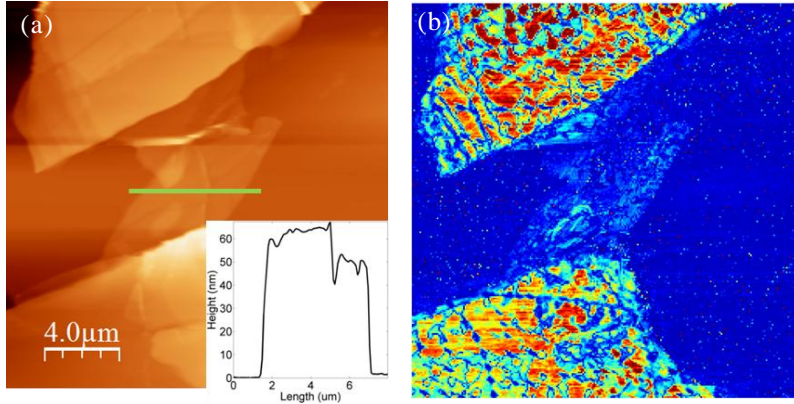


Figure 3: Ferroelectricity in CuInP_2S_6 layers. (a) 20x20 μm contact AFM image of an exfoliated piece of CITP on SiO_2 support, inset shows a line height profile for the green line in the image. (b) Band Excitation PFM Amplitude image of the area in (a).

Multimodal probing of Relaxation Dynamics in Ferroelectric Relaxors

Relaxor ferroelectrics display large dielectric dispersion and dramatic slowing down of dipole dynamics with lowering of temperature. Being of technological interest due to large electromechanical coupling coefficients, their dynamics in the ergodic and nonergodic phases has attracted much attention. The dispersion of relaxation behaviors at the mesoscopic level and the type of heterogeneity in the dynamic behavior of the polar nanoregions (PNRs) are less well studied, and require local probe methods. We developed a multimodal method using Band-Excitation voltage-time spectroscopy on a sample of $0.72\text{Pb}(\text{Mg}_{1/3}\text{Nb}_{2/3})\text{O}_3-0.28\text{PbTiO}_3$ (PMN-28PT), and multivariate statistical analysis to determine dynamic relaxation (Fig. 4).

Local piezoresponse was broken down into a function of voltage and time. After fitting the response to an exponential at each point, i.e. $R(x,y,V,t) = A(x,y,V) + R_0(x,y,V)\exp(-\tau/t)$ maps were produced for R_0 at different voltages. The response is clearly very heterogeneous (Fig. 4a). Analysis by standard functional fitting did not yield many useful clues pertaining to dynamic relaxation behaviors, and we

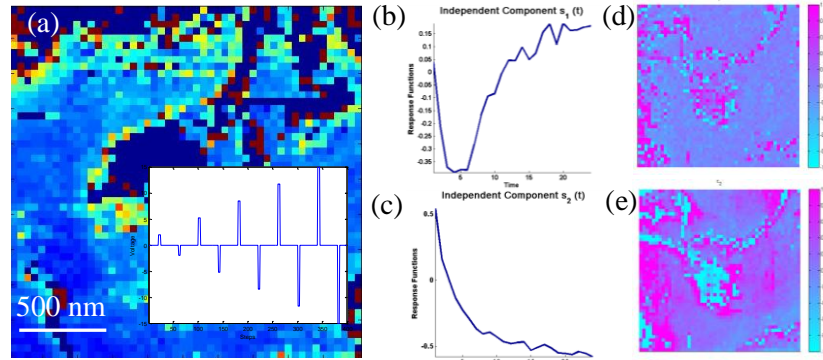


Fig. 4: BE-Spectroscopic Data on a ferroelectric relaxor. (a) Relaxing amplitude spatial map, with DC Voltage waveform applied to the tip inset. (b-e) ICA analysis, showing two distinct relaxation processes, for $V=8.5\text{V}$, with (b) ICA component 1, (c) ICA component 2, (d) c_1 , (e) c_2 .

turned to multivariate methods, specifically independent component analysis (ICA). We assumed that the dynamic behavior of the ferroelectric relaxor is governed by two relaxation processes that are independent of each other and whose components are spatially non-varying. Then we may write the response at each position $R = R(x, y, V, t)$ as $R(x, y, V, t) = c_1(x, y, V)s_1(t) + c_2(x, y, V)s_2(t)$ and ICA can be used to determine the independent components and the mixing coefficients c_1 and c_2 (Fig. 4b,c) The results of the ICA

analysis, are shown in Fig. 4(d,e) for $V = 8.5V$. The results clearly indicate the presence of two different relaxation processes that are occurring on the surfaces of PMN-28PT, with one being exponential (Fig. 4c) and the other appearing to peak after the pulse application (Fig. 4b) before decaying more rapidly. Notably, the spatial distribution of the respective components is very similar, verifying the original assumption and pointing to the amplitude rather than relaxation of the response as the dominant source of heterogeneity of the relaxor response.

Future plans:

Understanding of the fundamental physics of coupling between electronic properties and ferroic behaviors on strongly correlated oxide surfaces on the mesoscale necessitates a synergistic including (a) in-situ studies of deposited, cleaned, or cleaved surfaces, (b) development of data analytics tools that allow extraction of spatial variability of response from multidimensional data sets, and (c) theoretical framework that allows linking SPM data and relevant physical behaviors. Our research will pursue these directions, aimed at the following fundamental issues:

Mesoscopic phenomena. We will study hitherto unexplored regime of ferroelectric semiconductors in ferroic oxides with controlled dopants. We will look for transport signatures of phase transitions in related ferroics such as antiferroelectrics, where the conductance would be caused by an intriguing domain wall between a locally polar ferroelectric domain and parent antiferroelectric matrix and thin films with the composition near a morphotropic phase boundary. Stress-induced effects will be studied in detail, particularly with respect to penetration into bulk and modification of phase transitions in artificially poled structures. These studies will pursue the detailed atomistic origin of the local chemical changes associated with resistive, polarization and stress-induced modification with the aim of controlling complex oxides through defect chemistry. Equally important will be to establish the possibility to induce and control coupled resistive phenomena in meso- and macroscale contact geometries, such as capacitor and transistors based on phase-transition materials.

Local and mesoscale domain wall nonlinearity. We will utilize local scanning probe spectroscopic methods coupled with global measurements to determine global and local domain wall nonlinearity in ferroic materials, and correlate with minor and major local and mesoscale hysteretic phenomena. Through multivariate statistical analysis, relevant correlations between the nonlinear and hysteresis behaviors will be found, allowing connections to be drawn between descriptors specific to domain wall and its interaction with point defects, and the global hysteretic phenomena modelled by e.g. hysterons in the Preisach scheme. These studies have the potential to (a) provide the long-standing link between statistical descriptors of nonlinearity and hysteresis, (b) provide more insight into the interaction of domain walls and local minor hysteresis, which has not been studied, and (c) will allow scale limit-testing of macroscopic theories and determination of how micro and meso-scale phenomena average to provide the present macroscale description, allowing for optimization of material properties.

Research supported by the U.S. Department of Energy Office of Basic Energy Sciences Division of Materials Sciences and Engineering and performed at the Center for Nanophase Materials Sciences supported by Division of Scientific User Facilities (SVK, PM, WL, and AT).

DOE-sponsored publications 2012-2014 [27 peer-reviewed papers including 2 *Nature Mat.*, 1 *Sci Rep.*, 1 *Phys. Rev. Lett.*, 3 *ACS Nano*, 2 *Nano Lett.*, 5 *Adv. (Func, En.) Mat.*, 2 plenary, 2 keynote, and 12 invited talk at conferences]]

1. P. Maksymovych et al., *Tunable Metallic Conductance in Ferroelectric Nanodomains*, *Nano Letters* 12, 209 (2012).
2. Y. Kim et al, *Mechanical Control of Electroresistive Switching*, *Nano Lett.* **13**, 4068 (2013).
3. S. J. Kelly et al., *Controlled mechanical modification of manganite surface with nanoscale resolution*, *Nanotechnology* (in review), 2014.

3D Visualization of Emergent Behavior in Nanoscale Functional Heterostructures

Amanda K. Petford-Long, Seungbum Hong, Charudatta Phatak

Materials Science Division, Argonne National Laboratory, 9700 S Cass Avenue, Argonne, IL 60439

petford.long@anl.gov, hong@anl.gov, cd@anl.gov

Program Scope

The properties of ferroic materials at the nanoscale are governed by their complex energy landscape, which must be understood if emergent behavior is to be controlled. We are focusing on nanoscale heterostructures whose building blocks show ferromagnetic, ferroelectric, and resistance switching behavior. We aim to obtain a fundamental understanding of domain behavior and charge transport properties in these nanostructures through control of parameters that contribute to their energy landscape, such as interlayer coupling, geometric effects, and interactions between adjacent nanostructures. Further degrees of freedom can be achieved in 'designer' heterostructures, in which there is coupling between the order parameters in materials with different ferroic order. Our approach involves an interwoven combination of aberration-corrected Lorentz transmission electron microscopy (LTEM) and advanced scanning probe microscopy (SPM) and a particular focus is the use of three-dimensional (3D) analysis and imaging techniques that we have developed to visualize domain and transport behavior in nanostructures as a function of external stimuli such as applied fields, temperature and/or time.

Recent Progress

Three-dimensional magnetization in nanospirals

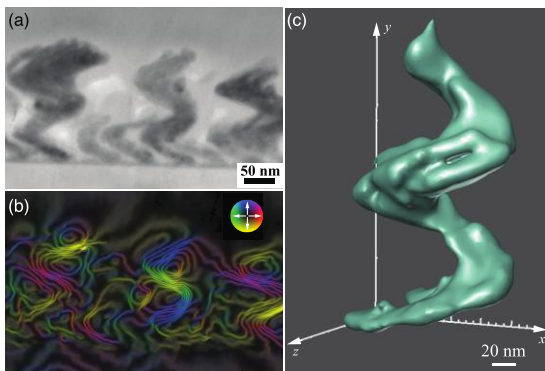


Figure 1 (a) TEM image of the nanospirals, (b) the magnetization map from the nanospirals, and (c) 3D morphology of an individual nanospiral.

3D nanostructures are critical building blocks for complex mesoscopic systems and the interplay between their energetics leads to these complex systems exhibiting novel behavior when compared with their bulk counterparts. We have successfully carried out the first direct 3D visualization of the magnetic domains in sculpted cobalt nanospirals of 20 nm in diameter. As a result, we were able to conclude that the shape anisotropy energy dominates over the magnetocrystalline energy of the nanostructures resulting in a checkerboard like magnetization pattern. Figure 1 shows (a) a bright-field TEM image of the nanospirals, (b) a magnetization map, and (c) the 3D morphology of an individual nanospiral. See publication [10]

Revealing the underlying polarization domain structures by collecting the screening charges

The polarization charge in ferroelectric materials is screened by equal amounts of surface charge with opposite polarity in ambient conditions. We have developed a new technique: charge gradient microscopy (CGM), that allows us to scrape, collect and quantify the surface screening

charge at high speed and reveal the underlying polarization domain structure (publication [14]).

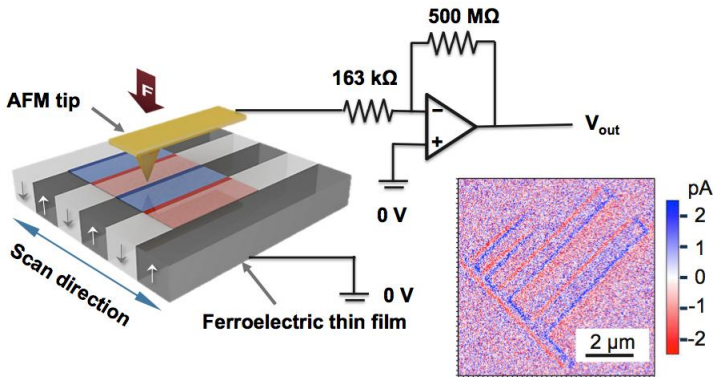


Figure 2 (left) Schematic diagram of CGM and (right) trace and retrace CGM images of artificially decorated ribbon domains with different sizes poled by 6 V to the bottom electrode of a 85 nm thick LiTaO₃ film scanned using a Pt tip at a scan frequency of 40 Hz.

We collected the current from a grounded CGM probe while scanning a periodically-poled single crystal LiTaO₃ thin film on a Cr electrode. We observed current signals at the domains and domain walls originating from the displacement current and the relocation or removal of surface charge. This enabled us to visualize the ferroelectric domains at a scan frequency >78 Hz over 10 μm. The scraped charge, measured as a current that scales with scraping rate, induces a charge gradient that leads to the immediate relocation or refill of the screening charges from the probe vicinity. CGM can be used to study the complex dynamics of domain nucleation and growth induced by a biased tip in the absence of surface screening charges.

CGM can be used to study the complex dynamics of domain nucleation and growth induced by a biased tip in the absence of surface screening charges.

X-ray irradiation induced reversible resistance change in resistive switching oxides

Previous studies of x-ray-induced resistance changes in binary oxides showed irreversible and permanent dielectric breakdown. However for Pt/TiO₂/Pt structures we observed a reversible

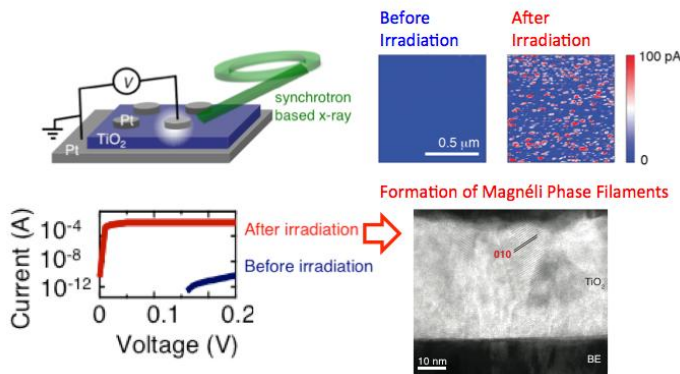


Figure 3 X-ray induced volatile and nonvolatile reversible changes in Pt/TiO₂/Pt heterostructures studied by conducting AFM and cross-section TEM.

volatile change of the pristine resistance state that can be related to a photovoltaic-like effect induced by the x-ray beam. We also found a reversible non-volatile conductance change that occurred when the photovoltaic-like effect is combined with a local phase transition into a Magnéli phase, which was confirmed by TEM and conducting AFM (c-AFM) analysis as shown in Figure 3. Our discovery of a reversible resistance change induced by x-rays is unexpected, as the scattering cross-

section of x-rays with TiO₂ is extremely small. However, our observations convincingly point towards the combined effects of a photovoltaic effect, Joule-heating and x-ray-induced defect generation. These findings provide insights into the detailed mechanisms of the electroforming process, such as local heating and defect generation leading to nanoscale metallic phase transition, by which the resistivity changes in resistive switching oxides. (Publication [9])

Future Plans

Exploring ferroic domain behavior at the nanoscale

We seek to develop a systematic understanding of the contribution and relative scale of various energy terms governing the domain behavior in vertically and laterally confined ferromagnetic heterostructures, and ferroelectric nanostructures. We will then build upon this research to explore more complex systems consisting of combined ferroelectric/ferromagnetic heterostructures. We are extending our work on artificial frustrated magnetic nanostructures to spin ice arrays with non-periodic lattices, as this will result in additional frustration that is not seen in periodic lattices such as those that we have explored to date. We will explore both the ground states of these lattices and the way in which defects such as magnetic monopole states propagate through the lattices. We will continue our research on coupled magnetic disks with the goal of generating artificial skyrmions through control of the layer interactions and exploring their quasistatic behavior in response to applied electric and magnetic fields.

In ferroelectric nanostructures we will explore the effect of boundary conditions such as size, shape and artificial defects on domain formation and structure. We will then explore the effect of screening charge on the resulting domain structure. Screening charges help compensate the effective depolarizing field acting on the FE nanostructure and the presence of the screening charges at a buried interface can lead to the appearance of spontaneous vortex nanodomain arrays at ferroelectric heterointerfaces. Our newly-developed technique of charge-gradient microscopy is ideally suited to quantifying the role of screening charges in controlling domain structure. We will also explore the domain switching in our patterned ferroelectric nanostructures to understand the local effects that hinder or facilitate domain motion. Our observations of domain nucleation and growth will allow us to understand the effects of confinement and pinning of domain boundaries by defects in ferroelectric nanostructures. For example we will explore the way in which local stress gradients influence ferroelastic switching, for which preliminary studies using CGM have shown great promise.

Resistive Switching oxides

Our exploration of resistive-switching oxide (RSO) materials will focus on understanding how confinement and the motion of charged defects control the 3D distribution of conduction pathways. We are developing a novel artificial resistive-switching network configuration [reference 1] that enables us to obtain exquisite control over the conduction pathways across the oxide. The goal of this research is to explore the ‘random circuit-breaker model’ for RSOs and to determine whether conducting filament formation is a self-limiting process.

In order to understand the effects of defect distribution in RSO films, we will extend our 2D studies of conducting filament distribution to three dimensions using a novel method involving the use of an AFM tip to first map current distribution and then serial section down through the filaments. These data will be combined with in-situ phase imaging of the electric field distribution using TEM.

References

1. J. W. Jeong, W.I. Park, M. Kim, C. A. Ross, and Y. S. Jung, “Highly tunable self-assembled nanostructures from poly(2-vinylpyridine-b-dimethylsiloxane) block copolymer,” *Nano Lett.* **11**, 4095-4101 (2011).

Selected Publications

1. **C. Phatak**, M. Pan, **A. K. Peford-Long**, **S. Hong**, and M. De Graef, “Magnetic interactions and reversal of artificial square spin ices,” *New. J. Phys.* **14**, 075028 (2012).
2. M. Pan, **S. Hong**, J. R Guest, Y. Liu and **A. Petford-Long**, “Visualisation of Magnetic Domain Structure Changes Induced by Interfacial Strain in $\text{CoFe}_2\text{O}_4/\text{BaTiO}_3$ Heterostructures”, *J. Phys. D: Appl. Phys.* **46**, 055001 (2013).
3. M. Park, K. No, and **S. Hong**, “Visualization and Manipulation of Metastable Polarization Variants in Multiferroic Materials”, *AIP Advances* **3**, 042114 (2013).
4. M. Narayanan, M. Pan, S. Liu, S. Tong, **S. Hong**, B. Ma, and U. Balachandran, “Effect of stress state on the domain configuration and switching behavior in ferroelectric thin films”, *RSC Advances* **2**, 11901 (2012).
5. S. O. Hruszkewycz, M. J. Highland, M. V. Holt, D. Kim, C. M. Folkman, C. Thompson, A. Tripathi, G. B. Stephenson, **S. Hong**, P. H. Fuoss, “Imaging local polarization in ferroelectric thin films by coherent x-ray Bragg projection ptychography,” *Phys. Rev. Lett.* **110**, 177601 (2013).
6. E. Humphrey, **C. Phatak**, M. De Graef, “Modified Transport-of-Intensity Approach for Electrostatic and Magnetic Phase Shift Separation”, *Microsc. & Microanal.*, **19**, S2 (2013).
7. J. P. Morgan, J. Åkerman, A. Stein, **C. Phatak**, R. M. L. Evans, S. Langridge, and C. H. Marrows, “Real and effective thermal equilibrium in artificial square spin ices”, *Phys. Rev. B*, **87**, 024405 (2013).
8. B. Kim, **S. Hong**, H. Choi, W.-H. Ryu, H. Paik, Y.-Y. Choi, H.-S. Kwon and K. No, “Fabrication and Characterization of Nanoscale Ferroelectric Honeycombs”, *J. Am. Ceram. Soc.* **96**, 1355 (2013).
9. S.H. Chang, J. Kim, **C. Phatak**, **K. D’Aquila**, S.J. Song, C.S. Hwang, J.A. Eastman, J.W. Freeland and **S. Hong**, “X-ray irradiation-induced reversible resistance change in Pt/TiO₂/Pt cells”, *ACS Nano* **8**, 1584 (2014).
10. **C. Phatak**, Y. Liu, E.B. Gulsoy, D. Schmidt, E. Schubert, **A.K. Petford-Long**, “Visualization of the magnetic structure in sculpted three-dimensional cobalt nanospirals”, *Nano Lett.* **14**(2), 759 (2014).
11. G. Lee, R. S. Katiyar, B.-K. Lai, **C. Phatak**, O. Auciello, “Dielectric behavior related to TiO_x phase change to TiO₂ in TiO_x/Al₂O₃ nanolaminate thin films”, *MRS Comm.* **4**, 67 (2014).
12. **K. D’Aquila**, **C. Phatak**, M.V. Holt, B.D. Stripe, S. Tong, **W.I. Park**, **S. Hong** and **A.K. Petford-Long**, “Bipolar resistance switching in Pt/CuO_x/Pt via local electrochemical reduction”, *Appl. Phys. Lett.* **104**, 242902 (2014).
13. **C. Phatak**, **A.K. Petford-Long**, M. Beleggia, M. De Graef, “Theoretical study of ferroelectric nanoparticles using phase reconstructed electron microscopy”, *Phys. Rev. B* **89**, 214112 (2014).
14. **S. Hong**, S. Tong, **W.I. Park**, Y. Hiranaga, Y. Cho and A. Roelofs, “Charge gradient microscopy”, *Proc. Nat. Acad. Sci. USA* **111**(8), 6566 (2014).
15. E. Humphrey, C. Phatak, **A.K. Petford-Long**, M. De Graef, “Separation of Electrostatic and Magnetic Phase Shifts using a Modified Transport-of-Intensity Equation”, *Ultramicrosc.* **139**, 5 (2014).

Understanding the Emergent Phenomena Arising from Competing Degrees of Freedom in Doped Manganites

Jing Tao and Yimei Zhu

Condensed Matter Physics and Materials Science Department,
Brookhaven National Laboratory, Upton, NY 11973

Program Scope

This research task under the FWP Number MA-015-MACA is aiming at understanding the role of competing degrees of freedom of spin, charge, orbital and lattice in the exotic materials' functionalities such as colossal magnetoresistance in doped manganites. Using integrated electron based approaches with emerging capabilities, this research is focused on i) probing the electronic structures in real space, momentum space and energy space at high resolution to quantitatively characterize the ordering states in manganites from electronic, atomic and symmetry perspectives; ii) direct imaging of local electronic structures and direct measurements of local material properties using scanning electron nanodiffraction, Lorentz phase imaging and other TEM tools to establish the structure-property relationship at the mesoscale; iii) studying a variety of correlated materials including cuprates, iron pnictides and nickelates that share intrinsic physics with doped manganites to unravel the coupling between competing orders. Emphasis will be placed on by applying stimuli including thermal, magnetic, electric, doping and strain variations for better interpretation of emergent phenomena. Experimental observations with synchrotron x-ray diffraction, neutron scattering, and theoretical calculation will be carried out to gain new insights into the underlying physics in correlated materials.

Recent Progress

From a symmetry perspective, electronic liquid-crystal (LC) phases, including electronic smecticity and nematicity, are considered to play a key role in emergent phenomena and functionalities in correlated materials¹. Despite the extensive research efforts devoted to these novel phases, no clear experimental evidence has been obtained to pin down the driving mechanisms for the electronic LC phase transitions. Experimentally, diffraction techniques have been widely used to characterize the global electronic LC phases, but real-space observations at the microscopic scale are lacking. Using a sharp electron probe with atomic real-space resolution, scanning tunneling microscopy provided many insights into the nature of the electronic LC phases but no observations were obtained from electronic smectic to nematic phase transition because disorder effects suppress long-range electronic nematic/smectic ordering in 2D materials.

Here we report the first experimental evidence in strongly correlated materials of the electronic LC phase transitions from electronic smectic to nematic and then to isotropic phase, with their driving mechanisms revealed in $\text{La}_{1/3}\text{Ca}_{2/3}\text{MnO}_3$ using TEM techniques. $\text{La}_{1/3}\text{Ca}_{2/3}\text{MnO}_3$ is a 3D material and electronic smecticity was observed at low temperatures. It is difficult to distinguish a transition from smecticity to nematicity by the electron diffraction measurements alone (black plots in Fig. 1b). However, the direct observations (Phase map and scanning electron nanodiffraction (SEND) maps in Fig. 1a) enable us to clearly identify the electron LC phase transition at $T = 220$ K (red plots in Fig 1b). In addition, high-resolution dark-

field images revealed the formation of dislocations suggesting the orbital disorder induced charge segregation which is initiated at the location of the dislocation pairs, as shown in Fig 1c and 1d. The proliferation of the dislocations was observed to further trigger electronic phase separation at higher temperatures and drive the electronic smecticity into nematicity². At the temperature range above $T = 245$ K, where the lattice constants of the crystal start to vary significantly, another phenomenon was seen to emerge with the electronic nematicity, i. e., nanoclusters with perpendicular electronic structure (purple clusters in the SEND maps in Fig 1a) formed with electronic phase separation, as a result of the strain effect induced by the lattice to minimize the total energy in the material. The coexistence of the melted “normal” nanoclusters (red in the SEND maps) and the anisotropic nanoclusters drive the electronic nematic phase into the isotropic phase at $T = 310$ K. Moreover, EELS results (Fig. 1e) agree with the charge segregation scenario suggested by electron nanodiffraction and simulations based on Ginzburg-Landau theory³. The electronic LC phases observed in doped manganites share common characteristics with other complex materials but bring additional features, demonstrating wide impact of the electronic LC phases and paving a path to a better understanding of the competing orders in strongly correlated materials.

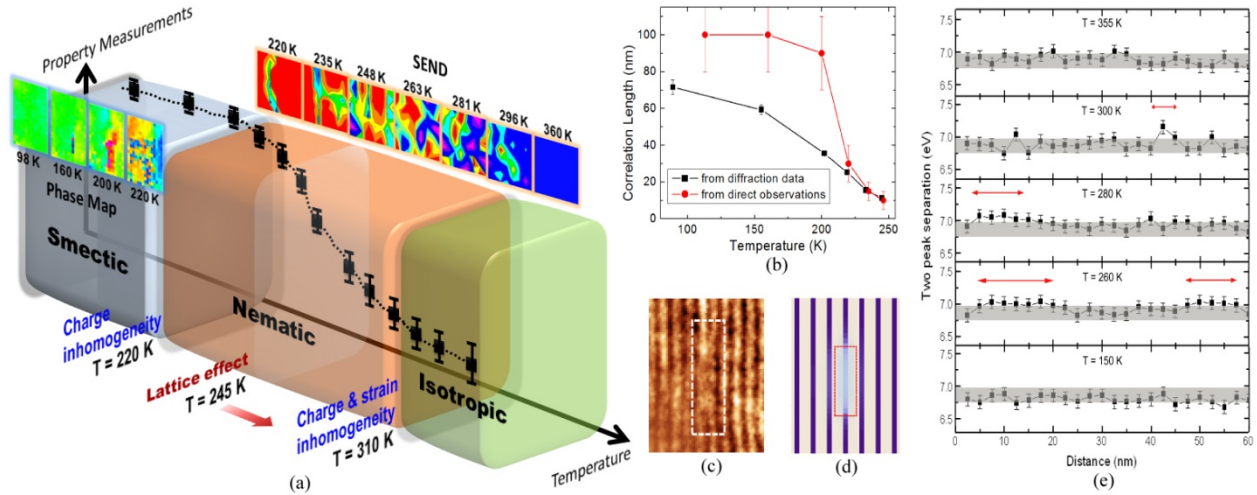


Fig. 1. (a) An electronic-LC-phase diagram of $\text{La}_{1/3}\text{Ca}_{2/3}\text{MnO}_3$ summarized from our in-situ TEM observations. Each phase map (reconstructed from high-resolution dark-field images) and SEND map is ~ 20 nm wide. An electronic smectic-nematic phase transition at $T = 220$ K was identified by the correlation length measurements in (b), which coincides with a commensurate-incommensurate phase transition characterized by wave number measurements (black plots). An electronic nematic-isotropic phase transition was identified at $T = 310$ K. (c) A TEM dark-field image shows a pair of dislocation in the electronic smecticity with a theoretical simulation (b) supporting the formation model. (e) Evolution of the electron LC phases probed by EELS.

Future Plan

Our strategy to unravel the role of competing orders in doped manganites is to study the response of the electronic structures by applying stimuli (Fig. 2, left panel) during the TEM observations. Coupling between the different orders is expected to have distinct response to the external excitations. For instance, magnetic field would directly modify the spin order in a correlated material as a principle effect and to influence the other ordering states as the secondary effect. We propose to investigate the phenomena under four stimuli in addition to thermal excitations in experimental observations, listed as follows.

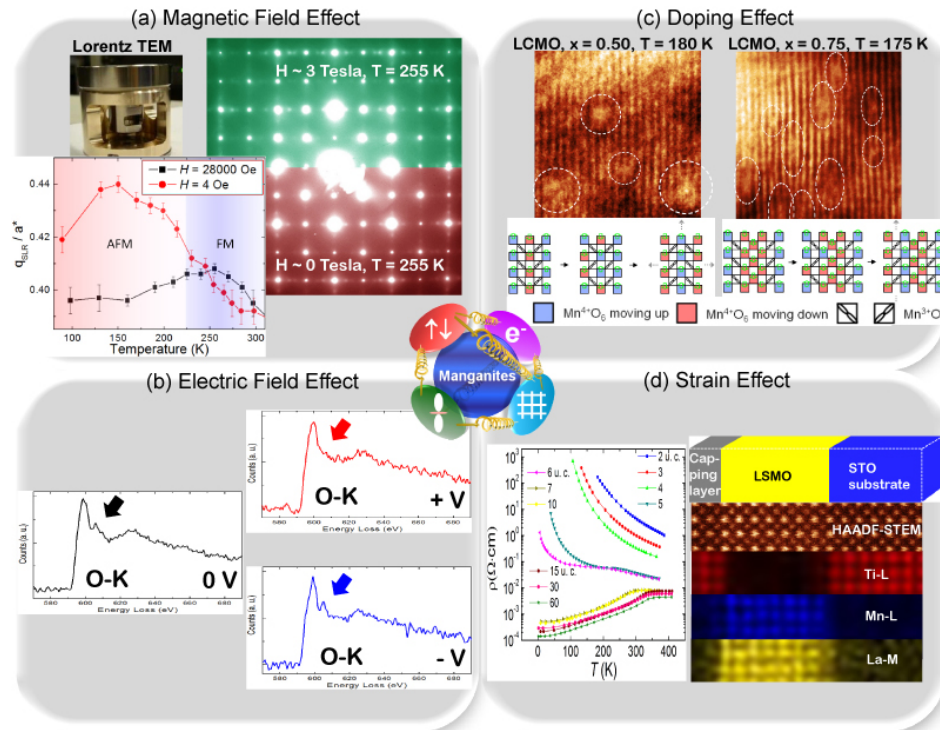


Fig. 2. Our future plan to unravel the role of competing orders by studying the following effects in correlated materials: magnetic field effect by comparing results obtained with and without magnetic field (a), electric field effect by exploring the change in electronic structures with applied electric voltage (b), doping effect by investigating at different doping levels in LCMO (c) and strain effect by tuning the LSMO film thickness on STO substrate (d).

Magnetic field effect Using our dedicated Lorentz TEM, experimental data can be acquired at nearly field-free environment compared to a field ~ 3 Tesla in conventional TEM. Fig 2a shows the electron diffraction patterns obtained from the same area in $\text{La}_{0.55}\text{Ca}_{0.45}\text{MnO}_3$ under different magnetic fields. The wave number of the short-range superstructure was measured to have unexpected variation in the antiferromagnetic and ferromagnetic regimes. We will continue to explore the phenomena by correlating the results with first principle calculations.

Electric field effect Fig. 2b shows that the main peak in Oxygen K-edge EELS obtained from a composite LSMO/STO sample disappeared after applying a positive voltage to the sample surface, and re-appear after applying a negative voltage. The observation might be attributed to charge accumulation or structural distortion induced by the electric field. We will explore the electric field effect by integrating more experimental observations together with other approaches such as density functional theory calculations.

Doping effect The electronic phase diagram of $\text{La}_{1-x}\text{Ca}_x\text{MnO}_3$ (LCMO; $0 \leq x \leq 1$) is rich and complex. Fig. 2c shows a simple case demonstrating the distinct defect formation in the superstructure in LCMO, $x = 0.50$ and $x = 0.75$, arising from different orbital/charge ordering. The doping effect will be studied by comparing direct imaging results with electron nanodiffraction and EELS data at various doping levels.

Strain effect By tuning the strain between the LSMO film and the STO substrate, the LSMO film can be altered from insulator to metal (left plot in Fig. 2d). EEL spectrum imaging (right images in Fig. 2d) provides chemical and electronic analysis which is necessary to understand the strain effect. Samples at different strain situations will be studied and correlated to physical property measurements (in collaboration with groups led by Prof. Jiandi Zhang and Prof. Ward Plummer at Louisiana State Univ.)

Reference

1. E. Fradkin, S. A. Kivelson, M. J. Lawler, J. P. Eisenstein, A. P. Mackenzie, *Annual Review of Condensed Matter Physics* **1**, 153 (2010)
2. J. Tao, K. Sun, W. G. Yin, Q. Meng, S. Pennycook, J. Tranquada and Y. Zhu, submitted;
3. J. Tao, K. Sun, H. Xin, J. Wen, W. Luo, J. Tranquada, S. Pennycook and Y. Zhu, manuscript under preparation

Publication

1. Tyson, T. A.; Yu, T.; Croft, M.; Scofield, M. E.; Bobb-Semple, D.; Tao, J.; Jaye, C.; Fischer, D. and Wong S. S., *Applied Physics Letters*, accepted (2014)
2. Ali, M. N.; Xiong, J.; Flynn, S.; Tao, J.; Gibson, Q.; Schoop, L.; Liang, T.; Haldolaarachchige, N.; Hirschberger, M.; Ong, N. P.; & Cava, R. J., *Nature*, accepted (2014)
3. Xia, X.; Figueroa-Cosme, L.; Tao, J.; Peng, H-C.; Niu, G.; Zhu, Y.; and Xia, Y., *Journal of the American Chemical Society* **136**, 10878 (2014).
4. Schoop, L.; Hirschberger, M.; Tao, J.; Felser, C.; Ong, N. P.; and Cava, R. J., *Physical Review B* **89**, 224417 (2014)
5. Chapler, B. C.; Post, K. W.; Richardella, A. R.; Lee, J. S.; Tao, J.; Samarth, N.; and Basov, D. N., *Physical Review B* **89**, 235308 (2014)
6. Lee, J. S.; Richardella, A.; Rench, D. W.; Fraleigh, R. D.; Flanagan, T. C.; Borchers, J. A.; Tao, J.; Samarth, N., *Physical Review B* **89**, 174425 (2014)
7. Chen, H. Y.; Yu, T.; Gao, P.; Bai, J. M.; Tao, J.; Tyson, T. A.; Wang, L. P.; Lalancette, R., *Inorganic Chemistry* **52**, 9692 (2013)
8. Lv, T.; Wang, Y.; Choi, S. I.; Chi, M. F.; Tao, J.; Pan, L. K.; Huang, C. Z.; Zhu, Y. M.; Xia, Y. N., *ChemSusChem* **6**, 1923 (2013)
9. Hirai, D.; Bremholm, M.; Allred, J. M.; Krizan, J.; Schoop, L. M.; Huang, Q.; Tao, J.; and Cava, R. J., *Physical Review Letters* **110**, 166402 (2013)
10. Taylor E.; Chen S.; Tao J.; Wu L.; Zhu Y.; and Chen J., *ChemSusChem* **6**, 1863 (2013)
11. Chen, S.; Jenkins, S.; Tao, J.; Zhu, Y.; Chen, J., *the Journal of Physical Chemistry C* **117**, 8924 (2013)
12. Shao, M. H.; He, G. N.; Peles, A.; Odell, J. H.; Zeng, J.; Su, D.; Tao, J.; Yu, T.; Zhu, Y. M.; Xia, Y. N., *Chemical Communications* **49**, 9030 (2013)
13. Si, R.; Tao, J.; Evans, J.; Park, B. J.; Barrio, L.; Hanson, J. C.; Zhu, Y.; Hrbek J.; and Rodriguez, J. A., *the Journal of Physical Chemistry C* **116**, 23547 (2012)
14. Xie, S.; Jin, M.; Tao, J.; Wang, Y.; Xie, Z.; Zhu, Y. and Xia, Y., *Chemistry: A European Journal* **18**, 14974, (2012)
15. Zhu, C.; Zeng, J.; Tao, J.; Johnson, M.; Schmidt-Krey, I.; Blubaugh, L.; Zhu, Y.; Gu, Z. and Xia, Y., *Journal of the American Chemical Society* **134**, 15823 (2012).
16. Tao J., *Nanotechnology Reviews*, vol **1**, issue 4, 301-311 (2012) (invited review article)
17. Neilson, J. R.; Llobet, A.; Stier, A. V.; Wu, L.; Wen, J.; Tao, J.; Zhu, Y.; Tesanovic, Z. B.; Armitage, N. P.; McQueen, T. M., *Physical Review B* **86**, 054512 (2012)

Scanning Transmission Electron Microscopy: Atomic Structure and Properties of Materials

Complex oxide functionality

Principal Investigators: Maria Varela, Matthew F. Chisholm, Andrew R. Lupini, Wu Zhou

Materials Science & Technology Division, Oak Ridge National Laboratory, TN 37831

Sub-Program Scope

Coupling of the electronic, spin and structural degrees of freedom in complex oxides can lead to fascinating behaviors. The potential of these materials has attracted significant interest in recent years but aberration corrected scanning transmission electron microscopy (STEM) offers unique access to structure and properties at the atomic scale. Local structural variations such as distortions of oxygen octahedra and anion/cation displacements or defects such as vacancies are revealed in real space images. Simultaneously, electron energy-loss spectroscopy (EELS) can now provide electronic and magnetic structure with atomic resolution. Developing the next generation of energy materials, where nanostructured architectures can be used to produce desired macroscopic behavior, will require understanding of complex interactions at the atomic scale. In this program, we investigate avenues to explore strongly correlated oxide materials by probing structural, chemical, and electronic properties with atomic-scale resolution in real space with exquisite detail.

Recent progress

In order to determine the connection between the local atomic landscape and resulting global properties we must explore in real space a number of open fronts such as atomic displacements, bond distortions, point defects, defect superstructures, interplay between different order parameters and magnetic quantities with improved spatial resolution. Examples of exciting recent progress along these lines include:

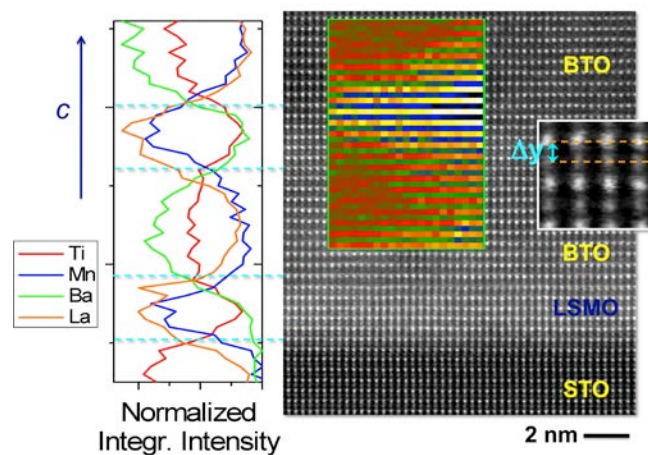


Fig. 1: Z-contrast image of a $\text{BTO}_9 \text{ u.c./LSMO}_6 \text{ u.c.}$ superlattice. On the left, the Ti L, Mn L, Ba M and La M line traces along the growth direction showing the stacking. The inset shows the spatial map of distortions.

1. Mapping of atomic displacements: new views of multiferroic heterostructures:

If the tilts and distortions of atomic bonds can be tuned at will in multiferroic composites, new macroscopic functionalities may arise [1-6]. An example can be found in $\text{BaTiO}_3/\text{La}_{0.7}\text{Sr}_{0.3}\text{MnO}_3$ (BTO/LSMO) heterostructures, such as the superlattice shown in **Fig. 1**.

By measuring the atomic column positions directly, we observe polarization gradients between the manganite and the ferroelectric. We find that in a nanometer thick ferroelectric tunnel barrier an unexpected ferroelectric state develops consisting of a head to head domain wall with a large polarization gradient extending over a large portion of the barrier. This is enabled by the presence of oxygen vacancies, which have a donor character supplying the charge carriers necessary to screen the polarization charges at the domain wall. The presence of a confined free electron gas within the nanometer thick domain wall results in resonant tunneling. This result points a new avenue for novel device concepts in oxide electronics based on exploiting the electronic properties of domain walls in ferroelectric tunnel barriers.

2. Interplay between order parameters:

Cobaltates exhibit complex behavior through cobalt's ability to adopt various valence and spin state configurations [7, 8]. The case of $\text{Sr}_3\text{YCo}_4\text{O}_{10+x}$ (SYCO) has attracted considerable attention because of persisting uncertainties about its structure and the origin of its observed room temperature ferromagnetism. Using aberration-corrected STEM we observe alternating Co-O bond lengths that are tied by DFT calculations to alternating high spin and intermediate spin cobalt atoms. This relatively direct observation of an intermediate spin state for cobalt provides new evidence for this controversial magnetic configuration. Our results provide clear insights into ferromagnetism in this cobaltite and should further our general understanding of magnetism in transition metal oxides.

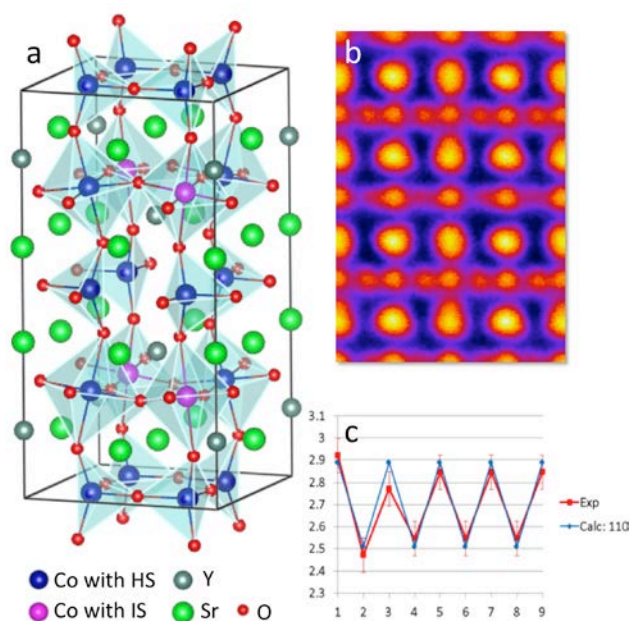


Fig. 2: a) schematic of atomic and magnetic structure of SYCO, b) ABF image (reversed contrast of $\langle 110 \rangle_p$ projections and c) experimental and theoretical O to O spacings in CoO_6 layer.

3. Magnetic quantity determination with atomic resolution: sub-nm mapping of magnetism in nanosystems:

For the first time, the electron microscope has been used to map the magnetization of nanoparticles in real space with sub-nanometer spatial resolution, along with their structure, chemistry and electronic properties (**Fig. 3**). Research on magnetic materials has been long hampered by the lack of real space probes capable of looking at these systems with true sub-nanometer eyes. Studies, for example, of the magnetic properties of defects in a crystal, or the surface magnetism in interfaces or nanoparticles were as limited as our understanding of the

underlying Physics. Electron magnetic circular dichroism (EMCD) [9] in the aberration corrected electron microscope, combined with density functional calculations, has shown that capping the surfaces of magnetite Fe_3O_4 iron-oxide nanoparticles with an organic acid restores magnetization on the surface layer. The bond to the organic acid prevents further oxidation to Fe_2O_3 and results in O-Fe atomic configuration and distances close to the bulk values, which has a strong effect on the magnetic state [10]. We conclude that the nature and number of molecules in the capping layer is an essential ingredient in the fabrication of nanoparticles with optimal magnetic properties.

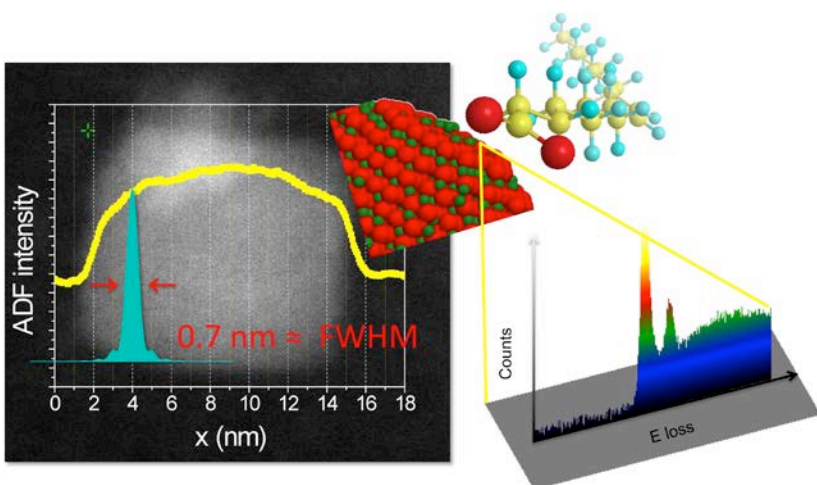


Fig. 3: Probing magnetism at the surface of nanoparticles with a sub-nanometer electron beam.

Future Plans

We plan to apply shaped electron beams for innovative measurements with high spatial and energy resolution and selective k-space sensitivity in both imaging and spectroscopy. This approach will provide improved understanding of the bridge from the atomic arrangements to macroscopic functionalities of complex oxides.

References

- [1] Cheong, S.-W., Mostovoy, M., *Nat. Mater.* **6**, (2007) 13.
- [2] Ramesh, R., Spalding, N. A., *Nat. Mater.* **6**, (2007) 21.
- [3] F. A. Cuellar et al., *Nature Communications* DOI:10.1038/ncomms5215 (2014).
- [4] G. Radaelli et al., *Nature Communications*. DOI: 10.1038/ncomms4404 (2014).
- [5] J. He et al., *Phys. Rev. Lett.* **105**, (2010) 227203.
- [6] G. Sanchez-Santolino et al., *Microscopy & Microanalysis*, **20**, (2014) 825-831.
- [7] J. Gazquez et al., *Nano letters* **11** (2011) 973.
- [8] N. Biskup et al., *Physical Review Letters* **112** (2014) 087202.
- [9] P. Schattschneider et al., *Nature* **441** (2006) 486.
- [10] J. Salafranca et al., *Nano Letters* **12** (2012) 2499.

Selected publications in the last two years

1. Choi, W. S., Chisholm, M. F., Singh, D. J., Choi, T., Jellison, G. E. & Lee, H. N. Wide bandgap tunability in complex transition metal oxides by site-specific substitution, *Nature Communications* **3** 689 (2012).
2. Salafranca, J., Gazquez, J., Perez, N., Labarta, A., Pantelides, S. T., Pennycook, S. J., Batlle, X. & Varela, M. Surfactant organic molecules restore magnetism in metal-oxide nanoparticle surfaces. *Nanoletters* **12**, 2499-2503 (2012).
3. Cantoni, C., Gazquez, J., Miletto Granozio, F., Oxley, M. P., Varela, M., Lupini, A. R., Pennycook, S. J., Aruta, C., di Uccio, U. S., Perna, P. & Maccariello, D. Electron transfer and ionic displacements at the origin of the 2D electron gas at the LAO/STO interface: Direct measurements with atomic-column spatial resolution. *Advanced Materials* **24**, 3952-3957 (2012).
4. Jeon, H., Seok, W. S., Biegalski, M. D., Folkman, C. M., Tung, I. C., Fong, D. D., Freeland, J. W., Shin, D., Ohta, H., Chisholm, M. F. & Lee, H. N. Reversible redox reactions in an epitaxially stabilized SrCoO_x oxygen sponge, *Nature Materials* **12** 1056-1062 (2013).
5. Jeon, H., Bi, Z., Choi, W. S., Chisholm, M. F., Bridges, C. A., Paranthaman, M. P. & Lee, H. N. Orienting oxygen vacancies for fast catalytic reaction, *Advanced Materials* **25** 6459-6463 (2013).
6. Bruno, F. Y., Schmidt, R., Varela, M., Garcia-Barriocanal, J., Rivera-Calzada, A., Cuellar, F. A., Leon, C., Thakur, P., Cezar, J. C., Brooks, N. B., Garcia-Hernandez, M., Dagotto, E. Pennycook, S. J. & Santamaria, J. Electron doping by charge transfer at LaFeO₃/Sm₂CuO₄ Epitaxial interfaces. *Advanced Materials* **25**, 1468-1473 (2013).
7. Gazquez, J., Bose, S., Sharma, M., Torija, M. A., Pennycook, S. J., Leighton, C. & Varela, M. Lattice mismatch accommodation via oxygen vacancy ordering in epitaxial La_{0.5}Sr_{0.5}CoO_{3-x} thin films, *Applied Physics Letters Materials* **1**, 012105 (2013).
8. Biskup, N., Salafranca, J., Mehta, V., Oxley, M. P., Suzuki, Y., Pennycook, S. J., Pantelides, S. T. & Varela, M., Insulating ferromagnetic LaCoO_{3.8} films: a phase induced by ordering of oxygen vacancies, *Physical Review Letters* **112**, 087202 (2014).
9. Radaelli, G., Petti, D., Plekhanov, E., Fina, I., Torelli, P., Salles, B., Cantoni, M., Rinaldi, C., Gutierrez, D., Panaccione, G., Varela, M., Picozzi, S. & Bertacco, R. Electric control of magnetism at the Fe/BaTiO₃ interface. *Nature Communications*. DOI: 10.1038/ncomms4404 (2014).
10. Salafranca, J., Rincon, J., Tornos, J., Leon, C., Santamaria, J., Dagotto, E., Pennycook, S. J. & Varela, M. Competition between covalent bonding and charge transfer at complex-oxide interfaces. *Physical Review Letters* **112**, 196802 (2014).
11. Cuellar, F. A., Liu, Y. H., Salafranca, J., Nemes, N., Iborra, E., Sanchez-Santolino, G., Varela, M., Garcia-Hernandez, M., Freeland, J. W., Zhernenkov, M., Fitzsimmons, M. R., Okamoto, S., Pennycook, S. J., Bibes, M., Barthelemy, A., te Velthuis, S. G. E., Sefrioui, Z., Leon, L. & Santamaria, J. Reversible electric-field control of magnetization at oxide interfaces, *Nature Communications* DOI:10.1038/ncomms5215 (2014).
12. Sanchez-Santolino, G., Cabero, M., Varela, M., Garcia-Barriocanal, J., Leon, C., Pennycook, S. J. & Santamaria, J. Oxygen octahedral distortions in LaMnO₃/SrTiO₃ superlattices. *Microscopy & Microanalysis*, **20**, 825-831, (2014).

Mapping Valence Electron Distribution using Quantitative Electron Diffraction to Understand Orbital Fluctuation and Superconductivity

Lijun Wu, Chao Ma and Yimei Zhu
 Condensed Matter Physics and Materials Science Department
 Brookhaven National Laboratory, Upton, NY 11973

Program Scope

The current focus of this research task under the FWP Number MA-015-MACA is to investigate the correlation between electron, spin, orbitals, and lattice that controls the functionalities of energy materials, such as the iron-based superconductors (FeSCs). It covers three major interconnected research areas to understand 1) doping effect on charge redistribution and superconductivity; 2) disproportionation reaction and valency change during charge/discharge processes in battery electrodes; and 3) phonon scattering mechanisms of thermoelectric materials. Emphasis is on revealing structure-property relationships. Quantitative electron microscopy techniques, including convergent beam electron diffraction (CBED), parallel recording of dark field imaging (PARODI) method¹, large angle CBED² and precession electron diffraction (PED) are developed to accurately retrieve the structure factors to map valence electron distribution as well as to measure static displacement and harmonic and anharmonic thermal atomic vibrations. Collaborations with theory groups at BNL are important ingredients of our research.

Recent Progress

The discovery of superconductivity with transition temperature (T_c) up to 56 K in iron-based pnictides and chalcogenides has provided a grand opportunity to explore high-temperature superconductivity besides cuprates. Like in the cuprates, superconductivity in FeSCs emerges when the parent antiferromagnetic phase is suppressed, typically by introduction of dopant atoms, such as Co-doped BaFe_2As_2 . On the other hand, FeSCs possess several unique features: (i) Their parent compounds are usually already metallic, not a Mott insulator. Introduction of charge carriers by doping is no longer a single primary driving force for superconductivity. (ii) The orbital degree of freedom on the Fe ions is active. Hund's rule coupling, an interorbital interaction, is at work and largely responsible for electronic correlation in FeSCs. Besides, orbital fluctuations induced by Fe-ion oscillation may

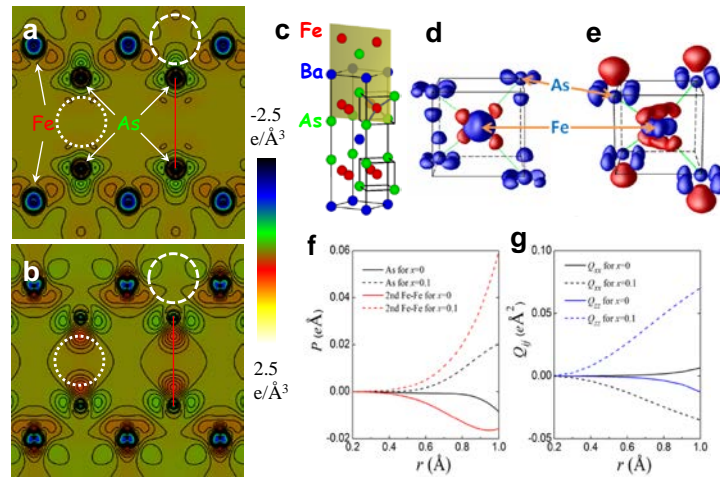


Fig. 1. Valence electron density maps of $\text{Ba}(\text{Fe}_{1-x}\text{Co}_x)_2\text{As}_2$ in (100) FeAs plane and in 3D for (a, d) $x=0$ and (b, e) $x=0.1$. (c) The structure model. (f) The radius dependence of the out-of-plane dipole moment at the As site and at the middle point of the next-nearest Fe-Fe bond. (g) The radius dependence of the quadrupole moments centered at the Fe anion [see ref.3 for details].

mediate electron pairing. Thus, the charge, spin, orbital, and lattice degree of freedom in the Fe planes are all active and understanding their interplay is the key to the resolution of FeSCs superconductivity. (iii) The anions' electronic polarizability in FeSCs is large, one order of magnitude larger than that of oxygen anions. Also unlike the oxygen anions sitting at the middle of the Cu-Cu bonds in the cuprates, the anions in FeSCs are positioned in a low-symmetry setup facilitates the anion polarization. The electronic oscillation of the anions has been shown to be a critical relevant degree of freedom in a one-orbital toy model for FeSCs. Whether this holds in real materials and how it interacts with the other active degree of freedom in the Fe planes are urgently needed to be elucidated. We address these important questions by probing the Co concentration dependence of the valence electron density distribution in $\text{Ba}(\text{Fe}_{1-x}\text{Co}_x)_2\text{As}_2$, a prototypical FeSC. Alteration in the electronic polarization of As^{3-} with Co substitution for Fe is expected to be subtle as the averaged total charge of Fe and Co cations remains 2^+ for any x . To detect such subtle change, we applied quantitative electron diffraction method to accurately measure low-order structure factors which are sensitive to the valence electron redistribution¹. With the combination of measured low-order structure factors and DFT calculated high-order structure factors, we retrieved the charge density for undoped ($x=0$, $T_c=0$) and optimally doped $\text{Ba}(\text{Fe}_{1-x}\text{Co}_x)_2\text{As}_2$ ($x=0.1$, $T_c=22.5\text{K}$) through multipole refinement. The resulting three-dimensional (3D) and two-dimensional (2D) valence electron density map (difference between experimentally measured total electron density and the core-electron density) are shown in Fig.1(a-e). The Co concentration dependence is characterized by a significant increase in the out-of-plane component of the dipole moment around the As anions and in the out-of-plane components of the quadruple moment around the Fe cations (Fig.1(f,g)), echoing the significant increase in T_c and indicating a strong dipole-quadruple interaction between As and Fe atoms. The observations show a strong correlation among T_c , the electronic polarization of the anions, interorbital charge transfer on the Fe cations, and Fe-Fe bond polarization in $\text{Ba}(\text{Fe}_{1-x}\text{Co}_x)_2\text{As}_2$. These observations provide direct support for the proposal that the large polarizability of the anions is critical to iron-based superconductivity by solvating the repulsive Coulomb interaction between electrons in the Fe plane, which could lead to the long-sought 'excitonic' high- T_c mechanism; they also reveal the stronger the electronic oscillation of the anions the stronger orbital fluctuations in the Fe plane, which could lead to orbital-fluctuation-mediated electron pairing³.

Future Plans

An essential step to detect strong orbital fluctuations in FeSCs is to verify the prediction of different orbital ordering in the parent compounds BaFe_2As_2 and LaOFeAs . Orbital polarization is in principle detectable as changes in the charge quadrupole around the Fe atoms. We plan to investigate the parent compound BaFe_2As_2 and map out the temperature dependence of the valence electron density distribution from room temperature to below the antiferromagnetic transition temperature (135 K). Since the orbital ordering may be difficult to detect with very weak discrete signal, the continuous measurement as a function of temperature will enable us to have access to the derivative information that can greatly amplify the signal. We anticipate our results to resolve this long-standing question. We will also systematically investigate the Ni-doping and temperature dependence of the valence electron distribution in $\text{Ba}(\text{Fe}_{1-x}\text{Ni}_x)_2\text{As}_2$ (Fig. 2). In this series of measurements, we will cover the whole regimes of doping levels, from undoped to optimally doped, and contrast the doping dependence of anion polarization, Fe-orbital fluctuation and T_c , to determine whether electronic polarization and

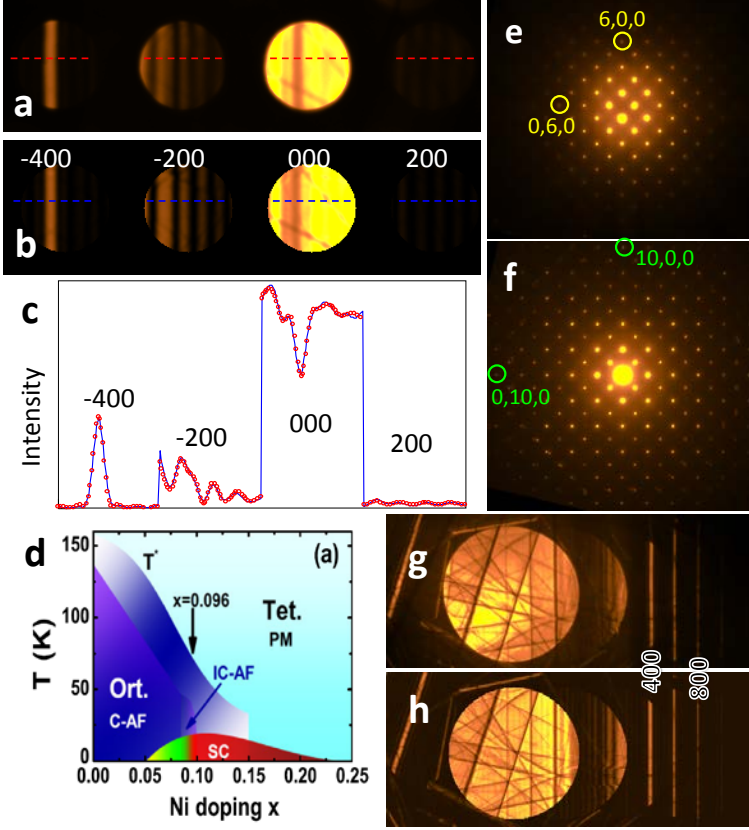


Fig. 2. Measurement of low-order and high-order electron structure factors using CBED and PED for $\text{BaFe}_{1-x}\text{Ni}_x\text{As}_2$ ($x=0.1$). (a) Experimental energy-filtered CBED pattern showing the $h00$ systematical row. (b) Calculated pattern using the dynamical Bloch wave method. (c) Line scans of the intensity profile from the experimental pattern (red dots) and calculated one (blue line) after the structure factors refinement for 200 and 400. (d) Electronic phase diagram of $\text{BaFe}_{2-x}\text{Ni}_x\text{As}_2$ as a function of Ni doping x^4 . (e,f) [001] electron diffraction patterns without precession (e) and with precession (f). With precession, not only more high-order reflections (up to 10,0,0) are visible, but also their intensities are close to the structure factor square, thus can be directly used for electron density refinement. (g,h) Energy-filtered large angle CBED with (g) experiment and (h) calculation for accurate measurement of high-order structure factors.

orbital fluctuation is directly correlated with superconductivity. These observations will provide quantitative information for parameterizing the theoretical model for the strong coupling between the anion charge dipole and Fe quadrupole polarizations as follows:

$$H_{d-p} = \sum_{i\alpha\beta\delta\epsilon} (g_{\alpha\beta\delta\epsilon} d_{i\alpha}^\dagger d_{i\beta} s_{i+\delta}^\dagger p_{i+\delta,\epsilon} + h.c.)$$

where $d_{i\alpha}^\dagger$ ($d_{i\beta}$) is the electron creation (annihilation) operator on the α -th (β -th) $3d$ orbital of the i th Fe atom, $s_{i+\delta}$ ($p_{i+\delta,\epsilon}$) is the electron annihilation operator on the $4s$ (ϵ -th $4p$) orbital of the δ -th neighboring As ion of the i th Fe atom, and $g_{\alpha\beta\delta\epsilon}$ is the coupling constant. Our experimental approach will be the use of the quantitative electron diffraction methods we developed at BNL in the past few years (Fig.2(a-c)). A new development with a recently installed precession camera on our instrument (Fig.2(f)) will enable us to measure a large number of high-order structure factors which was limited to single crystal x-ray diffraction in the past. This is particularly important especially for FeSCs because high quality large single crystal is not available.

References

1. Y. Zhu, J.C. Zheng, L. Wu, A. I. Frenkel, J. Hanson, P. Northrup and W. Ku, *Phys. Rev. Lett.* **99**, 037602 (2007).
2. K. Valsø, J. Taftø, L. Wu and Y. Zhu, *Phys. Rev. B* **84**, 220301(R) (2011).
3. C. Ma, L. Wu, W. Yin, H. Yang, H. Shi, Z. Wang, J. Li, C. C. Homes, and Y. Zhu, *Phys. Rev. Lett.* **112**, 077001 (2014).
4. H. Luo, M. Wang, C. Zhang, X. Lu, L. Regnault, R. Zhang, S. Li, J. Hu and P. Dai, *Phys. Rev. Lett.* **111**, 107006 (2007).

Publications

1. C. Ma, L. Wu, W. Yin, H. Yang, H. Shi, Z. Wang, J. Li, C. C. Homes and Y. Zhu, *Phys. Rev. Lett.* **112**, 077001 (2014).
2. D. A. Sokolov, M. C. Aronson, L. Wu, Y. Zhu, C. Nelson, J. F. Mansfield, K. Sun, R. Erwin, J. W. Lynn, M. Lumsden, and S. E. Nagler, *Phys. Rev. B* **90**, 035139 (2014).
3. S. Das, A. Rastogi, L. Wu, J.C. Zheng, Z. Hossain, Y. Zhu and R. C. Budhani, *Phys. Rev. B* **90**, 081107(R) (2014).
4. M. Li, Z. Dai, W. Cui, Z. Wang, F. Katmis, J. Wang, P. Le, L. Wu and Y. Zhu, *Phys. Rev. B* **89**, 235432 (2014).
5. V. F. Solovyov, T. Ozaki, A. Atrei, L. Wu, A. Al-Mahboob, J. T. Sadowski, X. Tong, D. Nykypanchuk & Q. Li, *Scientific Reports* | 4: 4627 | doi:10.1038/srep04627, (2014).
6. J. Liu, D. Chang, P. Whitfield, Y. Janssen, X. Yu, Y. Zhou, J. Bai, J. Ko, K.W. Nam, L. Wu, Y. Zhu, M. Feygenson, G. Amatucci, A. Van der Ven, X.Q. Yang and P. Khalifah, *Chem. Mater.* **26**, 3295–3305 (2014).
7. P. K. Rout, H. Pandey, L. Wu, Anupam, P. C. Joshi, Z. Hossain, Y. Zhu and R. C. Budhani, *Phys. Rev. B* **89**, 020401 (2014).
8. S.H. Bo, K.W. Nam, O.J. Borkiewicz, Y.Y. Hu, X.Q. Yang, P.J. Chupas, K.W. Chapman, L. Wu, L. Zhang, F. Wang, C.P. Grey and P.G. Khalifah, *Inorg. Chem.* **53**, 6585–6595 (2014).
9. H. Zhou, H.Q. Wang, Y. Li, K. Li, J. Kang, J.C. Zheng, Z. Jiang, Y. Huang, L. Wu, L. Zhang, K. Kisslinger and Y. Zhu, *ACS Appl. Mater. Interfaces*, doi: 10.1021/am503256p, (2014).
10. K.A. Kuttiyiel, K. Sasaki¹, D. Su, L. Wu, Y. Zhu, R.R. Adzic, *Nature Communications*, accepted (2014).
11. M.G. Han, M.S.J. Marshall, L. Wu, M.A. Schofield, T. Aoki, R. Twesten, J. Hoffman, F.J. Walker, C.H. Ahn and Y. Zhu, *Nature Communications*, 5:4693 (2014).
12. L. Wu, Q. Meng, Ch. Jooss, J.C. Zheng, H. Inada, D. Su, Q. Li, and Y. Zhu, *Adv. Funct. Mater.* **23**, 5728-5736 (2013).
13. M. B. Vukmirovic, Y. Zhang, J. X. Wang, D. Buceta, L. Wu and R. R. Adzic, *J. Serb. Chem. Soc.* **78** (12) 1983–1992 (2013).
14. Q. Meng, L. Wu and Y. Zhu, *Phys. Rev. B* **87**, 064102 (2013).
15. F. Wang, L. Wu, B. Key, X.Q. Yang, C. P. Grey, Y. Zhu and Jason Graetz, *Adv. Energy Mater.* **3**, 1324-1331 (2013).
16. F. Wang, L. Wu, C. Ma, D. Su, Y. Zhu and J. Graetz, *Nanotechnology* **24**, 424006 (2013).
17. Y.C. Hsieh, Y. Zhang, D. Su, V. Volkov, R. Si, L. Wu, Y. Zhu, W. An, P. Liu, P. He, S. Ye, R. R. Adzic & J.X. Wang, *Nature Communications* | 4:2466 | doi: 10.1038/ncomms3466, (2013).
18. K.W. Nam, S.M. Bak, E. Hu, X. Yu, Y. Zhou, X. Wang, L. Wu, Y. Zhu, K.Y. Chung and X.Q. Yang, *Adv. Funct. Mater.* **23**, 1047-1063 (2013).
19. M.G. Han, Y. Zhu, L. Wu, T. Aoki, V. Volkov, X. Wang, S.C. Chae, Y.S. Oh and S.W. Cheong, *Adv. Mater.* **25**, 2415–2421 (2013).
20. E. Taylor, S. Chen, J. Tao, L. Wu, Y. Zhu and J. Chen, *ChemSusChem*, 6, 1863 – 1867, (2013).
21. L. Wu, R. F. Egerton and Y. Zhu, *Ultramicroscopy* **123**, 66-73 (2012).
22. C. Ma, Y. Qin, H. Yang, H. Tian, J. Li, K. Sardar, R. I. Walton, D. Su, L. Wu, and Y. Zhu, *J. Appl. Phys.* **112**, 094105 (2012).
23. F. Wang, H.C. Yu, M.H. Chen, L. Wu, N. Pereira, K. Thornton, A. Van der Ven, Y. Zhu, G. G. Amatucci and J. Graetz, *Nature Communications* | 3:1201 | doi: 10.1038/ncomms2185 (2012).
24. Y. Zhu, and L. Wu, "Shadow Imaging for Charge Distribution Analysis", Book Chapter in "Electron Crystallography Meets Powder Diffraction", U. Kolb, K. Shankland, L. Meshi, A. Avilov, and W. David Eds., NATO Science for Peace and Security Series – B: Physics and Biophysics, Springer, 381 (2012).

Spin Physics and Nanoscale Probes of Quantum Materials

Shoucheng Zhang¹, Hari C. Manoharan¹, David Goldhaber-Gordon¹, Joseph Orenstein²

¹ *Stanford Institute for Materials and Energy Sciences, SLAC National Accelerator Laboratory & Department of Physics, Stanford University;* ² *Lawrence Berkeley National Laboratory & Department of Physics, University of California, Berkeley*

Program Scope

The main goals of this FWP are to discover new states of quantum matter and novel physical effects associated with the electron spin, to observe and to manipulate quantum spin degrees-of-freedom at the microscopic scale, and to design and predict materials with tailored functionality. The spin physics program investigates novel phenomena arising from spin coupling in solids. Recently, it was realized that spin-orbit coupling can lead to a fundamentally new state of matter, the topological insulator. These materials have an energy gap in the bulk, and a conducting topological state on the surface. The spin program develops theoretical concepts and experimental tools to investigate these novel effects.

Recent Progress

A new platform for topological superconductivity. Manoharan, Orenstein, and Zhang actively worked together on the half-metallic surface state of NaCoO₂ as a platform for topological superconductivity and Majorana fermions through the mechanism of *s*-wave superconductivity proximity effect. Manoharan performed STM measurements on the surface states of NaCoO₂, and distinguished the *p*-type doping surface region. The observed local density of states (LDOS) by STM experiments quantitatively agree with Zhang group's *ab initio* calculations, indicating the single Fermi surface on NaCoO₂. The single surface state was confirmed by ARPES experiments done by Yulin Chen. The magnetization of the surface states was confirmed by measurements of the magneto-optical Kerr effect by Orenstein group revealing a remnant magnetization of the state with a critical temperature $T \sim 15$ K, in agreement with *T*-dependent scanning tunneling spectroscopy performed by Manoharan group. Figure 1 shows a summary of these results.

Quantum anomalous Hall effect theory. Zhang group has theoretically predicted the quantum anomalous Hall (QAH) effect in magnetic topological insulators. Recently, this theoretical prediction has been confirmed experimentally in Cr doped topological insulator (Sb,Bi)₂Te₃. Zhang group published five papers on QAH effect. In the first paper, we present a general theory for QAH effect with higher Chern numbers, and show by first-principles calculations that thin film magnetic TI of Cr-doped Bi₂(Se,Te)₃ is a candidate for the *c*=2 QAH insulator. In the second paper, we predict by first-principles calculations that thin films of a Cr-doped (Bi,Sb)₂Te₃ magnetic topological insulator have gapless nonchiral edge states coexisting with the chiral edge state, which would explain dissipative transport in the quantum anomalous Hall (QAH) state experimentally observed in this system. In the third paper, we propose that in the ferromagnetic EuO/CdO quantum well, the QAH effect can be realized with high Curie temperature and larger band gap. In the fourth paper, we study the critical properties of the quantum anomalous Hall (QAH) plateau transition in magnetic topological insulators. We

predict that an intermediate plateau with zero Hall conductance could occur at the coercive field. σ_{xx} would have double peaks at the coercivity while ρ_{xx} only has single peak. In the fifth paper, we propose the QAH effect could be realized in heavily doped junction quantum wells due to inverted band structure induced by internal electric field, such as InSb and HgTe.

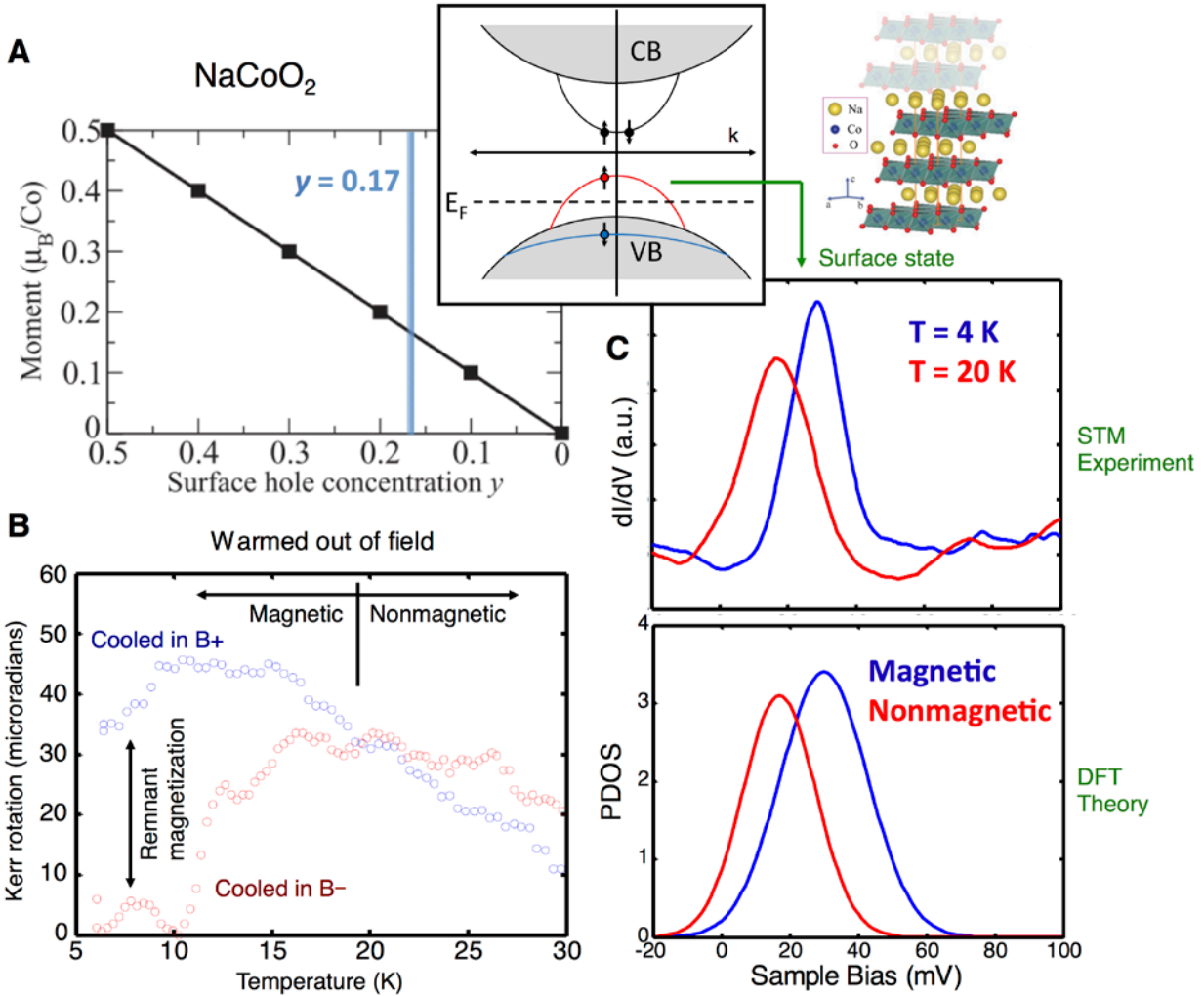


Figure 1 | Emergence of a half-metallic surface state on the bulk insulator NaCoO₂. (A) Predicted half-metallic surface state exhibiting spin polarization and magnetic moment on the surface of the bulk insulator NaCoO₂. Top inset: Band structure and spin structure. Right inset: atomic configuration of NaCoO₂ after cleaving, which exposes a sodium-terminated surface. Na vacancies lead to hole doping quantified by hole concentration y . (B) Surface Kerr rotation experiments showing the emergence of a remnant magnetization when cooled in a perpendicular magnetic field (oriented alternately up or down), and warmed in zero field. The sample undergoes a magnetic transition at ~ 18 K in this sample, above which it remains nonmagnetic. (C) The singular surface state is a flatband and manifests itself in STM/STS spectroscopy as a sharp peak in LDOS. This can be seen in experimental dI/dV and in the theory calculated PDOS. In addition, temperature-dependent STM reveals the magnetic-nonmagnetic transition at the same temperature observed by surface Kerr rotation, and in agreement with the theoretical energy bands.

Quantum anomalous Hall effect experiments. Orenstein, Goldhaber-Gordon, Manoharan, and Zhang actively worked together on the ferromagnetism of Cr doped topological insulator (Sb,Bi)₂Te₃. We performed measurements of magneto-optic Kerr effect in this material, which provides an alternative and accurate quantification of magnetization. Kerr rotation was measured

as a function of applied magnetic field and of temperature, as well as gate voltage. We made detailed investigations of Kerr response, first using a HeNe laser at 1.9 eV and more recently using Kerr spectroscopy. Using a recently acquired InGaAs detector we have measured the real and imaginary parts of κ as a function of probing energy from about 0.7 - 2.5 eV. We have also achieved nearly-quantized anomalous Hall effect in transport (to within 0.5%), as we prepare to build on last year's discovery of quantized anomalous Hall effect in Tsinghua and determine what are the sources of parallel conduction (and thus deviation from perfect quantization). STM experiments are being set up to explore new resonance observations spectroscopically.

Future Plans

Manoharan and Zhang plan to investigate the vortex state of the proximity coupled system of superconductor with NaCoO₂, and measure the tunneling spectrum of the core states, to observe possible signatures of the Majorana bound state at zero energy. Together with Manoharan and Harold Hwang of MSD/SLAC, Orenstein will perform optical measurements on systems with strong spin-orbit coupling, such as BiTeI and the interface of superconductors grown on small gap semiconductors. Goldhaber-Gordon will perform transport measurements on these systems, particularly the semiconducting ones.

Orenstein and Zhang plan to investigate the magnetic order in Cr-doped topological insulators, and study the mechanism for ferromagnetism in the insulating regime. Together with Manoharan and Goldhaber-Gordon, Orenstein will perform systematic magneto-optic Kerr measurements on this system. Zhang plans to perform detailed theoretical calculations on the ferromagnetic order and Kerr rotation angle at different chemical potential and compare with the experimental data.

Manoharan and Zhang plan to investigate the proximity coupling between superconductors and the quantum anomalous Hall state, and confirm the coupling by measuring the tunneling spectrum. Moreover, Manoharan and Zhang plan to investigate the vortex state of this proximity coupled superconductor, and measure the tunneling spectrum of the core states, to observe possible signatures of the Majorana bound state at zero energy. Goldhaber-Gordon will perform transport measurements on these systems, in order to confirm the chiral topological superconductivity in this system.

Publications

1. J. D. Koralek, L. Yang, D. R. Tibbetts, J. Orenstein, "Doppler velocimetry of spin and charge currents in the 2D Fermi gas," XVIIIth International Conference on Ultrafast Phenomena 8-12 July 2012, *EPJ Web of Conferences* **41**, 3017 (2013).
2. H. Zhang, S. C. Zhang, "Topological insulators from the Perspective of first-principles calculations," *Phys. Status Solidi RRL* **7**, 72 (2013).
3. Jing Wang, Biao Lian, Haijun Zhang, Yong Xu and Shou-Cheng Zhang, "Quantum Anomalous Hall Effect with Higher Plateaus," *Physical Review Letters* **111**, 136801 (2013).
4. Jing Wang, Biao Lian, Haijun Zhang, and Shou-Cheng Zhang, "Anomalous Edge Transport in the Quantum Anomalous Hall State," *Physical Review Letters* **111**, 086803 (2013).

5. Yong Xu, Binghai Yan, Haijun Zhang, Jing Wang, Gang Xu, Peize Tang, Wenhui Duan, Shou-Cheng Zhang, "Large-gap Quantum Spin Hall Insulators in Tin Films," *Physical Review Letters* **111**, 136804 (2013).
6. Haijun Zhang, Chao-Xing Liu, and Shou-Cheng Zhang, "Spin-Orbital Texture in Topological Insulators," *Physical Review Letters* **111**, 066801 (2013).
7. Katja C. Nowack, Eric M. Spanton, Matthias Baenninger, Markus König, John R. Kirtley, Beena Kalisky, C. Ames, Philipp Leubner, Christoph Brüne, Hartmut Buhmann, Laurens W. Molenkamp, David Goldhaber-Gordon and Kathryn A. Moler, "Imaging currents in HgTe quantum wells in the quantum spin Hall regime," *Nature Materials* **12**, 787 (2013).
8. Marco Polini, Francisco Guinea, Maciej Lewenstein, Hari C. Manoharan, and Vittorio Pellegrini, "Artificial honeycomb lattices for electrons, atoms and photons," *Nature Nanotechnology* **8**, 625 (2013).
9. Markus König, Matthias Baenninger, Andrei G. F. Garcia, Nahid Harjee, Beth L. Pruitt, C. Ames, Philipp Leubner, Christoph Brüne, Hartmut Buhmann, Laurens W. Molenkamp, David Goldhaber-Gordon, "Spatially Resolved Study of Backscattering in the Quantum Spin Hall State," *Physical Review X* **3**, 021003 (2013).
10. Jing Wang, Biao Lian, and Shou-Cheng Zhang, "Universal scaling of the quantum anomalous Hall plateau transition," *Physical Review B* **89**, 085106 (2014).
11. Haijun Zhang, Jing Wang, Gang Xu, Yong Xu, and Shou-Cheng Zhang, "Topological States in Ferromagnetic EuO/CdO Superlattices and Quantum Wells," *Physical Review Letters* **112**, 096804 (2014).
12. Jason C. Randel, Francis C. Niestemski, Andrés R. Botello-Mendez, Warren Mar, Georges Ndashimiye, Sorin Melinte, Jeremy E. P. Dahl, Robert M. K. Carlson, Ekaterina D. Butova, Andrey A. Fokin, Peter R. Schreiner, Jean-Christophe Charlier, and Hari C. Manoharan, "Unconventional Molecule-Resolved Current Rectification in Diamondoid-Fullerene Hybrids," *Nature Communications*, in press (2014).
13. Haijun Zhang, Yong Xu, Jing Wang, and Shou-Cheng Zhang, "Quantum Spin Hall and Quantum Anomalous Hall States Realized in Junction Quantum Wells," arXiv:1402.5167 (accepted by *Physical Review Letters*).
14. F. C. Niestemski, S. Johnston, A. W. Contryman, C. D. Camp, T. P. Devereaux, H. C. Manoharan, "Local Spectral Inversion and Bosonic Fine Structure Extraction via Superconducting Scanning Tunneling Spectroscopy," arXiv:1211.2244.
15. Jing Wang, Biao Lian, and Shou-Cheng Zhang, "Two-Dimensional Time-Reversal-Invariant Topological Superconductivity in Tin Films," submitted to *Physical Review Letters* (arXiv: 1402.4433, 2014/02/18).
16. P. Giraldo-Gallo, Y. Zhang, C. Parra, H. C. Manoharan, M. R. Beasley, T. H. Geballe, M. J. Kramer, and I. R. Fisher, "Stripe-like nanoscale structural phase separation and optimal inhomogeneity in superconducting $\text{BaPb}_{1-x}\text{Bi}_x\text{O}_3$," submitted to *Nature Communications* (2014).

Real Time TEM Imaging of Materials Transformations in Liquid and Gas Environments

Haimei Zheng Lawrence Berkeley National Laboratory

Program Scope

The objective of this project is to study the physical and chemical processes of materials with high spatial resolution using *in situ* liquid or gas environmental transmission electron microscopy (TEM). Understanding how materials grow and function at the nanometer or atomic scale in their working environments is essential to the development of efficient and inexpensive energy conversion and storage devices. In this project, we develop and apply the environmental cell TEM to study growth mechanisms of nanocrystals, mass transport in electrochemical processes and structural dynamics of nanocatalysts, which are important for energy applications.

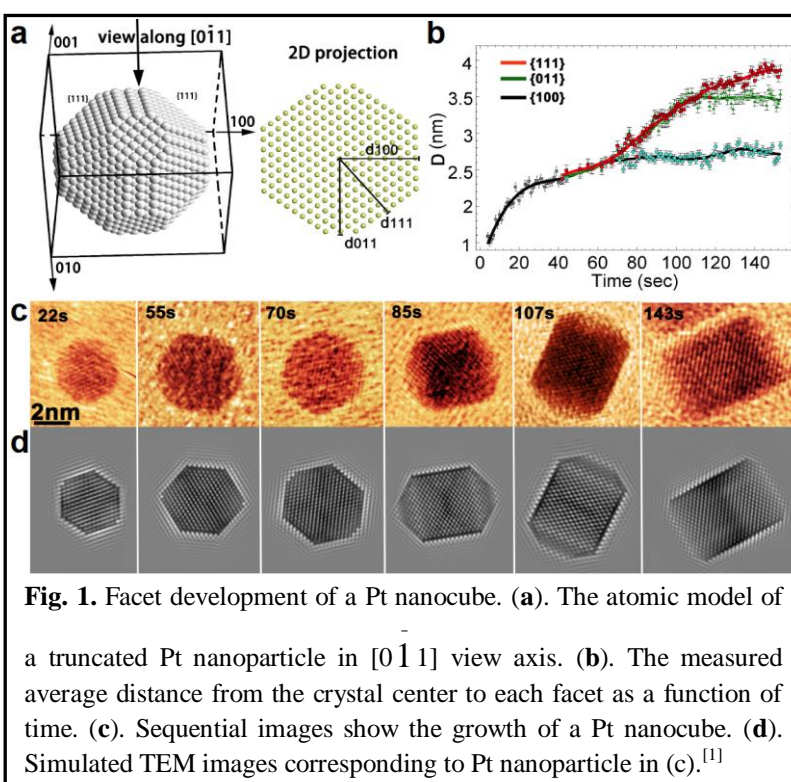
Recent Progress

In situ study of nanocrystal growth in solution

As one of the cutting edge developments in TEM, liquid cell TEM allowing for imaging through liquids with nanometer or atomic resolution provides many opportunities to address key questions related to the growth mechanisms of colloidal nanoparticles and hierarchical nanostructures. A liquid cell made from nanofabrication of silicon can maintain a thin liquid layer sandwiched between two silicon nitride membranes, with which single nanoparticle growth trajectories in the liquid can be examined by TEM.

In the past year, we have been continuing to explore the shape controlling

mechanisms of nanoparticles using liquid cell TEM. By using the advanced single electron direction Gatan K2 IS camera, we have been able to capture the facet development of Pt nanocubes with high spatial and temporal resolution (Fig. 1). The nucleation and attachment of Pt atoms on the individual facets of Pt nanocubes have been observed. We found that the shape



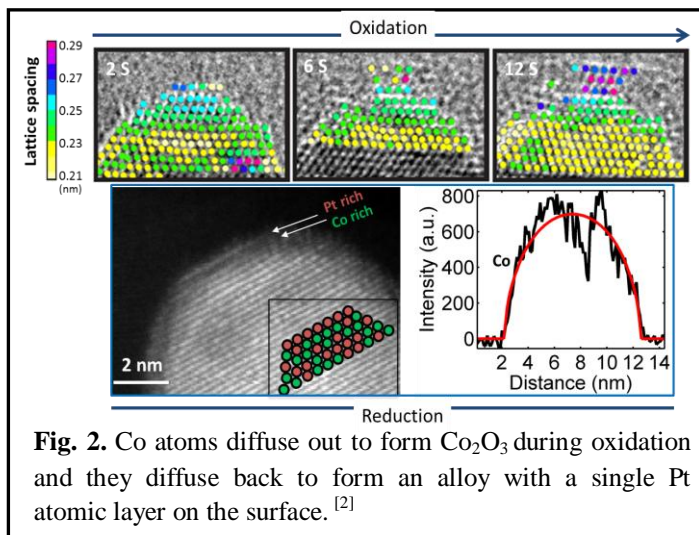
controlling mechanisms of nanocrystals drastically differ from the Wulff construction for bulk crystals with the stochastic characteristics dominant in the small length scale. For instance, the growth rates of all low index facets are similar until the {100} facets stop growth. The continuous growth of the rest facets leads to a nanocube. Our collaborators use ab initio density functional theory calculation to show that the oleylamine surfactant mobility on different facets is different which accounts for the nanocube shape evolution (*Science* 2014). Our proposed ligand mobility controlled selective facet arrested shape evolution may apply to many other systems. In addition to the above facet development of nanoparticles, we have also studied hollow nanoparticle formation by Kirkendall effects. Details of the hollowing process were reported in publication Nano Lett. 2014.

In situ probing gas reactions of nanocatalysts

Uncovering the chemistry and structure of materials under reaction conditions is of fundamental importance in establishing structure-property relationships and to assist designing new catalytic materials. We used an aberration-corrected environmental TEM to study Pt_{0.5}Co_{0.5} bimetallic nanoparticles during their reaction with O₂ and H₂ gases. The evolution of the atomic structure of the nanoparticles was captured in real time as the reaction was proceeding. The experiments were performed on a set of 10-12 nm Pt_{0.5}Co_{0.5} nanoparticles prepared by colloidal synthesis. The nanoparticles were supported on an 8-12 nm-thick silicon nitride membrane for TEM observation. The in situ experiments were carried out in the environmental TEM with post-specimen 3rd order aberration correction operated at 300 keV, with the $\pi/4$ phase plate tuned to >20 mrad prior to observation. A gas pressure range of 0.1-1 mbar was used during data acquisition where the temperature was at the 250-400°C.

During oxidation at 250 °C in 0.1 mbar O₂ gas environment, Co segregates from the Pt-Co alloy nanoparticle and forms oxide on the surface, which is confirmed to be CoO via lattice spacing measurement. The strain field and lattice relaxations were quantified with the well-established geometric phase analysis method (GPA) to map out the (111) interplane distance as a function of time and position.

In summary, using a differentially pumped gas cell TEM we have observed the atomic scale details of the segregation of Co in Pt-Co bimetallic nanoparticles in oxidizing environments and the re-absorption of Co in reducing environments. The ability to observe atomic scale details of the evolution of the structure of nanoparticles in their reactive environments opens the way to



a deeper understanding of the heterogeneous catalysis. It also allows for the study of a wider variety of nanoparticle systems where reaction pathways remain elusive.

In situ TEM study of electrochemical processes

Utilizing our newly designed electrochemical liquid TEM cells, we recently have been able to real time image morphology and structure change of electrode-electrolyte interfaces under an applied voltage program (Fig. 3). Our in situ study will greatly fulfill our understanding of detailed reaction process relevant to battery research. This systematic study of electrochemical reaction under TEM will also benefit the liquid environmental TEM community to better understand and control the electron beam effects during their experiments.

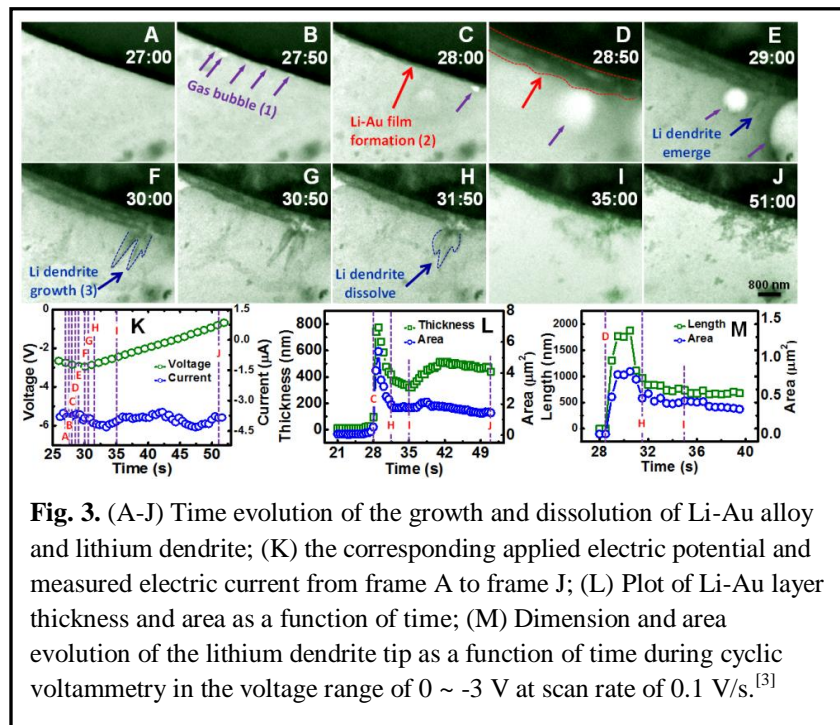


Fig. 3. (A-J) Time evolution of the growth and dissolution of Li-Au alloy and lithium dendrite; (K) the corresponding applied electric potential and measured electric current from frame A to frame J; (L) Plot of Li-Au layer thickness and area as a function of time; (M) Dimension and area evolution of the lithium dendrite tip as a function of time during cyclic voltammetry in the voltage range of 0 ~ -3 V at scan rate of 0.1 V/s.^[3]

In summary, we have made significant progress in using liquid cell TEM to study nanomaterials growth mechanisms and electrochemical processes and developing gas environmental cell TEM to probe heterogeneous nanocatalysts *in situ*. The materials of study are highly important for energy applications, such as fuel cells, batteries, etc. Within the scope of the proposed research, we have been also developing broad collaborations to apply liquid cell TEM or other TEM techniques to other areas of research. The success has been demonstrated in a number of recent publications (ref. 1-10). With the continuous support from DOE Office of Science Early Career Research Program, I expect we will be able to advance *in situ* liquid and gas environmental TEM for energy applications and contribute to the development of cutting edge sciences.

References

1. H. G. Liao, D. Zherebetsky, H. Xin, C. Czarnik, P. Ercius, H. Elmlund, M. Pan, L.W. Wang, H. Zheng, *Science* 345, 916 (2014).
2. H. L. Xin, S. Alayoglu, R. Tao, A. Genc, C. Wang, L. Kovarik, E. Stach, L -W. Wang, M. Salmeron, G. Somorjai, H. Zheng, *Nano Lett.* 14, 3203 (2014).

3. Z. Zeng, W. Liang, H. G. Liao, H. L. Xin, Y. H. Chu, H. Zheng*, "Visualization of electrode-electrolyte interfaces in LiPF₆/EC/DEC electrolyte for lithium ion batteries via in-situ TEM." *Nano Lett.* 14, 1745 (2014).

Publications

1. Z. Zeng, W. Liang, Y. H. Chu, H. Zheng* "In Situ TEM Study of Li-Au Reaction in an Electrochemical Liquid Cell" *Faraday Discussions* in press (2014).
2. H. G. Liao, D. Zherebetsky, H. Xin, C. Czarnik, P. Ercius, H. Elmlund, M. Pan, L.W. Wang, H. Zheng*, "Facet development during platinum nanocube growth" *Science* 345, 916 (2014).
3. H. L. Xin, S. Alayoglu, R. Tao, A. Genc, C. Wang, L. Kovarik, E. Stach, L -W. Wang, M. Salmeron, G. Somorjai, H. Zheng*, "Revealing the atomic restructuring of Pt-Co nanoparticles" *Nano Lett.* 14, 3203 (2014).
4. Z. Zeng, W. Liang, H. G. Liao, H. L. Xin, Y. H. Chu, H. Zheng*, "Visualization of electrode-electrolyte interfaces in LiPF₆/EC/DEC electrolyte for lithium ion batteries via in-situ TEM." *Nano Lett.* 14, 1745 (2014).
5. K. Niu, H. G. Liao, H. Zheng*, "Visualization of the coalescence of Bi nanoparticles." *Microsc. Microanal.* 20, 416 (2014).
6. M. Sun⁺, H. Liao⁺, K. Niu⁺, H. Zheng*, "Structural and morphological evolution of lead dendrites during electrochemical migration." *Scientific Reports* 3, 3227 (2013).
7. H. G. Liao, K. Niu, H. Zheng*, "Observation of growth of metal nanoparticles." *Chem. Comm.* 49, 11720 (2013).
8. K. Niu, J. Park, H. Zheng*, A. P. Alivisatos, "Revealing bismuth oxide hollow nanoparticle formation by the Kirkendall effect." *Nano Lett.* 13, 5715 (2013).
9. H. L. Xin, K. Niu, D. H. Alsem, H. Zheng*, "In situ TEM study of catalytic nanoparticle reactions in atmospheric pressure gas environment" *Microsc. Microanal.* 19, 1558 (2013).
10. H. Zheng, B. Sadtler, C. Habenicht, B. Freitag, A. P. Alivisatos, C. Kisielowski "Controlling electron beam-induced structure modifications and cation exchange in cadmium sulfide-copper sulfide heterostructured nanorods." *Ultramicroscopy* 134, 207 (2013).

Scanning Transmission Electron Microscopy: Atomic Structure and Properties of Materials

Nanomaterials: Defects in 2D materials

Principal Investigators: Wu Zhou, Matthew F. Chisholm, Andrew R. Lupini, Maria Varela
Materials Science & Technology Division, Oak Ridge National Laboratory, TN 37831

Sub-Program Scope

The objective of this research effort is to reveal the functionality of nano-materials at the atomic scale, with emphasis on defects, interfaces and surfaces. An important part of this effort is to explore, develop and optimize the best low-energy and low-dose techniques required to perform atomic-scale quantitative imaging and spectroscopy analysis in aberration-corrected scanning transmission electron microscopy (STEM) for materials that are electron beam sensitive, including two-dimensional (2D) materials, Li-based cathodes, heterogeneous catalysts. The low-energy and low-dose operation STEM, also known as “gentle” STEM, allows revealing the *true* atomic structure, chemistry, bonding and optical properties of materials with unprecedented spatial resolution and with single atom sensitivity. Theoretical studies, mainly in collaboration with Sokrates Pantelides, are then performed to establish a link between the microscopic structures and their functionalities.

2D materials have relatively simple structure for both electron microscopy and theoretical modeling, and contain rich new physics and novel properties. They serve as an excellent platform to explore the fundamental correlation of defect structure and local properties at the single atom level via *gentle* STEM imaging and spectroscopy.

Recent progress

1. Exploring defect landscape and their dynamics in 2D materials

Transition metal dichalcogenides (TMDC) are a new family of 2D materials, with most members displaying direct bandgaps and exceptional optoelectronic properties as monolayers. An important step towards practical application of these TMDC materials is to realize large-scale growth of monolayers and to understand the intrinsic structural defects present in these CVD-grown monolayers. However, obtaining the true intrinsic structural information from the semiconducting TMDC monolayer with atomic resolution is very challenging, as the material is prone to both knock-on damage at high electron beam energy and ionization damage at low voltage. In collaboration with Pulickel Ajayan and Jun Lou’s groups at Rice University, who were among the first to demonstrate CVD growth of centimeter size MoS₂ monolayers, we used *gentle* STEM imaging to systematically explore intrinsic structural defects, including point defects, defect complexes, dislocation cores, grain boundaries, and edges, in these CVD MoS₂ monolayers. Quantitative image analysis allows us to distinguish single Mo and S atoms, and enables such defect study with single atom sensitivity. We showed that both mono-vacancies of Mo and S as well as anti-site defects and vacancy complexes are naturally present during the CVD growth process (Fig. 1A). These point defects induce deep levels within the bandgap, and may contribute to the

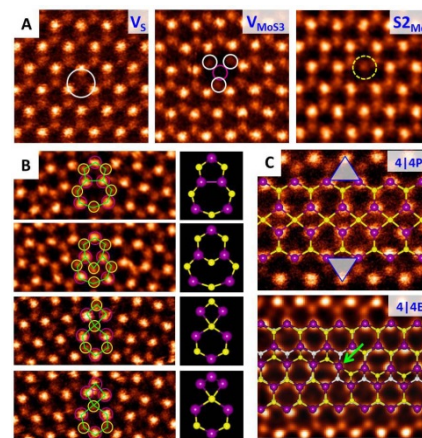


Figure 1. STEM annular dark field images of intrinsic defects in CVD-grown MoS₂ monolayer. (A) Point defects; (B) Dislocation cores; (C) 60° grain boundaries. [1]

omnipresence of n-type conductivity in CVD MoS₂. With quantitative *gentle* STEM, the various theoretically predicted dislocation core structures were experimentally observed for the first time (Fig. 1B). We also identified two new types of 60° grain boundaries, consisting of 4-fold rings (Fig. 1C), which are shown to be metallic by DFT calculations and can serve as conducting channels within the semiconducting matrix.

Chemical doping is a typical way to fine-tune the physical properties of a semiconducting material. Our collaborators at Rice University successfully synthesized MoS₂ atomic layers doped with selenium over a wide range of doping level, and demonstrated band-gap tuning over 0.2 eV. In order to understand the doping behavior and their influence on the optical properties, we developed a quantitative imaging analysis method to automatically map out the distribution of Se dopants in the MoS₂ atomic layers with single atom sensitivity (computer codes developed by Andrew Lupini).

Furthermore, our method allows for statistical analysis of the dopant distribution and clustering behavior, and with known crystallography symmetry, the dopant distribution of each layer in a bilayer structure can be imaged independently (Fig. 2). We demonstrate that each layer in the bilayer contains similar doping levels, randomly distributed, and that the fluctuation of local doping

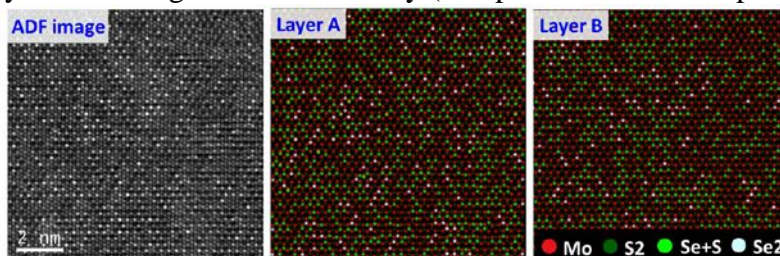


Figure 2. Mapping of Se-dopant distribution in MoS₂ atomic layers via quantitative ADF image analysis. Our method can decompose an ADF image from bilayer Se-MoS₂ into the dopant distribution map in the top and bottom layers. [2]

level contributes directly to the variation of local band-gap of the Se-doped MoS₂ monolayers.

Another important method for introducing new properties in semiconductors is to construct heterostructures. Ajayan's group demonstrated for the first time that both vertical and lateral heterostructures of WS₂ and MoS₂ monolayers can be obtained by controlling the growth temperature. Using *gentle* STEM imaging and spectroscopy, we show that both types of heterostructures are formed via epitaxial growth of WS₂, either on top of MoS₂ monolayer for vertical heterostructures or from fresh MoS₂ edges forming lateral heterojunctions. We further demonstrate that in the vertical bilayer heterostructure, the direct growth method results in preferred stacking and ultra-clean interfaces with strong interlayer coupling, which induces an additional direct bandgap at low energy. In the lateral heterojunction, we show that the lateral epitaxy generates atomically sharp interfaces along the preferred zigzag direction with minimal inter-diffusion (Fig. 3). Such atomically abrupt lateral interfaces induce a strong electric field from the type-II band alignment, contributing to the extraordinary photoluminescence enhancement observed experimentally at the interface.

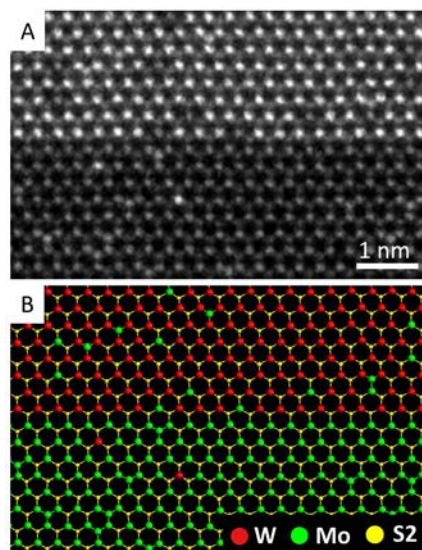


Figure 3. STEM ADF image (A) and the corresponding atomic structure (B) of a lateral interface between WS₂ and MoS₂ monolayers showing lateral epitaxy. [3]

Besides exploring the static atomic arrangement of intrinsic defects, we also use the electron beam to excite various defect dynamics via direct

energy transfer. This enables us to look at dynamic processes that are hard to observe under typical temperature ranges. For example, via dynamic *gentle* STEM imaging, we showed that the semiconducting MoS₂ layers can be locally converted into conductive nanowires using the electron beam, paving the way for direct patterning of conducting channels in semiconducting materials for flexible 2D integrated circuits.

2. Monochromatic EELS for optical properties beyond visible light regime

The introduction of a monochromator can drastically reduce the energy spread of the incident electron beam, and, thus, improve the energy resolution of electron energy loss spectroscopy (EELS). This becomes particularly important for exploring the optical properties of two-dimensional materials using low-loss EELS, where the optical absorption features are typically very weak and could easily be overwhelmed by the tail of the zero-loss peak (ZLP). Furthermore, combined with the imaging power available on an aberration-corrected STEM, simultaneous study and direct correlation of the local atomic structure and optical properties at the nm scale becomes feasible, a power not achievable with optical microscopy and spectroscopy methods.

We use twisted bilayer graphene (TBLG) as a model 2D material system to demonstrate the simultaneous study of the local atomic structure and optical properties with monochromatic STEM-EELS. The experiment was performed at 60 meV energy resolution on a monochromatic Nion UltraSTEM at Arizona State University. Figure 4a compares the ZLP acquired with and without the monochromator. While under our particular experimental setup, the monochromator improves the energy resolution only by a factor of 5, from 300 meV to 60 meV with 1 minute acquisition time, the relative intensity of the ZLP tail below 1 eV drastically decreases by more than two orders of magnitude. This suggests that for 2D materials, where plural scattering is negligible, the Nion monochromator can increase the information transfer capability by a factor of 100 for optical response in the near- and mid-infrared regime. This is further demonstrated in Fig. 4b, where the low-loss EEL spectra for a few TBLG samples acquired with and without the monochromator are presented. The spectra clearly reveal the presence of additional optical absorption peaks (highlighted), which shift consistently as a function of the twisted angle in TBLG and can be well described by tight-binding calculations. Noticeably, without the monochromator, this additional optical feature can only be identified in the visible and ultraviolet regime, while monochromatic EELS provides access to this new feature all the way down to the mid-infrared regime, superior to previous optical studies [4].

Figure 4b, where the low-loss EEL spectra for a few TBLG samples acquired with and without the monochromator are presented. The spectra clearly reveal the presence of additional optical absorption peaks (highlighted), which shift consistently as a function of the twisted angle in TBLG and can be well described by tight-binding calculations. Noticeably, without the monochromator, this additional optical feature can only be identified in the visible and ultraviolet regime, while monochromatic EELS provides access to this new feature all the way down to the mid-infrared regime, superior to previous optical studies [4].

Future Plans

We plan to combine *in-situ* holders with high spatial and energy resolution STEM imaging and spectroscopy to look at structural evolution and changes in local electronic structure and optical excitations under various external stimulations (heat/electric field) or gas/liquid environments.

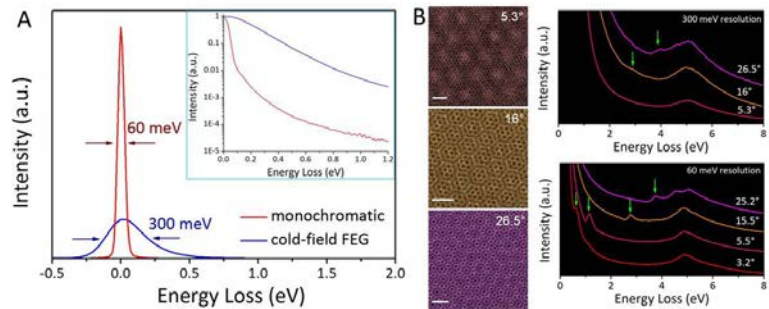


Figure 4. (A) Comparison of the ZLP taken on the Nion UltraSTEM with and without the monochromator. (B) (Left) ADF images of twisted bilayer graphene with different misorientation angles. Scale bars: 1 nm. (Right) Low-loss EEL spectra of the TBLG acquired using the Nion UltraSTEM with and without the monochromator. The misorientation angles are labeled on each spectrum.

References

- [1] Zhou *et al.* *Nano Letters* **13**, 2615-2522 (2013).
- [2] Gong *et al.* *Nano Letters* **14**, 442-449 (2014).
- [3] Gong *et al.* *Nature Materials* in press (2014).
- [4] Havener *et al.* *Nano Letters* **14**, 3353-3357 (2014).

Selected publications in the last two years

1. Salafrañca, J., *et al.*, Surfactant Organic Molecules Restore Magnetism in Metal-Oxide Nanoparticle Surfaces, *Nano Lett.* **12** 2499-2503 (2012).
2. Chisholm, M.F., Duscher, G., Windl, W. Oxidation Resistance of Reactive Atoms in Graphene, *Nano Lett.* **12** 4651-4655 (2012).
3. Zhou, W.*; Zou, X.; Najmaei, S.; Liu, Z.; Shi, Y.; Kong, J.; Lou, J.; Ajayan, P. M.; Yakobson, B. I.; Idrobo, J. C. Intrinsic structural defects in monolayer molybdenum disulfide. *Nano Letters*, **13**, 2615-2522 (2013).
4. Najmaei, S., *et al.*, Vapor phase growth and grain boundary structure of molybdenum disulfide atomic layers. *Nature Materials*, **12**, 754-759 (2013).
5. Wang, H.*; Zhou, W.*; Liu, J.* *et al.* Platinum-modulated cobalt nanocatalysts for low-temperature aqueous-phase Fischer-Tropsch synthesis. *Journal of the American Chemical Society*, **135**, 4149-4158 (2013).
6. Lin, J.; Fang, W.; Zhou, W.*; Lupini, A.R.; Idrobo, J.C.; Kong, J.; Pennycook, S.J.; Pantelides, S.T. AC/AB stacking boundaries in bilayer graphene. *Nano Letters*, **13**, 3262-3268 (2013)
7. Mishra, R.; Zhou, W.; Pennycook, S. J.; Pantelides, S. T.; Idrobo, J. C. Long-range ferromagnetic ordering in manganese-doped two-dimensional dichalcogenides. *Physical Review B* **88**, 144409 (2013).
8. X. Zhang, *et al.*, "Catalytically active single-atom niobium in graphitic layers," *Nature Comm.* **4** 1924 (2013).
9. Estrader, M., *et al.*, Robust antiferromagnetic coupling in hard-soft bi-magnetic core shell nanoparticles, *Nature Communications* **4** 2960 (2013).
10. Gong, Y., *et al.*, Band gap engineering and layer-by-layer mapping of selenium-doped molybdenum disulfide. *Nano Letters* **14**, 442-449 (2014).
11. Gong, Y. *et al.* Direct chemical conversion of graphene to boron- and nitrogen- and carbon-containing atomic layers. *Nature Communications* **5**, 3193 (2014).
12. Lu, X., *et al.*, Large-area synthesis of monolayer and few-layer MoSe₂ films on SiO₂ substrates. *Nano Letters* **14**, 2419-2425 (2014).
13. Mirtchev, P., *et al.*, Fe₂O₃/Cu₂O heterostructured nanocrystals, *J. Of Materials Chemistry A* **2** 8525-8533 (2014).
14. Gong, M., *et al.*, Ultrafast high-capacity NiZn battery with NiAlCo layered double hydroxide. *Energy & Environmental Science* **7**, 2025-2032 (2014).
15. Lee, J.; Yang, Z.; Zhou, W.; Pennycook, S.J.; Pantelides, S.T.; Chisholm, M.F. Stabilization of graphene nanopore. *PNAS* **111**, 7522-7526 (2014).
16. Lopez-Bezanilla, A.; Zhou, W.; Idrobo, J.C. Electronic and quantum transport properties of atomically identified Si point-defects in graphene. *J. Phys. Chem. Lett.* **5**, 1711-1718 (2014).
17. Lin, J.*; Cretu, O.; Zhou, W.* *et al.* Flexible metallic nanowires with self-adaptive contact to semiconducting transition-metal dichalcogenide monolayers. *Nature Nanotechnology* **9**, 436-442 (2014).
18. Zhou, W., Electron microscopy: A phase transition glides into view. *Nature Nanotechnology* **9**, 333-334 (2014).
19. Gong, M., *et al.*, Nanoscale nickel oxide/nickel hetero-structures for active hydrogen evolution electrocatalysis. *Nature Communications* **5**, 4695 (2014).
20. Z. Yang, *et al.*, "Direct Observation of Atomic Dynamics and Silicon Doping at a Topological Defect in Graphene, *Angewandte Chemie International Edition* **53** (34) 8908-8912 (2014).
21. Gong, Y, *et al.*, Vertical and in-plane heterostructures from WS₂/MoS₂ monolayers. *Nature Materials* in press (2014).
22. Shen, X., *et al.*, Interlaced crystals: Perfect Bravais lattices with interlaced chemical order revealed by real-space crystallography. *Nature Communications* in press (2014).
23. Liu, Z. *et al.* Strain and structure heterogeneity in MoS₂ atomic layers grown by chemical vapor deposition. *Nature Communications* in press (2014).

Dynamics of Topological Nano-Magnetism with Broken Symmetry

Shawn D. Pollard, Javier F. Pulecio, Vyacheslav V. Volkov, and Yimei Zhu
Condensed Matter Physics and Materials Science Department
Brookhaven National Laboratory, Upton, NY 11973

Program Scope

The focus of this research task under the FWP Number MA-015-MACA is to explore and elucidate the effects of symmetry breaking on the structure and dynamics of topological spin textures and their excitations. This focus area can be broken into three main research thrusts – (i) the determination of the spin structure of patterned magnetic materials with novel coupling mechanisms, (ii) the dynamic behavior of coupled spin structures under the influence of resonant and off-resonant magnetic fields and spin currents far from equilibrium, and (iii) the interplay between the spin ordering and electronic, orbital, and lattice degrees of freedom. Primary characterization tools used in this research are TEM-based quantitative Lorentz imaging including phase retrieval methods and electron holography, supplemented via other complementary experimental techniques, such as ferromagnetic resonance, atomic force microscopy to determine surface morphology and time-resolved synchrotron x-rays measurements. Under this FWP a variety of in-situ excitation capabilities such as microwave frequency (GHz) capable TEM holders were developed and a UHV compatible film-growth system and a multi-node computer system for micromagnetics calculations have been designed and built. Active collaborations within the department as well as with the researchers at NSLS and CFN at BNL are important ingredients to this research.

Recent Progress

Dynamic control of topological magnetic structures, such as magnetic vortices, skyrmions, and other domain walls, has received a great deal of attention due to their promising applications in low power spintronic applications such as microwave sources, signal processing, and magnetic memory and logic operations^{1,2}. A specific area of interest is the use of spin-transfer torque, the process by which an imbalance in spin populations of conduction electrons leads to a polarization of an electric current. This spin current can be used to excite the motion of magnetic domain walls without the use of magnetic fields, opening up possibilities for more energy efficient control of densely packed magnetic media. This spin-torque process can be broken into two components –adiabatic and non-adiabatic, with the non-adiabatic component being poorly understood with disagreement on orders of magnitude. To study this effect, as well as other high frequency spin processes such as damping phenomena, we have developed a unique capability by which high frequency electronic excitations could be applied to a sample in-situ and tuned to the resonance frequency for the in-plane gyrotropic mode of magnetic vortices³. By exploiting the symmetry of the magnetic vortex in a permalloy (Py) square disc, we were able to obtain measurements of the non-adiabatic spin torque with unprecedented precision, as well as utilize the spatial resolution unique to TEM in order to characterize off-resonance phenomena, allowing us to validate models for vortex core motion, such as predicting a tilt of the orbit off axis as well as an ellipticity that scales linearly with the ratio of the excitation to resonance frequencies. To further understand the dynamics of magnetic vortices we coupled a vortex pair

in a Py(15nm)/Cu(varied)/Py(15nm) trilayer stack geometry via the Ruderman-Kittel-Kasuya-Yosida (RKKY) interaction across the interface [Fig. 1a,b]. Resonant dynamics of these topological spin textures are determined by a combination of material parameters as well as their specific geometry. For two isolated discs of different thicknesses, the resonance frequencies differ. However, for thin Cu spacer layers, we found that RKKY interaction leads to the existence of only one resonance peak, and as the interaction strength increases, the two peaks converges to that of a slightly up-shifted 40nm single layer disc. This could allow for the use of an RKKY interaction to mode-couple large arrays of vortex states, yielding a new type of nanoscale magnetic vortex based antennae or signal processing devices ⁴.

While these measurements captured the dynamics of a vortex in symmetric potentials, measurements of topological spin structures with broken symmetry have been lacking despite the fact that far from equilibrium manipulation of magnetic domains have suggested novel means of controlling said structures, such as allowing for independent control of the polarity and chirality

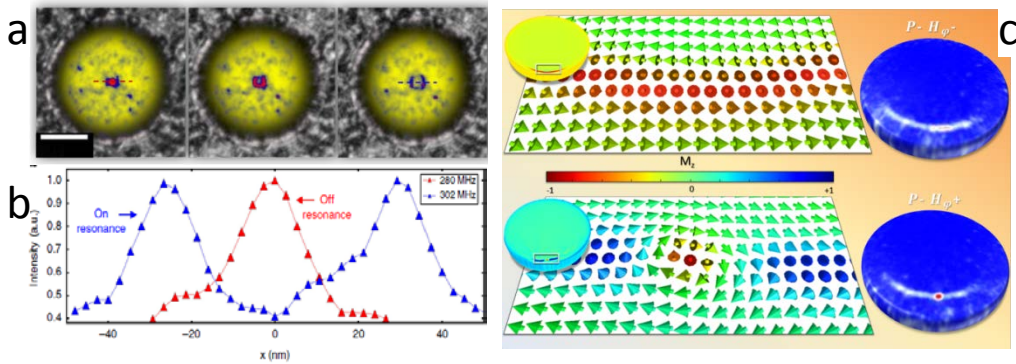


Fig. 1a.) Frequency sweep off, near, and on resonance of a magnetic vortex core showing the single orbital path of two strongly coupled vortices confined to a 1 μm permalloy/Cu/permalloy disc stack on a gold stripline. b.) Linescans indicated in (a), showing off resonance and on resonance behavior. c.) Simulated (left) and experimental (right) images of a magnetic vortex displaced far from equilibrium for a field parallel to the polarity (top) and anti-parallel (bottom). The vortex exhibits clearly different structure depending on the polarity and field direction. degrees of freedom. The lack of information on these asymmetric states is due to the fact that many of these effects are subtle, beyond the resolution of most techniques. With local electron probes, we have overcome some of these issues. For instance, we have used high resolution Lorentz TEM to analyze the breakdown of the magnetic vortex away from its zero-field equilibrium in the presence of a symmetry breaking out-of-plane field [Fig. 1c]. We showed that the breakdown is dependent on the relative orientation between the field and the vortex polarity, which has important implications for spintronic devices that rely on magnetic vortices in the presence of out-of-plane fields or polarizers⁵.

Future Plans

For the research thrust (i) and (ii) we will continue to study the dynamical properties of topological spin textures, and the role that broken symmetry plays in their evolution under a variety of stimuli including magnetic fields and spin-transfer torques, as well as temperature and strain. While previous work has focused on magnetic vortices, the vortex has strong limitations from a device perspective due to the fact that it is highly influenced by defects. In order to better understand the role that defects play in dynamical processes such as pinning and depinning, as well as vortex scattering, the ability to simultaneously image magnetic and physical structure

simultaneously is essential. This research will be carried out by implementing phase retrieval methods based on electron holography, the Transport-of-Intensity approach, as well as our newly developed hole-free phase plate that allows imaging of pure phase objects with an in-focus beam.

Beyond the magnetic vortex, the skyrmion represents a new type of spin texture which is predicted to be defect tolerant. These textures have been observed in single crystal continuous thin films in which a Dzyaloshinsky-Moriya interaction (DMI) is present, but not in patterned granular media. It was recently predicted that by tuning an RKKY interaction in a multilayer stack geometries, an effective DMI could be created, allowing for the design of skyrmions with controlled geometries. In continuous geometries, the resonant dynamics are inaccessible by conventional imaging techniques, but in patterned media, in which the resonant frequency can be tuned, it will be possible to study the dynamics in a controllable fashion. We have begun to fabricate magnetic structures in which the RKKY coupling between magnetic layers in multilayer stacks is tuned such that skyrmion and meron spin states should be created, the resonant dynamics can be studied. The process of designing a system such that the damping of displaced skyrmions (and vortices) may be studied is underway.

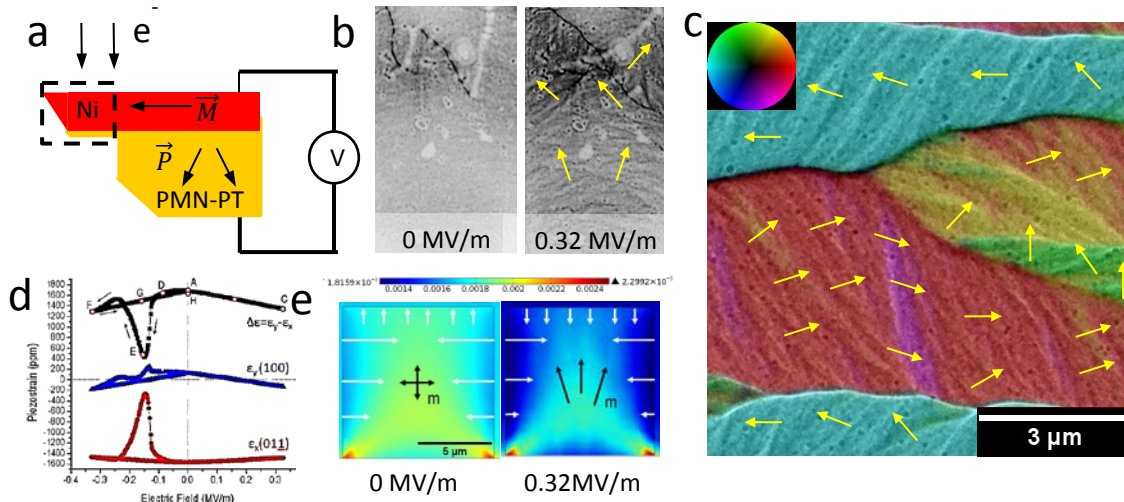


Fig. 2a.) Schematic of the experiment. A nickel film is deposited on a PMN-PT substrate, then milled at the edge to create an electron transparent window (highlighted by dashed black line). b.) The evolution of the magnetic structure of the nickel film with an applied field across the ferroelectric layer. Ripple contrast and visible changes in the domain structure are visible with increasing field. c.) Phase reconstruction showing subtle changes in magnetization associated with magnetization ripple contrast even in single domains. Color indicates the local magnetization direction and magnitude, with the direction at various points indicated by the arrows. d.) Lattice-strain measurements vs. field. Polarization reversal is associated with large jumps in strain near 0.16MV/m. e.) Simulated strain maps for the electron transparent window at 0MV/m and 0.32MV/m.

For thrust (iii), we will study strain coupled patterned-media with relaxor ferroelectric materials, such that an effective anisotropy can be added and controlled via interfacial strain coupling (Fig.2). It is well known that the voltage induced lattice distortions in relaxor ferroelectrics cause spin reorientation in conventional magneto-elastic materials, affording a novel means of manipulating the spin structure in magnetic materials. However, the effects of local coupling between ferroelectric polarization and spin textures has not been directly observed, and little is known about this effect at the nanoscale. We will use phase retrieval methods to image both simultaneously to study how the spin-lattice coupling effects the static and dynamic properties of these spin structures, including modifications to the effective

damping, the resonant dynamics, and local effective anisotropies. This coupling could lead to important advances in spintronics, such as the ability to continuously tune the resonance band of magnetic vortices and skyrmions over a large range via electrical biasing.

References

1. Jung, H. *et al.* Logic operations based on magnetic-vortex-state networks. *ACS nano* **6**, 3712–7 (2012).
2. Parkin, S. S. P., Hayashi, M. & Thomas, L. Magnetic domain-wall racetrack memory. *Science*, **320**, 190–4 (2008).
3. Pollard, S. D., Huang, L., Buchanan, K. S., Arena, D. a & Zhu, Y. Direct dynamic imaging of non-adiabatic spin torque effects. *Nature communications* **3**, 1028 (2012).
4. Pulecio, J. F., Warnicke, P., Pollard, S. D., Arena, D. A. & Zhu, Y. Coherence and modality of driven interlayer-coupled magnetic vortices. *Nature communications* **5**, 3760 (2014).
5. Pulecio, J. F., Pollard, S. D., Warnicke, P., Arena, D. A. & Zhu, Y. Symmetry breaking of magnetic vortices before annihilation. *Applied Physics Letters* (in press).

Publications

1. Pollard, S. D., Huang, L., Buchanan, K. S., Arena, D. a & Zhu, Y. Direct dynamic imaging of non-adiabatic spin torque effects. *Nature communications* **3**, 1028 (2012).
2. Pollard, S. D., Volkov, V. & Zhu, Y. Propagation of magnetic charge monopoles and Dirac flux strings in an artificial spin-ice lattice. *Physical Review B* **85**, 180402R (2012).
3. Hockel, J. L. *et al.* Electrically controlled reversible and hysteretic magnetic domain evolution in nickel film/Pb(Mg_{1/3}Nb_{2/3})O₃]_{0.68}-[PbTiO₃]_{0.32} (011) heterostructure. *Applied Physics Letters* **102**, 242901 (2013).
4. Pollard, S. D. & Zhu, Y. The Aharonov-Bohm effect, magnetic monopoles and reversal in spin-ice lattices. *Microscopy* **62 Suppl 1**, S55–64 (2013).
5. Pollard, S. D., Malac, M., Beleggia, M., Kawasaki, M. & Zhu, Y. Magnetic imaging with a Zernike-type phase plate in a transmission electron microscope. *Applied Physics Letters* **102**, 192401 (2013).
6. Pollard, S. D., and Zhu, Y., "Gauge theory and artificial spin ices,: imaging emergent monopoles with electron microscopy," in "In Memory of Akira Tonomura: Physicist and Electron Microscopist", K. Fujikawa and Y. A. Ono Eds., World Scientific Publishing Co. Pte. Ltd., p. 110-121 (2013)
7. Pulecio, J. F., Bhanja, S., and Sarkar, S., "Parallel energy minimizing computation via dipolar coupled single domain n", In J. E. Morris & K. Iniewski (Eds.), *Nanoelectronic Device Applications Handbook*, CRC Press, p. 940 (2013).
8. Volkov, V.V., Han, M.-G., and Zhu, Y., "Double-resolution electron holography with simple Fourier transform of fringe-shifted holograms", *Ultramicroscopy*, **134**, 175-184 (2013).
9. Pulecio, J. F., Warnicke, P., Pollard, S. D., Arena, D. A. & Zhu, Y. Coherence and modality of driven interlayer-coupled magnetic vortices. *Nature communications* **5**, 3760 (2014).
10. Pulecio, J. F., Pollard, S. D., Warnicke, P., Arena, D. A. & Zhu, Y. Symmetry breaking of magnetic vortices before annihilation. *Applied Physics Letters* (in press).

***UNIVERSITY GRANT
PROJECTS***

Discovery of Dielectric Response and Forces in Sub-Nanoscale Objects

P.E. Batson and M.J. Lagos

Institute for Advanced Materials, Devices and Nanotechnology

Departments of Physics, and Materials Science

Rutgers, the State University of New Jersey

607 Taylor Road, Piscataway, NJ 08854-8019

batson@physics.rutgers.edu

Program Scope

Nanoscale particles that support plasmonic and photonic modes are rapidly becoming crucial to the efficient coupling of light into sub-wavelength sized computational and energy gathering structures.[1] Electron beams are of course well positioned for the measurement of photonic fields and "hot" spots in candidate structures, using EELS in the electron microscope.[2] Recent theoretical spectral work is aimed at understanding basic mechanisms[3–5], and reconstruction of the plasmonic energy dependent potential using tomographic techniques. [6] Finally, time dependent information for investigation of dynamics, and phase relationships of nanoscale optical fields, is being studied at the pico-second level by many groups now following the pioneering work of Zewail. [7, 8]

This project seeks to explore the time resolved dielectric response of bulk and nano-scale structures in a fundamentally different way, using EELS. Conceptually, fourier transform techniques can connect EELS information to a fundamental physical quantity, the time dependent electronic density propagator, or density-density correlation function, $\chi(\vec{r}_1, \vec{r}_2, t_1, t_2)$. [9, 10] Understanding this dynamical quantity will allow us to expand understanding of dielectric behavior to a wider range of specimen excitations, both at higher and lower energies, and to explore how particular excitations evolve in time, couple to other specimen properties, and transfer energy in decay processes. The time scales that should be addressable range from a few atto-seconds, corresponding to the close approach of a kilo-volt electron to a nano- particle or molecule, with excitation of core losses, through femto- second times for plasmonic and photonic excitations and ultimately to pico-second times for phonon, IR and Raman transitions

This effort necessarily involves mastering new equipment which can obtain very accurate and reproducible EELS data to obtain single scattering spectral distributions that can be converted into the complex dielectric constant. Fourier transform techniques can then produce the density-density correlation function. Local behavior will emerge immediately. Non-local information will require some thought, but it seems likely that this will be accessible through tomographic [6] or in very small objects, phase retrieval techniques.[11]

Recent Progress

During the past 18 months, our understanding of the transverse forces has matured. The fundamental goal of the initial funding period was to understand the physical origin of an unexpected reversal in the transverse force felt by a metal nanoparticle during a very close

approach of a keV electron. Simple arguments suggest that this force should always be attractive, but as shown in Fig. 1c, extensive numerical calculation in the spectral domain demonstrated otherwise.[12, 13] Experimental work confirmed this,[14] but no simple physical explanation for the complicated behavior emerged.

We thought the best way to understand this was to calculate the microscopic, non-local forces on the particle, resolved in time and space during the passage of the swift electron. This is an interesting problem having several subtle features that have much in common with the well known Abraham-Minkowski debate over the partition of momentum flow between particles and fields within dielectric objects.[15] In Figs. 1a,b, we show approximate results for the instantaneous forces on the surface of a 1 nm radius Au nano-particle at times -3 and +3 attoseconds, before and after the closest passage of an 80 kV electron at $t=0$. Before passage, in Fig. 1a, a correlation hole builds on the surface, responding to the negative charge of the approaching electron, giving rise to an attractive, largely electrostatic force, as shown in Fig. 1d. This charge density is sluggish, lagging slightly behind the electron as it passes. After passage, in Fig 1b, a negative *force* appears in front of the lagging correlation hole. This force appears to contain both electric and magnetic components, and is responsible for the transition from attractive to repulsive shown in Figs. 1c,d. We believe that this surprising result fits the description of a plasmonic wake,[9] in this case restricted to the very small volume presented by the nanoparticle.

Instrumental work now supported by DOE includes bringing the Nion UltraSTEM, with high energy resolution EELS to routine operation. We have demonstrated a 9.7 meV zero loss peak and have obtained an optical phonon in SiC, with a publication submitted to Nature and under final review of minor modifications requested by referees. On the imaging side, we are very excited to demonstrate 0.9 Angstrom fringes in HAADF imaging at 60 kV, using a low field emission extraction voltage which reduces Boersch effect source broadening.

Future Plans

In the short term, we will carefully compare the atto-second behavior of the forces with the plasmonic, femto-second behavior, and then distill this information to produce a physical picture of the force reversal. This should be accomplished during the next couple months, and will finish our theoretical work in this part of the project. The knowledge we have gained feeds directly into the time dependent EELS derived dielectric behavior. While we have been evaluating the transverse forces previously, future theoretical work will involve longitudinal, energy loss behavior.

With the new instrument, we will be optimizing EELS measurement accuracy to allow us to obtain spatially resolved single scattering spectra which can be subjected to Kramers- Kronig transformation over a wide energy range, to allow time dependent information to be retrieved. This will be challenging, but it appears that all of the required tools are available to do this. Initial experiments will likely use plasmonic structures having Localized Surface Plasmon Resonances, to minimize non-local interactions.

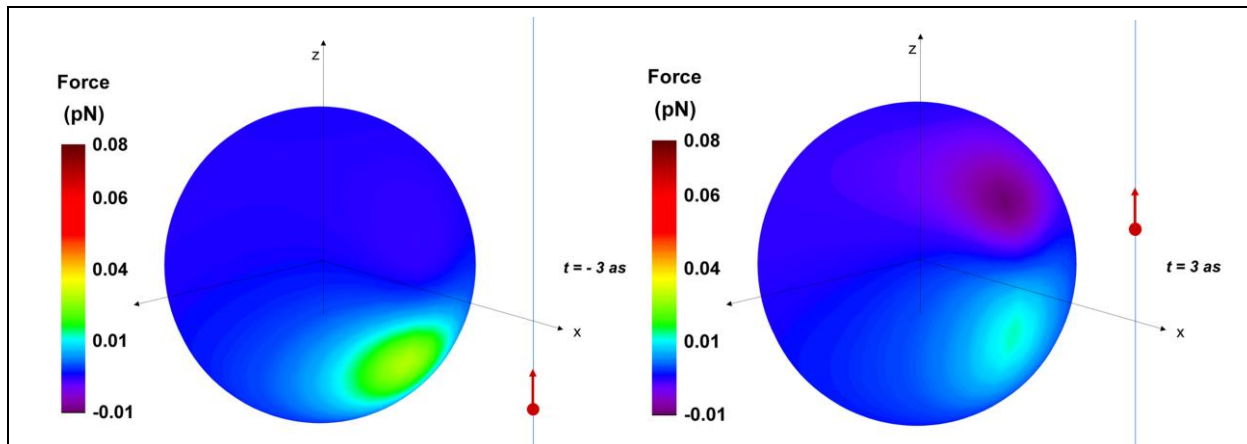


Fig. 1a. X component of the forces at -3 as. Green area is an electrostatic attractive force, caused by a correlation hole.

Fig. 1b. X component of the forces at +3 as. The correlation hole lags behind, and a purple area of negative force develops.

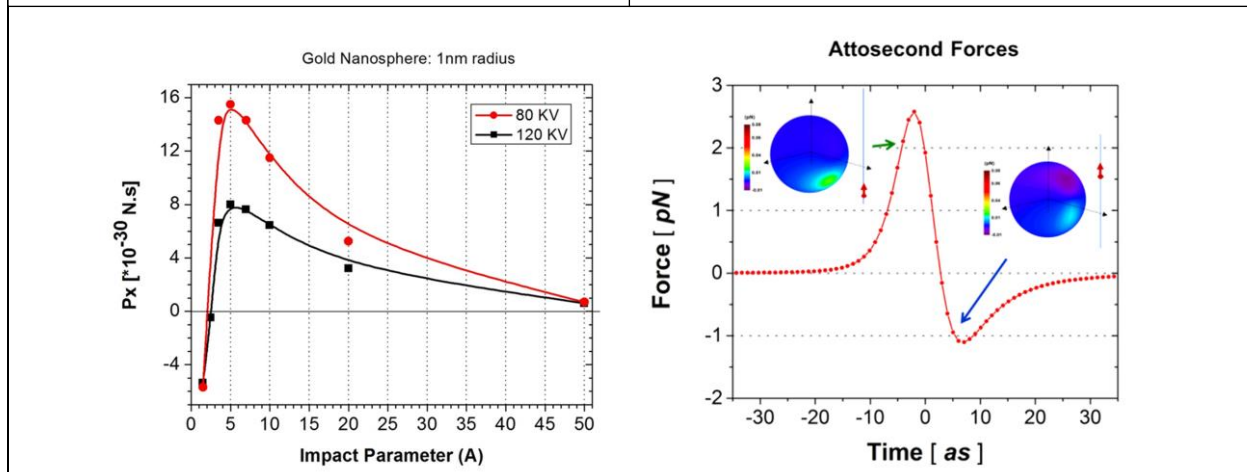


Fig. 1c. Transverse momentum given up to a metal sphere by a passing swift electron. A reversal occurs at small impact parameter.

Fig. 1d. Forces at attosec times are first attractive, then repulsive, as first electric, then magnetic interactions are dominant.

References

- [1] E.J.R. Vesseur, J. Aizpurua, T. Coenen, A. Reyes-Coronado, P.E. Batson and A. Polman, *Plasmonic excitation and manipulation with an electron beam*, MRS Bulletin, **37** 752 – 760 (2012) doi:10.1557/mrs.2012.174.
- [2] O. Nicoletti, F. Pena, R.K. Leary, D.J. Holland, C. Ducati and P.A. Midgley, *Three-dimensional imaging of localized surface plasmon resonances of metal nanoparticles*, Nature, **502** 80-84 (2013) doi:10.1038/nature12469.
- [3] F.J. García de Abajo and A. Howie, *Relativistic Electron Energy Loss and Electron-Induced Photon Emission in Inhomogeneous Dielectrics*, Phys. Rev. Lett., **80** 5180–5183 (1998) doi:10.1103/PhysRevLett.80.5180.
- [4] F.J. García de Abajo and M. Kociak, *Probing the Photonic Local Density of States with Electron Energy Loss Spectroscopy*, Phys. Rev. Lett., **100** 106804 (2008) doi:10.1103/PhysRevLett.100.106804.

- [5] F.J. Abajo and A. Howie, *Retarded field calculation of electron energy loss in inhomogeneous dielectrics*, Phys. Rev. B, **65** 115418 (2002) doi:10.1103/PhysRevB.65.115418.
- [6] A. Hörl, A. Trügler and U. Hohenester, *Tomography of Particle Plasmon Fields from Electron Energy Loss Spectroscopy*, Phys. Rev. Lett., **111** 076801 (2013) doi:10.1103/PhysRevLett.111.076801.
- [7] S. Park, M. Lin and A. Zewail, *Photon-induced near-field electron microscopy (PINEM): theoretical and experimental*, New Journal of Physics, **12** (2010) doi:10.1088/1367-2630/12/12/123028.
- [8] A.H. Zewail, *Four-Dimensional Electron Microscopy*, Science, **328** 187-193 (2010) doi:10.1126/science.1166135.
- [9] P.E. Batson, *Spatial Resolution in Electron Energy Loss Spectroscopy*, Ultramicroscopy, **47** 133-144 (1992) doi:10.1016/0304-3991(92)90190-U.
- [10] D. Pines and P. Nozieres, W. A. Benjamin(1966).
- [11] W. Van den Broek and C.T. Koch, *Method for Retrieval of the Three-Dimensional Object Potential by Inversion of Dynamical Electron Scattering*, Phys. Rev. Lett., **109** 245502 (2012) doi:10.1103/PhysRevLett.109.245502.
- [12] F.J. García de Abajo, *Momentum transfer to small particles by passing electron beams*, Phys. Rev. B, **70** 115422 (2004) doi:10.1103/PhysRevB.70.115422.
- [13] A. Reyes-Coronado, R. Barrera, P. Batson, P. Echenique, A. Rivacoba and J. Aizpurua, *Electromagnetic forces on plasmonic nanoparticles induced by fast electron beams*, Phys. Rev. B, **82** 235429 (2010) doi:10.1103/PhysRevB.82.235429.
- [14] P.E. Batson, A. Reyes-Coronado, R. Barrera, A. Rivacoba, P. Echenique and J. Aizpurua, *Plasmonic Nano-Billiards: Controlling Nanoparticle Movement Using Forces Induced by Swift Electrons*, Nano Letters, **11** 3388 – 3393 (2011) doi:10.1021/nl201795u.
- [15] S.M. Barnett and R. Loudon, *The enigma of optical momentum in a medium*, Proc R Soc A, **468** 1825 – 1838 (2012) doi:10.1098/rsta.2009.0207.

Publications during the past two years

- [1] P.E. Batson, A. Reyes-Coronado, R. Barrera, A. Rivacoba, P. Echenique and J. Aizpurua, *Nanoparticle Movement: Plasmonic Forces and Physical Constraints*, Ultramicroscopy, **123** 50 – 58 (2012) doi:10.1016/j.ultramic.2012.05.004.
- [2] P.E. Batson, A. Reyes-Coronado, R. Barrera, A. Rivacoba, P. Echenique and J. Aizpurua, *Nanoparticle Plasmonic Forces: Pulling and Pushing!*, Microscopy and Microanalysis, **18-S2** 296 – 297 (2012) doi:10.1017/S1431927612003339.
- [3] M. Lagos, A. Reyes-Coronado, P. Echenique, J. Aizpurua and P. Batson, *Atto-Second Forces Imposed by Swift Electrons on Metal nano-Particles*, Microscopy and Microanalysis, (in press 2014).
- [4] O. Krivanek, N. Dellby, T. Lovejoy, N. Bacon, G. Corbin, P. Hrcirik, Z. Szilagy, T. Aoki, R. Carpenter, P. Crozier, J. Zhu, P. Rez, R. Egerton and P. Batson, *Exploring phonon signals by high energy / high spatial resolution EELS*, Microscopy and Microanalysis, (in press 2014).

Towards Mapping Interactions in Hybrid Systems with Active Scanning Probes

Jesse Berezovsky, Case Western Reserve University, Department of Physics

Program Scope

The goal of this research is to explore nanoscale interactions in hybrid systems by harnessing the precision and flexibility of scanning probe microscopy. Projected applications in areas such as energy conversion, opto-electronics, and spintronics will involve hybrid nanosystems composed of two or more materials or nanostructures which interact electrically, optically, or magnetically. Progress in understanding these interactions has been held back by cumbersome and/or imprecise fabrication methods. To overcome this challenge, this work will employ cantilevers with integrated active magnetic and optical components. These active probes will be controllably scanned in proximity to metal or semiconductor nanoscale structures, essentially creating a highly tunable and versatile hybrid system. This technique will allow detailed studies of interactions between optical resonators and plasmonic or spintronic nanostructures, or between dynamic ferromagnetic elements and quantum-confined electron spins. Scanned probes with an integrated optical resonator will be used to spatially map the coupling of the resonator's evanescent modes to nanoscale emitters, such as semiconductor quantum dots. Probes with radio-frequency-driven ferromagnetic microstructures will allow us to study the effect of a highly localized, dynamic magnetic field on confined electron spins. The planned research offers a significant increase of flexibility and efficiency for investigating hybrid systems over traditional nanoassembly, accelerating progress towards future technology.

Recent Progress

As we move towards the objective of coupling nanostructures to optical and magnetic devices fabricated on scanned cantilevers, we have obtained results on the individual components separately, before they are ultimately combined. We have constructed a combined confocal optical/scanned probe microscope, and have used optical microscopy capabilities to study photoluminescence dynamics of individual nanocrystal quantum dots, and magnetization dynamics of driven ferromagnetic microstructures. We then use the optical microscopy and scanning probe microscopy capabilities to measure the effect of a local electric field on quantum dot emission dynamics.

We have used the optical spectroscopy capabilities of our recently constructed scanning probe/optical microscopy system to measure photoluminescence (PL) dynamics of individual semiconductor nanocrystal quantum dots (NCQDs) at room temperature. Because these materials provide a flexible platform for controllable, room-temperature confinement of individual electrons, they are of significant interest for opto-electronics and photovoltaics.

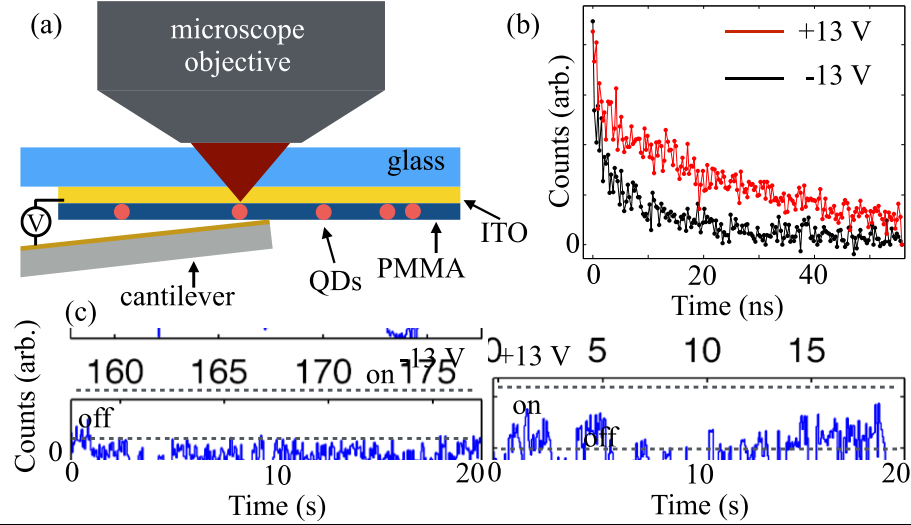


Figure 1. Local gating of single nanocrystal quantum dots. (a) Setup for gating quantum dots (QDs) with a scanned cantilever, and measuring luminescence. (b) Time-resolved photoluminescence from a single QD at two different applied local potentials. (c) Blinking traces corresponding to the measurements shown in (b).

Our supercontinuum pulsed laser-based system allows us to sweep excitation energy and intensity automatically. By monitoring photoluminescence of an individual NCQD via time-correlated single photon counting (TCSPC) while varying excitation energy and intensity, we gain information about the optical transition energies and their linewidths in these nanostructures [1]. Furthermore, by studying the statistics of NCQD blinking as these parameters are swept and comparing to a reaction kinetics model, we can extract information about the dynamics of charge transfer processes to defect states, which are of key importance for engineering these nanostructures for potential applications.

While measuring NCQD PL via the optical microscope and TCSPC setup, we use a metal-coated scanning probe cantilever to apply a local potential to NCQDs embedded in a polymer matrix on an ITO-coated glass cover slip (Fig. 1a). We find that the applied potential can significantly affect PL emission rate, resulting from a change in the charge state of the NCQD. A negative voltage applied to the cantilever causes a decreased PL lifetime as compared to a positive voltage (Fig. 1b). Likewise, the PL blinking (Fig. 1c) displays an increased time spent in the “off” (“on”) state at negative (“positive”) voltage. Together, these results indicate that the negative voltage tends to charge the NCQD with an extra charge carrier, leading to fast non-radiative Auger recombination. On the other hand, positive voltage quenches this short-lifetime component, due to a filling of trap states that, when un-filled, can lead to stochastic charging of the NCQD.

Ultimately, we plan to couple nanostructures such as the NCQDs described above to dynamically-driven micromagnets. We have used a sensitive scanning magneto-optical microscopy technique to study the response of a patterned micromagnet to an applied AC

magnetic field, with submicron spatial resolution and capable of measuring changes in magnetization $<0.1\%$. We have fabricated micron and sub-micron ferromagnetic disks and squares atop a metal stripline (see Fig. 2a). These structures display vortex-like domain structure. Typical data is shown in Fig. 2b, where we measure the change in magnetization of a 2- μm -diameter Permalloy disk to a small change in magnetic field along all three axes. Initial results from these experiments have uncovered new behavior of the magnetization dynamics in these structures.

An important factor in magnetic vortex dynamics is the tendency for the vortex core to be pinned at defects. Instead of translating the vortex continuously, an applied field causes the vortex core to jump from one pinning site to another. The standard assumption is that the vortex is completely rigid while pinned between jumps. Our dynamic differential probing technique results in a very sensitive measurement of the magnetization, and reveals the response of the magnetization while the core is pinned, as the magnetization pattern deforms to minimize the total energy.

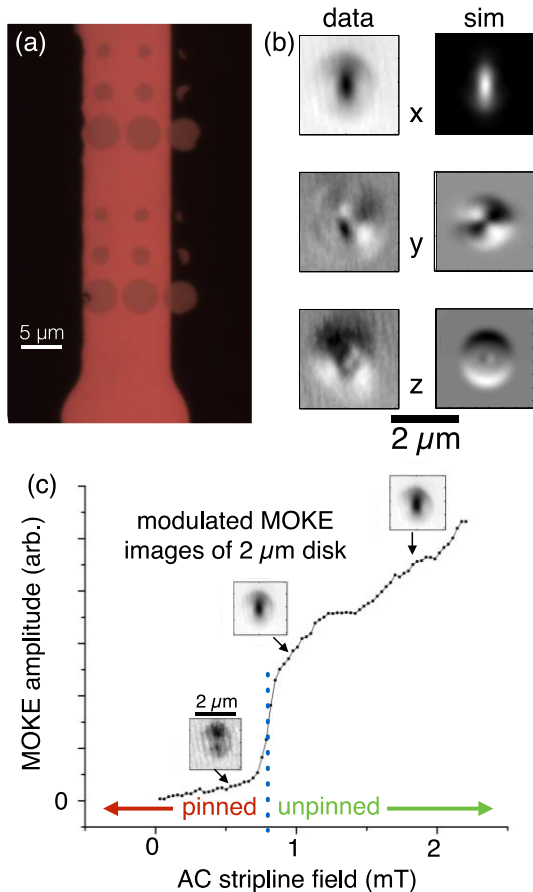


Figure 2. (a) Optical micrograph of Permalloy disks on a stripline. (b) Map of 3-D magnetization response of a 2 μm disk to an AC magnetic field in the x -direction (vertical). (c) Amplitude of central x -component signal vs. AC field strength. Insets show magnetization response map at selected driving voltages.

Our measurements have also allowed us to map out the pinning dynamics as the vortex is translated across the sample. As we increase the strength of the driving magnetic field, we see a strongly nonlinear response in the measured images (Fig. 2c), with a sudden jump corresponding to the depinning of the vortex core. Additionally, we have been able to measure the effects of thermal fluctuations on the depinning process. By pushing the system close to a depinning transition, and varying the dwell time under those conditions, we can measure the probability for a thermally-activated depinning transition to occur. These results will be importance for studying and controlling interactions between these systems and confined spins.

Future Plans

The next steps will be to complete the separate characterization of the nanostructures, and the devices we plan to couple to them. We will build upon our work on coherent spin dynamics in NCQD ensembles [2,3], and will extend these measurements to single NCQDs, as well as

exploring diamond nitrogen-vacancy spins in our system. Further characterization of magnetic vortices is also underway, aimed at mapping out the magnetization response at RF frequencies, using a frequency-domain technique similar to our previously demonstrated technique for probing spin dynamics in QDs [4]. We also plan to study optical interactions between nanostructures and integrated photonic devices. To this end, we are fabricating and characterizing silicon nitride waveguides, resonators, and grating couplers. Both the optical and magnetic devices will be fabricated on custom cantilevers. (The development of the cantilever fabrication process is underway.) Once these steps are complete, we will map out the coupling between the magnetic and photonic devices with individual quantum dots or NV centers. Photonic devices will allow us to study how the interaction of light with these nanostructures depends on the particular geometry, and how that interaction may be enhanced. Coupling dynamic magnetic structures with confined spins will allow a range of fast, local coherent spin manipulation techniques to be explored, with potential for addressable dynamic decoupling schemes or fast tunable coupling of neighboring spins.

References

1. Wolf, M. & Berezovsky, J. Homogeneous and inhomogeneous sources of optical transition broadening in room temperature CdSe/ZnS nanocrystal quantum dots. <http://arxiv.org/abs/1407.5548> (2014). (submitted to Appl. Phys. Lett.)
2. Fumani, A. K. & Berezovsky, J. Magnetic-field-dependent spin decoherence and dephasing in room-temperature CdSe nanocrystal quantum dots. Phys. Rev. B 88, 155316 (2013).
3. Fumani, A. K. & Berezovsky, J. Spin pumping efficiency in room-temperature CdSe nanocrystal quantum dots. <http://arxiv.org/abs/1407.5543> (2014).
4. Frey, J. A. & Berezovsky, J. Frequency-domain optical probing of coherent spins in nanocrystal quantum dots. Opt. Express 20, 20011 (2012).

Publications

Wolf, M. & Berezovsky, J. Homogeneous and inhomogeneous sources of optical transition broadening in room temperature CdSe/ZnS nanocrystal quantum dots. <http://arxiv.org/abs/1407.5548> (2014). (submitted to Appl. Phys. Lett.)

Application of STEM/EELS to Plasmon-Related Effects in Optical Spectroscopy

PI: Jon P Camden, Department of Chemistry and Biochemistry, University of Notre Dame, Notre Dame, IN 46556; Department of Materials Science, University of Tennessee, Knoxville, TN, 37996

Program Scope

We are currently studying the (1) plasmonic energy transfer from metallic nanoparticles to neighboring materials and (2) Localized surface plasmon resonance (LSPR) and plasmon coupling in alloy nanoparticles. Understanding plasmonic energy transfer is important as it is important for developing superior photocatalytic and photovoltaic devices. Using our monochromated STEM/EELS, we are able to probe the energy transfer process at single-particle level with high energy resolution ($\sim 120\text{meV}$). The second program is based on alloy nanoparticles synthesized via pulsed laser induced liquid thin film dewetting. With this method, we can control the mole fractions of the metal and perform comprehensive studies on the tuning effects of the alloy compositions on LSPRs. Also, we are able to design and pattern nanoparticle arrays to study the collective properties of the LSPRs.

Recent Progress

Plasmonic energy transfer: Previous studies suggest that LSPRs facilitate solar energy harvesting^{1,2} via the following mechanisms: (1) enhancing light trapping by concentrating the incident field and increasing the optical path length of the incoming light; (2) directly transferring plasmonic energy into the neighboring material through direct electron transfer (DET) and plasmon-induced resonant energy transfer (PIRET)². Mechanism (1) is only effective for photon energies above the band gap; while mechanism (2) allows for photon energies below and above the band gap, therefore, have drawn increased attention from researchers since they were proposed. For the DET process, hot electrons are generated via non-radiative LSPR decay and then injected into the conduction band of the neighboring material³. It requires the nanoparticle to be in contact with the semiconductor, and its efficiency relies on the relative energy of the hot electrons to the height of the Schottky barrier⁴. PIRET arises from the near field interaction between the LSPR dipole and the interband transition dipole of the neighboring material, similar to Förster resonant energy transfer. The strength of this process is determined by the overlap between the absorption band of the semiconductor and LSPR absorbance⁴, as well as the spacing between the nanoparticle and the semiconductor². The two plasmonic energy transfer schemes, DET and PIRET, inspire new development opportunities of plasmonic device designs.

Thanks to the advances in aberration-corrector and electron monochromator, sub-nanometer sized and monochromatic electron probe formation has made significant progress. This enables us to probe the plasmonic energy transfer process at single-particle level. By interrogating the

substrate-nanoparticle coupling mechanism with tomographic electron energy-loss spectroscopy (EELS), we obtained a nanoscale view of the plasmonic energy transfer process.

In the presence of a dielectric substrate, the primitive corner-dipole mode (D^0) and corner-quadrupole mode (Q^0) will hybridize to form bonding mode (D) and anti-bonding mode (Q), which dominates at the proximal corners and distal corners, respectively⁵. This is schematically described in Figure 1(a). The experimental setup of the tomographic EELS is illustrated in Figure 1(b). The two studied systems are: cube- SiN_x (insulator) and cube-Si (Semiconductor). For each cube-substrate system, we acquired EELS spectra at three positions: (1) the substrate alone, (2) a corner of the titled cube which is in contact with the substrate (proximal corner), and (3) a corner in the vacuum (distal corner). The EEL spectra of the two systems were compared in Figure 1(c).

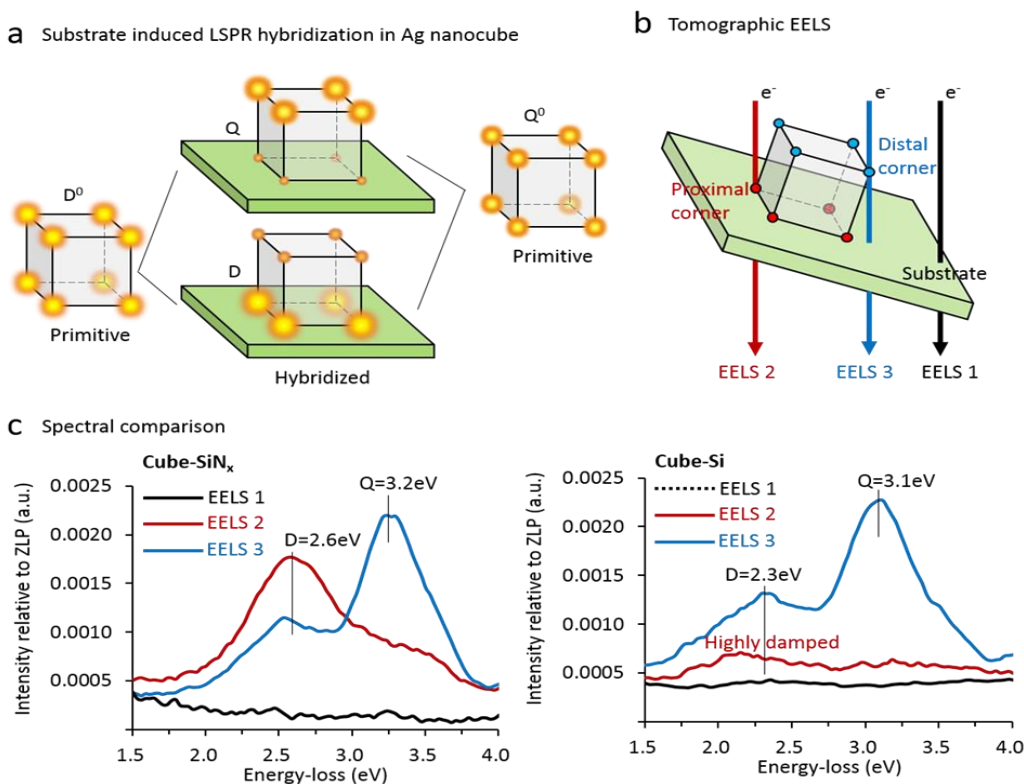


Figure 1. Tomographic EELS study of plasmonic energy transfer. (a) Schematic description of substrate-induced LSPR hybridization in Ag nanocube (Adapted from ref 8). (b) Illustration of tomographic EELS experiment. EEL spectra were acquired at three positions: the proximal corner, the distal corner and the substrate. (c) Spectral comparison between the cube- SiN_x and cube-Si systems.

According to the Figure 1(c), both of the D and Q modes of the cube-Si system experience red shift compared to those of cube- SiN_x . This is due to the higher dielectric constant of Si. In addition to the spectral shift, which provides the dielectric information of the substrate, the spectral line-shape can be used for LSPR lifetime analysis⁶. The D and Q modes of the cube-

SiN_x system exhibits standard proximal-distal splitting, as they dominate at the proximal and distal corners, respectively. The Q mode of the cube-Si system is similar to that of the cube-SiN_x system, however, its D mode is highly damped at the proximal corners, which is against previous understanding. The highly damped D mode serves as a strong evidence of plasmonic energy transfer from the cubes to the semiconductor substrates. This is the first time this process is directly observed at the nanoscale.

LSPR in alloy nanoparticles: The LSPRs in alloy nanoparticles can be tuned conveniently by varying the mole fractions of the metals^{7,8}. A local study of the LSPRs as a function of the particle size and alloy composition is very demanding. It has been reported that nanoparticles with variable size and composition can be synthesized via pulsed laser induced liquid thin film dewetting^{9,10}. This method yield cleaner nanoparticles compared to traditional chemical approach, as it does not employ organic ligands which serve as contamination source in the TEM column. We are also patterning particle arrays to study how the geometry, compositions, and arrangement of the particles modify the LSPR coupling.

Future Plans

For the energy transfer part, we plan to quantify the DET and PIRET processes by integrating our EELS results with theoretical simulations. A work from Cushing et al. distinguished the two pathways using ensemble optical spectroscopy in 2012¹¹. Their experimental object was a Au (core)-SiO₂ (shell)-Cu₂O (shell) structure, where the Au core converts incoming photons into local plasmonic energy; the SiO₂ shell serves as a spacing layer which blocks the DET process; Cu₂O is a semiconductor shell and it accepts the plasmonic energy via PIRET. With this design, they successfully observed the PIRET process. Since EELS provides nanometer-sized resolution and is quantifiable, it is capable of resolving the two pathways at the single-particle level. We plan to deposit insulating layers with different thicknesses (d) between the cube and the semiconductor and examine the EEL spectral line-shape as a function of the cube-semiconductor spacing (d). In the presence of a spacing layer, the DET pathway is shut off, therefore, the PIRET process can be investigated separately and quantitatively. This work will provide a deeper understanding of the plasmonic energy transfer process, and at the same time, demonstrate a way of tuning the energy transfer efficiency.

For the alloy part, more alloy systems (Au-Ag, Ag-Cu, Ni-Cu) with different elemental ratio will be characterized in the future. A systematic study of how metallic nanoparticles with different-leveled plasmon responses interact with each other will be performed.

References

1. Atwater, H. A. et al., Plasmonics for improved photovoltaic devices. Nat Mater 9, 205-213 (2010).
2. Cushing, S. K. et al., Plasmon-Enhanced Solar Energy Harvesting. Interface 22, 63-67 (2013).

3. Clavero, C. Plasmon-induced hot-electron generation at nanoparticle/metal-oxide interfaces for photovoltaic and photocatalytic devices. *Nat Photon* 8, 95-103, (2014).
4. Li, J. et al., Plasmon-induced photonic and energy-transfer enhancement of solar water splitting by a hematite nanorod array. *Nat Commun* 4, (2013).
5. Zhang, S. et al. Substrate-Induced Fano Resonances of a Plasmonic Nanocube: A Route to Increased-Sensitivity Localized Surface Plasmon Resonance Sensors Revealed. *Nano Letters* 11, 1657-1663, (2011).
6. Bosman, M. et al., Surface Plasmon Damping Quantified with an Electron Nanoprobe. *Scientific Reports* 3, 7, (2013).
7. Link, S. et al., Alloy Formation of Gold–Silver Nanoparticles and the Dependence of the Plasmon Absorption on Their Composition. *J. Phys. Chem. B*, 103, 3529-3533, (1999).
8. Verbruggen, S. W. et al., Predicting the Surface Plasmon Resonance Wavelength of Gold–Silver Alloy Nanoparticles. *J. Phys. Chem. C*, 117, 19142-19145, (2013).
9. Krishna, H. et al., Self-Organization of Nanoscale Multilayer Liquid Metal Films: Experiment and Theory. *ACS Nano* 5, 470-476, (2010).
10. Wu, Y. et al., Directed Liquid Phase Assembly of Highly Ordered Metallic Nanoparticle Arrays. *ACS Applied Materials & Interfaces* 6, 5835-5843, (2014).
11. Cushing, S. K. et al., Photocatalytic Activity Enhanced by Plasmonic Resonant Energy Transfer from Metal to Semiconductor. *J. Am. Chem. Soc.*, 134, 15033-15041, (2012).

Publications from BES support (2012-2014)

6. V. Iberi, N. W. Bigelow, N. Mirsaleh-Kohan, S. Griffin, P. D. Simmons Jr., B. S. Guiton, D. J. Masiello, J. P. Camden, "Resonance Rayleigh Scattering and Electron Energy-Loss Spectroscopy of Silver Nanocubes", *J. Phys. Chem. C*, **118**, 10254-10262, (2014).
5. N. W. Bigelow, A. Vaschillo, J. P. Camden, D. J. Masiello, "Signatures of Fano Interferences in the Electron Energy Loss Spectroscopy and Cathodoluminescence of Symmetry-Broken Nanorod Dimers", *ACS Nano*, **5**, 4511-4519 (2013).
4. D. Wang, W. Zhu, M. D. Best, J. P. Camden, K. B. Crozier, "Directional Raman Scattering from Single Molecules in the Feed Gaps of Optical Antennas" *Nano Letters*, **13**, 2194-2198 (2013).
3. [Invited Perspective] V. Iberi, N. Mirsaleh-Kohan, J. P. Camden, "Understanding Plasmonic Properties in Metallic Nanostructures by Correlating Photonic and Electronic Excitations" *J. Phys. Chem. Lett.*, **4**, 1070-1078, (2013).
2. N. Mirsaleh-Kohan, V. Iberi, P. D. Simmons, N. W. Bigelow, A. Vaschillo, M. M. Rowland, M. D. Best, S. J. Pennycook, D. J. Masiello, B. S. Guiton, J. P. Camden, "Single-Molecule Surface-Enhanced Raman Scattering: Can STEM/EELS Image Electromagnetic Hot Spots?" *J. Phys. Chem. Lett.*, **3**, 2303, (2012).
1. N. W. Bigelow, A. Vaschillo, V. Iberi, J. P. Camden, D. J. Masiello, "Characterization of the Electron- and Photon-Driven Plasmonic Excitations of Metal Nanorods," *ACS Nano*, **6**, 7497-7504 (2012).

Superconducting Properties of the LaAlO₃/SrTiO₃ Interface

Venkat Chandrasekhar, Department of Physics, Northwestern University

Program Scope

The primary focus of this project is to investigate the properties of a novel materials system using a combination of electrical transport and low temperature scanning probe techniques. The system being studied is the two-dimensional (2D) conducting gas that forms at the interface between the two band insulators LaAlO₃ (LAO) and SrTiO₃ (STO). As part of this effort, we continue to improve techniques for low temperature scanning probe microscopy [atomic force microscopy (AFM), electrostatic force microscopy (EFM) and magnetic force microscopy (MFM)], including the development of new software and hardware.

Recent Progress

Work in the past two years has focused on two areas. The first is improvements in software and hardware for low temperature scanning probe microscopy, and the second is investigating the magnetic and superconducting properties of the LAO/STO interface. Each is described in more detail below.

Scanning Probe Microscopy

The multiple feedback loops that are needed in scanning probe microscopy (SPM) require time-critical control. Earlier SPM control programs achieved this through analog electronics; recent SPM control programs use digital control. Since most modern computer operating systems use time-slicing for pre-emptive multitasking, feedback control loops that are implemented in conventional desktop software suffer from a slow feedback response, and more importantly, uncertain response times. Consequently, feedback control loops in commercial SPM control software are usually implemented through a dedicated digital signal processor (DSP). However, programming a DSP requires a substantial investment both in hardware and in software development. We have therefore implemented real-time SPM control software (RTSPM [3]) using a simple desktop computer running Linux with a real-time application interface (RTAI) and inexpensive data acquisition cards. The real-time kernel handles the time-critical z piezo feedback loop with a deterministic loop time of 50 μ s, and communicates with the user space interactive main program. The software is written entirely using open source programming tools, and we have made the program and the source code freely available on GitHub [8]. We have also used the real-time kernel to develop a SPM hardware simulator [6, 9] that enables us to test both the RTSPM program and to develop and test models for different scanning modes (e.g., AFM, EFM). This has proved extremely beneficial in sorting out bugs in

our scanning software without having to worry about crashing the tip of our SPM. In addition to software, we have developed a new hybrid analog-digital phase-locked-loop (PLL) controller for frequency-mode operation of our tuning-fork based SPM [4].

The custom-built software and hardware have been successfully used in our 4 K SPM. We are currently testing a new SPM that has been installed in our Kelvinox MX100 dilution refrigerator.

Superconductivity and magnetism at the LAO/STO interface

We have continued to focus on investigating superconductivity and magnetism at the LAO/STO interface. Earlier, we were the first to report the coexistence of superconductivity and magnetism at the LAO/STO interface,¹ an observation that has now been confirmed by other groups. In more recent work, measurements of the gate, temperature and magnetic field dependence of the resistance of the LAO/STO interface at millikelvin temperatures showed that the coexistence of magnetism and superconductivity in this system leads to a rather unique manifestation of charge-vortex duality in the gate-driven superconductor-to-insulator (SIT) transition [1]. In addition to a back-gate voltage, the system can be driven from the superconducting to the insulating state by a magnetic field, the so-called field-driven SIT. The coefficients obtained from a scaling analysis of the field-tuned SIT transition are those expected from quantum percolation [5], in accordance with the picture of an inhomogeneous two-dimensional superconductor that consists of isolated superconducting puddles coupled to each other by the Josephson effect.

The coexistence of superconductivity and magnetism at the LAO/STO interface raises the possibility that the superconductivity is of an unconventional nature, since magnetism and conventional *s*-wave superconductivity are antagonistic phenomena. In order to probe the nature of the superconducting state, we have been fabricating Josephson devices for spectroscopy and interferometry experiments. To do this, we have developed fabrication techniques to electrostatically gate the LAO/STO interface from the top. Such top gates are much more effective in controlling the density of the charge carriers since they are much closer to the interface (4-50 nm, as opposed to 500 μm for the global back gate). The proximity to the interface also means that we can modulate the density of charge carriers very locally, on length scales determined by the dimensions of the top gate, which can be made quite small by electron-beam lithography. Thus, top gating allows us to form local tunnel barriers and channels, with the overall charge density still being controlled by the global back gate. Figure 1 shows a SEM

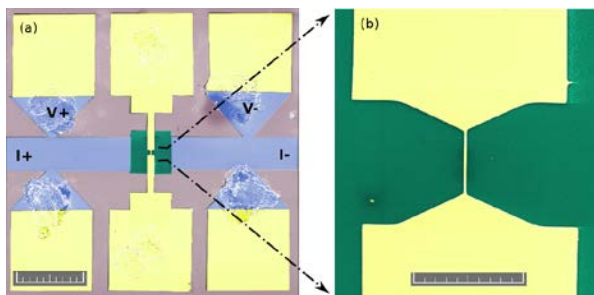


Figure 1 (a) Colorized SEM of a LAO/STO interface Hall bar (light blue). The green square is a blanket silicon oxide insulating layer that separates the gold top gate from the top LAO layer. The scale bar is 200 μm . (b) Narrowest part of top gate (yellow). The size of narrow part of the gate is 180 nm x 6 μm . The size bar is 10 μm .

image of one such LAO/STO Hall bar sample with a narrow top gate.

Varying the voltage on the top gate enables us to modulate the coupling between the two superconducting regions on either side of the gate, making a gate-tunable Josephson junction [7]. Figure 2(a) shows the differential resistance dV/dI of the junction of Fig. 1(b) with both top gate and back gate at zero volts. The red trace was taken after first cooling down; the black trace was taken after sweeping the top gate voltage over ± 40 V, showing that the top gate irreversibly modifies the region under it. Figure 2(b) shows the variation of the differential resistance as a function of the top gate voltage, showing that the critical current can be tuned over a wide range by the top gate. A more detailed analysis of the temperature dependence of the junctions showed that they behave like overdamped Josephson weak links [7]. We are currently making new samples to enable us to probe the superconducting gap with these devices.

Future Plans

In spite of a large number of experiments from various groups around the world, the nature of both the magnetism and the superconductivity at the LAO/STO interface is not clear. We plan to perform experiments to elucidate the nature of both these phenomena in LAO/STO interface samples, using both magnetotransport as well as scanning probe techniques.

There have been conflicting reports from various groups regarding magnetism in the LAO/STO system. Some groups report magnetism at room temperature; other groups report that it disappears at temperatures above a few Kelvin. Consequently, we propose to perform detailed electrical transport measurements on LAO/STO interface samples, looking in particular at the anisotropic magnetoresistance (AMR) and the anomalous Hall effect (AHE), focusing on the temperature regime above the superconducting transition since the small signatures of ferromagnetism will be swamped by the much larger response of the superconductor.

In order to investigate the superconductivity in this system, we will make devices using the top-gate fabrication techniques discussed above. Our goal is to make devices where we can probe the superconducting gap spectroscopically (for example, using NS point contacts), as there have been reports of the presence of a pseudogap in this system. Using the same techniques, we also plan to study interference effects by applying magnetic fields.

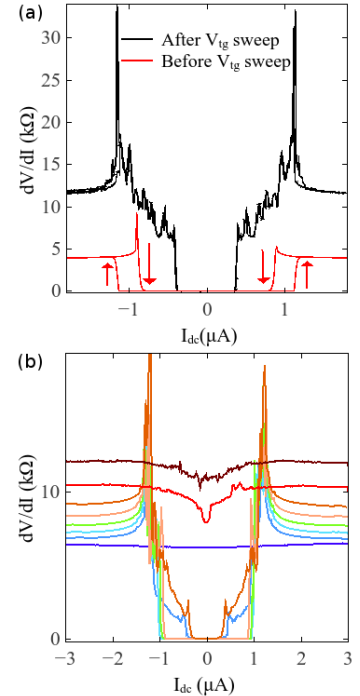


Figure 2 (a) Differential resistance dV/dI as a function of dc current I_{dc} for the LAO/STO sample of Fig. 1 at 30 mK with both back gate and top gate voltages at zero. The black trace was taken after the top gate was swept over the range ± 40 V. (b) dV/dI at a back gate voltage of 90 V, at various top gate voltages from +30 V to -40 V in steps of 10 V, showing the variation in critical current of the junction with top gate voltage.

In terms of scanning probe microscopy, we will use our millikelvin range scanning probe microscope, currently undergoing its first tests at low temperature, to investigate the magnetic properties of the LAO/STO interface. Our first goal would be to image superconducting vortices using MFM, particularly those induced by the underlying magnetism. Later, with improvements in sensitivity, we hope to directly image the magnetism itself.

Finally, we will undertake a substantial effort to develop techniques to fabricate piezoelectric cantilevers in order to increase our sensitivity, and to have the ability to make custom sensors on the ends of these cantilevers.

References

- i. D.A. Dikin, M. Mehta, C.W. Bark, C.M. Folkman, C.B. Eom and V. Chandrasekhar, 'Coexistence of Superconductivity and Magnetism in Two Dimensions,' Phys. Rev. Lett. **107**, 056802 (2011) (Selected for a Viewpoint in Physics).

Publications

1. M.M. Mehta, D.A. Dikin, C.W. Bark, S. Ryu, C.M. Folkman, C.B. Eom and V. Chandrasekhar, 'Evidence for charge-vortex duality at the LaAlO₃/SrTiO₃ interface,' Nature Comm. **3**, 955 (2012).
2. M. Mehta, D.A. Dikin, C.W. Bark, C.M. Folkman, C.B. Eom and V. Chandrasekhar, 'Hysteretic Hall resistance at the LaAlO₃-SrTiO₃ interface: interplay between superconducting and ferromagnetic properties,' Journal of Physics: Conference Series **400** 022071 (2012).
3. V. Chandrasekhar and M.M. Mehta, 'RTSPM: Real-time Linux control software for scanning probe microscopy,' Rev. Sci. Instrum. **84**, 013705 (2013).
4. M.M. Mehta and V. Chandrasekhar, 'A Hybrid Analog/Digital Phase-Locked Loop for Frequency Mode Non-contact Scanning Probe Microscopy,' Rev. Sci. Instrum. **85**, 013707 (2014).
5. M. M. Mehta, D.A. Dikin, C.W. Bark, S. Ryu, C.M. Folkman, C.B. Eom and V. Chandrasekhar, 'Magnetic field tuned superconductor-to-insulator transition at the LaAlO₃/SrTiO₃ interface,' under review at Physical Review Letters (arXiv:1309.3612).
6. V. Chandrasekhar and M.M. Mehta, 'A real-time software simulator for scanning probe microscopy,' submitted to Ultramicroscopy (<http://arxiv.org/abs/1307.7679>).
7. Varada V. Bal, Manan M. Mehta, Sangwoo Ryu, Hyungwoo Lee, Chad M. Folkman, Chang-Beom Eom, Venkat Chandrasekhar, 'Evidence of Josephson junction behavior in top-gated LaAlO₃-SrTiO₃,' arXiv:1407.5939.

Open Source Software Developed

8. RTSPM: Real-time Linux control software for scanning probe microscopy, <https://github.com/chandranorth/RTSPM>.
9. Real-time software simulator for scanning probe microscopy, <https://github.com/chandranorth/TFSimulator>.

Structure and Dynamics of Domains in Ferroelectric Nanostructures – Phase-field Modeling

Long-Qing Chen, Department of Materials Science and Engineering, The Pennsylvania State University, University Park, PA 16802; lqc3@psu.edu

Program scope

The program is centered on investigating the formation of mesoscale domain structures and their evolution in ferroelectric thin films and nanostructures under an electric and/or mechanical stress field. The main objective is to understand the fundamental thermodynamic stability of ferroelectric domain walls and multi-domain configurations as well as dynamic mechanisms of domain switching using the phase-field method. The focus will be on BiFeO_3 and $\text{PbZr}_x\text{Ti}_{1-x}\text{O}_3$ (PZT) systems. BiFeO_3 is one of the most promising single-phase candidates for magnetoelectric device applications and one of the most scientifically fascinating materials that may exhibit electric polarization, oxygen octahedral rotation, antiferromagnetic order, strain, and significant ionic/electronic charges while PZT is currently the most widely utilized class of ferroelectrics for piezoelectric device applications. The research is being carried out in close collaboration between the PI's group and a number of world-class experimental groups who use High Resolution Transmission Electron Microscopy (HRTEM), *in situ* TEM with Scanning Probe Microscopy (SPM), or Piezoresponse Force Microscopy (PFM) to characterize the domain structures and dynamics in high-quality ferroelectric BiFeO_3 and PZT thin films.

Recent Progress

Fundamental Understanding of BiFeO_3 Domain Wall Energies and Structures: A Combined Experimental and DFT+U Study [4]:

Bismuth ferrite (BiFeO_3) is to-date the only known room temperature, single-phase magnetoelectric multiferroic characterized by a large spontaneous electric polarization of $\sim 100 \mu\text{C}/\text{cm}^2$, a ferroelectric transition Curie temperature of ~ 1120 K, and an antiferromagnetic transition Néel temperature of ~ 640 K. One of the signatures of all ferroic materials is the formation of domains below their ferroic transition temperatures, dictated by the crystallographic symmetry group and subgroup relations between the parent phase and the ferroic phase. Accordingly, many applications of ferroic materials, such as data storage, spintronics, and microelectronic devices, are achieved through the control and manipulation of their domain structures, each of them is a micro- or nano-scale region with uniform spontaneous polarization, magnetization, or strain. We determined the atomic structures and energies of 109° , 180° and 71° domain walls in BiFeO_3 , combining DFT+U calculations and aberration-corrected transmission electron microscopy images. We find a substantial Bi sublattice shift and a rather uniform Fe sublattice across the walls (Fig. 1).

The calculated wall energies (γ) follow the sequence $\gamma_{109} < \gamma_{180} < \gamma_{71}$ for the 109° , 180° , and 71° walls. We attribute the high 71° wall energy to an opposite tilting rotation of the oxygen octahedra and the low 109° wall energy to the opposite twisting rotation of the oxygen octahedra across the domain walls. Indeed we recently proposed a rotational compatibility condition [14], to identify low-energy DWs in perovskites with oxygen octahedral tilt instability. It is derived from the strong DW energy anisotropy arising from the rigidity and corner-sharing feature of the octahedral network. We quantitatively analyze the DWs in BiFeO_3 and successfully explain the unusual ferroelectric DW width and energy in BiFeO_3 .

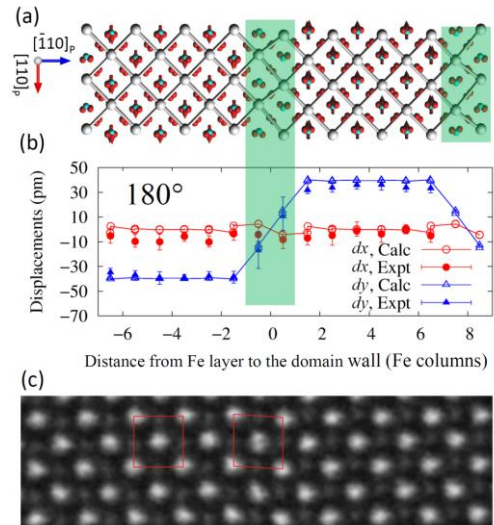


Fig. 1. Atomic structure of 180° domain wall in BiFeO_3 , from our combined DFT+U calculation and STEM measurements.

Understanding Ferroelastic Domain Switching Dynamics under External Excitations [1]:

Ferroelectric materials possessing a strong intrinsic coupling of spontaneous polarization and strain are in common usage for piezoelectric sensors and mechanical switches and under development as potential high-density non-volatile memories. For these materials, a long-standing controversial question is the behavior and mobility of the ferroelastic type of domain boundaries. Large scale ferroelastic switching altering the polarization and strain simultaneously could significantly enhance the electromechanical response, while a lack of such switching may hinder polarization reversal. Here we report the microscopic behavior of individual ferroelastic domains under electric fields and mechanical stress in a thin $\text{PbZr}_{0.2}\text{Ti}_{0.8}\text{O}_3$ film using *in situ* transmission electron microscopy and phase field modeling. We find that the mobility and switching behavior significantly depends on specific microstructures. Our results provide new insights into understanding of polarization switching dynamics and suggest a route to engineer electromechanical devices. Furthermore, the ability to control the polarization and strain by local ferroelastic domain switching provides a framework for exploring multiple local microstructure-related parameters such as charge, lattice and spin in strongly correlated materials.

Uncover the Atomic Scale Mechanisms of Ferroelastic Domain Wall Mediated Ferroelectric Switching [9]:

Ferroelectrics are characterized by a spontaneous polarization that can be re-oriented between energetically equivalent states (domains) by an electric field, providing applications for devices such as non-volatile memories. The polarization switching occurs via the nucleation and growth of 180° domains through a highly inhomogeneous process, and the switching kinetics is controlled by defects, interfaces, and pre-existing domain walls. For epitaxial $\text{Pb}(\text{Zr}_{0.2}\text{Ti}_{0.8})\text{O}_3$ (PZT) thin films, both 180° ferroelectric domain walls and 90° ferroelastic domain walls (twin boundaries) commonly exist due to substrate constraints. Given the high density of ferroelastic domains, the interaction between the newly switched 180° domains and the pre-existing, but immobile, ferroelastic domains dominates the polarization switching. Here, through a combination of *in situ* transmission electron microscopy (TEM) with local biasing, aberration-corrected TEM and phase field modeling (Fig. 2), we examine the atomic structure and dynamic behaviors of ferroelastic domain walls and their effects on polarization switching kinetics at the atomic scale in epitaxial PZT thin films. We directly observed that ferroelastic domain walls act as obstacles to 180° domain wall propagation, resulting in the formation of a charged ferroelastic domain wall and a ‘dead layer’ with a thickness of a few unit cells at their junction in which the local dipoles are disordered. These hindering effects can be overcome either by applying a higher bias or by removing the as-grown ferroelastic domains in fabricated nanostructures.

Discovered a First Order Morphological Transition of Ferroelastic Domains in Ferroelectric Thin Films [2]:

All materials in practical applications are structurally and/or compositionally inhomogeneous, containing mesoscale morphological patterns or microstructures. Depending on thermodynamic conditions, morphological patterns can be thermodynamically unstable, metastable, or stable. Ferroelastic domains are commonly observed in epitaxial thin films are often pinned by interfacial dislocations near

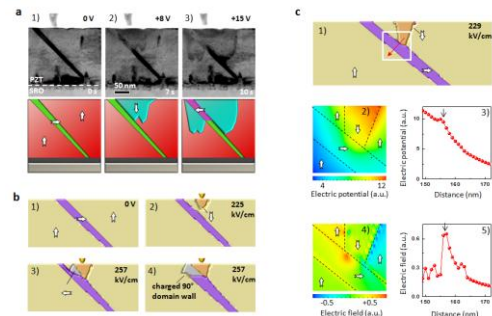


Fig. 2. **a**, *In situ* TEM observation of switching through an embedded 90° domain. **b**, Phase field simulation of switching around a 90° domain. **c**, Simulation of the switched $-c$ -domain impeded by an a -domain at an averaged field of ~ 229 kV/cm (image 1). Image 2 shows the local electric potential of the rectangle region in image 1. Image 3 shows the potential profile along the red arrow in image 1. The thin black arrow indicates the location of the charged domain wall. Image 4 shows the local distribution of in-plane electric field of the rectangle region in image 1. Image 5 is the in-plane electric field profile along the red

the film/substrate interface. Ferroelectric and ferroelastic domains have been extensively studied for their potential applications in electronic devices such as non-volatile memories. The morphology of a pinned ferroelastic domain in $\text{Pb}(\text{Zr}_{0.2}\text{Ti}_{0.8})\text{O}_3$ (PZT) thin films is investigated as a function of film thickness using phase field modeling in combination with transmission electron microscope (TEM) observations. It is found that the ferroelastic domain undergoes a first order morphological transition from a domain fully extended through the film thickness to one terminated inside the film as film thickness increases (Fig. 3 top). It is shown that such a transition results from the competing elastic and electrostatic energies. It is demonstrated that this transition is first-order associated with abrupt changes in thermodynamic properties of the domain structure at the transition (Fig. 3 bottom right), similar to first-order transitions of homogeneous systems with jumps in the first derivative of free energy with respect to thermodynamic variables. Such first order morphological transitions can also be induced by an external field such as electric field or stress/strain field, and thus expected to significantly impact domain switching in ferroelectric thin films.

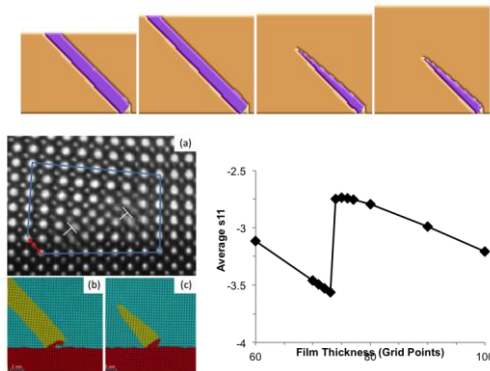


Fig.3. Morphology of a ferroelastic domain pinned by a pair of partial edge dislocations as a function of thickness 30, 36.5, 37, and 40 nm from phase-field simulations (top); TEM observations of dislocations near the interface between a PZT thin film and STO substrate; Ferroelastic domains were observed around the dislocation in thin and thick film sections; Average stress as a function of film thickness

Asymmetric Domain Wall Motion in a Ferroelectric Capacitor [5]: We discovered the preferential, but asymmetric, nucleation and forward growth of switched c-domains at the PZT/electrode interfaces during 180° polarization switching of a $\text{PbZr}_{0.2}\text{Ti}_{0.8}\text{O}_3$ (PZT) capacitor, arising from the built-in electric field induced at each interface. The subsequent sideways growth of the switched domains was inhibited by the depolarization field due to the imperfect charge compensation at the counter-electrode and also at the boundaries with preexisting a-domains, which contributed further to the asymmetric switching behavior. It was found that the preexisting a-domains split into fine a- and c-domains constituting a 90° stripe domain pattern during the 180° polarization switching process, revealing that these domains also actively participated in the out-of-plane polarization switching. The real-time experimental observations and phase-field simulations uncovered the origin of the switching asymmetry and further clarified the importance of charged domain walls and the interfaces with electrodes in ferroelectric switching.

Future Plans

The previous and current efforts by the PI's group have contributed to the fundamental understanding of the effects of strain and electric boundary conditions on the thermodynamic stability of ferroelectric domain structures in thin films as well as on the effect of ferroelastic domains on ferroelectric switching. The future research will be focused on the basic understanding of (1) the effects of dislocations and grain boundaries on polarization switching, including domain nucleation and growth kinetics, and thus switching mechanisms under electric fields; (2) the influence of ionic defects on domain wall mobility and on the electric conductivity along domain walls and topological defects such as domain vortices; and (3) the coupling between ferroelectric, antiferromagnetic, and oxygen octahedral rotation order parameters, and its effects on phase transition temperatures, domain patterns, and domain switching.

References and Publications of DOE sponsored research in 2012-2014

1. P. Gao, J. Britson, C.T. Nelson, J.R. Jokisaari, C. Duan, M. Trassin, S.H. Baek, H. Guo, L.Z. Li, Y.R. Wang, Y.H. Chu, A.M. Minor, C.B. Eom, R. Ramesh, L.Q. Chen, and X.Q. Pan, Ferroelastic Domain Switching Dynamics under Electrical and Mechanical Excitations. *Nature Communications*, 2014. 53801.

2. J. Britson, C. Nelson, X. Q. Pan, and L. Q. Chen, "First-order morphological transition of ferroelastic domains in ferroelectric thin films" *Acta Mater.* **75**, 188 (2014).
3. Y. Cao, J. Shen, C.A. Randall, and L.Q. Chen, Phase-Field Modeling of Switchable Diode-Like Current-Voltage Characteristics in Ferroelectric Batio3. *Applied Physics Letters*, 2014. **104**(18)182905
4. Y. Wang, C. Nelson, A. Melville, B. Winchester, S.L. Shang, Z.K. Liu, D.G. Schlom, X.Q. Pan, and L.Q. Chen, Bifeo3 Domain Wall Energies and Structures: A Combined Experimental and Density Functional Theory Plus U Study. *Physical Review Letters*, 2013. **110**(26).
5. J.K. Lee, G.Y. Shin, K. Song, W.S. Choi, Y.A. Shin, S.Y. Park, J. Britson, Y. Cao, L.Q. Chen, H.N. Lee, and S.H. Oh, Direct Observation of Asymmetric Domain Wall Motion in a Ferroelectric Capacitor. *Acta Materialia*, 2013. **61**(18):6765-77.
6. Y. Wang, L.A. Zhang, S.L. Shang, Z.K. Liu, and L.Q. Chen, Accurate Calculations of Phonon Dispersion in CaF₂ and CeO₂. *Physical Review B*, 2013. **88**(2)024304.
7. Y. Wang, S.L. Shang, L.Q. Chen, and Z.K. Liu, Density Functional Theory-Based Database Development and Calphad Automation. *Jom*, 2013. **65**(11):1533-39.
8. V.T. Tra, J.W. Chen, P.C. Huang, B.C. Huang, Y. Cao, C.H. Yeh, H.J. Liu, E.A. Eliseev, A.N. Morozovska, J.Y. Lin, Y.C. Chen, M.W. Chu, P.W. Chiu, Y.P. Chiu, L.Q. Chen, C.L. Wu, and Y.H. Chu, Ferroelectric Control of the Conduction at the Laalo3/Srtio3 Heterointerface. *Advanced Materials*, 2013. **25**(24):3357-64.
9. P. Gao, J. Britson, J.R. Jokisaari, C.T. Nelson, S.H. Baek, Y.R. Wang, C.B. Eom, L.Q. Chen, and X.Q. Pan, Atomic-Scale Mechanisms of Ferroelastic Domain-Wall-Mediated Ferroelectric Switching. *Nature Communications*, 2013. 42791.
10. J.C. Yang, Q. He, S.J. Suresha, C.Y. Kuo, C.Y. Peng, R.C. Haislmaier, M.A. Motyka, G. Sheng, C. Adamo, H.J. Lin, Z. Hu, L. Chang, L.H. Tjeng, E. Arenholz, N.J. Podraza, M. Bernhagen, R. Uecker, D.G. Schlom, V. Gopalan, L.Q. Chen, C.T. Chen, R. Ramesh, and Y.H. Chu, Orthorhombic Bifeo3. *Physical Review Letters*, 2012. **109**(24)247606.
11. Y. Wang, H.Z. Fang, C.L. Zacherl, Z.G. Mei, S.L. Shang, L.Q. Chen, P.D. Jablonski, and Z.K. Liu, First-Principles Lattice Dynamics, Thermodynamics, and Elasticity of Cr2o3. *Surface Science*, 2012. **606**(17-18):1422-25.
12. R.K. Vasudevan, A.N. Morozovska, E.A. Eliseev, J. Britson, J.C. Yang, Y.H. Chu, P. Maksymovych, L.Q. Chen, V. Nagarajan, and S.V. Kalinin, Domain Wall Geometry Controls Conduction in Ferroelectrics. *Nano Letters*, 2012. **12**(11):5524-31.
13. K. Kathan-Galipeau, P.P. Wu, Y.L. Li, L.Q. Chen, A. Soukiassian, Y. Zhu, D.A. Muller, X.X. Xi, D.G. Schlom, and D.A. Bonnell, Direct Determination of the Effect of Strain on Domain Morphology in Ferroelectric Superlattices with Scanning Probe Microscopy. *Journal of Applied Physics*, 2012. **112**(5)052011.
14. Fei Xue, Yijia Gu, Linyun Liang, Yi Wang, and Long-Qing Chen, "Orientations of Low-Energy Domain Walls in Perovskites with Oxygen Octahedral Tilts", submitted to *Physical Review Letters*, 2014
15. Linze Li, Jason Britson, Peng Gao, Jacob R. Jokisaari, Christopher T. Nelson, Carolina Adamo, Alexander Melville, Darrell G. Schlom, Long-Qing Chen, and Xiaoqing Pan "Atomic-Scale Imaging of Domain Wall Motion in Ferroelectrics." Under Review at *Nature Physics*, 2014
16. Koch, D.Y. Kim, J.K. Kim, W.Y. Jeong, C.G Park, Y. Cao, T.N. Yang, L.Q. Chen, and S.H. Oh "Correlative high resolution mapping of strain and charge density in a strained piezoelectric multilayer" submitted to *Nano Letters*, 2014
17. Linze Li, Jason Britson, Jacob R. Jokisaari, Yi Zhang, Carolina Adamo, Alexander Melville, Darrell G. Schlom, Long-Qing Chen, and Xiaoqing Pan, Large resistive switching via control of ferroelectric charged domain walls, to be submitted to *Science* before DOE program review, 2014
18. J. Britson, D. Marincel, S. T. McKinstry, C. A. Randall, and Long-Qing Chen "Domain Wall Clamping by Long Range Stress Fields in Lead Zirconate Titanate Thin Films." To be submitted to *Applied Physics Letters* before DOE program review meeting, 2014
19. D. M. Marincel, H. R. Zhang, J. Britson, A. Belianinov, S. Jesse, S. V. Kalinin, L. Q. Chen, W. M. Rainforth, I. M. Reaney, C. A. Randall, and S. Trolier-McKinstry. "Domain Pinning Near a Single Grain Boundary in Tetragonal and Rhombohedral Lead Zirconate Titanate Films", to be submitted to *Nature Materials* before DOE program review meeting, 2014
20. J. Britson and Long-Qing Chen "Nucleation Behavior around an Embedded Ferroelastic Domain" to be submitted to *APL* before DOE program review meeting, 2014
21. Y. Cao, J. Shen, C. Randall and L.Q. Chen, "Effect of multidomain structure on ionic transport, electric potential and current evolution in BaTiO₃ ferroelectric capacitor", to be submitted to *Applied Physics Letters* before DOE program review meeting, 2014

Combined microscopy studies of complex electronic materials

David H. Cobden

Department of Physics, University of Washington, Box 351560, Seattle, WA 98195

Program Scope

Many interesting electronic materials have very complex microstructure and exhibit high sensitivity to experimental conditions such as strain. Studies of small homogeneous single crystals under carefully controlled conditions are therefore needed for determining their fundamental properties. The goal of this program is to understand key aspects of important materials by combining multiple microscopy, scanning probe and transport techniques with simultaneous control of temperature, strain, magnetic field, and vapor environment. We focus on VO_2 as a prototypical strongly correlated material, and monolayer dichalcogenide semiconductors of formula MX_2 as examples of a rich new class of electronic materials that are only available as small crystals and are susceptible to substrate, strain and environmental influence.

Recent Progress

1. The metal-insulator transition in VO_2

In the first-order metal-insulator transition (MIT) in VO_2 , which involves strong correlations between electrons and phonons, multiple insulating phases (M1, M2 and T) compete with the metallic phase (R) as temperature is lowered. Such first-order transitions in solids are challenging to study because of the combination of change in unit cell shape, the long range of

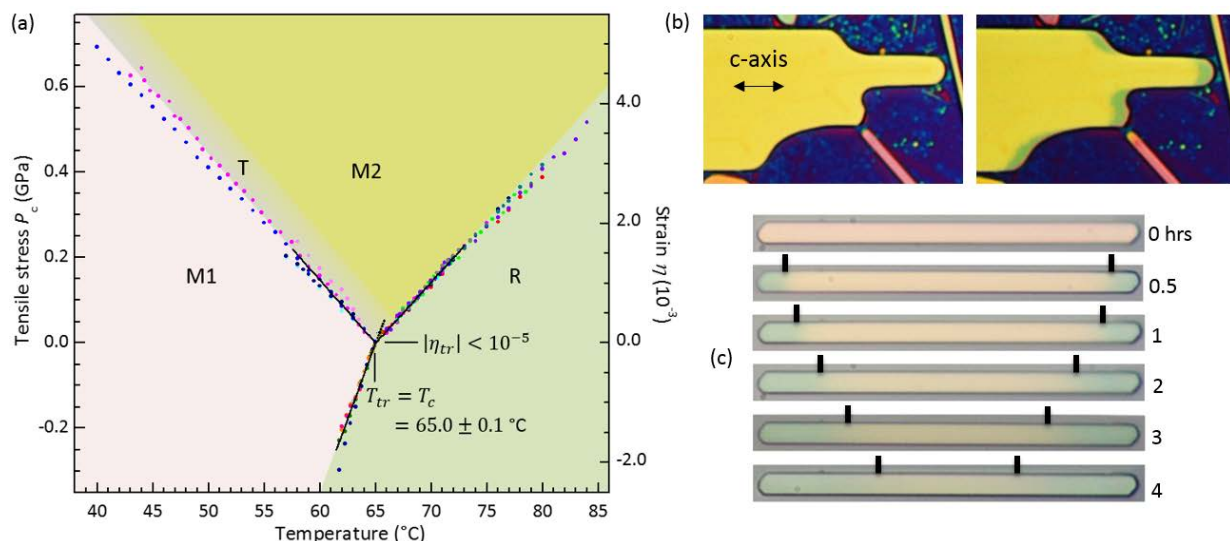


Figure 1. (a) The equilibrium stress-temperature phase diagram of VO_2 near the the metal-insulator transition, established using our nanomechanical strain setup incorporating optical microscopy and electrical transport. (b) Optical images of a VO_2 platelet at room temperature, as-grown (left), and after exposure to hydrogen gas at 100 $^{\circ}\text{C}$ for 15 minutes (right). The anisotropy of hydrogen diffusion is evident in the pattern of darker, doped regions here. The image width is 50 μm . (c) Images of one nanobeam (width 5 microns) after different hydrogen exposure times. From these the diffusion coefficient along the c-axis at 100 $^{\circ}\text{C}$ is determined to be $2 \times 10^{-11} \text{ cm}^2/\text{s}$.

elastic distortion, and the flow of latent heat, which lead to domain structure, nonuniform strain, hysteresis, and often cracking. To avoid these problems we developed a nanomechanical strain microscope, affording the unique ability to precisely control both temperature and axial stress in a nanobeam or nanowire. Using it we established for the first time the equilibrium phase boundaries in VO_2 (Fig. 1a). We found that the triple point of the R, M1 and M2 phases is right at the transition temperature (Fig. 1a), which we determined to be $T_{tr} = T_c = 65.0 \pm 0.1$ °C. With electrical contacts we also determined the strain dependence of the M1 phase resistivity and detected the triclinic distortion of M1. The findings have important implications for the mechanisms of the MIT in VO_2 and other oxides, and demonstrate the value of this approach for mastering phase transitions in complex materials.

The diffusion of hydrogen in solids is common and has many ramifications but is poorly understood. It is strongly affected by inhomogeneity such as grain boundaries and strain, and is also difficult to monitor. Hydrogen in VO_2 has recently been found to change the activation gap, MIT temperature, and color, allowing one to visualize its diffusion with optical microscopy. So motivated, we have begun to investigate the diffusion of hydrogen in VO_2 . Using suspended single-crystal VO_2 nanobeams we have, for example, determined that diffusion is orders of magnitude faster along the c-axis, as illustrated in Fig. 1b, and measured the diffusion coefficient, as illustrated in Fig. 1c.

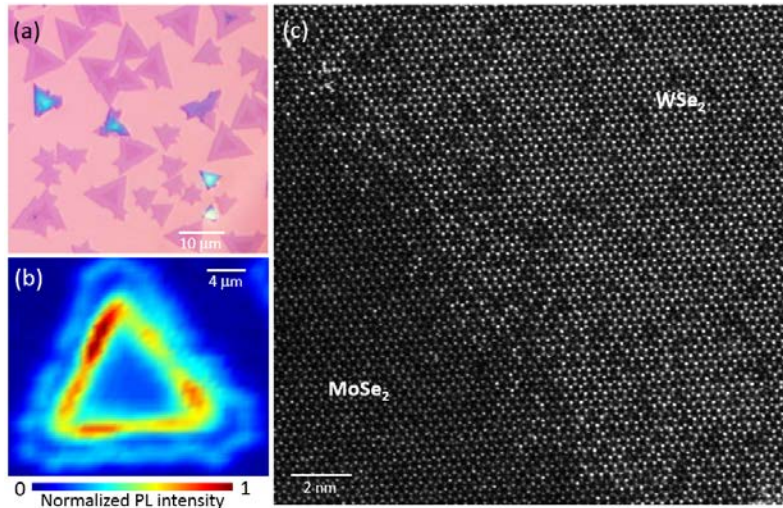


Figure 2. (a) Optical image of lateral monolayer semiconductor heterostructures grown by physical vapor transport. The darker inner triangles are MoSe_2 ; the paler surrounding bands are WSe_2 . (b) Photoluminescence map of a crystal showing enhanced emission from the heterojunction. (c) High resolution aberration-corrected TEM image of the heterojunction obtained at the University of Warwick, showing that the junction occurs in a defect-free honeycomb lattice, with a gradual replacement of Mo by W in the metal sites occurring over a few nm.

2. Monolayer MX_2 semiconductors

The semiconducting dichalcogenides with formula MX_2 , such as MoS_2 , MoSe_2 , and WSe_2 , have recently been recognized as having a direct band gap in monolayer form offering many potential applications with unique aspects related to strong spin-orbit coupling, acentricity, valley pseudospin, strong excitonic and many-body effects, and possible combinations in heterostructures with other 2D materials. We are employing our techniques to understand the fundamental properties of these materials, in collaboration with the group of Xiaodong Xu (UW Seattle).

Epitaxial heterojunctions between three-dimensional (3D) semiconductors are the basis of

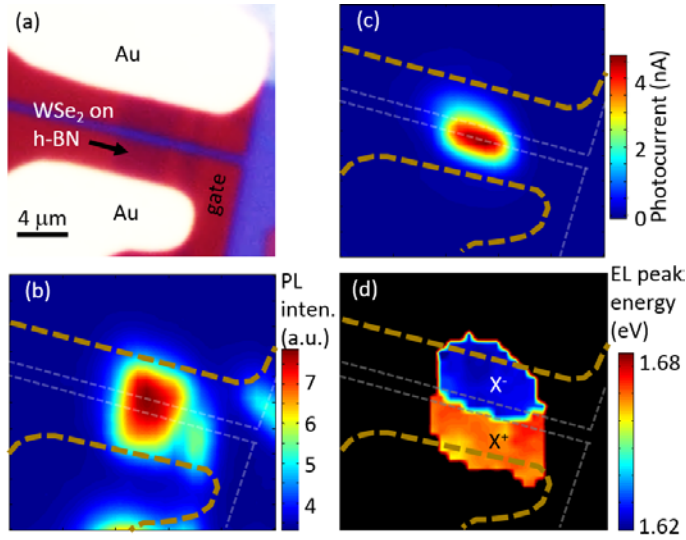


Figure 3. Monolayer WSe_2 photodiode and trion LED. (a) Optical image of a device. n- and p-regions are produced by oppositely biasing the sides of a split metal back gate underneath a thin h-BN dielectric supporting the monolayer. (b) Scanning photoluminescence image. (c) Scanning integrated photo-luminescence image. (d) Color scale map of the peak electroluminescence energy at 100 K, 20 nA, showing positive and negative trion peaks in the p- and n-doped contact regions respectively, effectively mapping the majority carrier type.

replaced in the metal sites by the other across the interface on a scale of a few nm (Fig. 2c). Lateral heterojunctions open up the possibility of band engineering within the 2D plane to make, for example, 1D quantum wires, superlattices, diodes and transistors.

Among the phenomena we have studied in MX_2 monolayers is electroluminescence from lateral p-n junctions (Fig. 3). The junctions were induced electrostatically in monolayer WSe_2 using a thin hexagonal boron nitride support as a dielectric layer with a pair of split metal gates beneath (Fig. 3a). The WSe_2 shows photoluminescence (Fig. 3b), and photocurrent is generated at the junction (Fig. 3c). The geometry allows effective injection of electrons and holes, and combined with the high optical quality of WSe_2 it yields bright electroluminescence with a low injection current (down to 1 nA) and smaller linewidth than reported in earlier simple MoS_2 devices. The X^+ and X^- trion peaks have different energies so that a map of the peak energy acts as a map of the majority carrier sign (Fig. 3d).

Future Plans

1. *Structural and time-resolved studies of the MIT in VO_2 .* We will complete studies of the infrared pump-probe response of single-crystal plates of VO_2 . We will determine the polarization dependence and any relationship to crystal shape, as not possible in films and bulk. We will investigate the coupling of the MIT to optical transitions in monolayers. Using high resolution TEM we will clarify the structures of the various phases using thin straight nanobeams mounted under tension. On increasing temperature such nanobeams will pass sequentially

modern light-emitting diodes, diode lasers, and high-speed transistors. We have synthesized analogous heterojunctions between different 2D semiconductors. The seamless lateral heterojunctions were formed between monolayer WSe_2 and MoSe_2 using physical vapor transport (PVT), as part of our continuing efforts in PVT growth of nanoscale materials including VO_2 , graphene, nanotubes and MX_2 s. The heterojunctions are visible in an optical microscope (Fig. 2a) and show enhanced photoluminescence compared with the homogeneous monolayers (Fig. 2b). Atomically resolved transmission electron microscopy (performed by Ana Sanchez, University of Warwick) reveals that their structure is an undistorted two-component honeycomb lattice in which one transition metal is

through all four phases. Questions to resolve include whether the M1-T transitions is continuous; whether M2 and T are centrosymmetric; the location of the spinodal lines for the R-M1 and R-M2 transitions; the nature of the interfaces; requirements for nucleation; and roles of defects and twinning.

2. *Scanning magneto-optical studies of monolayer semiconductors*. We will continue to develop facilities for combined scanning optical studies of complex materials in high magnetic field at low temperatures with environmental and strain control. We will investigate phenomena in MX_2 monolayers and heterostructures such as spin-valley-layer coupling, magnetic field dependence and photocurrent. We aim to improve control of growth of MX_2 monolayers and heterostructures and develop better, ambipolar, electrical contacts needed for detailed transport studies.

Publications

1. "Lateral heterojunctions within monolayer semiconductors", C. Huang, S. Wu, A.M. Sanchez, J.J.P. Peters, R. Beanland, J.S. Ross, P. Rivera, W. Yao, D.H. Cobden, and X. Xu. *Nature Materials* (2014), doi:10.1038/nmat4064.

2. "Electrically tunable excitonic light-emitting diodes based on monolayer WSe_2 p-n junctions", J.S. Ross, P. Klement, A.M. Jones, N.J. Ghimire, J. Yan, D.G. Mandrus, T. Taniguchi, K. Watanabe, K. Kitamura, W. Yao, D.H. Cobden, & X. Xu, *Nature Nanotechnology* (2014), doi:10.1038/nnano.2014.26.

3. "Measurement of a solid-state triple point at the metal-insulator transition in VO_2 ", J.H. Park, J.M. Coy, T.S. Kasirga, C. Huang, Z. Fei, S. Hunter, and D.H. Cobden, *Nature* 500, 431–434 (2013) doi:10.1038/nature12425.

4. "Vapor-solid growth of high optical quality MoS_2 monolayer with near unity valley polarization", S. Wu, C. Huang, G. Aivazian, J.S. Ross, D.H. Cobden, and X. Xu, *ACS Nano* 7, 2768 (2013) doi: 10.1021/nn4002038.

5. "Anisotropic infrared response of vanadium dioxide microcrystals", T.J. Huffman, P. Xu, M.M. Qazilbash, E.J. Walter, H. Krakauer, J. Wei, D.H. Cobden, H.A. Bechtel, M.C. Martin, G.L. Carr, D.N. Basov, *Phys. Rev. B* 87, 115121 (2013) doi:10.1103/PhysRevB.87.115121.

6. "Electrical tuning of valley magnetic moment via symmetry control", S. Wu, J.S. Ross, G.-B. Liu, G. Aivazian, A.M. Jones, Z. Fei, W. Zhu, D. Xiao, W. Yao, D.H. Cobden, and X. Xu, *Nature Physics* 9, 149 (2013) doi:10.1038/nphys2524.

7. "Photoresponse of a strongly correlated material determined by scanning photocurrent microscopy", T.S. Kasirga, D. Sun, J.H. Park, J.M. Coy, Z. Fei, X. Xu, and D.H. Cobden, *Nature Nanotechnology* 7, 723 (2012) doi:10.1038/nnano.2012.176.

Development and Application of *In Situ* Nanocharacterization to Photocatalytic Materials for Solar Fuel Generation

Principle Investigator: Peter A. Crozier

School for Engineering of Matter, Transport and Energy, Arizona State University,
Tempe, AZ 85287-6106

Email: crozier@asu.edu

Program Scope

We are developing a fundamental understanding of heterostructured semiconductor-based photocatalysts for H₂ generation via water splitting. Our catalysts are composite materials consisting of light harvesting semiconducting oxides supporting catalytic nanoparticles that facilitate the transfer of excited electrons/holes for water reduction/oxidation. We are working on titania and tantalate light harvesting oxides which are functionalized with metal and metal oxide nanoparticles yielding model systems which are active under ultraviolet light. The H₂ evolution is measured in a photoreactor and advanced electron microscopy techniques (including *in situ* and *operando* approaches) are employed to elucidate structure-reactivity relations. We are also developing and employing high energy resolution electron energy-loss spectroscopy to obtain new insights from high spatial resolution vibrational spectroscopy and band gap determinations.

Recent Progress

Titania-Based Water Splitting: *Figure 1* shows the overall architecture of the catalysts currently under investigation. The oxide semiconductor is functionalized with Ni metal and NiO nanoparticles which act as hydrogen and oxygen evolution sites respectively. The Ni metal/oxide core-shell architecture suppresses the reverse reaction because oxygen diffusion to the Ni metal surface is inhibited by the NiO shell. The core-shell structure is produced by first reducing the sample to Ni metal and then gently re-oxidizing to form an oxide skin.

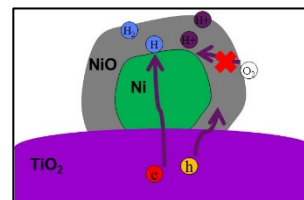


Figure 1: Architecture of photocatalyst.

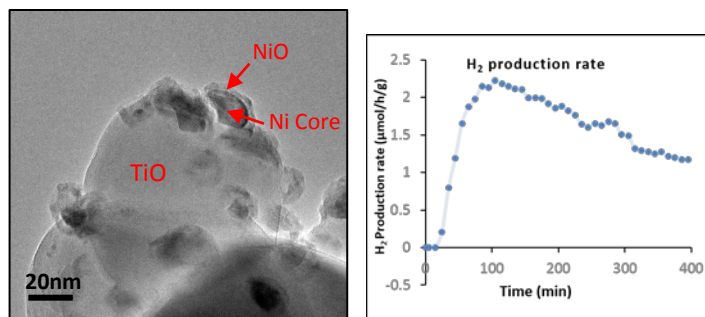


Figure 2: a) Photocatalyst consisting of Ni/NiO core-shells on anatase and H₂ evolution in liquid H₂O.

The structure and H₂ evolution of a titania based catalyst is shown in *Figure 2*. The structure shows a clear core-shell morphology and the hydrogen production rate drops by a factor of two over seven hours. Electron microscopy shows that the de-activation is associated with a significant change in the catalyst morphology. The most dramatic change is shown in *Figure 3a* where about 40% of the core-shell

structure evolves into NiO void structures. No metal remained in these structures resulting in termination of H₂ production. About 10% of the core-shells assumed a morphology shown in **Figure 3b**. In this case, a NiO layer grew between the TiO₂ and Ni metal acting as a barrier to electron transfer to the metal catalyst causing H₂ evolution to stop.

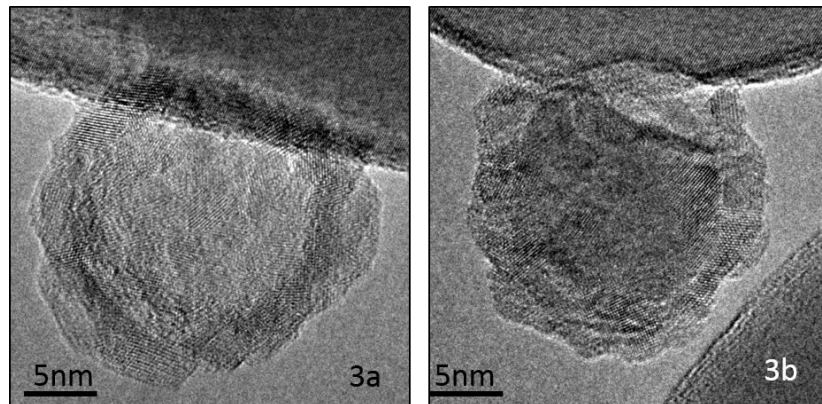


Figure 3: Deactivated catalyst showing NiO shell structure (left) and electrically insulating oxide layer between metal and TiO₂ (right).

Tantalate-Based Water Splitting: To facilitate the development of advanced *operando*

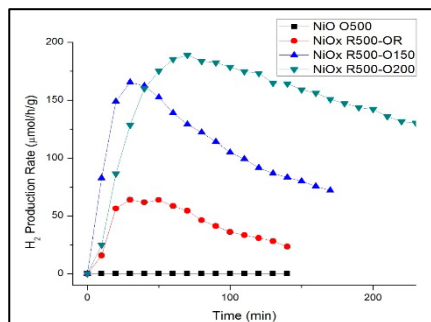


Figure 4: H₂ production rate from tantalate based Ni/NiO catalysts for different thermal oxidation step.

microscopy techniques, it is desirable to have a more active catalyst to make H₂ detection inside the electron microscopy easier. For this reason we are also working on Ta₂O₅ which shows very high activity. The rate of H₂ production is strongly influenced by the Ni re-oxidation step as shown in **Figure 4** with pure NiO being completely inactive for water splitting. The tantalate catalysts are up to a 100 times more active than the titania-based systems which is presumably the result of the high overpotentials associated with the larger bandgap (4.2 eV). The tantalate-based catalysts also deactivates via Ni metal conversion to NiO. In conclusion, the tantalate supported Ni/NiO coreshell structure is highly

active for water splitting but does not show long-term stability. *The loss of activity is associated with Ni metal conversion to NiO.*

Ultra-High Energy Resolution EELS for Band Gap Mapping: In early 2013, ASU received delivery of a unique ultra-high energy resolution monochromated electron microscope manufactured by Nion. The monochromator in this instrument represents a revolutionary advance in instrumentation allowing the energy resolution of electron energy-loss spectroscopy to be improved by almost an order of magnitude. *Over the last year, we have obtained an energy resolution of 12 meV.* The combination of high energy resolution as well as high spatial resolution should make localized band gap mapping possible. We have measured the band gap with EELS from rutile (direct gap 3.02 eV) and anatase (indirect gap 3.2 eV). The gap measured with EELS for these two materials comes out to be 3 and 3.5 eV. The 0.3 eV discrepancy for

anatase is presumably a result of the low momentum transfer to the scattered electrons for this experimental condition. Below the gap, structure is often observed in the spectrum which can in part be attributed to interband states, Cerenkov radiation and transition radiation. A great deal of work is required to realize the full potential of this approach for characterizing the localized optical properties of materials.

Localized Vibrational Spectroscopy and Phonon Detection in the TEM: The very high energy

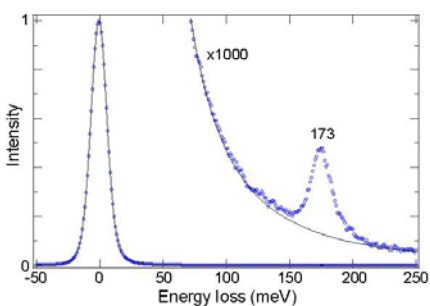


Figure 5: EELS from BN showing transverse optical phonon.

resolution of the system opens up the possibility of localized vibrational or phonon spectroscopy with electron probes down to 0.1 nm in size. Crozier's group and other scientist from ASU established a collaboration with Nion to search for phonons in the electron microscope earlier this year. In February 2014, we spectroscopically detected phonons in the electron microscope for the first time. Optical transverse phonons were first observed in hexagonal BN at 173 meV as shown in **Figure 5**. Since that time we have been able to observe phonons in several different oxides and a number of polymers. This approach

can be employed to detect hydroxide species on the surface of photocatalysts. **Figure 6** shows an atomic resolution STEM image from Ta₂O₅ along with the low-loss energy-loss spectrum. The spectrum shows an excitation at around 470 meV which is characteristic of the O-H vibrational stretch frequency showing that the surface of the oxide is covered with hydroxide. There are many fundamental questions that must be addressed to fully understand this new technique. Are the modes observed in EELS predominantly Raman or IR active modes? What is the spatial resolution of the technique? Can phonon modes associated with surfaces or interfaces be observed and if so how do they relate to atomic structure? **This clearly represents and exciting new frontier in electron beam characterization of materials.**

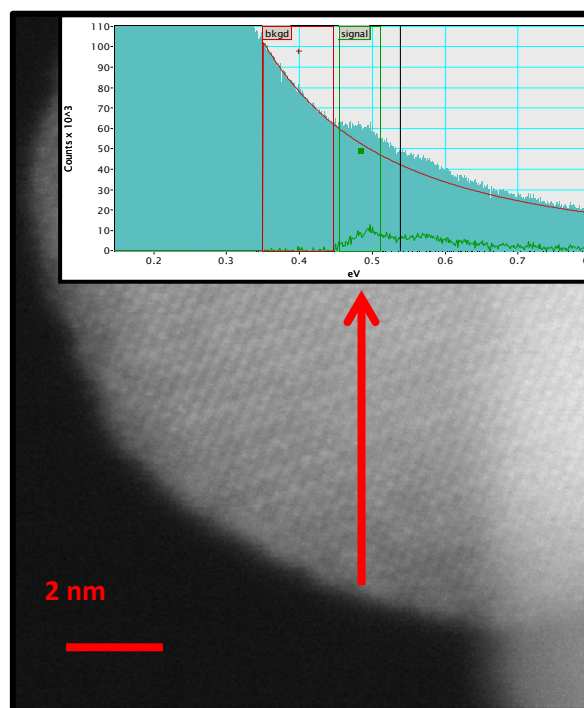


Figure 6: Z-contrast image and EELS from surface of Ta₂O₅ nanoparticle after exposure to water and UV light.

Future Plans

Instrumentation: We plan to construct a light illumination system for a newly delivered FEI Titan aberration corrected environmental TEM installed at ASU earlier this year. We will also continue to refine the *ex situ* reactor so that we can detect oxygen and optimize conditions for *operando* TEM experiments. *Structure-Reactivity:* We will perform a fundamental study of the structure-reactivity relations for a variety of functionalized titania and tantalate-based materials for water splitting. We are particularly interested in systems functionalized with NiO/Ni, Pt, Ru, Cu, Co and bimetallic systems. The work will employ *in situ* and *ex situ* aberration corrected electron microscopy with parallel *ex situ* reactor work. We will also attempt to perform *operando* TEM for water splitting in which H₂ and O₂ are detected in the microscope with simultaneous structure determination. We plan to fabricate our own thin membrane liquid cells to extend our *in situ* work to a liquid water environment. *Ultra-high Energy Resolution EELS:* We will apply novel high resolution EELS to a variety of materials including oxide catalysts. We will explore bandgap mapping, correction of Cerenkov and surface losses and determination of interband states. We will also perform a fundamental exploration of localized phonon mapping. At the moment this area of EELS research is a completely new field and so pioneering work must be undertaken to ascertain the potential of the technique.

Publications Supported by BES (2012- 2014)

References to publications of DOE sponsored research that have appeared in 2010-2012

1. V. Sharma, P.A. Crozier, R. Sharma and J.B. Adams, (2012) “*Direct Observation of Hydrogen Spillover in Ni-Loaded Pr-Doped Ceria*”, *Catalysis Today* **180**(2) 2-8.
2. P. P. Dholabhai, S. Anwar, J. B.Adams, P. A.Crozier, R. Sharma (2012) "*Predicting the optimal dopant concentration in gadolinium doped ceria: a kinetic lattice Monte Carlo approach.*" *Modelling and Simulation in Materials Science and Engineering* **20**(1): 13.
3. B. K. Miller and P. A. Crozier (2013). "*A System for In Situ UV-Visible Illumination of ETEM Samples*", *Microscopy and Microanalysis*, 19, 461-469,
4. L. Zhang, B. K. Miller and P. A. Crozier (2013). "*Atomic Level Observation of Surface Amorphization in Anatase Nanocrystals During Light Irradiation in Water Vapor* " *Nano Letters*, 13, 679-684.
5. O.L. Krivanek, T. C. Lovejoy, N. Dellby, Toshihiro Aoki, R.W. Carpenter, Jiangtao Zhu, Peter Rez, Ray F. Egerton, Philip E. Batson and Peter A. Crozier, “*Vibrational spectroscopy in the Electron Microscope*”, (Nature, in press).
6. L. Zhang and P. A. Crozier, “*In-situ and Ex-situ characterization of NiO-Ni-TiO₂ photocatalyst under in reaction conditions for development of structure-property relationships*”, (submitted).
7. Q. Liu and P.A. Crozier, “*Investigation on the structure-activity relationship of NiO/Ni loaded on Ta₂O₅ photocatalyst*”, (submitted)
8. L. Zhang and P. A. Crozier, “*In-situ and Ex-situ characterization of Pt/TiO₂ photocatalyst under in reaction conditions for development of structure-property relationship*”, (in preparation).
9. Q. Liu and P.A. Crozier, “*In situ observation on structural changes of Ta₂O₅ photocatalyst under reaction condition*”, (in preparation)

Materials Applications of Aberration-Corrected Lorentz Microscopy

Marc De Graef (PI), Emma Humphrey and Prabhat Kc (PhD students),
Department of Materials Science and Engineering,
Carnegie Mellon University, Pittsburgh, PA 15213

Program Scope

In this project (DOE# DE-FG02-01ER45893), we develop tomographic reconstruction methods that can be applied to the three-dimensional study of magnetic field distributions around nano-scale magnetic samples. The program consists of a strong modeling component, supported by an experimental component. In the modeling component, the ultimate goal is to be able to validate experimental observations, by using numerical simulations and analytical evaluation of error propagation. The experimental component makes use of a series of carefully selected samples, used in a series of increasingly more advanced electron microscopes, and on a series of length scales. The program also further develops methods for the computation of magnetostatic interactions between nano-particles, based on the shape amplitude formalism (developed with prior DOE support). This theoretical work has produced more than twenty publications in peer-reviewed journals over the past decade.

Recent Progress

During the past two years, we have focused on the development of numerical techniques for the 3D reconstruction of the magnetic vector potential, $\mathbf{A}(\mathbf{r})$, from Lorentz tilt series. In the past, we have succeeded in reconstructing the vector potential for simple geometries (rectangular islands and elliptical disks of Permalloy) using the standard filtered back projection (FBP) method adapted to vector field reconstruction [1]. Such reconstructions suffer from the fact that there is a missing wedge in the data (the tilt range is limited by the geometry of the sample holder and the limited space between the objective lens pole pieces) and also from the fact that the electrostatic and magnetic components of the electron phase shift have a different power spectrum. This latter problem is particularly serious, because it means that for phase reconstructions based on the Transport-of-Intensity Equation (TIE) formalism, there is an incomplete separation of electrostatic and magnetic phase contributions, limiting the resolution of the reconstruction near sample edges. Our theoretical progress has been in the area of separation of electrostatic and magnetic phase shift contributions and makes use of a modified Transport-of-Intensity Equation.

Modified Transport-of-Intensity Equation In [2], we describe a new approach for the separation of the electrostatic and magnetic components of the electron wave phase shift, based on the transport-of-intensity equation (TIE) formalism. We derived two separate TIE-like equations, one for each of the phase shift components. We used experimental results on FeCoB and Permalloy patterned islands to illustrate how the magnetic and electrostatic longitudinal derivatives can be computed. The main advantage of this new approach is the fact that the differences in the power spectra of the two phase components (electrostatic phase shifts often have signifi-

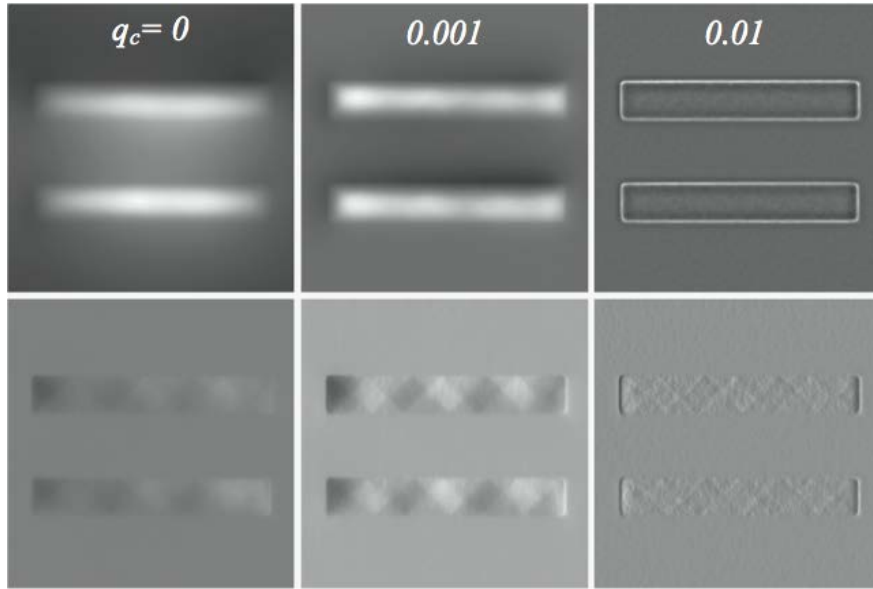
cant power in the higher frequencies) can be accommodated by the selection of two different Tikhonov regularization parameters for the two phase reconstructions. The extra computational demands of the method are more than compensated by the improved phase reconstruction results. Our approach makes use of the linearity of the TIE to accomplish the phase separation *before* the equation is solved. If $I^+(\Delta f)$ represent the image intensity for a defocus Δf and the sample in the upright position, and $I^-(\Delta f)$ for the sample flipped upside down, then the new TIEs are given by:

$$\begin{aligned}\nabla \cdot (I_0 \nabla \varphi_e) &= -k \partial_z^e I & [\text{TIE-e}]; \\ \nabla \cdot (I_0 \nabla \varphi_m) &= -k \partial_z^m I & [\text{TIE-m}],\end{aligned}$$

where the derivatives are defined in terms of the image intensities as:

$$\begin{aligned}\partial_z^e I &= \frac{1}{4\Delta f} (I^+(\Delta f) - I^+(-\Delta f) + I^-(\Delta f) - I^-(-\Delta f)); \\ \partial_z^m I &= \frac{1}{4\Delta f} (I^+(\Delta f) - I^+(-\Delta f) - I^-(\Delta f) + I^-(-\Delta f)),\end{aligned}$$

When these relations are applied to experimental CoFeB images, and Tikhonov regularization is applied to the inverse Laplacian operator needed to solve the TIEs, we obtain the reconstructions



shown to the left. Note that the reconstruction requires different regularization parameters for the electrostatic and magnetic phase shifts, due to differences in their power spectra. This new approach provides a more accurate phase reconstruction than the conventional TIE approach.

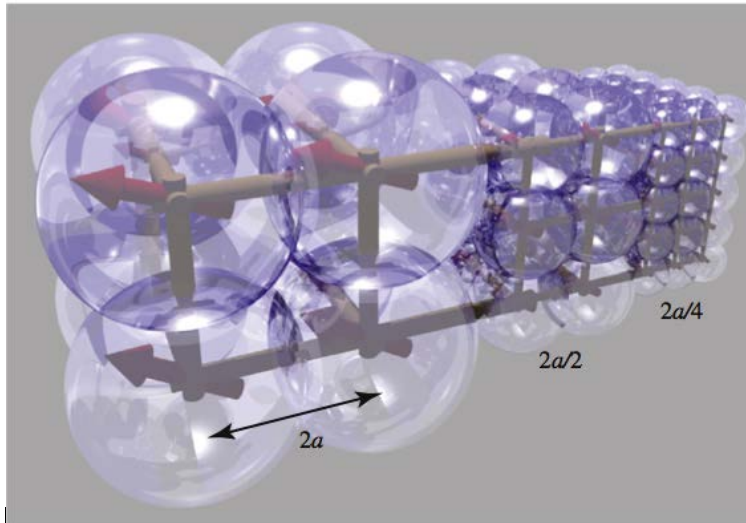
(Top row) Electrostatic phase shift for three different Thikonov regularization parameters; (Bottom row) magnetic B_y component, derived from the magnetic phase shift by a gradient operation. The islands are 1 mm wide, 5.6 mm long.

Phase shift computations for iterative tomographic reconstructions In [3], we proposed a new approach to the computation of magnetic phase shifts for objects of arbitrary shape and magnetization state. We consider the object to be made up of a collection of uniformly magnetized spheres arranged on the nodes of a cubic grid. In the limit of vanishing grid size, this approach becomes equivalent to other numerical approaches. We have derived update equations for the change of the magnetic phase shift when the magnetization of a single object voxel is modified. Example phase shift calculations were presented for a uniformly magnetized sphere, circular disks with an infinitely sharp vortex core and a smooth core, and an oval disk with a pair of vortices and an anti-vortex.

Our approach makes use of the fact that the projection of a sphere is independent of the projection direction, so that a regular lattice of identical spheres can serve as a model for tomographic reconstructions. The magnetic phase shift for a sphere is readily computed to be:

$$\varphi_m(k_x, k_y) = \mu_x S_y - \mu_y S_x \quad \text{where } S_\alpha = 4\pi^2 R^2 \frac{iB_0}{\varphi_0} \frac{j_1(k_\perp R)}{k_\perp^3} k_\alpha$$

the factors m_i are the in-plane components of the magnetic moment for the sphere with radius R ;



Representation of the object sampling lattice, with equal volume spheres superimposed and three multi-grid generations shown. Each sphere has a magnetic dipole moment at its center (red vectors).

$j_l(x)$ is a spherical Bessel function, B_0 the saturation induction and f_0 the flux quantum. These functions can be pre-computed once, and then re-used for each sphere that makes up the sample, as shown in the figure on the left. The total phase shift can be written as a sum of contributions for the individual spheres, and update equations can be derived that express how the overall phase shift changes when only a single sphere is modified.

Such update equations will prove to be useful for a fully iterative implementation of vector field tomographic reconstructions, which is currently under development in

this research program. This approach can also be used for the computation of the electrostatic phase shift, although other sampling approaches work equally well. A full numerical evaluation of the optimal grid size is currently underway, as is the integration of the method in a general Lorentz image simulation algorithm.

Future Plans

In the next year of this program, we plan to explore the use of forward modeling techniques in combination with Lorentz and STEM diffraction contrast transmission electron microscopy observation modes to determine quantitatively the 3-D spatial variations of vector-type quantities, such as magnetization and lattice displacement, and derived quantities, such as the magnetic vector potential and lattice strain, in modern engineering materials. The availability of spherical aberration correction combined with Lorentz transmission electron microscopy (LTEM) at both Carnegie Mellon University (CMU) and the Argonne National Laboratory (ANL) as well as at the Center for Electron Microscopy and Analysis at the Ohio State University (OSU) opens the door to quantitative 3D high resolution studies of both magnetic materials and complex microstructures in materials of importance for power generation and propulsion. We will build upon our earlier work in vector field electron tomography to expand the reconstruction of vector fields to the case of displacement fields in multi-phase engineering materials.

References

- [1] C. Phatak, A.K. Petford-Long, and M. De Graef, "Three-dimensional study of vector potential of magnetic structures," *PRL*, vol. 104, pp. 253901 (2010).
- [2] E. Humphrey, C. Phatak, A.K. Petford-Long, and M. De Graef, "Separation of electrostatic and magnetic phase shifts using the Transport-of-Intensity Equation," *Ultramicroscopy*, **139**, 5-12 (2013)
- [3] E. Humphrey and M. De Graef, "On the computation of the magnetic phase shift for magnetic nano-particles of arbitrary shape using a spherical projection model," *Ultramicroscopy*, **129**, 36-41 (2013)

Publications

- C. Phatak, A.K. Petford-Long, M. Beleggia, and M. De Graef, "Theoretical study of ferroelectric domain wall images using phase reconstructed electron microscopy," *Phys. Rev. B* **89**, 214112 (2014)
- E. Humphrey, C. Phatak, A.K. Petford-Long, and M. De Graef, "Separation of electrostatic and magnetic phase shifts using the Transport-of-Intensity Equation," *Ultramicroscopy*, **139**, 5-12 (2013)
- E. Humphrey and M. De Graef, "On the computation of the magnetic phase shift for magnetic nano-particles of arbitrary shape using a spherical projection model," *Ultramicroscopy*, **129**, 36-41 (2013)
- M. Beleggia, D. Vokoun, and M. De Graef, "Forces between a permanent magnet and a soft magnetic plate," *IEEE Magnetics Letters*, **3**, 0500204 (2012)
- A.K. Petford-Long and M. De Graef, "Lorentz Microscopy", Chapter in *Characterization of Materials*, ed. Kaufmann, Wiley-VCH, 1787-1801 (2012).
- C. Phatak, M. Pan, A.K. Petford-Long, S. Hong and M. De Graef, "Magnetic interactions and reversal of artificial square spin ices," *New Journal of Physics*, **14**, 075028 (2012).

In-Situ TEM Observations of Degradation Mechanisms in Next-Generation High-Energy Density Lithium-Ion Battery Systems

Shen J. Dillon, University of Illinois at Urbana-Champaign

Program Scope

Battery cycle life imposes severe cost limitations on the practical implementation of large battery packs such as those associated with electric vehicles or grid level storage. Improved insight into the fundamental mechanisms associated with battery degradation will inform strategies to extending their lifetime. A variety of potential degradation mechanisms exist and may have complex interactions with one another at the nanoscale. The need for dynamic experimental data at the nanoscale motivates our in-situ investigation of battery cycling in the electron microscope. We are working to characterize chemical, mechanical, and microstructural aspects of degradation in next generation Li-ion battery systems; such as high strain anode materials and high capacity cathode materials. This research involves three main components; in-situ cycling of high capacity electrodes in relevant commercial liquid electrolyte, characterization of electron beam effects in chemical environments to aid data analysis, and the development of novel in-situ environments.

Recent Progress

Our recent experiments focus on characterizing lithiation-induced strain accommodation in high capacity Sn-based electrodes, using in-situ techniques bridging multiple length scales (see Fig. 1 and Fig. 2). The reaction mechanism during initial lithiation was confirmed via x-ray computed tomography to be consistent with a 2-phase reaction front type mechanism, consistent with the phase diagram. For elastic-plastic response, such as observed in Si electrodes¹, there will be essentially no strain rate dependence for the occurrence of fracture². However, a significant strain rate

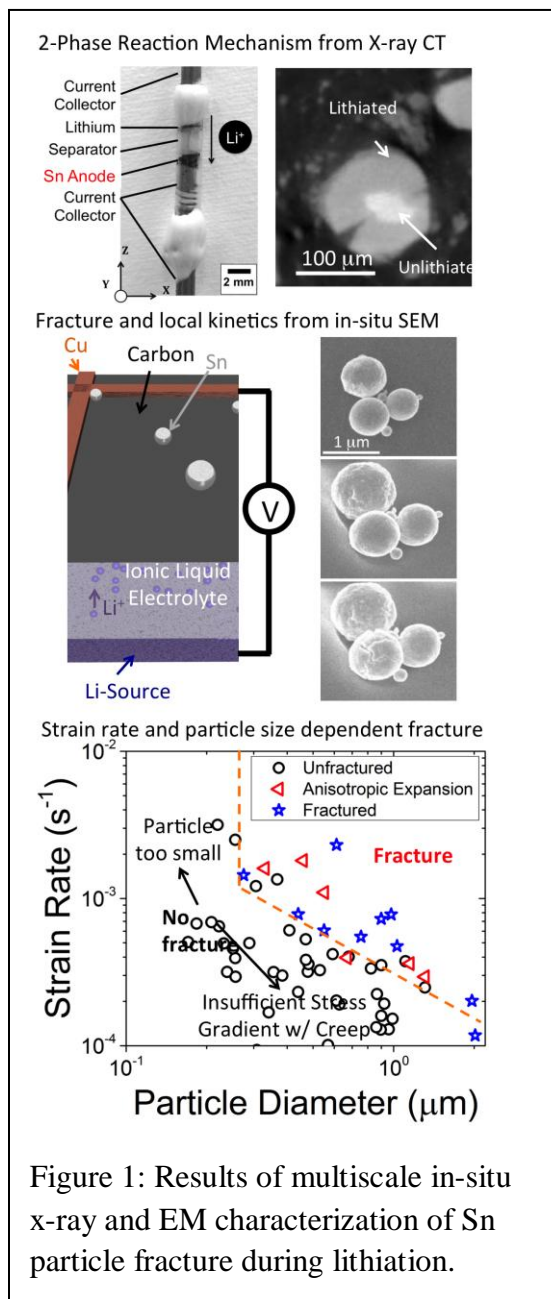


Figure 1: Results of multiscale in-situ x-ray and EM characterization of Sn particle fracture during lithiation.

dependence is observed in Sn electrodes and is correlated with the expected high creep compliance of the Sn-based materials at room temperature. Creep response has not previously been anticipated to be a governing factor in electrode mechanics and this is the first direct evidence of its importance.

Sn thin film electrodes were also observed during in-situ lithiation and delithiation in the commercially relevant ED:DMC 1M LiPF₆ environment. The length scales utilized here are too small to capture aspects of fracture behavior. However, details of interactions between the electrode and the electrolyte are clearly observed. Notably, porosity formation was observed during Li dealloying. The phenomena is associated with the enhanced surface diffusion of Sn in the liquid, which

enables surface diffusion to

mediate the tensile stresses evolved during delithiation. This phenomena is the surface analogue of Coble creep. The intensity change during delithiation correlates with the partial dissolution of the solid electrolyte interphase, which was confirmed via ex-situ characterization.

Temperature controlled platforms for environmental TEM studies are important for studying a diverse set of realistic materials and chemistry problems and extracting quantitative kinetics. We developed an environmental heating/cooling stage with electrochemical capabilities. The stage was demonstrated to characterize phase formation and the redistribution of solute and nanoparticles during crystallization of ice. The phenomena have broad implications in environmental, biological, chemical, and materials processes.

Initial application of this platform has been used to distinguish details of phase evolution during ice nucleation and growth that have been controversial for some time now. Specifically, we observe that cubic and hexagonal

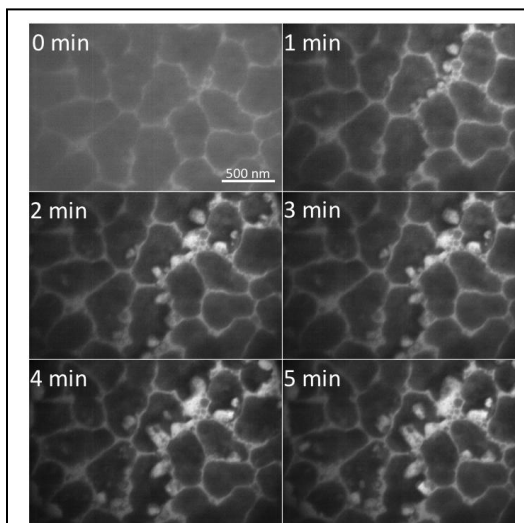


Figure 2: Time-lapse images depicting partial delithiation of a SnLi_x alloy at a constant voltage of 2.0 V.

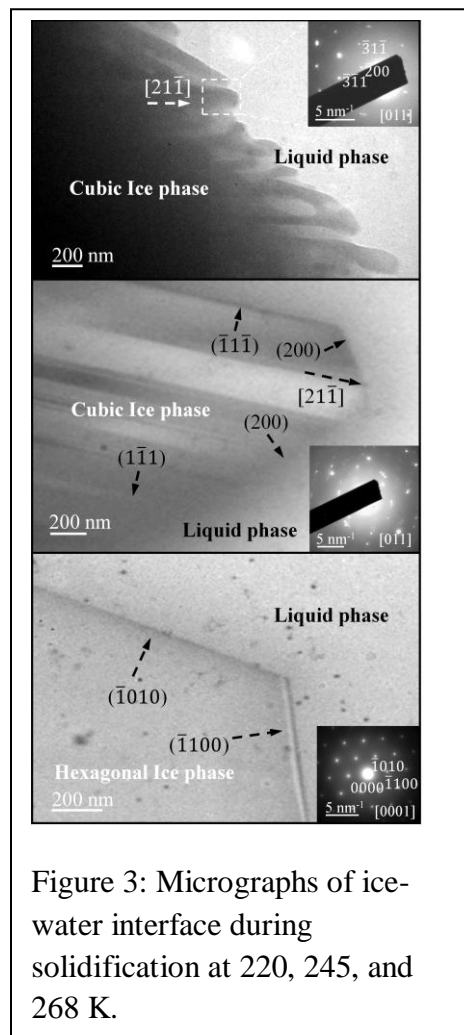
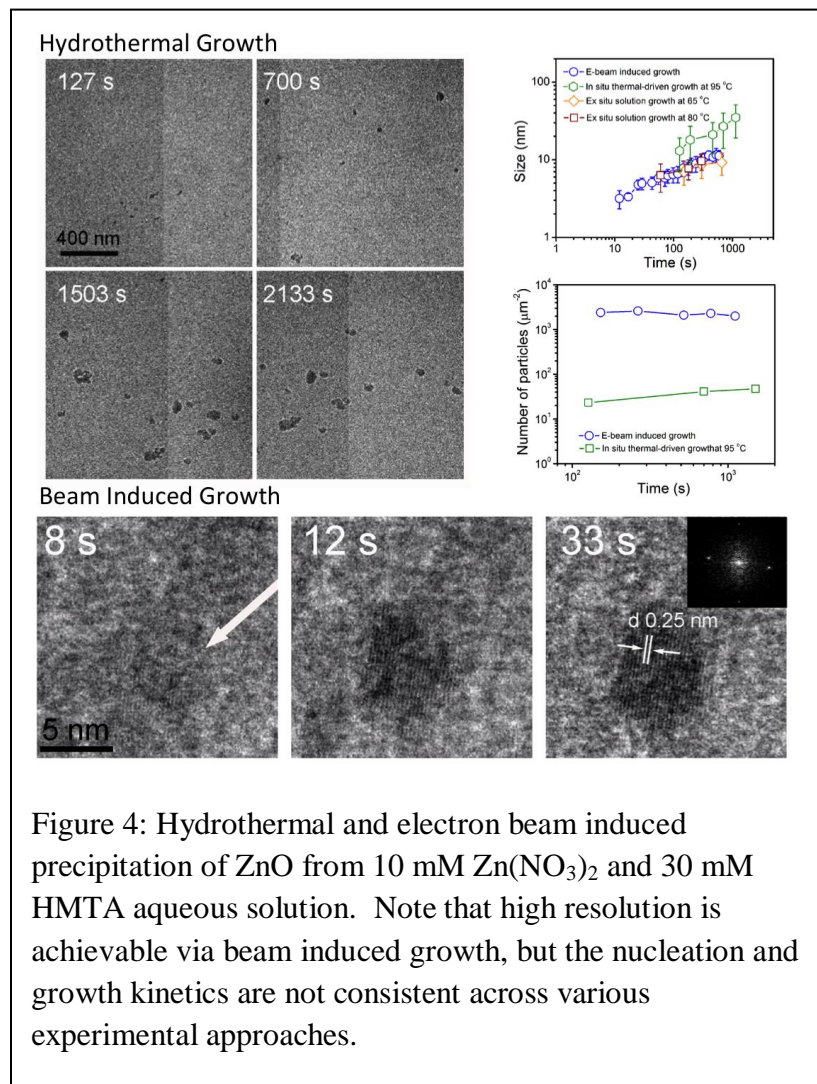


Figure 3: Micrographs of ice-water interface during solidification at 220, 245, and 268 K.

ice nucleate and grow separately and that one phase does not convert to the other during growth (Fig. 3).

In related experiments, we utilized sample heating to induce hydrothermal precipitation of ZnO from aqueous solutions under conditions of low beam current density, where no beam induced reactions occurred absent heating (Fig. 4). The results were quantitatively compared with beam induced precipitation from the same solution, and ex-situ hydrothermal precipitation. The results indicate that none of the experiments are in quantitative agreement, in terms of the nucleation and growth rates, due to confinement effects on liquid phase diffusion and particle aggregation.



Future Plans

Preliminary efforts have been made to characterize battery cycling, in-situ in the TEM, over multiple cycles. Many of the degradation processes critical to battery function do not occur until significantly into the cycle life of the electrode. We are currently designing improved in-situ testing configurations to more simply accommodate reliable characterization over multiple cycles.

References

¹Xiao Hua Liu, Li Zhong, Shan Huang, Scott X. Mao, Ting Zhu, and Jian Yu Huang, "Size-Dependent Fracture of Silicon Nanoparticles During Lithiation", *ACS Nano*, 6(2) 1522-1531 (2012).

²William H. Woodford, Yet-Ming Chiang, and W. Craig Carter, "Electrochemical Shock in Ion-Intercalation Materials with Limited Solid-Solubility," *Journal of The Electrochemical Society*, 160 (8) A1286-A1292 (2013).

Publications

1. K.-W. Noh, Y. Liu, L. Sun, and S.J. Dillon, "Challenges associated with in-situ TEM in environmental systems: The case of silver in aqueous solutions," *Ultramicroscopy*, 116, 34 (2012).
2. Y. Liu, X. Chen, K-W Noh, S.J. Dillon, "Electron beam induced deposition of silicon nanostructures from a liquid phase precursor," *Nanotechnology*, 23 385302 (2012).
3. K. Tai, T. Houlahan, J.G. Eden, and S.J. Dillon, "Integration of microplasma with transmission electron microscopy: Real-time observation of gold sputtering and island formation," *Scientific Reports*, 3, 1323 (2013).
4. B. Huang, K. Tai, and S.J. Dillon, "Structural evolution of α -Fe₂O₃ nanowires during lithiation," *J. Power Sources* 245 308 (2013).
5. Y. Liu, K. Tai and S.J. Dillon, "Growth kinetics and morphological evolution of ZnO precipitated from solution," *Chem. Mater.*, 25 2927 (2013).
6. K.-W. Noh, and S.J. Dillon, "Morphological changes in and around Sn electrodes during Li ion cycling characterized by in-situ environmental transmission electron microscopy," *Scripta Mater.*, 69 658 (2013).
7. K. Tai, Y. Liu, and S.J. Dillon, "In-situ cryogenic transmission electron microscopy for characterizing the evolution of solidifying water ice in colloidal systems," *Microscopy & Microanalysis*, 20 330 (2014).
8. B. Huang, K. Tai, M. Zhang, Y. Xiao and S.J. Dillon, "Comparative study of Li and Na electrochemical reactions with iron oxide nanowires," *Electrochimica Acta* 118 143 (2014).
9. K.W. Noh, K. Tai, S. Mao, and S.J. Dillon, "Grain Boundary Parting Limit during Dealloying," *Adv. Eng. Mater.* DOI: 10.1002/adem.201400179

The Nature of the Spin-Dependent Surface Chemical Bond: *The Role of Surface States*
Dan Dougherty, Department of Physics, North Carolina State University

Program Scope

Spin-dependent electronic interactions between molecular materials and magnetic surfaces are the decisive factor [1,2] permitting spin injection in new molecular spintronic devices [3]. Our program utilizes scanning tunneling microscopy and spectroscopy with special focus on spin polarized tunneling to directly observe spin dependent electronic coupling between single molecules and magnetic surfaces. The goal is to identify the types of interactions that optimize the formation of spin-polarized hybrid interface states [1] between the molecule and the magnetic electrode. This is achieved by comparative studies of different molecular structure motifs as well as different surface electronic structures.

Recent Progress

1.Organic Semiconductors on Magnetic Surfaces: PTCDA on Cr(001)

Several spin polarized STM studies have identified interactions between organic semiconductors and magnetic surfaces. These have focused primarily on molecules that have magnetic central ions (the phthalocyanines) that provide an active site for substrate interaction [4,5]. Our recent experiments have focused on molecules where the surface interaction may be more subtle (generally weaker) and yet device measurements have shown spintronic effects.

Particularly interesting is the case of perylene tetracarboxylic acid dianhydride (PTCDA) on Cr(001). The molecule has been recently observed to strongly modify the Shockley surface state derived from the bulk *sp* band on Ag(111) [6] and is thus a good candidate for creating new spin-dependent interfacial phenomena on Cr(001). Its covalent bonding to Ag(111) is through peripheral carbonyl oxygen atoms and a similar interaction is likely on Cr(001). This surface is chosen since it has a well-known pattern of in-plane surface magnetization reversals (see SPSTM image in Figure 1a) that can be used to directly assess coupling of adsorbates to different local spin directions in a single SPSTM image.

We have made several remarkable observations about this system. First, even a very low coverage of molecules on the Cr(001) surface, such as seen in Figure 1b, eliminates all observable spin contrast. It is unlikely that this small surface coverage can globally destroy the intrinsic surface magnetization pattern. Instead, we hypothesize that PTCDA molecules, have a strong tendency to coat the spin-polarized tip where magnetization is more delicate. This is an important technical challenge in spin polarized STM of relatively weakly-bound molecular adsorbates.

STM and STS studies of PTCDA/Cr(001) provide new insights about interfacial coupling. Near the Fermi level, the Cr(001) surface has a spin-polarized surface state [7] whose origin as a d_z^2 Shockley surface state or an "orbital" Kondo resonance has been debated in recent years [8]. At PTCDA adsorption sites on Cr(001), we find that this surface state is essentially *unperturbed* as shown in the STS spectra in Figure 1c. This observation favors an orbital Kondo

origin of the state since predominant d_z^2 symmetry would allow favorable overlap with p_z -derived frontier orbitals in the molecules. By contrast, the orbital Kondo resonance arise from a degenerate d_{xz}, d_{yz} orbitals that, by symmetry, have a non-bonding interaction with the molecular orbitals consistent with our observation of persistence of this state upon molecular adsorption.

In the STS spectra in Figure 1c, it is also clear that a molecular state exists at ~ 0.4 eV below the Fermi level (0 V) that is similar to the formerly unoccupied state for PTCDA on Ag(111) [6]. This similarity between Ag and Cr highlights an important fact to consider in the pursuit of efficient spin injection into organic semiconductor films: symmetry matching of electrode and molecular states is crucial and not all substrate states can hybridize with molecular states even if energy matching is good. We note in particular that for the planar PTCDA molecule efficient hybridization with the Cr sp band is implied by the direct similarities with Ag(111), but no evidence of hybridization with the d_{xz}, d_{yz} -derived surface state is observed.

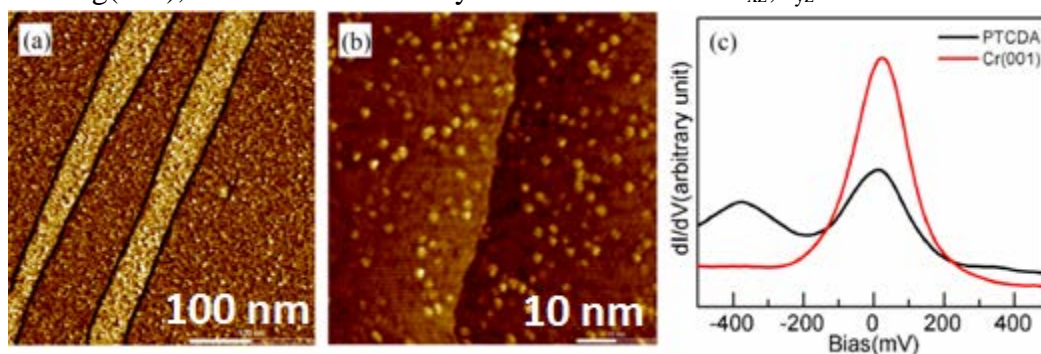


Figure 1. (a) SPSTM Conductance map of clean Cr(001) surface showing opposite magnetization direction (bright orange and dark orange) on adjacent terraces. (b) submonolayer coverage of PTCDA molecules on Cr(001) surface. No magnetic contrast has been observed at this coverage. (c) STS of PTCDA molecular sites and uncovered Cr(001) surface in the same local region.

2. Molecular Functionalization of Topological Insulator Surfaces

Our efforts to hybridize π electrons in organic semiconductors with magnetic surface states suggest an exciting new direction in magnetic molecule interactions with surfaces. The new class of materials known as topologically insulators (TI's) is characterized by surface states with well-defined "spin textures"[9] with spin constrained to be perpendicular to crystal momentum. This has the important consequence of suppressing backscattering from nonmagnetic surface impurities and has been proposed as a method to control spin transport in devices [10].

The integration of organic molecular materials with topological insulators has the advantage that planar aromatic molecules will easily wet the relatively inert topological insulator surfaces such as Bi_2Se_3 or Bi_2Te_3 driven by van der Waals interactions. In other words, weak intermolecular interactions are expected to be comparable in strength to interactions with the TI substrate surface. This leads to the likelihood of flat, continuous films suitable for device applications. We envision, for example, organic molecules as tunnel barriers to promote spin injection into TI materials for spintronics applications [10].

In the first project year, we directed significant effort to developing the materials science tools to explore these interesting spintronic interfaces. This has included new insights into complex, unexpected surface terminations (project publication 1) that will be useful in the future as a means of controlling spin-textured surface state properties to enhance electronic interactions with molecules. Initial work in on molecular films has identified a continuous wetting layer in films on F₄-TCNQ on Bi₂Se₃ that acts as a strong electron acceptor and partially removes the n-type doping in the that plagues bulk crystals (project publication 2) [11]. This indicates the general utility of the molecular approach to controlling TI surfaces and has been a proving ground for further molecular interface creation.

Our primary interest in exploring TI surfaces functionalized with molecules is as a special example of spin-dependent interfacial electronic interactions. We describe two important fundamental STM and SPSTM experiments in the Future Plans section below that will address directly the spin dependent interactions between these novel surface states and organic molecules.

Future Plans

1.SPSTM of Molecular Adsorbates: Bulk Cr tips for enhanced in-situ processing

Based on our experience with PTCDA on Cr(001), it is crucial to enhance in-situ processing of spin polarized STM tips during experiments to remove interfering molecules that have migrated to the tip. This is essentially impossible with Fe-coated tungsten tips currently in use since tip processing tends to remove or degrade the magnetic Fe coating.

We have started to etch bulk Cr tips in KOH using a Au wire counter electrode that will allow unlimited in-situ tip processing. If we can remove PTCDA molecules from magnetic tips, we will be able to add spin polarization to our characterization of PTCDA/Cr(001) interfacial hybridization. In turn, we will then be able to identify if the mixing with the *sp* bulk band has any magnetic impact on the nonmagnetic molecule. In addition, we will gain new access to out-of-plane magnetization directions near molecules due to the canted tip magnetization [12]. This will be important for measuring other molecules, with strong magnetic anisotropies.

2.Scattering and SPSTM of Controllable Paramagnets on TI Surfaces

We are particularly enthusiastic about identifying the magnetic consequences of molecular adsorption on TI surfaces. We note that many traditional magnetic surfaces are highly chemically reactive. This may lead to complex dissociative molecular adsorption processes. By contrast, TI surfaces are chemically relatively inert and we expect to maintain molecular functionality for most molecular adsorbates.

As part of this program we will be able to test important predictions related to scattering on TI surfaces with molecular adsorbates. First, we will take advantage of the tendency for molecules to aggregate on step edges on surfaces where they are mobile. On a TI surface suppressed backscattering results in a decay envelope for scattered surface state electrons from steps that is faster than the $1/\sqrt{x}$ found for typical surface states on metals [13]. An example of this scattering is shown in a conductance map for a Bi₂Te₃ surface in Figure 2a. If we adsorb

magnetic molecules such as Manganese Phthalocyanine at the step, the decay envelope will be changed from the rapid decay on TI's to the more typical decay and thus be direct evidence of the molecule-induced opening of the backscattering channel.

Apart from this step scattering envelope, calculations have predicted that *only* a spin polarized scattering experiment will be able to sense the impact of a local moment on allowed surface scattering wave vectors [14]. We will also test this prediction by applying SPSTM to magnetic molecules on TI surfaces. Using our routine SPSTM capability to first confirm tip polarization by SPSTM imaging of Cr(001), we will provide new information about topological surface state scattering from magnetic impurities. Molecular systems such as the phthalocyanines are particularly suited to systematic studies here because their molecular magnetic moment can be varied from $S=3/2$ (MnPc) to $S=0$ (ZnPc) with only minor changes to the molecular π system driving adsorption energetics.

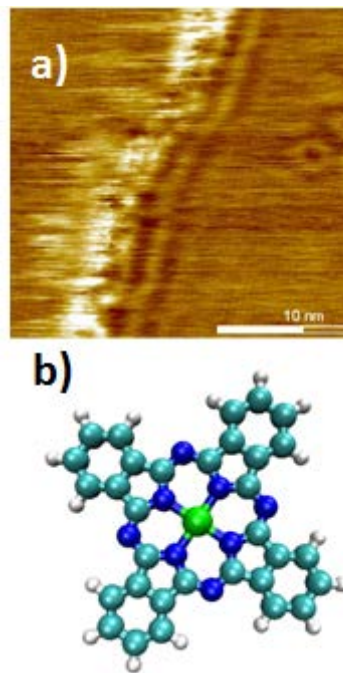


Figure 2. a) Differential conductance map showing surface state scattering from a Bi_2Te_3 step; structure of phthalocyanine molecules, MPc, where the central metal ion M (in green) may be varied from Mn to Zn to change the spin of the molecule.

References

- [1] Barraud et al., Nat. Phys. 6, 615 (2010).
- [2] Galbiati et al., MRS Bulletin 39, 602 (2014).
- [3] Sanvito, S. Chem. Soc. Rev. 40, 3336 (2011).
- [4]Iacovita et al., Phys. Rev. Lett. 101, 116602 (2008).
- [5]Brede et al., Phys. Rev. Lett. 105, 047204 (2010).
- [6] Temirov et al., Nature 444, 350 (2006).
- [7]Wiesendanger, Rev. Mod. Phys. 81, 1495 (2009).
- [8] Hänke et al., Phys. Rev. B 72, 085453 (2005).
- [9] Ando, J. Phys. Soc. Jpn. 82, 102001 (2013).
- [10] Ojeda-Aristizabal et al., Appl. Phys. Lett. 101, 023102 (2012).
- [11] Kim et al, Nat. Phys. 8, 459 (2012).
- [12] Schlenhoff et al, Appl. Phys. Lett. 97, 083104 (2010).
- [13] Biswas and Balatsky, Phys. Rev. B 83, 075439 (2011).
- [14] Guo and Franz, Phys. Rev. B 81, 041102R (2010).

Publications citing DOE-BES support 2013-2014

- 1) Andrew S. Hewitt, Jingying Wang, Jon Boltersdorf, Paul A. Maggard and Daniel B. Dougherty, “Coexisting Bi and Se surface terminations of cleaved Bi_2Se_3 single crystals”, J. Vac. Sci. Technol. B 32, 04E103 (2014).
- 2) Jingying Wang, Andrew S.Hewitt, Raj Kumar, Jon Boltersdorf, Tianshuai Guan, Frank Hunte, Paul A.Maggard, Joseph E.Brom, Joan M.Redwing, Daniel B.Dougherty, “Molecular Doping Control at a Topological Insulator Surface: $\text{F}_4\text{-TCNQ}$ on Bi_2Se_3 ” J. Phys. Chem. C 118. 1486 (2014).

Quantum control of spins in diamond for nanoscale magnetic sensing and imaging

Gurudev Dutt, Dept. of Physics & Astronomy, University of Pittsburgh

Program Scope

The goal of this research is to develop a magnetic field imaging technique with nanoscale resolution that would allow for non-invasive, non-destructive probing of a variety of important physical phenomena such as quantum tunneling in single molecule magnets and quantum bits encoded into spins in quantum dots. Diamond single spin magnetic sensors are a highly promising material platform featuring high magnetic field sensitivity, nanometer spatial resolution and the important ability to operate under ambient or harsh environmental conditions required to study many material systems. The proposed work will take a multi-faceted approach toward improving the accuracy, sensitivity and robustness of this platform through a unique combination of fundamental investigations into quantum control and precision quantum metrology coupled tightly to innovative design, sophisticated nano-fabrication and advanced measurement techniques.

Recent Progress

(i) Dual-channel lock-in magnetometer: The nitrogen-vacancy (NV) defect center in diamond shows great promise as an ultra-sensitive solid-state magnetometer and magnetic imager because it features potentially atomic-scale resolution, wide temperature range operation from 4 K -- 700 K, and long coherence times that allow for high magnetic field sensitivity.

Magnetometry with diamond spin sensors detects the frequency shift of the NV spin resonance caused by the magnetic field via the Zeeman effect. Highly sensitive quantum sensing techniques use multi-pulse dynamical decoupling (DD) sequences that are tuned to the frequency of a time-dependent field. The resulting fluctuating frequency shift is rectified and integrated by the pulse sequence to yield a detectable quantum phase, while effectively filtering out low frequency noise from the environment.

However, these state of the art quantum sensing methods also have significant drawbacks: the dynamic range is limited by the quantum phase ambiguity, the sensitivity is a highly nonlinear function of field amplitude requiring prior knowledge of a working point for accurate deconvolution, and the classical phase of the field has to be carefully controlled to obtain accurate field amplitude.

In our work, we presented an experimental method that incorporates the DD sequences with phase estimation algorithms (PEA) to address these fundamental problems. Our dual-channel lock-in magnetometer has linearized field readout and nearly decoherence-limited constant sensitivity, while offering significantly greater dynamic range. We demonstrated unambiguous reconstruction of the amplitude and phase of the magnetic field without prior knowledge of either value. Finally, we showed that our technique can be applied to measure random phase jumps in the magnetic field, and to obtain phase-sensitive field frequency readout. Fig. 1 summarizes one of the key results from our publication [1].

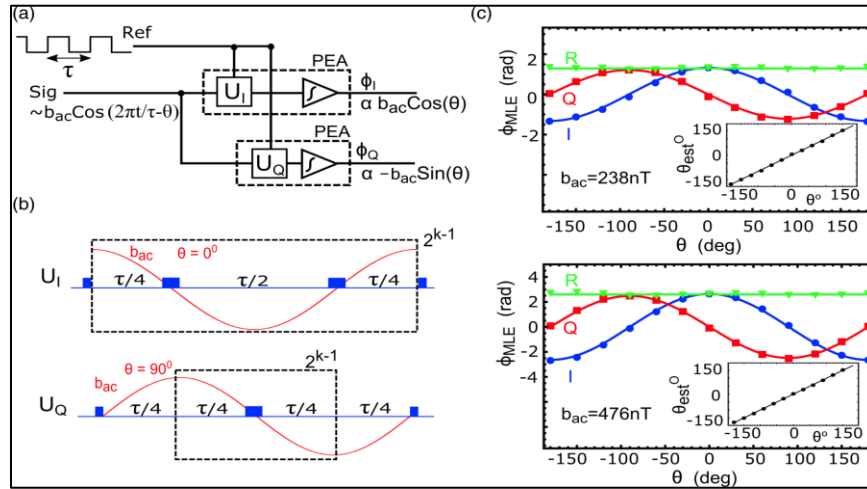


Figure 1: (a) Schematic illustration of the quantum dual-channel lock-in magnetometer. Via unitary evolution of the single spin, the applied magnetic field is multiplied with the lock-in reference signal set by the DD pulse sequences. The PEA is implemented for each channel as before to linearize the readout and yield the I and Q quantum phases. (b) DD pulse sequences for U_I and U_Q . (c), (d) Data for ϕ_I and ϕ_Q as θ is varied for different values of $b_{ac} = 238(476)$ nT. The estimator ϕ_R remains constant throughout; solid lines represent ideal sensing. Inset: Data for θ_{est} as a function of θ ; solid line represents ideal case $\theta_{est} = \theta$.

(ii) Optimization of phase estimation algorithms:

The essential idea of quantum probes is to detect a frequency shift $\delta\nu$ in the probe resonance caused by the external perturbation to be measured. The standard method to do this with maximum sensitivity is the Ramsey interferometry scheme.

The phase (or field) sensitivity in NV magnetometry is obtained by assuming that the quantum phase has been well localized between the values $(\varphi - \pi/2, \varphi + \pi/2)$, where φ is the actual quantum phase value, and in practice to much better than this by making a linear approximation to the inverse sinusoidal Ramsey distribution. Thus,

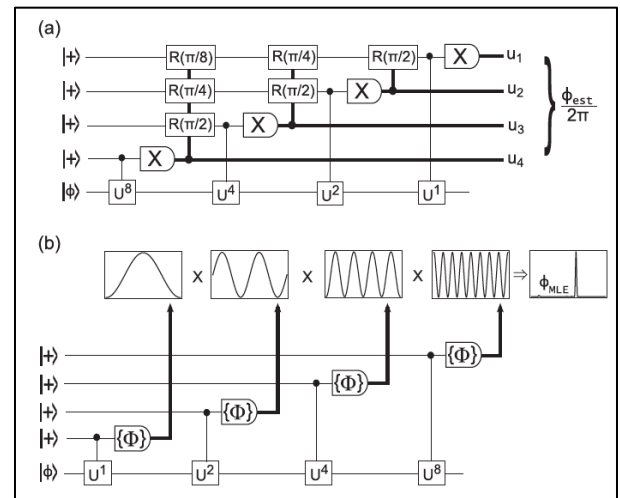


Figure 2: Quantum circuit diagrams: (a) QPEA, (b) NAPEA for the case $K = 4$. The dark lines represent the classical bits.

prior knowledge of the “working point” of the quantum sensor is key to obtaining the high sensitivity that makes the sensors attractive. When the actual phase φ is allowed to take the full range of values, then the quantum phase ambiguity (i.e., the multivalued nature of the inverse cosine function) results in much larger phase variance than predicted by the standard methods. To overcome the quantum phase ambiguity, we require an estimator φ_{est} that can achieve high precision (small phase variance) over the entire phase interval $(-\pi, \pi)$. In terms of field sensing, this translates to increasing the dynamic range for magnetometry.

Recently, phase-estimation algorithms (PEA) were implemented experimentally by our group with electron spin qubit in diamond to address this dynamic range problem. Fig. 2 shows the quantum circuit diagrams of the PEAs that were implemented. However, several questions remained about the exact nature of the improvement, and what were the optimal conditions for the PEA. In our work (publication [2]), we carried out detailed theoretical and numerical study discussing the application and optimization of the PEAs. We elucidated the importance of dynamic range to Ramsey magnetic imaging with diamond spins, and introduced the application of PEAs to time-dependent magnetometry. Some of the questions that we addressed in our work, and have not been studied earlier, include (i) the importance of control phases in the PEA, (ii) the dependence of sensitivity on the control phases, (iii) the dependence of sensitivity on the dynamic range, and (iv) the impact of measurement fidelity on the PEAs.

Fig. 3 shows results from our simulations, with only inputs as parameters taken from experimental data such as the evolution time, measurement fidelity and dephasing time. We compare standard Ramsey magnetometry, the non-adaptive PEA (NAPEA), and quantum PEA (QPEA) incorporating error checking. Our results show that the NAPEA requires lower measurement fidelity, has better dynamic range, and greater consistency in sensitivity.

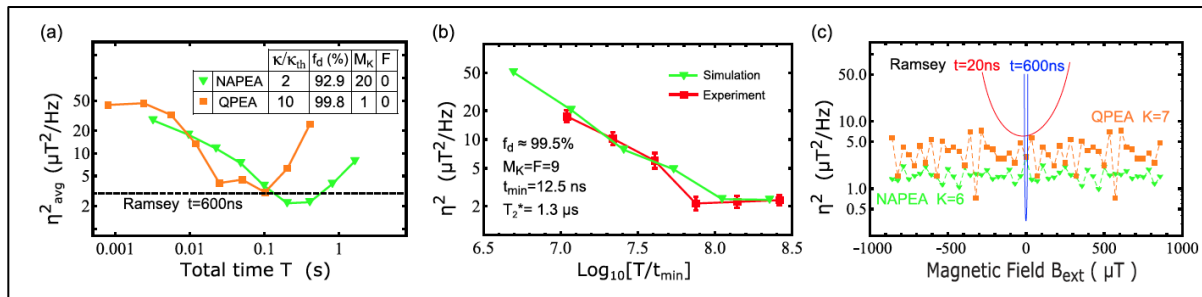


Figure 3: Magnetic field sensitivity. (a) Field sensitivity $\eta^2 = (\delta B)^2 T$ averaged over many different fields with the number of resources. The resources are increased by the increment of K and given in units of time. The best cases obtained from QPEA and NAPEA are compared with the optimum Ramsey sensitivity averaged over its full field range. (b) Field sensitivity with unitless number of resources $N = T/t_{\text{min}}$. The simulation here was performed with the exact experimental conditions and is in good agreement with experimental results. (c) The NAPEA sensitivity is roughly constant throughout the full field range, whereas QPEA sensitivity is not. The red (blue) curves show theoretical limits of Ramsey sensitivity for $t = 20 \text{ ns}$ ($t = 600 \text{ ns}$).

Future Plans

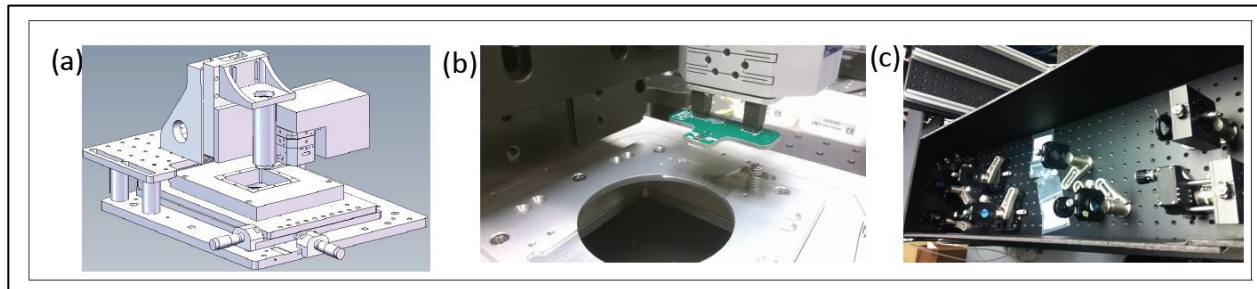


Figure 4 (a) Schematic design of the diamond QSM setup. (b), (c) Photographs of the assembled SPM, with combined confocal/SPM modes for exploring nanoscale spin physics.

A primary goal of our project was to build a quantum spin microscope with NV centers in diamond tips for the purpose of magnetic imaging to explore nanoscale spin physics. We have received all major components for the diamond QSM, and assembled together. The confocal optical setup for the diamond QSM has also been put together and are both shown in Figure 4. The next phase is to test the AFM and the optical setup together, and to take simultaneous AFM and confocal images of magnetic nanostructures and nanoparticles. Initially, we will use nano-diamonds instead of diamond tips, as they are easier to work with. Our fabrication of diamond tips is also in progress.

Publications (since 2012):

1. N. M. Nusran, M. V. Gurudev Dutt, "A Dual-Channel Lock-in Magnetometer with a Single Spin in Diamond", *Phys. Rev. B*, 88, 2201410R (2013)
2. N. M. Nusran, M. V. Gurudev Dutt, "Optimizing phase estimation algorithms for diamond spin magnetometry", *Phys. Rev. B*, 90, 024422(2014)

Time-resolved electrical, optical, and thermal probes of topological spin textures in magnetic nanostructures

Gregory Fuchs, Cornell University Applied & Engineering Physics, Ithaca, NY

Program Scope

The aim of this research is to investigate the interplay between charge, spin, heat, and light on the *dynamics* of nanoscale, topological spin textures. The prime example of a topological spin texture is a magnetic skyrmion, which is a “vortex-like” magnetic texture where the local magnetization vector can be topologically mapped to an outward facing vector on the surface of a sphere [1, 2] (Fig. 1). The topological nature of these magnetic textures makes them “particle-like” and gives them both protection from defects and extremely low critical current density for motion under spin-transfer torques [3, 4]. These remarkable properties, along with their nanoscopic extent (5 – 70 nm), makes them interesting for ultra-low power control of information at the nanoscale [5, 6].

Pioneering experiments [1, 2, 4, 7, 8] have revealed the robust magnetic phase space available for skyrmions and that skyrmion lattices move under applied current densities of $J_c \sim 10^2 \text{ A/cm}^2$. This compares very favorably, for example, to the spin-torque driven motion of a magnetic domain wall, which typically moves in a current density of $J_c \sim 10^7 \text{ A/cm}^2$ [9]. Additionally, micromagnetic simulation indicates that skyrmions are robust to motion through channels with imperfections [5, 6].

We will address the following basic science questions about the behavior and the dynamics of magnetic skyrmions:

1. How can we isolate and control single skyrmions and skyrmion lattices at the nanoscale?
2. What are the dynamics of skyrmion motion in nanostructures, particularly under applied magnetic fields, electrical currents, and thermal gradients?
3. How are the dynamics of individual skyrmions distinct from the dynamics of skyrmion lattices?
4. How does the topological spin texture of skyrmions influence electrical and thermal transport beyond the Hall Effect, including the Seebeck Effect and the Nernst Effect?
5. What new dynamical properties emerge because of the topological nature of skyrmions?

Recent Progress

This program has been active for only one month, and thus we are in the early stages of the research. We are the fabrication procedure for nanoscale magnetic wires that have widths comparable with the skyrmion diameter (<100 nm), enabling single skyrmions to be isolated and

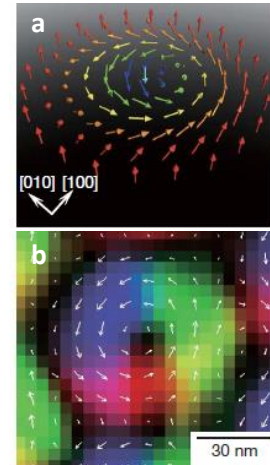


Fig. 1(a). Vector map of magnetization in an individual skyrmion. (b) Lorentz TEM image of an individual skyrmion in FeCoSi, taken from Ref. 2.

controlled. This geometry, which naturally lends itself to electrical measurements, also enables fully-electrical ferromagnetic resonance experiments. It also enables investigations into their behavior at boundaries and edges. Figure 2 (a) and (b) show scanning electron microscope and optical microscope images, respectively, of magnetic Hall devices fabricated in our group.

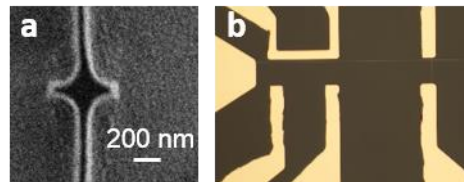


Fig. 2 (a) SEM image of a 30 nm thick, 100 nm wide magnetic nanowire with an 'anti-notch.' (b) Optical microscope image of a 200 nm magnetic nanowire with the "Hall cross" geometry, electrical contact, and microwave antenna for RF stimulation.

Future Plans

We plan to extend our fabrication procedure to enable Lorentz contrast transmission electron microscopy of electrically contacted nanoscale magnetic devices. These devices will be fabricated on thin (<50 nm) Si/SiN membranes. We will then combine experiments with Lorentz contrast electron microscopy and electrical transport to examine skyrmion dynamics in confined geometries.

References

- ¹ S. Mühlbauer, B. Binz, F. Joniez, C. Pfleiderer, A. Rosch, A. Neubauer, R. Georgii, and P. Böni, "Skyrmion Lattice in a Chiral Magnet," *Science* **323**, 915 (2009).
- ² X. Z. Yu, Y. Onose, N. Kanazawa, J. H. Park, J. H. Han, Y. Matsui, N. Nagaosa, and Y. Tokura, "Real-space observation of a two-dimensional skyrmion crystal." *Nature* **465**, 901 (2010).
- ³ F. Jonietz *et al.*, "Spin Transfer torques in MnSi at Ultralow Current Densities." *Science* **330**, 1648 (2010).
- ⁴ X. Z. Yu, N. Kanazawa, W. Z. Zhang, T. Hara, K. Kimoto, Y. Matsui, Y. Onose, and Y. Tokura, "Skyrmion flow near room temperature in ultralow current density." *Nat. Comm.* **3**, 988 (2012).
- ⁵ J. Iwasaki¹, M. Mochizuki and N. Nagaosa, "Current-induced skyrmion dynamics in constricted geometries." *Nat. Nano.* **8**, 742 (2013).
- ⁶ A. Fert, V. Cros, and J. Sampaio, "Skyrmions on the Track." *Nat. Nano.* **8**, 152 (2013).
- ⁷ T. Schulz *et al.*, "Emergent electrodynamics of skyrmions in a chiral magnet." *Nat. Phys.* **8**, 201 (2012).
- ⁸ S. X. Huang and C. L. Chien, "Extended skyrmion phase in epitaxial FeGe(111) thin films." *Phys. Rev. Lett.* **108**, 267201 (2012).
- ⁹ G. S. D. Beach, M. Tsoi, and J. L. Erskine, "Current-induced domain wall motion." *JMMM* **320**, 1272 (2008).

This is a new project started in 2014

Polarization-coupled tunable resistive behavior in oxide ferroelectric heterostructures

Alexei Gruverman¹ (PI), Chang-Beom Eom² and Evgeny Tsymbal¹

¹Department of Physics and Astronomy, University of Nebraska, Lincoln, NE 68588

²Department of Materials Science and Engineering, University of Wisconsin, Madison, WI 53706

E-mail: agruverman2@unl.edu

Program Scope

Strong interest in resistive switching phenomena is driven by a possibility to develop electronic devices with novel functional properties not available in conventional systems [1]. Bistable resistive devices are characterized by two resistance states that can be switched by an external voltage. Recently, memristors – electric circuit elements with continuously tunable resistance - have emerged as a new concept for nonvolatile memories and adaptive electronic circuit elements [2, 3]. Most of the existing memristor prototypes involve transition metal oxide layers where conductive filaments formation and/or the interface contact resistance control the memristive behavior. In this research we plan to implement the idea and investigate the mechanism of electrically and mechanically tunable nonvolatile resistive behavior in oxide ferroelectric heterostructures realized via polarization-coupled electroresistance effect and metal-insulator (M-I) transitions at oxide interfaces. We focus on investigating the effect of interface engineering on polarization-coupled electroresistance effect and metal-insulator (M-I) transitions to achieve nonvolatile and tunable resistance behavior in oxide ferroelectric heterostructures.

Recent Progress

At this stage of research, we are focusing on stabilization of ferroelectric polarization at the interface with semiconducting oxides, such as Nb-doped SrTiO₃ and other semiconductors. Semiconducting materials have a longer screening length as compared to metals and thus using them as electrodes in ferroelectric tunnel junctions (FTJs) may diminish ferroelectric stability. In particular, the incomplete screening of the depolarizing field in thin-film ferroelectrics and the presence of asymmetric interfaces may lead to the electric field reducing and/or pinning the ferroelectric polarization. A proper choice of the *interface termination* may, however, reduce this effect making the ferroelectric polarization switchable. Our recent first-principles calculations have demonstrated the effect of switchable polarization in electron-doped BaTiO₃ (*n*-BaTiO₃) on electronic and transport properties of the SrRuO₃/*n*-BaTiO₃ (001) interface. We found that ferroelectric polarization controls the accumulation or depletion of electron charge at the interface. For polarization pointing towards the SrRuO₃ metal the contact is metallic (Ohmic), whereas for polarization pointing away from the SrRuO₃ metal the contact exhibits a Schottky barrier. This leads to a five orders in magnitude change in the interface resistance. The associated interface resistances are $5.5 \times 10^2 \Omega \mu\text{m}^2$ for the Ohmic contact and $3.78 \times 10^7 \Omega \mu\text{m}^2$ for the Schottky contact [4].

We have expanded these studies to explore a possibility to control transport spin polarization by ferroelectric polarization. It is known that SrRuO₃ displays robust ferromagnetism

below the Curie temperature of about 160K. Using first-principles density functional calculations, we explored the effect of ferroelectric polarization switching on spin-polarized transmission across the SrRuO₃/*n*-BaTiO₃ interface. The interface transmission was calculated using a general scattering formalism implemented in the QUANTUM ESPRESSO code. Spin-polarization of the ballistic transmission was defined as $SP = (T_{\uparrow} - T_{\downarrow}) / (T_{\uparrow} + T_{\downarrow})$, where T_{\uparrow} and T_{\downarrow} and transmission functions for majority- and minority-spin electrons respectively. Figs. 1(a-d) show k_{\parallel} -resolved spin-dependent transmission, indicating that reversal of ferroelectric polarization results in a large resistance difference between Schottky and Ohmic conductance regimes, consistent with our non-spin-polarized calculations [1]. Figures 1 (c) and 1 (f) show spin-polarization distributions in the 2D Brillouin zone for each contact regime. In both cases the spin polarization is negative. When ferroelectric polarization is pointing to the interface the contact is Ohmic and the average spin polarization is -65% (Fig. 1 (e)). When the ferroelectric polarization is pointing away from the interface the contact is Schottky, the spin-polarization in this case is negatively enhanced to -98% (Fig. 1 (f)). This remarkable change in the spin polarization of the transmission across the interface driven by ferroelectric polarization reversal could provide an interesting mechanism to electrically control spin injection into semiconductor-based spintronic devices.

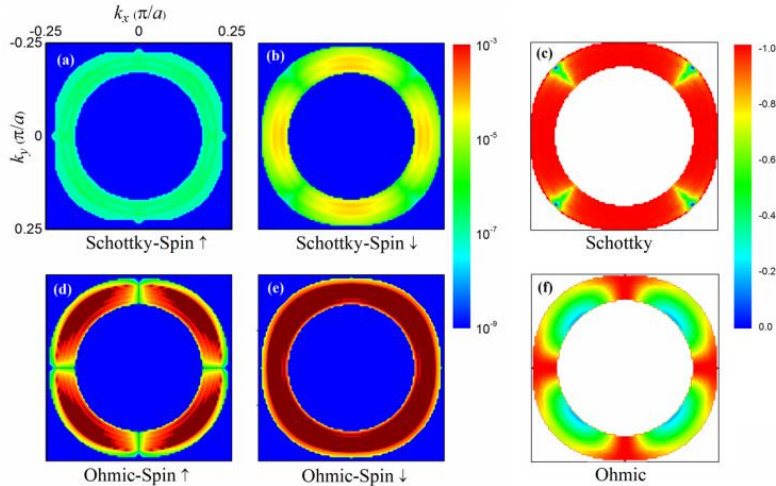


Figure 1. Calculated k_{\parallel} -resolved spin-dependent transmission (a-e) and spin-polarization (c, f) across the SrRuO₃/*n*-BaTiO₃ (001) interface in the 2D Brillouin zone.

It is known that the formation and retention of spontaneous polarization in thin ferroelectric films depend strongly on the properties of interfaces and involves a complex combination of interfacial chemistry, electrical screening and mechanical strain. Our recent studies also have shown that the film-electrode interface properties play a critical role in the TER effect resulting in tunable resistivity [4, 5]. To build up on this finding, we carried out interface engineering through the introduction of molecular layers (MLs) at the interface between the ferroelectric layer and graphene, which is used as a top electrode of a FTJ. A molecular layer forms during the transfer of graphene to the ferroelectric surface in different solvents. The 10×30 μm² graphene patches were fabricated by a combination of e-beam lithography and reactive ion etching on the SiO₂/Si wafer, which was subsequently spin-coated by PMMA and placed on the surface of HF solution to etch

away SiO₂. Introduction of the molecular layer at the graphene/BaTiO₃ interface was achieved by washing the PMMA/graphene film in a specific solution followed by its transfer to the BaTiO₃ surface after which the PMMA layer was removed by acetone.

The resistive switching behavior has been characterized by measuring the current-voltage (I-V) characteristics of the FTJs as a function of their polarization state using the conductive AFM (C-AFM) approach. Figure 2(a) shows the I-V curves measured after complete switching of the BaTiO₃ polarization either up or down by applying the +/-4 V voltage pulses. It is seen that there is a giant resistance change upon polarization reversal: the OFF/ON ratio $R_{\text{OFF}}/R_{\text{ON}}$ reaches a factor of more than 3300 in the zero-bias limit and can be as large as 6000 for the bias range of ± 0.2 V (Fig 2(b)). This effect is much stronger than that reported earlier for bare BaTiO₃ films of the same thickness (6 u.c.) with the TER magnitude of about 7. The observed effect is highly reproducible and stable: the I-V curves measured at different locations on the surface of the graphene patch display similar behavior and show no degradation with time within the period of polarization stability. In addition, C-AFM measurements performed on several different samples show little junction-to-junction variations. The obtained results suggest that the electrode/ferroelectric interface properties play a crucial role in the polarization-induced resistive switching behavior in FTJs. Introduction of the molecular layer at the graphene/BaTiO₃ interface not only stabilizes the polarization of BaTiO₃ but also significantly enhances the TER effect.

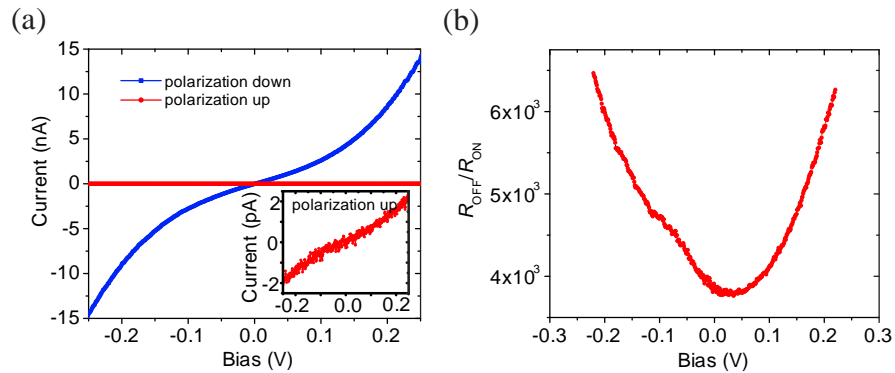


Figure 2. Electroresistance effect in the Gr/ML/BTO/LSMO junctions. (a) The I-V curves measured for the upward (red) and downward (blue) BaTiO₃ polarization states. The inset shows the rescaled I-V curve for the upward polarization state. (b) $R_{\text{OFF}}/R_{\text{ON}}$ resistance ratio as a function of the reading bias showing an increase of up to 6000 for ± 0.2 V read out voltage range. PFM testing of polarization after I-V measurements shows that polarization is not affected by the I-V measurements.

Future plans

1. Investigate mechanically-induced tunable resistive switching in ferroelectric tunnel junctions in conjunction with theoretical simulations.
2. Investigate the effect of the engineered interface parameters (thickness, termination structure, bonding chemistry, band-gap, etc) on resistive switching behavior.
3. Compute the changes in the tunneling conductance across the systems with the engineered interfaces.

References

1. R. Waser and M. Aono, "Nanoionics-Based Resistive Switching Memories", *Nat. Mat.* **6**, 833-840 (2007).
2. L. Chua, "Resistance switching memories are memristors", *Appl. Phys. A.* **102**, 765-783 (2011).
3. D. B. Strukov, G. S. Snider, D. R. Stewart, and R. S. Williams, "The missing memristor found", *Nature* **453**, 80-83 (2008).
4. X. Liu, Y. Wang, J. D. Burton, and E. Y. Tsymbal, "Polarization controlled Ohmic to Schottky transition at a metal/ferroelectric interface," *Phys. Rev. B* **88**, 165139 (2013).
5. D. J. Kim, H. Lu, S. Ryu, C. W. Bark, C. B. Eom, E. Y. Tsymbal, A. Gruverman, "Ferroelectric Tunnel Memristor", *Nano Lett.* **12**, 5697-5702 (2012).

Publications

1. D. J. Kim, H. Lu, S. Ryu, C. W. Bark, C. B. Eom, E. Y. Tsymbal, A. Gruverman, "Ferroelectric Tunnel Memristor", *Nano Lett.* **12**, 5697-5702 (2012).
2. H. Lu, D. J. Kim, C. W. Bark, S. Ryu, C. B. Eom, E. Y. Tsymbal, and A. Gruverman, "Mechanically-Induced Tunneling Electroresistance Effect in Ultrathin Ferroelectrics", *Nano Lett.* **12**, 6289-6292 (2012).
3. H. Lu, T. A. George, Y. Wang, I. Ketsman, J. D. Burton, C. W. Bark, S. Ryu, D. J. Kim, J. Wang, C. Binek, P. A. Dowben, A. Sokolov, C. B. Eom, E. Y. Tsymbal, and A. Gruverman, "Electric Modulation of Magnetization at Ferroelectric - Ferromagnetic Interfaces", *Appl. Phys. Lett.* **100**, 232904 (2012).
4. X. Liu, Y. Wang, J. D. Burton, and E. Y. Tsymbal, "Polarization controlled Ohmic to Schottky transition at a metal/ferroelectric interface," *Phys. Rev. B* **88**, 165139 (2013).
5. A. Stamm, D. J. Kim, H. Lu, C. W. Bark, C. B. Eom, and A. Gruverman, "Investigation of Polarization Relaxation Kinetics in Ultrathin Ferroelectric Capacitors", *Appl. Phys. Lett.* **102**, 092901 (2013).
6. S. Cao, P. Liu, J. Tang, H. Lu, C. W. Bark, S. Ryu, C. B. Eom, A. Gruverman, and P. A. Dowben, "Magnetoelectric coupling at the EuO/BaTiO₃ interface", *Appl. Phys. Lett.* **102**, 172402 (2013).
7. D. J. Kim, H. Lu, S. Ryu, S. Lee, C. W. Bark, C. B. Eom and A. Gruverman, "Retention of Resistance States in Ferroelectric Tunnel Memristors", *Appl. Phys. Lett.* **103**, 142908 (2013).
8. X. Liu, J. D. Burton and E. Y. Tsymbal, "Electric control of spin injection into a ferroelectric semiconductor," submitted to *Physical Review Letters* (2014).
9. H. Lu, A. Lipatov, S. Ryu, D. J. Kim, M. Y. Zhuravlev, C. B. Eom, E. Y. Tsymbal, A. Sinitskii, and A. Gruverman, "Ferroelectric Tunnel Junctions with Graphene Electrodes: Critical Role of the Interfacial Layer", in preparation.

Understanding microscopic mechanisms of spin pumping and magnetization dynamics in novel, tailored magnetic material systems

P. Chris Hammel, Department of Physics, Ohio State University, Columbus OH

Program Scope

Spin pumping—the transport of spin angular momentum into neighboring material from a ferromagnet (FM) driven out of equilibrium by microwave excitation—is receiving a great deal of attention because of its potential technological importance and the richness and breadth of the science involved. A powerful diagnostic for spin pumping is the transfer of energy from the precessing magnetization that accompanies the angular momentum transport. This energy transfer is evident in measurements of the damping of the mode, damping which is in addition to the better understood intrinsic damping. This damping is unusual because it is *non-local* making it an exciting scientific topic in its own right. The mechanisms underlying conventional, local damping, including Gilbert-damping and spin wave emission, in which excited ferromagnetic magnetization relaxes toward thermal equilibrium, have been extensively studied in bulk ferromagnets and individual FM films. Non-local damping has been observed as an additional damping that results when a metallic FM is located near normal metal in layered structures; this additional damping is associated with transfer of angular momentum to the neighboring material. There is now broad agreement that spin pumping (transfer of angular momentum) and enhanced damping are two aspects of the same phenomenon. In metallic FM/NM bilayer and multilayer systems in which itinerant electrons interact across a transparent (to charge and spin transport) interface, the relationship between non-local damping of the FM and the transfer of angular momentum have been well studied, particularly for bilayer systems consisting of a ferromagnet in contact with either a normal metal or another ferromagnetic metal. While these successes in explaining spin-pumping phenomena in layered metal systems separated by transparent interfaces demonstrate a rich scientific vein, it remains improve quantitative understanding of the dependence of the spin-mixing conductance on materials parameters. Contrary to expectations from models, experimentally determined values of the spin mixing conductance are found to vary only slightly across large variety of disparate FM and NM materials ranging from metals to semiconductors to insulators. Furthermore these models focus exclusively on the short-range exchange interaction appropriate for transparent contacts.

Recent Progress

We demonstrated tuning of magnetocrystalline anisotropy in high-quality Sr₂FeMoO₆ epitaxial films over a range of several thousand Gauss using strain induced by epitaxial growth on substrates of varying lattice constants. Spectroscopic measurements reveal a striking, linear dependence of the out-of-plane anisotropy on the strain-induced tetragonal distortion of the Sr₂FeMoO₆ lattice. This anisotropy can be tuned from +2000 to -3300 Oe, a range sufficient to rotate the easy axis from in plane to out of plane. Combined with its half-metallicity and high

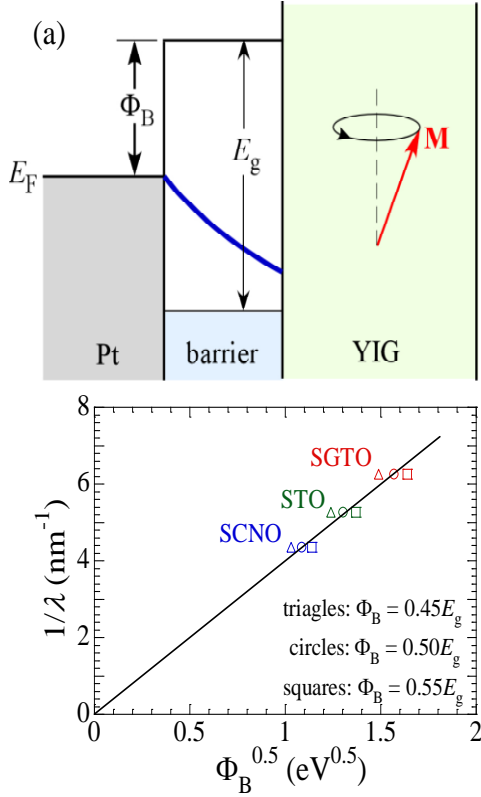


Figure 1. (a) Schematic of band structures of Pt/barrier/YIG heterostructures. The blue curve illustrates the quantum tunneling of the electron wavefunction from Pt into the barrier. (b) Inverse of decay length, $1/\lambda$, as a function of $\sqrt{\Phi_B}$ for Pt/Sr₂GaTaO₆/YIG, Pt/SrTiO₃/YIG and Pt/Sr₂CrNbO₆/YIG. The solid line connecting the three points and origin is a guide to the eye. See DOE publication 2.

and $2.30 \times 10^{14} \Omega^{-1}\text{-m}^{-2}$ for Pt/Y3Fe5O12 and W/Y3Fe5O12 bilayers, respectively.

We have investigated spin pumping from Y3Fe5O12 thin films into Cu, Ag, Ta, W, Pt, and Au with varying spin-orbit coupling strengths. From measurements of Gilbert damping enhancement and inverse spin Hall signals spanning 3 orders of magnitude, we determine the spin Hall angles and interfacial spin mixing conductances for the six metals. The spin Hall angles largely vary as Z^4 (Z : atomic number), corroborating the role of spin-orbit coupling. Amongst the four 5d metals, the variation of the spin Hall angle is dominated by the sensitivity of the d-orbital moment to the d-electron count, confirming theoretical prediction. We have also observed injection of spin currents from Y3Fe5O12 (YIG) films into Ni₈₁Fe₁₉ (Py), Fe, Co, and Ni, and detection of spin currents by inverse spin Hall effect (ISHE) in the FM metals. We obtain a high effective spin mixing conductance of $6.3 \times 10^{18} \text{ m}^{-2}$ in a YIG/Cu/Py trilayer and a spin Hall angle of 0.020 for Py. The spin pumping signals in Fe, Co, and Ni confirm the mechanism of ISHE in FMs is the inverse process of the anomalous Hall effect.

Curie temperature, this result implies a broad range of scientific and technological applications for this novel spintronic material. DOI: 10.1103/PhysRevLett.110.147204.

It is widely believed that the mechanism for spin pumping in ferromagnet-nonmagnet bilayers is the exchange interaction between the ferromagnet and nonmagnetic material. We observed 1000-fold exponential decay of spin pumping from thin Y3Fe5O12 films to Pt across insulating barriers, from which exponential decay lengths of 0.16, 0.19, and 0.23 nm are extracted for oxide barriers having band gaps of 4.91, 3.40, and 2.36 eV, respectively. This archetypal signature of quantum tunneling through a barrier underscores the importance of exchange coupling for spin pumping and reveals its dependence on the characteristics of the barrier material.

Epitaxial Y3Fe5O12 thin films deposited by off-axis sputtering exhibit excellent crystalline quality enabling observation of large spin pumping signals in Pt/Y3Fe5O12 and W/Y3Fe5O12 bilayers driven by cavity ferromagnetic resonance. The inverse spin Hall voltages reach 2.10 and -5.26 mV in 5-mm long Pt/Y3Fe5O12 and W/Y3Fe5O12 bilayers, respectively, excited by a radio-frequency magnetic field of 0.3 Oe. From the ferromagnetic resonance linewidth broadening, we obtain high interfacial spin mixing conductances of 4.56×10^{14}

We used FMR characterization of cobalt grown on chemical vapor deposition graphene and examined the validity of linewidth broadening as an indicator of spin pumping. In comparison to cobalt samples without graphene, direct contact cobalt-on-graphene exhibits increased FMR linewidth—an often used signature of spin pumping. Similar results are obtained in Co/MgO/graphene structures, where a 1 nm MgO layer acts as a tunnel barrier. We observe magnetic disorder that may account for the observed linewidth enhancement due to effects such as two-magnon scattering or mosaicity. It is unreliable to conclude successful spin injection into graphene from FMR linewidth measurements alone.

We have demonstrated strain tuning of magnetocrystalline anisotropy over a range of more than 1000 G in epitaxial Y₃Fe₅O₁₂ films of excellent crystalline quality grown on lattice-mismatched Y₃Al₅O₁₂ substrates. Ferromagnetic resonance (FMR) measurements reveal a linear dependence of both out-of-plane and in-plane uniaxial anisotropy on the strain-induced tetragonal distortion of Y₃Fe₅O₁₂. Importantly, we find the spin mixing conductance $G(r)$ determined from inverse spin Hall effect and FMR linewidth broadening remains large: $G(r) = 3.33 \times 10^{14} \Omega^{-1}\text{-m}^{-2}$ in Pt/Y₃Fe₅O₁₂/Y₃Al₅O₁₂ heterostructures, quite comparable to the value found in Pt/Y₃Fe₅O₁₂ grown on lattice-matched Gd₃Ga₅O₁₂.

Using ferromagnetic (FM) resonance spin pumping, we have observed injection of spin currents from Y₃Fe₅O₁₂ (YIG) films to FM metals, including Ni₈₁Fe₁₉ (Py), Fe, Co, and Ni, and detection of spin currents by inverse spin Hall effect (ISHE) in the FM metals. We obtain a high effective spin mixing conductance of $6.3 \times 10^{18} \text{m}^{-2}$ in a YIG/Cu/Py trilayer and a spin Hall angle of 0.020 for Py. The spin pumping signals in Fe, Co, and Ni confirm the mechanism of ISHE in FMs is the inverse process of the anomalous Hall effect.

We observed a dependence of the damping of a confined mode of precessing ferromagnetic magnetization on the size of the mode. The micron-scale mode is created within an extended, unpatterned YIG film by means of the intense local dipolar field of a micro-magnetic tip. The damping of the confined mode scales like the surface-to-volume ratio of the mode, indicating an interfacial damping effect (similar to spin pumping) due to the transfer of angular momentum from the confined mode to the spin sink of ferromagnetic material in the surrounding film. Though unexpected for insulating systems, the measured intralayer spin-mixing conductance $g = 5.3 \times 10^{19} \text{m}^{-2}$ demonstrates efficient intralayer angular momentum transfer.

Future Plans

In our future work we will continue to investigate the nature and the mechanisms of spin pumping. We will continue our experiments in electrical detection of spin pumping in multilayered magnetic systems with tailored magnetic properties. We will also continue the ongoing effort in investigating spin pumping using the localized FMR excitations with the help of the scanned probe technique of Ferromagnetic Resonance Force Microscopy (FMRFM). This approach allows us to separate the effects of spin pumping from the possible effects occurring at the interfaces of magnetic and nonmagnetic materials. We will also continue to develop new tools for performing magnetic resonance and ferromagnetic resonance imaging to reveal microscopic details of spin pumping and enhancement of damping in nanoscale hybrid materials.

Publications

1. "Control of Magnetocrystalline Anisotropy by Epitaxial Strain in Double Perovskite Sr₂FeMoO₆ Films," Chunhui Du, Rohan Adur, Hailong Wang, Adam J. Hauser, Fengyuan Yang, and P. Chris Hammel, *Physical Review Letters* 110 147204 (2013) DOI: 10.1103/PhysRevLett.110.147204
2. "Probing the Spin Pumping Mechanism: Exchange Coupling with Exponential Decay in Y₃Fe₅O₁₂/Barrier/Pt Heterostructures," C. H. Du, H. L. Wang, Y. Pu, T. L. Meyer, P. M. Woodward, F. Y. Yang, and P. C. Hammel, *Physical Review Letters* 111 247202 (2013) DOI: 10.1103/PhysRevLett.111.247202
3. "Scaling of spin Hall angle in 3d, 4d and 5d metals from Y₃Fe₅O₁₂/metal spin pumping," H.L. Wang, C. H. Du, Y. Pu, R. Adur, P. C. Hammel and F. Y. Yang *Physical Review Letters* 112 197201 (2014)
4. "Large Spin Pumping from Epitaxial Y₃Fe₅O₁₂ Thin Films to Pt and W Layers," H. L. Wang, C. H. Du, Y. Pu, R. Adur, P. C. Hammel, and F. Y. Yang, *Physical Review B Rapid Communications* 88 100406(R) (2013) DOI: 10.1103/PhysRevB.88.100406 URL: <http://link.aps.org/doi/10.1103/PhysRevB.88.100406>
5. "Spin current and inverse spin Hall effect in ferromagnetic metals probed by Y₃Fe₅O₁₂-based spin pumping," Hailong Wang, Chunhui Du, P. Chris Hammel and Fengyuan Yang, *Appl. Phys. Lett.* 104 202405 (2014) <http://dx.doi.org/10.1063/1.4878540>
6. "Strain-tunable magnetocrystalline anisotropy in epitaxial Y₃Fe₅O₁₂ thin films," Hailong Wang, Chunhui Du, P. Chris Hammel, and Fengyuan Yang, *Phys. Rev. B* 89 134404 (2014)
7. "Enhancement of Pure Spin Currents in Spin Pumping Y₃Fe₅O₁₂/Cu/metal Trilayers through Spin Conductance Matching," Chunhui Du, Hailong Wang, Fengyuan Yang, and P. Chris Hammel, *Physical Review Applied* 1 044004 (2014)
8. "Magnetization dynamics of cobalt grown on graphene," A.J. Berger, W. Amamou, S.P. White, R. Adur, Y. Pu, R. K. Kawakami and P. C. Hammel, *Journal Of Applied Physics* 115, 17C510 (2014)
9. "Ultra-narrow ferromagnetic resonance in organic-based thin films grown via low temperature chemical vapor deposition," H. Yu, M. Harberts, R. Adur, Y. Lu, P.C. Hammel, E. Johnston-Halperin, A.J. Epstein, *Applied Physics Letters* 105 012407 (2014) DOI: 10.1063/1.4887924
10. "Off-resonant manipulation of spins in diamond via precessing magnetization of a proximal ferromagnet," C. S. Wolfe, V. P. Bhallamudi, H. L. Wang, C. H. Du, S. Manuilov, R. M. Teeling-Smith, A. J. Berger, R. Adur, F. Y. Yang and P. C. Hammel, *Physical Review B Rapid Communication* 89 180406 (2014) (Editor's Suggestion and Physics Highlight) DOI:10.1103/PhysRevB.89.180406
11. "Anisotropy and Field-Sensing Bandwidth in Self-Biased Bismuth-Substituted Rare-Earth Iron Garnet Films: Measurement by Ferromagnetic Resonance Spectroscopy," Adur, R.; Lauback, S.; Banerjee, P.; Lee, I; Fratello, VJ; Hammel, PC, *IEEE Transactions On Magnetics* 49 2899–2902 (June 2013)
12. "Damping of Confined Modes in a Ferromagnetic Thin Insulating Film: Angular Momentum Transfer Across a Nanoscale Field-Defined Interface" Rohan Adur, Chunhui Du, Hailong Wang, Sergey A. Manuilov, Vidya P. Bhallamudi, Chi Zhang, Denis V. Pelekhov, Fengyuan Yang and P. Chris Hammel, arXiv:1405.4203

High Speed SPM of Functional Materials (DE-SC0005037)

Bryan D. Huey, University of Connecticut

Program Scope

The development and optimization of applications comprising functional materials necessitates a thorough understanding of their static and dynamic properties and performance. Leveraging High Speed SPM and concepts enabled by it, efficient measurements and maps with nanoscale and nanosecond temporal resolution are uniquely feasible. This includes recent enhancements for topographic, conductivity, ferroelectric, and piezoelectric properties as originally proposed, as well as newly developed improvements to AFM-based mechanical, thermal, and photoconductivity maps.

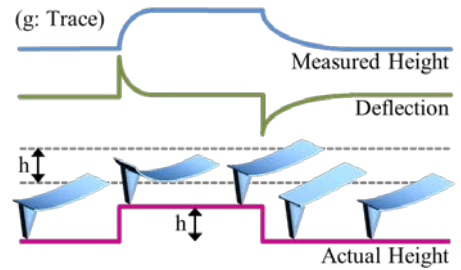
Recent Progress

Two advances from this ongoing work are particularly relevant to the ESPM community and presented below. The first includes a simple and widely applicable modification to AFM imaging that can greatly improve the accuracy of topographic and property maps, simplifies AFM training and operation, and enables high speed AFM imaging even on legacy systems. Leveraging such concepts, but investigating multiferroic switching, the behavior of ferroelectric domains in poly-domain epitaxial films are also thoroughly investigated. This statistically reveals and spatially resolves full ferroelectric polarization reversals occurring via multiple ferroelectric switches, with important implications for electromagnetic coupling in multiferroics.

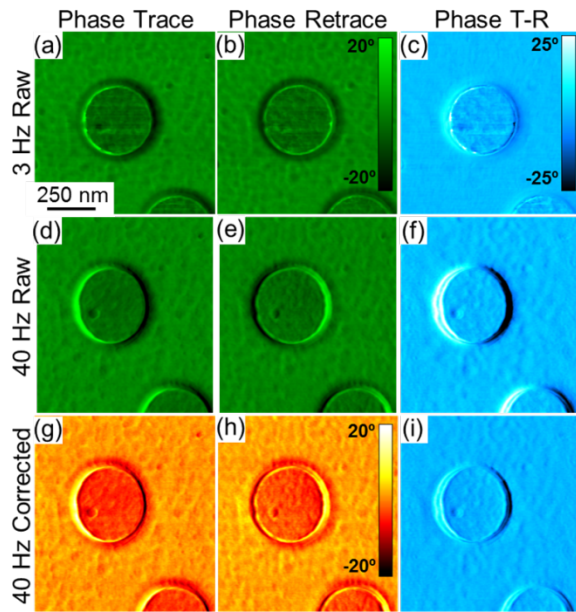
Error Corrected AFM ('True Topography')

For more than 25 years, quality AFM imaging has almost entirely been performed by trained users who monitor and attempt to minimize variations in a feedback channel, typically the deflection or AC amplitude signal. By maintaining a constant feedback parameter (setpoint force or force gradient, respectively), the surface topography and corresponding local properties can then accurately be mapped. In reality, however, the feedback never perfectly maintains the setpoint. While this is understood to result in image artifacts, as sketched in Figure 1 it is also clear that the actual height can still be recovered as long as the feedback channel can be appropriately calibrated and then simply summed with the measured height, correcting the initial flaws. This true topography additionally causes the trace and retrace signals to essentially perfectly overlap. Theoretically they always should, but practically they seldom do since the feedback channel typically inverts depending on the scan direction (trace or retrace), creating artificial lateral offsets and asymmetries in actually uniform topographic features.

Figure 1: Concept for error-corrected AFM to recover the true topography of a surface by simply summing the measured but incorrect height profile with the feedback (error) signal, i.e. the calibrated lever deflection or amplitude.



This concept is equally applicable to enhance property measurements as well, Figure 2. The relationship between error in the feedback channel (e.g. higher or lower force gradients) and the signal used to determine the property of

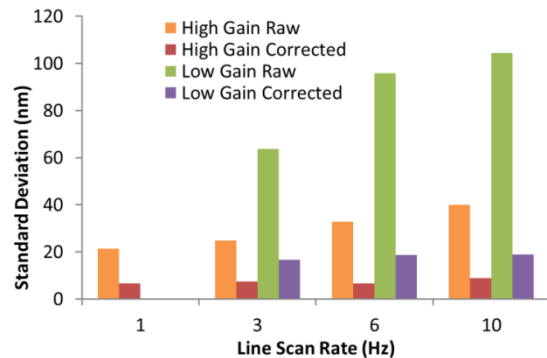


interest, e.g. how indentation influences phase contrast, can enhance property maps, again minimize trace/retrace offsets, and thus provide a more true representation of the studied surface.

Figure 2: AC imaged phase trace (left), retrace (right), and difference (trace minus retrace) with nearly ideal scanning settings (slow imaging, high gain) akin to an expert user running the AFM (a-c); results more common for an inexperienced AFM user (fast imaging, low gain) with strong scan direction dependent artifacts (e-f); and the error-corrected response (g-h) returning results that are nearly equivalent to the 13x slower images.

To quantify the benefits of ec-AFM, the rms roughness is calculated for the difference between trace and retrace images for raw, as well as corrected, images acquired under a variety of scanning settings. Figure 3 displays the results over an order of magnitude of scan rates, clarifying that corrected images are consistently better than raw, expert user scans (high gain). Furthermore, the images of beginning users (low gain) may initially be terrible initially (raw), but upon employing ec-AFM they improve to better than standard expert user images that took at least 10 times as long.

Figure 3: Chart of the standard deviation for trace minus retrace topography images, acquired with imaging rates that span an order of magnitude. Scanning parameters are considered that approximate expert AFM users (high gain) as well as AFM novices (low gain).

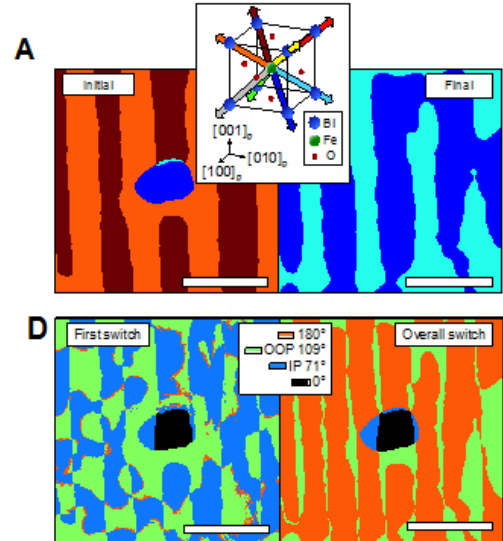


Practically, this approach therefore can enable more accurate high speed imaging, better property maps in general, and improve ease of use. There are caveats, of course, principally that the correction of images acquired with poor scanning parameters cannot remove artifacts caused by a possible increased likelihood of sample or tip damage. Since such flaws are characterizable and typically rapidly apparent, especially when scanning at high speeds, the outcome may simply be that more AFM tips are used, or the benefits of robust and low-friction probes become more pronounced.

Multiferroic Switching

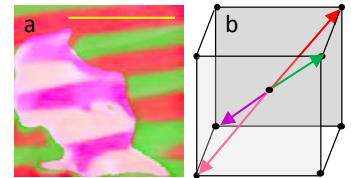
Following extensive previous work into ferroelectric and ferroelastic switching dynamics, a new study with a 2-polarization variant BiFeO_3 epitaxial film on DyScO_3 (110) has clearly resolved switching steps during poling (Figure 4). Comparing the initial (A, left) and the final (A, right) states, the overall reorientation (D, right) is 180° nearly everywhere, i.e. purely ferroelectric. Based on a movie of switching steps during the domain evolution, however, the first switching direction has also been determined (D, left) and is ferroelastic nearly everywhere. This includes both in-plane as well as out-of-plane first switches, even though the field is applied out of plane.

Figure 4: Domain orientation maps of the initial (A, left) and poled (A, right) states of a 2-variant BiFeO_3 film, along with maps of the first (D, left) as well as the overall (D, right) domain switching directions. 500 nm scale bars.



Crucially, if one terminates the poling process before the imaged region has completely switched, Figure 5, only 2 polarization variants (and thus 4 possible orientations) are present. This is expected for such 2-variant specimens, but important to ruling out other possible switching steps via the missing domain variant directions. Such results are crucial to understanding, and leveraging, electromagnetic coupling in multiferroics for real applications.

Figure 5: Overlaid in-plane domain contrast (a, stripes) and normal contrast (irregular patch), and a legend for the contrast scheme (b) for this partially switched 800 nm x 800 nm area. 500 nm scale bar.



Future Plans

In the remaining year of this effort, work will continue strengthened by collaborations with DOE scientists in two distinct areas: ferroelectric and ferroelastic switching dynamics in multiferroics, and performance mapping of photovoltaics. With J. L. Cruz-Campa (SNL) and including a student exchange, the grain and interface dependent PV performance is being directly mapped for polycrystalline solar cells. With P. Ashby (LBNL) and including Molecular Foundry user facility access, correlations between electric and magnetic domains and their relative switching dynamics will continue to be measured, even incorporating video-rate imaging.

References

1. Bosse, J.L. and B.D. Huey, "Error-corrected AFM: a simple and broadly applicable approach for substantially improving AFM image accuracy," *Nanotechnology*, 2014. 25(15).
2. J. T. Heron, M. Trassin, Y. Gao, J. Bosse, L. Ye, Q. He, J. Liu, C. Wang, S. Salahuddin, D. C. Ralph, D. G. Schlom, J. Iniguez, B. D. Huey, R. Ramesh, "Deterministic Electrical Switching of Magnetism at Room Temperature," *Nature Communications*, revision submitted, 2014.

Publications (BES recognized, since 2012)

Accepted

- A. Bosse, J.L. and B.D. Huey, "Error-corrected AFM: a simple and broadly applicable approach for substantially improving AFM image accuracy," *Nanotechnology*, 2014. 25(15).
- B. J. L. Bosse, I. Grishin, B. D. Huey, O. V. Kolosov, "Nanomechanical morphology of amorphous, transition, and crystalline domains in phase change memory thin films," *App. Surf. Sci.*, accepted, 2014.
- C. Bosse, J.L., P.D. Tovee, B.D. Huey, and O.V. Kolosov, "Physical mechanisms of megahertz vibrations and nonlinear detection in ultrasonic force and related microscopies." *Journal of Applied Physics*, 2014. 115(14).
- D. Bosse, J., S. Lee, B. Huey, A. Andersen, and D. Sutherland, "High Speed Friction Microscopy and Nanoscale Friction Coefficient Mapping. *Measurement Science and Technology*," accepted, 2014.

Submitted

- E. J. T. Heron, M. Trassin, Y. Gao, J. Bosse, L. Ye, Q. He, J. Liu, C. Wang, S. Salahuddin, D. C. Ralph, D. G. Schlom, J. Iniguez, B. D. Huey, R. Ramesh, "Deterministic Electrical Switching of Magnetism at Room Temperature," *Nature Communications*, revision submitted, 2014.
- F. P. Tovee, J. L. Bosse, B. Robinson, M. Timofeeva, B. D. Huey, O. V. Kolosov, "Nanothermal Characterization of Amorphous and Crystalline Phases in Chalcogenide Thin Films with Scanning Thermal Microscopy," *JAP*, revision submitted, 2014.
- G. Manuel Rivas, Varun Vyas, Aliya Carter, James Veronick, Flemming Besenbacher, Yusuf Khan, Oleg Kolosov, Ron Polcawich, Bryan D. Huey, "In Situ AFM of Electro-Mechanical Systems," *JMR*, submitted and Special Issue Co-Editor, 2014.
- H. Y. Kutes, J.L. Bosse, J.L. Cruz-Campa, E.D. Spoeke, D. Zubia, B.A. Aguirre, and B.D. Huey, "Mapping Photovoltaic Performance with Nanoscale Resolution," *Progress in Photovoltaics*, submitted, 2014.

For submission

- I. L. Ye, G. Santone, Y. H. Chu, P. Yu, R. Ramesh, and B. D. Huey, "Nanoscale Ferroelectric Switching Dynamics Resolved in Three Dimensions," *JAP*, submitting, 2014.
- J. N. A. Polomoff, A. Rakin, P. Yu, Y. H. Chu, R. Ramesh, B. D. Huey, "Influence of Pre-Existing Ferroelectric Domain Patterns on Domain Dynamics During Polarization Reversal," *J. Materials Science*, submitting, 2014.
- K. N. Polomoff, S. Lee, B. D. Huey, "Engineering Switching for Reduced Energy Consumption," *J. Appl. Phys.*, submitting, 2014.
- L. Y. Kutes, J.L. Bosse, J.L. Cruz-Campa, E.D. Spoeke, D. Zubia, B.A. Aguirre, B.D. Huey, "Grain, Grain Boundary, and Grain Orientation Dependent Photovoltaic Performance in a Micropatterned CdTe/CdS Solar Cell," *Nano Energy*, submitting, 2014.

Vortex Matter in Confined Superconductors and Mesoscopic Hybrid Heterostructures

Maria Iavarone
Physics Department, Temple University
Philadelphia, PA 19122
e-mail: iavarone@temple.edu

Project Scope

The primary emphasis of this project is on the physics of vortices in confined superconductors and hybrid heterostructures such as superconductor-ferromagnet (S/F) systems. The goal is to understand how the physics of vortex matter changes in order to be able to predict and control the electronic properties of new hybrid systems. The vortex configuration in confined superconductors and S/F systems can be probed with high spatial resolution by mapping the spatial variations in the electronic density of states with Scanning Tunneling Microscopy. The understanding of the local changes in the electronic density of states is crucial as it also affects all the thermodynamic properties of the material.

The proposed program is divided in two parts.

The first part will focus on studying the emergence of superconductivity and vortex matter in mesoscopic superconductors. Properties of superconducting materials differ greatly from the bulk properties when the size of the sample is small (compared to the coherence length and the London penetration depth). Critical parameters such as critical current and critical field can be greatly enhanced and the vortex configuration can be strongly influenced by the sample geometry. Despite many efforts over the last decade some fundamental issues are still open. In particular, we are still lacking a description of the emergence of superconductivity at the nanoscale.

The second part of this program focuses on the investigation of hybrid nanostructures incorporating superconducting and ferromagnetic components. Understanding of the physics involved will be combined with searching novel guiding principles to enhance materials and devices functionalities by combining specific properties of ferromagnets and superconductors. In proximity coupled structures the interplay between magnetism and superconductivity will lead to new physical phenomena with superconductivity coexisting with ferromagnetism at the interface. In magnetically coupled structures the inhomogeneous stray field of the ferromagnet will lead to an inhomogeneous superconducting state where superconductivity and vortices can be confined in channels determined by the underlying magnetic template.

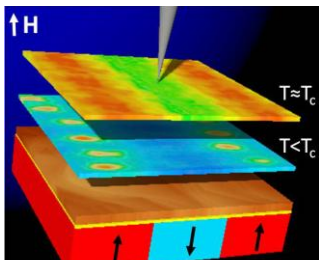


Figure 1 STM measurements taken at the surface of a F/S bilayer . The top image is the conductance map acquired just below the critical temperature in the presence of an applied magnetic field that compensates one type of magnetic domains of the ferromagnet. The middle image is the conductance map at the same location and in the same applied field at $T=1.5$ K. The bottom image is the topography of the superconducting layer. The cartoon shows the magnetic domains of the underlying ferromagnetic layer.

Recent Progress

Direct visualization of Domain Wall Superconductivity and Reverse Domain Superconductivity in S/F structures magnetically coupled

Magnetically coupled planar ferromagnet-superconductor (F/S) hybrid structures offer new avenues for manipulation of the superconductivity at the nanoscale and convenient means to control vortex dynamics. In this case the nonuniform magnetic field produced by the ferromagnet spatially confines superconductivity. When the temperature is decreased below T_c , the superconductivity is expected to nucleate first at the location where the stray field is minimum, *i.e.* at the domain wall, which is a realization of *domain wall superconductivity* (Fig. 2). Therefore, the superconductivity is confined in tiny channels that can more or less interact depending upon the distance between them. These channels can be positioned at different locations in the superconductors by applying an external magnetic field. These effects known as domain wall superconductivity and reverse domain superconductivity were theoretically predicted and inferred experimentally only by global measurements. *Our measurements provided the first direct visualization of the nucleation of the superconductivity in regions above the domain walls with a critical temperature that is function of location.*

On the other hand, when an external magnetic field is applied perpendicular to the film, the regions with minimum magnetic field will shift to a different position due to magnetic field compensation effect (Fig.1). Therefore the applied magnetic field will spatially shift the superconducting nucleus to the center of the compensated domain. Furthermore, by reversing the polarity of the applied field we observed the switching of a normal region in superconducting and viceversa.

Our results demonstrate that such F/S structures are attractive model systems that offer the possibility to control the strength and the location of the superconducting nucleus by applying an external magnetic field.

We fabricated F/S structures consisting of Co-Pd multilayers having different stripe domains width. The theoretical condition for the nucleation of the superconductivity at a domain wall is that the characteristic length scale for nucleation of superconductivity, *i.e.* the coherence length at the superconducting critical temperature of the S/F system $\xi(T_c)$, should be smaller than the domain half-width to avoid overlapping of the superconducting nuclei. We found that the nucleation of superconductivity at the domain wall is critically dependent upon the domain width. Indeed, if the domains are too narrow the superconducting nuclei overlap and the superconductivity will nucleate everywhere with slight spatial inhomogeneity.

Our results demonstrate that such F/S structures are attractive model systems that offer the possibility to control the strength and the location of the superconducting nucleus by applying an external magnetic field.

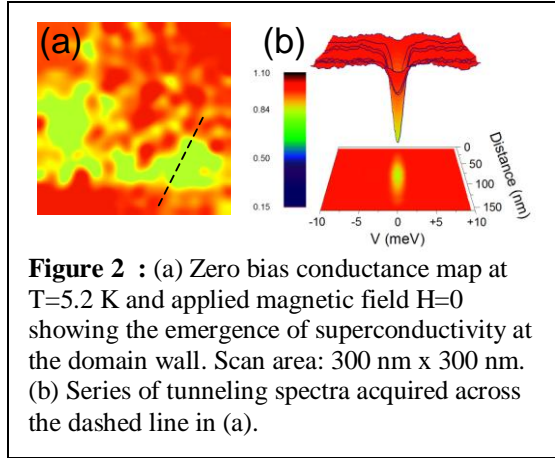
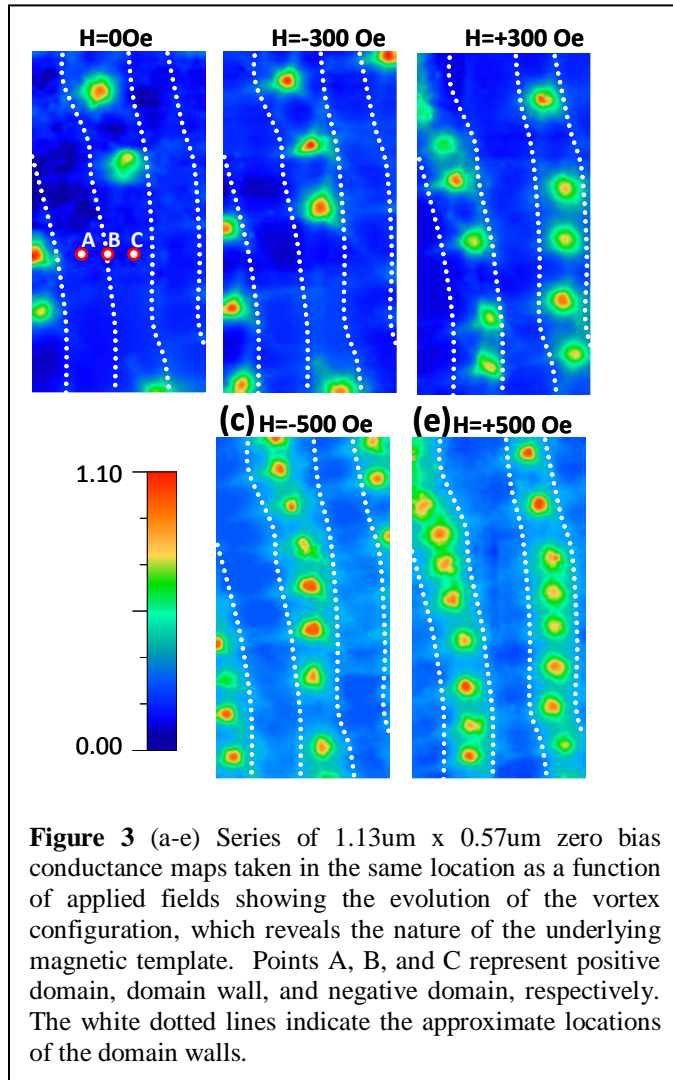


Figure 2 : (a) Zero bias conductance map at $T=5.2$ K and applied magnetic field $H=0$ showing the emergence of superconductivity at the domain wall. Scan area: 300 nm \times 300 nm. (b) Series of tunneling spectra acquired across the dashed line in (a).

Influence of Domain Width on Vortex Nucleation in Superconductor/Ferromagnet Hybrid Structures



We have investigated the effect of spatially inhomogeneous magnetic domain width on vortex nucleation in magnetically coupled superconductor/ferromagnet hybrid structures. Using low temperature scanning tunneling microscopy and spectroscopy (LT-STM/STS) we have studied Pb/[Co-Pd] systems. The ferromagnet is characterized by domains of opposite polarity having slight different width, with an average width of about 200 nm. When an external magnetic field is applied the domain antiparallel to the external field will be at least partially compensated and the domain width will decrease while the width of the domains parallel to the applied field will increase. Visualization of the underlying magnetic template structure is achieved through field dependent conductance maps. In the case of zero applied fields these maps reveal the absence of vortices below a threshold domain width. In those systems with insufficient domain width to support generation of vortices in zero

applied fields, nucleation can be restored through the application of an external magnetic field, with vortices nucleating above the domain parallel to the external field. In Figure 3 we report conductance maps acquired on the superconductor surface at various applied magnetic fields. *The images show that it is possible to locate vortices at different locations by changing the polarity of the applied magnetic field and by controlling the size of the domain width in the ferromagnet.*

Future Plans

We will continue to explore the physics of mesoscopic and S/F structures with an emphasis on the vortex matter and its impact on applications.

Specific planned activities include:

- Correlation of STM, MFM and transport of S/F structure in magnetically coupled regime to investigate vortex-antivortex dynamics.
- S/F structure in the regime of proximity effect to investigate the physics at the interface.
- We will explore mesoscopic superconductors on different substrates.

Publications supported by DOE-BES (2012-August 2014)

- [1] “Visualizing Domain Wall Superconductivity and Reverse Domain Superconductivity”, M. Iavarone, S.A. Moore, J. Fedor, S.T. Ciocys, G. Karapetrov, J. Pearson, V. Novosad, S.D. Bader, *Nature Communications* 2014 DOI: NCOMMS5766
- [2] “Influence of Domain Width on Vortex Nucleation in Superconductor/Ferromagnet Hybrid Structures”, M. Iavarone, S.A. Moore, J. Fedor, V. Novosad, J. A. Pearson, G. Karapetrov, *J. Supercond. Nov. Magn.* 2014 DOI: 10.1007/s10948-014-2650-9
- [3] “Vortex-Antivortex coexistence in Nb-based superconductor/ferromagnet heterostructures”, F. Bobba, C. Di Giorgio, A. Scarfato, M. Longobardi, M. Iavarone, S.A. Moore, G. Karapetrov, V. Yefremenko, and A.M. Cucolo, *Phys. Rev. B* **89**, 214502 (2014)
- [4] “Influence of topological edge states on the properties of Al/Bi₂Se₃/Al hybrid Josephson devices”, L. Galletti, S. Charpentier, M. Iavarone, P. Lucignano, D. Massarotti, R. Arpaia, Y. Suzuki, K. Kadowaki, T. Bauch, A. Taglaicozzo, F. Tafuri, and F. Lombardi, *Phys. Rev. B* **89**, 134512 (2014)
- [5] “Magnetization properties and vortex phase diagram of Cu_xTiSe₂ single crystals”, P. Husaniková, J. Fedor, J. Dérer, J. Šoltýs, V. Cambel, M. Iavarone, S.J. May, and G. Karapetrov, *Phys. Rev. B* **88**, 174501 (2013)
- [6] “Evidence of vortex jamming in Abrikosov vortex flux low regime”, G. Karapetrov, V. Yefremenko, G. Mihailović, J. E. Pearson, M. Iavarone, V. Novosad, and S.D. Bader, *Phys. Rev. B* **86**, 054524 (2012)
- [7] “Vortex Confinement in Planar Superconductor/Ferromagnet Hybrid Structures”, M. Iavarone, A. Scarfato, F. Bobba, M. Longobardi, S. A. Moore, G. Karapetrov, V. Yefremenko, V. Novosad, and A. M. Cucolo, *IEEE-transaction on Magnetics* **48 (11)**, 3275-3279 (2012)
- [8] “Visualizing vortex dynamics in Py/Nb thin film hybrids by low temperature magnetic force microscopy”, A.M. Cucolo, A. Scarfato, M. Iavarone, M. Longobardi, F. Bobba, G. Karapetrov, V. Novosad, V. Yefremenko, *J. Supercond. Nov. Magn.* **25(7)**, 2167-2171 (2012)
- [9] “Magnetic pinning in a superconducting film by a ferromagnetic layer with a stripe domain”, D. Mancusi, C. Di Giorgio, F. Bobba, A. Scarfato, A. Cucolo, M. Iavarone, S. Moore, G. Karapetrov, V. Novosad, V. Yefremenko, S. Pace and M. Polichetti, *Supercond. Sci. and Tech.*, Submitted (2014)
- [10] “Evolution of the superconducting properties of ultrathin Pb films as a function of the thickness”, S. A. Moore, J. Fedor, and M. Iavarone, *Supercond. Sci. and Tech.*, Submitted (2014)

Photon and surface plasmon dynamics studied in photoemission electron microscopy (PEEM)

Rolf Koenenkamp, Portland State University, Portland, OR 97201

Program Scope

The project addresses 2 main goals in photoemission electron microscopy (PEEM); one related to electron optical developments in aberration correction, the other addressing new microscope methodology in characterizing surface properties with ultrafast laser pulses.

(1) Spatial resolution and sensitivity are to be improved with the introduction of a new mirror-based aberration corrector. A 3-electrode electron mirror has been installed and is currently characterized and tested.

(2) Novel approaches for the imaging of optical and plasmonic processes are currently explored. Multi-photon photoelectron emission from laser pulses in the visible region is used to visualize photonic and plasmonic wave propagation at surfaces of metals and semiconductors. Coherent control techniques for the manipulation of localized surface plasmon resonances are being explored.

Recent Progress

Microscope development

A new 3-electrode mirror, based on our earlier calculations and design (P1), will provide adjustable aberration-correction for chromatic and spherical aberrations over a large operation regime. Software for utilizing this mirror in combination with a 3-electrode lens is being developed. Resolution improvement over the previous 2-electrode mirror that showed 4-5nm resolution, has not been achieved yet. The new mirror requires some adjustments of other instrument components, however, and this process has been very time-consuming. In our electrostatic lens system voltage stability is also known to be critical for resolution better than 2-3nm (R1).

In a separate instrument development, a spatial light modulator for wavelengths around 800nm and 100fs laser pulses has been installed in the optical system, and first experimental results for in-pulse polarization changes have been obtained (P9).

Electron microscopy of photonic wave propagation: We found that light propagation in semiconductors and transparent oxides can be visualized on nanometer scales using photoelectrons (P5,P6). Fig. 1 shows an example of 410nm light propagating in a micron-sized round disc defined in an indium-tin-oxide film on glass. Essentially, a stationary interference pattern is generated with the help of a coherent reference light beam. In a non-linear multi-photon process the created stationary pattern modulates the photoelectron emission from the sample surface. The photoelectrons are emitted with excess energies $\sim 0.5\text{V}$ and are accelerated, aberration-corrected and imaged in the microscope (P6). In the past months we developed a detailed quantitative description of these imaging process combining a general Fresnel-Kirchhoff

approach with a simple non-linear model for the photoemission process (P8). Fig. 1 compares experimental results and calculated results. Excellent agreement is typically obtained. The model then allows to extract optical constants, non-linear coefficients etc. We have applied this formalism to the description of optical surface waves on silicon and indium-tin-oxide (P5,P8).

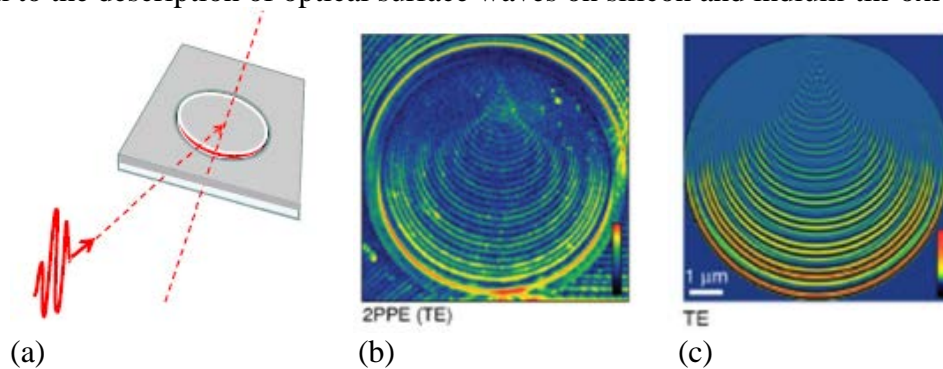


Figure 1 a: Schematic for optical wave-guiding set up in the microscope. A disk-shaped indium-tin-oxide waveguide is excited through a circular groove with laser pulses incident at 60° from the surface normal; b: Light propagation is observed in PEEM in a stationary interference pattern generated with the help of a coherent reference beam; c: The interference pattern calculated using a Kirchhoff-Fresnel approach and non-linear photoemission. Linear and non-linear optical constants for the waveguide can be extracted from the model fit.

Plasmonic wave propagation: A similar approach as outlined above can also be applied to describe the surface plasmon propagation at metallic surfaces. A PEEM image of surface plasmon modes at the surface of a single-crystalline gold flake is shown in Fig. 2. Further theoretical work has recently allowed us to quantitatively describe the energy transfer between photonic and plasmonic waves in samples where the plasmonic metal is adjacent to a dielectric or semiconducting film (P7).

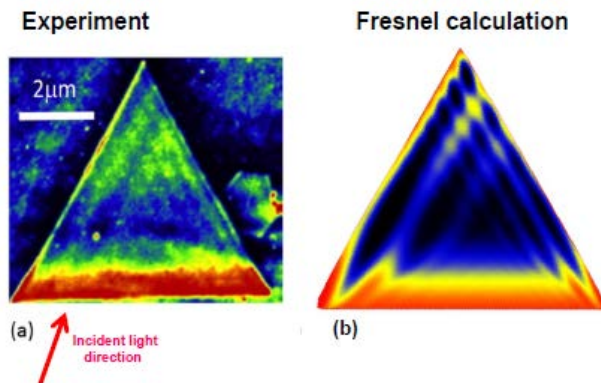


Figure 2a: PEEM micrograph showing propagating and reflected surface plasmon modes in a gold single crystal; b: calculated interference pattern using a Fresnel-Kirchhoff approach.

For the visualization of *localized* surface plasmon resonances a reference optical beam is not needed in PEEM, since the localized mode distributions are stationary. In these cases the PEEM images can directly be related to the stationary optical fields. In appropriately designed nano-structures optical fields can be strongly amplified near plasmonic resonances (R2). Photoelectron

emission can then often easily be detected in a photoelectron microscope (R3,R4). In our current work we are exploring ways to manipulate and steer the plasmonic response by applying coherent femtosecond pulse shaping to the exciting laser pulses (R5). Essentially, by varying amplitude, phase and polarization within the excitation light pulse in PEEM, a direct and in-situ observation of the induced plasmon mode changes is possible. As a first example, we show in Fig. 3 a sub-micron ring-type antenna structure; its plasmonic eigenmodes are expected to have axial symmetry. A linearly polarized optical beam breaks this symmetry and selects eigenmodes with specific orientations as shown in the figure. These selected eigenmodes can now be re-oriented in space by changing the polarization angle in the excitation light. Thus a motioning of localized mode patterns can be effected through polarization control (P9). The optical fields and the electron emission follow the spatial mode selection. Our experimental results are well corroborated by simulations carried out in finite element calculations utilizing the full dielectric constants and spatial dimensions of the sample. Thus a predictable, nanoscale mode-positioning can be achieved, which may become important for numerous applications in sensing, signal processing and controlled electron emission.

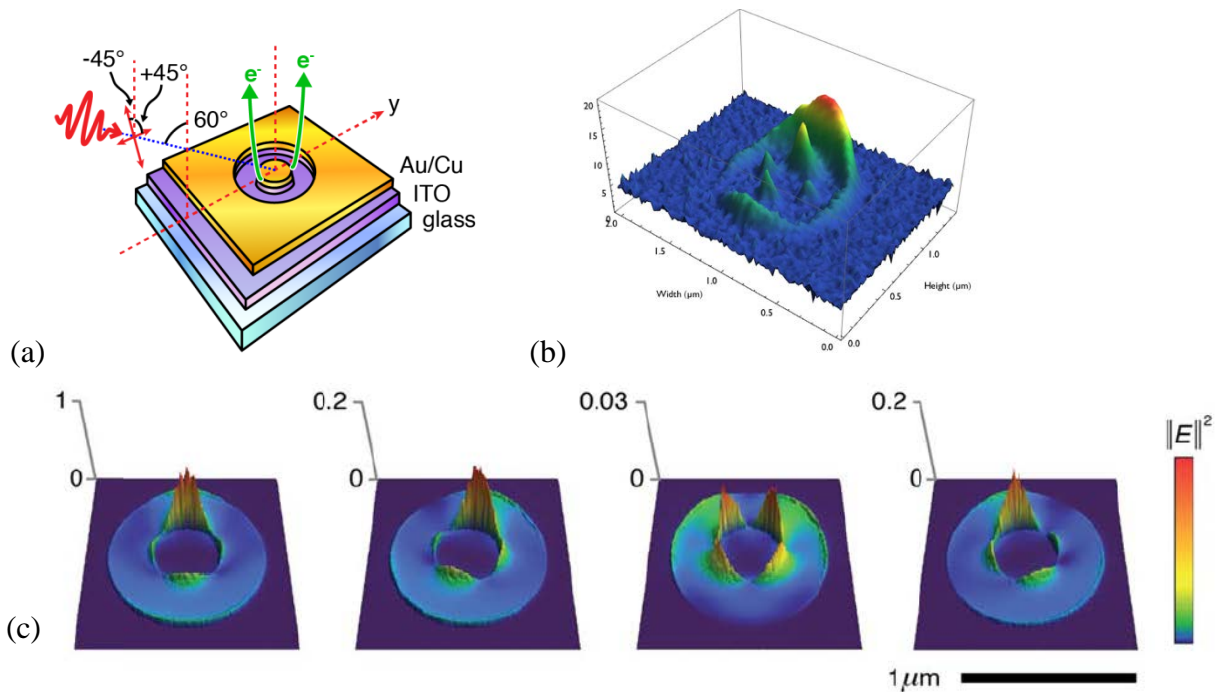


Figure 3: Control of localized surface plasmon resonances. A: plasmonic antenna structure allowing mode selection by polarization control; b: photoemission micrograph showing the eigenmode distribution in the antenna structure (experimental); c: motioning of the eigenmodes by polarization changes in the excitation light (calculation).

Future plans

Microscope development: We hope to complete the characterization and fine-tuning of the triode mirror in the year ahead, allowing us to obtain improved spatial resolution better than 4 nm for stationary excitation and around 15nm for femtosecond excitation. With the improved

resolution, we also expect increased sensitivity and contrast. These improvements will markedly improve the femtosecond imaging techniques explored in the photonic/plasmonic portion of the project.

Microscopy of photonic/plasmonic processes: Phase and amplitude control will be utilized to further enhance the control capabilities for photonic and plasmonic processes. Ultimately a coherent control of surface plasmon propagation, plasmonic resonance positioning and plasmonic energy transfer is envisioned using the pulse shaping capabilities of the newly installed spatial light modulator.

References

- (R1) S. Schramm, S. van der Molen and R. Tromp, Phys. Rev. Lett. 109, 163901 (2012)
- (R2) M. I. Stockman, S. Faleev and D. Bergman, Phys. Rev. Lett. 88, 067402 (2002)
- (R3) A. Kubo, N. Pontius and H. Petek, Nano Lett. 7, 470 (2007)
- (R4) T. Brixner and G. Gerber, Opt. Lett. 26, 557 (2001)
- (R5) M. Aeschlimann et al., PNAS 107, 5333 (2010)

Publications with DOE acknowledgement

- (P1) ***Simultaneous and independent dynamic correction of spherical and chromatic aberration in electron optics***
J.P.S. Fitzgerald, R.C. Word and R. Könenkamp, Ultramicroscopy 115, 35 (2012)
- (P2) ***Aberrations in asymmetrical electron lenses***
J.P.S. Fitzgerald, R.C. Word and R. Könenkamp, Ultramicroscopy 119, 40 (2012)
- (P3) ***Controlled spatial switching and routing of surface plasmons in designed single-crystalline gold nanostructures***, R. Könenkamp, R. C. Word, J. Fitzgerald, A. Nadarajah and S. Saliba, Appl. Phys. Lett. 101, 141114 (2012)
- (P4) ***Electron emission in the near-field of surface plasmons***
Robert C. Word, J. Fitzgerald and R. Könenkamp, Surface Science 607, 148 (2013)
- (P5) ***Direct imaging of optical diffraction in photoemission electron microscopy***
R.C. Word, J.P.S. Fitzgerald, R. Könenkamp, Appl. Phys. Lett. 103, 021118 (2013)
- (P6) ***Photonic near-field imaging in multiphoton photoemission electron microscopy***
J.P.S. Fitzgerald, R.C. Word, S.D. Saliba, R. Könenkamp, Phys. Rev. B 87, 205419 (2013)
- (P7) ***Direct coupling of photonic modes and surface plasmons observed in 2-photon PEEM***
R.C. Word, J.P.S. Fitzgerald, and R. Könenkamp, Opt. Express 21, 30507 (2013)
- (P8) ***Subwavelength visualization of light in thin film waveguides with photoelectrons***
J.P.S. Fitzgerald, R.C. Word, R. Könenkamp, Phys. Rev. B 89, 195129 (2014)
- (P9) ***Positional control of plasmonic fields and electron emission***
R. C. Word, J. P. S. Fitzgerald and R. Könenkamp (APL submitted)
- (P10) ***Photoemission electron microscope with a hyperbolic electron mirror as corrector for chromatic and spherical aberration***
R. Könenkamp, R. C. Word and J. Fitzgerald (in preparation)

Microscopy of Electrostatic Field Effect in Novel Quantum Materials

PI: Keji Lai (kejilai@physics.utexas.edu)

Department of Physics, University of Texas at Austin, Austin, TX 78712

Program Scope

The objective of this DOE supported Early Career program is to explore the nanoscale electronic properties when charge carriers in advanced quantum materials are electrostatically modulated in field-effect transistor (FET) structures. A unique microwave impedance microscope (MIM) [1], which is able to resolve the nanoscale dielectric and conductivity information, is utilized to image the buried transistor interface. The visualization of local conductivity variation in novel FETs is expected to address many fundamental issues in electron physics, material science, and electrical engineering, including (i) real-space evolution of electronic phase transitions induced by density modulation, (ii) difference between bulk chemical doping and surface electrostatic doping, and (iii) microscopic origin of sub-threshold behavior in FETs. In particular, three types of FET structures, as shown in Fig. 1, will be studied in this program. The conventional back-gated MOSFET is the most straightforward structure to modulate the density up to a range of $10^{13}\sim 10^{14}$ cm^{-2} . Using a vertically polarized ferroelectric layer as the gate dielectric [2], a strong electric field can be achieved at the ferroelectric-semiconductor interface, resulting in a large density change in the mid- 10^{14} cm^{-2} regime. Finally, electric-double-layer transistors (EDLTs) [3] using a spin-coated ion gel thin film (20 – 50 nm) as the gate dielectric have demonstrated a remarkable density modulation as high as 10^{15}cm^{-2} . Within the quantum-confined interface, this 2D density corresponds to a chemical substitution up to 10% or higher, at which the correlation effects become appreciable. Depending on the specific physics, all three FET structures will be explored to obtain a complete microscopic understanding of field effects in quantum materials.

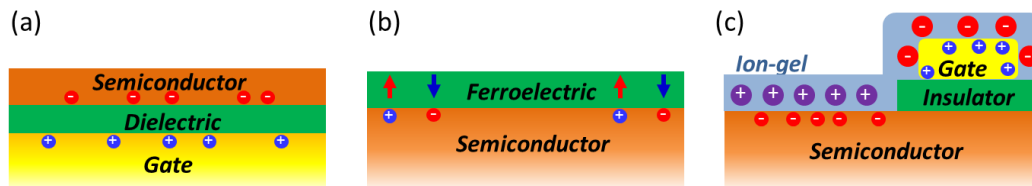


Fig. 1 (a) Conventional back-gated (a front gate would screen the electric fields) FET structure. (b) Ferroelectric FET (FerroFET) structure, in which the polarization can be locally switched by a biased tip. A much larger density change than that of the usual MOSFETs can be achieved. But generally only two states are available. (c) EDLT structure with a thin ion gel as the gate dielectric, achieving even higher (10^{15} cm^{-2}) density modulations. For simplicity, the source and drain contacts to the semiconductors are not shown in the schematics.

Recent Progress

1. Instrumentation

A crucial component of this program is to establish several MIM platforms for imaging electrical inhomogeneity at the mesoscopic (10~100nm) length scale. Thanks to the DOE support, we have now three up and running MIM systems: a room-temperature MIM based on a commercial atomic force microscope (AFM), a variable-temperature MIM based on the Janis cryostat, and a closed-cycle 4K/9T system from AttoCube Systems, as shown in Fig. 2. In addition, we have also improved the MIM performance in various aspects. The impedance detection electronics can now function at a wide range of 100MHz – 10GHz. For cryogenic environment, a tuning-fork based feedback loop has been tested and will be incorporated into the experimental platforms soon.

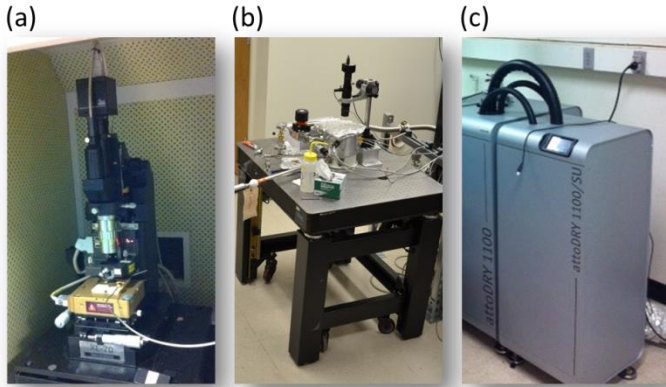


Fig. 2 (a) MIM based on room-T atomic-force microscope from Park Systems, Inc. The system will be used under ambient and elevated temperatures. (b) MIM based on variable-T cryostat from Janis Research Inc. The range of accessible temperatures is from 5K to 400K. (c) MIM based on closed-cycle 4K/9T system from AttoCube Systems. All three setups are now up and running in the PI’s laboratory.

2. Scientific Progress

2.1. Ferroelectric FET – carrier density modulation in semiconductors by polarization switching in the epitaxial ferroelectrics – has attracted much research interest due to the simple architecture and huge density modulation capability [2]. This seemingly straightforward approach has been extremely challenging because of the difficulty to combine a ferroelectric oxide directly with a semiconductor without any interfacial reaction. Our collaborator, Alex Demkov’s group at UT-Austin, has developed a method to strain the epitaxial BaTiO₃ (BTO) layer on Ge and force the polarization to be c-axis oriented. The density functional calculation, transmission electron micrograph (TEM), and piezo-force micrograph (PFM) all suggest that the BTO film is out-of-plane polarized. The challenge, however, is to demonstrate that the carrier density underneath the BTO is indeed modulated by the electrostatic field effect.

The MIM is capable of detecting the local conductivity of the underlying Ge substrate through capacitive coupling. The modulation of the carrier density at the ferroelectric-Ge interface results in appreciable impedance change of the tip, which is readily detected by the MIM electronics. As seen in Fig. 3, both PFM and MIM show clear contrast between the region written by $V_{tip} = -4V$ and the as-grown area. The PFM contrast confirms that BTO polarization is reversed by a large negative tip bias. More interestingly, the MIM contrast comes solely from the underlying Ge layer accompanied by the poling process. To our knowledge, this is the first time ferroelectric field effect is reported on semiconductors. And the observation will not be possible without the unique capability of the MIM.

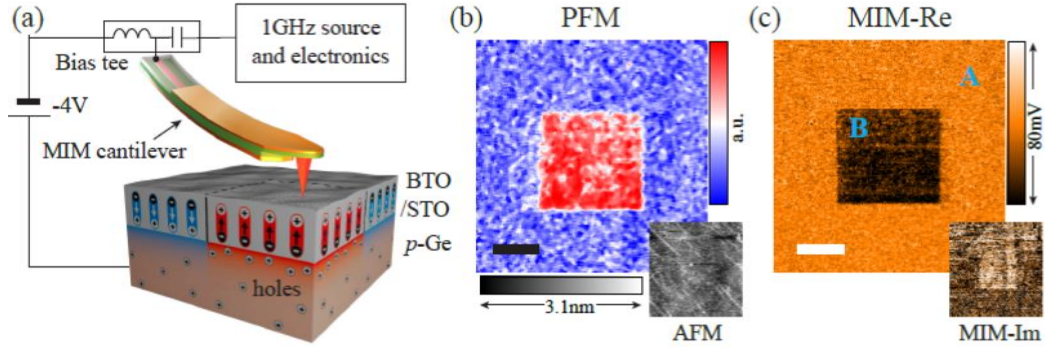


Fig. 3 (a) Schematic diagram illustrating the setup and configuration of samples. A negatively biased MIM probe locally switches the ferroelectric polarization of the BTO layer, resulting in substantial density modulation at the BTO/STO-Ge interface. (b) PFM and AFM (bottom right corner in b), (c) MIM real part and imaginary part (bottom right corner in c) images acquired after writing a $20\mu\text{m} \times 20\mu\text{m}$ square by applying -4V DC bias on the tip (Scale bars: $10\mu\text{m}$).

2.2. Electric-double-layer transistors (EDLTs) using electrolytes as gate dielectrics have shown an extremely wide range of density modulation, which is crucial for the emergent phenomena in quantum systems. Yet little is known microscopically when carriers are modulated due to the technical challenge to access the buried transistor interface with nanoscale resolution. Our variable-T MIM is ideal for this task because of the sub-surface imaging capability. Fig. 4 shows the experimental results on a prototypical semiconductor ZnO [4]. The gate voltage was applied at 230K before cooling down to 50K, at which the images were taken. When the ZnO is insulating with a channel resistance $> 1\text{G}\Omega$, the MIM data show very low signal on the ZnO region. As the transistor turns on with channel resistance $\sim 1\text{M}\Omega$, the MIM signal at the channel increases substantially, approaching that of the metal electrode. This preliminary result already contains all the necessary ingredients of the MIM study: (1) The field effect is seen for a thin ion gel $\sim 50\text{nm}$; (2) The gel freezes below $T_g \sim 220\text{K}$ and the scanning is possible; (3) The gel layer does not crack during the slow cooling process so the scan is not affected; (4) The conductivity change in the channel $\sim 50\text{nm}$ below the surface can be imaged by the MIM.

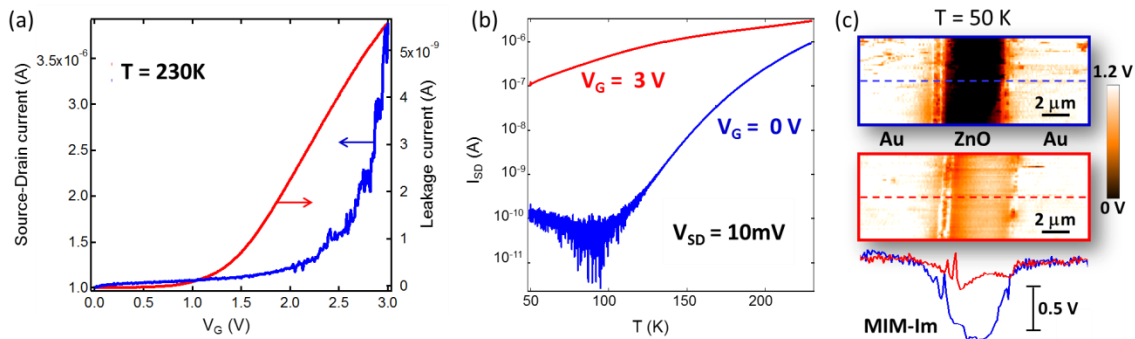


Fig. 4 (a) Transport characteristics of an EDLT on ZnO substrate. At 230K (slightly above T_g), the transistor turns on above $V_G = 2\text{V}$ with a low leakage current $I_{\text{leak}} \ll I_{\text{SD}}$. (b) Temperature dependence for the insulating ($V_G = 0\text{V}$) and conductive ($V_G = 3\text{V}$) states. A source-drain voltage of 10mV was applied for both (a) and (b). (c) MIM-Im images of the same EDLT device as described above taken at 50K. The top image was taken at $V_G = 0\text{V}$ and the bottom one at $V_G = 3\text{V}$ and $I_{\text{SD}}(230\text{K}) = 3\mu\text{A}$. The line cuts in both images are shown in the plot below.

To summarize, substantial progress has been achieved in the first year of DOE support. With instruments successfully installed and preliminary data obtained, we are excited to carry out the experiments in the coming years for profound scientific discoveries.

Future Plans

All three types of FET structures will be studied in the newly installed 4K/9T cryogenic MIM setup, which is crucial to determine the carrier densities. Besides, in addition to the standard 1GHz MIM electronics, we plan to use the new 100MHz and 10GHz circuits for frequency-dependent measurements.

EDLT experiment on the ZnO semiconductor will be finished soon and the results will be submitted. This will be the first report of electrical imaging on EDLTs and will attract a lot of attentions from the scientific community. We will then move on to more exotic materials such as colossal magnetoresistive manganites (LaCaMnO) and transition metal dichalcogenides (TMDCs, such as WSe₂, MoS₂). For TMDCs, both EDLT and conventional back-gated devices will be fabricated and the results compared. The spatially resolved information on these materials in the EDLT configuration has yet to be studied. We expect to enter an exciting and unexplored regime through the unique MIM measurements.

References

- [1] K. Lai, W. Kundhikanjana, M. A. Kelly and Z.-X. Shen, “Nanoscale microwave microscopy using shielded cantilever probes”, *Appl. Nanoscience* **1**, 13 (2011).
- [2] J. Hoffman, X. Pan, J. W. Reiner, F. J. Walker, J. P. Han, C. H. Ahn, and T. P. Ma, “Ferroelectric Field Effect Transistor for Memory Applications”, *Adv. Mater.* **22**, 2957 (2010).
- [3] K. Ueno, H. Shimotani, H. Yuan, J. Ye, M. Kawasaki, and Y. Iwasa, “Field-Induced Superconductivity in Electric Double Layer Transistors”, *J. Phys. Soc. Jpn.* **83**, 032001 (2014).
- [4] H. Shimotani, H. Asanuma, A. Tsukazaki, A. Ohtomo, M. Kawasaki, and Y. Iwasa, “Insulator-to-metal transition in ZnO by electric double layer gating”, *Appl. Phys. Lett.* **91**, 082106 (2007).

Publications

1. P. Ponath, K. Fredrickson, A. B. Posadas, Y. Ren, X. Wu, R. K. Vasudevan., M. B. Okatan., S. Jesse., T. Aoki, M. R. McCartney, D. J. Smith, S. V. Kalinin, K. Lai, and A. A. Demkov, “Carrier Density Modulation in Ge Heterostructure by Ferroelectric Switching”, Submitted to *Nature Communications*.

Scanning quantum gas atom chip microscopy of strongly correlated and topologically nontrivial materials

Prof. Benjamin Lev

Departments of Applied Physics and Physics and Ginzton Laboratory

Stanford University

benlev@stanford.edu

Program Scope:

Microscopy techniques co-opted from nonlinear optics and high energy physics have complemented solid-state probes in elucidating the order manifest in condensed matter materials. Up until now, however, no attempts have been made to use modern techniques of ultracold atomic physics to directly explore properties of strongly correlated or topologically protected materials. Our current program is focused on introducing a novel magnetic field microscopy technique into the toolbox of imaging probes. Our prior DOE ESPM program funded the development of a novel instrument using a dilute gas Bose-Einstein condensate (BEC) as a scanning probe capable of measuring tiny magnetic (and electric) DC and AC fields above materials. We successfully built the world's first “scanning cryogenic atom chip microscope” [1], and we now are in the process of characterizing its performance before *using* the instrument to take the first wide-area images of transport flow within unconventional superconductors, pnictides and oxide interfaces (LAO/STO), topological insulators, and colossal magnetoresistive manganites. We will do so at temperatures outside the capability of scanning SQUIDs, with $\sim 10x$ better resolution and without $1/f$ -noise. A notable goal will be to measure the surface-to-bulk conductivity ratio in topological insulators in a relatively model-independent fashion [2].

We have completed the construction of this magnetic microscope, shown in Figure 1. The instrument uses atom chips—substrates supporting micron-sized current-carrying wires that create magnetic microtraps near surfaces

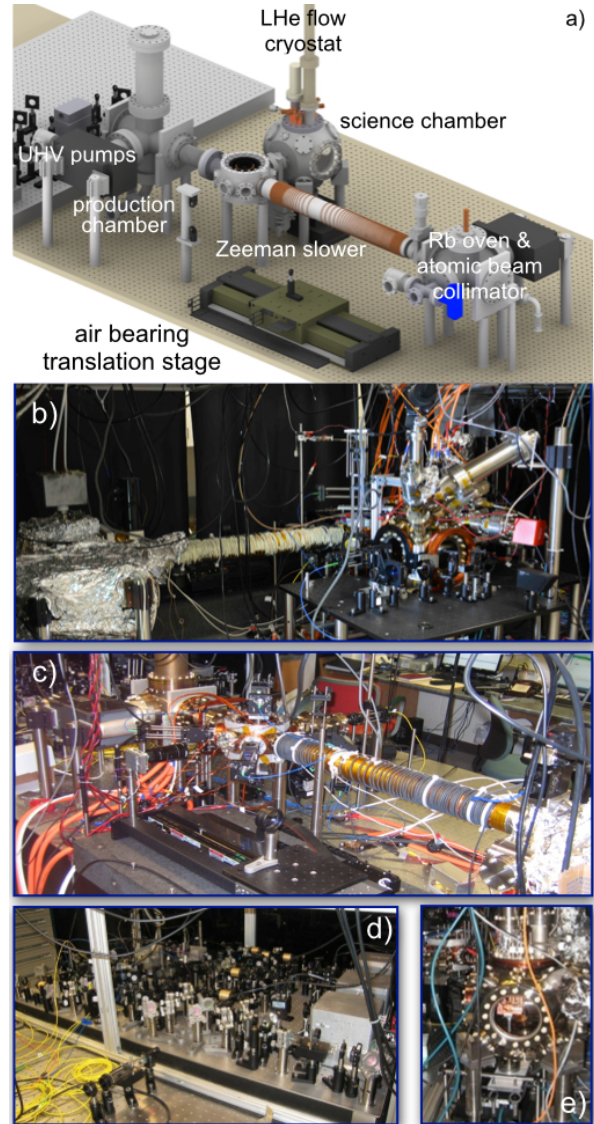


Figure 1: (a) 3D rendering of the cryogenic atom chip microscope we have designed and built (cooling and imaging optics not shown; another view shown in Fig. 2). (b-c) Picture of our functioning atom chip microscope. (d) Custom laser cooling system. (e) Image of science chamber and cryostat.

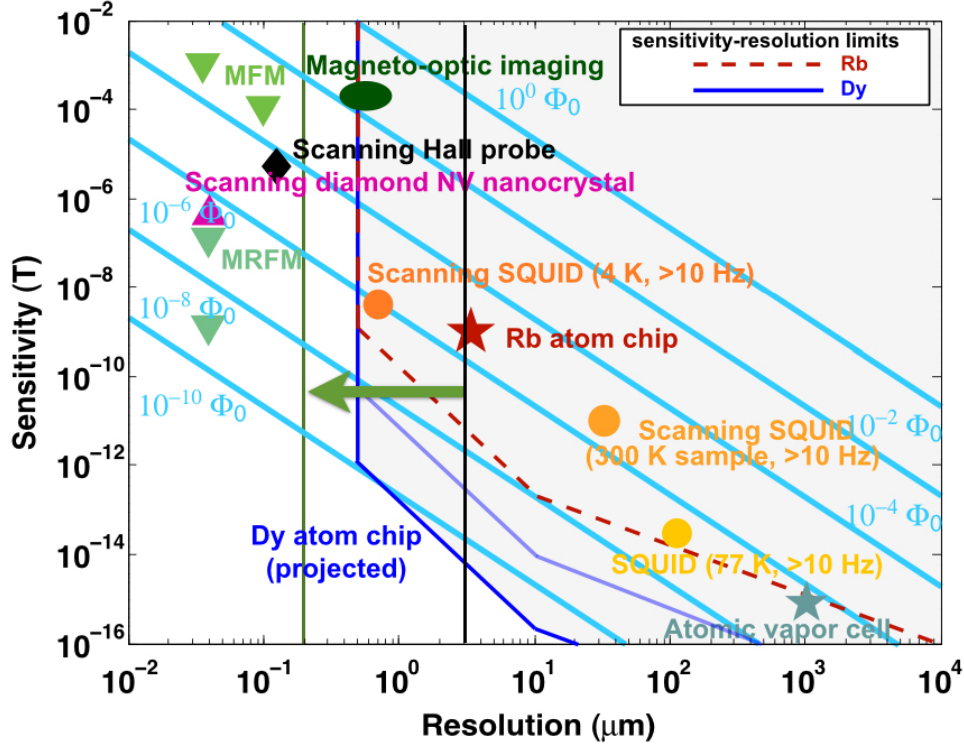


Figure 2: Comparison of techniques for high sensitivity, high-resolution magnetic field measurement. The red dashed (Rb) and blue solid (Dy) lines denote the sensitivity-resolution limits for atom chip microscopy with either Rb atoms or more exotic, highly magnetic atoms such as Dy that have recently been Bose-condensed by our group [5]. The leftmost blue and red boundary is due to a diffraction-limited ~ 600 -nm imaging resolution and the lower bounds arise from limits on obtainable trap frequencies vs gravity and BEC mean-field energies. In this program, we will work to push the resolution limit from the black line to the green vertical line through use of a novel super-resolution trapping technique.

for ultracold thermal gases and BECs—to enable single-shot and raster-scanned large-field-of-view detection of magnetic fields. The fields emanating from electronic transport may be detected at the 10^{-7} flux quantum (Φ_0) level and below (see Fig. 2); that is, few to sub-micron resolution of sub-nanotesla fields over single-shot, millimeter-long detection lengths.

By harnessing the extreme sensitivity of atomic clocks and BECs to external perturbations, we are now in a position to use atom chips for imaging transport in new regimes. Scanning quantum gas atom chip microscopy introduces three very important features to the toolbox of high-resolution scanning microscopy of strongly correlated or topological materials: simultaneous detection of magnetic and electric fields (down to the sub-single electron charge level [3,4]; no invasive large magnetic fields or gradients; simultaneous micro- and macroscopic spatial resolution; DC to MHz detection bandwidth; freedom from $1/f$ flicker noise at low frequencies; and, perhaps most importantly, the complete decoupling of probe and sample temperatures. The atom chip microscope can operate at maximum sensitivity and resolution without regard to the substrate temperature. While the BEC is among the coldest objects realizable (100 nK temperatures are typical), the atom chip substrate can be positioned $1 \mu\text{m}$ away from the BEC and be as hot as 400 K or as cold as the cryostat can cool. This is because unlike superconducting probes, whose temperature is closely coupled to nearby materials, quantum gases are immune to radiative heating¹. The energy gap between a Rb atom’s ground state and first excited state far exceeds the typical energy of room-temperature blackbody

¹ All experiments operate within an ultrahigh vacuum (UHV); convective heating is absent.

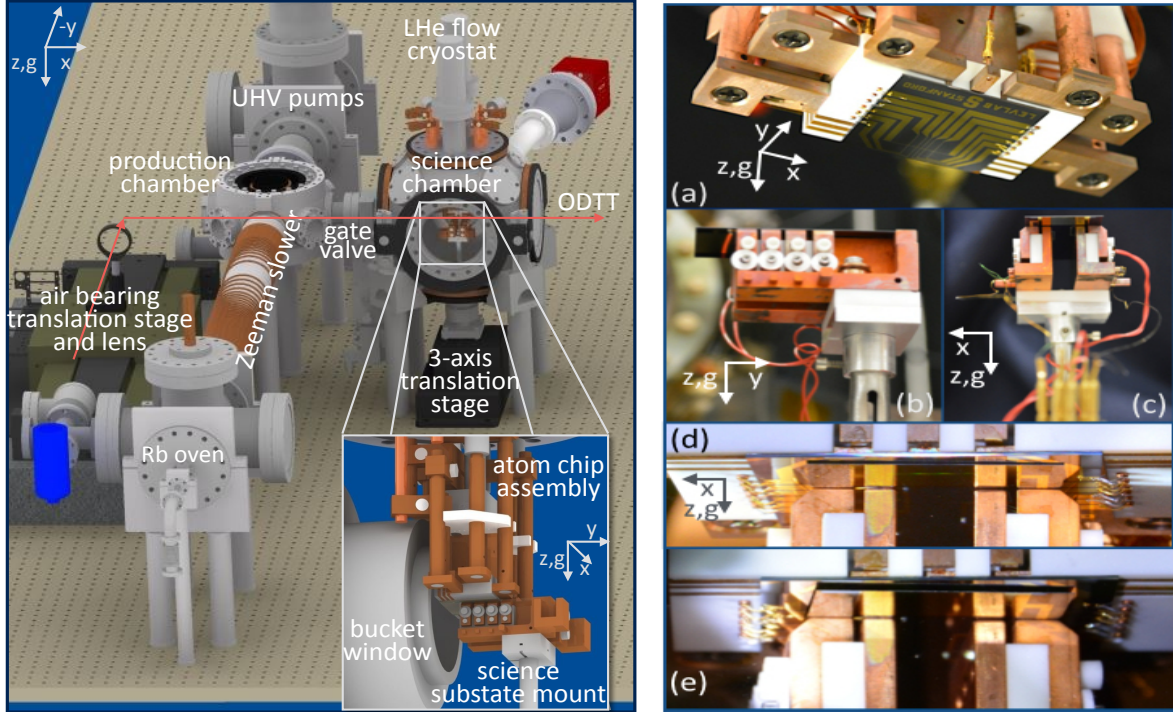


Figure 3: (Left) Rendering of experimental apparatus for laser cooling and trapping (cooling and imaging optics not shown). Inset: Intrachamber atom chip mount and electrical feedthroughs (top) along with the science substrate holder (bottom). The bucket window (left) allows high-NA lens placement. (Right) (a) Image of atom chip attached to macrowire-macor base chip and chilled-water block. View of science substrate mount from (b) the optical dipole trap viewpoint and (c) the imaging beam viewpoint. Science substrate (d) $d=120\ \mu\text{m}$ and (e) $d=300\ \mu\text{m}$ below atom chip.

radiation²; such atoms are therefore transparent to radiation heating by materials at room temperature or below.

Recent Progress:

We experimentally demonstrated a new atom chip trapping system that allows the placement and high-resolution imaging of ultracold atoms within microns from any $\leq 100\ \mu\text{m}$ -thin, UHV-compatible material, while also allowing sample exchange with minimal experimental downtime [1]. The sample is not connected to the atom chip, allowing rapid exchange without perturbing the atom chip or laser cooling apparatus. Exchange of the sample and retrapping of atoms has been performed within a week turnaround, limited only by chamber baking. Moreover, the decoupling of sample and atom chip provides the ability to independently tune the sample temperature and its position with respect to the trapped ultracold gas, which itself may remain in the focus of a high-resolution imaging system. See Fig. 3.

We confine 100-nK BECs of $10^4\ ^{87}\text{Rb}$ atoms near a gold-mirrored 100- μm -thick silicon substrate. The substrate can be cooled to 35 K without use of a heat shield, while the atom chip, 120- μm away, remains at room temperature. Atoms may be imaged with 1- μm resolution and retrapped every 16 s, allowing rapid data collection. Straightforward improvements will allow us to push sample temperatures close to 4 K, and improve imaging resolution from 1 μm down to a few-100 nm, thereby providing $10^{-9}\ \Phi_0$ detection sensitivity.

² At room temperature, blackbody radiation wavelength peaks at $\lambda = 10\ \mu\text{m}$; Rb electronic transitions are $\lambda < 1\ \mu\text{m}$.

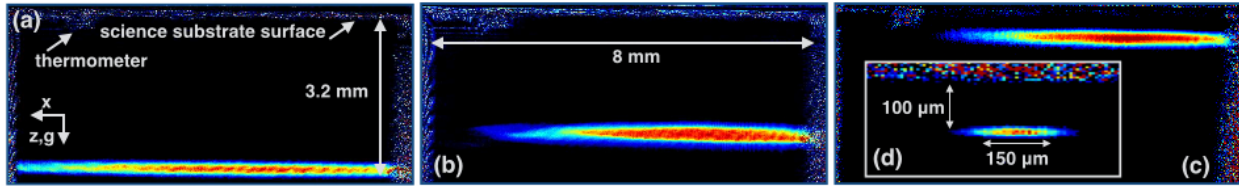


Figure 4: Time-of-flight absorption images of: (a) 1.1×10^7 atoms 2 ms after optical dipole trap release in science chamber; (b) atoms 5 ms after release from macrowire trap; (c) 8×10^6 atoms at $16 \mu\text{K}$ in compressed microwire trap at $h=350 \mu\text{m}$, 1 ms after release; (d) 8×10^4 atoms compressed and evaporatively cooled to near degeneracy.

Future plans:

We will test the utility of this technique by imaging the magnetic fields emanating from electronic transport and domain percolation in several interesting examples of strongly correlated or topologically protected materials. STM, transport, and x-ray scattering experiments have, among others, revealed the existence of a quantum liquid crystal state in iron (pnictide) and cuprate superconductors. This strongly correlated state of matter could also be detected by imaging the fluctuating transport (spatially and in time) of electrons as the phase/regime boundary is crossed between the pnictide non-Fermi liquid (cuprate strange metal) and the pnictide magnetic phase (cuprate pseudogap regime). Our ability to image wide-area inhomogeneous current flow from room-temperature to $<10 \text{ K}$ will allow us to study the developing domain structure and transport near twin boundary interfaces through the $T_N \sim 50\text{--}150 \text{ K}$ nematic transition recently identified in bulk transport experiments by Ian Fisher's group in underdoped Fe-arsenide superconductors [6]. Again, this highlights a main feature of our cryogenic atom chip microscope: the ability to image transport regardless of the sample temperature since the BEC, at nK temperatures, is transparent to blackbody radiation, even when held a microns from the surface.

These sets of experiments on iron-based superconductors, performed in collaboration with Ian Fisher at Stanford, will be followed by a relatively model-independent measurement of the surface-to-bulk conductivity ratio in topological insulators, in a scheme the PI recently proposed using our cryogenic atom chip microscope [2].

References:

- 3) S. Aigner *et al.*, *Long-range order in electronic transport through disordered metal films*, Science **319** 319 (2008).
- 4) S. Wildermuth, *et al.* *Sensing electric and magnetic fields with Bose-Einstein condensates*, Appl. Phys. Lett. **88**, 264103 (2006).
- 5) M. Lu, N. Q. Burdick, S.-H. Youn, and B. L. Lev, *Strongly Dipolar Bose-Einstein Condensate of Dysprosium*, PRL **107**, 190401 (2011).
- 6) J.-H. Chu, J. Analytis, K. De Greve, P. McMahon, A. Islam, Y. Yamamoto, and I. Fisher, *In-Plane Resistivity Anisotropy in an Underdoped Iron Arsenide Superconductor*, Science **329**, 824 (2010).

Publications:

- 1) M. A. Naides, R. W. Turner, R. A. Lai, J. M. DiSciacca, and B. L. Lev, *Trapping ultracold gases near cryogenic materials with rapid reconfigurability*, Applied Physics Letters **103**, 251112 (2013).
- 2) B. Dellabetta, T. L. Hughes, M. J. Gilbert, and B. L. Lev, *Imaging topologically protected transport with quantum degenerate gases*, Phys. Rev. B **85**, 205442 (2012).

Tailoring the electronic properties of graphene via nanostructuring: An integrated atomic resolution STM and non-contact AFM study

PI: Lian Li

Department of Physics, University of Wisconsin, Milwaukee, WI 53211

Program Scope

The focus of this program is to attain new functionalities in graphene by nano engineering and chemical modification using an integrated approach of STM/AFM imaging and spectroscopy and density functional theory calculations.

Recent Progress

1. Spatial fluctuations of barrier height at the graphene/semiconductor Schottky junctions

Unique to graphene, a 2D material with a negative coefficient of thermal expansion is that it is susceptible to deformation when interfaced with another material or under an electric field. In this part of the research, we have investigated the effect of these graphene “ripples” on the Schottky barrier height at graphene/semiconductor junctions.

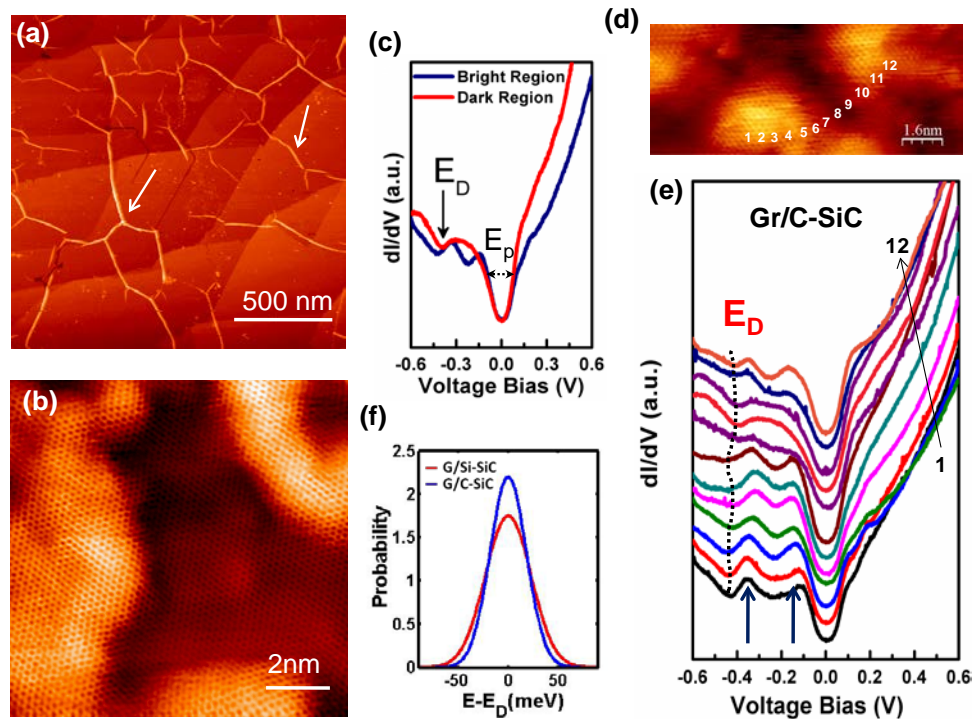


Fig. 1 **Spatial fluctuations of Dirac energy.** (a,b) STM images of graphene/Si-face ($V_s=-0.2V$, $I_t=1.0nA$). (c) Representative dI/dV spectra of graphene/C-face SiC. (d) STM image of graphene/C-SiC ($V_s=-0.2V$, $I_t=1.0nA$). (e) dI/dV spectra taken along positions 1-12 marked in (d). (f) Distribution of the E_D for graphene/Si- and C-face SiC.

Chemical vapor deposited graphene was transferred onto both Si- and C-faces of SiC, as confirmed by Raman spectroscopy and STM imaging (Fig. 1(a,b)). Tunneling spectroscopy

indicates that for graphene/C-SiC, the Dirac point is at 0.42 eV below E_F (Fig. 1(c)), while on the Si-face it is 0.35 eV above (not shown), a direct consequence of the larger work function at the Si-face. In addition, we observe spatial fluctuations in the Dirac energy caused by the intrinsic rippling at the graphene/SiC interface (Fig. 1(c)). The spatial variation of the Dirac energy directly follows the undulation of the ripples (Fig. 1(e)), exhibiting a Gaussian distribution with a full-width-at-half-maximum of 42 and 51 meV for graphene transferred on C- and Si-SiC (Fig. 1(f)), respectively. This result – in direct contrast to graphene/SiO₂, where fluctuations in the Dirac energy is not correlated to topographic variations, but to charge impurities in the SiO₂ substrate – reflects an intrinsic effect inherent for graphene/semiconductor Schottky contacts. This work has been published in *Nature Communications* (Nat. Commun. **4**, 2752 (2013)).

We have also investigated the intrinsic spatial inhomogeneity in barrier height at graphene/SiC Schottky junctions using transport measurements. Temperature dependent I-V

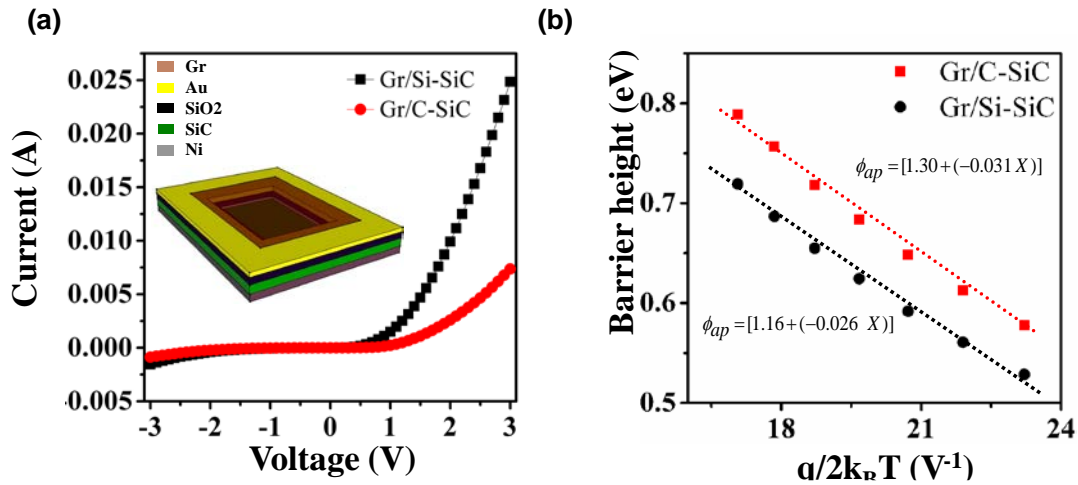


Fig. 2 **Spatial fluctuations of barrier height at the graphene/SiC Schottky junctions.** (a) Rectifying I-V characteristics of Gr/C-SiC and Gr/Si-SiC Schottky junctions at 310 K (Inset shows device schematic diagram). (b) Plot of apparent zero bias barrier height ϕ_{ap} vs. $q/2k_B T$.

measurements clearly show indicate rectifying behaviors (Fig. 2(a)). Nevertheless, we find that non-ideal behavior - increase of zero bias Schottky barrier height and decrease of ideality factor with increasing temperature - is directly related to the three main types of spatial inhomogeneities as revealed by STM: atomic scale ripples, nanometer ridges, and deformation caused by SiC steps. Using the modified thermionic emission model, assuming a Gaussian distribution of the barrier, mean Schottky barrier heights of 1.30 ± 0.18 eV and 1.16 ± 0.16 eV are found for graphene/SiC junctions on the C- and Si-face, respectively. This work is the first such study that directly relates the spatial inhomogeneities at graphene semiconductor junctions to the fluctuations in Schottky barrier height. These findings have been published in *Applied Physics Letters* (APL **105**, 021607 (2014)).

2. Semiconducting graphene zigzag nanoribbons with H-termination

While pristine graphene is a semimetal with linear dispersion at the Dirac point, graphene nanoribbons provide new functionalities, such as tunable energy gap and spin-polarized edge states. In this part of the research, we have fabricated H-terminated zigzag nanoribbons using Fe

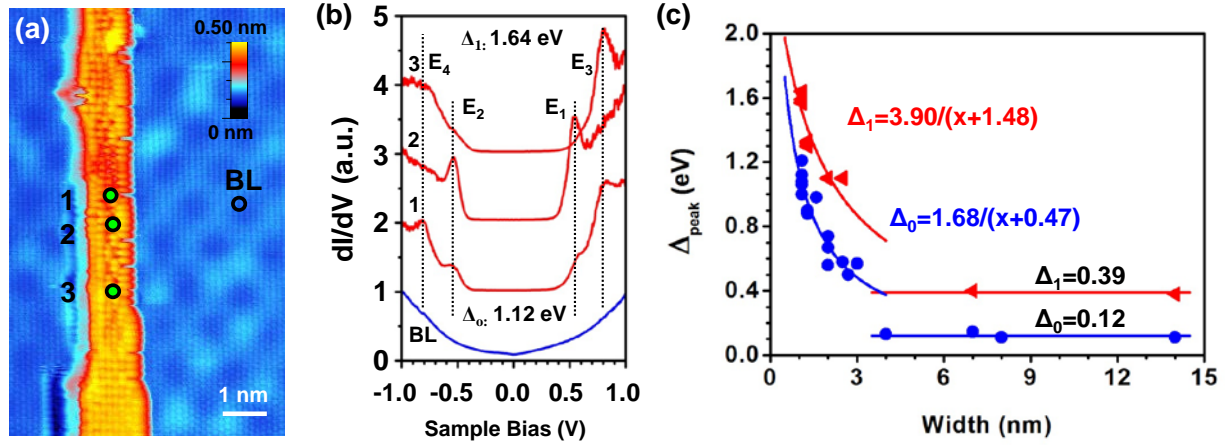


Fig. 3 **Semiconducting H-terminated zigzag nanoribbons.** (a) STM image of a variable width ribbon supported on BL graphene ($V_s = -0.5$ V, $I_t = 0.1$ nA). (b) dI/dV spectra taken at positions marked 1, 2, and 3 in (a). (c) Plot of the two gaps in the LDOS as a function of ribbon width.

nanoparticles (NPs)-assisted etching of epitaxial graphene/SiC(0001) in hydrogen. Nanoribbons as small as 1 nm can be made using this method as shown in Fig. 3(a).

We find two gaps in their local density of states by tunneling spectroscopy as shown in Fig. 1(b). In addition, the gaps are found to be strongly dependent on their width (w). For ribbons wider than 3 nm, gaps up to 0.39 eV are found independent of w , consistent with DFT calculations. For ribbons narrower than 3 nm, however, much larger gaps are obtained, which also scale inversely with w , supporting the need for quasiparticle corrections to the calculated gap (Fig. 3(c)). A 1.6 eV gap is found for a 1 nm ribbon. These results provide the first direct experimental confirmation of electron-electron interactions in the gap opening of graphene zigzag nanoribbons, and reveal a critical width of 3 nm for the onset of such interactions.

The finding of a critical threshold for the onset of the quasiparticle corrections to the gap for narrower ribbons is fully consistent with the fact that the interior of wider ribbons (>5 nm) are nominally graphene, a zero gap semiconductor. Therefore, quasiparticle corrections to the gap are not relevant since there is no gap to begin with. This work has been published in *Nature Communications* (Nat. Commun. **5**, 4311 (2014)).

3. Revealing the origin of the linear dispersion of silicene/Ag(111)

In this part of the research, we have theoretically investigated the formation and electronic properties of silicene – the silicon analog of graphene – which forms a (3×3) structure on (4×4) Ag(111). Although there have been reports from angle-resolved photoemission spectroscopy (ARPES) of linearly dispersing Dirac states, the calculations clearly show that the (3×3) reconstruction opens a gap. We have used a k -projection technique that accounts for the photon

(k_z) dependence which allows a consistent comparison of the ARPES experiments and the calculations. Our calculations not only reproduce the observed gap and linear dispersion across the K point of (1×1) silicene, but also demonstrate that these originate from the k -dependence of Ag(111) substrate states (modified by interactions with the silicene) and not from a Dirac state. Our theoretical results thus provide a consistent explanation of the available experimental data, and thus resolve the controversy concerning the (non)existence of Dirac states in silicene/Ag(111). This work has been published in *Nano Letters* (DOI: 10.1021/nl502107v).

Future Plans

We will continue the systematic studies already underway to investigate 1) the electronic properties of oxygen-terminated graphene nanoribbons synthesized by Ag NPs-assisted etching of epitaxial graphene/SiC(0001); 2) the intrinsic electronic properties of graphene grain boundaries; and 3) proximity effects in graphene.

Publications

1. “Revealing the substrate origin of the linear dispersion of silicene/Ag(111)”, M. X. Chen and M. Weinert, *Nano Lett.* (2014) (DOI: 10.1021/nl502107v).
2. “Direct experimental determination of onset of electron-electron interactions in gap opening of zigzag graphene nanoribbons”, Y. Y. Li, M. X. Chen, M. Weinert, and L. Li, *Nat. Commun.* **5**, 4311 (2014).
3. “Intrinsic inhomogeneity in barrier height at monolayer graphene/SiC Schottky junction”, D. Tomer, S. Rajput, L. J. Hudy, C. H. Li, and L. Li, *Appl. Phys. Lett.* **105**, 021607 (2014).
4. “Direct experimental evidence for the reversal of carrier type upon hydrogen intercalation in epitaxial graphene/SiC(0001)”, S. Rajput, Y. Y. Li, and L. Li, *Appl. Phys. Lett.* **104**, 041908 (2014).
5. “Spatial fluctuations in barrier height at the graphene-SiC Schottky contact”, S. Rajput, M. X. Chen, Y. Y. Li, Y. Liu, M. Weinert, and L. Li, *Nat. Commun.* **4**, 2752 (2013).

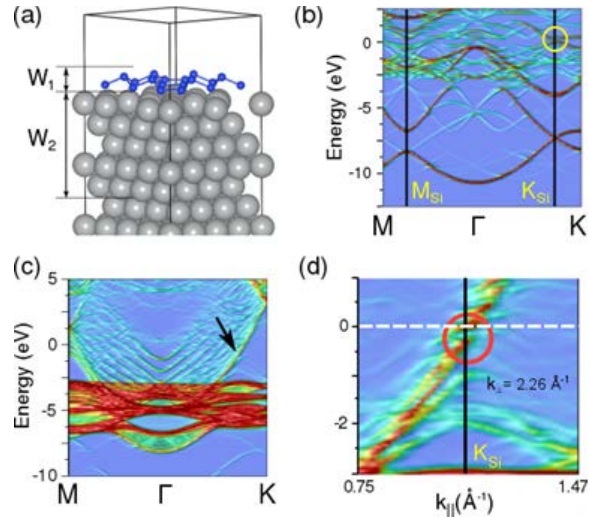


Fig. 4 DFT calculations of silicene/Ag(111). (a) Model of the relaxed structure of (3×3) silicene on (4×4) Ag(111). W_1 (centered on the silicene) and W_2 (substrate) are the regions used for integrating wave functions in the k -projection. (b) k -projected bands for the silicene layer (W_1) in silicene/Ag(111). The yellow circle highlights the gap opening at K_{Si} . (c) Bands k -projected to (1×1) Ag(111); the arrow indicates the silicene-induced Ag surface state. (d) $E(k)$ around K_{Si} for silicene/Ag(111) along Γ – K for $k_z = 2.26 \text{ \AA}^{-1}$, corresponding to the experimental photon energy. The circle indicates the apparent gap opening at this photon energy.

STM Studies of Spin-Orbit Coupled Phases in Real- and Momentum-Space

Vidya Madhavan, Department of Physics, Boston College and Department of Physics, University of Illinois Urbana-Champaign

Program Scope

Our goal is to investigate the electronic properties of new topological materials such as topological crystalline insulators in bulk and in thin film form. To explore these materials we use scanning tunneling microscopy and spectroscopy, Fourier Transform spectroscopy and Landau level spectroscopy.

Recent Progress

1. Coexistence of massless and massive Dirac Fermions in topological crystalline insulators.

The recently discovered topological crystalline insulators (TCIs) belong to a new category of materials whose topological characteristics rely on crystal symmetry. The interplay between topology and crystalline symmetry creates unique surface states consisting of two generations of spin-polarized Dirac cones at different energies. In this work we carried out scanning tunneling microscopy studies of a TCI $\text{Pb}_{1-x}\text{Sn}_x\text{Se}$. By combining Landau level data with a theoretical model for the band structure, we map out the electronic structure of surface states with meV resolution. We demonstrate that the low-energy Dirac nodes are separated from high-energy ones by a Van-Hove singularity associated with a change of Fermi surface topology. In addition, we observe unexpected non-dispersing peaks located symmetrically on both sides of the low-energy Dirac point. Comparison with theory reveals that these peaks arise from a distortion of the crystal structure, which breaks reflection symmetry with respect to one mirror plane. This type of broken symmetry endows mass to one pair of Dirac fermions, while leaving the other pair massless. Our results demonstrate the formation of zero mass Dirac fermions protected by crystal symmetry and the mechanism of mass generation via symmetry breaking, which constitute the defining characteristics of TCIs. Our work paves the way for engineering the Dirac band gap and realizing interaction-driven topological quantum phenomena by manipulating the crystal structure. (Published *Science*, 2013¹)

2. Mapping the unconventional orbital texture in topological crystalline insulators

A fundamental property predicted for topological crystalline insulator (TCI) family of materials is that due to symmetry constraints the orbital character of the surface state (SS) bands is

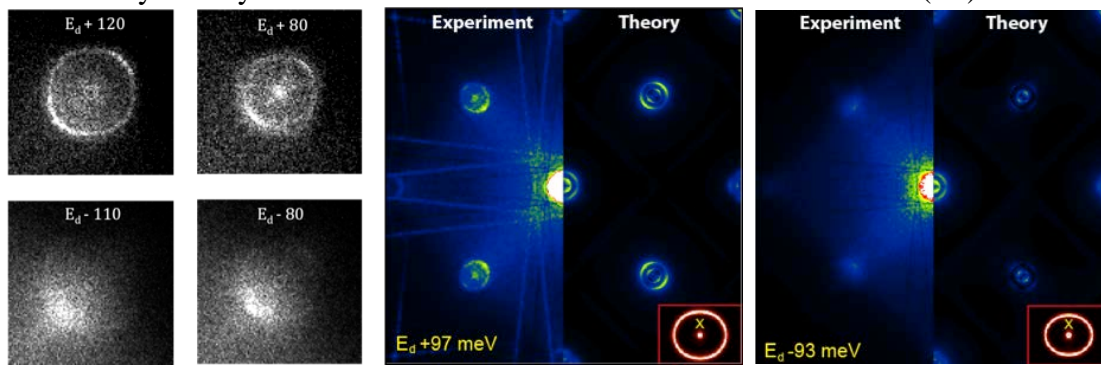


Fig. 1 (Left) STM Fourier transforms above and below the Dirac point showing the effects of orbital depending scattering. (Middle and right) Comparison between STM data and theory.

different above and below the Dirac point. Both orbital- and spin-texture are therefore essential for a complete description of the TCI SS band structure. To experimentally probe this, we measured the interference patterns produced by the scattering of SS electrons of $\text{Pb}_{1-x}\text{Sn}_x\text{Se}$ in the topological regime by scanning tunneling spectroscopy (STS). Fourier transforms (FTs) of the interference patterns show a marked change with energy across the Lifshitz transition. Importantly, we find that the intensity and energy dependence of the FTs show distinct characteristics, which by comparison with theory can be attributed to orbital effects (Fig. 1). Our results demonstrate the impact of orbital texture in scattering processes measured by STS and reveal the distinct orbital nature of the Dirac bands in this new class of topological materials. (Published *Nature Physics*, 2014²)

3. Evolution of Dirac Surface States across the Quantum Phase Transition in a Topological Crystalline Insulator

A central question in the field of topological insulators involves the fate of the Dirac surface states when band inversion is undone and the material becomes non-topological. The transition of topological

surface states into the trivial phase has remained elusive in part due to lack of suitable materials. Here, we use scanning tunneling microscopy to track the quantum phase transition in a topological crystalline insulator (TCI), $\text{Pb}_{1-x}\text{Sn}_x\text{Se}$, tuned by Sn content. We discover the existence of surface states in the trivial phase that have the characteristics of gapped, double-branched Dirac

fermions (Fig. 2). We demonstrate how these states induced by proximity to the topological phase, morph into robust topologically protected Dirac surface states across the critical composition. Our new theory for the non-topological SS indicates that this transformation is created by the reversal of Dirac fermion chirality, which naturally accompanies the topological phase transition in the bulk. Furthermore, we image the symmetry breaking distortion that leads to massive Dirac Fermions and track the evolution of the mass across the phase transition. Our results establish the highly tunable nature of TCIs with constantly evolving fermiology as a function of composition, which goes beyond topology and crystalline symmetries and shows unexpectedly rich behavior. (Paper under review at *Nature Materials*³)

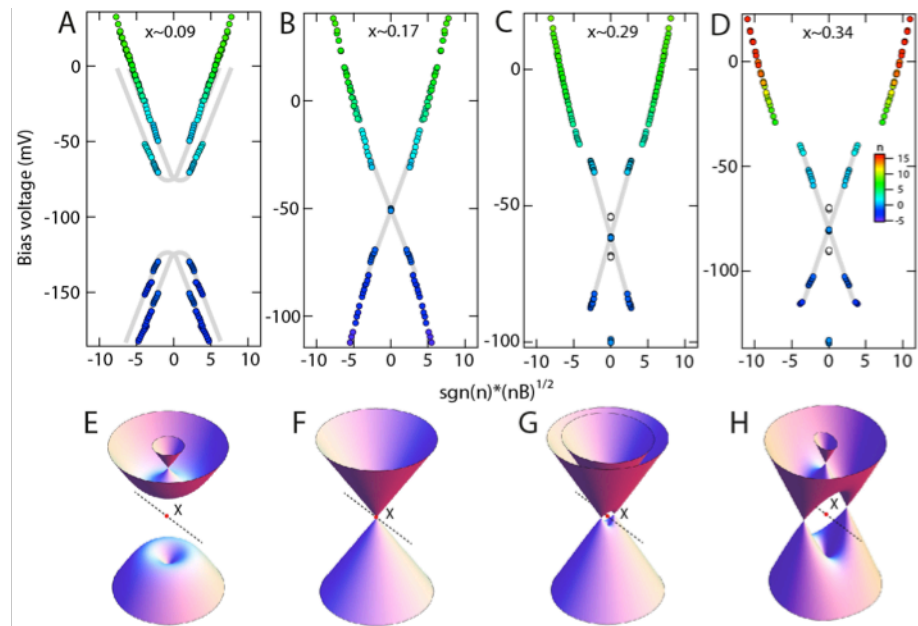
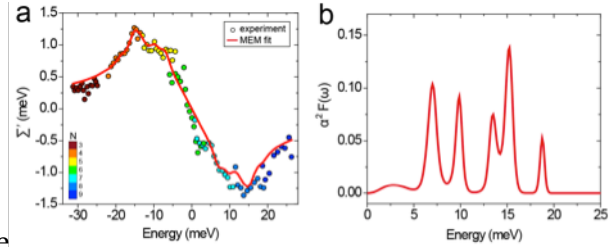


Fig.2 Landau level data showing the evolution of the Dirac surface states from the trivial to the topological regime. The schematic band structure from our data is shown below.

4. Nanoscale Determination of the Mass Enhancement Factor in Lightly-Doped n-type PbSe

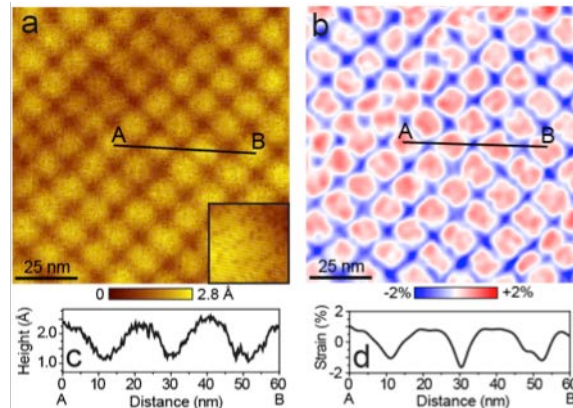
Before the discovery of topological surface states in bismuth chalcogenides and lead telluride/selenide alloys, these systems were heavily investigated due to exceptional thermoelectric properties which could be harnessed for power generation and device applications¹. Recent evidence suggests that lattice vibrations (phonons) play a significant role in achieving these desired properties², so quantifying the interaction between phonons and electrons is of immense importance for complete understanding of these systems. Nearly all information about electron-phonon coupling (EPC) is contained in the Eliashberg function of the material, but its precise extraction has in part been limited due to the lack of local experimental probes. By utilizing Landau level spectroscopy, we construct a method to directly extract the Eliashberg function, and demonstrate its applicability to lightly-doped thermoelectric bulk insulator PbSe. In addition to high energy resolution only limited by thermal broadening, and access to both occupied and unoccupied electronic states, this novel experimental method could be used to detect variations in mass enhancement factor (λ) on microscopic length scales, which opens up a unique pathway for investigating the effects of chemical defects, surface doping and strain on λ . (submitted to *Nature Communications*⁴)



Real part of the self-energy (Σ') and the extraction of the Eliashberg function. (a) Experimentally determined Σ' (open circles) and the maximum entropy method (MEM) fit (red line). (b) The extracted Eliashberg function (red) obtained by using the experimental data in (a).

Future Plans

Our thin film effort is focused on growing topological materials which are susceptible to being tuned by doping, strain or gating, allowing us to explore their electronic properties at the nanoscale in the most interesting regimes. We plan to grow various kinds of topological thin films on various substrates and study this by STM. In our first experiments we have successfully grown SnTe thin films on PbSe substrates resulting in a strained thin film. Strain in TCIs is predicted to be an *in-situ* tuning equivalent of alloying composition change, which can be used to alter the momentum position of the surface state (SS) Dirac cones away from the time-reversal-invariant (TRI) points. However, experimental realization of this unique tunability of TCI SS via strain engineering is yet to be achieved. We are currently growing heteroepitaxial thin films of SnTe and studying them using Fourier-transform (FT) scanning tunneling



Mapping the local lattice strain. (a) STM topograph of the region of the sample used for QPI measurements in Figure 2. Atomically-resolved inset in (a) acquired over a 10 nm square region demonstrates the high quality of our samples. (b) 'Strain' map calculated from the topograph in (a). (c) Line cut through topograph in (a) and strain map in (b)

microscopy (STM). Our preliminary measurements indicate that in-plane strain induces a distinct spatial changes in the surface state dispersion. In our studies of bulk TCIs our next step will be to study magnetically doped TCIs to explore the effects of broken time-reversal symmetry on the TCI surfaces states.

Publications

¹Y. Okada, et.al , Observation of Dirac node formation and mass acquisition in a topological crystalline insulator, *Science* **341**, 1496-1499 (2013)

²Ilija Zeljkovic, et.al , Mapping the unconventional orbital texture in topological crystalline insulators, *Nature Physics* **10**, 572–577 (2014)

³Ilija Zeljkovic, et.al , Dirac mass generation from crystal symmetry breaking on the surfaces of topological crystalline insulators, *under review Nature Materials*, , arXiv:1403.4906

⁴Ilija Zeljkovic, et.al , Nanoscale Determination of the Mass Enhancement Factor in Lightly-Doped Bulk Insulator PbSe,, *submitted to Nature communications*

New Strategies to Image Surfaces

L. D. Marks, Department of Materials Science and Engineering, Northwestern University, Evanston, IL 60208

Program Scope

Oxide surfaces are an important frontier, with numerous energy-related applications in areas ranging from catalysis to the emerging field of oxide electronics. Despite this, our understanding of oxide surfaces is relatively primitive and more often than not it is assumed that they are essentially the same as the bulk. This is not true. There is a large body of evidence indicating that many oxide surfaces reconstruct with large unit cells, some of which make the reconstructions found for elemental metals or semiconductors look simple. Indeed, the simplest perovskite SrTiO₃ has many more reconstructions than silicon, and some of them (those on the (111) surface) are almost certainly more complicated than the Si (111) 7x7 reconstruction. The atomic structure of most of these reconstructions is not known, in large part due to a combination of experimental complications in fabricating them reproducibly and the fact that the workhorses of structure determination for conductors (low energy electron diffraction (LEED) and scanning tunneling microscopy (STM)) are much less effective with insulators.

It would be invaluable to have local information about oxide surfaces where one could read of the atomic structure, independent of whether they are insulators or conductors. For instance, with an oxide supported catalyst or an oxide which is itself used as an active catalyst, knowledge of the detailed atomic structure of the surface as well as its chemical composition is needed to fill the gap between structure and performance paving the way for better catalysts to be engineered. As a second example, there is substantial evidence that the exact structure of the initial surface often plays a critical role in determining the subsequent growth. Without detailed atomic-scale information it is hard to explain or predict properties with much confidence, and one often has to fallback to a trial-and-error approach.

The focus of this work is:

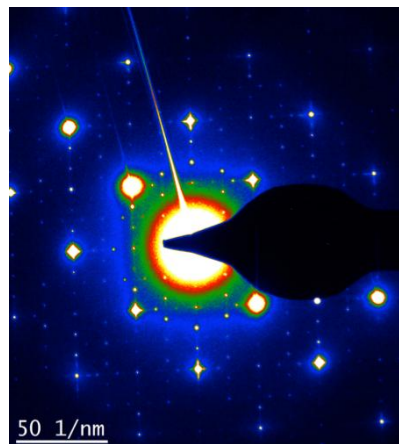
- To take advantage of recent advancements in electron microscopy to evolve and improve our methods for imaging oxide surfaces.
- To test and refine our methods for imaging oxide surfaces by applying them to scientifically relevant materials such as SrTiO₃ and LaAlO₃.
- To deepen the scientific community's understanding of how oxide surfaces behave and how that knowledge can be used to beneficially manipulate surfaces for specific applications.

A specific target of the work is to see to what extent new aberration-corrected instruments can be used to obtain better information about surfaces, both in plan-view as well as

profile view, other techniques such as HAADF and new methods still under development such as high-resolution scanning electron microscopy (HRSEM) [1].

Recent Progress

The work has been highly collaborative, involving not just the group at Northwestern but also James Ciston at NCEM, Yimei Zhu at BNL and the group of Les Allen in Melbourne. The original intent was to calibrate HRSEM using a known reconstruction on SrTiO₃ (001), specifically the c(6x2) (see Figure 1) but it has evolved into a more complicated project from which a series of papers are being reviewed or are being prepared for publication. The main new science to come out is:

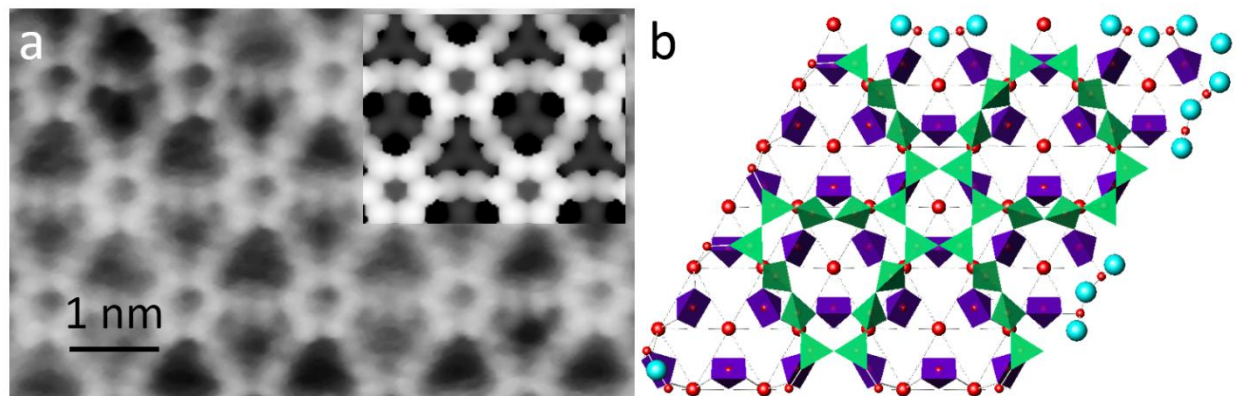


Pseudocolor diffraction pattern of the c(6x2) (001) surface

1. HRSEM is a powerful technique with true surface sensitivity, and can be used to obtain surface information on essentially any material with parallel collection of bulk information. The current limit is signal-to-noise which may involve detector design.
2. The prior theories for HRSEM [2, 3] needed to be extended to account for the role of dielectric screening in attenuating the signal from valence and to a lesser extent semi-core electrons. The image contrast is not simply related to the atomic number as originally suggested with a $Z^{0.53}$ dependence [2], it is much more complicated with some very interesting potential for new spectroscopies.
3. The previously published model for the c(6x2) reconstruction [4] was incorrect, having the wrong registry on the underlying bulk. A new structure has been derived combining imaging and DFT
4. Conventional plan view imaging works well with aberration-corrected instruments, but unfortunately it is not significantly better; the image resolution may be better but dynamical diffraction and projection problems remain.
5. HAADF is surprisingly insensitive to surface structure in plan view mode.

A second significant piece of work has been the reconstruction of the SrTiO₃ (111) surface. While a family of nxn reconstructions such as (9/5 x 9/5)[5-7], ($\sqrt{7}\times\sqrt{7}$ R19.1°)[8], (3x3)[5-7], ($\sqrt{13}\times\sqrt{13}$ R13.9°)[8], (4x4)[5-7], (5x5)[7], and (6x6)[5-7] had been known to exist for some years, what they were beyond the unit cells was completely unknown. By combining STM images from Martin Castell in Oxford as well as TED data, DFT calculations and STM simulations we have been able to solve the 4x4, 3x3, and several 2x2 reconstructions. While the structures by themselves are interesting, see Figure 2, there is much more from the details. Based upon an extensive analysis of about 100 different possibilities we have been able to determine

that there is a order-disorder transition from the simpler 4x4 and 3x3 to glass-like 2x2 structures which can be described via a Potts model, the more disorder structures being entropically favored at high temperatures. This has quite interesting implications for thin film growth of



oxides, it changes substantially how one considers such problems.

Figure 2: STM image and simulation in a) of the 3x3 structure, atomic structure in b).

Future Plans

I believe that HRSEM has gone a long way in a short time, but there is still a vast amount to be done and many potential opportunities. We intend to test it on a large range of systems such as heterogeneous catalysts, oxide thin films from oxidative or aqueous corrosion both with a lower performance microscope at Northwestern as well as with collaborators at BNL and NCEM.

There are also many other ways to image surfaces in plan view which we intend to test. One is to investigate the performance of off-zone HREM imaging with aberration-corrected instruments. Another is to look at ABF, where it is unclear whether or not surfaces can be better imaged.

Another planned work is to investigate further some aspects of HRSEM imaging using more sophisticated dielectric response methods such as BSE calculations of specific structures using DFT calculated electronic structure. This will be important to better understand possible spectroscopic possibilities.

Finally, a new collaboration has opened up with the group of Dillon Feng at ANL who is currently funding two graduate students to do in-situ growth work at APS. The intent is to jointly look into the role of the initial surface structure on subsequent growth. The generic structure of this work is that methods and samples of known reconstructions for SrTiO_3 as well as other materials such as LaAlO_3 or KNdO_3 would be produced at Northwestern then used for thin film growth at ANL.

References

1. *Imaging single atoms using secondary electrons with an aberration-corrected electron microscope.* Zhu, Y., H. Inada, K. Nakamura, and J. Wall, *Nature Materials*, 2009. **8**(10), 808-812.
2. *Image simulation for atomic resolution secondary electron image.* Wu, L.J., R.F. Egerton, and Y.M. Zhu, *Ultramicroscopy*, 2012. **123**, 66-73.
3. *Secondary electron imaging at atomic resolution using a focused coherent electron probe.* Brown, H.G., A.J. D'Alfonso, and L.J. Allen, *Physical Review B*, 2013. **87**(5), 054102.
4. *Atomic-scale structure of the SrTiO₃(001)-c(6×2) reconstruction: Experiments and first-principles calculations.* Lanier, C.H., A. van de Walle, N. Erdman, E. Landree, O. Warschkow, A. Kazimirov, K.R. Poeppelmeier, J. Zegenhagen, M. Asta, and L.D. Marks, *Physical Review B*, 2007. **76**(4), 045421.
5. Chiaramonti, A.N., *Structure and Thermodynamics of Model Catalytic Oxide Surfaces*, in *Materials Science and Engineering*. 2005, Northwestern: Evanston, USA.
6. *Time, temperature, and oxygen partial pressure-dependent surface reconstructions on SrTiO₃ (1 1 1): A systematic study of oxygen-rich conditions.* Chiaramonti, A.N., C.H. Lanier, L.D. Marks, and P.C. Stair, *Surface Science*, 2008. **602**, 3018-3025.
7. *The surface of sputtered and annealed polar SrTiO₃(111): TiO_x rich (n×n) reconstructions.* Russell, B.C. and M.R. Castell, *Journal of Physical Chemistry C*, 2008. **112**, 6538.
8. *(root 13X root 13)R13.9 degrees and (root 7X root 7)R19.1 degrees reconstructions of the polar SrTiO₃ (111) surface.* Russell, B.C. and M.R. Castell, *Physical Review B*, 2007. **75**(15), 155433.

Publications (partially or fully BES supported)

1. *Surface transmission electron diffraction for SrTiO₃ surfaces.* Kienzle, D.M. and L.D. Marks, *CrystEngComm*, 2012. **14**(23), 7833-7839.
2. *Structure refinement from precession electron diffraction data.* Palatinus, L., D. Jacob, P. Cuvillier, M. Klementova, W. Sinkler, and L.D. Marks, *Acta Crystallographica Section A*, 2013. **69**(2), 171-188.
3. *Structure of the c(6x2) surface on SrTiO₃ (001) by plan-view HREM and atomic resolution SEM.* Ciston, J., P. Koirala, H. Galloway, L. Allen, and M.L. D., Submitted, 2014.
4. *Lanthanum Aluminate (110) 3x1 surface reconstruction.* Kienzle, D. and L.D. Marks, Submitted, 2014.
5. *Structure of the LaAlO₄ (001) 5x2 Reconstruction.* Kienzle, D.M. and L.D. Marks, In Preparation, 2014.
6. *Conditions for Atomic Resolution Plan View Imaging of Surfaces.* Koirala, P., Y. Lin, and L.D. Marks, In Preparation, 2014.
7. *Surface Structure of the n×n (111) reconstruction on SrTiO₃ by direct methods, STM and plan-view HREM.* Marks, L.D., A. Chiaramonti, J. Ciston, Y. Lin, and M.R. Castell, Submitted, 2014.
8. *The 2xn family of octahedral structures on SrTiO₃ (110).* Zheng, Z., A. Loon, M. Hieckel, D. U., and L.D. Marks, In Preparation, 2014.

Electron Microscopy With Vortex Beams Carrying Orbital Angular Momentum

Benjamin J. McMorran, Department of Physics, University of Oregon

Program Scope

The goal of this project is to develop new electron microscopy capabilities using electron vortex beams. Electron microscopy is one of the most widely used tools for studying energy-related materials at atomic lengthscales, yet the information that it can typically provide is limited by the types of physical interactions occurring between the electron beam and the sample. Electron vortex beams possess quantized, programmable orbital angular momentum (OAM) and can interact with matter in new ways compared to conventional electron beams. The project investigates methods for using the electron vortex beam to directly probe magnetization and electronic orbital structure within materials. Methods are also being explored for using these beams to enhance image contrast of carbon-based materials at the nanoscale. To accomplish these goals, the project advances a new technology: nanofabricated diffractive optical elements (DOEs) that can be used inside existing microscopes to sculpt electron beams^{1,2}.

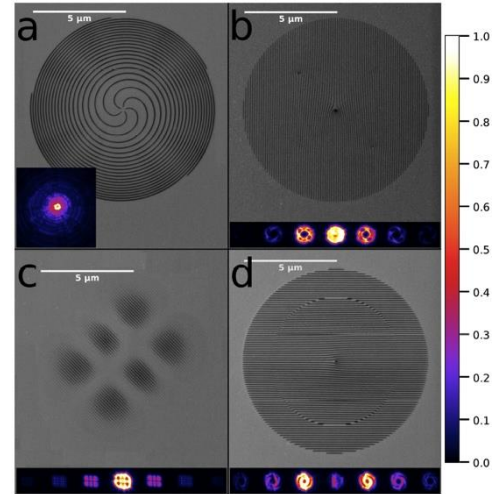


Figure 1 – Examples of phase grating designs that produce electron beams with nontrivial phase structure, together with the corresponding diffraction patterns.

Recent Progress

1. *Systematic optimization of efficient diffractive optics for electrons* – We made significant progress improving the size, spatial resolution, spatial coherence and diffraction efficiency of nanofabricated DOEs for electrons. An additional advance has been the invention of high efficiency, electron-transparent *phase* gratings. In the first year of this project, we have optimized the diffraction efficiency and quality of electron DOEs using different fabrication parameters. We have developed a theoretical model of phase gratings for electrons, to show that our demonstrated diffraction efficiency of 34% is close to the expected maximum (Fig. 2). We have also demonstrated blazed diffraction gratings. We have published¹² and presented this work at several oral presentations at international conferences³⁻⁵.

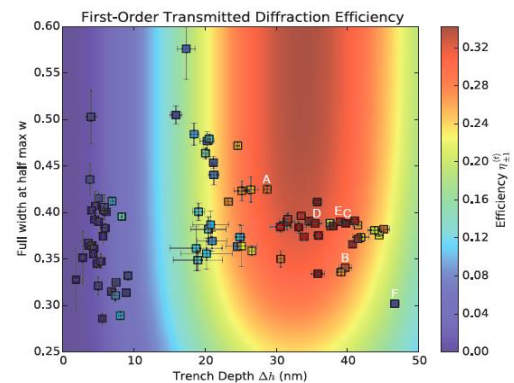


Figure 1 – Diffraction efficiencies ($\equiv I_{\pm 1}/I_{\text{tot}}$) for diffractive optical elements (DOEs) as a function of the depth and width of nanofabricated grooves. Each data point represents a measurement of an individual DOE constructed with different fabrication parameters. The background color map represents a theoretical model. The data indicates the maximum balanced diffraction efficiency has been achieved.

2. *Demonstration of atomic resolution STEM using electron vortex probes* – We created modified condenser lens apertures capable of producing electron vortex probe beams, and installed them in four STEM instruments: TEAM I at NCEM, the FEI Titan at UO, the aberration-corrected JEM-ARM200CF at University of Illinois-Chicago (a new collaboration with Robert Klie), and a Nion UltraSTEM (a new collaboration with Ondrej Krivanek). Through a close collaboration with Peter Ercius at NCEM and at UO, we developed techniques for collecting STEM images of specimens using individual vortex beam probes, demonstrating Angstrom-resolution (Fig. 3). The most promising technique is to look at the edge of a sample, such that just one of the multiple probe beams from the grating interacts with the specimen. A post-specimen aperture (SAD) is used to block the unwanted beams. We have demonstrated atomic resolution vortex STEM images of Si nanowires, STO, Co nanoparticles, and NiO nanoparticles using this technique, and have discussed this progress at M&M⁶. We are in the process of optimizing the beam characteristics and experiment geometry to observe a dichroism signal with atomic resolution.

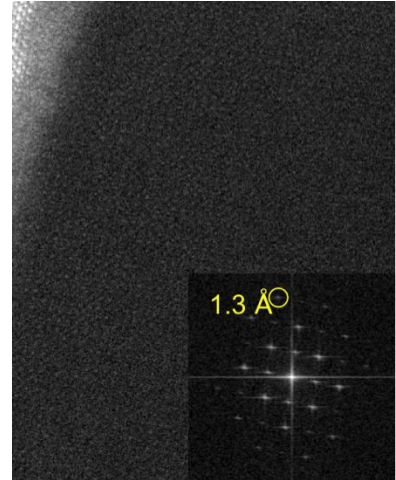


Figure 3 – Atomic-resolution STEM image of STO using aberration-corrected vortex beams.

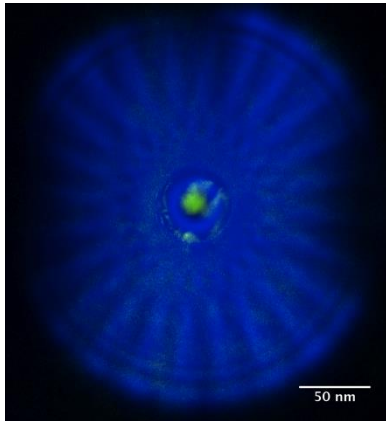


Figure 4 – Color map representing change in intensity of an electron vortex beam skimming a gold nanoparticle. A vortex beam carrying OAM (blue) is incident on the NP. The exit wave is imaged, and the new zero-OAM component of outgoing wave (green) is calculated from image differences.

3. *Demonstration of OAM-dependence of surface plasmon excitation using STEM-EELS with vortex beams* – We observed the transfer of OAM from an electron vortex beam to surface plasmon modes in two studies of nanoparticle systems^{7,8}. Several optical studies have induced plasmon vortices using optical vortices and circularly polarized light and suggested their use in nanophotonic and plasmonic devices^{9,10}. Direct observation of angular momentum transfer from electron vortices allows for unique identification of the OAM associated with localized plasmon excitations down to the nanometer scale.

Electron vortex beams were produced in an FEI Titan TEM at 300 kV with large spot size and strong gun lens to maximize the coherence of the beam. A forked diffraction grating is located in the condenser lens aperture of the microscope. The +1 and -1 diffracted probe beams each carry one unit (\hbar) of OAM per electron, with opposite handedness in the two beams¹¹. They are alternately focused in the plane of the

sample to be analyzed, such that the inner radius of the beam grazes the sample.

The intensity of the dark spot at the center of a vortex beam can be used to detect a transfer of OAM. A vortex probe beam features a persistent, topologically stable dark spot due to the phase singularity. However, in a regular electron beam with no OAM and no phase singularity, the peak intensity is at the center of the beam. Thus, when an electron vortex beam

with one unit of OAM transfers that angular momentum to a system, the phase singularity “collapses” and the scattered component of the beam is distinguishable as an increase in the intensity at the center of the beam. We used this technique to detect a transfer of OAM from the vortex beam to a spherical gold nanoparticle (NP). Figure 5 shows a clear increase in intensity in the initially dark vortex core. This effect is largest when the inner radius of the hollow vortex beam is adjusted to match the diameter of the Au NP.

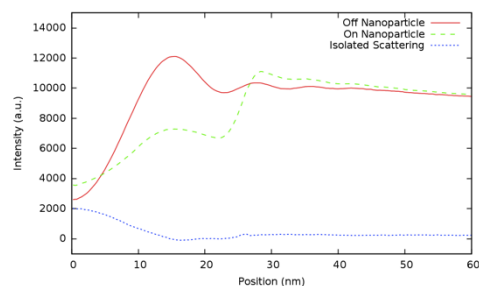


Figure 5 – Comparison of the radial integrated intensity of the electron vortex positioned off the nanoparticle (Fig. 4, blue image), on the nanoparticle, and the isolated scattering due to the electron vortex-nanoparticle interaction.

We also observed a clear OAM dependence in low-loss EELS in a chiral distribution of Al/Al₂O₃ core-shell nanoparticles (Fig. 6). The cluster was illuminated by +1, 0, and -1 OAM vortex beams. EEL spectra were acquired using electrons in the optical axis of each beam. It was found that illumination of a -1 OAM beam generated an additional plasmon peak at approximately 3.5 eV, whereas illumination by a +1 OAM beam *with identical intensity distribution* did not produce the plasmon. This signal (and lack thereof, under +1 illumination) was fairly robust against relative beam-cluster alignments. Therefore, we conclude this plasmon mode was only generated by a transfer of angular momentum of a particular handedness.

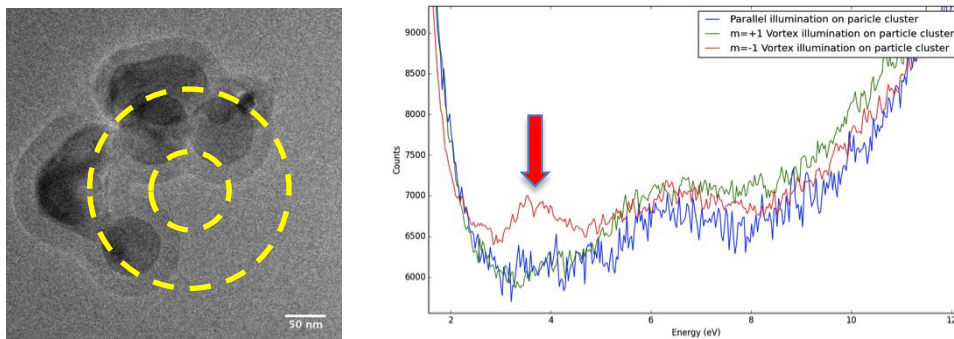


Figure 6 – OAM-dependent interaction of electron vortex beams with a chiral system. (Left image) A chiral cluster of Al/Al₂O₃ core-shell nanoparticles was illuminated by +1, 0, and -1 OAM vortex beams. The outer yellow dashed line represents the location of max intensity of the ring-shaped beams. The inner yellow dashed line represents the diameter of the central dark spot of the vortex core in the ± 1 vortex beams. (Right image) Low-loss EEL spectra were acquired for each illumination. The EELS entrance aperture was positioned to only accept electrons within the inner dashed line in the left image. The usual Al NP surface plasmon and bulk plasmon resonances were excited by all beams, but an additional resonance at 3.5 eV was excited by a -1 OAM (left-handed) vortex beam (red arrow).

Future Plans

Plasmonic studies using electron vortex beams – We plan to perform numerical modeling to verify chiral nanoparticle cluster plasmon resonances from vortex beams. We will expand on this research by studying nanofabricated plasmonic structures with prepared anisotropy and chiral asymmetry. To this end, we are contacting with research groups with expertise in nanoplasmonics that exhibit polarization-dependent optical activity.

Atomic resolution orbital interactions of vortex STEM probes – We have used the vortex STEM probe on TEAM I to capture EELS signals from specimens of iron, cobalt/cobalt oxide nanoparticles, and nickel/nickel oxide nanoparticles, but have not conclusively measured OAM dependence of the spectra. We attribute this to imperfections in the grating and lower-order aberrations in the probe beam (coma and stigmatism). To solve this, we plan to use a higher-OAM beam to align and stigmatize the diffracted probe, then switch to another grating that produces the desired probe with one unit of OAM for dichroism experiments. Our intermediate goal is to verify the presence of a clean vortex mode in the focused, aberration corrected probe by demonstrating STEM images with hollow spots at atomic column positions.

Phase microscopy – In collaboration with Prof. Robert Glaeser at UC-Berkeley, we plan to demonstrate spiral phase microscopy by placing a spiral phase grating in a modified TEM with a post-specimen drift tube for providing larger camera lengths. This collaboration has been on hiatus while we optimize diffraction efficiency of the gratings. We also plan to begin experimenting with low angle bright field STEM configurations using hollow vortex beams.

References

1. McMorran, B. *et al.* Sculpting Electron Beam Profile and Phase with Nanofabricated Diffractive Optics. in *EIPBN Proc.* P04–16 (2012).
2. McMorran, B. United States Patent: 8680488 - *System and method for producing and using multiple electron beams with quantized orbital angular momentum in an electron microscope.* (2014).
3. Pierce, J. S., Harvey, T. R., Yahn, T. S. & McMorran, B. J. High Efficiency Electron Diffractive Optics. *Microsc. Microanal.* **19**, 1188–1189 (2013).
4. Pierce, J. S., Harvey, T. R., McMorran, B. J., Agrawal, A. & Ercius, P. A. Efficient Diffractive Phase Optics for Electrons. in *M&M Proc.* (2014).
5. Pierce, J. S., Wright, C., Harvey, T. R. & McMorran, B. J. Creation of High Resolution Electron Diffraction Gratings using FIB and E-Beam Techniques. in *EIPBN Proc.* (2014).
6. Ercius, P. *et al.* Atomic-resolution Imaging Using Cs-corrected Vortex Beams. in *M&M Proc.* (2014).
7. Harvey, T. R. *et al.* Electron Orbital Angular Momentum Transfer to Nanoparticle Plasmon Modes. *Microsc. Microanal.* **19**, 1186 (2013).
8. Harvey, T. R., Chess, J., Pierce, J. & McMorran, B. J. Characterization of Electron Orbital Angular Momentum Transfer to Nanoparticle Plasmon Modes. in *M&M Proceedings* (2014).
9. Tan, P. S. *et al.* Phase singularity of surface plasmon polaritons generated by optical vortices. *Opt. Lett.* **36**, 3287–3289 (2011).
10. Gorodetski, Y., Niv, A., Kleiner, V. & Hasman, E. Observation of the Spin-Based Plasmonic Effect in Nanoscale Structures. *Phys. Rev. Lett.* **101**, 043903 (2008).
11. McMorran, B. J. *et al.* Electron Vortex Beams with High Quanta of Orbital Angular Momentum. *Science* **331**, 192–195 (2011).

Publications (2013 – 2014)

12. T. R. Harvey, J. Pierce, A. Agrawal, P. A. Ercius, M. Linck, and B. J. McMorran, Efficient Diffractive Phase Optics for Electrons, *New Journal of Physics*, **in press**, (2014).

New *In Situ* Analytical Electron Microscopy for Understanding Structure Evolution and Composition Change in High Energy Density Electrode Materials in Lithium Ion Batteries

PI: Shirley Meng Department of NanoEngineering, University of California, San Diego

Collaborators: Feng Wang and Huolin Xin, Brookhaven National Lab
Nancy Dudney and Nina Balke, Oak Ridge National Lab
Oleg Shpyrko, UC San Diego

Program Scope

In this project, we focus on the development and optimization of *in situ* analytical electron microscopy to quantitatively understand the dynamic changes in the bulk and interfaces of electrodes and electrolytes within all solid state batteries. The objectives of the proposed research are 1) to design and fabricate all solid state batteries with a new electrochemical materials family; 2) to develop the fundamental understanding of the dynamic chemical and electronic processes at the solid/solid interfaces of electrode/electrolyte; and 3) to make significant inroads towards understanding the basic science of ion transport and related phase transitions in electrochemical systems at the nanometer scale.

Recent Progress

I. Successful *in situ* TEM Biasing of Nanobattery

To enable *in situ* TEM biasing of nanobatteries, we have successfully optimized the Focused Ion Beam fabrication procedures used to preserve the electrochemical activity of nanobatteries made from rf-magnetron sputtered thin film batteries.^[1-4] In order to retain electrochemical activity, ion beam current and pixel dwell time must be carefully controlled. Electrical connections to the nanobattery are made by Pt-deposition to the cathode side and a piezo-controlled STM tip on the specialized Nanofactory TEM holder to the anode layer as shown in Figure 1b-d. Successful biasing of a nanobattery at approximately 1C rate in the TEM was conducted for 60 minutes (Fig. 1a) with the beam on, and a video was recorded simultaneously to observe morphological changes. Figures 1b-d show the morphology of the nanobattery layers at 30 minute intervals throughout the charging process. It is apparent that there are little morphological changes that occur during electrochemical biasing. Small morphological changes are advantageous as the long term cycling performance of the thin film battery depends on reversible lithium insertion and extraction. Under such conditions, characterization of the elemental composition and chemical bonding with high spatial resolution become much more crucial to identifying the underlying interfacial phenomena that occur during thin film battery cycling that could affect its performance. Therefore, we were able to apply the *in situ* TEM experimental setup to STEM/EELS characterization and observe interfacial phenomena and quantify the changes at the LiPON/LCO interface as shown in part II.

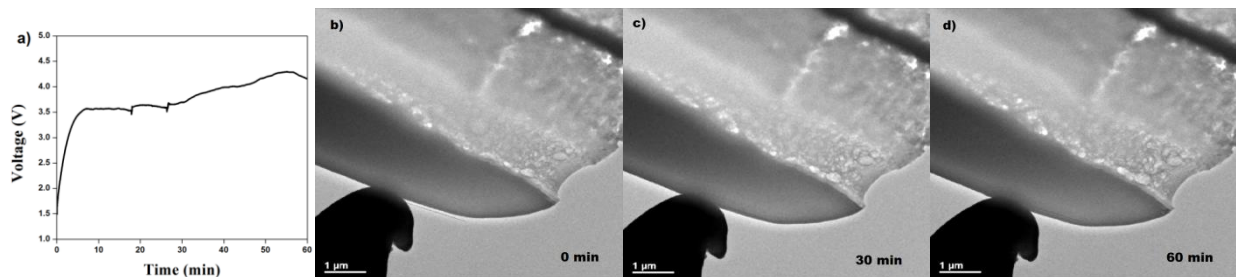


Figure 1. (a) Charging profile of in situ TEM biased nanobattery for 60 minutes, the spikes in voltage curve are due to the vibrations. (b)-(d) TEM snapshots extracted from the video taken at 30-minute intervals.

II. STEM/EELS Characterization of Interfacial Phenomena during *ex situ*/*in situ* TEM

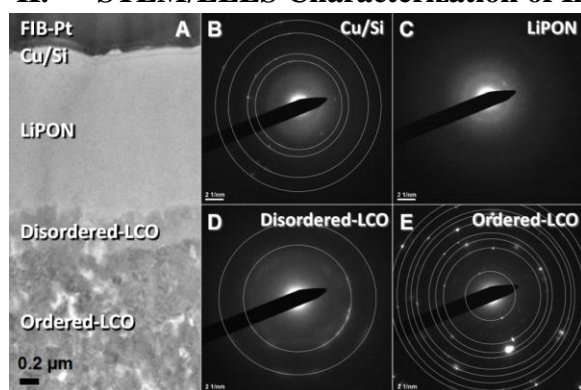


Figure 2. (a) STEM imaging of the electrode layers of the solid state battery SAED of (b) silicon/copper layers showing amorphous silicon. (c) LiPON showing amorphous LiPON. (d) the disordered LCO layer showing weak different spots forming rings. (e) the ordered LCO layer showing polycrystalline

Scanning transmission electron microscopy (STEM) enables quantitative elemental composition and chemical bonding information on the interfacial phenomena that occurs in thin film solid state batteries. Selected area electron diffraction on the electrode layers shows amorphous silicon anode layer, amorphous LiPON electrolyte layer, polycrystalline bulk lithium cobalt oxide cathode layer, and a highly disordered lithium cobalt oxide layer that exists between the cathode and electrolyte layers figure 2a-e. During cycling elemental composition and chemical bonding changes within this disordered LCO layer is of high interest and is shown to have profound effects on the solid state battery's performance.

To fully capture the distinction between *ex situ* and *in situ* characterization, three samples were compared: pristine, *ex situ* charged nanobattery, *in situ* charged nanobattery. Through Li-K edge mapping, lithium is deficient in the pristine disordered LCO layer (Figure 3a); while upon charging, lithium accumulates in the disordered LCO layer in both the *ex situ* and *in situ* cases (Figure 3a-c). Such disordered structure could form during RF magnetron deposition of LiPON which produces high energy ions that collide with ordered LCO layer resulting in a disordered layer or reaction of the ordered LCO layer with LiPON over time. High loss EELS conducted on the LCO layers showed chemical changes in the Co-O bonding structure upon charging as reflected in changes of the O-K edge.^[5] Analysis of the high loss region shows that O-K pre-edge is present in the disordered LCO layer of the pristine sample. However, it has decreased significantly in the disordered LCO layer of the *ex situ* sample, while the O-K pre-edge has shifted to a higher energy in the disordered LCO layer of the *in situ* sample. Through theoretical calculations and experimental results, the O-K pre-edge is a strong indicator of the bonding nature between the cobalt atom and oxygen atom.^[6, 7] Disappearance of the oxygen K pre-edge is normally accompanied by formation of oxygen vacancies and reduction of cobalt.^[8] The kinetics of CoO formation and oxygen evolution cannot be de-convoluted with *ex situ* observation; but with *in situ* insight, we were able to show the dynamics of each reaction in the disordered layer. The detailed analysis is still underway and the working manuscript will be submitted shortly.

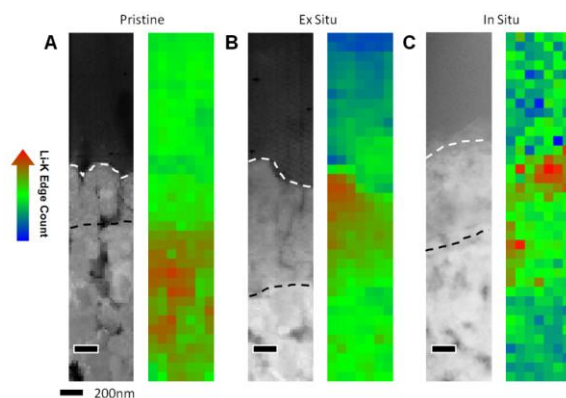


Figure 3. (a) Li-K edge mapping of the pristine sample. (b) Li-K edge mapping of the *ex situ* sample. (c) Li-K edge mapping of the *in situ* sample.

III. Conductive Atomic Force Microscopy of $\text{Li}_4\text{Ti}_5\text{O}_{12}$ Thin Films

Thin-film $\text{Li}_4\text{Ti}_5\text{O}_{12}$ (LTO) as anode material for lithium ion battery was studied using conductive atomic force microscopy (cAFM) in order to elucidate aspects of its reversible phase transition to $\text{Li}_7\text{Ti}_5\text{O}_{12}$ upon cycling. Quite interestingly, LTO has extremely high rate capability that retains more than 70% capacity at 100C.^[9] One reason is because its beginning ($\text{Li}_4\text{Ti}_5\text{O}_{12}$) and end ($\text{Li}_7\text{Ti}_5\text{O}_{12}$) members possess identical space groups, Fd-3m. LTO, as a “zero strain” material, makes many conventional characterizations, such as x-ray diffraction, problematic.^[10] The electronic properties of $\text{Li}_4\text{Ti}_5\text{O}_{12}$ and $\text{Li}_7\text{Ti}_5\text{O}_{12}$, the former being insulating and the later being conducting, can be used for characterization. We aimed to monitor the transition between each phase at the single particle level, therefore, by measuring the materials conductivity as a function of state of charge, using AFM. Figure 4 shows a representative voltage profile of LTO thin-film vs Li/Li+. Figure 5a shows AFM height images of LTO surface morphology upon cycling. Though the material is considered to undergo no strain and form no SEI, we observe expansion of grain size upon discharge below 1.5V, and size reduction upon charge. Figure 5b demonstrates that larger grains lose conductivity. These measurements allow us to directly observe the formation of a percolation network of electronic conduction and its eventual deterioration, which may be a possible degradation mechanism not yet reported.

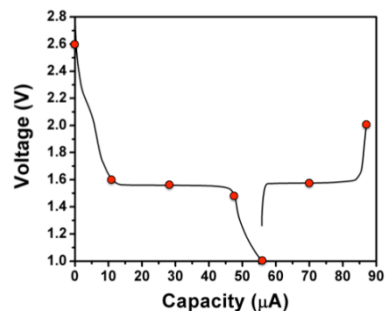


Figure 4. Discharge/Charge profile of LTO. Red dots show points of analysis

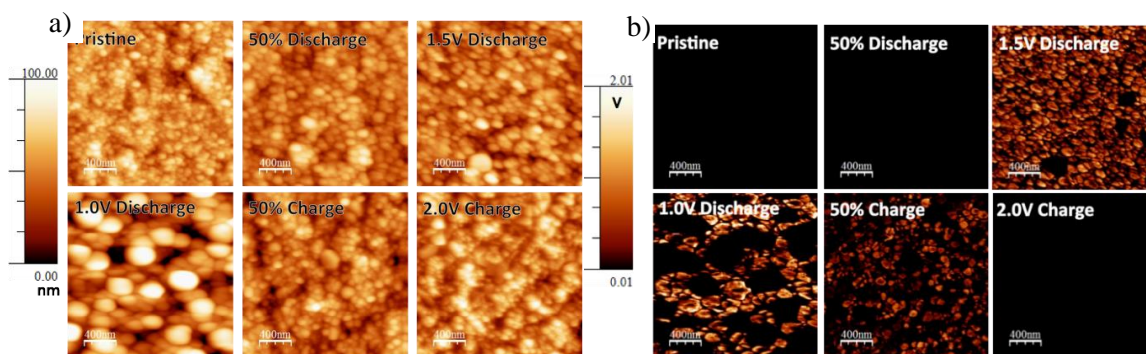


Figure 5. a) height images of LTO cycled to different states of charge. b) cAFM conductivity map of LTO cycled to different states of charge

IV. Exploration of Lithium Lanthanum Titanate as Solid State Electrolyte

Lithium lanthanum titanate perovskite (LLTO) was synthesized in two Li:La ratios that have shown the highest ionic conductivity, $\text{Li}_{0.5}\text{La}_{0.5}\text{TiO}_3$ and $\text{Li}_{0.27}\text{La}_{0.57}\text{TiO}_3$. The recipes are taken from Furusawa et al. and Sutorik et al. respectively.^[11, 12] $\text{Li}_{0.27}\text{La}_{0.57}\text{TiO}_3$ by Sutorik et al.’s method has the lowest grain boundary conductivity of $4.7\text{e-}5$ S/cm with powder packing and lowest lattice conductivity of $9.1\text{e-}4$ S/cm without packing.

Future Plans

- **In Situ High Loss EELS of disordered LCO layer with time evolution:** After the initial STEM/EELS analysis on the a-Si/LiPON/LCO nanobatteries, we are working to observe the O-K edge changes as the system relaxes.

- **EELS Simulation of Coordination changes and Bonding distances of Co-O octahedron:** The shift of the O-K pre-edge in *in situ* biasing of the nanobattery could be attributed to partial coordination changes of the Co-O octahedron or Co-O bond distance.
- **Fabrication and testing of all-PLD solid-state battery with LLTO electrolyte:** The all-PLD solid-state batteries are under fabrication and would enable us to investigate different chemistry namely TiO₂ or Si/LLTO/LiNi_{0.5}Mn_{1.5}O₄.

References

1. Santhanagopalan, D., et al., *Interface Limited Lithium Transport in Solid-State Batteries*. The Journal of Physical Chemistry Letters, 2013: p. 298-303.
2. Balke, N., et al., *Real space mapping of Li-ion transport in amorphous Si anodes with nanometer resolution*. Nano Lett., 2010. **10**: p. 3420 – 3425.
3. Bates, J.B., et al., *Thin-film lithium and lithium-ion batteries*. Solid State Ionics, 2000. **135**(1–4): p. 33-45.
4. Neudecker, B.J., N.J. Dudney, and J.B. Bates, "*Lithium-Free*" Thin-Film Battery with *In Situ Plated Li Anode*. J. Electrochem. Soc., 2000. **147**: p. 517-523.
5. Graetz, J., et al., *Electronic Structure of Chemically-Delithiated LiCoO₂ Studied by Electron Energy-Loss Spectrometry*. The Journal of Physical Chemistry B, 2002. **106**(6): p. 1286-1289.
6. Aydinol, M.K., et al., *Ab initio study of lithium intercalation in metal oxides and metal dichalcogenides*. Physical Review B, 1997. **56**(3): p. 1354-1365.
7. Ceder, G., et al., *First-principles alloy theory in oxides*. Modelling and Simulation in Materials Science and Engineering, 2000. **8**(3): p. 311.
8. Stemmer, S., et al., *Characterization of oxygen-deficient SrCoO_{3-δ} by electron energy-loss spectroscopy and Z-contrast imaging*. Solid State Ionics, 2000. **130**(1–2): p. 71-80.
9. Liu, J., et al., *Self-Supported Li₄Ti₅O₁₂-C Nanotube Arrays as High-Rate and Long-Life Anode Materials for Flexible Li-Ion Batteries*. Nano Letters, 2014. **14**(5): p. 2597-2603.
10. Ohzuku, T., A. Ueda, and N. Yamamoto, *Zero-Strain Insertion Material of Li[Li_{1/3}Ti_{5/3}]O₄ for Rechargeable Lithium Cells*. Journal of The Electrochemical Society, 1995. **142**(5): p.1431-1435.
11. Furusawa, S.-i., et al., *Ionic conductivity of amorphous lithium lanthanum titanate thin film*. Solid State Ionics, 2005. **176**(5–6): p. 553-558.
12. Sutorik, A., et al., *The comparative influences of structural ordering, grain size, Li-content, and bulk density on the Li⁺-conductivity of Li_{0.29}La_{0.57}TiO₃*. Journal of Materials Science, 2012. **47**(19): p. 6992-7002.

Publications

1. D. Santhanagopalan, D. Qian, T. Mcgilvary, Z. Wang, F. Wang, F. Camino, J. Graetz, N. Dudney, Y. S. Meng, "*Interface Limited Lithium Transport in Solid-State Batteries*", J. Phys. Chem. Lett., 2014, **5**, 298-303. DOI: 10.1021/jz402467x
2. Z. Wang and Y.S. Meng, "*Analytical Electron Microscopy – Study of All-Solid-State Batteries*", Handbook of Solid State Batteries, Editors Nancy Dudney, William West, and Jagjit Nanda, 2nd edition, World Scientific Publishing, Book Chapter in Print.
3. A. Singer, A. Ulvestad, H-M Cho, J.W. Kim, J. Maser, R. Harder, Y. S. Meng and O. G. Shpyrko "*Nonequilibrium Structural Dynamics of Nanoparticles in LiNi_{1/2}Mn_{3/2}O₄ Cathode under Operando Conditions*", Nano Letters, Just accepted, 2014, DOI: 10.1021/nl502332b
4. Z. Wang, D. Santhanagopalan, W. Zhang, F. Wang, J. Li, N. Dudney, Y.S. Meng, "*Mechanisms of Interfacial Phenomena in All-Solid-State Battery Observed by in situ STEM/EELS*", Manuscript Submitted, 2014.
5. M.G. Verde, N. Balke, L. Baggetto, G.M. Veith, Danna Qian and Y.S. Meng, "*Nanoscale Resolution of Strain and Li Ion Diffusion within Li₄Ti₅O₁₂ Anode Material*", Manuscript Under Preparation.

ATOMIC RESOLUTION ELECTRON TOMOGRAPHY

Jianwei (John) Miao

Department of Physics & Astronomy and California NanoSystems Institute, University of California, Los Angeles, CA 90095-1547. Tel: 310 206 2645, Email: miao@physics.ucla.edu.

Program Scope

Electron tomography was originally developed in 1968, and has been primarily applied to determine the 3D structure of biological systems¹. In the last decade, electron tomography has been increasingly applied in materials science and nanoscience through the use of scanning transmission electron microscopy (STEM)^{2,3}. Previously, the highest resolution achieved by STEM tomography was around 1 nm in three dimensions³. However, improving the 3D resolution from ~1 nm to the atomic level remained a challenging task, which requires new tomographic reconstruction algorithms, better projection alignment methods, state-of-the-art STEM instruments, and more robust data-acquisition procedures. Over the past few years, we have made important progress towards achieving atomic resolution STEM tomography. We developed a novel tomographic method, termed equally sloped tomography (EST)^{4,6}, which allows the 3D image reconstruction of a tilt series with a limited number of projections and a “missing wedge” (i.e. specimens cannot usually be tilted beyond $\pm 79^\circ$)^{1,3}. We have also developed a center of mass (CM) alignment method that can be used to align the projections of a tilt series with atomic level accuracy⁷. Using an FEI Titan 80-300 S/TEM at UCLA, we have implemented more robust data acquisition procedures and have obtained several tomographic tilt series of atomic-resolution projections from nanoparticles.

Building upon these developments, the scope of this project is:

- To conduct a comprehensive numerical study of the non-linear diffraction and dynamical scattering effects by incorporating multislice STEM calculations⁸ into the EST reconstruction^{4,6}. We will optimize the experimental parameters for 3D characterization of nanomaterials at atomic resolution.
- To develop methods for identifying all atoms in nanoparticles through a combination of high-quality tilt series, the EST reconstruction, and 3D atomic structure refinement.
- To establish STEM tomography as a general tool for 3D characterization of crystal defects, polycrystalline and potentially disordered materials at atomic resolution.

Recent Progress

Achieving electron tomography at 2.4 Å resolution. Transmission electron microscopy (TEM) is a powerful imaging tool that has found broad applications across several disciplines⁹. With the introduction of aberration-corrected electron lenses, both the spatial resolution and the image quality in TEM have been significantly improved and resolution below 0.5 Å has been demonstrated¹⁰. A TEM image, however, represents a 2D projection of a 3D object. To reveal the 3D structure of materials, electron tomography is the method of choice. We have recently applied the CM and EST methods to electron tomography and achieved a 3D resolution of 2.4 Å, the highest resolution ever obtained in any 3D imaging method⁷. Individual atoms are observed in some regions of the particle and several grains are identified in three dimensions (Fig. 1). The 3D surface morphology and internal lattice structure revealed are consistent with a distorted icosahedral multiply twinned particle.

Three-dimensional imaging of dislocations in a nanoparticle at atomic resolution.

More recently, we have combined this general electron tomography method with Fourier filtering to observe nearly all the atoms in a multiply-twinned Pt particle (Fig. 2)¹¹. Figure 2a and b show the 3D volume rendering of the Pt nanoparticle in two different orientations in which the individual atoms are visible. Also, the existence of atomic steps at 3D twin boundaries of the Pt nanoparticle were found, and the 3D core structure of edge and screw dislocations in the nanoparticle were imaged at atomic resolution. Figure 2c shows the zoomed view of a 2.6 Å thick internal slice, exhibiting an edge dislocation where red dots represent the position of the atoms. The dislocation line is in the direction of $[10\bar{1}]$. The Burgers vector of the edge dislocation was determined to be $1/2[101]$.

Figure 2d shows the zoomed view of a 5.3 Å thick slice where the zigzag pattern, a characteristic feature of a screw dislocation, is clearly visible. The atoms in green are on the top layer and those in red in the bottom layer. The Burgers vector of the screw dislocation was determined to be $1/2[01\bar{1}]$. These dislocations and the atomic steps at the twin boundaries are hidden in conventional 2D projections, and appear to be a significant stress-relief mechanism. Nature has produced a video featuring these results (www.youtube.com/watch?v=yqLlgIaz1L0), which has been viewed more than 445,000 times on YouTube.

Towards three-dimensional structural determination of amorphous materials at atomic resolution. Through numerical experiments, we demonstrate an electron tomography method for

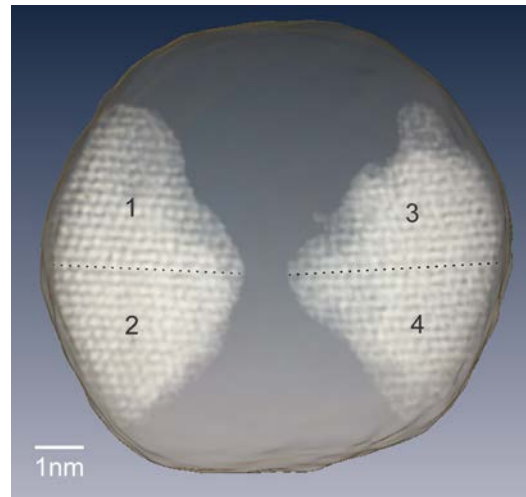


Figure 1. Identification of four major grains inside a gold nanoparticle at atomic scale resolution in three dimensions. Grains 1, 2 and grains 3, 4 are related by mirror-reflection across the horizontal interfaces marked by dotted lines. The angle enclosed by close-packed planes across these interfaces was measured to be $\sim 69.9^\circ$ between grains 1 and 2, and $\sim 71.3^\circ$ between grains 3 and 4, both of which are consistent with the angle for an FCC twin boundary (70.53°). [Nature 483, 444-447 (2012)]

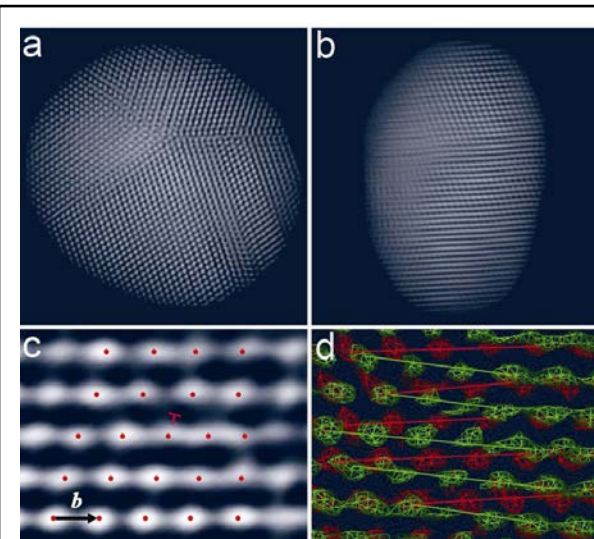


Figure 2. Three-dimensional imaging of dislocations in a nanoparticle at atomic resolution. **a** and **b**, 3D reconstruction of a Pt nanoparticle where nearly all the atoms are observed in 3D. **c** and **d**, 3D imaging of the core structure of an edge dislocation and a screw dislocations at atomic resolution (the data, detailed procedures and source codes of our work can be freely downloaded: www.physics.ucla.edu/research/imaging). [Nature 496, 74-77 (2013)]

3D structural determination of amorphous materials at atomic resolution¹². By combining multislice simulations of an aberration-corrected STEM with EST, we have determined the 3D atomic structure of a simulated glass particle, consisting of 334 Si and 668 O atoms, from a tilt series of 55 noisy projections. An atomic model refinement method has been implemented to locate the positions of the Si and O atoms in the reconstruction (Fig. 3).

Future Plans

- We have performed a series of STEM tomographic experiments on FePt nanocrystals. As synthesized, the FePt nanocrystals exhibit a chemically disordered face-centered cubic (FCC) phase. After thermal annealing at 600°C for ~30 minutes, the nanocrystals change to a chemically ordered face-centered tetragonal (FCT) phase and also show very strong ferromagnetism. A tilt series from an annealed FePt nanocrystal was measured. Our goal is to use electron tomography to determine the position of the atoms inside the nanocrystal. Figure 4 shows a preliminary result on element-resolved 3D structure determination of the FePt nanoparticle at atomic resolution, showing the position of the Pt (fuchsia) and Fe (yellow) atoms.

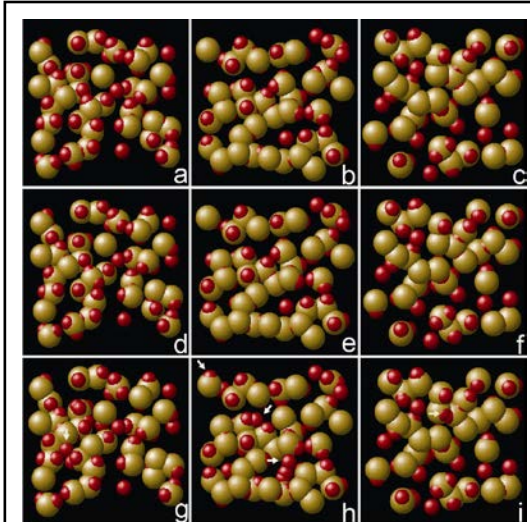


Figure 3. **a-c**, Three 3 Å thick central slices in the YZ, XZ and XY planes of a MD simulated silica structure (yellow spheres: Si atoms and red spheres: O atoms). **d-f**, Corresponding slices of the EST reconstruction with an electron dose of $1.43 \times 10^6 \text{ e}/\text{Å}^2$, where the atomic positions are very well traced. **g-i**, Corresponding slices of the reconstruction with a dose of $3.0 \times 10^5 \text{ e}/\text{Å}^2$, in which only several O atoms are misplaced as indicated by arrows. [*Phys. Rev. B* **88**, 100201 (2013)]

- Core/shell structured quantum dots, where the core and shell are constructed using different semiconductor materials, demonstrate interesting electronic and optical properties that can be harnessed for applications in LEDs, solar cells and bio-imaging, quantum computation, and photo-detection. For example, a type-I quantum dot, where the shell has a wider band gap than that of the core can strongly confine the charge carriers, leading to enhanced quantum efficiency for luminescence¹³. Knowledge of the heterostructure interface, e.g. the facets at the interface and strain induced by lattice mismatch is important to understand the band alignment. Defects at the interface also strongly affect recombination pathways and carrier dynamics. They can act as charge trap centers, or provide pathways for non-radiative recombination. Thus 3D atomic resolution imaging of quantum dots can be an indispensable tool to render detailed information of the interface for the first time, guiding the theoretical prediction of the properties of colloidal quantum dots where defects associated with growth conditions are abundant. In this project, we aim to resolve the location of all the atoms and defects in CdSe and (CdSe)ZnS quantum dots and other nanoscale

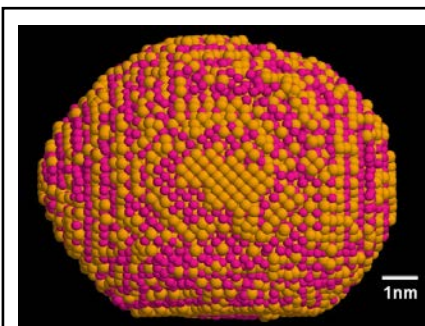


Figure 4. Element-resolved 3D structure determination of a FePt nanoparticle at atomic resolution using STEM tomography. Showing the position of the Pt (fuchsia) and Fe (yellow) atoms; unpublished work.

heterostructures such as Mn-doped PbS and Au-PbS nanoparticles. We will obtain the 3D atomic models of the nanostructures by using high-quality tilt series, the EST reconstruction and 3D atomic structure refinement. The refined 3D atomic models will be compared with the known crystallographic structure of the bulk materials, from which we will deduce the defects and atomic vacancies in the nanoparticle.

References

1. J. Frank. *Electron Tomography*. (Plenum, New York, 1992).
2. S. J. Pennycook & P. D. Nellist. *Scanning Transmission Electron Microscopy: Imaging and Analysis* 1st ed. (Springer, 2011).
3. P. A. Midgley & R. E. Dunin-Borkowski. Electron tomography and holography in materials science. *Nature Materials* **8**, 271-280 (2009).
4. J. Miao, F. Förster & O. Levi. Equally Sloped Tomography with Oversampling Reconstruction. *Phys. Rev. B*. **72**, 052103 (2005).
5. Y. Zhao, E. Brun, P. Coan, Z. Huang, A. Sztrókay, P. C. Diemoz, S. Liebhart, A. Mittone, S. Gasilov, J. Miao & A. Bravin. High resolution, low dose phase contrast x-ray tomography for 3D diagnosis of human breast cancers. *Proc. Natl. Acad. Sci. USA* **109**, 18290–18294 (2012).
6. H. Jiang, R. Xu, C.-C. Chen, W. Yang, J. Fan, X. Tao, C. Song, Y. Kohmura, T. Xiao, Y. Wang, Y. Fei, T. Ishikawa, W. L. Mao & J. Miao. Three-Dimensional Coherent X-Ray Diffraction Imaging of Molten Iron in Mantle Olivine at Nanoscale Resolution. *Phys. Rev. Lett.* **110**, 205501 (2013).
7. M. C. Scott, C. C. Chen, M. Mecklenburg, C. Zhu, R. Xu, P. Ercius, U. Dahmen, B. C. Regan & J. Miao. Electron tomography at 2.4-ångström resolution. *Nature* **483**, 444–447 (2012).
8. E. J. Kirkland. *Advanced Computing in Electron Microscopy* 2nd edition. (Springer, 2010).
9. J. C. H. Spence. *Experimental High-Resolution Electron Microscopy* 3rd edition. (Oxford University Press, New York, 2003).
10. R. Erni, M. D. Rossell, C. Kisielowski & U. Dahmen. Atomic-resolution imaging with a sub-50-pm electron probe. *Physical Review Letters* **102**, 096101(2009).
11. C. C. Chen, C. Zhu, E. R. White, C.-Y. Chiu, M. C. Scott, B. C. Regan, L. D. Marks, Y. Huang & J. Miao, “Three-dimensional imaging of dislocations in a nanoparticle at atomic resolution”, *Nature* **496**, 74–77 (2013).
12. C. Zhu, C.-C. Chen, J. Du, M. R. Sawaya, M. C. Scott, P. Ercius, J. Ciston, and J. Miao, “Towards three-dimensional structural determination of amorphous materials at atomic resolution”, *Phys. Rev. B (Rapid Commun.)* **88**, 100201 (2013).
13. D. Bimber, M. Grundmann & N. N. Ledentsov. *Quantum Dot Heterostructures* 1st ed. (Wiley, 1999).

Publications supported by BES (the project has been funded by DOE since Aug. 1, 2013)

1. C. Zhu, C.-C. Chen, J. Du, M. R. Sawaya, M. C. Scott, P. Ercius, J. Ciston, and J. Miao, “Towards three-dimensional structural determination of amorphous materials at atomic resolution”, *Phys. Rev. B (Rapid Commun.)* **88**, 100201 (2013).
2. J. Miao, C.-C. Chen, M. C. Scott, P. Ercius, C. Zhu, M. Mecklenburg, E. R. White, C.-Y. Chiu, B. C. Regan, Y. Huang, L. D. Marks and U. Dahmen, “Three-Dimensional Imaging of Dislocations and Defects in Materials at Atomic Resolution Using Electron Tomography”, *Microsc. Microanal.* in press.
3. Z. Huang, S. Jiang, F. Louis, M. C. Scott, Q. Cao, W. Wen, M. Mecklenburg, P. Ercius, Z. Amghouz, Y. Chen, X. Gu, P. Hu, F. Xu, M. Springborg, J. Miao, and X. Tang, “Suspended Single-Atom Metallic Chains Created from Silver Nanoparticles”, submitted.
4. J. Miao, C.-C. Chen, M. C. Scott, P. Ercius, and U. Dahmen, “Atomic Resolution Electron Tomography” (invited review), *Chem. Soc. Rev.*, in preparation.

Using Interfaces to Create Strongly-Coupled Magnetic-Ferroelectrics

David A. Muller¹, Craig J. Fennie¹, Darrell G. Schlom¹, Peter Schiffer³

¹Cornell University, Ithaca, NY 14853

²University of Illinois at Urbana Champaign, IL 61802, USA

I. PROGRAM SCOPE

Our objective is to create a ferromagnetic ferroelectric that can be deterministically switched between symmetry equivalent states using an electric field. The electric-field switching of a magnetization between 180° symmetry equivalent states has not been demonstrated in any material. The required coupling between ferroelectric and ferromagnetic domains allowing such switching is a missing feature in most multiferroics and is key to advancing the field both scientifically and technologically. Starting at the level of electrons and atoms our goal is to rationally design complex oxide heterostructures and interface-materials with this targeted emergent behavior. Using a combination of symmetry arguments and first-principles calculations to explore the connection between structural distortions and ferroelectricity in the perovskite family of materials, we have predicted electrical control of magnetism in the hexagonal rare earth ferrites¹. These realizations are created with atomic-layer precision, microscopically interrogated to see if there are competing mechanisms to the intended realization, and finally their macroscopic properties are measured. Here we will develop the scientific ideas and experimental tools necessary to apply this design paradigm to the creation of multiferroics with unprecedented coupling between ferroelectric and magnetic order parameters.

II. RECENT PROGRESS

Materials that exhibit simultaneous order in both their electric and magnetic ground states hold tremendous promise for use in next-generation memory devices. Full exploitation of these properties demands a material that has both a coherent orientation of the electronic dipoles—a ferroelectric—as well as alignment of the spin states in a ferromagnetic state. As a starting point

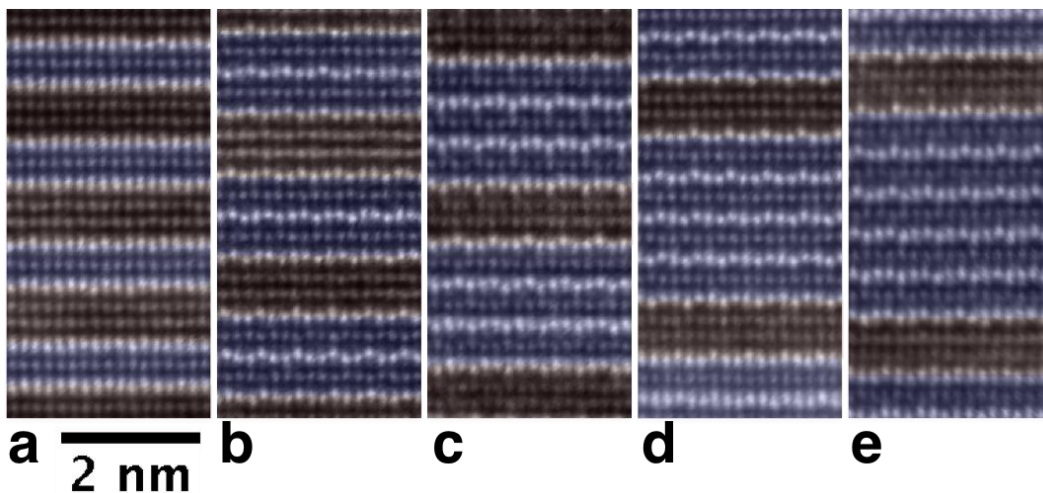
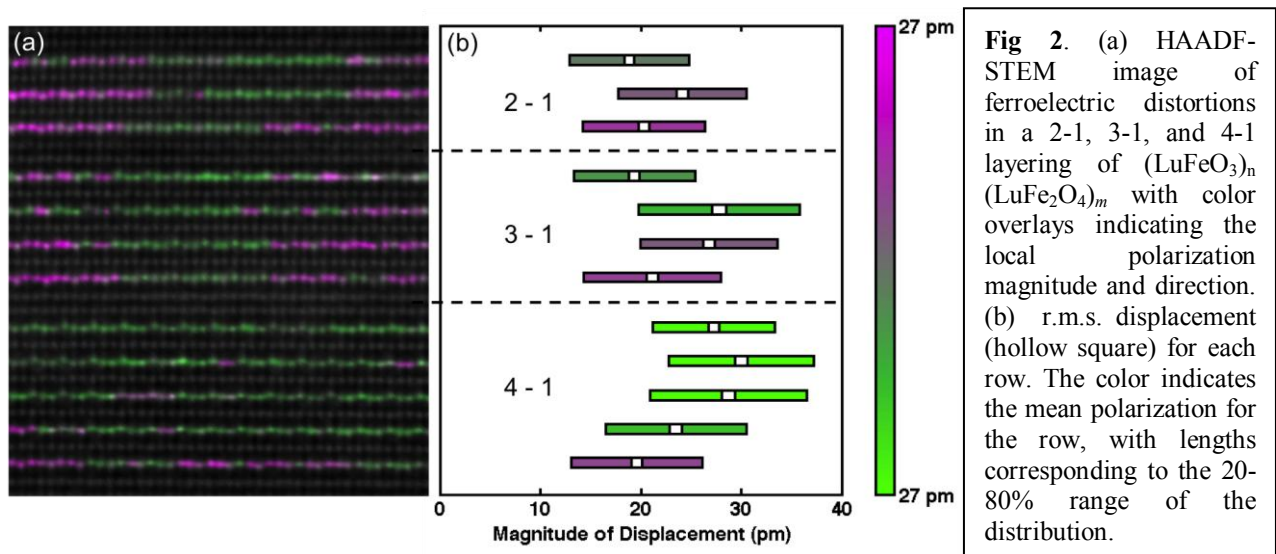


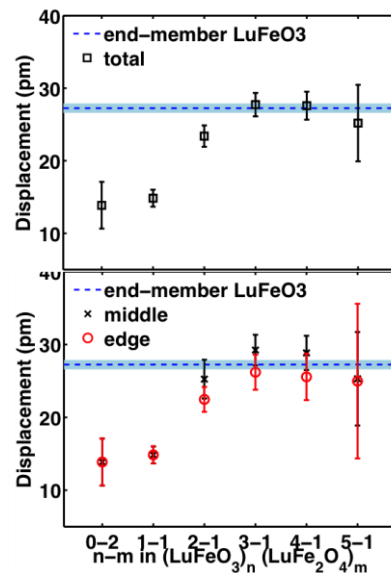
Fig 1. ADF-STEM images of the $(\text{LuFeO}_3)_n(\text{LuFe}_2\text{O}_4)_m$ superlattices, with the $(\text{LuFeO}_3)_n$ blocks highlighted in blue, for the $n=1, m=1$ structure (a), $n=2, m=1$ (b), $n=3, m=1$ (c), $n=4, m=1$ (d) and $n=5, m=1$ (e). The brightest atoms are Lu. The buckling of the Lu-O layer leads to a displacement of Lu atoms and resulting polarization in (b)-(e) compared to the non-polar structure in (a).



we combine LuFe_2O_4 which is ferrimagnetic below 240 K, although it is not ferroelectric, with hexagonal LuFeO_3 that is a robust high-temperature ferroelectric with a closely related structure. The properties of LuFe_2O_4 and hexagonal LuFeO_3 depend sensitively on composition² and to obtain true single-phase films, we developed a way to grow single-phase epitaxial films by MBE in an adsorption-controlled regime.³

Here we use precise atomic layer-by-layer control to engineer a new strong ferrimagnet-ferroelectric with the highest-known simultaneous transition temperatures. These $(\text{LuFeO}_3)_n(\text{LuFe}_2\text{O}_4)_m$ superlattices (Fig 1) are constructed through integration of the ferroelectric, yet antiferromagnetic, LuFeO_3 and paraelectric, ferrimagnetic LuFe_2O_4 . Our results show that the superlattices have a *higher* ferrimagnetic ordering temperature (T_C) than either of the end members, LuFe_2O_4 and LuFeO_3 , from which they are created. T_C increases to nearly room temperature with simultaneous ferroelectricity, suggesting the tantalizing prospect of the existence of the world's first single-phase room-temperature ferrimagnetic ferroelectric.

We use scanning transmission electron microscopy imaging and spectroscopy to map the material structure and chemistry with atomic precision⁴. A two-dimensional analysis of the fine structure of the O-K edge yielded distinct signals for the two inequivalent oxygen sites in the crystal. Comparison to an *ab initio* simulation showed that these two components can be interpreted in terms of the differing hybridization of the O *p* orbitals to the Lu and Fe *d* orbitals, thus producing an atomic-resolution map of the local oxygen bonding environment. The hexagonal LuFeO_3 end member is an improper ferroelectric where a Lu-O buckle and the accompanying tilt of the Fe-O bipyramids leads to a polar structure. Here we quantify the buckling of the Lu-O layers—manifest as a displacement of the lutetium atoms—through the superlattice structure. We show that the $(\text{LuFeO}_3)_n(\text{LuFe}_2\text{O}_4)_1$ superlattices are ferroelectric with an increasing polarization from the $n=1$ to $n=5$ structures (Fig 2). Our atomic probe also shows a damping of the polarization in $(\text{LuFeO}_3)_n(\text{LuFe}_2\text{O}_4)_1$



superlattices in the proximity of the LuFe_2O_4 layers (Fig 3). We measure a variation in the iron valence through the structure to correspond to the nominal $\text{Fe}^{+2.5}$ and Fe^{+3} formal valences in the LuFe_2O_4 and LuFeO_3 respectively. We do not see evidence for charge ordering in bulk LuFe_2O_4 .

III. FUTURE PLANS

We are growing $(\text{ABO}_3)_1/(\text{A}'\text{BO}_3)_1$ perovskite superlattices with $B=\text{Fe}$ and A and A' being different rare-earth ions. Our calculations indicate that this ordered superlattice is a hybrid improper multiferroic (both ferroelectric and weakly ferromagnetic) at room temperature. We will synthesize these superlattices and measure their properties including whether they can be switched, whether switching them with an electric field leads to deterministic switching of their magnetization, and their linear magnetoelectric performance. We plan to study the temperature dependence of antiferroic distortions by electron diffraction and direct imaging using a new, high-resolution double-tilt heating holder, and correlate with the ferroelectric phase. The magnetic order will be established by neutron diffraction and microscopically by Lorentz Microscopy. Cryoelectron microscopy will also allow us to study the ground state structure and electronic structure at the atomic scale.

IV. REFERENCES

- ¹ H. Das, A.L. Wysocki, Y. Geng, W. Wu, and C.J. Fennie, “Bulk Magnetoelectricity in the Hexagonal Manganites and Ferrites,” *Nature Communications* **5** (2013) 1–11.
- ² J.A. Moyer, R. Misra, J.A. Mundy, C.M. Brooks, J.T. Heron, D.A. Muller, D.G. Schlom, and P. Schiffer, “Intrinsic Magnetic Properties of Hexagonal LuFeO_3 and the Effects of Nonstoichiometry,” *APL Materials* **2** (2014) 012106.
- ³ C.M. Brooks, R. Misra, J.A. Mundy, L.A. Zhang, B.S. Holinsworth, K.R. O’Neal, T. Heeg, W. Zander, J. Schubert, J.L. Musfeldt, Z.K. Liu, D.A. Muller, P. Schiffer, and D.G. Schlom, *Appl. Phys. Lett.* **101** (2012) 132907.
- ⁴ J.A. Mundy, Q.Y. Mao, C.M. Brooks, D.G. Schlom, and D.A. Muller, “Atomic-Resolution Chemical Imaging of Oxygen Local Bonding Environments by Electron Energy Loss Spectroscopy,” *Appl. Phys. Lett.* **101** (2012) 042907.

V. PUBLICATIONS RESULTING FROM THIS WORK

1. J.A. Mundy, Y. Hikita, T. Hidaka, T. Yajima, T. Higuchi, H.Y. Hwang, D.A. Muller, and L.F. Kourkoutis, “Visualizing the Interfacial Evolution from Charge Compensation to Metallic Screening Across the Manganite Metal–Insulator Transition,” *Nature Communications* **5** (2014) 3464.
2. J.A. Moyer, R. Misra, J.A. Mundy, C.M. Brooks, J.T. Heron, D.A. Muller, D.G. Schlom, and P. Schiffer, “Intrinsic Magnetic Properties of Hexagonal LuFeO_3 and the Effects of Nonstoichiometry,” *APL Materials* **2** (2014) 012106.
3. Y. Geng, H. Das, A.L. Wysocki, X. Wang, S.W. Cheong, M. Mostovoy, C.J. Fennie, and W. Wu, “Direct Visualization of Magnetoelectric Domains,” *Nature Materials* **13** (2014) 163–167.
4. Y. Zhu, A. Soukiassian, D.G. Schlom, D.A. Muller, and C. Dwyer, “Towards Artifact-Free Atomic-Resolution Elemental Mapping with Electron Energy-Loss Spectroscopy,” *Applied Physics Letters* **103** (2013) 141908.
5. X. Ke, T. Birol, R. Misra, J.-H. Lee, B.J. Kirby, D.G. Schlom, C.J. Fennie, and J.W. Freeland, “Structural Control of Magnetic Anisotropy in a Strain-Driven Multiferroic EuTiO_3 Thin Film,” *Physical Review B* **88** (2013) 094434.
6. H. Das, A.L. Wysocki, Y. Geng, W. Wu, and C.J. Fennie, “Bulk Magnetoelectricity in the Hexagonal Manganites and Ferrites,” *Nature Communications* **5** (2013) 2998.

7. A.T. Mulder, N.A. Benedek, J.M. Rondinelli, and C.J. Fennie, "Turning ABO₃ Antiferroelectrics into Ferroelectrics: Design Rules for Practical Rotation-Driven Ferroelectricity in Double Perovskites and A₃B₂O₇ Ruddlesden-Popper Compounds," *Advanced Functional Materials* **23** (2013) 4810–4820.
8. T. Birol and C.J. Fennie, "Origin of Giant Spin-Lattice Coupling and the Suppression of Ferroelectricity in EuTiO₃ from First Principles," *Physical Review B* **88** (2013) 094103.
9. N.A. Benedek and C.J. Fennie, "Why Are There So Few Perovskite Ferroelectrics?" *Journal of Physical Chemistry C* **117** (2013) 13339–13349. Cover of the July 4, 2013 issue.
10. A. Melville, T. Mairoser, A. Schmehl, T. Birol, T. Heeg, B. Holländer, J. Schubert, C.J. Fennie, and D.G. Schlom, "Effect of Film Thickness and Biaxial Strain on the Curie Temperature of EuO," *Applied Physics Letters* **102** (2013) 062404.
11. P.J. Ryan, J.-W. Kim, T. Birol, P. Thompson, J.-H. Lee, X. Ke, P.S. Normile, E. Karapetrova, P. Schiffer, S.D. Brown, C.J. Fennie, and D.G. Schlom "Reversible Control of Magnetic Interactions by Electric Field in a Single-Phase Material," *Nature Communications* **4** (2013) 1334.
12. N.A. Benedek, A.T. Mulder, and C.J. Fennie, "Polar Octahedral Rotations: A Path to New Multifunctional Materials," *Journal of Solid State Chemistry* **195** (2012) 11–20.
13. L.W. Martin and D.G. Schlom, "Advanced Synthesis Techniques and Routes to New Single-Phase Multiferroics," *Current Opinion in Solid State and Materials Science* **16** (2012) 199–215.
14. T. Birol, N.A. Benedek, H. Das, A.L. Wysocki, A.T. Mulder, B.M. Abbett, E.H. Smith, S. Ghosh, and C.J. Fennie, "The Magnetoelectric Effect in Transition Metal Oxides: Insights and the Rational Design of New Materials from First Principles," *Current Opinion in Solid State and Materials Science* **16** (2012) 227–242.
15. C.M. Brooks, R. Misra, J.A. Mundy, L.A. Zhang, B.S. Holinsworth, K.R. O'Neal, T. Heeg, W. Zander, J. Schubert, J.L. Musfeldt, Z.K. Liu, D.A. Muller, P. Schiffer, and D.G. Schlom, "The Adsorption-Controlled Growth of LuFe₂O₄ by Molecular-Beam Epitaxy," *Applied Physics Letters* **101** (2012) 132907.
16. M. Stengel, C.J. Fennie, and P. Ghosez, "Electrical Properties of Improper Ferroelectrics from First Principles," *Physical Review B* **86** (2012) 094112.
17. K. Kathan-Galipeau, P.P. Wu, Y.L. Li, L.Q. Chen, A. Soukiassian, Y. Zhu, D.A. Muller, X.X. Xi, D.G. Schlom, and D.A. Bonnell, "Direct Determination of the Effect of Strain on Domain Morphology in Ferroelectric Superlattices with Scanning Probe Microscopy," *Journal of Applied Physics* **112** (2012) 052011.
18. P. Cueva, R. Hovden, J.A. Mundy, H.L. Xin, and D.A. Muller, "Data Processing for Atomic Resolution Electron Energy Loss Spectroscopy," *Microscopy and Microanalysis* **18** (2012) 667–675.
19. J.A. Mundy, Q.Y. Mao, C.M. Brooks, D.G. Schlom, and D.A. Muller, "Atomic-Resolution Chemical Imaging of Oxygen Local Bonding Environments by Electron Energy Loss Spectroscopy," *Applied Physics Letters* **101** (2012) 042907.
20. J.M. Rondinelli and C.J. Fennie, "Octahedral Rotation-Induced Ferroelectricity in Cation Ordered Perovskites," *Advanced Materials* **24** (2012) 1961–1968.
21. S. Kamba, V. Goian, M. Orlita, D. Nuzhnyy, J.H. Lee, D.G. Schlom, K.Z. Rushchanskii, M. Ležaić, T. Birol, C.J. Fennie, P. Gemeiner, B. Dkhil, V. Bovtun, M. Kempa, J. Hlinka, and J. Petzelt, "Magnetodielectric Effect and Phonon Properties of Compressively Strained EuTiO₃ Thin Films Deposited on (001)(LaAlO₃)_{0.29}-(SrAl_{1/2}Ta_{1/2}O₃)_{0.71}," *Physical Review B* **85** (2012) 094435.

Structure and Dynamics of Domains in Ferroelectric Nanostructures – *In-situ* TEM Studies

Xiaoqing Pan

**Department of Materials Science and Engineering
University of Michigan, Ann Arbor, MI 48109**

Program Scope

The main goal of the proposed research is to explore the structure and dynamic behaviors of ferroelectric domains in ferroelectric thin films and nanostructures by advanced transmission electron microscopy (TEM) techniques in close collaboration with phase field modeling. The experimental techniques used include aberration-corrected sub-Å resolution TEM and *in-situ* TEM using a novel scanning tunneling microscopy (STM) - TEM holder which allows the direct observation of nucleation and dynamic evolution of ferroelectric domains under applied electric field. Specifically, we propose (1) to study the roles of static electrical boundary conditions and electrical charge in controlling the equilibrium domain structures of BiFeO₃ thin films with controlled substrate constraints, (2) to explore the fundamental mechanisms of ferroelectric domain nucleation, growth, and switching under an applied electric field in both uniform thin films and nanofabricated nanostructures, and to understand the roles of crystal defects such as dislocations and interfaces in these processes, (3) to understand the physics of ferroelectric domain walls and the influence of defects on the electrical switching of ferroelectric domains. The nucleation and dynamic evolution of ferroelectric domains observed by *in-situ* TEM under applied external electric field are quantitatively analyzed and directly compared with phase field simulations in Professor Long-Qing Chen's group at Penn State University.

Recent Progress

We have conducted a systematic study of static and dynamic behaviors of domains and domain wall motion in ferroelectric thin films using *in-situ* TEM techniques and analysis tools previously developed under this project. Some of the findings are highlighted here.

Changes in crystal structure and symmetry induced by charged domain walls

A ferroelectric domain wall can become electronically active, as a result of charged domain walls (CDWs) with a “head-to-head” or “tail-to-tail” polarization configuration. Such domain walls carrying net bound charge can have distinct properties from uncharged domain walls, such as a metallic conductivity. The atomic structures of CDWs, however, remain rarely explored. Using our previously developed quantitative atomic displacement and strain mapping techniques based on Cs corrected HAADF STEM imaging, we analyzed the local structural changes induced by the CDWs in ferroelectric BiFeO₃ thin films [1]. In such films, 71° CDWs are observed above triangular 109° /180° domain wall junctions. The HAADF image is processed to obtain mapping of the lattice parameter and the atomic displacement of Fe ions from the center of four Bi neighbors (D_{FB}). The electric polarization is proportional to $-D_{\text{FB}}$. Fig. 1a shows the spatial distribution of $-D_{\text{FB}}$ overlaid on the HAADF image. A CDW with

“head-to-head” polarization configuration is clearly seen above the triangular junction. Interestingly, the polarization rotates gradually from $\langle 111 \rangle$ directions beside the CDW to the out-of-plane orientation at the CDW. The lattice parameter mapping (Fig. 1b) also shows a local increase of the c/a ratio at the CDW. These results suggest the formation of a tetragonal (T)-like structure at the CDW, surrounded by the regular rhombohedral (R)-like phase. The T-like CDW also leads to changes in structures of the nearby domains. The tip region of the triangular domain below the CDW is found to possess an unexpected ferroelectric state, as its c/a ratio is close to 1.00, but its polarization has rotated from the $\langle 111 \rangle$ direction to the in-plane direction. This avoids a direct “tail-to-tail” configuration at the triangular tip and thus releases some of the electrostatic energy. Due to the unique polarization configuration in this nano-sized region, the rotation angle of polarization across the domain walls formed with the neighboring domains is no longer 180° or 109° , although they do return to those angles in the region far below the T-like CDW. The inclined wall (on the left side) of the triangular domain near the triangular tip becomes slightly charged itself.

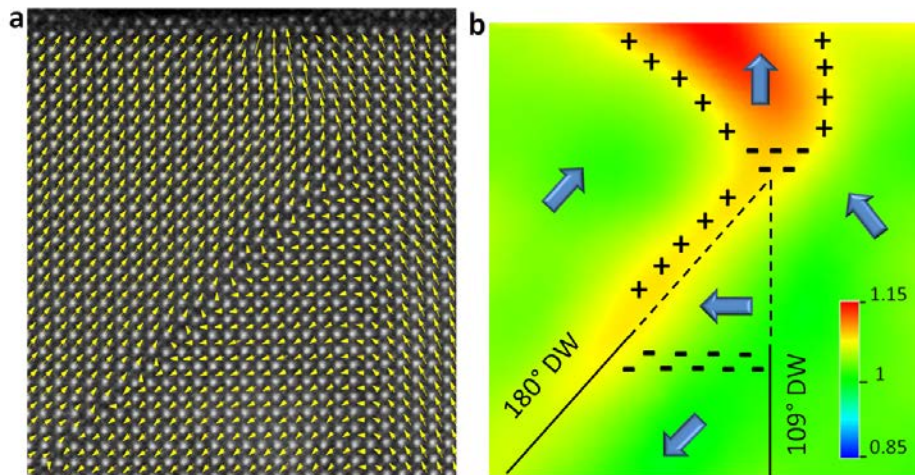


Fig. 1 | Charged domain wall induced changes of atomic structure – a, Plot of the $-\mathbf{D}_{\text{FB}}$ vectors overlaid on HAADF image of a $109^\circ/180^\circ$ domain wall junction near the free surface of the 20 nm thick BiFeO_3 film. **b,** The corresponding color map of the c/a ratios. The polarization orientation and bound charge are indicated.

We found that for sufficiently thin films an increased T/R ratio and CDWs traversing the full thickness of the film can be achieved. Arrays of T-like CDWs with unusual triangular domains were observed. Due to the effect of charges, such CDWs can provide conducting channels running through the whole film in ferroelectric thin films.

Ferroelastic domain-wall-mediated ferroelectric switching

Polarization switching in ferroelectric thin films occurs via nucleation and growth of 180° domains through a highly inhomogeneous process in which the kinetics are largely controlled by defects, interfaces and pre-existing domain walls. Our *in-situ* TEM studies provides direct experimental evidence that domain switching can be hindered by pre-existing, but immobile, ferroelastic domains in $\text{Pb}(\text{Zr}_{0.2}\text{Ti}_{0.8})\text{O}_3$ (PZT) thin films [2]. The switched c -

domain grew with increasing voltage. Under a constant voltage, the domain grew slowly, resulting from a relatively high density of dislocations acting as weak pinning centers in the film. Once the created c-domain reached the edge of the a-domain, the 180° domain wall motion ceased, showing the ferroelastic domain wall acted as an obstacle to the ferroelectric switching.

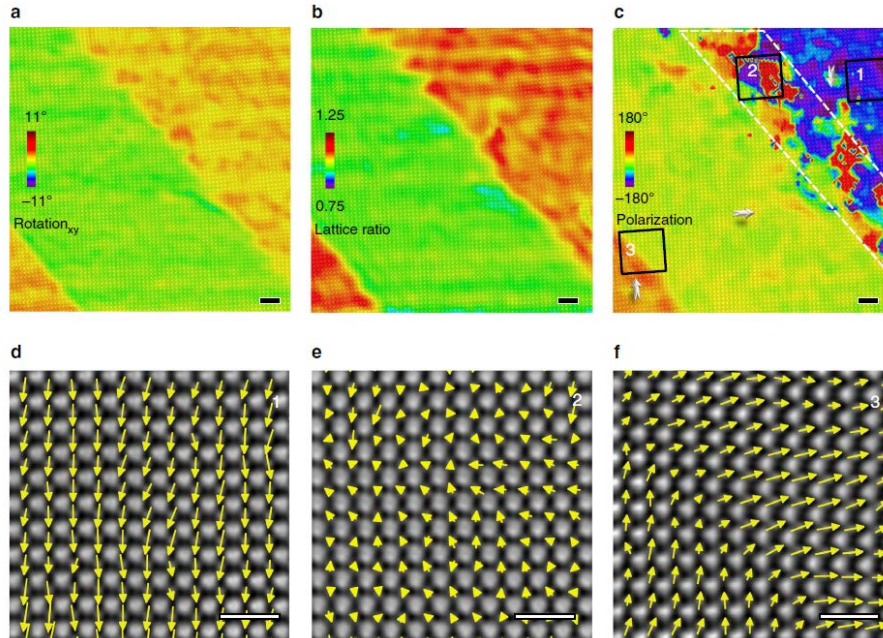


Fig. 2 | Charged ferroelastic domain boundary between c-domain and a-domain – **a**, A map of lattice tilt angle based on GPA calculations overlaid on its atomic resolution HAADF image. The region consists of three domains: c-domain (upper right), a-domain (middle) and c-domain (lower left). Scale bar, 2 nm. **b**, The map of lattice ratios of out-of-plane to in-plane calculated from the Pb sublattice of the same region. Scale bar, 2 nm. **c**, Polarization angle map showing the transition zone, highlighted by the white-dashed line, between c-domain and a-domain. Scale bar, 2 nm. **d**, Polarization vector map of the switched a-domain corresponding to the rectangle number 1 in c. Scale bar, 1 nm. **e**, Polarization vector map from the transition zone corresponding to the rectangle number 2 in c. Scale bar, 1 nm. **f**, Polarization vector map at the a-domain/c-domain boundary corresponding to the rectangle number 3 in c. Scale bar, 1 nm.

We analyzed the structure of 90° domain walls around the ferroelastic domain after switching using atomically resolved HAADF images (Fig. 2), and found that the hindering effect of the ferroelastic domain walls for the ferroelectric switching is caused by the formation of a transient layer with a thickness of several unit cells at an otherwise charged interface between a ferroelastic domain and a switched domain. This transient layer possesses a low-magnitude polarization, with a dipole glass structure, resembling the dead layer (Fig. 2c and e). The present study provides an atomic level explanation of the hindering of ferroelectric domain motion by ferroelastic domains. Hindering can be overcome either by applying a higher bias or by removing the as-grown ferroelastic domains in fabricated nanostructures.

Future Plans

In the next year we will continue exploring the static and dynamic properties of ferroelectric

heterostructures to elucidate atomic structures and switching behavior of ferroelectrics, using *in situ* TEM techniques in combination with theoretical modeling and simulations performed in Professor Long-Qin Chen's group at Penn State University. We will expand upon our analytical and *in-situ* TEM characterization of the prototypical BiFeO₃ and PbZr_{0.2}Ti_{0.8}O₃ ferroelectrics, supplied through collaboration with Dr. Chang-Beom Eom from the University of Wisconsin and Dr. Darrell Schlom from Cornell University. Specifically, we will continue atomic structures characterizations of interfaces of ferroelectric heterostructures to explore the interaction of polarization, strain, and octahedron rotations and their effects on the properties of ferroelectrics. We also plan to further explore the interplay between applied and built-in electric fields, strain, defects, and ferroelectric domains in switching behavior, and expand our measurements to explore the atomic-scale mechanism of domain walls switching dominated by charging effect or pinning of lattice potentials. We will also continue the *in-situ* study of mechanical switching of ferroelectrics through the flexoelectric effects to discover the underlying dynamics.

References

- [1] L.Z. Li et al. *Nano Letters* **13**, 5218-5223 (2013).
- [2] P. Gao et al., *Nature Communications*. **4**, 2791 (2013).

Publications

1. Gao, P., Britson, J., Nelson, C. T., Jokisaari, J. R., Duan, C., Trassin, M., Baek, S. H., Guo, H., Li, L., Wang, Y., Chu, Y. H., Minor, A. M., Eom, C. B., Ramesh, R., Chen, L. Q., & Pan, X. Q. "Ferroelastic Domain Switching Dynamics under Electrical and Mechanical Excitations", *Nature Communications* **5**, 3801 (2014). DOI: 10.1038/ncomms4801.
2. Gao, P., Britson, J., Jokisaari, J. R., Nelson, C. T., Baek, S. H., Wang, Y., Eom, C. B., Chen, L. Q., & Pan, X. Q. "Atomic-scale mechanisms of ferroelastic domain-wall-mediated ferroelectric switching", *Nature Communications* **4**, 2791 (2013). DOI: 10.1038/ncomms3791.
3. Li, L., Gao, P., Nelson, C. T., Jokisaari, J. R., Zhang, Y., Kim, S. J., Melville, A., Adamo, C., Schlom, D. G., & Pan, X. Q. "Atomic Scale Structure Changes Induced by Charged Domain Walls", *Nano Letters* **13**, 5218-5223 (2013).
4. Britson, J., Nelson, C. T., Pan, X. Q., & Chen, L. Q., "First Order Morphological Transition of Ferroelastic Domains in Ferroelectric Thin Films," *Acta Materialia*, in press.
5. Wang, Y., Nelson, C. T., Melville, A., Winchester, B., Shang, S. L., Liu, Z. K., Schlom, D. G., Pan, X. Q., & Chen, L. Q., "BiFeO₃ Domain Wall Energies and Structures: A Combined Experimental and Density Functional Theory+U Study", *Phys. Rev. Lett.* **110**, p. 267601 (2013).
6. C. Beekman, W. Siemons, T. Z. Ward, M. Chi, J. Howe, M. D. Biegalski, N. Balke, P. Maksymovych, A. K. Farrar, J. B. Romero, P. Gao, X. Q. Pan, D. A. Tenne, and H. M. Christen, "Phase transitions, phase coexistence, and piezoelectric switching behavior in highly strained BiFeO₃ films", *Adv. Mater.* **25**, 5561–5567 (2013).
7. Lee, S., Tarantini, C., Gao, P., Jiang, J., Weiss, J. D., Kametani, F., Folkman, C. M., Zhang, Y., Pan, X. Q., Hellstrom, E. E., Larbalestier, D. C., & Eom, C. B., "Artificially engineered superlattices of pnictide superconductors", *Nature Materials* (2013), doi:10.1038/nmat3575.

Physics of complex materials systems through theory and microscopy/EELS

Principal Investigators: Sokrates T. Pantelides, Mark P. Oxley, Kalman Varga
Department of Physics and Astronomy, Vanderbilt University, Nashville, TN 37235

Program Scope

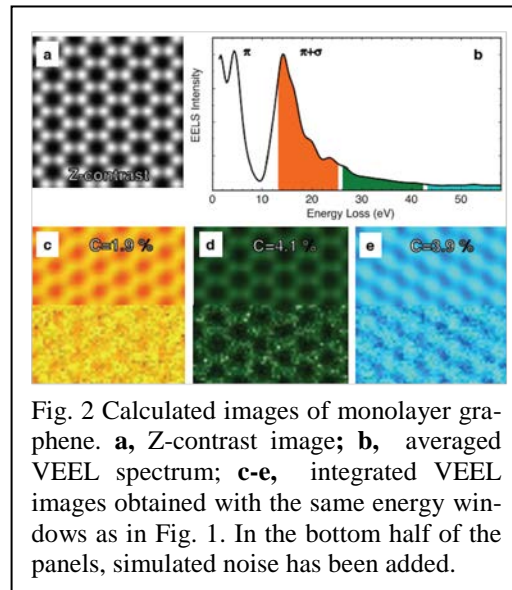
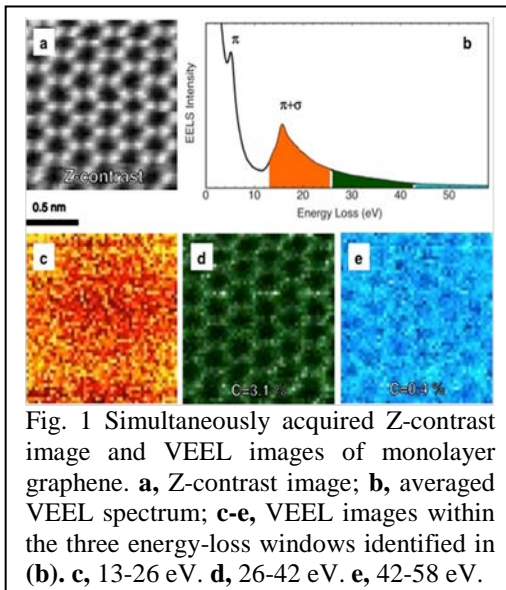
The main objective is to combine density functional theory (DFT) with Z-contrast imaging and electron-energy-loss spectroscopy, obtained with scanning transmission electron microscopes (STEMs), to elucidate structure property relations in complex materials structures. A key subtask has been the development of computer codes that combine DFT calculations of electron excitations in solids with dynamical scattering theory that tracks the microscope's finely focused electron beam as it undergoes diffraction in the sample, exits, and gets collected in the detector, including all interference effects. These simulations are aimed at the new capabilities of aberration-corrected STEMs, which provide high-resolution two-dimensional maps of EELS spectral features, generated by collecting probe-position-dependent EELS. We have primarily collaborated with the STEM group at Oak Ridge National Laboratory that was led until recently by Stephen J. Pennycook and is currently led by Matthew F. Chisholm.

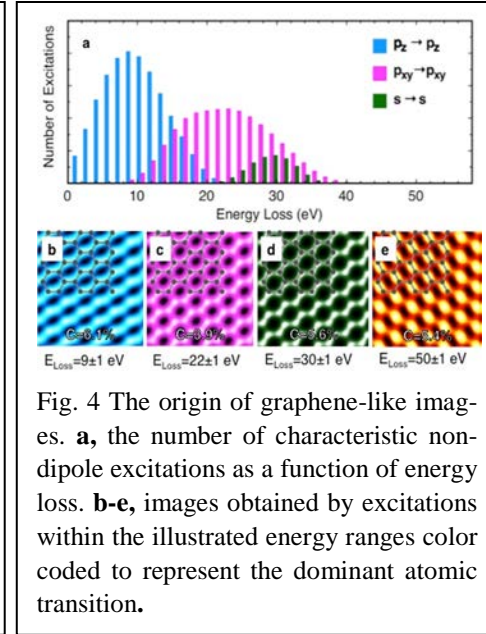
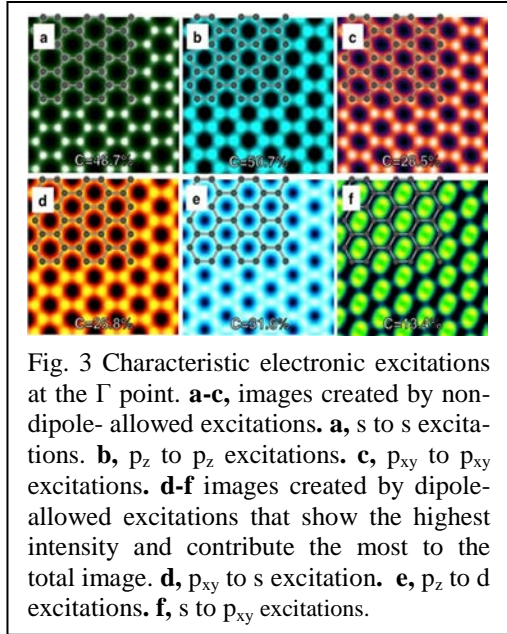
Recent progress

1. Valence-electron-energy-loss spectroscopy (VEELS) maps in graphene

A major accomplishment during the present grant period is the joint theory/experiment demonstration that VEELS contains atomic-resolution contrast and thus can rival photon-based spectroscopies, which have low spatial resolution, for the study of complex, inhomogeneous structures. There has been a widely held belief that VEEL spectra are not likely to exhibit atomic-scale contrast because of the inherent delocalization of low-energy-loss scattered electrons.¹

Our ORNL collaborators (post doc and subsequently Wigner Fellow Wu Zhou, working with Juan Carlos Idrobo and Steve Pennycook) obtained VEELS from monolayer graphene that in some energy regions exhibit atomic-scale contrast, with almost the resolution of a Z-contrast image (Fig. 1). We developed a computational tool and simulated the same spectra (Fig. 2), confirming the presence of atomic-scale contrast and elucidating its origin, heralding an era in which two-dimensional VEELS maps can play the same role for complex, inhomogeneous materials structures that optical spectra played in the past for perfect crystals and surfaces.





In prior work for this grant, we developed integrated computer codes combining DFT calculations of core-level excitations with dynamical scattering theory for the simulation of core-loss two-dimensional maps of spectral features. New coding was needed for excitations involving two Bloch functions and the new codes were again integrated with dynamical-scattering codes by post-doc Myron Kapetanakis and co-PI Mark Oxley. The first results using this methodology are shown in Fig. 2 in full reciprocity with Fig. 1. The overall agreement is excellent, given the following observations. The contrast in Fig. 2c is only 1.9%, which explains why it is not detectable in the experimental data of Fig. 1c. In Fig. 2d, the theoretical contrast is 3.9% while the experimental contrast in Fig. 1d is only 0.4% probably because the signal is so small.

The power of the theory is that we can examine the transitions that contribute within each of the energy windows and explore the origin of the contrast. In Fig. 3 we focus on excitations at the Γ point in the Brillouin zone (BZ) - where the atomic character of the states is highest - and show images from excitations between states with maximum atomic character, exhibiting contrast exceeding 50%. Figures 3 a-c are images of non-dipole allowed excitations, exhibiting a graphene-like structure with high contrast. They contribute the most to the total VEEL image contrast. Figure 3d is an image of a dipole-allowed transition. The image of Fig. 3e shows strong atomic contrast, but reduced localization on C sites than the excitations of Fig. 3b.

In Fig. 4a we show the number of valence excitations as a function of the transition energy and the images of excitations in 2-eV windows at energies where the graphene band structure consists mostly of delocalized d states with a weak atomic character. The contrast in these images is reduced compared to Fig. 3 and are much closer to that observed experimentally. Figure 4e shows an image in which the intensity is not localized about individual atomic sites, but blurs two atomic sites together, consistent with Fig. 2e.

The power of the new methodology will be fully realized as detectors with lower noise levels and new monochromators with better energy resolution become available, new instrumentation is designed to allow collections of electrons at selective momentum transfer, and computer performance increases.

This work was presented at the Microscopy Society of America conference in Hartford, CT, August 4-7, 2014. A full-length paper has been submitted to *Science*.

2. Investigations of complex materials systems with a combination of theory and STEM/EELS

We describe here briefly two out of several case studies (see complete publication list).

2.1 Ultrathin metallic nanowires in semiconducting transition metal dichalcogenides

Graduate student Junhao Lin, working with Wu Zhou at ORNL, used the STEM's electron beam to sculpt ultrathin nanowires, including ramified Y-junctions, connecting designated points within a semiconducting transition-metal-dichalcogenide (TMDC) monolayer (Fig. 5). The data also revealed that the nanowire formation is a self-regulating and self-healing process that is insensitive to precise beam parameters and that the resulting ultrathin nanowires are mechanically very robust while flexing and rotating under the electron beam. *In-situ* electrical measurements, performed by Dr. Kazu Suenaga's group in Japan, found that the nanowires are intrinsically metallic. Junhao carried out DFT calculations and confirmed that the nanowires are metallic, whereby they can potentially serve as interconnects in 2D circuits.² He also predicted that the metal-semiconductor contacts are Ohmic to p-type TMDC monolayers. He finally accounted for the observed robustness of the nanowires by showing that the fast switching between several specific rotation angles corresponds to switching between different stable states of the junction.

This work was published in *Nature Nanotech*.

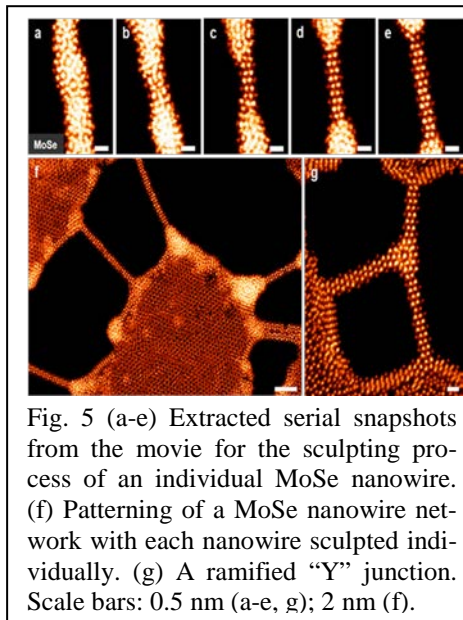


Fig. 5 (a-e) Extracted serial snapshots from the movie for the sculpting process of an individual MoSe nanowire. (f) Patterning of a MoSe nanowire network with each nanowire sculpted individually. (g) A ramified “Y” junction. Scale bars: 0.5 nm (a-e, g); 2 nm (f).

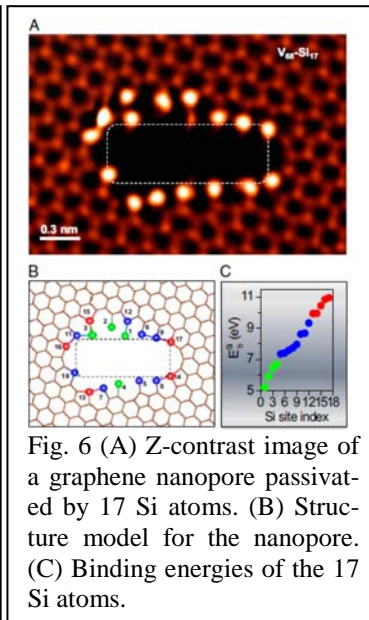


Fig. 6 (A) Z-contrast image of a graphene nanopore passivated by 17 Si atoms. (B) Structure model for the nanopore. (C) Binding energies of the 17 Si atoms.

2.2 Stabilization of graphene nanopores by Si atoms

Holes in graphene are known to fill quickly by C atoms. Stable holes, however, are highly desirable for applications involving molecular translocation, e.g., water filtering, gas separation, DNA sequencing, etc. Z-contrast images taken by our ORNL collaborators show multivacancies that are passivated by Si impurities (Fig. 6A). DFT calculations by Jaekwang Lee found that the Si atoms are strongly bound (Fig. 6 C) and that C atoms do not fill multivacancies but rather form dendrites attached to Si atoms, which can be avoided altogether by passivating Si dangling bonds with H atoms (binding energies >3 eV), resulting in robust, stable nanopores.

This work has been published in PNAS in 2014 and a patent application has been filed.

Future Plans

We plan to explore VEEL maps for several prototype al systems (impurities, defects, interfaces) to establish the new methodologies. Experimental VEELS maps showing atomic-scale contrast are available for a Si impurity, for edges, and for grain boundaries in graphene. We will also continue exploring other systems combining theory and microscopy/EELS.

References

1. D. Muller, and J. Silcox, *Ultramicrosc.* **59**, 195 (1995); R. Egerton, *ibid.* **107**, 575 (2007).
2. B. Radisavljevic et al., *ACS Nano* **5**, 9934 (2011).

Publications in the last 2 years

1. W. Zhou, M. D. Kapetanakis, M. P. Prange, S. T. Pantelides, S. J. Pennycook, and J.-C. Idrobo, "Direct determination of the chemical bonding of individual impurities in graphene", *Phys. Rev. Lett.* **109**, 206803 (Nov. 15, 2012)
2. S. T. Pantelides, Y. Puzyrev, L. Tsetseris, B. Wang, "Defects and doping and their role in functionalizing graphene", *MRS Bull.* **37**, 1187-1194 (Dec. 2012)
3. M. P. Prange, M. P. Oxley, M. Varela, S. J. Pennycook, and S. T. Pantelides, "Simulation of spatially resolved electron energy loss near-edge structure for scanning transmission electron microscopy", *Phys. Rev. Lett.* **109**, 246101 (Dec. 2012)
4. J. Lee, W. Zhou, S. J. Pennycook, J.-C. Idrobo, and S. T. Pantelides, "Direct visualization of reversible dynamics in a Si₆ cluster embedded in a graphene pore", *Nature Comm.* **4**, 1650 (April 2013)
5. S. Ma, P. R. Cantwell, T. J. Pennycook, N. Zhou, M. P. Oxley, D. N. Leonard, S. J. Pennycook, J. Luo, and M. P. Harmer, "Grain boundary complexion transitions in WO₃-and CuO-doped TiO₂ bicrystals", *Act. Mat.* **61**, 1691-1704 (March 2013)
6. J. Lin, W. Fang, W. Zhou, A. Lupini, J.-C. Idrobo, J. Kong, S. J. Pennycook, and S. T. Pantelides, "AC/AB stacking boundaries in bilayer graphene", *Nano Lett.* **13**, 3262 (July 2013)
7. Y. Gong, Z. Liu, A. Lupini, G. Shi, J. Lin, S. Najmaei, Z. Link, A. L. Elias, A. Berkdemir, G. You, H. Terrones, M. Terrones, R. Vajtai, S. T. Pantelides, S. J. Pennycook, J. Lou, W. Zhou, and P. M. Ajayan, "Band gap engineering and layer-by-layer mapping of selenium-doped molybdenum disulfide", *Nano Lett.* **14**, 442-449 (Feb. 2014)
8. N. Biskup, J. Salafranca, V. Mehta, M. P. Oxley, Y. Suzuki, S. J. Pennycook, S. T. Pantelides, and M. Varela, "Insulating Ferromagnetic LaCoO_{3-δ} films: A phase induced by ordering of oxygen vacancies", *Phys. Rev. Lett.* **112**, 087202 (Feb. 2014)
9. C. Li, Y. Wu, J. Poplawsky, T. J. Pennycook, N. Paudel, W. Yin, S. J. Haigh, M. P. Oxley, A. R. Lupini, M. Al-Jassim, S. J. Pennycook, and Y. Yan, "Grain-boundary-enhanced carrier collection in CdTe solar cells", *Phys. Rev. Lett.* **112**, 156103 (April 2014)
10. X. Lu, M. I. B. Utama, J. Lin, X. Gong, J. Zhang, Y. Zhao, S. T. Pantelides, J. Wang, Z. Dong, Z. Liu, W. Zhou, and Q. Xiong, "Large-area synthesis of monolayer and few-layer MoSe₂ films on SiO₂ substrates", *Nano Lett.* **14**, 2419-2425 (May 2014)
11. J. Lee, Z. Yang, W. Zhou, S. J. Pennycook, S. T. Pantelides, and M. F. Chisholm, "Stabilization of graphene nanopore", *Proc. Nat. Acad. Sci. USA* **111**, 7522-7526 (May, 2014)
12. J. Lin, O. Cretu, W. Zhou, ...and S. T. Pantelides, "Flexible metallic nanowires with self-adaptive contacts to semiconducting transition-metal dichalcogenide monolayers", *Nature Nanotech.* **9**, 436-442 (June 2014)
13. M. P. Oxley, M. D. Kapetanakis, M. P. Prange, M. Varela, S. J. Pennycook, and S. T. Pantelides, "Simulation of probe position-dependent electron energy-loss fine structure", *Microsc. Microanal.* **20**, 784-797 (2014)
14. Y.-M. Kim, A. N. Morozovska, E. A. Eliseev, M. P. Oxley, ...S. T. Pantelides, S. V. Kalinin, and A. Y. Borisevich, "Direct observation of ferroelectric field effect and vacancy-controlled screening at the BiFeO₃-La_xSr_{1-x}MnO₃ interface", *Nature Mater.* in press (2014)
15. Y. Gong, J. Lin (co-first author), ... S. T. Pantelides, Z. Liu, W. Zhou, and P. M. Ajayan, "Vertical and in-plane heterostructures in WS₂/MoS₂ monolayers", *Nature Mater.*, in press
16. M. D. Kapetanakis, W. Zhou, M. P. Oxley, J. Lee, M. P. Prange, S. J. Pennycook, and S. T. Pantelides, "Atomically resolved maps of valence electron excitations with application to graphene", submitted to *Science*

Emerging Functionality in Transition-Metal Compounds Driven by Spatial Confinement

Ward Plummer, Department of Physics and Astronomy, Louisiana State University

Program Scope: The exotic properties displayed by correlated electronic materials (CEMs) such as the cuprates, manganites, ruthenates, Fe-based pnictides, and heavy-fermion compounds are intimately related to the coexistence of competing nearly degenerate states which couple simultaneously active degrees of freedom—charge, lattice, orbital, and spin states. This project focuses on the exploration of novel behavior induced by spatial confinement, strain, and chemical or physical modification of the surface or interface. Thin films will be grown and characterized *in situ* in an ultra high vacuum environment, using a combination of techniques, such as scanning tunneling microscopy and spectroscopy, low energy electron diffraction, high-resolution X-ray photoemission, angle-resolved photoemission spectroscopy, and low energy electron loss spectroscopy. High resolution scanning transmission electron microscopy, electron loss spectroscopy (BNL), x-ray diffraction, and electrical and magnetic transport measurements will be conducted *ex situ*. We focus on complex doped manganites and ruthenates, exploring the coupled structural, magnetic and electronic transitions. By combining local modifications to order parameters across the range of correlation length scales, we will investigate where the interplay of combinations of spin-charge-orbital-lattice contributions dominate or break down. New nanofabrication capabilities at the Center for Nanophase Materials Sciences at ORNL will be utilized to push the size of spatial confinement into the nanometer range. The electronic and magnetic properties can be tuned in these spatially confined films by depositing electronic donors or acceptors or by patterning of magnetic nano-clusters. Strain also gives a non-thermal parameter to be used to tune electronic or magnetic phase transitions. In essence we are combining two of the grand challenges of the 21st century —Complexity and Nano-structured materials to explore and exploit emergent behavior.

Recent Progress

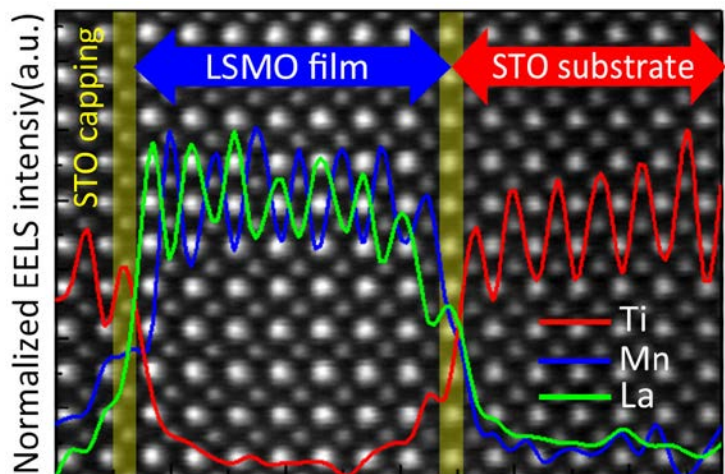
What is behind the metal-nonmetal transition in thin films of oxides?*

An intriguing property of many transition metal oxide thin films is that their physical properties are fundamentally different from what is observed for the bulk. One outstanding example is the nonmetallic behavior in ultrathin films of metallic oxides: *a thickness-induced metal-nonmetal transition*. We explore the origin of such transition by manipulating thin film growth and combining both macroscopic and microscopic characterization techniques, for $\text{La}_{2/3}\text{Sr}_{1/3}\text{MnO}_3$ (LSMO) ultrathin films. We have isolated several key driving forces -- lattice strain, oxygen vacancies, disorder, chemical segregation and interfacial charge transfer, all of which have noticeable contribution to the metal-nonmetal transition.

We find that both tensile and compressive substrate strain increase the critical metal-nonmetal transition thickness. By minimizing strain effect through inserting strained buffer layers, we are able to approach the minimum critical thickness of 4 unit cell (u.c) for the transition. Further capping with a SrTiO_3 overlayer further reduces critical thickness down to 3 u.c. However, the ferromagnetism of LSMO is more robust against reducing thickness. The ferromagnetic ground state persists down to 2 u.c. films. In particular, with decreasing film thickness, the film exhibits a weak to strong localization crossover behavior with a characteristic onset temperature (T^*) and such crossover is strongly tied with oxygen vacancies. As T^* increases and approaches to the

Curie temperature (T_C), the film eventually becomes insulating. Both Scanning Transmission Electron Microscopy (combining atomically-resolved STEM imaging with electron energy loss spectroscopy as shown in the figure) data confirms surface of the films is terminated with La/Sr-O layer rather than MnO_2 -layer. ARXPS results also suggest that Sr segregation tends to be stronger with reduced film thickness, providing new aspects in understanding the metal-nonmetal transition.

In conclusion, while several parameters such as strain and doping level are important for the nonmetallic behavior, the unavoidable existence of oxygen vacancies is the main driving force for the thickness-dependent metal-nonmetal transition in thin films of metallic oxide materials.



High-angle annular dark image (HAADF) STEM image of STO(capping layer)/LSMO/STO film along [100] zone-axis direction and the normalized integrated intensities of the La M (green), Ti L (red) and Mn L (blue) edges extracted from the EELS spectrum at room temperature.

* This work is supported by DOE DE-SC0002136 (Zhaoliang Liao, Zhen Wang, Lina Chen, Hangwen Guo, Gaomin Wang, and Jiandi Zhang) with collaboration with Brookhaven National Laboratory (Jing Tao and Yimei Zhu), supported by the US DOE, BES, through the Materials Sciences and Engineering Division under Contract No. DE-AC02-98CH10886).

Future Plans

We have demonstrated that we are able to grow complex materials such as oxides with atomic precision and characterize these materials with in-situ (RHEED, LEED, STM/AFM, ARPES, ARXPS and EELS) and ex-situ STEM through our close collaboration with BNL. With such growth and characterization capabilities in truly atomic scale, we plan to explore following several issues in near future:

- **Measure the layer-by-layer lattice distortion in the crystalline oxide thin films.** In order to full understand the thickness-dependent metal to nonmetal transition, as well as the thickness-dependent functionalities in general, in many metallic oxide films, it is essential to reveal the thickness-dependent lattice distortion. We plan to use atomically-resolved STEM imaging at BNL to characterize the layer-by-layer lattice distortion of LSMO films on STO (100) and other substrates. In addition, we will use *in-situ* LEED $I(V)$ to refine the lattice structure at the surface of films, thus providing systematically the thickness dependence of lattice distortion.
- **Reveal the thickness dependence of electronic structure of oxide thin films:** By using in-situ ARPES and ARPES, we would like to study both valence and relevant core-level electronic structure as a function of film thickness. We are able to control both dimensionality (thickness) and the relative oxygen vacancy density of oxide films like LSMO.

We plan to reveal the dimensionality effect and defect induced electronic structure, as we have revealed that oxygen vacancy-induced disorder effect is the primary driving force for thickness-dependent metal to nonmetal transition.

- **Study microscopic magnetic structures and possible domain manipulation:** In many thin films of oxides like manganites, unusual magnetic properties are linked to the nanoscale magnetic domain behaviors. We plan to use Lorentz TEM to characterize the magnetic domain structure and evolution for different film thickness in real space imaging. Eventually, we hope we can manipulate these microscopic structures and reveal their relationship with macroscopic magnetic properties.
- **Explore the lattice and charge dynamics in the doped oxide thin films:** Because of unusual electronic and magnetic properties with changing film thickness, we plan to explore the lattice and charge dynamics in real time as well as lattice and charge excitation spectroscopy. The experiments include time-resolved TEM currently being developed in BNL (collaborated with Yimei Zhu's group) and in-situ EELS. It will include the characterization of charge/magnetic domain fluctuations, phonon and electron excitation spectroscopy.
- **Development of STEM for interface and thin film studies:** A technical development in our future plane is, through the close collaboration with BNL, to combine intra-unit-cell convergent-beam electron diffraction (CBED) and scanning technique to determine the structure symmetry at the interface and in the film. CBED is a technique with high sensitivity on the crystal symmetry, strain and charge density. We propose to image the quantitative results including the strain and charge density from CBED in real space. Together with the EEL spectrum imaging, we believe that such technical development will provide great insight into the physics at interfaces and in film materials.

Publications

- “*Tuning Properties of Columnar Nanocomposite Oxides*”, Zhaoliang Liao, Peng Gao, S. Stadler, R. Jin, X. Pan, E.W. Plummer, and Jiandi Zhang, *Appl. Phys. Lett.* **103**, 043112 (2013).
- “*Strain-Mediated Defect Superstructure on a Complex Oxide Surface*”, Zhiming Wang, Fengmiao Li, Sheng Meng, Jiandi Zhang, E. W. Plummer, Ulrike Diebold, and Jiandong Guo, *Phys. Rev. Lett.* **111**, 056101 (2013).
- “*Electrophoretic-like gating used to control metal–insulator transitions in electronically phase separated manganite wires*”, Hangwen Guo, Joo H. Noh, Shuai Dong, Philip D. Rack, Zheng Gai, Xiaoshan Xu, Elbio Dagotto, Jian Shen and T. Zac Ward, *Nano Lett.* **13**, 3749 (2013)
- “*Room temperature multiferroic hexagonal LuFeO₃*”, Wenbin Wang, Zheng Gai, Miaofang Chi, Nina Balke, Ho Nyung Lee, Leyi Zhu, Xuemei Cheng, David J. Keavney, Jiyu Yi, Thomas Z. Ward, Jun Zhao, Paul C. Snijders, Hans M. Christen, Jian Shen, and Xiaoshan Xu, *Phys. Rev. Lett.* **110**, 237601 (2013).
- “*Growth diagram of La_{0.7}Sr_{0.3}MnO₃ thin films using pulsed laser deposition*”, Hangwen Guo, Dali Sun, Wenbin Wang, Zheng Gai, Ivan Kravchenko, Jian Shao, Lu Jiang, Thomas Z. Ward, Paul C. Snijders, Lifeng Yin, Jian Shen, and Xiaoshan Xu, *J. Appl. Phys.* **113**, 234301 (2013).

- “*Persistent metal-insulator transition at the surface of oxygen deficient, epitaxial $La_{5/8-x}Pr_xCa_{3/8}MnO_3$ films*”, P.C. Snijders, M. Gao, H. Guo, G. Cao, W. Siemons, H.-J. Gao, T.Z. Ward, J. Shen, and Z. Gai, *Nanoscale* **5**, 9659 (2013).
- “*Active control of magnetoresistance of organic spin valves using ferroelectricity*”, Dali Sun, Mei Fang, Xiaoshan Xu, Lu Jiang, Hangwen Guo, Yanmei Wang, Wenting Yang, Lifeng Yin, Paul C. Snijders, T. Z. Ward, Zheng Gai, X.-G. Zhang, Ho Nyung Lee, and Jian Shen, *Nature Comm.* **5**, 4396 (2014).
- “*Strain driven anisotropic magnetoresistance in antiferromagnetic $La_{0.4}Sr_{0.6}MnO_3$* ”, A.T. Wong, C. Beekman, H. Guo, W. Siemons, Z. Gai, E. Arenholz, Y. Takamura, T.Z. Ward, *Appl. Phys. Lett.* **105**, 052401 (2014).
- “*Epitaxial Growth of Complex Metal Oxides*”, Hangwen Guo and Jiandi Zhang, “Scanning tunneling microscopy of epitaxial oxide films” Book Chapter (Chap. 21), eds. Gertjan Koster and Guus Rijnders, Woodhead Publishing Limited, in press.
- “*A new non-destructive readout by using photo-recovered surface potential contrast*”, Le Wang, Kui-juan Jin, Jun-xing Gu, Chao Ma, Xu He, Jiandi Zhang, Can Wang, Yu Feng, Qian Wan, Jin-an Shi, Lin Gu, Meng He, Hui-bin Lu, and Guo-zhen Yang, Submitted to Nature Scientific Report.
- “*Controlling the length of a single axis in a complex oxide lattice via helium implantation and extraction*”, Hangwen Guo, Shuai Dong, Philip D. Rack, John D. Budai, Christianne Beekman, Zheng Gai, Wolter Siemons, Anthony T. Wong, Paul C. Snijders, Elbio Dagotto, Thomas Z. Ward, submitted
- “*Toward the ultimate critical thickness for metal-nonmetal transition in $La_{2/3}Ca_{1/3}MnO_3$* ”, Zhaoliang Liao, Fengmiao Li, Peng Gao, Jiandong Guo, Xiaoqing Pan, E. W. Plummer and Jiandi Zhang, submitted.
- “*Ferromagnetism and nonmetallic transport of a stabilized metastable material: α -FeSi₂ thin film*”, Guixin Cao, D. J. Singh, Xiaoguang Zhang, German Samolyuk, Liang Qiao, Chad Parish, Ke Jin, Yanwen Zhang, Hangwen Guo, Siwei Tang, Wenbin Wang, Jieyu Yi, Claudia Cantoni, Wolter Siemons, E. Andrew Payzant, Michael Biegalski, T. Z. Ward, David Mandrus, G.M. Stocks and Zheng Gai, submitted.

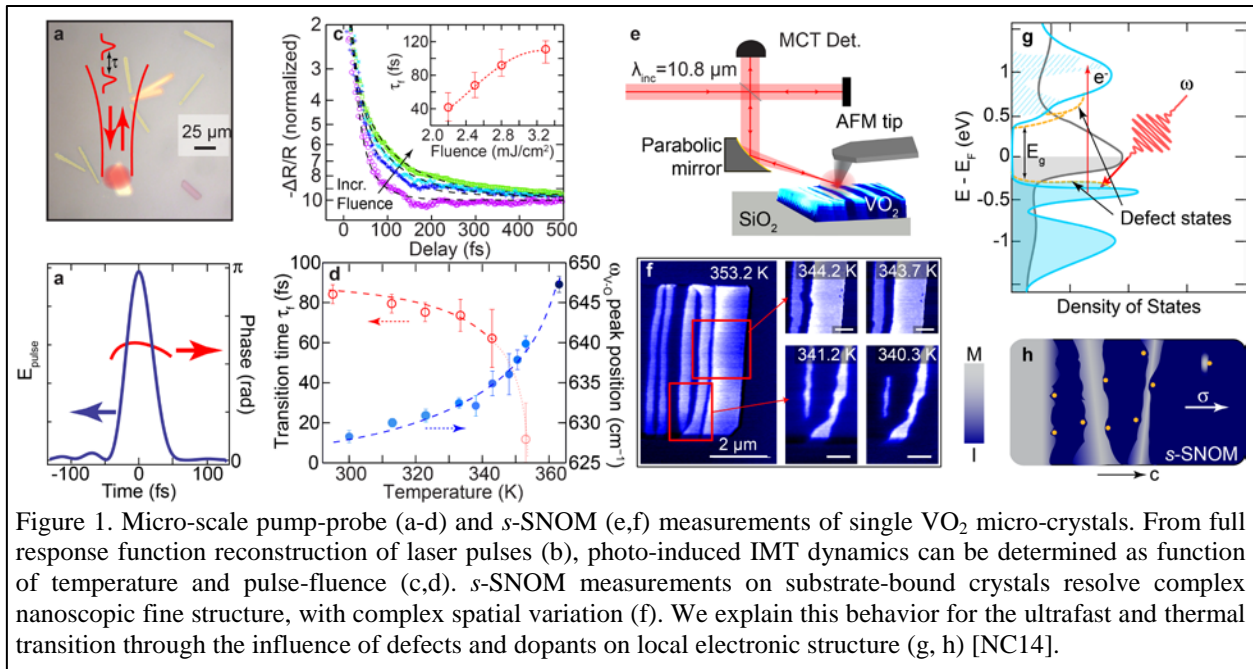
Nano-imaging and -spectroscopy of complex and correlated materials

Markus B. Raschke, Department of Physics, and JILA, University of Colorado, Boulder

Program Scope: The combination of optical spectroscopy with scanning probe microscopy has emerged as a new frontier of optical ultra-microscopy with few nanometer spatial resolution. We have generalized this approach of *scattering scanning near-field optical microscopy* (*s*-SNOM) to *any optical modality* including linear (mid-IR to vis), inelastic (Raman), nonlinear (SHG), and ultrafast spectroscopy [AP12], and extended it to variable and cryogenic temperatures [RSI13]. On that basis we have demonstrated a unique application potential for probing nanoscale behavior in correlated, complex, and 2D materials. We pursue the multi-modal and multi-spectral nano-imaging of electronic and vibrational (including Drude and polaronic) resonances, structural symmetry, and ultrafast dynamics to gain insight into properties, mechanisms, and functions of correlated electron materials (CEM), domain formation in multiferroics, polaronic thermal properties, and finite-size effects, and multivariable and optical control of 2D materials.

Recent Progress: In our project we pursue method development, demonstration and application of *s*-SNOM in our lab, as well as in collaboration with EMSL/PNNL and ALS/LBL to disseminate the technique making it available as user facilities. In addition to the application to problems in complex materials our work ties into new fundamental questions of optical physics that enables, e.g., the combination of *s*-SNOM with femtosecond spectroscopy to access ultrafast dynamics, or taking advantage of the enhanced electromagnetic density of states of the thermal near-field or the coherence of mid-IR synchrotron radiation, for broadband spectroscopy within the only nanoscale sample volumes inherent with the increase in spatial resolution. Specific examples of our work over the past 2 years include:

Inhomogeneity in the ultrafast insulator-to-metal transition dynamics of VO₂ Vanadium dioxide (VO₂) is one of the prototypical CEM, exhibiting an insulator-metal transition (IMT). A wide variety of photon and electron probes have been applied in search of a satisfactory mechanistic



explanation, but the IMT has remained puzzling since its discovery more than five decades ago. In our previous work we have studied single micro-crystals of VO₂ to resolve the nano-domain

mation and competition of the metallic with different insulating phases [NL10, PRB12]. We extended this work to address the ultrafast dynamics of the photoinduced IMT, where past studies by different groups on thin film samples yielded conflicting results. We reveal inherently inhomogeneous behavior in the photoinduced bandgap reorganization as fast as 40 ± 8 fs, shorter than a suggested phonon bottleneck¹. A variation in time scales is uncorrelated with crystal size, orientation, and initial insulating phase. Surprisingly, however, the average value of 80 ± 25 is similar to results from previous studies on polycrystalline thin films^{1,2}. This together with the nano-domain behavior during the thermally induced phase transition, suggests a high sensitivity to local variations, such as doping, defects, and strain. These could alter the density of available states and change the rate of electron delocalization. Similarly, disruption in the free energy uniformity could produce complex domain topology in the thermal transition. The combination of results point to an electronic mechanism dominating the photoinduced IMT, obscured in previous polycrystalline ensemble-averaging investigations. This study in general demonstrates the importance of probing homogeneous, well-characterized sub-systems in CEM [NC14].

Phase-resolved plasmon interferometry on graphene The surface plasmon polaritons (SPPs) of graphene reflect the spatial variations of its underlying electronic structure. Using near-field plasmon interferometry, we excite and image the graphene SPP response in phase and amplitude, and develop an analytic cavity model that can self-consistently describe the SPP response function for edge, grain boundary, and defect SPP reflection and scattering [PRL14]. In contrast to earlier work, the phase contrast provides additional constraints for theoretical models and is more robust to changes in signal intensity due to, e.g., bilayer graphene or surface contaminants.

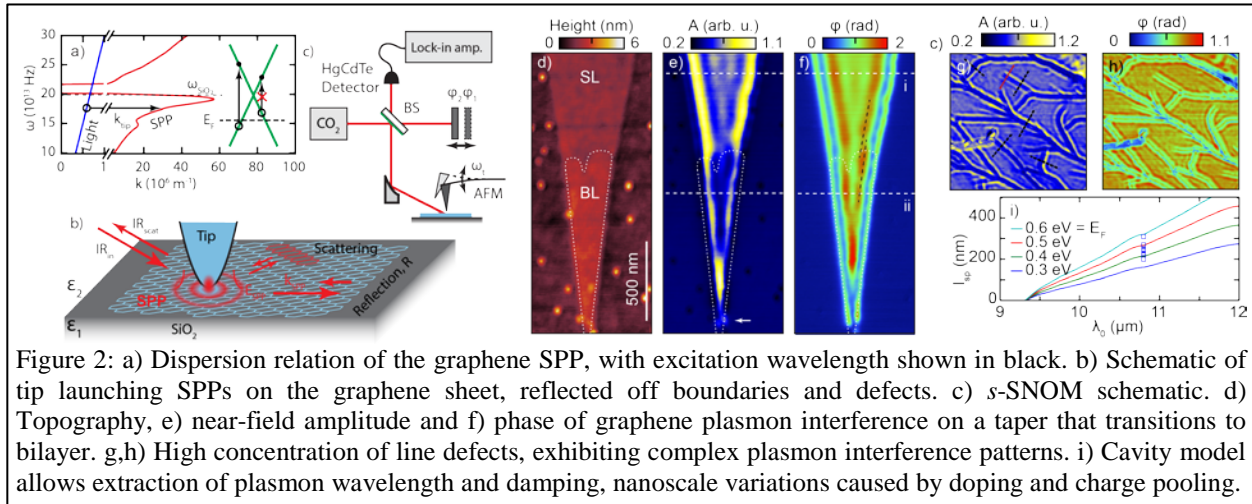


Figure 2: a) Dispersion relation of the graphene SPP, with excitation wavelength shown in black. b) Schematic of tip launching SPPs on the graphene sheet, reflected off boundaries and defects. c) *s*-SNOM schematic. d) Topography, e) near-field amplitude and f) phase of graphene plasmon interference on a taper that transitions to bilayer. g,h) High concentration of line defects, exhibiting complex plasmon interference patterns. i) Cavity model allows extraction of plasmon wavelength and damping, nanoscale variations caused by doping and charge pooling.

We see changes in SPP wavelength due to local variations in the Fermi level of $E_F \approx 0.4 - 0.6$ eV, corresponding to variations in the carrier concentration n ranging from 1.2 to $2.6 \times 10^{13} \text{ cm}^{-2}$. SPP phase contrast imaging thus opens a new degree of freedom for spatial and spectral graphene SPP tuning and modulation for optoelectronics applications.

Phonon-polariton coherence and control in the thermal near-field We have previously used *s*-SNOM to achieve spectroscopic access to the fundamentally distinct spectral, spatial, and coherence properties of the thermal near-field [NL12]. Using SiC as an example, we study its thermal phonon polariton (SPhP) response [PRB14]. In contrast to the strongly surface-confined thermal near-field of localized vibrational modes, an extended exponential distance dependence is observed reflecting the spatial coherence of the SPhP thermal field. We observe pronounced spectral frustration with spectral shifts ranging from ~ 5 to $\sim 50 \text{ cm}^{-1}$ that can be describing by

effective medium change by the tip. The results highlight the possibility for local spectral and spatial tuning of the thermal SPhP resonance for control of the light-matter interaction [PSS13].

Synchrotron infrared near-field spectroscopy Characterizing and ultimately controlling the heterogeneity underlying complex matter, photonic materials, catalysis, or biological functions requires imaging with sensitivity to structure, phase, and chemical composition at nanometer spatial resolution. However, as with any ultrahigh spatial resolution microscopy technique, the demand for an increase in both spatial and spectral bandwidth often leads to a decrease in sensitivity. In collaboration with the ALS/LBL we overcome this limitation in *s*-SNOM using synchrotron radiation. The localized light-matter interaction is induced by low-noise, broadband, and spatially coherent synchrotron light with a high spectral irradiance, and the near-field signal is sensitively detected using heterodyne interferometric amplification. We achieve sub-40 nm spatially resolved molecular, and phonon vibrational spectroscopic imaging, with rapid spectral acquisition, spanning the full mid-IR (700 – 5000 cm^{-1}) with few cm^{-1} spectral resolution [PNAS14]. The setup we developed is available for and open for user proposals at beamline 5.4.

Future Plans: We will continue our nano-optical investigations of correlated and complex materials with an emphasis on new materials with emergent properties:

Transition metal dichalcogenides Transition metal dichalcogenides (TMDCs) have attracted attention in recent years due to their complex electronic properties, which can be tailored through stacking of layers. Some of these materials can also display correlated behavior such as superconducting and charge density wave phases⁴. The edges and grain boundaries of these 2D materials may have different electronic structure, as has been suggested recently for MoS_2 ⁵. These edge states have been studied using second-harmonic generation, which lacks the spatial resolution to directly investigate their properties. We plan to probe edge states and other inhomogeneities in TMDCs with a combination of micro-Raman and tip-enhanced SHG (TE-SHG) [PRB09], in order to resolve structure and electronic property variations.

2D polaronic materials Hexagonal boron nitride (hBN) with its 2D graphene-like structure shows promise as a high-temperature stable and electrically insulating substrate for many nanotechnology applications. Its layer thickness dependent and boundary controlled surface phonon polariton (SPhP) allows for the tuning its far- and near-field infrared response for superlensing and metamaterials and control of nano-scale heat transport. Recently, a first *s*-SNOM study identified the basic SPhP properties of hBN⁶. We have started to extend these studies to measure the phase-resolved full spatio-spectral SPhP response, to reveal reflection at grain boundaries and defects, temperature dependence and phonon softening, thermal near-field tuning of the SPhP response, and pump-probe ultrafast dynamics, using a combination of ultrafast laser based, broad-band synchrotron, and thermal-near-field *s*-SNOM.

Nonlinear and ultrafast graphene dynamics The interband excitation of carriers in graphene directly influences its electrical and optical properties, affecting potential applications in photovoltaic devices and saturable absorbers. Plasmons coupled to infrared light also lead to free carrier absorption and may result in variations in the plasmonic response, as detectable by plasmon interferometry experiments. We study this response in the form of intensity dependent nonlinear plasmon interferometry measurements. In addition, we plan to investigate fs spatially-resolved nonequilibrium carrier dynamics and other inhomogeneous phenomena⁶.

VO_2 pump-probe As our single-crystal IMT results indicate [NC14], VO_2 exhibits a high degree of sensitivity to defects, impurities, and strain. We therefore plan to extend our far-field pump probe experiments to the near-field, and perform above band-gap pump and mid-IR probe

experiments with ~ 10 nm spatial resolution. This will allow us to probe local variations in the dynamical response for both single crystal and polycrystalline thin film samples in order to access the intrinsic, homogeneous response.

Coupled ferroic order in multiferroics We will continue to develop our work on tip-enhanced second harmonic generation (TE-SHG) [PRB09], which will enable us to probe charge, spin, and lattice degrees of freedom in multiferroic systems and ferroic nanoparticles such as BiFeO_3 and hexagonal manganites, in a variety of forms.

Other strongly-correlated electron materials Phase separation in strongly-correlated electron materials is a phenomenon of high fundamental and technological significance. However, probing mesoscale variations in e.g. conductivity, spin organization, and energy gap remains difficult. We plan to image pseudogap variations in nickelate and other superconducting systems using resonant IR excitation for gaps of 60 – 200 meV, at a range of temperatures.

References

- [NL10] A. C. Jones, S. Berweger, J. Wei, D. Cobden, and M. B. Raschke, “Nano-optical investigations of the metal-insulator phase behavior of individual VO_2 , microcrystals”, *Nano Lett.* **10**, 1574 (2010).
[PRB12] J. M. Atkin, S. Berweger, E. K. Chavez, and M. B. Raschke, “Strain and temperature dependence of the insulating phases of VO_2 near the metal-insulator transition”, *Phys. Rev. B*, **85**, 020101(R) (2012).
[NL12] A. C. Jones and M. B. Raschke, “Thermal infrared near-field spectroscopy”, *Nano Lett.* **12**, 1475 (2012).
[PRB09] C. C. Neacsu, B. B. van Aken, M. Fiebig, and M. B. Raschke, “Second-harmonic near-field imaging of ferroelectric domain structure of YMnO_3 ”, *Phys. Rev. B* **79**, 100107 (2009).
[1] A. Cavalleri, T. Dekorsy, H. H. W. Chong, *et al.*, *Phys. Rev. B* **70**, 161102 (2004).
[2] S. Wall, L. Foglia, D. Wegkamp, *et al.*, *Phys. Rev. B*, **87**, 115126 (2013).
[3] Q. H. Wang, K. Kalantar-Zadeh, A. Kis, *et al.*, *Nat. Nanotech.* **7**, 699 (2012).
[4] J. A. Wilson, F. J. Disalvo, and S. Mahajan, *Adv. Phys.* **24**, 117–201 (1975).
[5] X. Yin, Z. Ye, D. A. Chenet, *et al.*, *Science* **344**, 488 (2014).
[6] S. Dai, Z. Fei, Q. Ma, *et al.*, *Science*, **343**, 1125 (2014).
[7] D. Brida, A. Tomadin, C. Manzoni, *et al.*, *Nature Comm.* **4**, 1987 (2013).

Publications (supported by BES, past 2 years)

- [AP12] J. M. Atkin, S. Berweger, A. C. Jones, and M. B. Raschke, “Nano-optical imaging and spectroscopy of order, phases, and domains in complex solids”, *Adv. Phys.* **61**, 745 (2012)
[PSS13] A. C. Jones, B. T. O’Callahan, H. U. Yang, and M. B. Raschke, “The thermal near-field: coherence, spectroscopy, heat-transfer, and optical forces”, *Prog. Surf. Sci.*, **88**, 349 (2013).
[RSI13] H. U. Yang, E. Hebestreit, E. E. Josberger, and M. B. Raschke, “A cryogenic scattering-type scanning near-field optical microscope”, *Rev. Sci. Instrum.* **84**, 023701 (2013).
[NC14] B. T. O’Callahan, J. M. Atkin, A. C. Jones, J. H. Park, D. Cobden, and M. B. Raschke, “Inhomogeneity in the ultrafast insulator-to-metal transition dynamics of VO_2 ”, *Nature Commun.* (submitted).
[PRL14] J. A. Gerber, S. Berweger, B. T. O’Callahan, and M. B. Raschke, “Phase-resolved surface plasmon interferometry of graphene”, *Phys. Rev. Lett.* **113**, 055502 (2014).
[PRB14] B. T. O’Callahan, W. E. Lewis, A. C. Jones, and M. B. Raschke, “Spectral frustration and spatial coherence in thermal near-field spectroscopy”, *Phys. Rev. B* **89**, 245446 (2014).
[PNAS14] H. A. Bechtel, E. A. Muller, R. L. Olmon, M. C. Martin, and M. B. Raschke, “Ultrabroadband infrared nanospectroscopic imaging”, *PNAS* **111**, 7191 (2014).

Study of Nanoscale Heat Transport and Dissipation
Pramod Reddy, University of Michigan

Program Scope

The goal of this project is to experimentally investigate radiative and conductive thermal transport as well as heat dissipation (generation) in nanoscale gaps and circuits. In macroscale devices, heat transport via radiation and conduction is well described by the Stefan-Boltzmann law and the Fourier's law, respectively. However, recent studies have highlighted that both these laws fail to adequately describe heat transport at the nanoscale. For example, recent computational studies of radiative heat transport in nanoscale gaps have suggested that the radiative heat flux in a one-nanometer sized gap between suitably chosen planar dielectric surfaces could be five orders of magnitude larger than what is predicted by the Stefan-Boltzmann law! This large deviation arises primarily due to contributions from evanescent waves that decay exponentially on a length scale comparable to their wavelength. Heat transport is expected to be greatly enhanced when objects are in the extreme near-field of each other (i.e. gap sizes of a few nanometers) because contributions from the evanescent modes increase dramatically as the gap size decreases. However, extreme near-field radiative properties have not been systematically explored due to a number of experimental challenges. Such enhancements in radiative heat transport, if realized, could be leveraged for a variety of technological applications. In addition, computational work on heat transport in nanometer-sized atomic and molecular junctions (devices where a few atoms or a molecule bridge macroscopic electrodes) has also suggested intriguing properties, including length independent thermal conductance, which indicates a breakdown of Fourier's law, and quantization of the electronic thermal conductance, all of which remain experimentally untested. Experimentally elucidating these important nanoscale heat transport and dissipation phenomena is key to the rational design of novel electronic, photonic, and thermoelectric devices that are a major focus of current nanotechnology research.

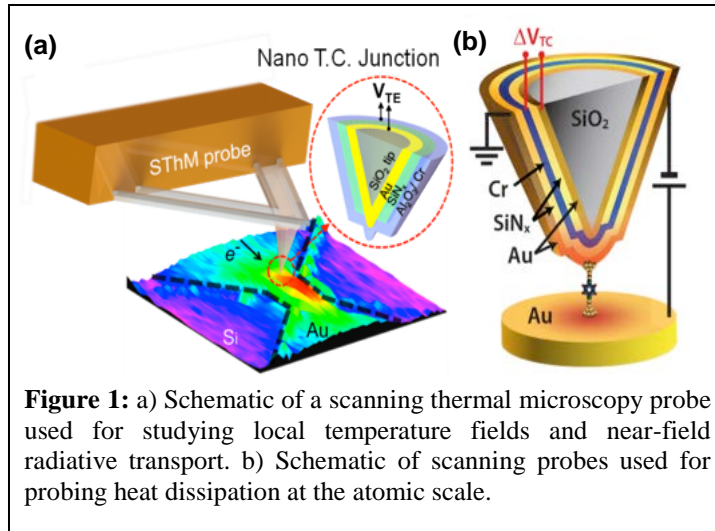


Figure 1: a) Schematic of a scanning thermal microscopy probe used for studying local temperature fields and near-field radiative transport. b) Schematic of scanning probes used for probing heat dissipation at the atomic scale.

This project seeks to leverage novel scanning thermal microscopy tools (Fig. 1) to answer several questions regarding nanoscale heat transport and dissipation: 1) How do the radiative transport properties of nanometer-sized gaps (1 - 10 nm) depend on the dielectric properties of the surfaces? 2) Can radiative heat transport be enhanced by orders of magnitude in the extreme near-field? 3) What are the heat transport characteristics of atomic and molecular junctions? 4) Are quantum limited thermal transport properties realizable at room temperatures in metallic atomic chains? 5) What are the heat dissipation characteristics of atomic and molecular scale junctions? 6) Can Peltier cooling be experimentally realized in molecular junctions?

Recent Progress

In the first few years of the project we invested a substantial amount of effort into developing scanning probes (Fig. 2) with integrated nanoscale thermocouples that are compatible with operation in a UHV environment. Using these probes we demonstrated that it is possible to quantitatively map temperature fields with ~ 15 mK temperature resolution and ~ 10 nm spatial resolution¹. Further, we also developed novel calorimetric techniques, by taking advantage of ultra-high resolution thermometry and microfabrication techniques, to enable measurements of heat currents with picowatt resolution^{2,3}. These high-resolution heat-flow techniques are necessary to perform fundamental studies of nanoscale conductive and radiative heat transport. Finally, we have recently adopted (unpublished work) the principles of picowatt-resolution calorimeters to create scanning probes that can simultaneously measure topography with nm resolution and heat currents with picowatt resolution.

In addition, we have also used scanning probes to study thermoelectric properties of molecular junctions. Specifically, we performed experiments on a variety of molecular junctions to study the effect of contact coupling strength and contact chemistry on their thermoelectric properties. We demonstrated that the thermoelectric of molecular junctions are relatively insensitive to coupling strength but depended strongly on the chemical identity of the contacting end-groups⁴. These results demonstrate the possibility of tuning the thermoelectric properties of molecular junctions via contact chemistry and molecular structure.

In the past two years year we used custom-fabricated probes with integrated nanoscale thermocouples to study heat dissipation in atomic-scale junctions⁵. In these studies, we elucidated—for the first time—the fundamental relationships between the electronic structure of atomic and molecular junctions and the asymmetries in the heat dissipated in their electrodes. Specifically, we showed that that heat dissipation in the electrodes of molecular junctions, whose transmission characteristics are relatively strongly dependent on energy is asymmetric, *i.e.* unequal and dependent on both the bias polarity and the identity of majority charge carriers (electrons vs. holes). In contrast, we showed that atomic contacts whose transmission characteristics show very weak energy dependence do not exhibit appreciable asymmetries.

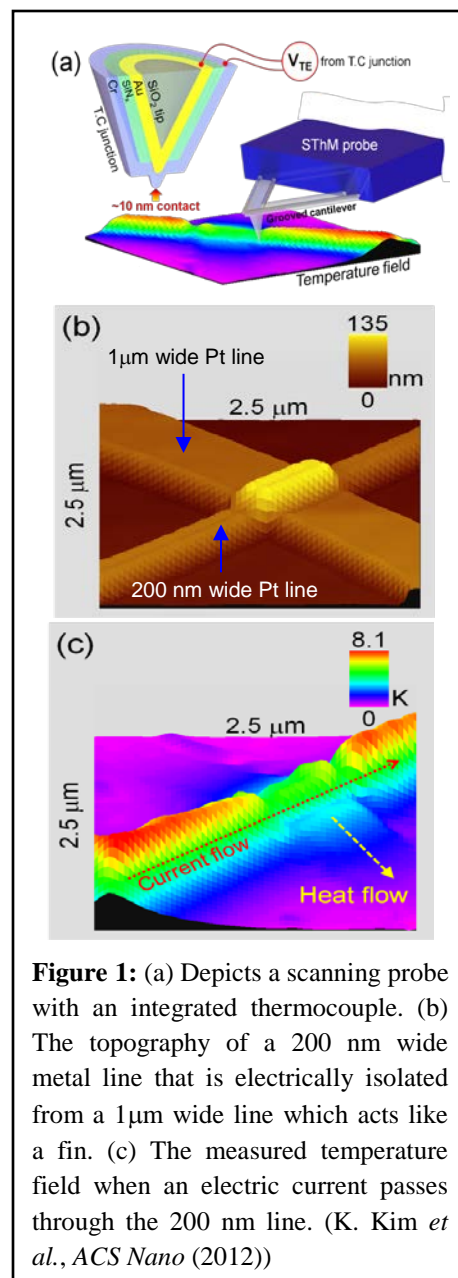


Figure 1: (a) Depicts a scanning probe with an integrated thermocouple. (b) The topography of a 200 nm wide metal line that is electrically isolated from a 1 μ m wide line which acts like a fin. (c) The measured temperature field when an electric current passes through the 200 nm line. (K. Kim *et al.*, *ACS Nano* (2012))

Recently, we studied radiative heat transfer in the extreme near-field regime (gaps of 1 – 10 nm). Specifically, we employed scanning thermal probes with integrated nanoscale thermocouples, which were coated with dielectrics (SiO_2 or SiN_x) to study heat transport between the spherical tip of the scanning probes and a flat substrate coated with dielectrics, in an ultra-high vacuum environment. These experiments⁶ unambiguously show that heat transport is dramatically enhanced in the extreme near-field. Further, the measured enhancement in heat flows between dielectric surfaces was found to be in reasonable agreement with computational predictions—thus establishing the validity of using fluctuational electrodynamics in modeling near-field heat transport even at single-digit nanometer separations.

Future Plans

We are currently developing novel scanning probe calorimeters that will enable us to study local heat flows with unprecedented heat flow resolutions (picowatt) to explore both near-field radiative heat transport and heat transport at the atomic scale. Using these probes in conjunction with other scanning probes (already developed by us) we seek to address the following questions:

- 1) How do the radiative transport properties of nanometer-sized gaps (1 – 10 nm) depend on the electrical conductivity and the dielectric properties of the surfaces?
- 2) What are the heat transport characteristics of atomic chains and short molecular junctions? Are their thermal transport properties quantized? Can one relate the thermal conductance of such junctions to the quantum thermal conductance observed in recent pioneering measurements? Further, is there a breakdown of Fourier's law in such junctions?
- 3) What are the heat dissipation characteristics of atomic and molecular scale junctions? Are asymmetries in heat dissipation that were observed recently¹, robust even when transport in the junctions is inelastic? Can the study of such asymmetries lead to new insights into the energy dissipation characteristics of nanoscale junctions? Can Peltier cooling be experimentally realized in atomic and molecular junctions?

References

1. K. Kim, W. H. Jeong, W. C. Lee, and P. Reddy, "Ultra-High Vacuum Scanning Thermal Microscopy for Nanometer Resolution Quantitative Thermometry," *ACS Nano*, 6, 4248-4257 (2012).
2. S. Sadat, Y-J. Chua, W. Lee, Y. Ganjeh, K. Kurabayashi, E. Meyhofer, P. Reddy, "Room Temperature Picowatt-Resolution Calorimetry," *Appl. Phys. Lett.*, 99, 0443106 (2011)
3. S. Sadat, E. Meyhofer, and P. Reddy, "Resistance thermometry-based picowatt-resolution heat-flow calorimeter," *Appl. Phys. Lett.*, 102, 163110 (2013).
4. A. Tan, J. Balachandran, S. Sadat, V. Gavini, B. Dunietz, S-Y. Jang, P. Reddy, "Effect of Length and Contact Chemistry on the Electronic Structure and Thermoelectric Properties of Molecular Junctions," *J. Amer. Chem. Soc.*, 133, 8838 (2011).

5. W. Lee, K. Kim, W. Jeong, L. A. Zotti, F. Pauly, J. C. Cuevas, P. Reddy, "Heat dissipation in atomic-scale junctions," *Nature*, 498, 209-212 (2013).
6. K. Kim, B. Song, W. Lee, W. Jeong, J. Feist, V. Fernandez, F. J. G. Vidal, J. C. Cuevas, E. Meyhofer, P. Reddy, "Radiative heat transfer in the extreme near-field," *To be submitted*.

Publications

1. Y. Kim, W. Jeong, K. Kim, W. Lee, P. Reddy, "Electrostatic control of thermoelectric properties in molecular junctions," *Nature Nanotechnology*, In Press.
2. W. Jeong, K. Kim, Y. Kim, W. Lee, P. Reddy, "Characterization of nanoscale temperature fields during electromigration of nanowires," *Scientific Reports*, 4 (2014)
3. L. A. Zotti, M. Burkle, F. Pauly, W. Lee, K. Kim, W. Jeong, Y. Asai, P. Reddy, J. C. Cuevas, "Heat dissipation and its relation to thermopower in single-molecule junctions," *New Journal of Physics*, 16, 015004 (2014).
4. W. Lee, K. Kim, W. Jeong, L. A. Zotti, F. Pauly, J. C. Cuevas, P. Reddy, "Heat dissipation in atomic-scale junctions," *Nature*, 498, 209-212 (2013).
5. S. Sadat, E. Meyhofer, and P. Reddy, "Resistance thermometry-based picowatt-resolution heat-flow calorimeter," *Applied Physics Letters*, 102, 163110 (2013).
6. J. Balachandran, P. Reddy, B. Dunietz, V. Gavini, "End-Group Influence on Frontier Molecular Orbital Reorganization and Thermoelectric Properties of Molecular Junctions," *Journal of Physical Chemistry Letters*, 4, 3825 (2013).
7. K. Kim, W. H. Jeong, W. C. Lee, and P. Reddy, "Ultra-High Vacuum Scanning Thermal Microscopy for Nanometer Resolution Quantitative Thermometry," *ACS Nano*, 6, 4248-4257 (2012).

Four-Dimensional Characterization of Dislocation-Defect Interactions in Aggressive Environments - A New Approach

Ian M Robertson, Department of Materials Science and Engineering, University of Illinois, Urbana, IL. 61801. Department of Materials Science and Engineering, University of Wisconsin-Madison WI. 53706

Program Scope

The scope of this program is to first develop the technique of electron tomography of defect structures in metallic systems and to couple it with in-situ TEM deformation capabilities. Successful combination of the two will permit four-dimensional (time and three spatial dimensions) characterization of the microstructure evolution processes. Critical to the success is the ability to include the real space coordinate system in the tomogram, resolving the defect invisibility issue and drastically reducing the number of images acquired to produce a useful tomogram. The second component is to apply this method to determine the evolution pathway of the deformation microstructure and to discovery how this is transmitted across interfaces and influenced by precipitates.

Recent Progress

Previous work demonstrated the viability of using low resolution electron tomograms as the basis for constructing a three-dimensional model of the evolved dislocation structure with prior knowledge of dislocation properties and image contrast theory providing the missing information^{1,2}. Spatial information extracted from diffraction patterns enabled inclusion of the real space coordinate system in the tomogram and the model. By using a low resolution tomogram as a template, the number of images that must be acquired to permit reconstruction could be reduced and the need for limited contrast variability across and between images could be relaxed. This method was originally applied to FCC metals²⁻⁵ but has now been successfully applied to dislocation interactions with grain boundaries in HCP Ti⁶. It was found that the slip transfer rules developed for FCC systems apply to HCP Ti.

An example of slip transfer of pure screw $\langle a \rangle$ -type dislocations that are glissile on a prismatic plane across a random high-angle tilt boundary in Ti is shown in Fig. 1⁶. The outgoing dislocations were $\langle a \rangle$ type and were glissile on a prismatic plane. The result of the impinging dislocations is seen first in the form of elastic distortions emanating from the grain boundary into the adjoining grain; examples are marked by arrowheads in Fig. 1a. With continued straining, slip transfer occurs although there is no indication of the formation of dislocation pile-ups; the arrowhead in Fig. 1b shows slip traces. The number of grain boundary

locations from which dislocations are emitted increases with increasing deformation. This observation suggests the determining factor might be related to a critical but unknown strain energy density being achieved in the grain boundary due to the accommodation of lattice dislocations. The activated slip system was predicted based on the minimization of the magnitude of the Burgers vector of the residual grain boundary dislocation is the smallest for the emitted system. The conclusions drawn from this work are at variance with those drawn from macroscale in-situ x-ray

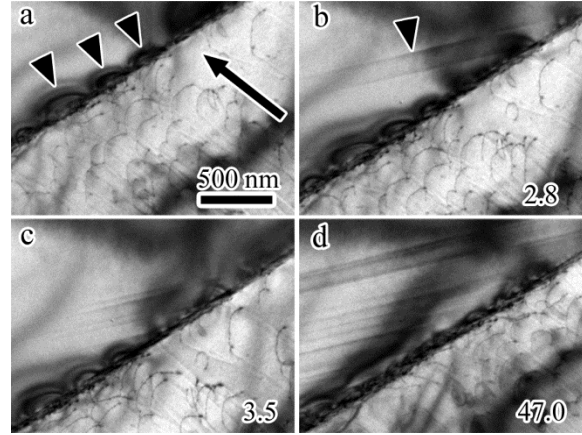


Figure 1. Slip transfer processes in Ti.

diffraction deformation experiments that suggested either a geometric factor⁷ or the extent of the prior deformation in the initiating grain⁸ was deterministic in predicting slip transfer.

Although it appears that minimization of the Burgers vector of the residual grain boundary dislocation is deterministic in FCC and HCP system, it is unclear if it is applicable to BCC systems. Macroscale deformation experiments point to slip transfer occurring when active slip systems are favorably oriented across the grain boundary and the Schmid factors are high. For boundaries at which the slip systems are not favorably oriented and the Schmid factors are low, the response at the grain boundary involves the formation of topographical discontinuities and dislocation pile-ups⁹. Others suggest that the magnitude of the Burgers vector of the dislocation left in the boundary determines the propensity for slip transmission but does not necessarily predict the activated system¹⁰. Preliminary in-situ TEM straining experiments of BCC V and Mo have shown that significant numbers of lattice dislocations can be accommodated in the grain boundary without slip transmission, dislocation pile-up formation is not necessary for slip transmission at some boundaries and dislocation emission occurs from multiple sources along the length of the boundary as opposed to the limited volume seen in FCC metals. The reasons for these response differences are under investigation.

From computational and experimental studies it has been shown that classic dislocation precipitate bypass processes constitute a small subset of the total number of possible pathways^{11, 12}. Factors such as the nature and size of the precipitate, the character of the dislocations, and the location at which the slip system intersects the precipitate either directly or through its stress field are important. In-situ TEM straining experiments involving dislocation interactions with vanadium carbides show the bypass mechanism is dependent on particle size. At small particle sizes looping is the preferred by-pass mechanism although no loop is left behind as a result of the bypass process. At thin platelet precipitates, dislocations approaching the edge of the precipitate cross-slip at significant distances from it to avoid intersecting it. In contrast, dislocations of the same type approaching the central region of the precipitate interact with and become trapped in the precipitate interface. There was no evidence for dislocations emerging from the opposite

side of the precipitate, although discontinuities are seen to develop within the precipitate. Examples of these different dislocation behaviors are shown in the time-resolved series of images presented in Figure 2. Electron tomography is being used to understand the spatial dependence of these different interactions. These results will be compared with models of the precipitate stress field distributions to determine the cause of the different reactions especially the distance at which the dislocations cross-slip.

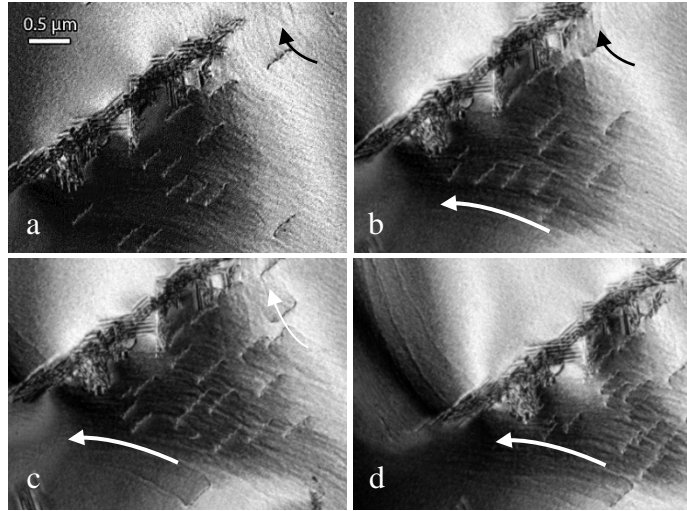


Figure 2. Time resolved interaction of dislocations with precipitates in vanadium. Frames are roughly 2 seconds apart. Arrows indicate direction of motion.

Future Plans

Determine, using a combination of in-situ TEM straining and electron tomography, the slip transfer rules for grain boundaries in bcc alloys to determine if they are general and consistent with those developed for FCC and limited HCP systems.

Discover, using a combination of in-situ TEM straining, electron tomography and modeling, the role of precipitates and the attendant stress field in determining the dislocation bypass mechanisms.

Develop further the coupling of electron tomography and in-situ TEM deformation technique to minimize the number of images required to form a tomogram.

References

1. G. S. Liu, S. D. House, J. Kacher, M. Tanaka, K. Higashida, and I. M. Robertson: 'Electron tomography of dislocation structures', *Mater Charact*, 2014, **87**(0), 1-11.
2. G. S. Liu and I. M. Robertson: 'Three-dimensional visualization of dislocation-precipitate interactions in a Al-4Mg-0.3Sc alloy using weak-beam dark-field electron tomography', *J. Mater. Res.*, 2011, **26** (4), 514 -522.
3. J. Kacher, G. S. Liu, and I. M. Robertson: 'In situ and tomographic observations of defect free channel formation in ion irradiated stainless steels', *Micron*, 2012, **43**(11), 1099-1107.
4. J. Kacher, G. Liu, and I. M. Robertson: 'Three-dimensional characterization of dislocation-defect interactions', 3D Materials Science 2012, Seven Springs, Pennsylvania, 2012, TMS.
5. J. P. Kacher, G. S. Liu, and I. M. Robertson: 'Visualization of grain boundary/dislocation interactions using tomographic reconstructions', *Scripta Mater.*, 2011, **64**(7), 677-680.

6. J. Kacher and I. M. Robertson: 'In situ and tomographic analysis of dislocation/grain boundary interactions in titanium', *Phil. Mag.*, 2014, **94**(8), 814-829.
7. L. Wang, Y. Yang, P. Eisenlohr, T. R. Bieler, M. A. Crimp, and D. E. Mason: 'Twin nucleation by slip transfer across grain boundaries in commercial purity titanium', *Metall. and Mater. Trans A*, 2010, **41**(2), 421-430.
8. T. R. Bieler, L. Wang, A. J. Beaudoin, P. Kenesei, and U. Lienert: 'In Situ Characterization of Twin Nucleation in Pure Ti Using 3D-XRD', *Metall. and Mater. Trans A*, 2013, 1-14.
9. T. R. Bieler, S. C. Sutton, B. E. Dunlap, Z. A. Keith, P. Eisenlohr, M. A. Crimp, and B. L. Boyce: 'Grain Boundary Responses to Heterogeneous Deformation in Tantalum Polycrystals', *JOM*, 2013, 1-8.
10. L. Patriarca, W. Abuzaid, H. Sehitoglu, and H. J. Maier: 'Slip transmission in bcc FeCr polycrystal', *Mater. Sci. and Engin. A*, 2013, **588**, 308-317.
11. X. Yang, C. Li-Tien, D. J. Srolovitz, and E. Weinan: 'A level set method for dislocation dynamics', *Acta Mater.*, 2003, **51**(18), 5499-5518.
12. Y. Xiang and D. J. Srolovitz: 'Dislocation climb effects on particle bypass mechanisms', *Phil. Mag.*, 2006, **86**(25-26), 3937-3957.

Publications

- 1 G.S. Liu, S.D. House, J. Kacher, M. Tanaka, K. Higashida, I.M. Robertson, Electron tomography of dislocation structures, *Mater Charact*, 87 (2014) 1-11.
- 2 J. Kacher, I.M. Robertson, In situ and tomographic analysis of dislocation/grain boundary interactions in titanium, *Phil. Mag.*, 94 (2014) 814-829.
- 3 J. Kacher, B. Eftink, B. Cui, I.M. Robertson, Dislocation interactions with grain boundary interactions, *Current Opin. Solid State and Mater. Sci.*, 18 (2014) 227-243.
- [4] M. Briceño, J. Kacher, I.M. Robertson, Dynamics of dislocation interactions with stacking-fault tetrahedra at high temperature, *J. Nucl. Mater.*, 433 (2013) 390-396.
- [5] J. Kacher, I.M. Robertson, Quasi-four-dimensional analysis of dislocation interactions with grain boundaries in 304 stainless steel, *Acta Mater.*, 60 (2012) 6657-6672.
- [6] J. Kacher, G. Liu, I.M. Robertson, Three-dimensional characterization of dislocation-defect interactions, in: *3D Materials Science 2012*, TMS, Seven Springs, Pennsylvania, 2012.
- [7] J. Kacher, P. Elizaga, S.D. House, K. Hattar, M. Nowell, I.M. Robertson, Thermal stability of Ni/NiO multilayers, *Mater. Sci. and Engin. A*, 568 (2013) 49-60.

Dynamical Nanoscale Electron Crystallography

Chong-Yu Ruan

Michigan State University, East Lansing, MI 48824. E-mail: ruan@pa.msu.edu

Program Scope:

This research seeks to employ femtosecond electron crystallography to investigate the complex material processes of correlated oxides and plasmonics-enhanced surface dynamics on metal nanoparticles, with atomistic spatial and temporal resolutions. Ultrafast electron crystallography is well suited for the investigation of complex materials due to high scattering cross-section over large momentum space, which allows simultaneously accessibility to various Bragg and non-Bragg diffraction features (satellites, stripes, etc.) for the emergence of collective quantum orders rich in correlated oxides. In addition, the photonic control using tunable femtosecond pulses allow us to control such emergence, and provide us an unique way to dissect various competitive or cooperative processes far from equilibrium through in situ observation with atomic details. In nanomaterial plasmonics, by manipulating the local morphology, we aim to control the field-enhancement and prioritize either local charge-transfer-induced or remote resonance-transfer-mediated reaction channels. These efforts build on recent successful ultrafast electron microdiffraction investigations of vanadium dioxide nanobeams and the surface supported plasmonic nanocrystals. The proposed research further benefits from an emerging ultrafast electron microscope with RF recompression system to significantly enhance the probe's deployable brightness (>100 improvement) to reach a very high level of signal level and resolution to elucidate the key mechanisms proposed to investigate here.

Recent Progress

1. Ultrafast nonthermal insulator-metal switching in VO₂

We have investigated VO₂ nanobeam system and uncovered a decoupling between the structural and electronic phase transitions induced by interface charge doping [3]. It is generally believed that the competitive nature of Mott and Peierls physics is what drives the strongly first-order phase transition, where the critical temperature T_c is highly tunable by applying pressure or charge doping. Therefore breaking of this cooperativity as evidenced in the nanoscale system [3], where VO₂ is metallic and yet retains distorted monoclinic structure, suggests a complicated energy landscape that may host various metastable states with unusual properties. The existence of such states has strong implication in the ultrafast measurement as one may access such states nonthermally for instigating insulator-metal switching in VO₂ electronic crystal without the typical structure-bottleneck effect in the cooperative regime, which limits its high-speed applications. As the lattice enthalpy is a significant part of the free energy, bypassing excessive structural dynamics could provide an alternative pathway for a more efficient switching.

Using femtosecond electron crystallography, we have addressed this question by mapping out the sequence of optically induced phase transition under different photoexcitation conditions. The dynamics show several steps, but the initial most notable

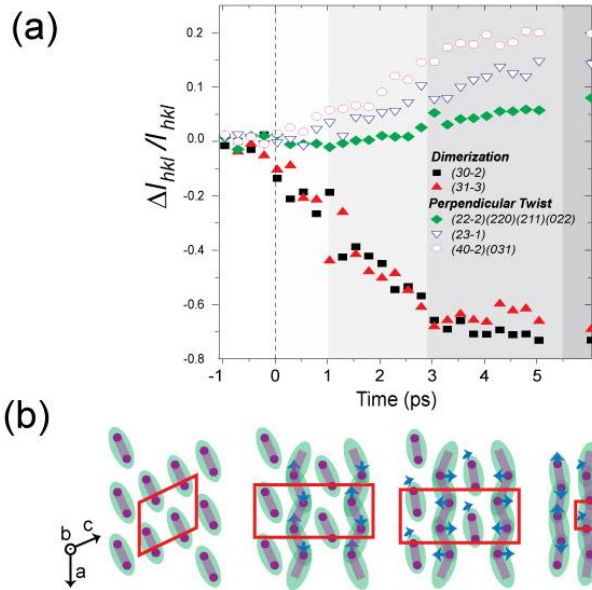


Fig. 1 Ultrafast electron crystallography investigation of nanocrystalline VO₂. (a) The detailed Bragg peak intensity changes as a function of time. The dynamics show several steps, but notably the initial dominant changes are related to the symmetry recovery along the monoclinic (M1)-a axis, and ~ 1 ps later joined by an untwisting along the bc-plane, leading to a rutile-like structure (R) as early as 3ps. (b) Based on structure refinement of the diffraction patterns, the dynamics can be visualized as occurring in four major steps. The two intervening transient structures can be categorized as 50% dimerized and partially twisted, resembling a M2 structure.

dominant changes [e.g. the strong suppression of (3,0,-2) and (3,1,-3) peaks] are related to the symmetry recovery, namely the relaxation of dimerization along the monoclinic-*a* axis, and joined by the *bc*-plane atomic motion ~ 1 ps later, as indicated in the reconstructed motion sequences in Fig. 1(b). The rutile structure emerges just above ~ 3 ps. These sequences of events can be associated with a descent from a fully dimerized M1 phase to the more symmetric R phase, where it must cross over the intervening other topologically stable states. We also found that while exciting VO₂ from monoclinic phase (insulating) to rutile phase (metallic) using high-energy photons (above gap) requires energy density similar to that of the thermal, using low-energy photons (near gap) we observed suppression of lattice latent heat, and the phase transition is nonthermal with a well-defined critical photon density that translates to a lower energy deposition than the thermodynamic threshold. This new finding thus points to an exciting new pathway for efficient photonic control of electronic and structural states in VO₂ at fractional cost in energy consumption.

2. Competitive Charge-Density Wave Phase Transitions

Using femtosecond electron crystallography, we have examined some of the open questions involving materials with Mott phase entangled with complex charge orders in 1T-TaS₂, in contrast to an earlier study of a weakly correlated CDW[4]. First, in photoinduced near-commensurate (NC)-to-incommensurate (IC) transition, we were able to resolve dynamics pertaining to domain proliferation. We unveiled a hidden phase – characterized by a wave-vector between the NC and IC near room temperature in the nonequilibrium evolution, which is unstable under thermal heating. Most importantly, at far from thermal equilibrium, driven under photodoping *x* with nearly no excess heat, we observed hitherto-hidden “staircases” connecting various low-temperature topologically stable CDW configurations. These phase transitions involve rearrangement of domain structure. We were able to directly resolve ballistic domain-wall soliton dynamics into

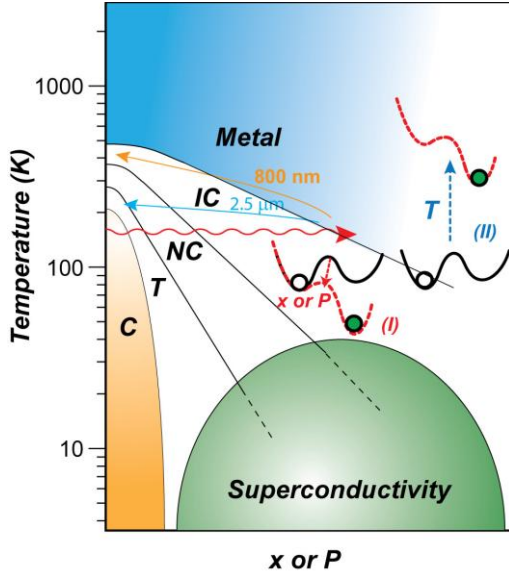


Fig. 2 The phase diagram of 1T-TaS₂ under chemical doping (x) or applying pressure (P). In the pristine 1T-TaS₂ (x , or $P = 0$) crystal, the CDW undergoes four consecutive phase transitions. Upon doping the crystal (or applying pressure), a superconducting phase (SC) emerges within the NC (or T) phases. The charge doping generally suppress the transition temperatures between different CDW states, and yet the detailed structural pathway between these various transitions are unknown in general.

applying this methodology on Si/SiO₂ interface, and surfaces decorated with nanostructures, we are able to elucidate localized charge injection, dielectric relaxation, carrier diffusion, and enhancements on such processes through surface plasmon resonances, with direct resolution in the charge state and possibly correlated structural dynamics at these interfaces. These new results highlight the high sensitivity of the interfacial charge transfer to the nanoscale modification, environment, and surface plasmonics enhancement and demonstrate the diffraction-based ultrafast surface voltage probe as a unique and powerful method to resolve the nanometer scale charge carrier dynamics.

Future Plans

Work is in progress on single-crystal VO₂ in the direction of doped VO₂ nanobeam. The nanobeam is gradient-doped, which means that we can investigate the shift of transition temperature as a function of chemical doping and optical doping systematically. We will also conduct optical, TEM, and ultrafast electron crystallography investigation on these systems to draw comparison between nanoparticle and nanobeam systems. Drawing

different meta-stable CDWs. The prevailing sub-ps to ~ 1ps switching between distinct macroscopic phases is interlocked with suppression of charge order, presenting a highly cooperative step at few photon timescale on macroscopic scale. These various novel features were explained based on interconnected dynamics of optically pumped charge carriers, electron-hole-asymmetry-driven chemical potential, polaron interlocking, and domain-wall solitons. Meanwhile, the establishment of these staircases promises high-fidelity controls over ultrafast switching between different electronic states, which may have a range of applications in photonics and electronics.

3. Light-induced charge carrier dynamics at interfaces

We have formulated the ultrafast interfacial charge transfer processes examined using refraction-based ultrafast electron diffraction technique along with experimental results from interfaces and nanomaterials studies based on effective circuit model, as exemplified in Fig. 3 on charge transfer dynamics at /SiO₂/Si interface [5]. From

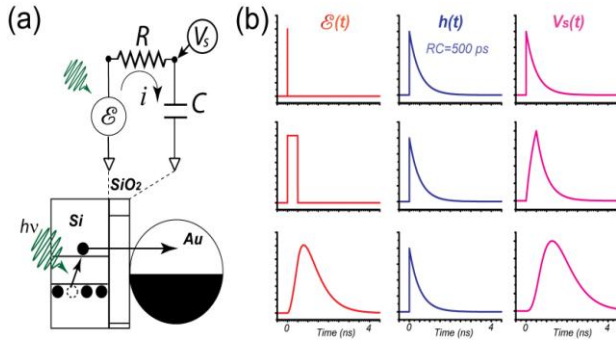


Fig. 3 (a) An effective circuit model depicting the transient surface voltage $V_s(t)$ measurement via the refraction shift across the SiO_2 slab at SiO_2/Si interface. The electromotive potential $E(t)$ comes from the hot carriers generated at the Si substrate. (b) Examples showing the photovoltage $V_s(t)$ measured at the interface as a function of $E(t)$. The relationship can be seen as a convolution with kernel function $h(t)$ characteristic of the RC circuit.

powder pattern with higher spatial and temporal specificity (no convolution due to insight from our recent experiments of the ultrafast powder diffraction from multi-grain samples (see Fig. 1), we will be able to zoom in on the critical dynamics observed in the inhomogeneity) in the single-crystal systems to separate the inherent versus the strain-induced effects, and contrast them to charge doping effects. Work is under preparation for optical exploration of novel phases in V_2O_3 , which also has a rich phase diagram encompassing the metal-insulator transition and structural phase transitions. In particular, temperature, doping or pressure induces a metal-to-insulator transition between different electronically ordered phases, similar to those in VO_2 .

Publications (DOE sponsored)

1. Z. Tao, H. Zhang, M. Berz, P.M. Duxbury, and C.-Y. Ruan, ‘Space-charge effects in ultrafast electron diffraction and imaging’, *J. Appl. Phys.* 111, 044316 (2012).
2. C.-Y. Ruan, Four-Dimensional Electron Nanocrystallography, Research in Optical Sciences, *OSA Technical Digest* (Optical Society of America, 2012), paper IT3D.5.
3. Z. Tao, T.-R. T. Han, S. D. Mahanti, P. M. Duxbury, F. Yuan, and C.-Y. Ruan, K. Wang, and J. Wu, ‘Decoupling of Structural and Electronic Phase Transitions in VO_2 ’, *Phys. Rev. Lett.* 109, 166406 (2012).
4. T.-R. T. Han, Z. Tao, S.D. Mahanti, K. Chang, and C.-Y. Ruan, C. D. Malliakas, and M. G. Kanatzidis, ‘Structural dynamics of two-dimensional charge-density waves in CeTe_3 investigated by ultrafast electron crystallography’, *Phys. Rev. B* 86, 075145 (2012).
5. K. Chang, R.A. Murdick, T.-R. T. Han, F. Yuan, and C.-Y. Ruan, ‘Light-induced charge dynamics at nanostructured interfaces investigated by ultrafast electron diffractive photovoltammetry’, Eds. J. Wu, Z.M. Wang, Chapter 13, *Quantum Dot Solar Cell*, pp. 313-347 (Springer, New York, 2013).
6. Z. Tao, T.-R. T. Han, C.-Y. Ruan, ‘Anisotropic electron-phonon coupling investigated by ultrafast electron crystallography: Three-temperature model’, *Phys. Rev. B* 87, 235124 (2013).
7. C.-Y. Ruan, P.M. Duxbury, M. Berz, ‘The perspectives of femtosecond imaging and spectroscopy of complex materials using electrons’, *Proceedings of SPIE: Ultrafast Nonlinear Imaging and Spectroscopy II*, in press (2014).

1. Title: ER46317: “Spin-Polarized Scanning Tunneling Microscopy Studies of Nanoscale Magnetic and Spintronic Nitride Systems”

PI: Arthur R. Smith

Co-PI: Jeongihm Pak

Address: Ohio University
Nanoscale & Quantum Phenomena Institute
Department of Physics & Astronomy
Athens, OH 45701

E-mail: smitha2@ohio.edu

2. Program Scope

The scope of this project is to investigate the electronic and spin magnetic properties of nitride-based material systems, in particular specific bi-layer systems consisting of atomic layers of magnetic materials on semiconducting nitride surfaces. The material systems include ferromagnetic binary alloys, magnetic nitrides, and dilute magnetic nitride semiconductors. Such spintronic systems are of high interest as advanced materials for future energy-related applications. In order to probe these systems, this project is focused on the use of scanning tunneling microscopy (STM) and spin-polarized STM (SP-STM). The latter is a powerful technique which can provide spin information on surfaces with atomic-scale resolution. Combining ultra-high vacuum SP-STM together with molecular beam epitaxial growth in the same system, diverse nitride material systems can be explored in a pristine state.

3. Recent Progress

- “Heteroepitaxial Growth and Surface Structure of L10-MnGa(111) Ultra-thin Films on GaN(0001)” *published in Applied Physics Letters*

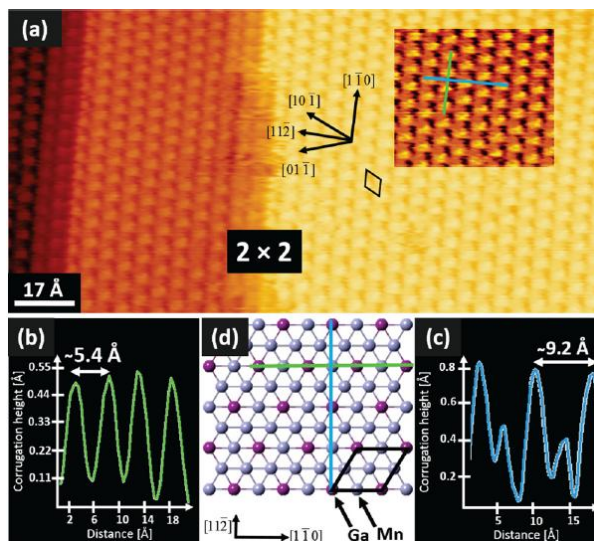


Fig. 1. (a) STM image showing 2×2 (hexagonal-like) surface reconstruction; (b) and (c) line profiles taken along the indicated lines shown in the contrast-enhance part of (a); (d) atomic model indicating the crystal lattice directions corresponding to the line profiles.

This study involved very careful STM imaging of the surface domains of the material in which we found primarily 3 different surface reconstructions, depending on the surface stoichiometry, including 1×2, 2×2, and 2×3. Since we believe that the magnetism is dependent on the stoichiometry, identifying the region corresponding to a specific stoichiometry is very important. For the given growth conditions we used (slightly Mn rich conditions), we found that the dominant surface reconstruction for that sample surface is the 2×2. Combining with first-principles theory (via our collaborators), it was possible to identify that this 2×2 corresponds to a Mn-rich 2×2.

Figure 1(a) shows a stepped 2×2 surface corresponding to the Mn-rich 2×2. Line profiles taken across the region highlighted in

(a) are displayed in (b) and (c) and indicated on the atomic model in (d). We find that the corrugation amplitude ranges from ~ 0.4 Angstrom (along $[1\bar{1}0]$) to ~ 0.8 Angstrom (along $[11\bar{2}]$). A unit cell is shown as well in (d). As we find from the theoretical calculations, the protrusions seen in the STM image, as also indicated by the line profile peaks compared to the atomic model, correspond to the Ga atoms.

The energies of various theoretical models were compared to the experimental results. It is found that the energetically most favorable structures are the stoichiometric 1×2 , the Mn-rich 2×2 , and the Ga-rich 2×2 . STM simulations for both 2×2 structures were compared to the actual STM 2×2 images, and the best agreement was found for the Mn-rich 2×2 .

We also concluded based on the combination of experiment and theory that the Mn-rich surface most likely results from Mn-segregation at the surface during growth, although the bulk of the sample remains very close to stoichiometric. Therefore, what we see at the surface is a very sensitive indicator of the conditions during growth.

• **“Iron on GaN(0001) pseudo-1x1 ($1 + 1/12$) Investigated by Scanning Tunneling Microscopy and First Principles Theory” *published in Applied Physics Letters***

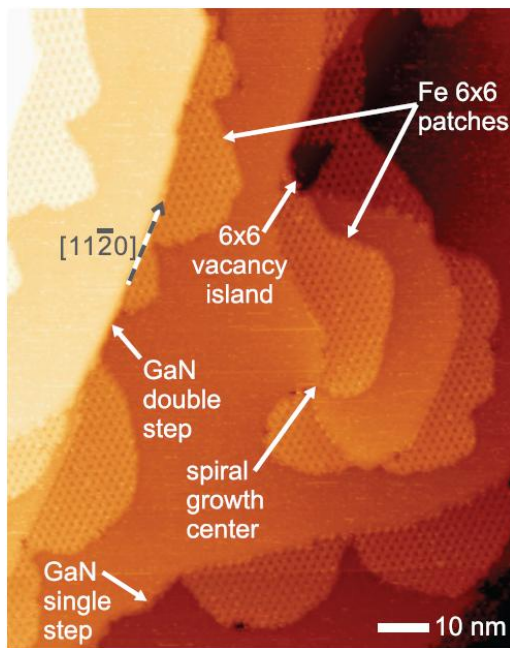


Fig. 2. STM image of the Fe/GaN ($1 + 1/12$) surface showing hexagonal-like regions adjacent to GaN single and double height steps, including also two steps emerging from a spiral growth center located around a screw-type dislocation. Sample bias $V_s = -1.75$ V, tunnel current $I_T = 0.10$ nA.

monolayer Fe is deposited. Shown in Fig. 2 is the resulting STM image of the surface after deposition of $\sim 1/3$ monolayer Fe. We see 6×6 reconstructed regions adhered to the step edges of the GaN pseudo- 1×1 surface. The 6×6 regions adhere to both single

We find the formation of iron-containing reconstructed regions observed at the surface of GaN after deposition of sub-monolayer amounts of Fe. The sample is prepared by first forming a very specific reconstruction on GaN(0001), namely the pseudo- 1×1 ($1 + 1/12$). This surface has a high concentration of excess Ga residing in a double Ga layer. Once this special surface is created, the sample is heated to ~ 360 °C, and then sub-

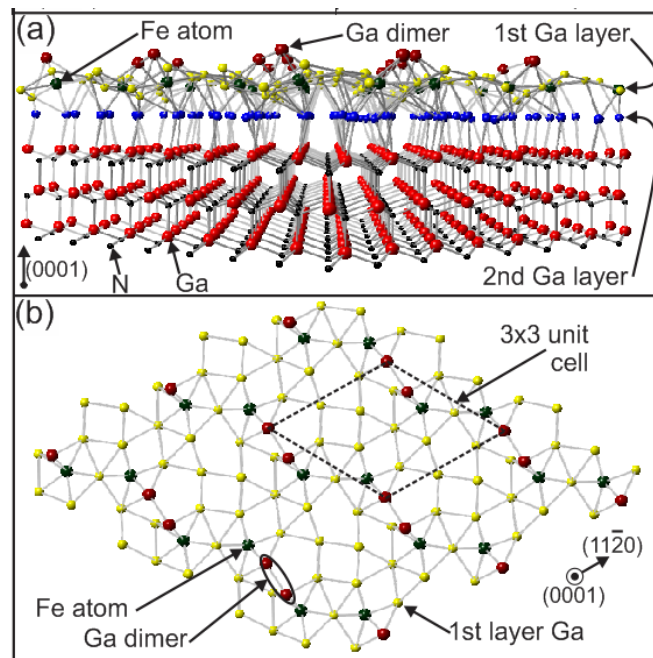


Fig. 3. (a) perspective view of the $2/9$ ML Fe + $7/3$ ML Ga dimer model showing all atoms including 3 GaN layers; (b) top view of the $2/9$ ML Fe + $7/3$ ML Ga dimer model showing only the top highly distorted Fe+Ga layer.

and double height GaN steps on the surface, and they also emanate outward from the step edges, including the leading step edges of a *spiral growth center*.

Via our theory collaborators, a model for the 6×6 Fe-containing structure was found. It turns out that Fe does not easily stick to this GaN surface, and the resulting Fe content is quite small. The best model turns out to be a $2/9$ ML Fe + $7/3$ ML Ga dimer model, as shown in Fig. 3. Very interestingly, Ga atoms displaced by the Fe atoms go to the top where they form Ga dimers. This dimer surface is highly distorted and corrugated, and the corrugation agrees very well with the STM measurements of the surface.

- **“Direct Observation of Condensed Gallium Atom Gas Showing Chiral Asymmetry at LHe Temperature on the GaN surface” *to be submitted to Nano Letters***

Unexpectedly this year, while performing atomic resolution STM measurements at LHe temperature on GaN surfaces, we discovered surface features suggesting gallium atom condensation. These features are illustrated in Fig. 4 where we see a random-looking distribution of what appear as “L-shapes”. We obtained very high resolution images of these L-shapes at a variety of tip-sample biases. Upon imaging the surfaces which were grown using 3 different Ga/N flux ratios, we found that the areal density of the L-shapes varies with the flux ratio.

Therefore, we hypothesize that the L-shapes are Ga atoms condensed from a quasi-2-dimensional surface

gas phase, which is thus inferred to exist at room temperature or higher temperatures at the surface. Their density at LHe temperature is very small, only just around 0.003 monolayer or so.

We also find that there are two orientations of the L-shapes. One can be arrived at by rotation of the other by 180° . We refer to these two as ‘L-up’ and ‘L-down’. Additionally, one of the two orientations is about 4 times more likely to occur than the other one, but this asymmetry reverses upon crossing a bilayer height step. Furthermore, we find that within a given domain, there is only one kind of chirality of the L-shapes (say, 100% right-handed), but the left-handed chirality is found to exist on the opposite type of domain. This result may have wide reaching importance for understanding N-polar GaN growth.

- **“STM Study of 1-D Atomic Chains and 2-D Manganese Gallium Quantum Height Islands on Wurtzite GaN(000 $\bar{1}$)” *to be submitted to Journal of Applied Physics***

We have previously reported that two-dimensional MnGa quantum-height islands with two unique heights are formed spontaneously during the deposition of less than 1 ML manganese onto the gallium-rich, nitrogen polar GaN(000 $\bar{1}$). Last year, we have made additional analysis of the STM images and reflection high energy electron diffraction (RHEED) patterns. The structural evolution is followed from the beginning of growth using RHEED, in which a dotted

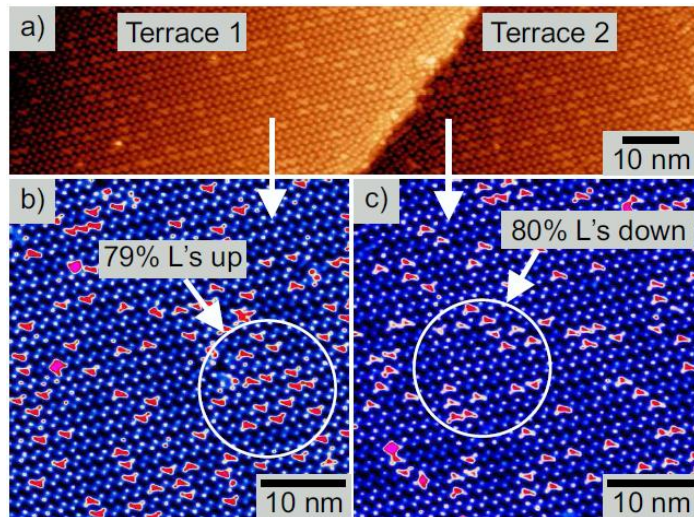


Fig. 4. (a) STM image at LHe temperature showing L-shape features on 2 terraces; (b) zoom-in on upper terrace showing predominance of L-ups; (c) zoom-in on lower terrace showing predominantly L-downs.

2× pattern is observed to form. *In-situ* STM is also used to investigate the islands' structures with atomic resolution. Based on all the observations, we derived a possible model for the islands from the face-centered tetragonal (fct) CuAu type-I ($L1_0$) MnGa crystal structure.

Our model is consistent with the RHEED analysis suggesting a pseudo-morphic growth mode. One possible bonding structure at the substrate/island interface is revealed using this model. Manganese atoms substitute for Ga atoms in the Ga adlayer, thus making the MnGa islands bonded to the GaN substrate. The *in-plane* epitaxial relationship to GaN is ideal, with $[1\bar{1}0]_{\text{MnGa}} \parallel [11\bar{2}0]_{\text{GaN}}$ and $[11\bar{2}]_{\text{MnGa}} \parallel [10\bar{1}0]_{\text{GaN}}$.

4. Future Plans

In general, each project in our lab should move from the initial growth study, to the structural investigation, and then on to the measurement of electronic and spin magnetic properties. Current and future efforts are therefore to be focused on the use of spectroscopy and SP-STM to obtain the electronic and spin magnetic properties for these nitride-related spintronic materials.

5. Publications of DOE sponsored research (2012-2014)

Papers listed below are shown in reverse chronological order, with the numbering defined based on paper #1 = A.R. Smith's first paper. Full publication list can be seen at <http://www.phy.ohiou.edu/~asmith/publist.html>.

75. [Iron on GaN\(0001\) pseudo-1x1 \(1 + 1/2\) Investigated by Scanning Tunneling Microscopy and First Principles Theory](#), Wenzhi Lin, Andrada-Oana Mandru, Arthur R. Smith, Noboru Takeuchi, and Hamad A. H. Al-Britthen, *Applied Physics Letters* **104**, 171607 (2014).
74. [Facility for Low-Temperature Spin-Polarized-Scanning Tunneling Microscopy Studies of Magnetic/Spintronic Materials Prepared In-situ by Nitride Molecular Beam Epitaxy](#), Wenzhi Lin, Andrew Foley, Khan Alam, Kangkang Wang, Yinghao Liu, Tianjiao Chen, Jeongihm Pak, and Arthur R. Smith, *Review of Scientific Instruments* **85**, 043702 (2014).
73. [Heteroepitaxial Growth and Surface Structure of L10-MnGa\(111\) Ultra-thin Films on GaN\(0001\)](#), Andrada-Oana Mandru, Reyes Garcia Diaz, Kangkang Wang, Kevin Cooper, Muhammad Haider, David C. Ingram, Noboru Takeuchi, and Arthur R. Smith, *Applied Physics Letters* **103**, 161606 (2013).
72. [Manganese 3x3 and sqrt3 x sqrt3-R30° Structures and Structural Phase Transition on w-GaN\(000-1\) Studied by Scanning Tunneling Microscopy and First-principles Theory](#), Abhijit V. Chinchore, Kangkang Wang, Meng Shi, Andrada Mandru, Yinghao Liu, Muhammad Haider, Arthur R. Smith, Valeria Ferrari, Maria Andrea Barral, and Pablo Ordejon, *Physical Review B* **87**, 165426 (2013).
71. [Formation of Manganese Delta-doped Atomic Layer in Wurtzite GaN](#), Meng Shi, Abhijit Chinchore, Kangkang Wang, Andrada-Oana Mandru, Yinghao Liu, and Arthur R. Smith, *Journal of Applied Physics* **112**, 053517 (2012).

Trimodal Tapping Mode Atomic Force Microscopy: Simultaneous 4D Mapping of Conservative and Dissipative Probe-Sample Interactions of Energy-Relevant Materials

Santiago D. Solares, George Washington University, Department of Mechanical and Aerospace Engineering, Washington, DC 20052

Program Scope

The overall goal of this project is to develop a trimodal, intermittent-contact atomic force microscopy (AFM) method for the rapid and simultaneous mapping of probe-sample conservative and dissipative forces in four dimensions (three spatial dimensions plus the probe's normal velocity). This new method will be applied to characterize the time-dependent degradation of energy-relevant materials and nanostructures, including fuel cell alkaline anion exchange membranes (AAEMs), fuel cell proton exchange membranes (PEMs) and solid-electrolyte interfaces on battery electrodes (SEIs). Measurements will be carried out both in liquid and air environments. Where applicable, the degradation studies will evaluate the effect of temperature, environmental humidity, sample moisture content and applied mechanical strain. This project includes experimental work as well as multi-scale simulation ranging from the atomistic to the continuum scales, with special emphasis on virtual AFM methods.

Recent developments in multifrequency AFM [1] have enabled the rapid mapping of the cumulative effect of conservative and dissipative interactions in two dimensions (2D). However, while these advances are significant, they still do not enable a full description of the elastic or viscoelastic properties of the sample surface, because the 2D maps they provide depend on the hardware and imaging parameters used, and the acquired information can be distorted by the non-constant, not-directly-controllable depth at which all contact and intermittent-contact AFM methods explore the surface. Instead, the quantitative acquisition of the tip-sample junction properties, from which the surface properties can be inferred, requires that the conservative forces be measured as a function of the 3-dimensional (3D) probe position and that the dissipative forces be mapped as a function of 4 dimensions (4D) including the three Cartesian dimensions plus the vertical probe velocity, as proposed in this work (inclusion of the fourth dimension is critical in the study of materials that exhibit rate-dependent properties).

Recent Progress

The most significant development has so far been a trimodal intermittent-contact AFM method, whereby the three active eigenmodes are driven using either the amplitude- or frequency-modulation control methods, and where each eigenmode is used as a 'control knob' that carries out a different task [1,2]. Specifically, in this scheme the fundamental vibrational mode of the AFM cantilever is optimized for topographical acquisition, while a higher mode (not necessarily the second) is optimized for compositional contrast mapping, and another higher

mode is utilized to modulate the depth of penetration of the tip into the sample. Figure 1 illustrates the application of this method to study a poly-dimethylsiloxane (PDMS) polymer film with glass nanoparticles embedded in it at depths on the order of 20 nm (see Figure 1a). The successive images in Figures 1c to 1e gradually reveal the glass nanoparticles and hard substrate as the AFM tip explores the sample at greater depths. This method is ideal for characterizing any soft samples that have subsurface features, allowing the user to gradually and reversibly modulate imaging depth, focusing on different surface or subsurface features, much like the focus and zoom functions of a camera.

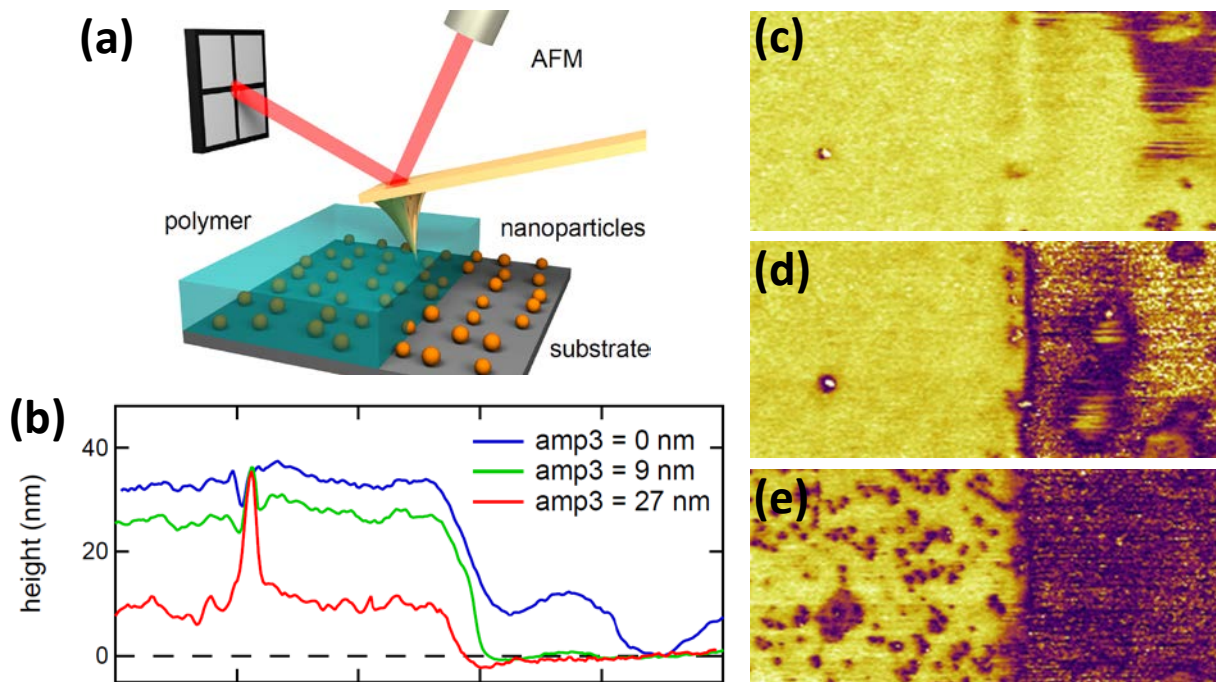


Figure 1. (a) Schematic of PDMS film sample with glass nanoparticles in the subsurface and exposed silicon substrate; (b) successive depth-modulated experimental scan lines for the sample in (a) with varying third mode amplitude; (c)-(e) successive experimental contrast images gradually revealing the subsurface (compare to (a)).

Studies have also been conducted aiming to understand the trade-offs in imaging sensitivity and indentation depth when using bimodal AFM methods, with only two instead of three active eigenmodes. Bimodal methods are simpler to implement and interpret than trimodal methods and can be carried out with off-the-shelf instruments. However, despite their apparent simplicity, ambiguities in parameter selection and modifications inflicted on the sample during measurement can complicate the interpretation of the results due to the existence of an inverse relationship between the sensitivity of the instrument (defined as the smallest detectable tip-sample force) and the indentation depth at which the sample is studied by the AFM tip. Figure 2 illustrates the variation in the shape of a feature on a Nafion® fuel cell membrane surface when it is characterized with monomodal and bimodal AFM under different imaging conditions. Clearly the measured morphology depends on the imaging parameters. An extensive discussion

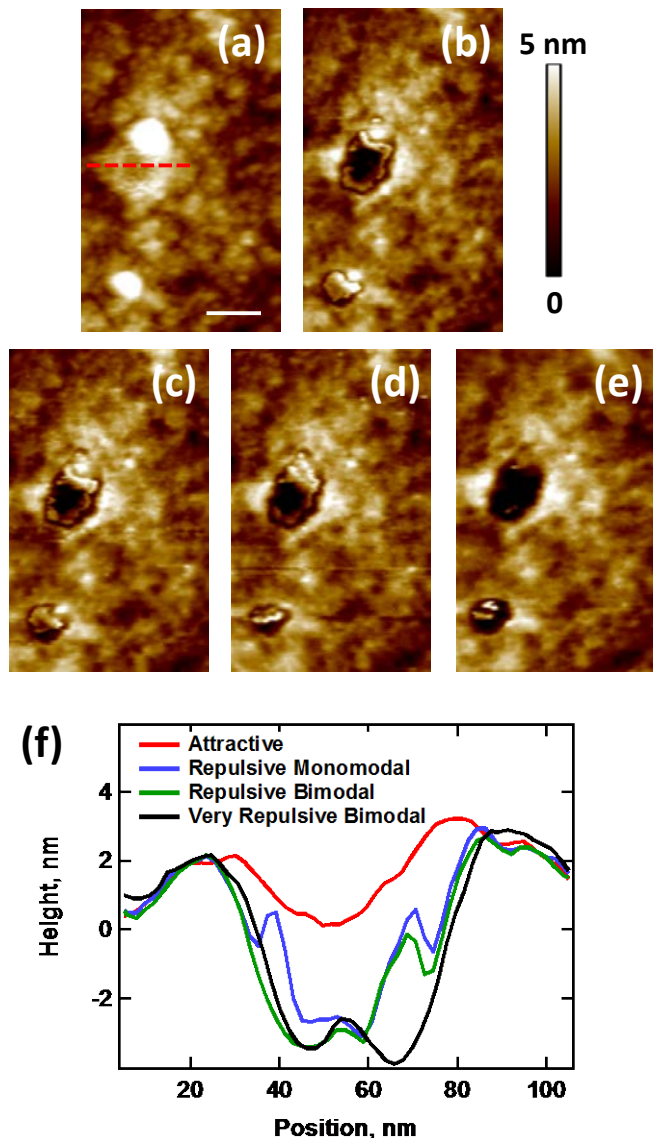


Figure 2. Comparison of Nafion® feature morphology under different AFM imaging conditions: (a) monomodal attractive regime; (b) monomodal repulsive regime; (c) – (e) bimodal tapping-mode with increasing higher mode amplitude setting; (f) scan lines along the dashed line in (a) for (a), (b), (c) and (e).

of the corresponding trade-offs between sensitivity and sampling depth is provided in reference [3].

Future Plans

The major future activities for this project are the following:

- Implementation of the above trimodal AFM method in liquid environments for the characterization of SEIs. Liquid environments offer additional challenges with respect to ambient air environments [4], which may require modifications in the method.
- Extension of the trimodal AFM method to a 3D representation of the sample contrast through the incorporation of multiple depth-modulated profile scans into a tip-sample force model.
- Further computational development of existing spectral inversion techniques [5-6] in order to extend the above 3D method to 4D. This will require theoretical work for the development of viscoelastic models that are more realistic than those currently used in AFM. Existing models, despite their usefulness for theoretical developments and in linear techniques such as contact resonance AFM, are either too simple [5] or non-physical [4] in the context of intermittent-contact measurements.

References

- [1] Ebeling, D.; Eslami, B.; Solares, S.D.; *ACS Nano* **2013**, *7*, 10387-10396.
- [2] Solares, S.; Chawla, G.; *J. Appl. Phys.* **2010**, *108*, 054901.
- [3] Eslami, B.; Ebeling, D.; Solares, S.D.; *Beilstein J. Nanotech.*, **2014**, *5*, 1144–1151.

[4] Solares, S.D.; *Beilstein J. Nanotech.* **2014**, *5*, 298-307.

[5] Solares, S.D.; Holscher, H.; *Nanotechnology* **2010**, *21*, 075702.

[6] Williams, J.C.; Solares, S.D.; *Beilstein J. Nanotech.* **2013**, *4*, 87-93.

Publications

1. Diaz, A.J.; Eslami, B.; Lopez-Guerra, E.A.; Solares, S.D.; “*Selection of Higher Eigenmode Amplitude Based on Dissipated Power and Virial Contrast in Bimodal Atomic Force Microscopy*,” submitted.
2. Solares, S.D.; An, S.; Long, C.J.; “*Multifrequency tapping-mode atomic force microscopy beyond three eigenmodes in ambient air*,” *Beilstein J. Nanotech.* **2014**, in press (Thematic Series “Multifrequency AFM II”).
3. Solares, S.D.; “*Probing viscoelastic surfaces with bimodal tapping-mode atomic force microscopy: Underlying physics and observables for a standard linear solid model*,” *Beilstein J. Nanotech.* **2014**, in press (Thematic Series “Advanced atomic force microscopy techniques II”).
4. Eslami, B.; Ebeling, D.; Solares, S.D.; “*Trade-offs in sensitivity and sampling depth in bimodal atomic force microscopy and comparison to the trimodal case*,” *Beilstein J. Nanotech.*, **2014**, *5*, 1144–1151 (Thematic Series “Advanced atomic force microscopy techniques II”).
5. Solares, S.D.; “*Challenges and complexities of multifrequency atomic force microscopy in liquid environments*,” *Beilstein J. Nanotech.* **2014**, *5*, 298-307 (Thematic Series “Noncontact AFM II”).
6. Ebeling, D.; Eslami, B.; Solares, S.D.; “*Visualizing the subsurface of soft matter: simultaneous topographical imaging, depth modulation, and compositional mapping with triple frequency atomic force microscopy*,” *ACS Nano* **2013**, *7*, 10387-10396.
7. Ebeling, D.; Solares, S.D.; “*Amplitude modulation dynamic force microscopy imaging in liquids with atomic resolution: comparison of phase contrasts in single and dual mode operation*,” *Nanotechnology* **2013**, *24*, 135702 (Feature article of the November 2013 issue – podcast available on the journal website).
8. Ebeling, D.; Solares, S.D.; “*Bimodal atomic force microscopy driving the higher eigenmode in frequency-modulation mode: Implementation, advantages, disadvantages and comparison to the open-loop case*,” *Beilstein J. Nanotech.* **2013**, *4*, 198-207 (Thematic Series “Multifrequency AFM I”).

Probing Correlated Phenomena in Oxide Structures with Quantitative STEM

Susanne Stemmer, Materials Department, University of California, Santa Barbara

Program Scope

The goals of this project are to further our understanding of the role of structure and coupling to the lattice in strong electron correlation phenomena in complex oxide materials, and to advance quantitative methods for atomic scale imaging of functional oxide materials and interfaces. The project utilizes advances made by our group in quantitative scanning transmission electron microscopy (STEM) techniques and in the synthesis of oxide heterostructures to establish quantitative relationships between atomic structure and the electrical and magnetic properties of correlated oxide interfaces. Key parameters of these interfaces are varied in systematic film growth experiments. Experimental techniques include STEM-based diffraction techniques that allow for mapping of small lattice distortions and changes in the oxygen octahedral tilt patterns, with unit cell spatial resolution, at oxide interfaces. These are correlated with phenomena caused by strong electron correlation physics that occur in these structures, such as metal-insulator transitions and magnetism. The program further seeks to advance quantitative analysis of STEM image intensities to elucidate local arrangements of point defects and nonstoichiometries.

Recent Progress

a) Quantitative STEM for visualizing the three-dimensional configuration of individual dopant atoms [4]

Obtaining the complete three-dimensional (3D) configuration of defects with atomic spatial resolution is the ultimate goal of any microstructure characterization technique. In TEM and STEM, sub-Å lateral resolution is obtained but depth resolution in techniques such as through-focal series or confocal approaches had been limited by the depth of focus (at least 5 nm). In our recent study [4] we showed that quantitative HAADF-STEM, previously developed by us, can be used for complete 3D imaging of individual Gd dopant atoms in a thin foil of SrTiO₃. Information is extracted from a single image, thereby avoiding alignment issues of approaches that require multiple images. We show that uncertainties in the depth positions of individual dopants are less than one unit cell, and provide fully quantitative information of expectation values and establish a quantitative criterion for the dopant visibility. The overall dopant concentration measured from atom column intensities agrees quantitatively with electrical measurements. The method is applied to analyze the 3D arrangement of dopants within small clusters containing 4-5 Gd atoms (Fig. 1). Sufficiently thin TEM foils are key for unambiguous interpretation.

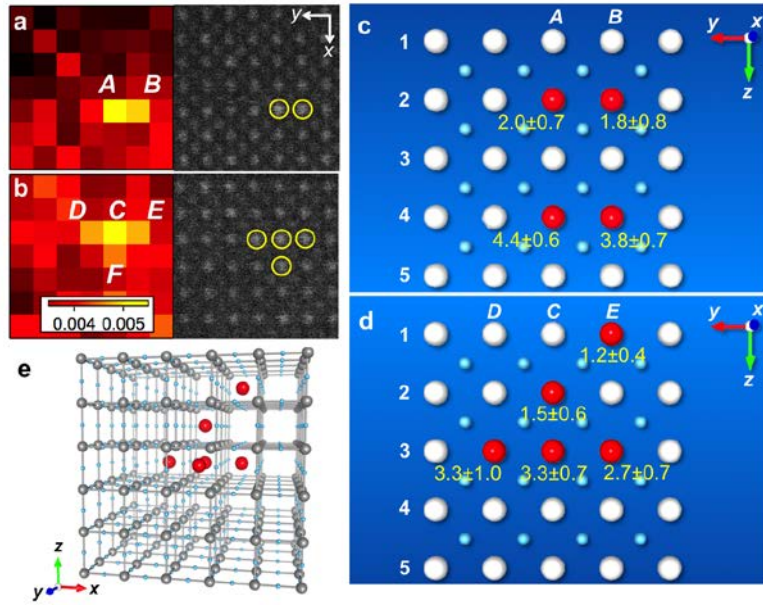


Figure 1: Determining individual Gd dopant atom configurations in SrTiO₃ using quantitative STEM. (a-b) Sr column intensity maps (left) and HAADF images (right) of the areas containing columns labeled A-B (a) and C-F (b). Yellow circles in the images indicate the areas over which the intensities were averaged. (c-d) Schematics showing the configurations of dopant atoms in A-B (c) and C-E (d) columns. The most probable dopant position is shown in red and the expectation values and uncertainties are labeled (yellow numbers). (e) 3D illustration of the area in (b) with the most probable Gd dopant configuration in columns C-F. For clarity, Sr atoms are not shown and some Ti and O atoms were also removed. From ref. [4].

b) Role of transition metal-oxygen octahedral tilts in properties of quantum confined, correlated oxide structures

Strongly correlated “Mott” materials often feature structural distortions. The rare earth titanates (RTiO₃, R = rare earth ion) exhibit oxygen octahedral tilts, or Ti-O-Ti bond angle distortions, away from the 180° angle in the ideal cubic perovskite structure. Properties are intimately coupled with the structural distortion. For example, the magnetic ordering temperature, the type of magnetic and orbital order, and the critical doping density needed for metallic conduction, are all correlated with the tilt of the TiO₆ octahedron. Unlike bulk materials, thin film heterostructures allow for *separately* controlling the contributions of lattice distortions and electronic configuration to electron correlation phenomena. We have investigated the strongly modified octahedral tilts in RTiO₃/SrTiO₃ heterostructures (superlattices and quantum wells), and phenomena such as magnetism and metal-insulator transitions. We quantified the structural distortions in extreme-electron-density (containing $\sim 6 \times 10^{14} \text{ cm}^{-2}$ carriers), confined quantum wells of SrTiO₃ embedded in GdTlO₃, which were grown by molecular beam epitaxy [3]. Column displacements are measured using HAADF-STEM. Orthorhombic-like Sr-site displacements are observed when SrTiO₃ quantum wells are thinner than 4 SrO layers, in precise agreement with the observed metal-to-insulator transition. This is remarkable, because *bulk* SrTiO₃ is a band insulator with cubic symmetry. We showed that the structural displacements are absent in thicker quantum wells, even in the immediate proximity to the orthorhombic

GdTiO₃. The results support true “Mott” physics in the quantum wells. In a subsequent publication [8] we showed that SrTiO₃ quantum wells embedded in SmTiO₃ remain metallic down to a single SrO layer thickness. Symmetry-lowering structural distortions, measured by quantifying the Sr-column displacements, are present only in the insulating quantum wells, but are either absent or very weak in metallic quantum wells, independent of whether they are embedded in SmTiO₃ or in GdTiO₃. The results provided insights into the roles of orthorhombic distortions, orbital ordering, and electron correlations in the transition to the insulating state.

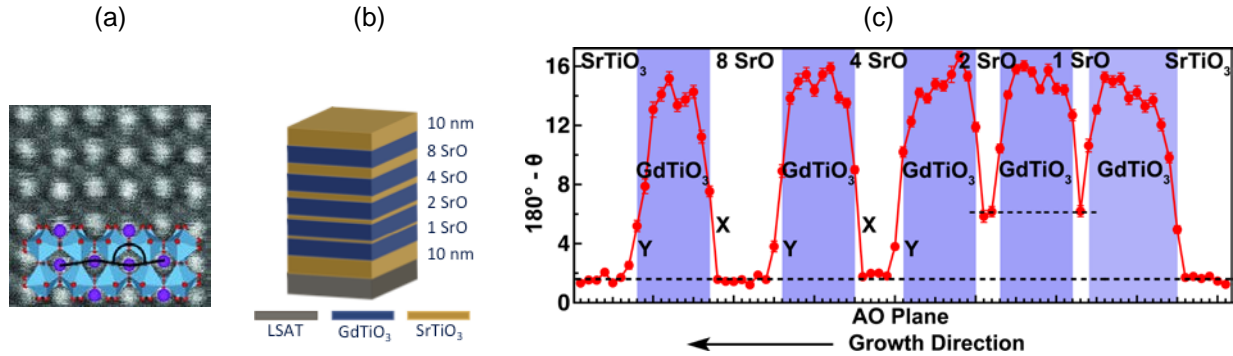


Figure 2: (a) HAADF image of GdTiO₃. In the Pbnm space group, oxygen octahedral tilts are accompanied by Gd displacements. The angle $180^\circ - \theta$ (solid black line) is measured between successive Gd columns. In the cubic structure $\theta = 0$. (b) Schematic of the sample. The SrTiO₃ quantum well thickness is specified by the number of SrO layers they contain. (c) Measured deviation angle, $180^\circ - \theta$, of each GdO and SrO layer in the sample. The error bars represent the standard error of the mean. Note the abrupt increase in the deviation angle at 2-SrO layers, which coincides with the metal-insulator transition. From ref. [3].

In a recent study [6], we showed that with decreasing GdTiO₃ film thickness, structural distortions are reduced, concomitant with a reduction in the ferrimagnetic Curie temperature. Ferromagnetism persists to smaller deviations from the cubic perovskite structure than for the bulk rare earth titanates. The results indicate that the ferromagnetic ground state is controlled by the narrow bandwidth, exchange and orbital ordering, and only to second order depends on amount of the GdFeO₃-type distortion. By combining PACBED, a technique developed by us, with STEM-HAADF imaging, the R-site displacements and oxygen octahedral tilts are measured independently from each other. PACBED patterns are only sensitive to the latter (Fig. 3).

Future Plans

Our future plans include low-temperature STEM imaging and diffraction experiments of the structures described in b) above, for better correlations with properties. For example, the SrTiO₃ quantum wells may exhibit structural distortions at lower temperatures, above the thickness where a structural distortion was detected at room temperature. Because of the significant drift of cold stage holders, we plan to investigate non-rigid registration methods, in collaboration with ESPM funded PI Voyles, to obtain atomic resolution information. We will also continue to develop quantitative methods for 3D point defect imaging. We are particularly interested in angle-resolved methods, to improve the contrast.

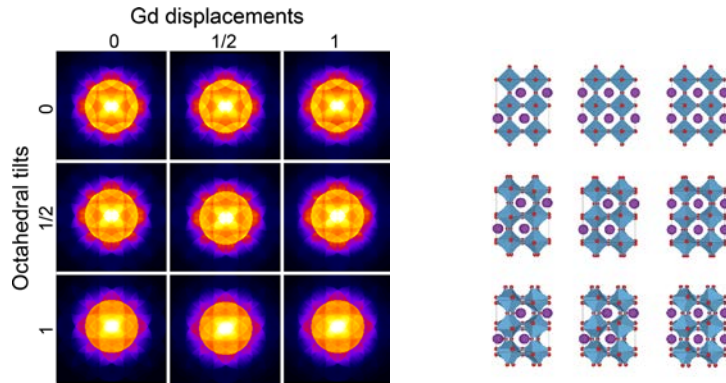


Figure 3: (right) Simulated “GdTiO₃” PACBED patterns for different Gd displacements and octahedral tilts. The numbers indicate the degree of distortion, with 0 signifying no distortion, 1 the distortion in GdTiO₃, and ½ corresponding to the intermediate distortion. The top-left panel corresponds to the cubic structure, while the bottom-right panel is bulk GdTiO₃. (Left) Different structures used for simulations. From ref. [6].

DOE Sponsored Journal Publications (2012 – 2014)

- [1] J. Hwang, J. Y. Zhang, J. Son, and S. Stemmer, *Nanoscale quantification of octahedral tilts in perovskite films*, Appl. Phys. Lett. **100**, 191909 (2012).
- [2] J. Hwang, J. Son, J. Y. Zhang, A. Janotti, C. G. Van De Walle, and S. Stemmer, *Structural origins of the properties of rare earth nickelate superlattices*, Phys. Rev. B **87**, 060101(R) (2013).
- [3] J. Y. Zhang, J. Hwang, S. Raghavan, and S. Stemmer, *Symmetry lowering in extreme-electron-density perovskite quantum wells*, Phys. Rev. Lett. **110**, 256401 (2013).
- [4] J. Hwang, J. Y. Zhang, A. J. D'Alfonso, L. J. Allen, and S. Stemmer, *Three-Dimensional Imaging of Individual Dopant Atoms in SrTiO₃*, Phys. Rev. Lett. **111**, 266101 (2013).
- [5] S. Stemmer and A. J. Millis, *Quantum confinement in oxide quantum wells*, MRS Bulletin **38**, 1032-1039 (2013).
- [6] J. Y. Zhang, C. A. Jackson, S. Raghavan, J. Hwang, and S. Stemmer, *Magnetism and local structure in low-dimensional, Mott insulating GdTiO₃*, Phys. Rev. B **88**, 121104(R) (2013).
- [7] D. G. Ouellette, P. Moetakef, T. A. Cain, J. Y. Zhang, S. Stemmer, D. Emin, and S. J. Allen, *High-density Two-Dimensional Small Polaron Gas in a Delta-Doped Mott Insulator*, Sci. Rep. **3**, 3284 (2013).
- [8] J. Y. Zhang, C. A. Jackson, R. Chen, S. Raghavan, P. Moetakef, L. Balents, and S. Stemmer, *Correlation between metal-insulator transitions and structural distortions in high-electron-density SrTiO₃ quantum wells*, Phys. Rev. B **89**, 075140 (2014).
- [9] S. Stemmer and S. J. Allen, *Two-Dimensional Electron Gases at Complex Oxide Interfaces*, Ann. Rev. Mater. Res. **44**, 151-171 (2014).

Medium-range order in amorphous materials studied by fluctuation electron microscopy

M. M. J. Treacy

Arizona State University, Dept. of Physics, P.O. Box 871504, Tempe, Arizona 85287-1504

Program Scope

Fluctuation electron microscopy (FEM) studies the variation in electron diffraction between small volumes of the sample. The average diffraction pattern tells us information about the average structure of the material, whereas the variance of the diffraction patterns tells us about the way the structure the structure changes between regions. Any medium-range order (MRO) that is present will show up as correlations between patterns and the diffraction variance will reflect this sensitively. The length scale of the MRO can be explored by varying the probe size.

Despite successes in applying FEM to amorphous materials, the technique remains qualitative. The principal impediment to quantitation is the complexity of the data, which reflects 4-body, or pair-pair, correlations in the sample. However, there is also a significant discrepancy between the data and simple kinematical diffraction theory – experimental variance is about a factor of 100 lower than predicted.

Our research over the past period has been focused on identifying the reason for the large discrepancy. We have identified *decoherence* of electron phase during the scattering as the primary culprit. The primary source of decoherence are large atomic motions induced by interactions with the electron beam, which includes, but is not restricted to, beam damage. In addition, multiple scattering of electrons in thicker samples also contributes. One of the key techniques that helped us identify the source of the problem was *interferometry* between two diffracting regions. Our longer-term goal has been to develop this methodology as a holographic technique in a scanning transmission electron microscope. In the interim, we found a way to implement a variant of the method by examining diffraction from overlapping sample layers.

Recent Progress

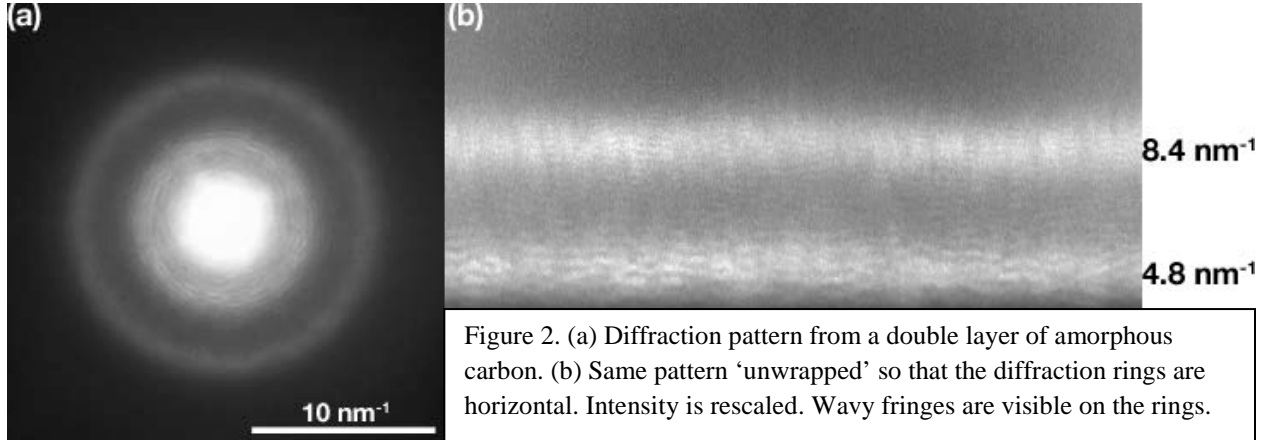
To explore the FEM signal as a function of thickness, we fabricated amorphous carbon and silicon samples that were made from layers of equal thickness. The layers did not lie in perfect contact with each other. We believe that the layers rest on each other in a manner similar to the way cling-film attaches to itself, with many gaps and wrinkles. Consequently, instead of an amorphous sample



Figure 1. Double layer of amorphous material, each of thickness t , with a gap, L .

of thickness $2t$, we obtained a sample with a gap L between layers along the beam direction, as depicted in Figure 1.

Amorphous diffraction patterns exhibited fringes whose spacing decreased with increasing scattering vector (Figure 2a).



The layer separation, L , can be inferred from the fringe spacing Δk via

$$L = \frac{1}{\lambda k \Delta k} - \left(n + \frac{1}{2} \right) \lambda \quad (1)$$

where k is the wavevector, λ the electron wavelength and n is the fringe number counting from the origin. The last term in n makes a small contribution and can be ignored when k (and therefore n) is small.

The fringes arise because of interference between the diffracted waves arising in the two layers. They are wavy and broken because the form factor of the double-layer itself has a complicated structure and intercepts the Ewald sphere irregularly. It is striking that the fringe contrast fades rapidly as wavevector k increases. This indicates that the two interfering patterns become increasingly mutually incoherent as k increases. This is not a simple Debye-Waller attenuation as the contrast fades away too rapidly. Kinematically, the fringe spacing Δk should decrease as k increases (since L is constant) while the fringe contrast should remain constant. Decoherence is arising that is significantly stronger than the Debye-Waller diffuse scattering.

Until recently, this decoherence was confused with spatial incoherence in the illumination. It had always been assumed that speckle contrast in dark-field images was limited by illumination coherence. Kinematical theory predicts negative-exponential intensity statistics, but instead we obtain Gamma Distribution statistics,

$$P(I) = \frac{m^m}{\Gamma(m)} \frac{I^{m-1}}{I_0^m} \exp(-mI / I_0) \quad (2)$$

where I_0 is the mean intensity. The normalized variance of this distribution is $1/m$. m should equal 1 under kinematical diffraction theory when the illumination is fully coherent. However, experimentally we obtain m values much greater than 1. Figure 2 shows the speckle statistics from a tilted dark-field image of amorphous carbon.

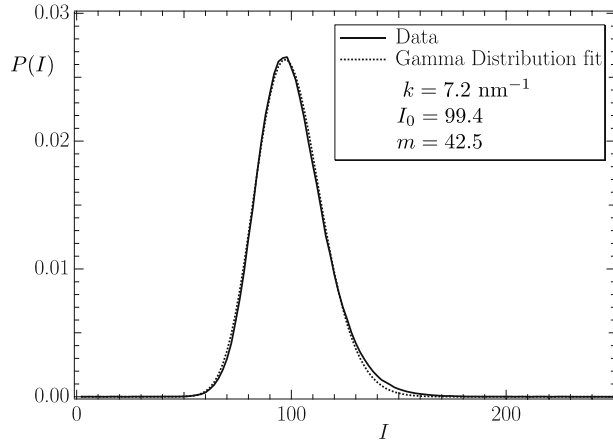


Figure 3. Speckle intensity histogram from a tilted dark-field image of amorphous carbon, using 200 kV electrons. The data are fitted impressively by a Gamma Distribution, with $m = 42.5$. Under ideal kinematical scattering theory, with fully coherent illumination, m should equal 1. Since the illumination was fully coherent, the source of incoherence must lie in the scattering process itself.

In FEM, the normalized variance is examined as a function of the scattering vector, $V(k)$. In Figure 4 we compare theoretical variance for three models of amorphous silicon with the data.

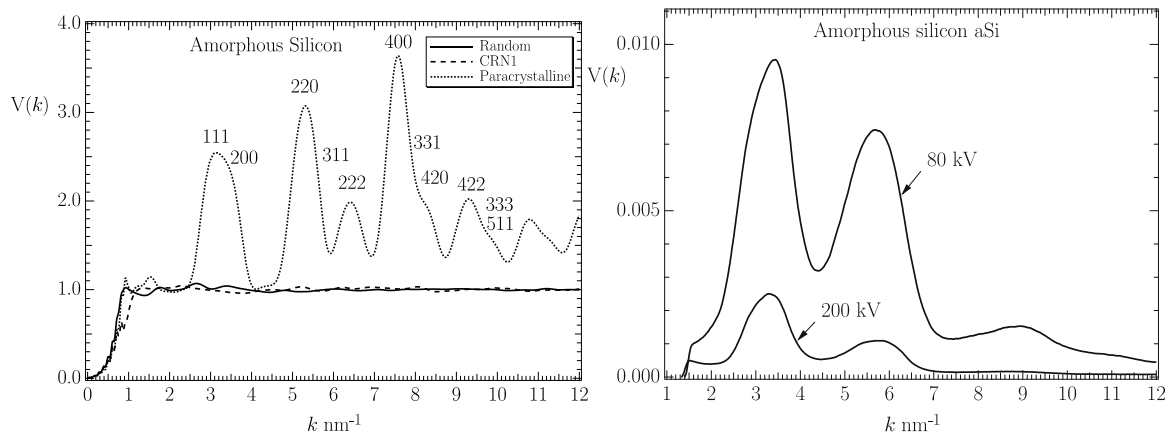


Figure 4. Left. The simulated variance for three different models of amorphous silicon. Both the continuous random network (CRN) and the random model give a uniform variance of 1. The model with paracrystallinity shows peaks in the vicinity of the crystallographic cubic Si reflections. The variance is everywhere greater than 1. Right. FEM normalized variance data for amorphous silicon obtained at two different beam voltages. The sample is believed to be paracrystalline, since it exhibits peaks near 111, 220 and 422 reflections of cubic silicon. However, the higher- k peaks are missing. Also, the experimental variance is over two orders of magnitude lower than the theory predicts. The variance decreases further as the beam energy increases.

If we modify the simulations to include large, Einstein-type, atomic motions, the calculations resemble the data (Figure 5). In addition, multiple scattering also suppresses variance, but does so uniformly for all k values.

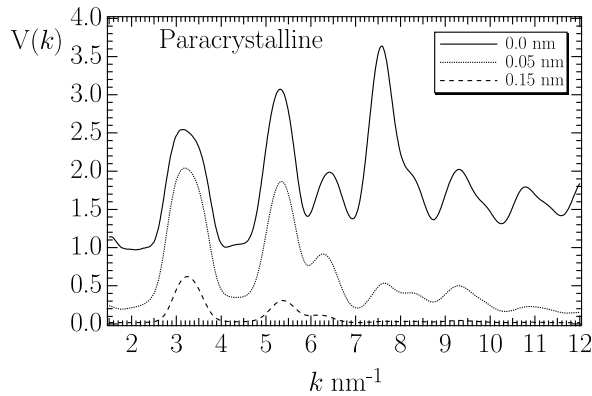


Figure 5. Left. The simulated variance for amorphous silicon assuming a paracrystalline structure, with large atomic vibration amplitudes. R.M.S. amplitudes of 0.15 nm, which is more than half of the Si-Si bond distance (0.235 nm) suppresses the high- k peaks, as observed, and suppresses the overall variance. Multiple scattering also contributes to variance suppression.

We conclude that *displacement decoherence* is a major factor in suppressing speckle variance, while not affecting the mean intensity significantly. Consequently, the mean diffraction intensity follows kinematical theory fairly well, whereas the variability of the scattering does not.

Future Plans

We will implement an interferometric version of FEM. We will use holographic methods to generate two separated, mutually coherent, probes and examine the correlations in scattering as a function of probe separation. The main hold up has been the absence of a suitable low-noise diffraction camera on the ASU Nion microscope. A suitable high-vacuum-compatible camera, is has been designed and is being tested.

We will use this new technology to explore the detailed structure of ultra-nanocrystalline diamond films.

Publications

T. Sun, F. A. M. Koeck, A. Rezikyan, M. M. J. Treacy, and R. J. Nemanich

Thermally enhanced photoinduced electron emission from nitrogen-doped diamond films on silicon substrates, PHYSICAL REVIEW B, in press, 001300(R) (2014)

A. Rezikyan, Z. Jibben, B. A. Rock, G. Zhao, F. A. M. Koeck, R. F. Nemanich, and M. M. J. Treacy,

The Dominant Role of Decoherence in the Suppression of Speckle Contrast in Quantitative Fluctuation Electron Microscopy,

in preparation for Phys. Rev. B.

A. Rezikyan and M. M. J. Treacy,

Interferometric diffraction studies from multiple-layer amorphous thin films

in preparation for Microscopy and Microanalysis.

P. Rez and M. M. J. Treacy,

Three-dimensional imaging of dislocations,

Nature 503, <http://dx.doi.org/10.1038/nature12660> (2013).

Imaging Point Defects with Quantitative STEM

Paul M. Voyles and Dane Morgan

Materials Science and Engineering, University of Wisconsin, Madison

1509 University Avenue, Madison, WI 53706, voyles@engr.wisc.edu, ddmorgan@wisc.edu

Program Scope

The goal of this project is to advance the state of the art in quantitative electron microscopy for characterization of defects, focusing on scanning transmission electron microscope (STEM) imaging of point defects. We apply methods from applied mathematics and image processing to overcome instrumental limitations and achieve low distortion, low noise intensity data. Low distortion and noise enables high precision location of atomic columns in aberration-corrected images and detailed quantitative matching between experiment and image simulations. We combine quantitative imaging and density functional theory (DFT) to study point defects and defect clusters, including the details of defect structures, and defect populations and their evolution under various conditions in semiconductors and complex oxides.

Recent Progress

High Precision STEM

We have demonstrated sub-picometer precision in the location of atomic columns in high-resolution Z-contrast STEM images.^B High precision is achieved by non-rigid registration and averaging of a large number of short exposure STEM images, resulting in an image with extremely high signal to noise ratio (SNR). Unlike the more common rigid registration method, non-rigid registration can correct for sample and scan instabilities within the images, enabling improved averaging of a large number of frames without loss of resolution and better preservation of the correct atomic column position information in the image.

Figure 1 demonstrates sub-picometer precision STEM imaging of Si [110]. Figure 1(a) is the first image in a series of 512 STEM images. Figure 1(b) is the average image after non-rigid registration. Atom positions were located by fitting to Gaussian peaks. The precision is determined by measuring repeated, known crystallographic distances, x and y in Figure 1(b), parallel and perpendicular to the scan. Figure 1(c) and (d) show histograms of the x and y distances,. In both directions, the standard deviation of the measurements is <1 pm. Rigid registration of the same data set yields precision ~ 5 times worse.

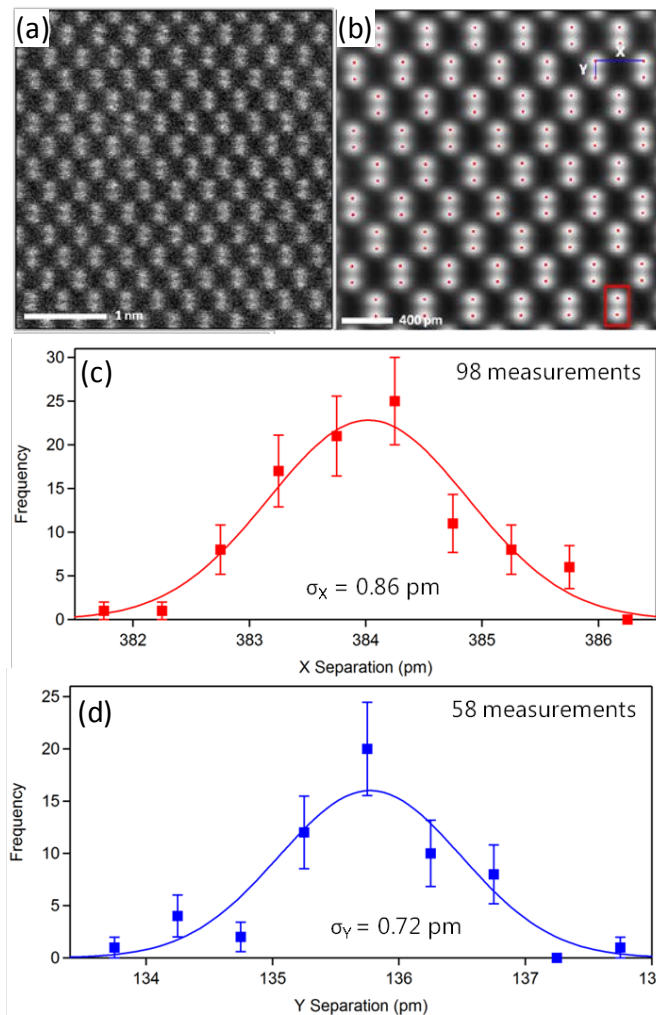


Figure 1: (a) first frame of a series of Si [110] STEM images. (b) the average image after non-rigid registration. (c) and (d) histograms of the x and y interatomic separations measured in (b).

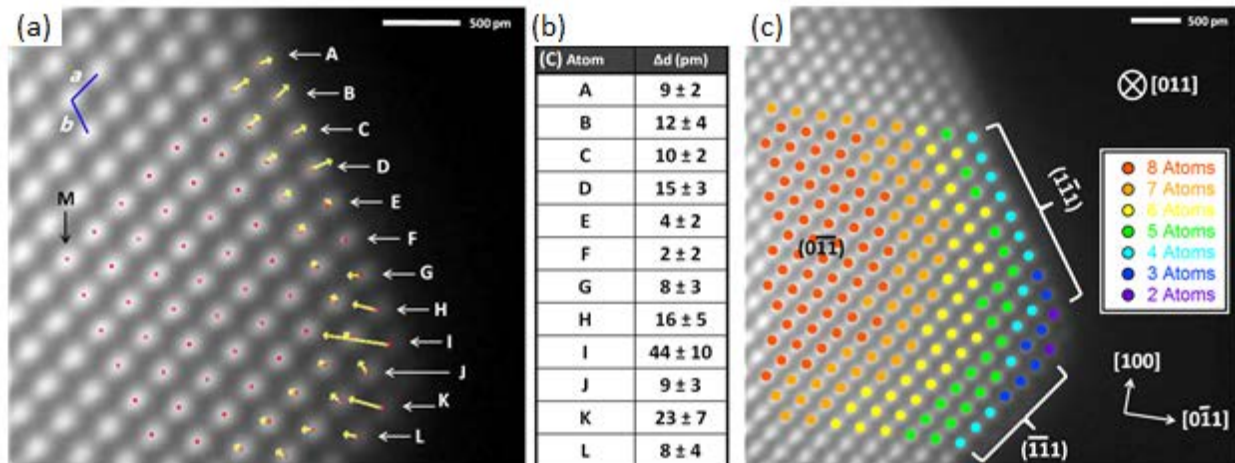


Figure 2: (a) Average image of a Pt nanocatalyst after non-rigid registration. The arrows represent the (magnified) displacement vectors of the surface atoms. (b) Surface atom displacements. (c) Atom column thickness from standardless atom counting.

We also tested non-rigid registration against simulated STEM distortions applied to a simulated image of a dislocation as an example inhomogeneous strain field. Non-rigid registration preserves the strain field, with rms displacements of <1 pm between the reconstructed positions after non-rigid registration and averaging and the positions in the original, undistorted simulated STEM image.

We applied high precision STEM imaging to measuring the surface atom displacements of a Pt nanocatalyst on a SiO_2 support, as shown in Figure 2. The catalyst nanoparticle is more dose sensitive than the Si crystal, so only 56 frames at lower dose per frame were averaged. More frames were acquired, but surface atoms became mobile at higher dose. As a result of the lower dose and the smaller scattering power of the thin nanocrystal, the precision in Figure 2 is ~ 1.5 pm. We find that flat $\{111\}$ facets bulge outward from the particle center, and that a reconstructed corner between two $\{111\}$ facets has a large contraction toward the particle center. There is a smooth transition between expansion and contraction, and the first subsurface layer has a similar pattern of displacements. Numerical values of the displacements in Figure 2(b) are generally consistent with previous DFT calculations on similar structures.¹

High SNR from non-rigid registration also enables improved quantification of images, reducing the uncertainty in standardless atom counting. Figure 2(c) shows the result of comparing the integrated intensity in each column in Figure 2(a) to frozen-phonon multislice calculations for a Pt $[110]$ crystal as a function of thickness. If we assume a flat interface between the Pt and the underlying SiO_2 ,² Figure 2(c) is a map of the top surface of the nanocrystal showing natural terraces and single-atom high steps. 60% of the atomic columns can be assigned uniquely to one particular thickness, with an uncertainty in the thickness of <1 atom. The other 40% could contain either one more or one less atom, but not both. The dominant contribution to the uncertainty in atom counting is the variation in support scattering underneath the Pt particle; Poisson noise in the image intensity is no longer a limit.

Limits to Precision from Electron Scattering

Picometer-precision STEM images like Figure 1 raise the question, what are the fundamental limits to precision imposed by electron scattering? At finite spatial resolution, the atomic column images will be slightly shifted from the projected positions of the atomic columns, since each image will sit on the sloping tails of nearby columns, but are there further shifts imposed by dynamical electron scattering? We have addressed this question using multislice simulations of Z-contrast and annular bright-field (ABF) STEM images of Si $[110]$, GaN $[11-20]$ and LaMnO_3 $[110]$ (pseudocubic notation). For the two simpler crystals, Si and GaN, the Z-contrast image shows only small, ~ 0.5 pm, channeling-induced

variation in the position of the atomic columns in the images as a function of the sample thickness. The ABF image shows a periodic breathing mode of the atom images moving closer together, then farther apart, with a peak-to-peak amplitude of ~ 4 pm and a periodic in thickness of ~ 30 nm. Thus, for ABF STEM, accurate knowledge of the sample thickness and careful simulations are necessary to extract atomic column positions to 1 pm or better precision.

In contrast, LaMnO_3 exhibits a ~ 10 pm change in the distance between neighboring La columns as a function of thickness in Z-contrast, as shown in Figure 3. The large shift arises from the intensity of the unresolved O columns that lie between the La columns in this projection. As the O column intensity oscillates with thickness, it changes the position of the center of intensity of the La column.

The same set of simulations demonstrates that achieving convergence comparable to the data quality in Figure 1 using the frozen-phonon method requires a large number of frozen phonon configurations. The noise level in Figure 1 is much less than 1%. If we define convergence as an intensity standard deviation of the mean of every pixel over ten independent simulations $< 1\%$, then a minimum of 96 phonon configurations is required for convergence of a Z-contrast STEM image of LaMnO_3 $[110]_{\text{pc}}$. (Figure 3 was calculated with 128 configurations.) 96 configurations also provides good convergence in the atomic column positions, with the standard deviation of the mean over ten simulations < 0.7 pm. 96 or 128 phonon configurations is significantly larger than commonly undertaken (e.g.^{3,4}), increasing computational cost.

Clustering Formation Tendencies in LaMnO_{3-d}

We are pursuing the application of our unprecedented resolution capabilities to the challenge of directly observing isolated and clustered point defect in perovskites, with an initial focus on LaMnO_{3-d} . LaMnO_{3-d} is widely used as a base material for solid oxide fuel cell cathode alloys, where generation of free mobile O vacancies is critical to performance. La-site deficient materials (e.g., $\text{La}_{0.95}\text{MnO}_{3-d}$) have been synthesized with intent to yield excess O vacancies, but they do not yield the expected increase in performance. It has been proposed that the La and O vacancies are bound, making the O vacancies unavailable to activate O transport and catalysis. Figure 4 shows results of DFT calculations on the La-O and Mn-O vacancy binding energy (the energy to bring the isolated point defects together), demonstrating

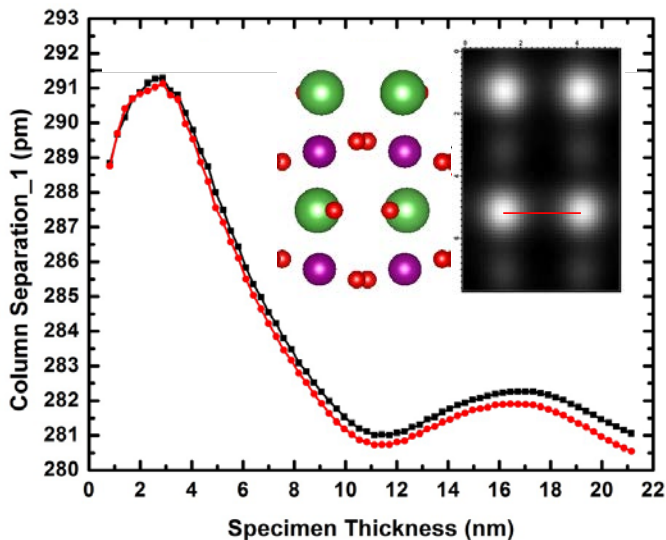


Figure 3: Simulated La-La separation in a Z-contrast STEM image for two camera lengths.

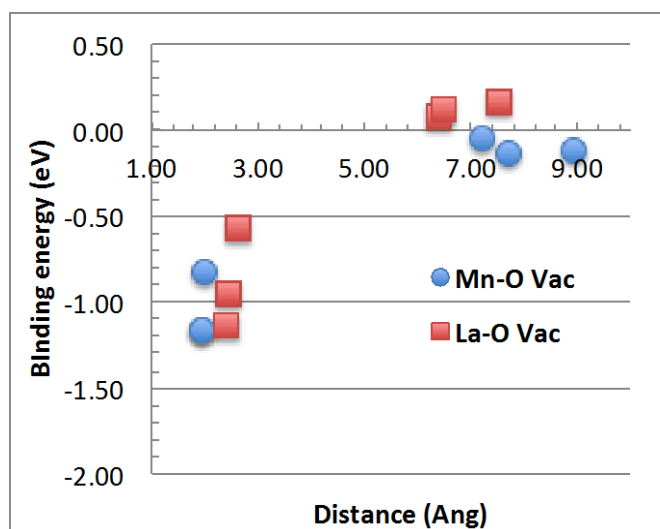


Figure 4: Binding energy of La and Mn vacancies with O vacancies as a function of their separation.

that these defects bind with energies of over 1 eV per pair. This large value will bind almost all vacancies at any reasonable temperature, supporting the hypothesis that that La and O vacancies are bound together.

Future Plans

We plan to combine high precision STEM, image simulations, and DFT simulations to characterize point defects and point defect complexes in off-stoichiometric complex oxides, starting with LaMnO₃. DFT simulations will be used to determine defect structures for vacancies on all sites, vacancy clusters, and antisite defects. Image simulations from these structures will be matched to high precision STEM experiments to rigorously identify defects. DFT calculated formation and reaction energies will be used to develop a thermokinetic model of defect densities as a function of composition, annealing temperature, and oxygen partial pressure. The model will be tested against quantitative STEM results.

We will also address the most significant limitation of our high precision STEM technique: the extremely high dose to the sample. Our current method achieves high SNR by brute-force averaging. It may be possible to use the redundancy inherent in most lattice images for single-image denoising using an approach like non-local means.^A However, such methods bring significant potential for introducing artifacts or failing on the aperiodic regions of a lattice image which are often the most interesting because they contain the defects. Developing these methods will require careful validation.

References

1. L. Y. Chang, A. S. Barnard, L. C. Gontard, R. E. Dunin-Borkowski, Resolving the structure of active sites on platinum catalytic nanoparticles. *Nano Lett.* **10**, 3073–3076 (2010).
2. P. Ajayan, L. Marks, Evidence for sinking of small particles into substrates and implications for heterogeneous catalysis. *Nature* **338**, 139–141 (1989).
3. J. Hwang, J. Y. Zhang, A. J. D'Alfonso, L. J. Allen, S. Stemmer, Three-Dimensional Imaging of Individual Dopant Atoms in SrTiO₃ *Phys. Rev. Lett.* **266101**, 266101 (2013).
4. D. A. Blom, Multislice frozen phonon high angle annular dark-field image simulation study of Mo–V–Nb–Te–O complex oxidation catalyst “M1.” *Ultramicroscopy* **112**, 69–75 (2012).

Publications Supported by this Program

- A. N. Mevenkamp, B. Berkels, A. B. Yankovich, P. M. Voyles, Non-local Means for Scanning Transmission Electron Microscopy Images and Poisson Noise based on Adaptive Periodic Similarity Search and Patch Regularization, *Vision, Modeling, and Visualization*, J. Bender, A. Kuijper, T. von Landesberger, and P. Urban (Eds.) (to be published).
- B. A. B. Yankovich, B. Berkels, W. Dahmen, P. Binev, S. I. Sanchez, S. A. Bradley, A. Li, I. Szlufarska, P. M. Voyles, Picometre-precision analysis of scanning transmission electron microscopy images of platinum nanocatalysts. *Nat. Commun.* **5**, 4155 (2014).
- C. A. B. Yankovich, A. V. Kvit, X. Li, F. Zhang, V. Avrutin, H. Liu, N. Izyumskaya, U. Özgür, B. Van Leer, H. Morkoç, P. M. Voyles, Thickness Variations and Absence of Lateral Compositional Fluctuations in Aberration-Corrected STEM Images of InGaN LED Active Regions at Low Dose. *Microsc. Microanal.* **20**, 864–8 (2014).
- D. H. Y. Liu, N. Izyumskaya, V. Avrutin, U. Özgür, A. B. Yankovich, A. V. Kvit, P. M. Voyles, H. Morkoç, Donor behavior of Sb in ZnO. *J. Appl. Phys.* **112**, 033706 (2012).
- E. A. V. Kvit, A. B. Yankovich, V. Avrutin, H. Liu, N. Izyumskaya, U. Özgür, H. Morkoç, P. M. Voyles, Impurity distribution and microstructure of Ga-doped ZnO films grown by molecular beam epitaxy. *J. Appl. Phys.* **112**, 123527 (2012).

Beneath and Between: Structural, Functional, and Spectroscopic Measurements of Buried Interfaces and Interactions – DE-FG02-10ER46734 (DE-SC0005025-002)

**Paul S. Weiss, California NanoSystems Institute and Departments of Chemistry & Biochemistry and Materials Science & Engineering, UCLA, Los Angeles, CA 90095.
psw@cnsi.ucla.edu; www.nano.ucla.edu**

Program Scope

Spectroscopic imaging tools and methods, based on scanning tunneling microscopes (STMs), are being developed to examine buried layers and interfaces with ultrahigh resolution. These new methods will measure molecule-substrate bonds, buried dipoles in molecular layers, and key structural aspects of adsorbed molecules, such as tilt angles. We are developing the ability to locate lateral projections of molecular parts as a means of determining the structures of molecular layers. We are developing the ability to measure the locations and orientations of buried chemical functionality.

Recent Progress

We have developed methods, in collaboration with mathematicians Bertozzi and Osher, for the segmentation of domains of carboranethiol self-assembled monolayers, which form two-dimensional plastic lattices.¹ We have ascertained that proximate molecular domains often have aligned dipoles that cross features such as domain boundaries and substrate step edges. Thus, developing new real-time analysis tools has been critical for testing whether the offset between maxima in topographic, which follows the exposed molecular surface in this case, and in barrier-height imaging, which measures the largest buried dipoles (due here to the dipole of the cage), are due to artifacts or dipole alignment. We have found alignment both within and between domains. Our molecular dynamics simulations are consistent with the experimental results. These segmentation and analysis methods are now being applied to many other systems in our laboratory. Initial indications are that the new imaging and analysis methods enable us to image directional hydrogen bonds buried within monolayers.

We have used chemical lift-off lithography to produce metal monolayers.² We are studying these monolayers, elucidating their chemistry, electronic, and optical properties as well as their potential as substrates for scanning probe and electron microscopy.

We have used the segmentation methods, both total variation and empirical wavelets in the analysis of amyloid-forming peptides. We have accelerated the methods such that analyses now take place in real time (our first such structural analysis³ without these tools took two years!) such that missing information can be collected while the sample is still available. We have

now advanced this work to the point where we are able to locate metal ions associated with the peptides, which cannot be done crystallographically, because these ions are not arranged periodically.

We have found that we can measure and change the valency of the interactions between bifunctional carboranedithiol/diselenol molecules on Au{111}. The scanning tunneling microscope can be used to measure the number of surface bonds, once calibrated with X-ray photoelectron and infrared spectroscopies. The interconversion between one and two surface bonds can be performed through protonation and deprotonation with simple acid-base reactions.

Future Plans

We are combining STM, spectroscopic, and microwave-frequency polarizability imaging to locate buried functionality, interactions, and contacts in a diverse range of molecular systems on surfaces.

In collaboration with our math colleagues, we are developing and applying routines for stacking, associating, and interpreting these multi-spectral data sets.

References

1. Defect-Tolerant Aligned Dipoles within Two-Dimensional Plastic Lattices, J. C. Thomas, J. J. Schwartz, J. N. Hohman, S. A. Claridge, A. C. Serino, H. S. Auluck, G. Tran, K. F. Kelly, C. A. Mirkin, J. Gilles, S. J. Osher, and P. S. Weiss, submitted.
2. Subtractive Patterning via Chemical Lift-Off Lithography, W.-S. Liao, S. Cheunkar, H. Cao, H. Bednar, P. S. Weiss, and A. M. Andrews, *Science* **337**, 1517 (2012).
3. Differentiating Individual Amino Acid Residues and Side Chain Orientations in Peptides Using Scanning Tunneling Microscopy, S. A. Claridge, J. J. Schwartz, M. A. Silverman, J. C. Thomas, Y. Yang, C. Wang, and P. S. Weiss, *Journal of the American Chemical Society* **135**, 18528 (2013).

Publications (2012-2014)

1. Subtractive Patterning via Chemical Lift-Off Lithography, W.-S. Liao, S. Cheunkar, H. Cao, H. Bednar, P. S. Weiss, and A. M. Andrews, *Science* **337**, 1517 (2012).
2. Design, Control, and Measurement of Molecular and Supramolecular Assemblies, B. K. Pathem, Ph.D. Thesis, Department of Chemistry & Biochemistry, University of California, Los Angeles, Los Angeles, CA, USA (2012).
3. Molecular Self-Assembly for Biological Investigations and Nanoscale Lithography, S. Cheunkar, Ph.D. Thesis, Department of Chemistry, The Pennsylvania State University, University Park, PA, USA (2013).

4. From the Bottom Up: Dimensional Control and Characterization in Molecular Monolayers, S. A. Claridge, W.-S. Liao, J. C. Thomas, Y. Zhao, H. Cao, S. Cheunkar, A. C. Serino, A. M. Andrews, and P. S. Weiss, *Chemical Society Reviews* **42**, 2725 (2013).
5. Defect-Tolerant Aligned Dipoles within Two-Dimensional Plastic Lattices, J. C. Thomas, J. J. Schwartz, J. N. Hohman, S. A. Claridge, A. C. Serino, H. S. Auluck, G. Tran, K. F. Kelly, C. A. Mirkin, J. Gilles, S. J. Osher, and P. S. Weiss, submitted.

Project Title: Electron Density Determination, Bonding and Properties of Tetragonal Ferromagnetic Intermetallics

Principal Investigator: Jörg M.K. Wiezorek

Address: Department of Mechanical Engineering and Materials Science,
John A. Swanson School of Engineering,
University of Pittsburgh,
636 Benedum Hall, 3700 O'Hara Street, Pittsburgh, PA 15261.

E-mail: wiezorek@pitt.edu

Program Scope

Ordered intermetallic phases offer unique properties, often superior to those of elemental metals and compositionally equivalent solid solution alloys, which are directly related to their chemically ordered crystal structures and can be understood most fundamentally in terms of electron density and bonding. Electronic structure calculations based on DFT require some critical approximations, which often are empirically justified by comparison of property predictions, e.g. bulk modulus, phase stability, unit cell dimensions or planar fault energies, to available experimental data. For many materials such data is lacking, encumbering validation of DFT calculations, which is particularly critical when elements with d- and/or f-electron related bonding contributions are involved. Establishing robust and facile methods for probing experimentally the electron density, an intrinsic result of DFT calculations, of crystalline solids with d-electron effects remains a high impact goal of basic science research.

This project uses transmission electron microscopy (TEM) experimentation by quantitative convergent-beam electron diffraction (QCBED) and DFT based electronic structure calculation for study of the electron density and interatomic bonding in transition metals, alloys and intermetallic compounds. Since QCBED permits study of nano-scale volumes a broad range of crystalline phases can be studied. The methods developed here focus on the electron charge difference or bonding charge distribution, $\Delta\rho(r)$, as one of the quantum mechanical characteristics central for understanding of properties and validation of DFT calculations. Charge difference distributions, $\Delta\rho(r)$, the difference between the QCBED measured or DFT calculated electron density and those based on the independent atom model (IAM), $\rho(r)^{\text{CBED/DFT}} - \rho(r)^{\text{IAM}} = \Delta\rho(r)$, can be visualized in electron density difference maps (EDDM) and help elucidate details of interatomic bonding in the transition metal based crystals.

Multiple structure (F_{hkl}) and temperature (Debye Waller, B_i) factors are measured simultaneously from high-quality crystal volumes by QCBED with sufficient accuracy and precision for comparison with electron density calculations by DFT. The often anisotropic Debye-Waller factors (DWF) for the different atoms and atom sites in chemically ordered phases can differ significantly from those known for the respective pure element crystals due to bonding effects. Therefore, the DWF need to be measured, ideally from the same crystal volumes as the structure factors to facilitate robust electron density determination. The ferromagnetic ordered intermetallic phases FePd and FePt have been selected as model systems for 3d-4d and 3d-5d electron interactions, while the intermetallic phases NiAl and TiAl are used to probe 3d-3p electron interactions. Additionally, transition metal elements up to Ta with 5d electrons have been studied. This effort advances the state of the art in quantitative TEM experimentation, provides original experimental data uniquely suited for new validation approaches of DFT calculations of d-electron affected transition metals and intermetallics.

Currently the research team includes the P.I., Prof. Jörg Wiezorek, graduate student, Can Liu, and post-doctoral research associate Dr. Mauricio Gordillo (since 6/2014). Former team members Dr. Xiahan Sang (PhD, 8/2012, post-doctoral research associate 8/12-7/13) and Dr. Andreas Kulovits (until 3/2012) have joined the STEM workforce at North Carolina State University and the Alcoa Technical Center, respectively. The project continues to benefit from collaboration regarding DFT calculations with Prof. Guofeng Wang (MEMS, University of Pittsburgh).

Recent Progress

It has been established that the improved robustness of the multi-beam off-zone axis QCBED method used in this effort for electron density determination via simultaneous measurement of high precision and accuracy F_g 's and DWF's stems from an increased number and increased amplitudes of excited Bloch wave branches when compared to other zero-order Laue zone QCBED methods [1]. QCBED experiments have been performed for transition metals, the Fe-Pd transition metal based chemically disordered concentrated solid solution phase γ -(Fe,Pd) with FCC structure, and the off-stoichiometric Al-rich composition chemically ordered intermetallic γ -TiAl phase with the tetragonal $L1_0$ -structure. The iso-structural chemically ordered equiatomic composition γ 1-FePd and γ -TiAl phases have been studied previously [2-4] and can be used in comparisons with recent studies to elucidate effects of chemical ordering in equiatomic composition Fe-Pd and of Al-substitution on Ti sites in off-stoichiometric ordered γ -TiAl. The elements studied included the 3d transition metals Cr, Fe (bcc, anti- and ferromagnetic), Co (hcp, ferromagnetic), Ni and Cu (fcc, ferro- and paramagnetic), and the 5d transition metal Ta. QCBED data sets of sufficient quality and precision for comparison with electron density calculation by DFT have been obtained [4-6]. The use of low-order F_g from QCBED as facile experimental metrics for comparison and use in validation of aspects of DFT calculations has been explored [5]. Differences between the experimental QCBED and DFT calculated F_g have been evaluated by the mean unassigned error (MUE) [5]. The MUE is the average uncertainty of the respective data set (Table 1). MUE values smaller than the respective CBED MUE indicate good agreement of the calculated F_g from theory (e.g. IAM, LDA or GGA-PBE) with the experiments (Table 1). For example, for Cr and Fe the DFT LDA and GGA-PBE results agree well with the CBED data and the IAM and GGA-EV93 results do not. For Ni and Cu only the F_g calculated with the EV93 DFT functional and the LDA+U approach agree with the CBED data. Generally, the DFT calculations for the 3d metal elements achieve significantly better agreement with the CBED measured low-order F_g than for the intermetallics (see average MUE values rows M and IM, Table 1) [5]. Utilizing the LDA+U approach enables inclusion of onsite Coulomb-repulsion effects. This generally improved the MUE for the DFT calculated low-order F_g (Table 1) [5]. Fig. 1 illustrates and summarizes the MUE reduction in the low-order F_g from the DFT calculations (for clarity only PBE and EV93 shown) achievable when using LDA+U. This implies that onsite Coulomb repulsion effects become non-negligible as the d-orbitals fill. Notably, none of the current GGA functionals or the LDA+U implementations in the popular Wien2K code used here for DFT calculations succeeded in predicting simultaneously well the low-order F_g , bonding effects and other properties, e.g. magnetic moments for Ni [5]. The use of easily measured low-order F_g as an additional metric combined with more conventional property based metrics has been proposed for use in validation of DFT calculation in order to capture better both total energy related properties and details of the interatomic bonding in system with d-electron orbital contributions.

Table I. MUE CBED and theoretical datasets ([5])

MUE	CBED ^a	IAM	LDA	PBE	EV93	LDA+U
Cr	0.030	0.280	0.024	0.029	0.059	0.024
Fe	0.019	0.116	0.014	0.008	0.048	0.014
Ni	0.020	0.068	0.053	0.044	0.003	0.005
Cu	0.035	0.262	0.079	0.069	0.025	0.003
TiAl	0.021	0.201	0.034	0.040	0.047	0.034
FePd	0.052	0.340	0.127	0.121	0.152	0.094
M ^b	0.027	0.158	0.037	0.033	0.032	0.014
IM ^c	0.033	0.254	0.076	0.077	0.089	0.054
Total	0.030	0.208	0.057	0.056	0.062	0.035

$${}^a\text{MUE} = \frac{1}{N} \sum_{i=1}^N \sigma_i. \text{ Other, MUE} = \frac{1}{N} \sum_{i=1}^N |F_i^{\text{CBED}} - F_i^{\text{theor}}|$$

^bMUE for metals, ^cMUE for intermetallics

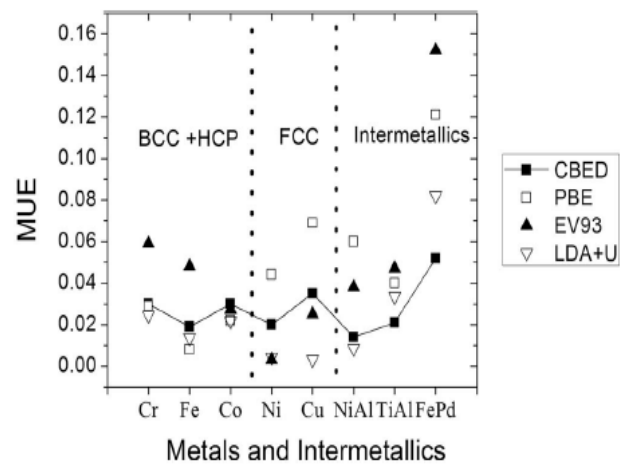


Fig. 1: MUE for low-order F_g from CBED and for different DFT functionals for a range of materials, after [5].

For the metals and intermetallic crystals studied here the CBED measured F_g with $h^2+k^2+l^2>4$, e.g. F_{211} and higher in Cr and Fe, become equal to the IAM calculated F_{hkl} (e.g. Table in Fig.2 for Fe).

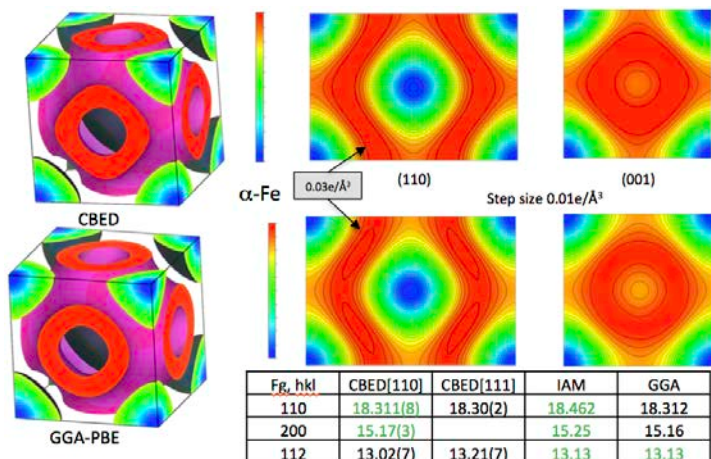


Fig. 2: EDDM for bcc α -Fe from CBED and DFT GGA-PBE F_g . The F_g from CBED, IAM and DFT are equal for F_{112} and higher. Yellow to red increased and green to blue diminished electron charge.

Hence, the low-order $F_g = F_{hkl}$ with $h^2+k^2+l^2 \leq 4$ suffice to capture interatomic bonding effects and are used in EDDM visualizations (e.g. Fig 2). Relative to the CBED results the DFT EDDM for the bcc, fcc, hcp transition metals showed slightly enhanced bonding related delocalized charge between nearest neighbor atoms [3-6]. For the fcc and fcc-related crystal structures quite well defined delocalized bonding charge density is observed in tetrahedral sites [e.g. 3,5], while the charge density appears less directional, more distributed for the bcc transition metals (e.g. Fig. 2).

Effects of composition on changes in bonding in binary intermetallics have been revealed by QCBED measurements of low-order F_g and DWF for the chemically ordered intermetallic phase γ -TiAl with slightly Al-rich composition, i.e., Ti-52at%Al. The lattice parameters of the off-stoichiometric γ -TiAl phase, with the tetragonal $L1_0$ structure, and the elemental composition have been determined by combining X-ray diffraction, locally resolved CBED HOLZ line analyses [7] and analytical electron microscopy using binary standards [3,6]. For equiatomic γ -TiAl DFT calculations based on the local density approximation (LDA) fail to treat accurately the 3d-electron system related bonding effects,

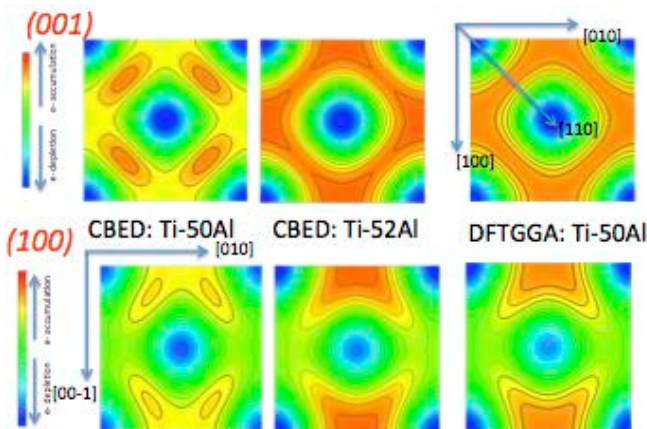


Fig. 3: EDDM for γ -TiAl phase for 50at.% Al, 52at.% Al from CBED and calculated by DFT GGA-PBE for 50at.% Al, (001)-section, Ti atoms only, and (100)-section, Ti at corners and Al in center.

while using the generalized gradient approximations (GGA-PBE) considerably improves agreement with CBED measurements but predicts larger electron charge delocalization to the octahedral sites [3]. EDDM have been obtained from the CBED experiments for Ti50Al50 and Ti48Al52, and for Ti50Al50 by DFT calculation (Fig. 3). Differences between the CBED EDDM for the Al-rich and equiatomic composition intermetallic phase γ -TiAl are discernible for the compositionally all-Ti ((001)- and the mixed Ti-Al (100)-sections (Fig. 3). Substitution of excess 2at.% Al on the Ti sites appears to redistribute charge from the tetrahedral sites between nearest neighbor atoms, e.g. along $\langle 110 \rangle$, to enhance charge delocalization to octahedral sites, e.g.

between second nearest neighbor Ti atoms along $\langle 010 \rangle$. The excess Al substitution to the Ti sites also affects the charge density in the vicinity of the Al atoms, e.g. in the (100) EDDM section, stretching it along [010], relative to the Ti50-Al50 CBED EDDM.

Initial QCBED study of the electron density in equiatomic composition, solid solution chemically disordered γ -phase Fe-Pd with the fcc structure have been performed. DWF have been measured to be isotropic and of much larger magnitude ($0.403(4)\text{\AA}^2$) than for the chemically ordered $L1_0$ -FePd $\gamma 1$ -phase (~ 0.2 to 0.3\AA^2) and EDDM have been compared. The increased DWF has been rationalized in

terms of lattice distortion theory. CBED measurements performed with systematically varied probe size, range from 0.5nm to 5.0nm, indicated that sensitivity to local compositional (structural short-range order) variations affected larger scatter and uncertainty in data obtained for probes smaller than 2nm for the fcc γ -phase Fe-Pd. Since this correlates with the apparent size of coherency strain related contrast and patches of ordered regions in HREM observations, this phenomenon has been attributed speculatively to pre-ordering and short-range ordering present in the concentrated solid solution Fe-Pd.

Future Plans

- Perform experiments and DFT calculations to probe for the origin(s) of the differences in the EDDM and structure factors for the transition metal based crystals, inclusive of effects of off-stoichiometric compositions in binary TiAl and FePd systems. Include site-specific treatments of atomic properties, such as the temperature factors, which are expected as excess species transition metals substitute to the minority species sub-lattices in the off-stoichiometric intermetallic phases.
- Extend the QCBED based experimentation and comparison to predictions from DFT calculations to concentrated solid solution states of the Fe-Pd system where short-range ordering and pre-ordering phenomena are expected. These may become accessible by CBED probe size dependent mapping experiments using high quality crystal volumes.
- Extend the effort to 5d-transition metal based crystals, e.g. Ta and beyond.

References

1. X. Sang, A. Kulovits, J. Wiezorek, "Comparison of convergent beam electron diffraction methods for simultaneous structure and Debye Waller factor determination", *Ultramicroscopy* (2013) Vol 126, 48-59.
2. X.H. Sang, A. Kulovits and J.M.K. Wiezorek, "Simultaneous determination of highly precise Debye-Waller factors and multiple structure factors for chemically ordered tetragonal FePd", *Acta Crystallographica A67* (2011) 229-239.
3. X. Sang, A. Kulovits, G. Wang, J. Wiezorek, "High Precision Electronic Charge Density Determination for L1₀ ordered γ -TiAl by Quantitative Convergent Beam Electron Diffraction", *Philosophical Magazine* (accepted 7/2012).
4. X. Sang, PhD Dissertation, "*ELECTRON DENSITY DETERMINATION AND BONDING IN TETRAGONAL BINARY INTERMETALLICS BY CONVERGENT BEAM ELECTRON DIFFRACTION*", University of Pittsburgh, Pittsburgh, PA 15261, USA (July 2012).
5. X. Sang, A. Kulovits, G. Wang, J. Wiezorek, "Validation of density functionals for transition metals and intermetallics using data from quantitative electron diffraction", *J. Chem. Phys.* 138, 084504 (2013); doi: 10.1063/1.4792436.
6. X. Sang, A.K. Kulovits, G. Wang, J.M.K. Wiezorek, "Charge density determination for Al-rich Composition L1₀-ordered TiAl intermetallic Phase by Convergent Beam Electron Diffraction", *Microscopy and Microanalysis* (accepted 4/2014).
7. M. Tanaka, M. Terauchi, *Convergent Beam Electron Diffraction*, JEOL, Tokyo (1985) p1.

DOE-sponsored publications (2012 - 2014)

- X. Sang, A. Kulovits, J. Wiezorek, "Comparison of convergent beam electron diffraction methods for simultaneous structure and Debye Waller factor determination", *Ultramicroscopy* (2013) Vol 126, 48-59.
- Xiahuan Sang, Andreas Kulovits, Guofeng Wang, and Jörg Wiezorek, "Validation of density functionals for transition metals and intermetallics using data from quantitative electron diffraction", *J. Chem. Phys.* 138, 084504 (2013); doi: 10.1063/1.4792436.
- X. Sang, A.K. Kulovits, G. Wang, J.M.K. Wiezorek, "Charge density determination for Al-rich Composition L1₀-ordered TiAl intermetallic Phase by Convergent Beam Electron Diffraction", *Microscopy and Microanalysis* (accepted 4/2014).
- X. Sang, A.K. Kulovits, G. Wang, J.M.K. Wiezorek, "Charge density determination in transition metals and intermetallics by convergent beam electron diffraction and density functional theory validation", *Proceedings International Microscopy Congress, Open Access via Google Scholar* (2014), Extended Abstract from IMC18, Prague, Czech Republic (September 2014);

Program Title: *in situ* scanning probe microscopy studies of cross-coupled domains and domain walls

Principal Investigator: Weida Wu

Email: wdwu@physics.rutgers.edu

Rutgers Center for Emergent Materials (R-CEM)

Department of Physics and Astronomy

136 Frelinghuysen Road, Piscataway, NJ 08854, USA

Program Scope

The objective of this project is to explore the nanoscale emergent phenomena and to understand the unconventional properties of cross-coupled domains and domain walls in multiferroics, where both ferroelectricity and magnetism coexist. The giant magnetoelectric effect due to coupled ferroic orders in multiferroics is of both fundamental and technological interest, and is promising for energy-efficient multifunctional applications. The presence of domains and domain walls is a distinguishing feature of any ferroic order; their responses to external stimuli determine the macroscopic properties and the functionalities of ferroic materials. To address the challenges and to directly visualize the cross-coupled domains and domain walls and their responses to the applied electric and magnetic fields, the PI proposed and developed a unique, magnetoelectric force microscopy (MeFM). The real space imaging of domains and domain walls by SFM aims to fundamentally understand the nature of magnetoelectric cross-coupling in representative multiferroic and magnetoelectric materials.

Program Progress

- Instrumentation development

- *Development of Magnetoelectric Force Microscopy (MeFM)*

We have developed unprecedented Magnetoelectric Force Microscopy (MeFM) technique that combines Magnetic Force Microscopy (MFM) with in-situ modulating high electric fields. This method allows us to visualize local magnetoelectric response for the **first** time. Figure 1 shows the basic principle of the MeFM, which can be summarized as a lock-in detection of electric field induced magnetic signal \mathbf{M}_E . The top electrode (a thin metal film deposited on the sample surface) was grounded to screen all \mathbf{E} -fields. A modulated voltage $V(\omega)$ is applied to the bottom electrode to generate a modulated \mathbf{E} -field across the sample. Our MeFM

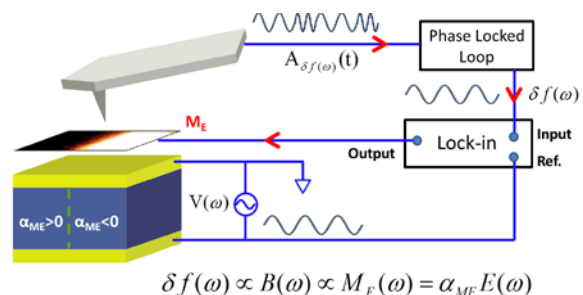


Figure 1 | Schematic of MeFM setup. The basic principle of MeFM is the lockin detection of the demodulated MFM signal from the \mathbf{E} -field induced magnetization (\mathbf{M}_E). The domains with different magnetoelectric coefficients would have different image contrast.

technique is demonstrated by imaging the magnetoelectric response of multiferroic domains in *h*-ErMnO₃ single crystals¹. In addition, we have performed several control experiments to exclude possible extrinsic origins of MeFM signals. The key results were published in **Nature Materials** (**13**, 163-167, 2014).

➤ *Background-Free Piezo-response Force Microscopy (PFM)*

In addition to the development of MeFM, the PI's group also optimized the PFM setup configuration which effectively removes the background signal. PFM detects small mechanical deformation of a specimen by applying an AC voltage between a conductive AFM tip (as a top electrode) and the back electrode. It has been widely used for visualizing ferroelectric domain patterns with high lateral resolution. In nominal or commercial setups, the PFM signal is contaminated by the so-called “system-inherent background” with a complex frequency spectrum which consists of many cross-talk resonances with peak amplitude over 10 pm/V, which severely distorts the PFM contrast (especially the phase signal) and the domain pattern in PFM images. Using our background-free PFM setup, we have been able to obtain quantitative measurements of diagonal piezoelectric response in ferroelectric (LiNbO₃, 5.6 pm/V), improper ferroelectric (ErMnO₃, 0.89 pm/V) and piezoelectric (*x*-cut α -quartz, 2.3 pm/V)². High quality PFM images of LiNbO₃ and ErMnO₃ are shown in Fig. 2. Furthermore, we are able to write and read PFM domains in a newly discovered room temperature multiferroics LuFeO₃ thin film³.

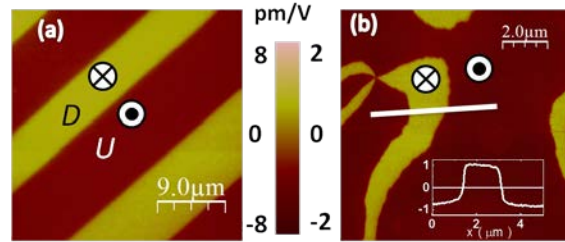


Figure 2 | high quality images of Background-Free PFM setup. (a) and (b) PFM images without any image processing on the (001) surfaces of PPLN and *h*-ErMnO₃, respectively. The inset shows the profile of PFM signals along solid line in panel (b).

- Scientific accomplishments

➤ *Lattice-mediated magnetoelectric response in hexagonal manganites and ferrites*

Our MeFM results of hexagonal manganites are in excellent agreement with the theoretical studies carried out by Fennie's group at Cornell and M. Mostovoy at Groningen, providing a textbook example of the microscopic mechanism of lattice-mediated magnetoelectric coupling^{1,4}. Here the “bridging” degree of freedom is the condensed trimerization mode, which couples to both polar mode and 120° AFM order of Mn³⁺ spins, as shown in Fig. 3. The collaboration leads to 2 joint publications, one in *Nature Materials* and the other in *Nature Communications*. The same microscopic mechanism is predicted to be present in related system, hexagonal ferrites (e.g. LuFeO₃), which can only be stabilized in thin films by state-of-the-art PLD or MBE. More interestingly, the ground state of LuFeO₃ is predicted to be the magnetoelectric A₂ phase without application of magnetic field⁴. The PI's group has performed PFM studies to demonstrate the existence of ferroelectricity in PLD grown films in last reported period³. The PI is currently collaborating with D. Schlom (Cornell) on high quality hexagonal ferrite films synthesized by MBE to reveal the intrinsic magnetoelectric properties⁵.

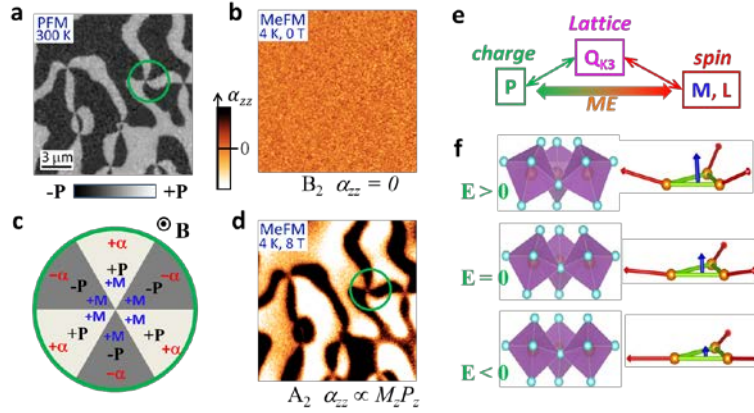


Figure 3 | MeFM results of *hex*-ErMnO₃. **a, b** and **d**, room temperature PFM image, low temperature (4 K) MeFM images at zero magnetic field and 8.0 T, were taken at the same location on the (001) surface of a *h*-ErMnO₃ single crystal, respectively. The white (dark) color in PFM image represents up (down) ferroelectric domain. **c**, a cartoon of the magnetoelectric coefficient (α_{zz}) of the A_2 phase in different ferroelectric domains in *h*-ErMnO₃. **e**, a cartoon illustration of the effective magnetoelectric coupling via structural instability. **f**, cartoon illustrations of the mechanism of lattice-mediated ME response.

➤ *Fluctuation enhanced magnetoelectric response*

Our MeFM studies not only confirm the intriguing magnetoelectric response of hexagonal manganites, but also reveal a giant enhancement of magnetoelectric response in the proximity of tri-critical point which separates continuous (via a mixture A_2' phase) and first-order spin reorientation transition ($B_2 \rightarrow A_2$) of Mn^{3+} spins. The experimental data are in excellent agreement with a phenomenological Landau theory proposed by our collaborator M. Mostovoy (Groningen), as shown in Fig. 4b. Our results suggest that critical fluctuations of competing orders may be harnessed for colossal E-induced magnetic responses¹.

Future plans

MeFM studies of hexagonal manganites and ferrites

We will continue to optimize our unique MeFM technique and to apply it to visualization of mesoscopic magnetoelectric effect of domains or domain walls in either single-phase multiferroics (e.g. *hex*-REMnO₃, *hex*-REFeO₃) and magnetoelectrics (e.g. DyFeO₃), or heterostructural thin films where interfacial strain or exchange bias provide the cross-coupling. Our preliminary MeFM results of *hex*-YbMnO₃ reveal striking sign change of the divergent magnetoelectric response in the intermediate phase (A_2'). Furthermore, the comparison of magnetization and magentoelectric response between *hex*-ErMnO₃ and *hex*-YbMnO₃ provides

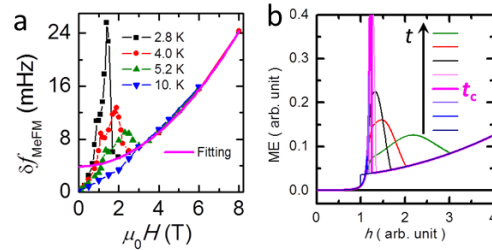


Figure 4. a, H -dependence of the MeFM signal at 2.8, 4.0, 5.2, and 10 K. The solid curve (magenta) is the polynomial fitting $MeFM(H) = a + c \cdot (\mu_0 H)^2$ of the high field A_2 phase. **b**, the simulated magnetic field (h) dependence of ME responses at various effective temperatures (t) using a phenomenological Landau theory of the re-orientation transition. t_c is the critical temperature at which the order of the transition changes from second to first.

insights on the magnetoelectric contributions from Mn spins and RE spins, respectively. Our systematic studies of magnetoelectric effect in hexagonal manganites would shed new light on the fundamental mechanism of magnetoelectric response in hexagonal systems. In collaboration with D. Schlom at Cornell, the PI will explore magnetoelectric effect in hexagonal ferrite (e.g. LuFeO_3) and related superlattice thin films.

Magnetic imaging of multiferroic domains/walls

We will continue to investigate coupled domain walls in multiferroics, using our unique VT-MFM with *in situ* high field capabilities. How the domain wall moments respond to external magnetic field is an interesting question to address. Observation of alternating net moments on vortex domain walls in rare-earth manganites (e.g. TmMnO_3 or YbMnO_3) will provide a unified picture for the *hex-REMnO₃*. Also, we will study the domain wall state (chiral or not) of stripe domains in hexagonal manganites to explore the origin of stripes (from vortex-pair annihilation or not). We will apply this powerful technique to other multiferroics to understand the mechanism of cross-coupling between different ferroic orders.

Background-Free PFM on new piezoelectric materials

We will continue to optimize our background-free PFM setup for quantitative piezoelectric responses, both out-of-plane and in-plane PFM measurements. The PI acquired a used multi-mode AFM for dedicate PFM measurements and general surface characterization. Our background free PFM would also be very powerful to extract quantitative information on polycrystalline samples when single crystals are not available or difficult to make. We will apply our innovated background-free PFM to other new ferroelectric or piezoelectric materials to study their domain structure and piezoelectric properties. E.g. our preliminary PFM results indicate that LuFeO_3 thin is in single domain state. We will explore poling experiments to understand the intrinsic ferroelectric/piezoelectric properties of these potentially strong multiferroics at room temperature.

Design and construction of LT-AFM

A dedicate state-of-the-art SPM controller (SPECS) was ordered for expanding the capabilities and flexibility of current VT-MFM and MeFM. The PI will design new LT-AFM head for potential ultra-low temperature operation. Once the new LT-AFM is constructed, it will be combined with the new controller for multimodal operations at extreme conditions.

Reference (*publications of DOE sponsored research)

- 1* Geng, Y. et al., Direct visualization of magnetoelectric domains. *Nat. Mater.* **13**, 163 (2014).
- 2* Wang, W., Geng, Y., and Wu, W., Background-free Piezoresponse Force Microscopy for quantitative measurements. *Appl. Phys. Lett.* **104**, 072905 (2014).
- 3* Wang, W. et al., Room-temperature multiferroic hexagonal LuFeO_3 films. *Phys. Rev. Lett.* **110**, 237601 (2013).
- 4* Das, H. et al., Bulk magnetoelectricity in the hexagonal manganites and ferrites. *Nature Comm.* **5**, 2998 (2014).
- 5 Moyer, J. A. et al., Intrinsic magnetic properties of hexagonal LuFeO_3 and the effects of nonstoichiometry. *APL Materials* **2**, 012106 (2014).

Transport and Imaging of Mesoscopic Phenomena in Single and Bilayer Graphene

Yacoby, Amir - Harvard University, yacoby@physics.harvard.edu
Jarillo-Herrero, Pablo – MIT, pjarillo@mit.edu

Project Scope

The research objective of this project is to investigate novel quantum phenomena in single and few layer graphene. Special emphasis is given to the role of Coulomb interactions and to spatially varying phenomena where geometry and boundary conditions play an important role. Our experimental approach consists of both conventional transport methods as well as sophisticated local probe techniques capable of imaging the local thermodynamic and transport properties of these spatially varying quantum phenomena. We explore both naturally occurring inhomogeneities due to intrinsic disorder as well as spatially dependent phenomena arising from patterning graphene into nanostructures, introducing inhomogeneous charge densities or magnetic fields using local electrostatic gates, superconducting contacts, and contacting graphene with novel materials. Our focus will be on extremely high quality few layer graphene fabricated either by suspending above a substrate or using hBN as a support structure. Such devices have very small disorder where mesoscopic and relativistic-like phenomena in the ultra-low density regime may be studied. A few examples include the investigation of the fractional quantum Hall effect and the effects of screening on such correlated phenomena, and the investigation of hybrid superconductor-graphene (S-G) devices.

Recent Progress

Fractional quantum Hall effect in bilayer graphene

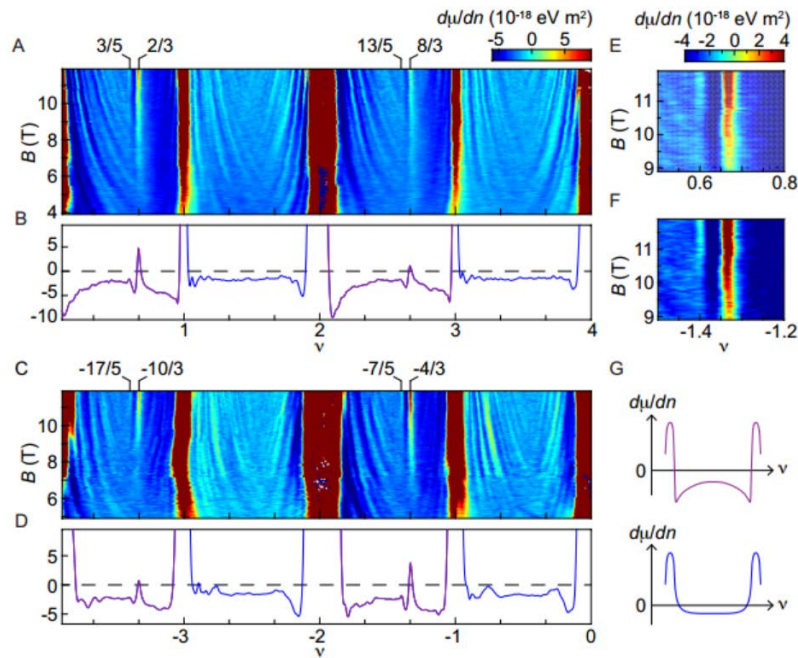
The charge carriers in bilayer graphene obey an electron-hole symmetric dispersion at zero magnetic field. Application of a perpendicular magnetic field B breaks this dispersion into energy bands known as Landau levels (LLs). In addition to the standard spin and valley degeneracy found in monolayer graphene, the $N = 0$ and $N = 1$ orbital states in bilayer graphene are also degenerate and occur at zero energy. This results in a sequence of single-particle quantum Hall states at $\nu = 4Me^2/h$, where M is a nonzero integer.

When the disorder is sufficiently low, the eightfold degeneracy of the lowest LL is lifted by electron-electron interactions, which results in quantum Hall states at all integer filling factors. The nature of these broken-symmetry states has been studied extensively both experimentally and theoretically. Multiple groups have been able to induce transitions between different spin and valley orders of the ground states using external electric and magnetic fields, which indicates the extensive tunability of many-body states in bilayer graphene. Particular attention has been given to the $\nu = 0$ state, which is a canted antiferromagnet at large perpendicular magnetic field, but can be tuned into a ferromagnetic state by a large parallel magnetic field or a layer-polarized state under large perpendicular electric field. However, the order in which orbital states are filled as well as the nature of fractional quantum Hall states remains an open question, with suggestions of full polarization or orbitally coherent states depending on system parameters. The interplay between externally applied fields and intrinsic electron-electron interactions, both of which break the degeneracies of bilayer graphene, produces a rich phase diagram not found in any other system.

Knowledge of the ground state at integer filling factors is especially important for investigating the physics of partially filled LLs, where in exceptionally clean samples, the charge carriers condense into fractional quantum Hall (FQH) states. The above-mentioned degrees of freedom as well as the strong

screening of the Coulomb interaction in bilayer graphene are expected to result in an interesting sequence of FQH states in the lowest LL.

Here, we report local compressibility measurements of a bilayer graphene device fabricated on hexagonal boron nitride (h-BN), performed using a scanning single-electron transistor (SET). Our technique allows us to directly probe the thermodynamic properties of the bulk of the sample. We measure the local chemical potential μ and the local inverse compressibility $d\mu/dn$ by changing the carrier density n with a proximal graphite gate located 7.5 nm from the graphene and monitoring the resulting change in SET current. Remarkably, the observed sequence of FQH states and the background inverse compressibility pattern break particle-hole symmetry and instead follow a $\nu \rightarrow \nu + 2$ pattern (see Fig. 1). The $\nu \rightarrow \nu + 2$ symmetry that we observe indicates that the orbital degeneracy uniquely present in bilayer graphene is playing an important role. Recent theoretical work on the FQH effect in the lowest LL has predicted the presence of FQH states with a $\nu \rightarrow \nu + 2$ symmetry in bilayer graphene based on a model that incorporates the strong screening and LL mixing present in the lowest LL of bilayer graphene. The absence of FQH states between $\nu = -3$ and -2 as well as its $\nu \rightarrow \nu + 2$ symmetric counterparts suggests a difference in electron-electron interactions between partial filling when both the $N = 0$ and $N = 1$ LLs are empty and partial filling of the $N = 1$ LL when the $N = 0$ LL is full. The increased LL mixing present when the $N = 0$ LL is full may be weakening the strength of FQH states in



the $N = 1$ LL.

Figure 1. Fractional quantum Hall states in bilayer graphene. (A) and (C) Inverse compressibility as a function of filling factor and magnetic field. The color scales are the same in both panels. (B) and (D) Average inverse compressibility between $B = 7.9$ and 11.9 T as a function of filling factor. Colors indicate regions of similar behavior in the background inverse compressibility. (E) and (F) Inverse compressibility as a function of filling factor and magnetic field near $\nu = -7/5$ and $3/5$. (G) Schematic diagram highlighting the differences in background inverse compressibility between $\nu = 2p$ and $\nu = 2p + 1$ in purple and $\nu = 2p + 1$ and $\nu = 2p$ in blue.

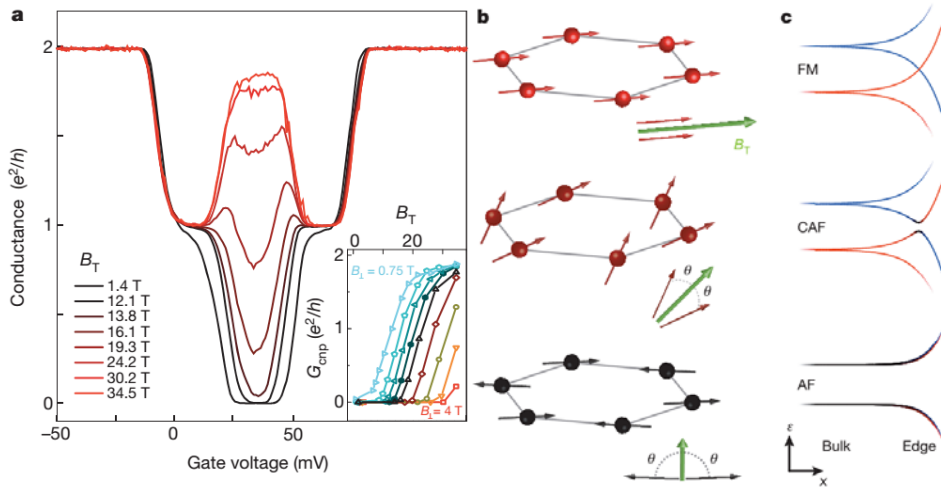
Tunable symmetry breaking and helical edge transport in a graphene quantum spin Hall state

Low-dimensional electronic systems have traditionally been obtained by electrostatically confining electrons, either in heterostructures or in intrinsically nanoscale materials such as single molecules,

nanowires and graphene. Recently, a new method has emerged with the recognition that symmetry-protected topological phases can host robust surface states that are protected by a global symmetry. The primary example in two dimensions is the quantum spin Hall (QSH) state: a bulk insulator with metallic edge states that counter-propagate with opposite spin polarizations.

We have induced a QSH state in monolayer graphene by subjecting a high quality graphene sample to a large magnetic field angled with respect to the graphene plane. Unlike previous realizations of QSH states observed in HgTe and InAs/GaSb quantum wells, this graphene QSH state is fundamentally built upon the graphene quantum Hall effect and the effects of electron-electron interactions. This approach is inspired by the similarity between the quantum spin Hall state and overlapping electron- and hole-like copies of the quantum Hall effect, with the two copies having opposite spin polarizations. We have demonstrated that such a state can be induced in graphene by inverting its electron- and hole-like Landau levels through the effect of Zeeman splitting, which is induced by a large in-plane magnetic field and exchange interactions.

The observed graphene quantum spin Hall state is evidenced by a transition with applied in-plane magnetic field from an insulating state to a metallic state with conductance $\sim 2e^2/h$ due to conduction through nearly ballistic edge states (Figure 2a). This conclusion is supported by bulk capacitance measurements which demonstrate that the bulk remains gapped throughout this transition. Moreover, non-local transport measurements prove that the large conductance in the QSH regime occurs exclusively at the edge of the sample. Such observations reproduce the expected phenomenology of a quantum spin Hall state, where current is carried by a pair of counter-propagating edge states which are



protected from back scattering due to spin conservation.

Figure 2. Transition from a band insulator to the QSH state. **a**, Conductance of a graphene device at a fixed perpendicular magnetic field. As the in-plane magnetic field increases the conductance at charge neutrality transitions from an insulating state to nearly $2e^2/h$ due to the formation of edge states. **b**, Schematic of the bulk spin order as a function of increasing in-plane magnetic field. The quantum spin Hall state corresponds to a bulk ferromagnetic state **c**, Band structure near the physical edge of the graphene sample. For fully perpendicular field the bulk and edge are gapped (bottom). As in-plane field increases, the gap at the edge continuously decreases to zero resulting in the QSH state (top).

The observed continuous transition from a band insulator to a quantum spin Hall state can be understood as being due to the continuous breaking of a spin-rotation symmetry which protects the gapless edge structure of the QSH state (Figure 2b and c). In a purely perpendicular magnetic field, an inherent anti-ferromagnetic instability breaks this symmetry, resulting in a gapped edge state and the observed

insulating behavior. With increasing in-plane field, this symmetry breaking effect is reduced, resulting in the continuous closing of the edge gap to zero. In the intermediate regime where the edge is slightly gapped, we are able to observe edge state transport which is partially protected, suggesting that the edge state in this intermediate regime has a nontrivial spin texture.

Our observation of a graphene QSH state expands the notion of possible 2d symmetry-protected topological insulators beyond the previously considered time reversal symmetry-protected cases. It also introduces a highly tunable QSH system where electron-electron interactions play a major role; as a result, the protecting symmetry can be continuously broken to create novel gapped edge states which are observed in transport. These results should inspire future experimental and theoretical work, both to understand the true nature of the edge states and to use them as a building block for realizing novel quantum circuits.

Future Plans

Our research effort for the next years will focus on the following topics:

1. Transport and imaging of ultra-high mobility in hBN encapsulated single and few layer graphene.
2. Induced superconductivity and Andreev bound states spectroscopy in single layer and few layer graphene.
3. Proximity effect between superconductivity and quantum Hall physics.
4. Engineering topological phases in graphene by tuning electron-electron interactions. Such phases include quantum spin Hall and non-Abelian fractional quantum Hall states.

Publications from DOE supported research

1. A. Kou, B. E. Feldman, A. J. Levin, B. I. Halperin, K. Watanabe, T. Taniguchi, A. Yacoby, “*Electron-Hole Asymmetric Integer and Fractional Quantum Hall Effect in Bilayer Graphene*”, *Science* **345**, 6192 (2014).
2. A. F. Young, J. D. Sanchez-Yamagishi, B. Hunt, S. H. Choi, K. Watanabe, T. Taniguchi, R. C. Ashoori, P. Jarillo-Herrero, “*Tunable symmetry breaking and helical edge transport in a graphene quantum spin Hall state*”. *Nature* **505**, 528 (2014).
3. M. Yankowitz, J.I-J. Wang, A.G. Birdwell, Y.-A. Chen, K. Watanabe, T. Taniguchi, P. Jacquod, P. San-Jose, P. Jarillo-Herrero, P. Jacquod, B.J. LeRoy, “*Electric Field Control of Soliton Motion and Stacking in Trilayer Graphene*”. *Nature Materials* **13**, 786 (2014).
4. M. Yankowitz, J.I-J. Wang, S. Li, A.G. Birdwell, Y.-A. Chen, K. Watanabe, T. Taniguchi, S.Y. Quek, P. Jarillo-Herrero, B.J. LeRoy, “*Band Structure Mapping of Bilayer Graphene via Quasiparticle Scattering*”. *APL Materials* **2**, 092503 (2014).
5. B. Hunt, J. D. Sanchez-Yamagishi, A. F. Young, M. Yankowitz, B. J. LeRoy, K. Watanabe, T. Taniguchi, P. Moon, M. Koshino, P. Jarillo-Herrero, R. C. Ashoori, “*Massive Dirac fermions and Hofstadter butterfly in a van der Waals heterostructures*”. *Science* **340**, 1427 (2013).
6. D. Abanin, B. E. Feldman, A. Yacoby and B. I. Halperin, “*Fractional and Integer Quantum Hall Effect in the Zeroth Landau Level in Graphene*”, *Phys. Rev. B* **88**, 115407 (2013).
7. B. E. Feldman, A. J. Levin, B. Krauss, D. Abanin, B. I. Halperin, J. H. Smet, A. Yacoby, “*Fractional Quantum Hall Phase Transitions and Four-flux Composite Fermions in Graphene*”, *Phys. Rev. Lett.* **111**, 076802 (2013).

Probing Correlated Superconductors and their Phase Transitions on the Nanometer Scale

Ali Yazdani

Department of Physics

Princeton University, Princeton, NJ 08544

Grant #: DE-FG02-07ER46419

Program Monitors: Dr. James Horwitz & Dr. Jane Zhu

Reporting Period: May 2013-May 2014

Program Scope:

Our experimental program provides an atomic scale perspective of unconventional superconductivity — how it evolves from an unconventional conducting state and how it competes with other forms of order in correlated electronic systems. Such phenomena are at the heart of some of the most debated issues in condensed matter physics, and understanding these phenomena is an intellectual driver for many of the DOE-BES projects for the development of novel materials, including the search for higher temperature superconductivity. Our aim is to provide a microscopic view of these exotic materials and their phase transitions into the superconducting state using some of the most sophisticated scanning tunneling microscopy (STM) and spectroscopy techniques. The results of the experiments proposed here provide important evidence that will help constrain theoretical models of unconventional superconductivity, the normal states from which it emerges from, and electronic states with which it competes.

The proposed program is divided into three parts. The first part will focus on examining how heavy electron states emerge in compounds in which localized f orbitals interact with more itinerant electronic states and the process by which such heavy electronic states give rise to unconventional superconductivity. Although heavy fermions do not superconduct at very high temperatures, their transition temperature is a substantial fraction of the heavy electron state bandwidth, hence making these materials among the most strongly correlated superconductors discovered to date. More importantly, the parallels between the puzzles in heavy fermions and high- T_c cuprates superconductors suggest that heavy fermions might provide important clues to a more general understanding of correlated electronic states and their superconductivity. For example, like cuprates or Fe-based superconductors, superconductivity in a heavy fermion system is often found in the vicinity of anti-ferromagnetism in the phase diagrams of these systems.

The second part of the proposed program will focus on how charge ordering competes with superconductivity in high- T_c cuprates. One of the key questions is to determine whether there is universality in the way charge ordering occurs in doped Mott insulators and to study the connection between different forms of charge ordering now observed in different cuprate families. Overall, the precise determination of charge ordering in Bi-based compounds as a function of temperature examined in our program, and contrasting the results of such studies with experiments on other cuprates is establishing the universality of charge ordering in the cuprates.

The third and more exploratory part of this program is focused on the development of techniques for local Josephson tunneling with superconducting STM tips at millikelvin temperatures. Development of such techniques can provide important details about the nature of the superfluid response and phase of the superconducting order parameter on the nanoscale, with broad applicability for the study of superconductivity in a wide range of materials. The three components of the proposed program provide a

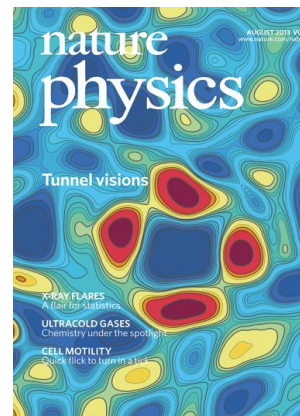


Figure 1. Cover of August 2013 issue of Nature Physics showing our group's results for mapping impurity bound states in the superconducting state of CeCoIn₅. This work demonstrates that the pairing mechanism has $d_{x^2-y^2}$ symmetry. This work is described below and in [1].

broad attack on some of the most important problems in the physics of correlated materials and the emergence of superconductivity in these systems.

Recent Progress:

Visualizing Nodal Heavy Fermion Superconductivity—Nature Physics (2013) and covered in News and Views [1]

Last year we had a major breakthrough by performing the first STM experiments to study the emergence of heavy electron superconductivity with the lowering of temperature. With this study, we uncovered the first direct spectroscopic and spatially resolved evidence for $d_{x^2-y^2}$ gap symmetry in a heavy fermion system. These experiments, which were also carried out on CeCoIn₅, were made possible by our recent development of an advanced ultra-low temperature, high magnetic field UHV STM system (also supported by DOE-BES).

STM can probe the symmetry of the superconducting order parameter through scattering of quasi-particles from impurities as well as when the impurity is strong enough to trap a localized quasi-particle state in its immediate vicinity. We have performed comprehensive STM measurements probing the interplay between quasi-particles and impurities in a Ce-115 system in both its superconducting and normal state. For weak impurities, probing symmetry of the superconducting order parameter requires understanding the interference of quasi-particle scattering from the impurities—a task that requires an assumption about the band structure and the way in which pairing gaps in the Fermi surface of the superconductor. The complex three-dimensional Fermi surface of CeCoIn₅ makes such analysis unreliable. In contrast, if the impurity is strong enough to trap an electron-like or hole-like quasi-particle, direct mapping of this impurity bound state provides direct visual evidence for the pairing symmetry. The results of such experiments on CeCoIn₅ are shown in Figure 1, which was featured on the cover of Nature Physics in their August 2013 issue. As shown in this figure, the impurity bound state leaks out away from the impurity along the minima of pairing potential, thereby pinpointing the nodes to occur at a diagonal to the crystal axis in $d_{x^2-y^2}$ form.

These experiments firmly establish the pairing symmetry in CeCoIn₅ to be similar to that of high- T_c cuprates superconductors and extend for the first time the power of the STM to another class of extraordinary superconductors, the heavy fermions. In fact, the parallels to the high- T_c cuprates go even further as our spectroscopy reveals that the superconductivity gap develops within a depression of the density of states near the Fermi level that persists above T_c and above the critical magnetic field. Further experiments are required to fully understand the interplay between our discovery of a pseudogap and other electronic correlations in this heavy fermion system.

Ubiquitous Interplay Between Charge Ordering and High Temperature Superconductivity in Cuprates, Science 2014 and covered in Perspective [2]

For the past several years, each year, our group has had a major breakthrough in understanding the properties of high- T_c cuprates superconductors. This past year our group had major experimental results showing the ubiquity of charge ordering in cuprates and its competition with superconductivity. To put this work in context, we should first note that in 2004 (Vershinin et al. Science 2004), our group reported the first observation of a charge-ordering signal in temperature range above T_c in underdoped Bi-based cuprates. In the interim years, we also established that this signal can be first detected at the onset of the pseudogap state at T^* and has the strongest signal near 1/8 doping, similar to the stripe phase in La-based cuprates found in the late 1990s by Tranquada. During the last few years,

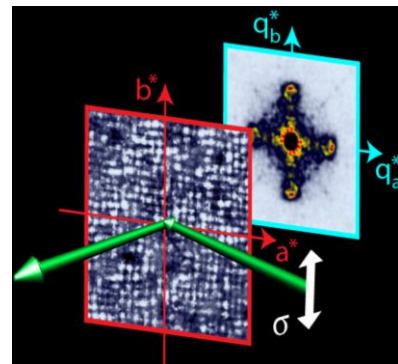
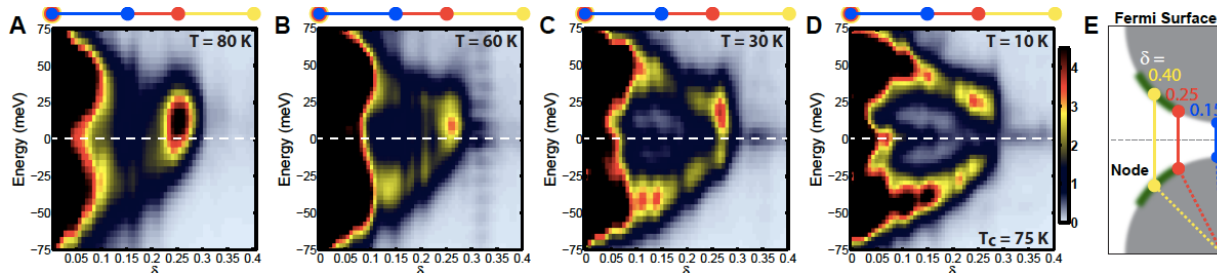


Figure 2. Our group was the first to combine STM and REXS measurements, enabling us to establish that the charge ordering signature found with the STM at the surface of Bi-based cuprates is the same as that found in the bulk of the sample. [2]

Figure 3. (A-D) Energy-momentum structure of the modulations seen in the STM along the Cu-O bond direction, extracted from line cuts along the $(2\pi/a, 0)$ direction of the discrete Fourier transforms for an underdoped $T_c = 75$ sample measured at selected temperatures. The data shows the opposite temperature dependence between the particle-hole symmetric BdG-QPI and the particle-hole asymmetric charge order. (E) Schematic layout of the Fermi surface in Bi-2212 UD75 sample. The green segment represents the Fermi arc as determined by ARPES above T_c . The vertical lines (also reproduced horizontally in A-D) correspond to QPI wavevectors connecting with the Fermi surface (consistent with ARPES, see at different regions. From [2].



resonant x-ray scattering has also been used to find charge ordering in Y-based cuprates and to show that cooling the sample into the superconducting state the charge ordering signal gets weaker.

In a recent combined study of charge ordering, using both high-resolution, temperature dependent spectroscopic mapping with the STM as well as resonant elastic x-ray scattering (REXS) on the same sample, we have made several important contributions. First, we have established that the charge ordering observed with the STM is present at the same wavevector in the REXS measurements. Depending on doping, we find this wavevector to be the same as that of Y-based cuprates or La-based cuprates, thereby establishing a universality of charge ordering mechanism across all families of cuprates. Second, we found that both the STM and REXS signals confirmed that the charge ordering competes with superconductivity as it becomes weaker with decreasing temperature below T_c , where superconductivity gets stronger. Third, using the energy resolution of the STM together with its ability to obtain information about momentum of the quasi-particles using their interference, we established a connection between the end of the arcs of the pseudogap in momentum space and the charge ordering wavevector (Figure 3). Finally, by demonstrating that charge ordering signatures in the STM measurements is particle-hole asymmetric, we show that it is likely caused by the organization of holes and is very much connected to Mott physics as opposed to some weak-coupling nesting mechanism.

New Techniques: Spin Polarized and Josephson STM capabilities

Over the last two years we have commissioned two different STM instruments, one for spin-polarized STM work with a vector field, and the other for ultra-low temperature experiments and high magnetic fields. We have now fully developed the capability to do spin-polarized STM with Cr tips. Currently, we are using these tips to study model magnetic nanostructures and are learning how to probe spin-orbit coupling using these techniques. We will be applying this technique to the study of heavy fermions systems in the coming year. In the ultra-low temperature system, we have managed to get very high quality STM tunneling into conventional superconductors using a superconducting tip. We are still improving the electron temperature in this system, as that is the only barrier to achieving coherent Josephson tunneling using STM. Overall, this is progressing well and in the coming year a focus for our group will be to demonstrate local Josephson coupling.

Future Plans:

We will continue to explore the physics of correlated superconductors through various experiments on heavy fermion and cuprates superconductors, with an emphasis on understanding the competition between superconductivity and other types ordering phenomena that are possible in these systems. One area of focus will be to study the so-called Q-phase in the 115 compound in which anti-ferromagnetism (AFM) and superconductivity co-exist and there is the possibility that there is an FFLO

state with pairing at a finite wavelength. Also, application of spin-polarized STM to detect AFM in heavy fermions would be quite interesting and complement spatially averaged techniques such as neutron scattering.

Publications Supported by the DOE-BES (2013-2014):

In addition to publications directly related to DOE-BES projects, the DOE funding that supports the instrumentation in our lab have assisted other projects. The publications from these projects benefiting from DOE support are also included in the list below (marked as partially supported by DOE).

1. B. Zhou, S. Misra, E. H. da Silva Neto, P. Aynajian, R. E. Baumbach, J. D. Thompson, E. D. Bauer, and A. Yazdani, “Visualizing Nodal Heavy Fermion Superconductivity,” *Nature Physics*, **9**, 474 (2013). (Cover story & also discussed in News & Views). Fully supported by DOE.
2. E. H. da Silva Neto, P. Aynajian, A. Frano, R. Comin, E. Schierle, E. Weschke, A. Gyenis, J. Wen, J. Schneeloch, Z. Xu, S. Ono, G. Gu, M. Le Tacon, and A. Yazdani, “Ubiquitous Interplay between Charge Ordering and High-Temperature Superconductivity in Cuprates,” *Science*, **343**, 393 (2014). (Also covered in Perspective). Fully supported by DOE.
3. E. H. da Silva Neto, P. Aynajian, R. E. Baumbach, E. D. Bauer, J. Mydosh, S. Ono, and A. Yazdani, “Detection of electronic neumaticity using scanning tunneling microscope,” *Physical Review B*, **87**, 161170 (2013). (Editors choice). Fully supported by DOE.
4. Pegor Aynajian, Eduardo H. da Silva Neto, Brian B. Zhou, Shashank Misra, Ryan E. Baumbach, Zachary Fisk, John Mydosh, Joe D. Thompson, Eric D. Bauer, and Ali Yazdani, *Journal of the Physical Society of Japan* **83**, 061008 (2014), invited review paper. Fully supported by DOE.
5. Ilya K. Drozdov, A. Alexandradinata, Sangjun Jeon, Stevan Nadj-Perge, Huiwen Ji, R. J. Cava, B. A. Bernevig, and Ali Yazdani, “One-dimensional topological edge states of bismuth bilayers,” available at arXiv:1404.2598, to appear in *Nature Physics* (2014). Partial support by DOE.
6. Sangjun Jeon, Brian B. Zhou, András Gyenis, Benjamin E. Feldman, Itamar Kimchi, Andrew C. Potter, Quinn D. Gibson, Robert J. Cava, Ashvin Vishwanath, Ali Yazdani, “Landau quantization and quasiparticle interference in the three-dimensional Dirac semimetal Cd_3As_2 ,” available at arXiv:1403.3446, to appear in *Nature Materials* (August 2014). Partial support by DOE.

Electron Nanocrystallography of Complex Materials and Processes

Jian-Min Zuo

Dept. of Materials Science and Engineering and Materials Research Laboratory,
University of Illinois, Urbana-Champaign, IL 61801

Program Scope

Ferroelectric crystals possess spontaneous polarization; the direction and magnitude of spontaneous polarization can be determined by convergent beam electron diffraction (CBED). The principle is based on crystal symmetry and symmetry breaking induced by polarization. Under the DOE BES support, we have developed a quantitative method for quantifying and mapping crystal symmetry using scanning CBED. Using this technique, polar domains can be imaged using a nanometer-sized electron beam. Here, we propose a further development of this technique for a quantitative measurement of polarization and its application to the relaxor-ferroelectric crystals of PMN-xPT ($\text{Pb}(\text{Mg}_{1/3}\text{Nb}_{2/3})\text{O}_3$ - $x\text{PbTiO}_3$) and PZN-xPT ($\text{Pb}(\text{Zn}_{1/3}\text{Nb}_{2/3})\text{O}_3$ - $x\text{PbTiO}_3$). Specifically, we propose to map the spatial distribution of monoclinic phases and investigate their response under external mechanical forces. For the measurement, we propose to measure local polarization by measuring the structure factor phase to the accuracy of $1/10$ degree or better so the atomic positions can be determined with precision better than 1 picometer, beyond the resolution of electron direct imaging. We expect the significant improvement in the measuring accuracy will have a major impact on the study of polar crystals in general, including highly doped materials.

The experiment will be carried out using the scanning electron nanodiffraction (SEND) technique developed here at University of Illinois by recording electron diffraction patterns at every probe positions. Electron beams of 1 nm or less in full-width at half-maximum (FWHM) will be obtained using a field emission gun TEM. Electron diffraction patterns are recorded on a CCD camera. For local structure factor measurement, we use the so-called refinement method by comparing experimental and theoretical intensities and optimizing for the best fit. A JEOL2200FS TEM with an in-column energy filter will be used for this study.

Recent Progress

Background: The symmetry of piezoelectric materials has been widely studied for the simple reason that symmetry controls displacements of ionic charge and position, which, in turn, determines directions of spontaneous polarization (\mathbf{P}_s) and spontaneous strain ($\boldsymbol{\epsilon}_s$), and field (E)-induced orientations of ferroelectric and piezoelectric properties. The

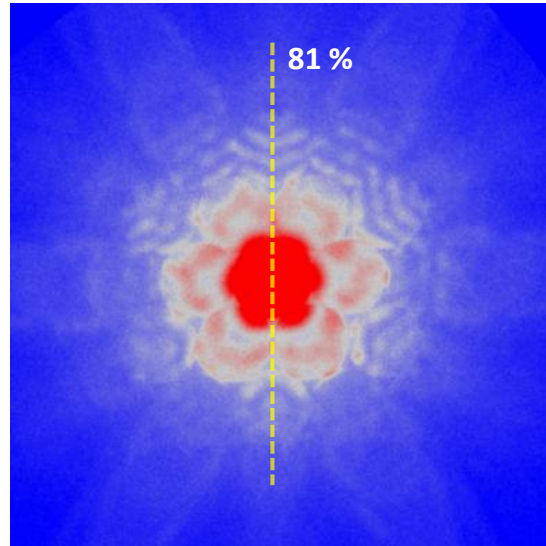


Fig. 1 A CBED pattern recorded from the ferroelectric crystal of PMN-31%PT using an nm-sized electron probe. The pattern reveals a single mirror symmetry containing the polarization direction.

high-temperature (HT) phase of PMN-xPT and PZN-xPT is cubic $Pm3m$ with no spontaneous distortions. According to published x-T phase diagrams for PMN-xPT and PZN-xPT, the prototypic HT phase spontaneously distorts to rhombohedral (R) $R3m$ symmetry on cooling at low x, or tetragonal (T) $P4mm$ symmetry at higher x, in which \mathbf{P}_S and $\boldsymbol{\varepsilon}_S$ are constrained to the cubic (noted by the subscript 'C') $[111]_C$ and $[001]_C$ directions for the R and T phases, respectively. The R and T phases are initially separated by a vertical boundary termed the morphotropic phase boundary (MPB), i.e., a chemically (x)-driven change in morphology. The MPB of PMN-xPT and PZN-xPT is defined in a narrow composition region where the R and T phases meet. This phase boundary composition has attracted much attention because displacements maximize as the lattice softens and transforms, giving rise to large enhancements in piezoelectric properties.

A large body of work has been reported on the structural origin of the piezoelectric properties of PMN-xPT at the MPB. A new phase with monoclinic (M) symmetry was proposed in the vicinity of MPB as identified using X-ray and neutron diffraction studies. Several research groups, however, have disputed whether the observed M phase truly has the monoclinic symmetry at the local (microscopic) scale. The adaptive phase model proposed by Viehland and coworkers states that the M phase found in the MPB region is not a local symmetry but an averaged symmetry obtained from twin-related domain structures.[1] Another point-of-view, put forward by Kisi et al., suggests the M phase is not a true phase but a distorted structure resulting from residual stress.[2] Thus, a determination of symmetry, from the local to macroscopic level, in the MPB region, is therefore critical to settle these disputes, and is the purpose of this investigation.

Results: We have made major breakthroughs in CBED quantification of symmetry and in the applications of our method to the study of PMN-xPT crystals as follows:

- 1) *Symmetry quantification and mapping using convergent beam electron diffraction:* We proposed a new algorithm to quantify symmetry recorded in convergent beam electron diffraction (CBED) patterns and use it for symmetry mapping. Experimental and simulated CBED patterns recorded from a Si single crystal are used to calibrate the proposed algorithm for the symmetry quantification. The proposed algorithm is then applied to a Si sample with defects. Using the mirror symmetry as an example, we demonstrated that the normalized cross-correlation coefficient provides an effective and robust measurement of the symmetry recorded in experimental CBED patterns.
- 2) *Symmetry determination in ferroelectric single crystals of PMN-PT:* By quantifying the symmetry recorded in the experimental CBED patterns, we show that the symmetry of PMN-31%PT is triclinic at few nm length scales, and becomes monoclinic (M_B)-like symmetry at the length scale of few tens of nm. The macroscopic symmetry determined by X-ray diffraction suggests multiple domains of different sizes in PMN-31%PT single crystal. Thus, the high piezoelectric response of PMN-31%PT single crystal at the MPB region is underlined by the structure that lacks local symmetry, which has an averaged monoclinic symmetry over tens of nanometers in some regions of the crystal.
- 3) *Fluctuations in local symmetry revealed by CBED:* Direct evidence for the volume dependence and spatial dependence of symmetry fluctuations was

obtained in PMN-31%PT by CBED with help of energy dispersive x-ray (EDX) spectroscopy. Fluctuations in symmetry were determined by using different electron beam probe sizes ranging from ~2 to 25 nm from a crystal ~62 nm thick. The symmetry of PMN-31%PT was found to increase linearly as the average volume increased, and the local symmetry fluctuated from one location to another at the nanoscale. The EDX spectroscopy results indicate chemical fluctuations are significant only when the probe size decreases to ~2nm. We attributed the symmetry fluctuation to locally varying composition, composition dependent ionic displacements, and spontaneous polarization.

Future Plans

The results we have achieved so far shows clearly that 1) the recorded symmetry of PMN-31%PT in CBED increases with sampling volume, 2) the local symmetry fluctuates from one location to another at the nanoscale and 3) CBED is a sensitive technique for measuring local symmetry. Since symmetry is ultimately determined by polarization and local strain in ferroelectric crystals, we plan to develop further of scanning CBED for quantitative measurement and mapping of polarization in ferroelectric crystals. The hypothesis is that in a small diffraction volume, the local atomic displacements do not average to zero and $\Delta\vec{r} = \Delta\vec{r}_S + \Delta\vec{r}_R$; one is systematic (S) and one is random (R). Their separation leads to the modified atomic scattering factor of $\langle f \rangle = f \exp(2\pi i \vec{g} \cdot \Delta\vec{r}_S) \exp(-2\pi g^2 \langle \Delta r_R^2 \rangle)$, where Δr_S gives rise to the structure factor phase. We will measure the structure factor phase (as well as amplitude) using the so-called refinement method [3-5]. The refinement method works by comparing experimental and theoretical CBED intensities and optimizing for the best fit. Multiple scattering effects can be taken into consideration by using dynamical theory to calculate diffraction intensities during the refinement. To obtain the phase map, we will further apply structure factor refinement to scanning CBED data.

Recent breakthrough in the direct electron detection camera enables detection of every single electron and recording at ~1000 frames per second for up to 15 minutes recording. Using this, we carried out initial experiments on oxidation of Fe, the results are promising [6]. We plan to further explore the applications of fast electron imaging and diffraction in in-situ studies.

References

- [1] D. Viehland, Journal of Applied Physics 88, 4794 (2000).
- [2] E. H. Kisi, R. O. Piltz, J. S. Forrester, and C. J. Howard, Journal of Physics-Condensed Matter 15, 3631 (2003).
- [3] J. M. Zuo, Acta Crystallographica Section A49, 429 (1993).
- [4] K. Tsuda, Y. Ogata, K. Takagi, T. Hashimoto, and M. Tanaka, Acta Cryst. A58, 514 (2002).
- [5] J. M. Zuo, Reports on Progress in Physics 67, 2053 (2004).
- [6] Aram Yoon et al., Microscopy and Microanalysis, in print, (2014).

DOE Sponsored Publications in 2012-2014

Publications in refereed journals:

- 1) K. Ran, X. Mi, Z. J. Shi, Q. Chen, Y. F. Shi, and J. M. Zuo, "Molecular packing of fullerenes inside single-walled carbon nanotubes," *Carbon* 50 (15), 5450-5457 (2012).
- 2) K. Ran, Q. Chen, and J. M. Zuo, "Fabrication and structure characterization of quasi-2-dimensional amorphous carbon structures," *Acta Phys. -Chim. Sin.* 28 (7), 1551-1555 (2012).
- 3) K. Ran, J. M. Zuo, Q. Chen, and Z. J. Shi, "Electrons for single molecule diffraction and imaging", *Ultramicroscopy* 119, 72 (2012).
- 4) Kyou-Hyun Kim, David A. Payne, and Jian-Min Zuo, "Symmetry of piezoelectric (1-x)Pb(Mg_{1/3}Nb_{2/3})O-3-xPbTiO(3) (x=0.31) single crystal at different length scales in the morphotropic phase boundary region," *Physical Review B* 86 (18), 184113 (2012).
- 5) Kyou-Hyun Kim and Jian-Min Zuo, "Symmetry quantification and mapping using convergent beam electron diffraction," *Ultramicroscopy* 124, 71-76 (2013).
- 6) A. B. Shah, S. T. Sivapalan, B. M. DeVetter, T. K. Yang, J. G. Wen, R. Bhargava, C. J. Murphy, and J. M. Zuo, "High-index facets in gold nanocrystals elucidated by coherent electron diffraction," *Nano Letters* 13 (4), 1840-1846 (2013).
- 7) Kyou-Hyun Kim, David A. Payne, and Jian-Min Zuo, "Determination of fluctuations in local symmetry and measurement by convergent beam electron diffraction: applications to a relaxor-based ferroelectric crystal after thermal annealing", *J. Appl. Cryst.* 46, 1331-1337 (2013).
- 8) K. Kim and J. M. Zuo, "Convergent-beam electron diffraction pattern symmetry of nanodomains in complex lead-based perovskite crystals", *Acta Crystallographica Section A*, in print (2014).

Publications in conference proceedings:

- 1) Y Hu, J Li, and J-M Zuo, "Reducing transient electric fields effect in ultrafast electron diffraction using multiple laser pulse train", *Microscopy and Microanalysis* 19 (S2), 1170 (2013).
- 2) Jianbo Wu, Wenpei Gao, Hong Yang, and Jian-Min Zuo, "Imaging shape-dependent corrosion behavior of pt nanoparticles in H₂AuCl₄ solution over extended time using a liquid flow cell and TEM", *Microscopy and Microanalysis*, in print, (2014).
- 3) Aram Yoon, Xiaofeng Zhang, Wenpei Gao, Jianbo Wu, Yung-Tin Pan, Hong Yang and Jian-Min Zuo, "Oxidation of Fe whiskers and surface diffusion observed by environmental TEM", *Microscopy and Microanalysis*, in print, (2014).
- 4) Wenpei Gao, Jianbo Wu, Aram Yoon, J. Mabon, W. Swiech, W.L. Wilson, H. Yang and Jian-Min Zuo, "Surface atomic diffusion processes observed at milliseconds time resolution using environmental TEM", *Microscopy and Microanalysis*, in print, (2014).

Book Chapter

J.M. Zuo, W.J. Huang, Coherent Electron Diffractive Imaging, in: G. Van Tendeloo, D. Van Dyck and S. J. Pennycook (Eds) *Handbook of Nanoscopy*, Wiley-VCH, Weinheim, Germany, 2012

AUTHOR INDEX
AND
PARTICIPANT LIST

Balke, Nina.....	162	Lupini, Andrew R.	30, 46, 62
Balsara, Nitash.....	2	Ma, Chao	50
Batson, P. E.....	72	Madhavan, Vidya.....	150
Berezovsky, Jesse	76	Maksymovych, P.	26, 34
Borisevich, Albina Y.	6	Manoharan, Hari C.	54
Camden, Jon P.....	80	Marks, L. D.	154
Campbell, Geoffrey H.....	10	McKeown, Joseph T.	10
Chandrasekhar, Venkat	84	McMorrان, Benjamin J.	158
Chen, Long-Qing	88	Meng, Shirley	162
Chisholm, Matthew F.	30, 46, 62	Miao, Jianwei (John).....	166
Cobden, David H.	92	Minor, Andrew	2
Crozier, Peter A.	96	Mishra, Rohan	6
Davis, J. C. Séamus	14	Morgan, Dane	218
De Graef, Marc.....	100	Muller, David A.....	170
Dillon, Shen J.	104	Nguyen, Linh.....	10
Dougherty, Dan	108	Orenstein, Joseph.....	54
Downing, Kenneth.....	2	Oxley, Mark P.....	178
Dudney, Nancy	162	Pak, Jeongihm.....	202
Dutt, Gurudev.....	112	Pan, Xiaoqing	174
Eom, Chang-Beom	118	Pantelides, Sokrates T.	6, 178
Fennie, Craig J.....	170	Petford-Long, Amanda K.	38
Fuchs, Gregory	116	Phatak, Charudatta	38
Garlow, Joseph	22	Plummer, Ward.....	182
Gianfrancesco, A.	26, 34	Pollard, Shawn D.	66
Goldhaber-Gordon, David	54	Prendergast, David.....	2
Gozar, Adrian	18	Pulecio, Javier F.....	66
Gruverman, Alexei	118	Raschke, Markus B.	186
Hammel, P. Chris	122	Reddy, Pramod	190
Han, Myung-Geun.....	22	Robertson, Ian M.	194
He, Qiuán	6	Ruan, Chong-Yu	198
Heo, Tae Wook.....	10	Rudd, Robert E.	10
Hong, Seungbum	38	Santala, Melissa K.	10
Huey, Bryan D.....	126	Schiffer, Peter	170
Humphrey, Emma.....	100	Schlom, Darrell G.	170
Iavarone, Maria	130	Shpyrko, Oleg.....	162
Jang, Jae Hyuck.....	6	Smith, Arthur R.	202
Jarillo-Herrero, Pablo	233	Solares, Santiago D.....	206
Kalinin, S. V.....	26, 34	Stemmer, Susanne.....	210
Kc, Prabhat.....	100	Tao, Jing	42
Könenkamp, Rolf	134	Treacy, M. M. J.	214
Kortright, Jeffrey	2	Tselev, A.	26, 34
Lagos, M. J.....	72	Tsymbal, Evgeny	118
Lai, Keji	138	Varela, Maria.....	30, 46, 62
Lev, Benjamin	142	Varga, Kalman.....	178
Li, Lian.....	146	Vasudevan, R.....	26, 34
Lin, W.	26, 34	Volkov, Vyacheslav V.	66

Voyles, Paul M.	218
Wang, Feng	162
Weiss, Paul S.	222
Wiezorek, Jörg M. K.	225
Wu, Lijun	50
Wu, Weida	229
Xin, Huolin.....	162
Yacoby, Amir	233
Yazdani, Ali	237
Zhang, Shoucheng	54
Zheng, Haimei	58
Zhou, Wu	30, 46, 62
Zhu, Yimei	22, 42, 50, 66
Zuckermann, Ronald.....	2
Zuo, Jian-Min	241

Nitash Balsara
Lawrence Berkeley National Laboratory
nbalsara@berkeley.edu

Philip Batson
Rutgers University
batson@physics.rutgers.edu

Jesse Berezovsky
Case Western Reserve University
jab298@case.edu

Albina Borisevich
Oak Ridge National Laboratory
albinab@ornl.gov

Jon Camden
University of Notre Dame
jon.camden@gmail.com

Geoffrey Campbell
Lawrence Livermore National Laboratory
ghcampbell@llnl.gov

Long-Qing Chen
The Pennsylvania State University
lqc3@psu.edu

Matthew Chisholm
Oak Ridge National Laboratory
chisholmmf@ornl.gov

Tammy Click
ORAU
tammy.click@orau.org

David Cobden
University of Washington
cobden@uw.edu

Peter Crozier
Arizona State University
crozier@asu.edu

John Cumings
University of Maryland
cumings@umd.edu

JC Séamus Davis
Cornell University/Brookhaven Nat'l Lab
jcdavis@ccmr.cornell.edu

Marc De Graef
Carnegie Mellon University
degraef@cmu.edu

Shen Dillon
University of Illinois Urbana-Champaign
sdillon@illinois.edu

Daniel Dougherty
North Carolina State University
dbdoughe@ncsu.edu

Gurudev Dutt
University of Pittsburgh
ljp14@pitt.edu

Gregory Fuchs
Cornell University
gdf9@cornell.edu

David Goldhaber
Stanford University
goldhaber-gordon@stanford.edu

Adrian Gozar
Brookhaven National Laboratory
agozar@bnl.gov

Alexei Gruverman
University of Nebraska-Lincoln
agruverman2@unl.edu

Nathan Guisinger
Argonne National Laboratory
nguisinger@anl.gov

P Chris Hammel
Ohio State University
hammel@mps.ohio-state.edu

Myung-Geun Han
Brookhaven National Laboratory
mghan@bnl.gov

Seungbum Hong
Argonne National Laboratory
hong@anl.gov

Bryan Huey
University of Connecticut
bhuey@ims.uconn.edu

Maria Iavarone
Temple University
iavarone@temple.edu

Juan Idrobo
Oak Ridge National Laboratory
idrobojc@ornl.gov

Sergei Kalinin
Oak Ridge National Laboratory
sergei2@ornl.gov

Rolf Könenkamp
Portland State University
rkoe@pdx.edu

Keji Lai
University of Texas at Austin
kejilai@physics.utexas.edu

Benjamin Lev
Stanford University
benlev@stanford.edu

Lian Li
University of Wisconsin, Milwaukee
lianli@uwm.edu

Andrew Lupini
Oak Ridge National Laboratory
9az@ornl.gov

Vidya Madhavan
University of Illinois, Urbana-Champaign
vm1@illinois.edu

Petro Maksymovych
Oak Ridge National Laboratory
maksymovychp@ornl.gov

Harindran Manoharan
Stanford University
manoharan@stanford.edu

George Maracas
U.S. Department of Energy
george.maracas@science.doe.gov

Laurence Marks
Northwestern University
L-marks@northwestern.edu

Benjamin McMorran
University of Oregon
mcmorran@uoregon.edu

Shirley Meng
University of California San Diego
shirleymeng@ucsd.edu

Jianwei Miao
University of California, Los Angeles
miao@physics.ucla.edu

Karren More
Oak Ridge National Laboratory
morekl1@ornl.gov

David Muller
Cornell University
dm24@cornell.edu

Jeongihm Pak
Ohio University
pakj@ohio.edu

Xiaoqing Pan
University of Michigan
panx@umich.edu

Sokrates Pantelides
Vanderbilt University
pantelides@vanderbilt.edu

Amanda Petford-Long
Argonne National Laboratory
petford.long@anl.gov

Ward Plummer
Louisiana State University
wplummer@phys.lsu.edu

Markus Raschke
University of Colorado
markus.raschke@colorado.edu

Pramod Reddy
University of Michigan
pramodr@umich.edu

Aram Rezikyan
Arizona State University
arezikya@asu.edu

Ian Robertson
University of Wisconsin-Madison
enr-dean@enr.wisc.edu

Chong-Yu Ruan
Michigan State University
ruan@pa.msu.edu

Eric Schwegler
Lawrence Livermore National Laboratory
schwegler1@llnl.gov

Arthur Smith
Ohio University
smitha2@ohio.edu

Santiago Solares
The George Washington University
ssolares@gwu.edu

Susanne Stemmer
University of California, Santa Barbara
stemmer@mrl.ucsb.edu

Jing Tao
Brookhaven National Laboratory
jtao@bnl.gov

John Christopher Thomas
University of California, Los Angeles
jct197@ucla.edu

Maria Varela
Oak Ridge National Laboratory
mvarela@ornl.gov

Paul Voyles
University of Wisconsin-Madison
voyles@enr.wisc.edu

Haiyan Wang
National Science Foundation (on leave from TAMU)
hawang@nsf.gov

Jorg Wiezorek
University of Pittsburgh
wiezorek@pitt.edu

Lijun Wu
Brookhaven National Laboratory
ljwu@bnl.gov

Weida Wu
Rutgers University
wdwu@physics.rutgers.edu

Amir Yacoby
Harvard University
yacoby@physics.harvard.edu

Ali Yazdani
Princeton University
yazdani@princeton.edu

Shoucheng Zhang
Stanford University
sczhang@stanford.edu

Haimei Zheng
Lawrence Berkeley National Laboratory
hmzheng@lbl.gov

Wu Zhou
Oak Ridge National Laboratory
zhouw1@ornl.gov

Jane Zhu
U.S. Department of Energy
jane.zhu@science.doe.gov

Yimei Zhu
Brookhaven National Laboratory
zhu@bnl.gov

Jian Min Zuo
University of Illinois
jianzuo@illinois.edu